Spent Nuclear Fuel Final Disposal Program

Preliminary Development of Pre-Siting Safety Case

Taiwan Power Company

Feb 2023

Table of Contents

1. Introduction 1-1

1.1. SPENT NUCLEAR FUEL FINAL DISPOSAL PROGRAM 1-1

1.2. PURPOSE OF THE PRELIMINARY SAFETY CASE REPORT 1-1

1.3. FEEDBACK FROM SNFD2017 REPORT 1-2

1.4. LAWS AND REGULATIONS 1-4

1.5. EXECUTIVE TEAMS (ORGANIZATIONS) 1-12

1.6. PREVIOUS RESEARCHES 1-14

2. Methodology 2-1

2.1. CURRENT STATUS OF DISPOSAL PROGRAM IN OTHER COUNTRIES 2-1

2.2. METHODOLOGY OF SAFETY CASE 2-3

2.3. DEFINITION OF SYSTEM BOUNDARY 2-8

2.4. TIMESCALES 2-10

2.5. SAFETY OF THE REPOSITORY 2-15

2.6. EXPERT JUDGMENTS 2-17

2.7. INFORMATION/UNCERTAINTY MANAGEMENT 2-18

2.8. QUALITY ASSURANCE 2-23

2.9. RISK ASSESSMENT 2-25

3. Features/Events/Processes (FEPs) 3-1

3.1. INTRODUCTION 3-1

3.2. FEPS DATABASE OF THE REFERENCE CASE 3-1

3.3. FEPS LIST OF THE REFERENCE CASE 3-3

3.4. COMPREHENSIVE ANALYSES 3-16

4. Initial State of the Repository 4-1

4.1. INTRODUCTION 4-1

4.2. SOURCE TERM AND INITIAL STATE 4-2

4.3. INITIAL STATE OF GEOSPHERE AND BIOSPHERE 4-45

4.4. LAYOUT OF THE REPOSITORY 4-60

4.5. MONITORING 4-70

5. External Factors 5-1

5.1. INTRODUCTION 5-1

5.2. CLIMATE 5-1
5.3. TECTONIC EVOLUTION 5-11
5.4. FUTURE HUMAN ACTIONS 5-25

6. Internal Processes 6-1
6.1. INTRODUCTION 6-1
6.2. COUPLING OF THE INTERNAL PROCESSES 6-1
6.3. ASSESSMENT MODEL FLOWCHART (AMF) 6-25

7. Safety Functions and Safety Function Indicators 7-1
7.1. INTRODUCTION 7-1
7.2. SAFETY FUNCTIONS, SAFETY FUNCTION INDICATORS, AND SAFETY FUNCTION INDICATOR CRITERIA 7-2
7.3. CONTAINMENT SAFETY FUNCTION INDICATORS 7-4
7.4. RETARDATION SAFETY FUNCTION INDICATORS 7-12
7.5. KEY ISSUES OF EVOLUTION OVER TIME 7-20
7.6. FACTORS AFFECTING SAFETY FUNCTION INDICATORS OVER TIME 7-21

8. Compilation of Input Data and Data Uncertainty 8-1
8.1. INTRODUCTION 8-1
8.2. REFERENCE REQUIREMENTS AND CRITERIA FOR JUDGMENT 8-3
8.3. INVENTORY OF DATA 8-3
8.4. PROCEDURE FOR ASSIGNING VALUES 8-14

9. Evolution Analyses of the Repository 9-1
9.1. INTRODUCTION 9-1
9.2. EXCAVATION AND OPERATION PERIOD 9-10
9.3. THE INITIAL PERIOD AFTER CLOSURE (POST-CLOSURE 1,000 YEARS) 9-30
9.4. THE REMAINING GLACIAL PERIOD AFTER CLOSURE (POST-CLOSURE 120,000 YEARS) 9-103
9.5. THE SUBSEQUENT GLACIAL CYCLES 9-149
9.6. GLOBAL WARMING 9-154
9.7. CONCLUSION OF THE EVOLUTION ANALYSIS 9-156

10. Selection of Scenarios 10-1
10.1. INTRODUCTION 10-1
10.2. DESIGN-BASIS EVOLUTION SCENARIOS 10-2

10.3. NON-DESIGN-BASIS EVOLUTION SCENARIOS 10-10
10.4. FUTURE HUMAN ACTIONS (FHA)..10-11
10.5. WHAT-IF SCENARIOS..10-12
10.6. CONCLUSION 10-14

11. Containment safety function Analyses of the Selected Scenarios 11-1
11.1. INTRODUCTION 11-1
11.2. BUFFER ADVECTION...11-3
11.3. BUFFER TRANSFORMATION 11-6
11.4. CONCLUSION FOR BUFFER SCENARIOS 11-7
11.5. CANISTER FAILURE DUE TO CORROSION...11-7
11.6. CANISTER FAILURE DUE TO ISOSTATIC LOAD 11-10
11.7. CANISTER FAILURE DUE TO SHEAR FORCE 11-13
11.8. SCENARIOS SYNTHESIZING ANALYSIS 11-17

12. Retardation safety function Analyses of the Selected Scenarios 12-1
12.1. INTRODUCTION 12-1
12.2. ASSESSMENT OF THE BIOSPHERE 12-1
12.3. CRITICALITY 12-21
12.4. RADIONUCLIDE TRANSPORT AND DOSE ESTIMATION 12-24
12.5. QUANTITATIVE ASSESSMENT OF CANISTER FAILURE DUE TO CORROSION 12-31
12.6. QUANTITATIVE ASSESSMENT OF CANISTER FAILURE DUE TO SHEAR FORCE..12-47
12.7. ANALYSES OF WHAT-IF SCENARIOS 12-64
12.8. SUMMATION OF THE RISK 12-76
12.9. UNCERTAINTIES OF THE RISK ASSESSMENT...12-78
12.10. SUMMARY OF THE RETARDATION SAFETY FUNCTION ANALYSES..........12-80
12.11. CONCLUSION OF SENSITIVITY ANALYSES 12-81

13. Additional Analyses and Supporting Arguments..13-1
13.1. INTRODUCTION 13-1
13.2. FUTURE HUMAN ACTIONS SCENARIOS 13-1
13.3. NON-DESIGN-BASIS EVOLUTION SCENARIOS 13-8
13.4. DEMONSTRATION OF OPTIMIZATION OF THE ANALYSES AND THE USE OF BEST AVAILABLE TECHNIQUES 13-10

13.5. IMPACT ON SCENARIOS AND RISK ASSESSMENT AFTER FEPS SCREENING 13-13
13.6. SAFETY OF THE DISPOSAL SYSTEM BEYOND ONE MILLION YEARS 13-16
13.7. STUDY OF NATURAL ANALOGUES 13-16

14. Conclusions 14-1
14.1. INTRODUCTION 14-1
14.2. SUMMARY OF THE ASSESSMENT 14-1
14.3. DEMONSTRATION OF THE COMPLIANCE 14-5
14.4. DESIGN BASIS 14-11
14.5. FEEDBACK TO REFERENCE DESIGN AND DESIGN PREMISES 14-14
14.6. FEEDBACK TO DETAILED SITE INVESTIGATION AND SDM 14-25
14.7. FEEDBACK TO R&D PROGRAM 14-34
14.8. CONCLUSION RELEVANT TO SAFETY ASSESSMENT METHODOLOGY 14-51

15. References 15-1
Appendix A: Process models for terrestrial module 1
Appendix B: Process models for aquatic module 3
Appendix C: Ingestion exposure pathways model for dose calculation model 6
Appendix D: Inhalation and external exposure pathways model for dose calculation model 8
Appendix E: Dataset for Biosphere Assessment 9

List of Figures

Figure 1-1: Work plan for the SNF final disposal program in Taiwan. 1-3
Figure 1-2: Organization of the Spent Nuclear Fuel Final Disposal Program. 1-13
Figure 2-1: Flowchart of the safety case. 2-7
Figure 2-2: KBS-3 disposal concept 2-9
Figure 2-3: Radiotoxicity of SNF over time. 2-14
Figure 2-4: Classification of uncertainty. 2-21
Figure 4-1: Screening process of the major radionuclides. 4-6
Figure 4-2: Specifications of copper shell of the canister. 4-14
Figure 4-3: Specifications of cast iron lining of the canister. 4-15
Figure 4-4: Specifications of steel lid of the canister. 4-15
Figure 4-5: Specifications of copper shell and cast iron lining of the canister. 4-16
Figure 4-6: Cross-section of the canister 4-16
Figure 4-7: Geometry specifications of the buffer blocks and rings. 4-22
Figure 4-8: Installation of canister and buffer in the deposition hole. 4-23
Figure 4-9: Saturated densities of buffer in the deposition hole. 4-24
Figure 4-10: Swelling pressure versus bentonite dry density for different water solutions. 4-25
Figure 4-11: Hydraulic conductivity versus bentonite dry density for different water solutions. 4-25
Figure 4-12: Geometry design requirements of the deposition hole. 4-28
Figure 4-13: Bevel design of the deposition hole and demonstration of the installation of the canister. 4-29
Figure 4-14: Specifications of the disposal tunnel. 4-36
Figure 4-15: Geometry specifications of the backfill blocks. 4-36
Figure 4-16: Installation of backfill in the disposal tunnel. 4-37
Figure 4-17: Geometry specifications of the plug. 4-41
Figure 4-18: Profile of the plug. 4-41
Figure 4-19: Schematic view of the borehole seal. 4-44
Figure 4-20: The geological map and borehole location in one of the granitic area in Taiwan 4-58

Figure 4-21: Comprehensive analysis map of geophysical survey in one of the granitic area in Taiwan. 4-58
Figure 4-22: Three dimensional distribution of geologic units in the reference case and schematic profile. 4-59
Figure 4-23: Recharge volume from 1991 to 2019 of the reference case. 4-59
Figure 4-24: Estimation steps of thermal dimensioning. 4-63
Figure 4-25: Extended Full Perimeter InterSection Criterion (EFPC). 4-63
Figure 4-26: Hybrid DFN/ECPM model. 4-64
Figure 4-27: Maximum temperature in the buffer versus canister spacing under different geothermal gradient and different initial power output. 4-68
Figure 4-28: Layout of the underground facility. 4-69
Figure 4-29: Layout of deposition holes in the disposal tunnel. 4-69
Figure 5-1: Estimated climate evolution and sea-level changes. 5-6
Figure 5-2: Global temperature changes in different RCP scenarios. 5-6
Figure 5-3: Observation data of temperature changes of Taiwan (from 1900 to 2017). 5-7
Figure 5-4: Location of Binhai fault (blue line) and reference case (red triangle) 5-16
Figure 5-5: Logic tree for seismic hazard analysis. 5-16
Figure 5-6: Boundaries of the three diffuse seismicity. 5-17
Figure 5-7: Accumulated seismicity rate versus earthquake magnitude within the range of 200 km radius from the reference case. 5-17
Figure 5-8: Accumulated seismicity rate versus earthquake magnitude within AS_K01 region. 5-18
Figure 5-9: Accumulated seismicity rate versus earthquake magnitude within DS_K01 region. 5-18
Figure 5-10: Impact on long-term safety of the repository due to uplifting and denudation. 5-20
Figure 5-11: Volcanism distribution in Taiwan. 5-23
Figure 5-12: Distribution and eruption probability for volcanoes in Taiwan. 5-24
Figure 6-1: Concept of process diagram (buffer/backfill). 6-3
Figure 6-2: Assessment model flowchart (AMF). 6-26

Figure 8-1: Input data parameters for radionuclide transport in safety assessment. 8-2
Figure 8-2: The distributions of solubility limits for strontium, radium, zirconium, and niobium in probabilistic analyses. 8-12
Figure 8-3: The distributions of solubility limits for technetium, nickel, palladium, and tin in probabilistic analyses. 8-12
Figure 8-4: The distributions of solubility limits for selenium, thorium, protactinium and uranium in probabilistic analyses. 8-13
Figure 8-5: The distributions of solubility limits for neptunium, plutonium, americium, curium and lead in probabilistic analyses. 8-13
Figure 9-1: Hydrogeological model with sea-level equals to 0 m. 9-8
Figure 9-2: Hydrogeological model with sea-level dropping to -20 m. 9-8
Figure 9-3: Hydrogeological model with sea-level dropping to -120 m. 9-9
Figure 9-4: Safety factors of the disposal tunnel after excavation. 9-14
Figure 9-5: Safety factors of the disposal tunnel during an earthquake. 9-15
Figure 9-6: Total water pressure results in near-field outputted by DarcyTools. 9-18
Figure 9-7: FracMan imports the near-field fractures exported by DarcyTools and analyzes the fracture connectivity. 9-18
Figure 9-8: Total head for each node on the fractures of FracMan. 9-19
Figure 9-9: Deposition hole DH-61 and the intersecting fracture. 9-19
Figure 9-10: Hydrostatic pressure of DH-61 deposition hole and the fracture. 9-20
Figure 9-11: Velocity and direction of flow in the fracture. 9-20
Figure 9-12: Flow rate in the fracture. 9-21
Figure 9-13: Demonstration of water flow into the disposal tunnel and deposition hole through fracture. 9-26
Figure 9-14: Accumulated eroded material versus accumulated water flow of horizontal erosion test. 9-26
Figure 9-15: Accumulated eroded material versus accumulated water flow of vertical erosion test. 9-27
Figure 9-16: Accumulated eroded material versus accumulated water flow. 9-27

Figure 9-17: Peak buffer temperature at the top of the canister over time with different canister spacing (thermal conductivity of the host rock: 2.3 W/mK). 9-34
Figure 9-18: Peak buffer temperature at the top of the canister over time with different canister spacing (thermal conductivity of the host rock: 3.0 W/mK). 9-34
Figure 9-19: Grids of the site scale model. 9-41
Figure 9-20: Effective hydraulic conductivity values of the site scale model. 9-41
Figure 9-21: Dynamic pressure of the site scale model. 9-42
Figure 9-22: Salinity of the site scale model. 9-42
Figure 9-23: Concept of Q1 and Q2 release paths. 9-43
Figure 9-24: Dynamic pressure and salinity of Q1 release paths of the site scale model. 9-43
Figure 9-25: Dynamic pressure and salinity of Q2 release paths of the site scale model. 9-44
Figure 9-26: Cumulative distribution functions of flow related transport resistance for Q1 and Q2 paths of the site scale model. 9-44
Figure 9-27: Cumulative distribution functions of equivalent flow rate for Q1 and Q2 paths of the site scale model. 9-45
Figure 9-28: Salinity distribution at the depth of canisters. 9-48
Figure 9-29: The 3D numerical model. 9-51
Figure 9-30: Initial dry density of the buffer and backfill. 9-51
Figure 9-31: Fracture positions and initial state of saturation (the fractures intersect with both the disposal tunnel and the deposition hole). 9-52
Figure 9-32: Average saturation versus time (when fractures intersect with both the disposal tunnel and the deposition hole). 9-52
Figure 9-33: Fracture position and initial state of saturation (the fracture only intersects with the deposition hole). 9-53
Figure 9-34: Average saturation versus time (when fracture only intersects with the deposition hole). 9-53
Figure 9-35: Fracture positions and swelling pressure when saturated (the fractures intersect with both the disposal tunnel and the deposition hole). 9-59

Figure 9-36: Fracture positions and swelling pressure when saturated (the fracture only intersects with the deposition hole). 9-59
Figure 9-37: Swelling pressure distribution when saturated. 9-60
Figure 9-38: Initial dry density distribution. 9-60
Figure 9-39: Distribution of vertical displacement after canister sinking. 9-61
Figure 9-40: Distribution of dry density after canister sinking. 9-61
Figure 9-41: Redistribution of bentonite at different times after loss of 1,200 kg bentonite. 9-62
Figure 9-42: Distribution of pore water, porosity, and pH value of the plug and backfill after 1 year of closure. 9-71
Figure 9-43: Distribution of pore water, porosity, and pH value of the plug and backfill after 100 years of closure. 9-72
Figure 9-44: Relationship between axial displacement of the backfill behind the plug and time 9-73
Figure 9-45: Groundwater infiltrates into the deposition hole through water-conducting fracture. 9-89
Figure 9-46: Banana shape deposition hole due to over-excavation or collapse of rock. 9-89
Figure 9-47: Stress distribution of cast iron lining and copper shell due to uneven swelling pressure when the buffer is not saturated (cylindrical deposition hole, $\delta 1$=0 mm, $\delta 2$=0 mm). 9-90
Figure 9-48: Stress distribution of cast iron lining and copper shell due to uneven swelling pressure when the buffer is not saturated (banana shape deposition hole, $\delta 1$=8 mm, $\delta 2$=0 mm). 9-90
Figure 9-49: Stress distribution of cast iron lining and copper shell due to uneven swelling pressure when the buffer is saturated (cylindrical deposition hole, $\delta 1$=0 mm, $\delta 2$=0 mm). 9-91
Figure 9-50: Stress distribution of cast iron lining and copper shell due to uneven swelling pressure when the buffer is saturated (banana shape deposition hole, $\delta 1$=8 mm, $\delta 2$=0 mm). 9-91
Figure 9-51: Stress distribution of cast iron lining and copper shell due to uneven swelling pressure when the buffer is saturated (banana shape deposition hole, $\delta 1$=8 mm, $\delta 2$=33 mm). 9-91

Figure 9-52: Corrosion depth of the copper canister versus time due to the existing sulfides in groundwater. 9-92
Figure 9-53: Maximum shear displacement and max. Permanent shear displacement of fracture induced by fault source and diffuse seismicity of a single earthquake event. 9-113
Figure 9-54: Maximum accumulated shear displacement of each fracture cluster over the safety assessment timescale under conservative assumptions. 9-113
Figure 9-55: Average accumulated shear displacement of each fracture cluster over the safety assessment timescale under conservative assumptions. 9-114
Figure 9-56: Canister failure rate due to shear displacement over the safety assessment timescale. 9-117
Figure 9-57: Relative position of the three fracture sets. 9-118
Figure 9-58: Grids of the regional model with sea-level equal to -20 m. 9-129
Figure 9-59: Grids of the regional model with sea-level equal to -120 m. 9-129
Figure 9-60: Effective hydraulic conductivity values of the regional model with sea-level equal to -20m. 9-130
Figure 9-61: Effective hydraulic conductivity values of the regional model with sea-level equal to -120m. 9-130
Figure 9-62: Dynamic pressure of the regional model with sea-level equal to -20 m. 9-131
Figure 9-63: Dynamic pressure of the regional model with sea-level equal to -120 m. 9-131
Figure 9-64: Dynamic pressure of the regional model with sea-level equal to -120 m. 9-132
Figure 9-65: Dynamic pressure and Q1 paths from the repository of the regional model with sea-level equal to -20 m. 9-132
Figure 9-66: Dynamic pressure and Q2 paths from the repository of the regional model with sea-level equal to -20 m. 9-133
Figure 9-67: Dynamic pressure and Q1 paths from the repository of the regional model with sea-level equal to -120 m. 9-133

Figure 9-68: Dynamic pressure and Q2 paths from the repository of the regional model with sea-level equal to -120 m. 9-134
Figure 9-69: Dynamic pressure and Q1 paths from the repository of the regional model with sea-level equal to -120 m. 9-134
Figure 9-70: Dynamic pressure and Q2 paths from the repository of the regional model with sea-level equal to -120 m. 9-135
Figure 9-71: Cumulative distribution functions of flow related transport resistance for Q1 and Q2 paths of the regional model with sea-level -20 m. 9-135
Figure 9-72: Cumulative distribution functions of equivalent flow rate for Q1 and Q2 paths of the regional model with sea-level -20 m. 9-136
Figure 9-73: Cumulative distribution functions of equivalent flow rate for Q1 and Q2 paths of the regional model with sea-level -120 m. 9-136
Figure 9-74: Cumulative distribution functions of flow related transport resistance for Q1 and Q2 paths of the regional model with sea-level -120 m. 9-137
Figure 9-75: Cumulative distribution functions of equivalent flow rate for Q1 and Q2 paths of the regional model with sea-level -120 m. 9-137
Figure 9-76: Mass loss of the bentonite versus time after closure. 9-141
Figure 9-77: Rainfall versus temperature changes under global warming. 9-154
Figure 10-1: Establishment of design-basis evolution scenarios. 10-5
Figure 10-2: Flowchart of the development of canister failure due to corrosion. 10-6
Figure 10-3: Storyboard of canister failure due to corrosion. 10-7
Figure 10-4: Flowchart of the development of canister failure due to shear force. 10-9
Figure 10-5: Storyboard of canister failure due to shear force. 10-9
Figure 11-1: Number of canister failure due to shear force and its corresponding probability. 11-17
Figure 12-1: Approach and concept for biosphere assessment. 12-3
Figure 12-2: Relation between exposure pathways and environmental media. 12-10
Figure 12-3: The terrestrial landscape module. 12-16
Figure 12-4: The aquatic landscape module. 12-16
Figure 12-5:The radial-inward displaced fuel assemblies 12-23

Figure 12-6: Materials of the compartments and the release paths in the near-field. 12-26
Figure 12-7: Cumulative density distribution of the flow-related parameters. 12-34
Figure 12-8: Near-field annual effective doses for corrosion variant case (current sea-level, deterministic case). 12-38
Figure 12-9: Far-field annual effective doses for corrosion variant case (current sea-level, deterministic case). 12-38
Figure 12-10: Near-field annual effective doses for corrosion variant case (sea-level falls to -120 m, deterministic case). 12-39
Figure 12-11: Far-field annual effective doses for corrosion variant case (sea-level falls to -120 m, deterministic case). 12-39
Figure 12-12: Near-field mean annual effective doses for corrosion variant case (probabilistic case). 12-40
Figure 12-13: Far-field mean annual effective doses for corrosion variant case (probabilistic case). 12-40
Figure 12-14: The mean value, medium value, and 95th and 99th percentiles of far-field annual effective doses for corrosion variant case (probabilistic case). 12-41
Figure 12-15: Near-field annual effective doses for corrosion variant case (current sea-level, deterministic case, and analytical model). 12-44
Figure 12-16: Far-field annual effective doses for corrosion variant case (current sea-level, deterministic case, and analytical model). 12-44
Figure 12-17: Results of the sensitivity analyses for corrosion variant case (probabilistic case). 12-46
Figure 12-18: Compartments and release paths in the near-field for canister failure due to shear force. 12-49
Figure 12-19: Near-field annual effective doses for shear load case (current sea-level, deterministic case). 12-53
Figure 12-20: Far-field annual effective doses for shear load case (current sea-level, deterministic case). 12-53
Figure 12-21: Near-field annual effective doses for shear load case (sea-level falls to -120 m, deterministic case). 12-54

Figure 12-22: Far-field annual effective doses for shear load case (sea-level falls to -120 m, deterministic case). 12-54
Figure 12-23: Near-field mean annual effective doses for shear load case (probabilistic case). 12-55
Figure 12-24: Far-field mean annual effective doses for shear load case (probabilistic case). 12-55
Figure 12-25: The mean value, medium value, and 95th and 99th percentiles of far-field annual effective doses for corrosion variant case (probabilistic case). 12-56
Figure 12-26: Near-field mean annual effective doses for shear load variant case (probabilistic case). 12-59
Figure 12-27: Far-field mean annual effective doses for shear load variant case (probabilistic case). 12-59
Figure 12-28: Near-field annual effective doses for shear load basic case (current sea-level, deterministic case, and analytical model). 12-61
Figure 12-29: Far-field annual effective doses for shear load basic case (current sea-level, deterministic case, and analytical model). 12-61
Figure 12-30: Results of the sensitivity analyses for shear load basic case (probabilistic case). 12-63
Figure 12-31: Flow-related transport resistance of Q1 and Q2 paths of each deposition hole (the evaluation results of current sea-level, sea-level -20 m, and sea-level -120 m). 12-63
Figure 12-32: Near-field annual effective doses for initial canister defect case. 12-68
Figure 12-33: Far-field annual effective doses for initial canister defect case (1). 12-69
Figure 12-34: Far-field annual effective doses for initial canister defect case (1) to (4). 12-69
Figure 12-35: Far-field annual effective dose for corrosion variant case with (right) and without (left) colloid facilitated transport (current sea-level, deterministic case, and the concentration of colloid is 10 kg/m^3). 12-72
Figure 12-36: Annual risk from the repository. 12-77

Figure 12-37: Annual risk of different PEGs of shear load variant case (probabilistic case). 12-79
Figure 12-38: Annual risk of the “fruit and vegetable grower group” of shear load variant case (probabilistic case). 12-80
Figure 13-1: Dose estimation of the drilling staff when drilling occurred during post-closure 300 to 1 million years. 13-6
Figure 13-2: Dose estimation of occupants using the polluted well water when drilling occurred during post-closure 300 to 1 million years. 13-6
Figure 13-3: Dose estimation of farming using the contaminated soil when drilling occurred during post-closure 300 to 1 million years. 13-7

List of Tables

Table 1-1: Estimated amount of SNF in Taiwan. 1-3
Table 1-2: Name, schedule and target of each phase of the Spent Nuclear Fuel Final Disposal Program. 1-1
Table 1-3: Summary of researches of the program in recent years. 1-17
Table 2-1: Safety case/safety assessment of disposal program in other countries. 2-2
Table 2-2: Summary of dose/risk limits and assessment timescale of post-closure repositories in other countries. 2-12
Table 3-1: FEPs List of the Reference Case 3-5
Table 4-1: Initial inventory of the major radionuclides (34 in total). 4-7
Table 4-2: Design functions and requirements of the canister. 4-11
Table 4-3: Design specifications of the canister. 4-11
Table 4-4: Material specifications of the canister. 4-13
Table 4-5: Design functions, properties, and design requirements of the buffer 4-20
Table 4-6: Chemical composition of the synthetic groundwater. 4-21
Table 4-7: Reference specifications of the buffer blocks and pellets. 4-21
Table 4-8: Design requirements for manufacturing and installation of the buffer. 4-22
Table 4-9: Design requirements of the deposition hole. 4-27
Table 4-10: Design requirements of the disposal tunnel. 4-33
Table 4-11: Design functions, properties, and design requirements of the backfill 4-34
Table 4-12: The design requirements for manufacturing and installation of the backfill. 4-34
Table 4-13: Reference specifications of the backfill blocks and pellets. 4-35
Table 4-14: Design parameters, specifications, and installation requirements of the backfill. 4-35
Table 4-15: The estimated dry density of backfill after installation. 4-35
Table 4-16: Parameters of geologic units of the reference case. 4-55
Table 4-17: DFN parameters of the reference case. 4-55

Table 4-18: Thermal properties and mechanical properties of the reference case. 4-56
Table 4-19: Hydraulic characteristics of the reference case. 4-56
Table 4-20: Composition of groundwater of the reference case. 4-57
Table 4-21: In-situ stress of the reference case. 4-68
Table 4-22: Main monitoring items at each stage. 4-1
Table 5-1: Human actions that may affect long-term safety of the repository. 5-26
Table 5-2: Purposes, depth, and targeted formations of drilling. 5-26
Table 6-1: Concept of influence table of the internal processes of the geosphere. 6-1
Table 6-2: Concept of process mapping/process table of the source term and relevant development status in Taiwan. 6-9
Table 6-3: Concept of process mapping/process table of the canister and relevant development status in Taiwan. 6-12
Table 6-4: Concept of process mapping/process table of the buffer and relevant development status in Taiwan. 6-14
Table 6-5: Concept of process mapping/process table of the backfill and relevant development status in Taiwan. 6-18
Table 6-6: Concept of process mapping/process table of geosphere and relevant development status in Taiwan. 6-20
Table 7-1: Containment safety functions, containment safety function indicators, and containment safety function indicator criteria. 7-5
Table 7-2: Retardation safety functions, containment safety function indicators, and containment safety function indicator criteria. 7-13
Table 8-1: Fuel dissolution rate. 8-6
Table 8-2: Release duration of the metal assemblies of corroded fuel. 8-6
Table 8-3: Corrosion release fraction (CRF). 8-6
Table 8-4: Instant release fraction (IRF). 8-6
Table 8-5: The material parameters of the disposal system. 8-7
Table 8-6: Element specific effective diffusion coefficients. 8-7
Table 8-7: Diffusion-available porosity of the system units. 8-8
Table 8-8: Solubility limits for each element. 8-9

Table 8-9: Partition coefficients for each element of the system units (deterministic analysis). 8-10
Table 8-10: Partition coefficients for each element of buffer and backfill (probabilistic analysis). 8-10
Table 8-11: Partition coefficients for each element of host rock (probabilistic analysis). 8-11
Table 9-1: Parameters of the hydrogeological model at different evolution periods. 9-9
Table 9-2：Material parameters of the rock. 9-14
Table 9-3: Evaluation results of chemical evolution of the five deposition holes. 9-48
Table 9-4: Relevant parameters in the evaluation of mass loss of the bentonite. 9-69
Table 9-5: Mass loss of bentonite during the initial period after closure. 9-69
Table 9-6: Maximum tensile stress of the cast iron lining due to uneven swelling pressure when the buffer is not yet saturated. 9-87
Table 9-7: Maximum tensile stress of the cast iron lining due to uneven swelling pressure when the buffer is saturated. 9-87
Table 9-8: Hydrogeological input parameters of sea-level 0 m. 9-87
Table 9-9: Hydrogeological input parameters of sea-level -20 m. 9-87
Table 9-10: Hydrogeological input parameters of sea-level -120 m. 9-87
Table 9-11: Corrosion rate of the copper canister due to the existing sulfides in groundwater (when the buffer is intact). 9-88
Table 9-12: Corrosion rate of the copper canister due to the existing sulfides in groundwater (when substances transport through advection in the buffer). 9-88
Table 9-13: Maximum corrosion depth of the copper canister in the initial aerobic environment after closure. 9-88
Table 9-14: Maximum corrosion depth of the copper canister in the anaerobic environment after closure. 9-88
Table 9-15: Safety functions of the canister during the initial period after closure. 9-98
Table 9-16: Safety functions of the buffer and the backfill during the initial period after closure. 9-99

Table 9-17: Safety functions of the geosphere during the initial period after closure. 9-101
Table 9-18: Earthquake-induced shear displacement of fracture clusters by fault source and diffuse seismicity in a single earthquake event. 9-110
Table 9-19: Earthquake-induced accumulated shear displacement of fracture clusters by fault source and diffuse seismicity in the remaining glacial period after closure. 9-111
Table 9-20: Earthquake-induced accumulated shear displacement of fracture clusters by fault source and diffuse seismicity over the safety assessment timescale. 9-112
Table 9-21: Five cases of canister failure due to shear displacement in 50,000 DFN realizations. 9-117
Table 9-22: Parameters of the three fracture sets leading to canister failure. 9-117
Table 9-23: Evaluation results of TDS, ionic strength, pH, and the concentration of sulfide and iron. 9-139
Table 9-24: Parameters used to evaluate mass loss of the bentonite at sea-level -20 m. 9-141
Table 9-25: Parameters used to evaluate mass loss of the bentonite at sea-level -120 m. 9-141
Table 9-26: Safety functions of the canister during the remaining glacial period. 9-145
Table 9-27: Safety functions of the buffer/backfill during the remaining glacial period. 9-146
Table 9-28: Safety functions of the geosphere during the remaining glacial period. 9-148
Table 9-29: Safety functions of the canister during the remaining glacial period. 9-150
Table 9-30: Safety functions of the buffer/backfill during the remaining glacial period. 9-151
Table 9-31: Safety functions of the geosphere during the remaining glacial period. 9-153
Table 10-1: List of the scenarios. 10-15
Table 12-1: The radionuclide transport model of each release type. 12-8

Table 12-2: Potentially exposed groups of each release type. 12-8
Table 12-3: Exposure pathways of the potentially exposed groups. 12-9
Table 12-4: BDCFs of the potentially exposed groups ($SvyBqy$). 12-18
Table 12-5: Median values of the flow-related parameters. 12-34
Table 12-6: Geometry of the compartments in the near-field. 12-49
Table 12-7: Summarized cases for Canister failure due to initial defect 12-68
Table 12-8: Parameters used in the case of radionuclide transport in gas phase. 12-75
Table 12-9: Parameters for dose estimation of C-14 ingestion. 12-75
Table 12-10: Parameters for dose estimation of C-14 and Rn-222 inhalation. 12-75
Table 12-11: Annual mean life risk from C-14 and Rn-222 gaseous release from a single canister. 12-75

1. Introduction

1.1. Spent Nuclear Fuel Final Disposal Program

Nuclear energy technology has been widely applied in agriculture, industry, medical science and nuclear power for years, and is closely integrated with people's life in Taiwan. However, it produces radioactive waste inevitably. Safety management of radioactive waste has become a topic of public concern in recent years. Above all, radioactive waste final disposal is the focus of attention from society. Radioactive waste management has been not only a technical issue but also a political, economic and social issue.

Nuclear power has been used in Taiwan since 1978, with three nuclear power plants and each comprising two reactors. The four nuclear reactors in Chinshan and Kuosheng are boiling water reactors (BWRs), and the two nuclear reactors in Maanshan are pressurized water reactors (PWRs). Under the condition of permanent shutdown for Chinshan, Kuosheng and Maanshan nuclear plants, it is expected to generate about 4,913 MTU spent nuclear fuel (SNF) in total, including 17,890 BWR SNF assemblies and 4,320 PWR SNF assemblies respectively (as shown in Table 1-1) (台電公司, 2019c).

According to the "Radioactive Waste Management Policy" revised and issued on September 2nd, 1997, the plan for storage and final disposal of SNF was required to be strengthened. The requirements included active implementation of SNF on-site interim storage program, searching for the possibility of SNF reprocessing abroad under the compliance of international safeguards, continuously implementing the SNF final disposal program, and proposing early feasible plans and implementation plans as soon as possible.

The SNF strategy of Taiwan is direct final disposal in Taiwan territory and isolation from human life to decrease the risk of human and environmental hazards.

Sea floor disposal, deep hole disposal, ice layer disposal, space disposal and deep geological repository have been studied in the previous researches in the world. Among them, deep geological repository has been widely deemed as the most feasible method for SNF. In Taiwan, the "Regulations on the Final Disposal of High-Level Radioactive Waste and Safety Management of the Facilities" has also prescribed a deep geological repository as the most feasible disposal method. (Note: according to the definition of “The Nuclear Materials and Radioactive Waste Management Act,” the high-level radioactive waste is SNF for final disposal or the extraction residue produced by reprocessing. Since there is no SNF reprocessing operation in Taiwan, high-level radioactive waste refers to SNF.)

Taiwan Power Company (TPC) has performed researches on SNF final disposal since 1986. According to the “Nuclear Materials and Radioactive Waste Management Act,” TPC submitted the “Spent Nuclear Fuel Final Disposal Program” in 2004. The program has been implemented after approval from the Atomic Energy Council (AEC), and will be reviewed and revised every 4 years in accordance with relevant regulations. Currently, the “Spent Nuclear Fuel Final Disposal Program (2018)” is the latest version approved by AEC in 2020.

According to the “Spent Nuclear Fuel Final Disposal Program (2018),” the final disposal of SNF is divided into five phases from 2005 to 2055 until the completion of the repository. They are “survey and evaluation of the potential host rock,” “candidate site selection and approval,” “detailed site investigation and test,” “repository design and safety analysis,” and “repository construction” (Figure 1-1). The target of each phase is presented in Table 1-2.

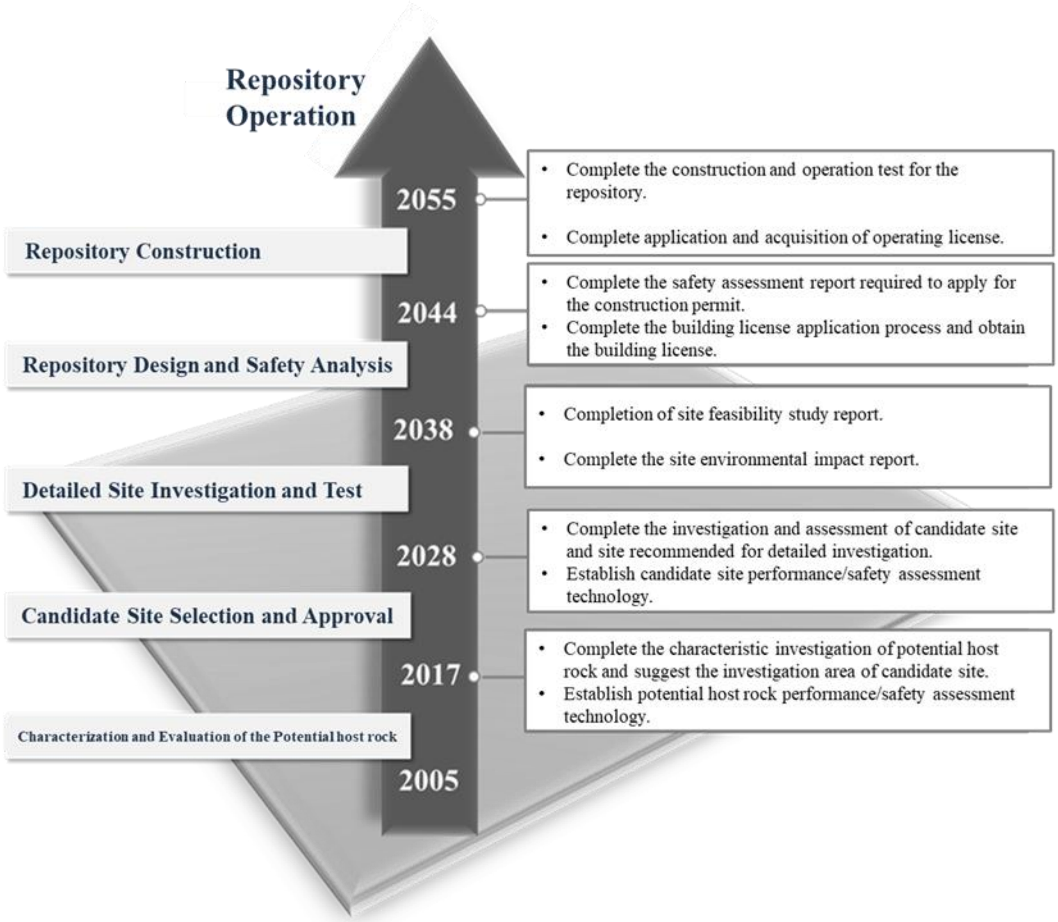

Figure 1-1: Work plan for the SNF final disposal program in Taiwan.

Table 1-1: Estimated amount of SNF in Taiwan.

Reactor type	Power Plant	Unit 1 fuel assemblies	Unit 2 fuel assemblies	Total of fuel assemblies
BWR	Chinshan	3,482	3,484	17,890
	Kuosheng	5,462	5,462	
PWR	Maanshan	2,160	2,160	4,320

Note: the amount of SNF is estimated by Kuosheng and Maanshan power plant operating for 40 years based on the statistical data of May 2018.
Reference: 台電公司 (2019c).

Table 1-2: Name, schedule and target of each phase of the Spent Nuclear Fuel Final Disposal Program.

Phase	Characterization and Evaluation of the Potential Host Rock	Candidate Site Selection and Approval	Detailed Site Investigation and Test	Repository Design and Safety Analysis	Repository Construction
Schedule	2005 to 2017	2018 to 2028	2029 to 2038	2039 to 2044	2045 to 2055
Target	Complete the characteristic investigation and assessment of potential host rock. Establish potential host rock performance/safety assessment technology.	Complete the investigation and assessment of the candidate site and site recommended for detailed investigation. Establish candidate site performance/safety assessment technology.	Completion of site feasibility study report (FR). Complete the site environmental impact report (EIS).	Complete the safety assessment report (SAR) required to apply for the construction permit. Complete the building license application process and obtain the building license.	Complete the construction and operation test for the repository. Complete application and acquisition of the operating license.
Milestone*	Preliminary Technical Feasibility Study for Final Disposal of Spent Nuclear Fuel was released in 2009. Potential host rock performance/safety assessment technology was established in 2016. The Technical Feasibility Assessment Report on Spent Nuclear Fuel Final Disposal was released in 2017. Candidate site recommendation for detailed investigation was proposed in 2017.	Complete the conceptual design of the repository in 2025. Complete the characteristic investigation and assessment of the candidate site in 2026. Establish the performance/safety assessment technology of the candidate site in 2027. Propose prior detailed investigation site in 2028.	Complete the ground geological survey of the disposal site in 2033. Start the planning and construction of vertical well test and underground test facility in 2033. Complete preliminary repository design in 2036. Complete site feasibility report (FR) in 2037. Complete site environmental impact report (EIS) in 2038.	Complete the safety assessment report (SAR) in 2043. Complete underground technology verification in 2043. Complete the detail design of the repository and receiving staging facility and transportation planning design in 2043. Complete the building license application process and obtain the building license in 2044.	Complete the construction and obtain the operation license of receiving staging facility in 2052. Complete the construction of the repository and transportation facility in 2054. Complete the application and obtain the operation license of the repository in 2055.

Note: the schedule may be delayed due to factors such as public opinions and land acquisition. The schedule will be revised every 4 years in accordance with “The Nuclear Materials and Radioactive Waste Management Act.”

Reference: 台電公司 (2019c).

1.2. Purpose of the Preliminary Safety Case Report

In order to prove that the design and operation of the repository conform to safety requirements, International Atomic Energy Agency (IAEA) published safety standards “SSG-23” (IAEA, 2012) which provides guidance and advice for repository development and indicates that it is the repository operator’s responsibility to develop safety case and safety assessment. The safety case, which integrates arguments and evidences of science, technology, management and operation proving the safety of the repository, is established by iteration and collection of the latest information. The safety case includes site and repository design, suitability of construction and operation, radiation safety assessment, and suitability and quality assurance of all safety-related works for the repository. It can act as the basis for demonstrating safety and applying license. Safety cases can provide comprehensive information for stakeholders (such as government authorities, regulatory agencies, general public and local people) to obtain understanding, recognition, faith and consensus of the disposal program.

In accordance with the requirements of the competent authority, the disposal technologies need to be continuously reviewed. According to the safety case guidance proposed by IAEA, and with the international peer review and AEC review of “The Technical Feasibility Assessment Report on Spent Nuclear Fuel Final Disposal” (SNFD2017 Report), and considering the disposal program phase and host rock geological properties in Taiwan, the “Preliminary Safety Case Report” (hereinafter referred to as SNFD2021 report”) would be proposed at the end of 2021. Because candidate sites of Taiwan have not been chosen yet, experience from countries that do not complete site selection process such as the United States, the United Kingdom, Canada, and Japan have been referred to, for the development of a generic safety case. Also, a “reference case” has been established based on international experience and geological data from previous surveys. The reference case in SNFD2021 report was established based on all the data TPC has from the investigation data and research data of the program. Detailed investigation reports can be found in the database of TPC. Applying relevant analysis technologies, quantitative evidences have been proposed. These evidences will be reviewed by the authority and domestic and international peers, to make sure that disposal technology in Taiwan is in line with international standards, and to make sure that the safety of the repository is ensured.

The main purposes of the SNFD2021 Report are as follows:

(1) Advanced international disposal technologies have been referred to, and the reference case has been assessed to ensure the safety of the repository.

(2) Results and findings from the report will be fed back to future R&D program, site survey work, development of engineering design and related safety assessment activities.

(3) The aim of this report is to strengthen communication with the stakeholders and build a social consensus on implementing the disposal program.

1.3. Feedback from SNFD2017 Report

Taiwan Spent Nuclear Fuel Final Disposal Program published the SNFD2017 Report in 2017, which integrated the researches of "site survey and description," "repository design and engineering technology," and "safety assessment technology." The SNFD2017 Report studied three potential host rock in Taiwan (granites, mudstones, Mesozoic basement) and achieved three requirements of the competent authority: (1) whether a suitable granitic rock mass for final geological disposal could be identified in Taiwan; (2) whether adequate engineering capabilities for constructing a geological repository have been established in Taiwan; and (3) whether adequate capabilities for assessing the long-term safety for a repository site have been established in Taiwan. The SNFD2017 Report confirmed that Taiwan has the feasibility to develop disposal technology, and completed the important target of Phase I – "Characterization and Evaluation of the Potential Host Rock." The advanced international experience and disposal concept were referred in the SNFD2017 Report, which can prove the feasibility and the safety of deep geological repository to the program manager, competent authority and stakeholders. In 2018, the SNFD2017 Report passed international peer review and competent authority review in Taiwan.

The competent authority considered that each disposal technology in final disposal program in Taiwan should be continuously improved to ensure relevant disposal technology reaches to the best and international level. The safety of the repository should be enhanced to protect people's safety and environment quality. The main feedbacks from the competent authority are presented as below:

(1) "To confirm whether a suitable granitic rock mass for geological final disposal could be identified in Taiwan."

The results have shown that there are sufficient volume of granitic rock mass in western Taiwan offshore island and eastern Taiwan, which is worth further characteristic investigation for the deep geological repository. The geological information should be continuously collected, and conceptual model should be applied to repository design and assessment technology for the following site selection.

(2) "To confirm whether adequate engineering capabilities for constructing a geological repository have been established in Taiwan."

The SNFD2017 Report has preliminarily introduced the KBS-3 disposal concept and established the engineering arrangement, design and verification of the repository in Taiwan. The optimization and feasibility should be continuously refined for the following application to every candidate disposal site.

(3) "To confirm whether adequate capabilities for assessing the long-term safety for a repository site have been established in Taiwan."

The SNFD2017 Report has fully understood the methodology and technology of the safety case. The latest international technology development should still be focused and advanced. In addition, geological survey has been difficult in Taiwan, leading to the lack of parameters, which is necessary for ensuring safety of the repository.

1.4. Laws and Regulations

The safety management of radioactive waste is not only an environmental and technological issue, but also a subject matter that involves political, economic and social considerations. Regarding the final disposal of SNF, there are laws and regulations for candidate site selection, repository construction, operation and closure. Above all, the Nuclear Materials and Radioactive Waste Management Act (announced in December 2002), Regulations on the Final Disposal of High-Level Radioactive Waste and Safety Management of the Facilities (amended in January 2013) and Regulations on Siting of High-level Radioactive Waste Final Disposal (amended in March 2017), are elaborated as Section 1.4.1 to Section 1.4.3.

1.4.1. Nuclear Materials and Radioactive Waste Management Act

The act is enacted to administer radioactive material, preventing radioactive hazard and secure public safety. The main provisions are as follows:

(1) Article 17: For the construction of treatment, storage and final disposal facilities of radioactive waste, an application for a construction license shall be filled with the competent authorities. After the application has been reviewed and approved (by the competent authorities) to satisfy the following prescription and the competent authorities have issued a construction license, the construction would be permitted:

   (a) The construction is consistent with the prescription of relevant international conventions.

   (b) The equipment and the facilities are sufficient to secure public health and safety.

   (c) The impact on the environment complies with the prescription of relevant regulations.

(d) The technology, the management capacity and the financial basis of the applicant are competent to operate the facilities.

(2) Article 29: The treatment, transportation, storage and final disposal of radioactive waste shall be done by the producer of radioactive waste itself solely or be entrusted to the domestic or foreign operator who is of technical capacity or holds the facilities for disposal. The producer shall be responsible for minimizing the generation amount and the volume reduction of radioactive waste. The final disposal program shall be actually proceeded in accordance with the planned schedule.

(3) Article 37: One who fails to implement the final disposal plan in accordance with the planned schedule referred to in Paragraph 1 of Article 29 shall be punished with an (administrative) fine of more than New Taiwan Dollars Ten Million (NT$10,000,000) but not more than NT Fifty Million (NT$50,000,000), and the punishment may be respectively imposed annually.

(4) Article 46: The operator of nuclear power shall raise from the nuclear back end operation funds, by way of setting aside at least two percent (2%) thereof, and transfer funds to carry on the research and(/or) the development of operating technology of radioactive materials and(/or) final disposal.

(5) Article 49: After this law comes into effect, the competent authorities shall supervise and urge the producer of radioactive waste to plan the construction of the domestic final disposal facilities, and ask the producer to resolve the issues as to the final disposal of radioactive waste.

1.4.2. Regulations on the Final Disposal of High-Level Radioactive Waste and Safety Management of the Facilities

The main provisions are as follows:

(1) Article 1: These Regulations are enacted pursuant to Article 21 of the Radioactive Materials Management Act (following abbreviated as “the Act”).

(2) Article 2: The terms used in these Regulations are defined as follows:

   (a) High-level radioactive waste repositories (hereinafter referred to as “repositories”): repositories located in a proper geological environment at a proper depth under the ground surface, which can safely separate the radioactive nuclides from the biosphere for a long time, including the buildings, structures and equipment on the related ground surface and in the disposal area of underground tunnels as well as the underground disposal area used to isolate high-level radioactive wastes.

   (b) Host rock for disposal: the geological rock mass used to place high-level radioactive wastes

   (c) Multiple barriers: the multiple combination of natural and engineered barriers used to isolate or retard the filtering, leakage and transplantation of radioactive nuclides, including the waste itself, container, buffering and backfill, and stratum.

   (d) Personal annual risk: the product of the annual probability of accidents incurring to the disposal facilities multiplied by the probability of death due to exposure to the radiation caused by the accident.

   (e) Controlled area for disposal: the area of the ground surface and the underlayer of the ground surface within the scope of the repositories, marked with proper signs indicating the boundary of the repositories.

(3) Article 3: The final disposal of high-level radioactive wastes shall be conducted in the deep stratums.

(4) Article 4: The disposal facilities must not be located in the following areas:

   (a) Active faults or areas in which the geological conditions would affect the safety of the disposal facilities.

   (b) Areas with geochemical conditions not favorable for effectively controlling the spreading of pollution caused by radionuclides and likely to affect the safety of the disposal facilities.

(c) Areas with surficial or underground hydrographical conditions likely to affect the safety of the disposal facilities.
(d) Areas with high population density.
(e) Other areas in which development is prohibited according to any law.

(5) Article 5: It shall be avoided that the disposal facilities be located in the following areas:
(a) Where landslide, subsidence, and volcanic activities are likely to occur.
(b) Where the geological structure is likely to change obviously.
(c) Where the hydrological conditions are prone to change.
(d) Where the host rock for disposal is being deteriorated obviously.
(e) Where the bedrock is uplifting or eroding obviously.

If the disposal facilities are located in any of the above areas, the operators shall bring forward solutions to ensure the facilities meet the safety requirements.

(6) Article 6: The operators of repositories shall submit a plan for detailed site investigation and then start the detailed investigation after the plan is approved by the competent authority.
The plan of detailed site investigation referred to in the preceding paragraph shall include the following contents:
(a) Description of the site.
(b) Conceptual design of the operating area of the repositories.
(c) Necessity of drilling or excavation and operation planning.
(d) Research and test plan.
(e) Plan for investigating and controlling the factors likely to influence the capability of the site to isolate high-level radioactive wastes.
(f) Quality assurance plan.
(g) Restoration plan.
(h) Financial description.
(i) Other contents specified by the competent authority.

(7) Article 7: The operators of the repositories shall, during the period of detailed site investigation, report the investigation progress and results to the competent authority before the end of February every year.

During the period of detailed site investigation, the competent authority may dispatch personnel to conduct an inspection at any time.

(8) Article 8: Multiple barriers approach shall be designed for the disposal facilities.

(9) Article 9: The disposal facilities shall be designed to ensure that the annual effective dose to any individual in the critical group outside the facilities is not more than 0.25 mSv.

(10) Article 10: The disposal facilities shall be designed to ensure that the risk constraint to any individual in the critical group outside the facilities is not more than $1x10^{-6}$ per year.

(11) Article 11: The disposal facilities shall be designed to ensure that the high-level radioactive wastes can be safely retrieved within 50 years after disposal.

(12) Article 12: The design of the important structures, systems and components of the repositories shall meet the following requirements:

(a) Support inspection, maintenance and test, and meet the requirements for nuclear protection operations.

(b) Prevent expected natural disasters.

(c) Provided with emergency response functions.

(d) Ensure the operations of high-level radioactive wastes can be kept at subcritical status under normal operating and expected accidents.

(e) Provided with protective functions against fire and gas explosion.

(f) Other requirements specified by the competent authority.

(13) Article 13: The closure of the repositories shall be designed to ensure that the underground passages and drilled holes, after being

sealed, would not become the key routes for the transportation of radioactive nuclides.

(14) Article 14: The operators shall acquire the right to use the lands within the controlled area for disposal prior to the construction of the repositories.

(15) Article 15: During the operation of the repositories, the operators shall renew the safety analysis report and submit it to the competent authority for examination every five years.

(16) Article 16: For the closure of the repositories, the operators shall bring forward a closure plan and a supervision plan according to the provisions of Article 32 and Article 33 of the Enforcement Rules of the Act, and submit them to the competent authority for approval prior to implementation.

(17) Article 17: To apply for exemption from supervision, the operators of the repositories shall follow the provisions of Article 34 of the Enforcement Rules of the Act.

(18) Article 18: Where the repositories are exempted from supervision, the operator shall store the following data permanently and submit them to the competent authority for examination:

(a) Data about surficial characteristics, boundary monuments, tunnels, and drilling holes.

(b) Construction methods, materials, structures and important construction data.

(c) Geological map and geological profile.

(d) Hydrological data.

(e) Position and characteristics of high-level radioactive wastes.

(f) Data about abnormities or accidents.

(g) Radiation monitoring data.

(h) Other data specified by the competent authority.

(19) Article 19: These Regulations shall become effective as of the date of promulgation.

1.4.3. Regulations on Siting of High-level Radioactive Waste Final Disposal

The regulations provide the following requirements for potential sites to ensure the safety of the final repository of high-level radioactive waste.

Main provisions are as follows:

(1) Article 1: "Regulations on Siting of High-level Radioactive Waste Final Disposal" are enacted to ensure the safety of the final repository site (following abbreviated as "site") of high-level radioactive waste, and be a reference for site selection and management.

(2) Article 2: The site shall provide natural barriers to retard the transportation of radionuclides, and prevent the repository from natural hazard, so as to ensure the repository meet safety requirements.

(3) Article 3: The site shall not be located in areas near active faults or where geological conditions may affect the safety of the repository.
   (a) Areas within 1 km on both sides and belt-like area extending for 3 km at both ends of the main fault zone of an active fault.
   (b) Areas within a radius of 15 km from the center of Quaternary active volcanic.
   (c) Areas within a radius of 1 km from the eruption of hervideroes.
   (d) Areas of a single landslide area are greater than 0.1 km^2 and cannot be overcome by engineering.

(4) Article 4: Geochemical conditions cannot inhibit the transport of radionuclides and thereby adversely affect the safety of the repository.
   (a) Areas where the pH of groundwater lower than 4.
   (b) Areas where the distribution coefficient of stratum to key cationic nuclide less than 3 ml/g.

(5) Article 5: Hydrologic conditions of surface water and groundwater cannot adversely affect the safety of the repository.
   (a) Water course, including river, lake, reservoir storage area, drainage facilities, canals, flood channels and flood detention ponds.

(b) Catchment area of existing, under construction reservoir.

(c) Groundwater control area.

(6) Article 6: The site shall not be located in areas of high population density, where the population density is higher than 600 people/km^2 in a town, district or city.

(7) Article 7: The site shall not be located in areas of potential for landslides, subsidence or volcanic activity.

(8) Article 8: The site shall not be located in areas of potential for structural deformation, such as uplift, subsidence, folding, or faulting.

(9) Article 9: The site shall not be located in areas of potential for foreseeable human action and natural phenomena.

(10) Article 10: The site shall not be located in areas of potential for regional uplift and erosion.

(11) Article 11: The host rock characteristics listed below shall be under consideration for site selection.

(a) The depth of the host rock shall be greater than 300 m from the ground surface.

(b) The host rock has the appropriate depth and horizontal distribution to contain the underground facilities of the repository.

(c) The thermal properties of the host rock are conducive to removing the decay heat generated by the high-level radioactive waste.

(d) The hydrological properties of the host rock are low hydraulic conductivity and low permeability.

(e) The mechanical properties of the host rock are conducive to safe construction, operation and closure of the repository.

(f) The chemical properties of the host rock are able to precipitate, absorb, or retard the transportation of nuclides.

(12) Article 12: The site hydrological characteristics listed below shall be under consideration.

(a) Hydrogeological structures are conducive to the limitation of groundwater flow and retardation of nuclide transportation.

(b) The groundwater flow field is stable and has a low hydraulic gradient so as not to accelerate the flow of groundwater.

(c) Hydrogeological environment may not adversely affect the repository of high-level radioactive waste.

(13) Article 13: The site geochemical characteristics listed below shall be under consideration.

(a) The long-term geochemical evolution of sites shall not adversely affect barriers of the repository.

(b) The redox characteristics of the sites and the chemical composition of the groundwater shall not accelerate the corrosion and damage of the canister.

(14) Article 14: The site shall not be located in areas that cannot be developed according to other laws. The scope and recognition criteria are in accordance with the provisions of the other laws.

(15) Article 14-1: The selection of the site shall comply with Article 31 of "The Indigenous Peoples Basic Law", and high-level radioactive waste shall not be disposed of in the areas of indigenous peoples against their wishes.

1.5. Executive Teams (Organizations)

In this report, program management and technology integration are implemented by TPC. Analyses and report writing are conducted by the Institute of Nuclear Energy Research (INER). This report includes the research results through years contributed by all executive teams cooperating with TPC, which include Industrial Technology Research Institute (ITRI), the domestic academic units, and the domestic engineering consulting agency. The research results consist of multiple professional fields such as geology, hydrogeology, civil engineering, mechanical engineering, materials engineering, chemical analysis, nuclear engineering, radiation protection and information management. The executive teams of the SNF final disposal program also cooperate with international institutions, for example, Finnish Posiva Oy company, Southwest Research Institute (SwRI), Sandia National Laboratories

(SNL), Canadian Nuclear Waste Management Organization (NWMO) and Nuclear Waste Management Organization of Japan (NUMO). In addition, TPC contracted with Swedish SKB as a technical consultant to ensure this report meet the basic framework of international safety case (Figure 1-2).

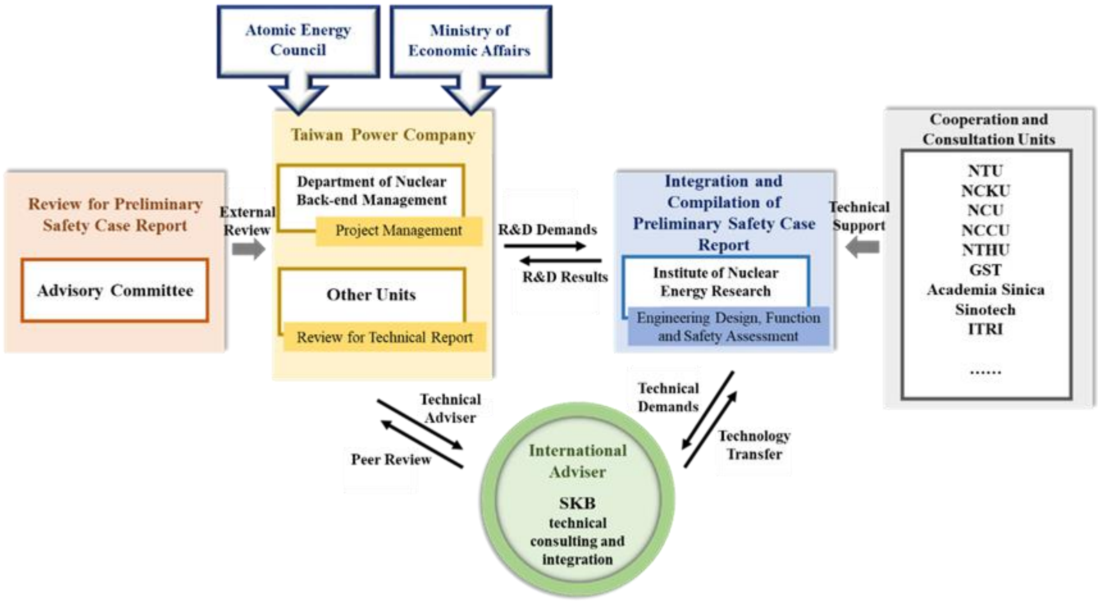

Figure 1-2: Organization of the Spent Nuclear Fuel Final Disposal Program.

1.6. Previous Researches

TPC completed the “Research Program of Spent Nuclear Fuel from Nuclear Reactors” in 1983, and delivered it to Executive Yuan for approval and implementation. Soon after, relevant industrial, governmental, academic and research agencies invested in the planning, management and research of SNF’s final disposal. In accordance with “The Nuclear Materials and Radioactive Waste Management Act” and “Enforcement Rules for the Nuclear Materials and Radioactive Waste Management Act,” TPC delivered the “Spent Nuclear Fuel Final Disposal Program” in 2004, and the program was approved by the competent authority in July 2006. The history and results of the disposal program are divided into two parts by the “Spent Nuclear Fuel Final Disposal Program” in 2004, which are “Final Disposal Pilot Program” from 1986 to 2004, and the “Final Disposal Program” from 2004.

The “Final Disposal Pilot Program” had gone through 4 stages, which were Preliminary Research of Disposal Concept, Initial Planning, Preparation of Regional Survey, and Investigation and Technology Development. The results of each stage are as follow:

(1) Preliminary Research of Disposal Concept (1986/05~1988/06):
The basic concepts of site guidelines, site investigation and design were determined. The possible methodology and technology of international SNF final disposal were systematically studied and understood.

(2) Initial Planning (1988/11~1991/06):
The full work plan (1991 version) was completed and proposed that crystalline rocks, Mesozoic basements, and mudstones are potential host rock in Taiwan, which became the basis of the following work plan.

(3) Preparation of Regional Survey (1993/08~1998/10):
The investigation technology drill of the crystalline rock test site was completed, and became the basis for the host rock characteristic survey. Meanwhile, the technology could support the site investigation and assessment requirements of low-level radioactive waste final disposal plan. In this stage, the conceptual system of

safety assessment for uncertainty and sensitivity analysis was developed as well.

(4) Investigation and Technology Development (1999/05~2003/09): The integrated investigation of the deep geological cross-hole test was implemented in this stage in Taiwan. The research of repository design concept, preliminary planning of repository layout, and establishment of a database of granite properties, references, parameters and scenario analysis were implemented as well. Those works became references for the following field survey, nuclide transportation and safety function assessment. The “Spent Nuclear Fuel Final Disposal Program” was also delivered to the competent authority for review in this stage, reaching the requirements of “Enforcement Rules for the Nuclear Materials and Radioactive Waste Management Act” Article 37.

“Final Disposal Program”: According to “Spent Nuclear Fuel Final Disposal Program,” each planning of the program has been implemented since 2005. Two milestones of the “Characterization and Evaluation of Potential Host Rock” phase have been completed, which are the SNFD2009 Report and the SNFD2017 Report. The SNFD2009 and SNFD2017 Reports demonstrated the development and capability of disposal technology, and established the basis of the “Candidate Site Selection and Approval” phase. Above all, the result of the “Characterization and Evaluation of Potential Host Rock” phase can refer to “Spent Nuclear Fuel Final Disposal Program (2018)” (台電公司, 2019c). The research results since 2018 are presented in Table 1-3 in this report. Additionally, according to “Enforcement Rules for the Nuclear Materials and Radioactive Waste Management Act” Article 37, TPC has to deliver the implementation result report of the former year, and the working plan report for the next year to the competent authority, which will be published on the AEC website.

For the “Characterization and Evaluation of Potential Host Rock” phase, the main results included integrating the definition and investigation technology (including geology, groundwater, rock and water chemistry and engineering characteristic) of potential host rock characteristics. The geological structure of the investigation area was constructed, and a safety assessment of the repository in the potential host rock was established, which proposed the characteristic investigation of the potential host rock and the evaluated condition suitable for a deep geological repository in Taiwan.

For the “Candidate Site Selection and Approval” phase, the development of disposal technology will continue to be reviewed and improved. On condition that no candidate site has been selected, the SNFD2017 Report will be the basis to make good use of domestic and foreign experiences and R&D resources to improve “geological survey technology assessment,” “geological disposal engineering technology,” “long-term safety assessment of geological disposal facilities” and other related technologies, and complete this report before the end of 2021 according to the requests of competent authority.

Table 1-3: Summary of researches of the program in recent years.

Year	Subject	Summary of important achievements
2018	(1) Improvement of regional characteristics survey technology	Based on the study of the anomalous zone of magnet susceptibility and resistivity, and geological linear structure distribution, the regional and structural geological survey technology of the offshore island crystalline rock area (K-area) is improved. Based on the study of granite mineral composition and the age comparison of igneous rocks, the geochemistry of the offshore island crystalline rock has been completed. With tidal station observation data, satellite altimetry data, microseismic observation data in the main island crystalline rock test area of the island, and hypocenter rupture scale analysis, long-term monitoring information is obtained.
	(2) Improvement of the suitability of the repository and evaluation of the design project	The technical establishment of the SNF database implementation and the integration of the web interface database are completed. The analysis of the α, β, and γ radiation source in the SNF, the preliminary study on the related reaction mechanism of the radiation source and the underground radiation hydrolysis mechanism, and the exploration of the corrosion effects of the radiation hydrolysate on the canister are completed. The establishment of 4 sets of hypocenter models, obtainment of the simulated waveforms of the target station by the simulate method of strong ground motion seismic wave, and comparison of the relevant data to understand the possible hypocenter parameters of the 1920 Hualien offshore earthquake are completed. The life prediction analysis and construction of the copper shell of the canister, the study of the corrosion resistance of the copper shell in the detection rate environment, the development of the friction stir welding and testing technology of copper materials, and the development of the manufacture and testing technology of cast iron lining of the canister are completed. The preliminary establishment of design concepts and design requirements of the backfill are completed, as a reference for backfill design. The comparison and correction of the results of the stylised compaction experiment and the settlement of the Swedish SKB canister are completed, as well as the simulation of the settlement of the canister in the fluid mechanics cycle. The numerical model that simulates strain and stress of the large-size triaxial test equipment, and manufacture of the large-size triaxial equipment, and the process of assembly, leakage test and axial force application are completed. Long-term safety analysis and verification study of tunnel support materials are completed.
	(3) Improvement of safety assessment	The practices of IAEA SSG-23 and other countries were referred to, the process of post-closure safety assessment methods was proposed, and a safety assessment database was initially established. Based on the simulation analysis of the SNFD2017 report, the reason for choosing the numerical model was proposed, the benchmark verification process was explained, and the uncertainty handling process and the application interface relevance were discussed. The GoldSim model for the evaluation of colloids was established to promote the migration of radionuclides. The gas permeability test process and experiments were established and discovered that buffer and backfill are affected by hydraulic effects and chemical effects. The long-term safety analysis and verification of low-alkali concrete or low-alkali mortar as the tunnel support material were completed.

	(4) Integrated technology	technical research on the crystalline rock area of the main island and offshore islands are preliminarily integrated as below: The long-term safety assessment of the geosphere was completed. Groundwater flow analysis model verification and technical improvement was completed. The numerical model of groundwater flow for the sea-level drop was completed. The migration behavior of the radionuclides in buffer, backfill, and disposal host rock was completed.
2019	(1) Improvement of regional characteristics survey technology	Regional geological survey technology and data analysis were developed and the spatial distribution of granite rock mass in Taiwan was studied. Aerial magnetic survey technology and data analysis were improved. The reference case was updated. 3D geological unit modelling and display technology were built, and the evaluation technology for the impact of deep fluids was established. The granitic gneiss tunnel was taken as the technical construction site, which was a preliminary research on the detection and evaluation technology of the domestic tunnel excavation damage zone. Improvement of the statistical study on the fracture parameter distribution characteristics and the analysis technology of fractured rock mass groundwater flow of the granite in Taiwan were completed. Long-term monitoring, GPS continuous observation and time series analysis, microseismic monitoring and data analysis were continuously carried out. The construction process and survey technology requirements of the rock mechanics description model, and the parameter characteristics required for the rock mechanics description model at different stages were studied.
	(2) Improvement of engineering design and safety assessment technology of the repository	The updated statistics of the use history data of the SNF in the Chinshan, Kuosheng and Maanshan nuclear power plant were complete, and the decay heat sensitivity analysis and the decay heat relationship curve under different conditions were completed. MCNP nuclear criticality safety analysis model was established, including SNF, canisters and deposition holes. The parameter sensitivity analysis and proposed conservative parameter combinations were completed. The specification adjustment of the canister and buffer preliminary design was complete based on the length of domestic SNF. The analysis of uniform isostatic load generated by the hydrostatic pressure and the swelling pressure after disposal according to domestic canister specification was completed. The von Mises stress value of the cast iron lining was within the allowable stress value. The performance analysis of the shear displacement based on the domestic canister specifications was completed to confirm that the canister can meet the performance requirements. The mechanical behavior simulation analysis of the unsaturated bentonite under stress was complete, including the analysis of the instantaneous deformation and fracture cutoff caused by the weight of the canister and backfill. The evaluation of saturation time and the calculation of swelling pressure distribution were completed. Calculation of the backfill's capability to resist uplift of the buffer was completed, and the distribution of the swelling pressure and the amount of swelling in the buffer were analyzed. Based on the decay heat information of the SNF of power plants in Taiwan and relevant local geological conditions, the thermal distance analysis of the repository was completed. The analysis of the layout design of the underground facility was completed, including the amount of fracture shear displacement

		caused by earthquake, and the quantitative evaluation of the deposition holes and fracture cutoff. The objects of 3 simulation areas were completely generated. DarcyTools was adopted to perform 4 cases of steady-state groundwater flow field simulation. The shear force and corrosion effects of canisters analysis were completed in order to explore the reference evolution assessment on a long-term scale. According to the engineered barrier design, underground repository layout design and localized geological parameters, the nuclide release path and near-field, far-field and biosphere transport analysis were carried out. The research and analysis of the safety function indicators of the engineered barrier were completed. The classification and development of the scenarios, analysis of the post-closure safety assessment dose and risk based on the design of the domestic repository were completed.
2020	(1) Investigation and survey technology of site suitability	The investigation of the characteristics of the Mesozoic basement in Taiwan waters had been preliminarily completed. The rock mechanical analysis was carried out with the existing crystalline rock samples of Taiwan, so as to obtain the related rock mechanical parameters and study the uncertainties. Temporary broadband seismic stations and GPS continuous observation stations for surface deformation were deployed in the Taiwan plate boundary area to conduct long-term continuous monitoring of seismic activity and surface deformation in the plate boundary area.
	(2) Safety assessment technology	The research on nuclides inventory and decay heat analysis of SNF in PWR was preliminarily studied, as well as nuclear criticality analysis technology. Based on the laboratory test results of Taiwan crystalline rock and the measurement data of the geothermal gradient, a three-dimensional thermal characteristic evaluation simulation was carried out, and the release path (Q3 path) analysis technology of the fracture cutoff and disposal tunnel was established.
	(3) Database	The database was designed according to the type, property, format, and existing form of the data. The reports, data, parameters and related quality files generated by the projects during the execution were digitally preserved, which can be searched and retrieved through the web interface to facilitate the retrospective process of the experimental data generation and quality assurance records to ensure visibility and traceability.

2. Methodology

2.1. Current Status of Disposal Program in Other Countries

There has been an international reference for developing safety cases since the SSG-23 Guideline was published by IAEA in 2012 (IAEA, 2012). The integration group for the safety case (IGSC) of Organisation for Economic Co-operation and Development (OECD) / Nuclear Energy Agency (NEA) raised a number of relevant international seminars to promote international technical exchange. The overall international trend has gradually formed a consensus on the practice of developing safety cases. The development of SNF disposal safety case and safety assessments all over the world in recent decade provides references for Taiwan’s technology development, including important cases in Table 2-1.

According to the document published by OECD/NEA in December, 2020 (NEA, 2020), the key features and activities for developing a safety case include: (1) integration of science and technology information, (2) clarifying the safety case of the repository system, (3) excluding and decreasing the uncertainty, (4) systematically deducing the scenario development, (5) tracing and storage of knowledge management record. In addition, the safety case should promote communication and interaction with stakeholders, and promote the disposal program implemented safely.

Nuclear safety regulatory agencies of various countries have also continued to improve the regulatory requirements for safety cases. For example, the Radiation and Nuclear Safety Authority (STUK) of Finland published Nuclear Waste Disposal Guidelines (YVL D.5) in February 2018, which describes the regulatory requirements for the safety case of the repository in Chapter 9 (STUK, 2018). In addition, the Canadian Nuclear Safety Commission (CNSC) also revised and published a radioactive waste disposal safety case regulatory document (CNSC, 2021) in January 2021, reflecting the latest international viewpoints on safety cases.

Table 2-1: Safety case/safety assessment of disposal program in other countries.

Year	**Country**	**Instituti on**	**Program**	**Site**	**Report No.**	**Assessment purpose**
2011	Sweden	SKB	SR-Site	Forsmark	SKB TR-11-01	Construction license application
2012	Finland	Posiva Oy	TURVA-2012	Olkiluoto	Posiva 12-12	Construction license application
2014	Netherlands	COVRA	OPERA	Site has not been decided. (Focusing on the of clay rock and halite)	OPERA-PU-TUD311	General safety case, technological development
2016	France	Andra	Cigeo	Meuse/Haute-Marne	DOS-AF	Stakeholder communication
2016	UK	RWM	DSSC	Site has not been decided. (Focusing on the crystalline rock)	DSSC-101-01	General safety case, technological development
2017	Canada	NWMO	APM	Crystalline rock	NWMO-TR_2017_02	General safety case, technological development
2018	Japan	NUMO	-	Site has not been decided. (Focusing on the plutonite, Neogene sedimentary rock, Pre-Neogene sedimentary rock, volcanic rocks and metamorphic rocks)	NUMO TR-18-02 and NUMO TR-18-03	General safety case, technological development

2.2. Methodology of Safety Case

Compared to SNFD 2017, this report is a generic safety case report. This report refers to general safety case process of the NEA MeSA report (NEA, 2012a) and establishes the Taiwan safety case method, which can be widely applied to different disposal concepts and geological environments. This safety case method not only focuses on the safety analysis and its result, but also integrates more evidences, discussion and analysis. Furthermore, the safety case flowchart (Figure 2-1), which includes safety case elements, can illustrate the relationship and feedback between the safety assessment component and the safety case.

The methodology of safety case adopted in this report can be divided into (1) background, (2) assessment basis, (3) safety assessment, (4) integration of evidence, arguments and analyses, (5) feedback to project management and (6) others.

(1) Background

(a) Repository development strategy:

Define a timeline for the design and construction of the repository, including milestones and decision points in the disposal plan in accordance with the “Spent Nuclear Fuel Final Disposal Program” approved by the competent authority in stages.

(b) Disposal and assessment principles:

Disposal and assessment principles describe the “disposal principles” of repository development in the safety strategy and “assessment principles” of safety assessment guidelines in the assessment strategy. This report refers to the Swedish KBS-3 disposal concept that uses crystalline rock as the disposal host rock to construct a deep repository system, and complies with the safety principles of the repository to achieve safe disposal.

(c) Assessment regulatory basis:

The relevant laws and regulations on high-level radioactive disposal in Taiwan can be found in Section 1.4. Assessment regulatory basis provides the safety indicators.

(2) Assessment basis

(a) Site description and design specification:

Site description and design specification describe the repository design and geological environment in detail, and provide boundary conditions for the safety assessment. In this report, the initial state of the repository is described in Chapter 4 (including engineered barriers and natural barriers). The external factors that may affect the safety of the repository (including climate evolution, geological evolution and future human actions) are described in Chapter 5, which provides a reference for the scenario evolution hypothesis of the safety assessment.

(b) The synthesis of process understanding and influences between processes:

First of all, the features/events/processes (FEPs) that may affect the repository must be identified and collected, and interaction between FEPs should be studied. In FEPs, features are the objects, structures or environmental conditions which might affect the repository. Events are transient weather phenomena or human actions which might affect the repository. Processes are the long-term and gradual phenomena which might affect the repository. By studying coupled processes of thermal (T), hydraulic (H), mechanics (M), and chemistry (C), the safety impact on the repository can be evaluated. The establishment, processing, and analysis of Taiwan's FEPs database are presented in Chapter 3. The complex interaction among FEPs and the coupling of T-H-M-C processes, as well as current analysis and research of internal processes in Taiwan are shown in Chapter 6.

(c) Methodology, model, computer codes and database:

The repository, geological environment, interaction and impact between features, events and processes should be described. The assessment model and parameter introduction in this report are shown in Section 6.5. In addition, in order to improve the quality of the quantitative calculation of safety assessment, it is necessary to freeze the key parameters used before the safety assessment so that the key parameters used in the subsequent safety assessment can be traced and ensure the consistency of the used parameters. The list of key parameters of the safety assessment of this report is presented in Section 8.3.

(3) Safety assessment

The assessment basis, including site description, design specification and coupling research of internal processes, can describe the expected initial state of the repository system, the evolution of the repository, uncertainty, and the correlation between the FEPs and the safety functions of the repository.

Safety assessment covers the uncertainty assessment of safety functions and the evolution of the repository, and constructs different scenarios. Quantitative analysis of the scenario can be carried out through a conceptual model, mathematical model, and assessment model.

Safety functions of the disposal concept currently established in Taiwan will be presented in Chapter 7 of this report. The initial state, external factor, internal process and interactive process of the repository system are compiled in the assessment basis provided in Chapters 4 to Chapter 6. With the assessment model and key data in Chapter 8, the evolution impact of the repository system in the safety case timescale is quantified and discussed. The possible impact of each action on the safety functions at different times is evaluated as well. Then the evaluation of the repository system, the result of uncertainty assessment, and the safety functions are integrated in Chapter 9. The factors of FEPs related to safety functions are also connected in this chapter. In Chapter 10, the main scenario is constructed, and the evaluation extreme value of the FEPs scenario is screened. The containment safety function analysis and retardation safety function analysis of the main scenario are presented in Chapters 11 and Chapter 12. The interference scenario is analyzed in Chapter 13, which supplements other relevant arguments supporting the safety of the repository (such as natural analogue).

(4) Integration of evidence, arguments and analyses

Various arguments related to the safety of the repository are compiled in Chapter 14. It illustrates confidence and completeness of the analyses of the program, review current results, and feed uncertainties that can be improved back to future R&D projects. Finally, whether the program has reached the goals at this phase would be discussed through peer review domestically and internationally.

(5) Feedback to project management

The relationship between safety assessment and repository development is iteration. Safety assessment provides key information for site characterization and engineering design. Relatively, the data generated by the development and research of site characterization and engineering design can support high-quality safety assessment. The uncertainty in the safety assessment can provide research instruction for the following site investigation and engineering design. The results of the investigation, design and assessment in this report will provide feedback for the arrangement of the following development.

(6) Others

During safety assessment and construction of the safety case, it is also necessary to strengthen the implementation of quality assurance (NEA, 2012a), such as the use of the same and consistent data, application of “standard” protocol of assessment, and using FEPs to check the comprehensiveness in the safety assessment. Such inspections can be regarded as part of a "bias audit". The purpose of the bias audit is a comprehensive check, which should be separated from the main line of the safety assessment and maintain a certain degree of independence, such as inviting external experts to conduct a peer review. If bias audit can be recognized by the competent authority, and relevant domestic and foreign technical review groups, it will further promote the realization of subsequent phases of the disposal program and become an important basis for decision-making.

According to the geological characteristic of the reference case (Section 4.3.2), this report constructs the preliminary concept of the repository system and completes a post-closure safety assessment based on the methodology of the safety case and disposal concepts of advanced countries in the world are referred to.

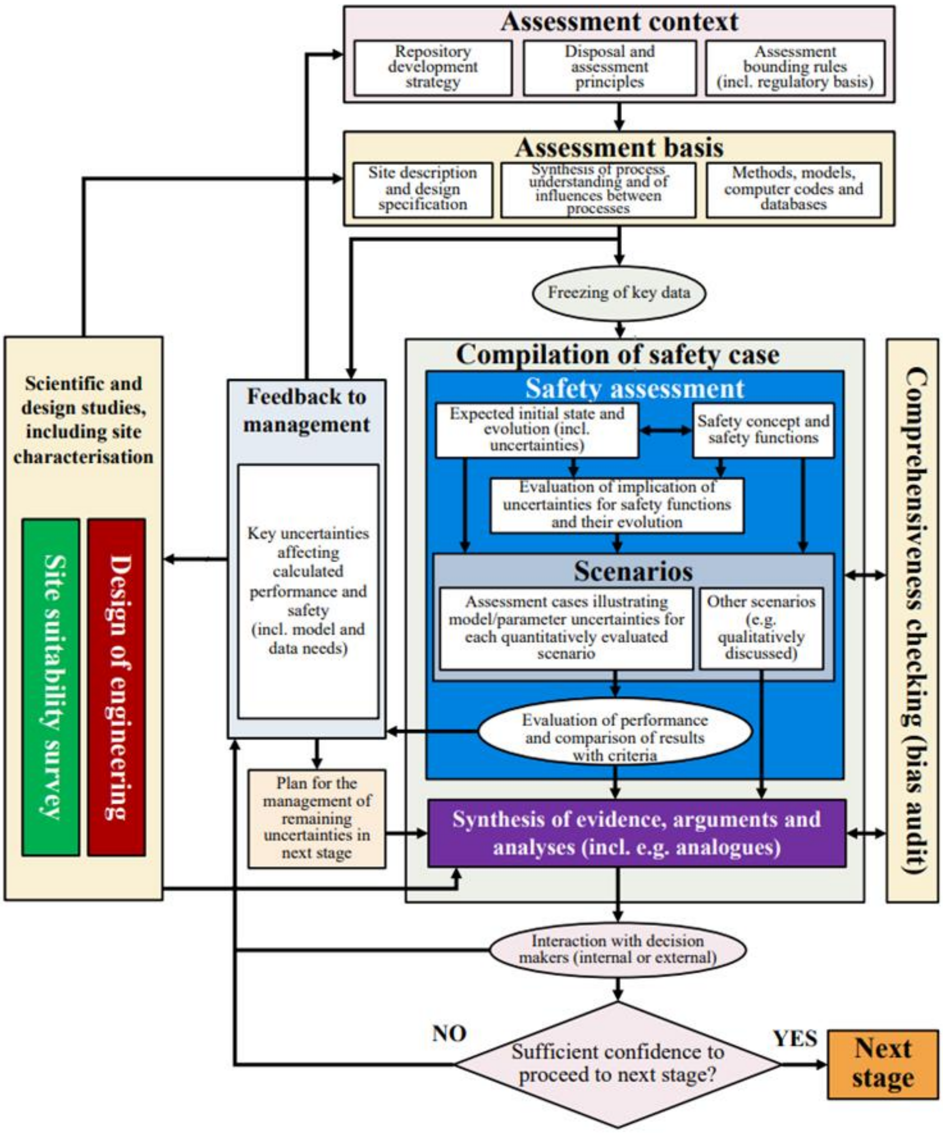

Figure 2-1: Flowchart of the safety case.

2.3. Definition of System Boundary

The disposal concept approved by the competent authority used in this report refers to the KBS-3 disposal concept proposed by Swedish SKB (Figure 2-2). The KBS-3 disposal system includes: (1) near-field: areas affected by the decay heat and radiation of spent nuclear fuel. Near-field contains the engineered barrier system covering canister, which contains spent nuclear fuel, buffer, backfill, deposition hole and disposal tunnel; (2) far-field: natural barriers such as geosphere and host rock outside the repository area unaffected by decay heat and radiation; (3) biosphere: the area of the environment inhabited by humans and other organisms.

The boundaries of the disposal system shall be defined prior to the safety assessment. The assumptions of boundary conditions of the repository system are listed below.

(1) Generally, it is hard to specifically define boundary conditions of the deep geological repository, which should be flexible. While implementing safety assessment, different factors correspond to different boundary conditions.

(2) In this report, the adjacent catchment area of the radionuclide release point, including the repository, is defined as the assessment range of the biosphere. Outside of this range is considered as external factors. The depth of the biosphere ranges to the surface of the host rock. The range can be adjusted according to the requirements during the assessment.

(3) Geosphere ranges to 1,000 m depth, which can be adjusted according to the requirements of assessment. For instance, the boundary condition of the local groundwater model and regional groundwater model is different.

(4) Future human actions near the repository are considered as a part of the repository system, but future human actions and behaviors outside the regional area are not directly related to the repository system.

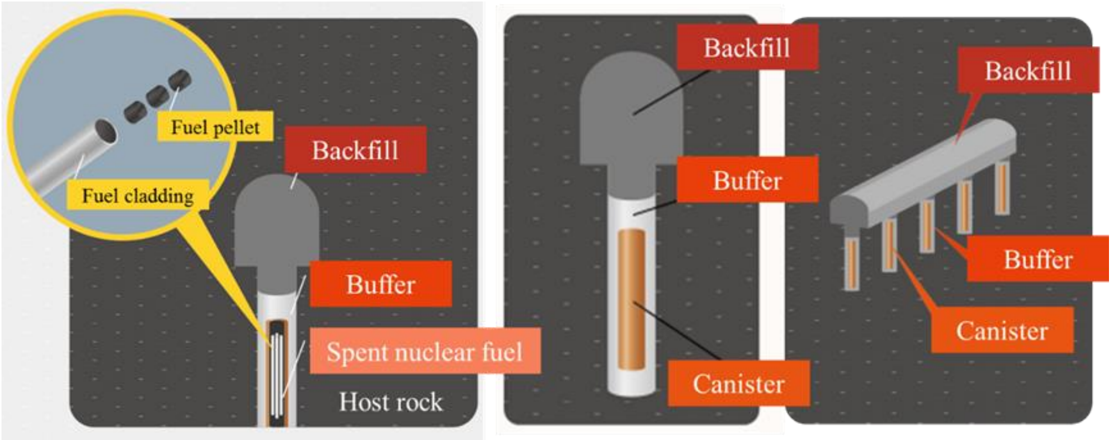

Figure 2-2: KBS-3 disposal concept

2.4. Timescales

2.4.1. Regulatory Requirements

In terms of the timescales of safety assessment, Taiwan's current regulations do not specify the timescale of safety assessment for the spent nuclear fuel repository.

2.4.2. Timescale of Safety Assessment

The radiation of 1 tonne SNF can attenuate to the level of 8 tonnes of natural uranium ore after 250,000 years of decay (SKB, 2011). For the safety assessment, the timescale should be set with a reasonable margin.

The international safety standard and timescale can be referred to Table 2-2. The international dose limitation of high-level waste final disposal repository is between 0.1 mSv/yr and 0.3 mSv/yr. The dose limitation in Taiwan is 0.25 mSv/yr which is within the international standards. The international requirement for the risk is between 10^{-5} /year and 10^{-6} /year. The requirement for the risk in Taiwan is 10^{-6} /year, which is a high standard all over the world.

Considering the relevant international experience and the radiation effects caused by the SNF, the timescale of the safety assessment in this report is set to 1,000,000 years post-closure.

2.4.3. Timescale of Repository Evolution

The timescale of repository evolution is an important issue. For example, the internal processes description in Chapter 6 and the evolution analysis in Chapter 9 are related to the timescale issue. The repository evolution is related to the following timescales, which are described as follows:

(1) Changes of radionuclide species over 1 million years:

(a) As described in Section 2.4.2, the basic safety assessment timescale is related to the radiotoxicity of spent nuclear fuel. The radiation of 1 tonne SNF can attenuate to the level of 8 tonnes of natural uranium ore after 250,000 years of decay. The timescale of the safety assessment of this report is set to 1,000,000 years post-closure.

(b) The doses from spent nuclear fuel are dominated by radionuclide species and their daughter nuclei with long half-life and should be isolated for long periods to reduce the risk of radiation exposure. For long-term safety, direct radiation to humans is only a concern in scenarios addressing unintentional intrusion into the repository.

(2) Timescales of long-term geological processes occurring over millions of years, including tectonic movements caused by plate movement.

(3) Timescale of climate change: the timescale range from decades to millions of years. On the million-year timescale, the timescale of climate change is related to the glacial cycle, so the glacial cycle is used as the timescale basis in this report.

(4) Timescale of human social change: The record of human history covers thousands of years. Over the past 100 years, many aspects of society have changed dramatically, either suddenly or within a few years.

(5) Timescale of bentonite saturation: under the conditions of crystalline rock environment, saturation of buffer, backfill and host rock usually takes more than several decades.

(6) Timescale of chemical conditions in host rock returning to natural conditions after the repository operation: it is expected that chemical conditions in the host rock can return to close to natural conditions approximately several hundred years after the repository operation.

Table 2-2: Summary of dose/risk limits and assessment timescale of post-closure repositories in other countries.

Nations	Dose/Risk limit post-closure of repository	Timescale of safety assessment	Reference
Belgium	Practical evaluation experience: Dose 0.1 - 0.3 mSv/yr. Risk 10^{-5}/yr.	Practical evaluation experience: over 1,000,000 years.	[1][2]
Bulgaria	Regulation: Dose 0.3 mSv/yr.	No specific regulation.	[3]
Canada	Regulation: Dose 0.3 mSv/yr. Risk 10^{-5}/yr.	Regulation: include the time when the greatest impact occurs.	[1][2][4]
China	No specific regulation.	No specific regulation.	[2]
Czech Republic	Regulation: Dose 0.25 mSv/yr.	No specific regulation.	[1][5]
Finland	Regulation: Dose 0.1 mSv/yr.	Regulation: At least thousands of years.	[1][2][6]
France	Regulation: Dose 0.25 mSv/yr (constrain value within 10,000 years, reference value for 10,000 to 1,000,000 years).	Regulation: At least 1,000,000 years.	[1][2]
Germany	Regulation: Dose 0.1 mSv/yr. Risk 10^{-5}/yr.	Regulation: Should have covered 1,000,000 years.	[1][2][7]
Hungary	Regulation: Dose 0.1 mSv/yr. Risk 10^{-5}/yr.	No specific regulation.	[1][8]
Japan	Practical evaluation experience: 0.1 - 0.3 mSv/yr	Practical evaluation experience: at least 1,000,000 years.	[1][2]
South Korea	practical evaluation experience: Dose 0.1 mSv/yr (normal evolution), 1 mSv/yr (human intrusion). Risk 10^{-6}/yr (Probability analysis).	No specific regulation.	[1]
Netherlands	Regulation: Dose 0.1 mSv/yr.	No specific regulation.	[1]
Slovakia	Regulation:	No specific regulation.	[1]

Nations	Dose/Risk limit post-closure of repository	Timescale of safety assessment	Reference
	Dose 0.1 mSv/yr.		
Spain	Regulation: Dose 0.1 mSv/yr. Risk 10^{-6}/yr.	No specific regulation.	[1][2]
Sweden	Regulation: Risk 10^{-6}/yr.	1,000,000 years.	[9][10]
Switzerland	Regulation: Dose 0.1 mSv/yr. Risk 10^{-6}/yr.	Regulation: Over 1,000,000 years.	[1][2][11]
United Kingdom	Regulation: Dose 0.15 mSv/yr. Risk 10^{-6}/yr.	No specific regulation.	[1][2][12]
United States	Regulation: Dose 0.15 mSv/yr within 10,000 years. 1 mSv/yr between 10,000 to 1,000,000 years.	Regulation: 1,000,000 years.	[1][13]
Taiwan	Regulation: Dose 0.25 mSv/yr. Risk 10^{-6}/yr.	No specific regulation.	[14]

Reference:
[1] OECD/NEA (2007)
[2] Journal of University of South China (2020)
[3] Bulgaria Government (2004)
[4] CNSC (2006)
[5] Czech Republic (2002)
[6] STUK (2013)
[7] BMUB (2010)
[8] Hungary Government (2003)
[9] SSI (1998)
[10] SSM (2008)
[11] ENSI (2009)
[12] SEPA and NIEA (2009)
[13] EPRI (2010b)
[14] AEC (2013)

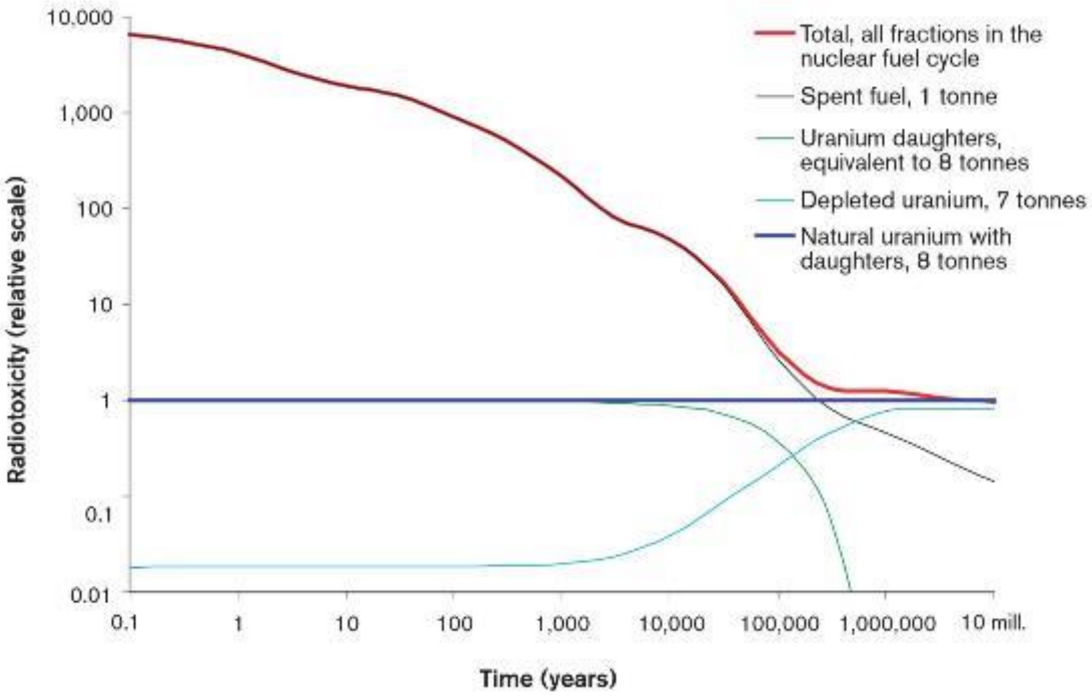

Figure 2-3: Radiotoxicity of SNF over time.

Reference: SKB (2011)

2.5. Safety of the Repository

2.5.1. Safety considerations for the Repository

This report refers to the Swedish KBS-3 disposal concept, and establishes the following safety principles for the repository:

(1) The repository is in a long-term stable deep geological environment. The SNF is isolated from human and ground environments to prevent the impact of human society changes and long-term climate changes.

(2) The repository should be located in a place where there is no economic benefit to future generations in order to reduce the risk of human intrusion.

(3) Several engineered barriers and the natural barrier are used to contain SNF (multiple barriers).

(4) The primary safety function of the barriers is to contain the SNF in the canister.

(5) If the safety function of containment fails, the secondary safety function of the barriers is to retard the release of radionuclides from the repository.

(6) The design and manufacture of the engineered barrier should use natural materials in order to maintain long-term safety in the environment of the repository system.

(7) The design and construction of the repository should avoid serious harm to the long-term performance of the barrier caused by high temperature.

(8) The design and construction of the repository should prevent radiation-induced reactions from serious harm on the long-term behavior of the engineered barrier and the host rock.

(9) The design of the barrier should be passive, that is, it can perform its safety functions without any intervention by human.

2.5.2. Safety Functions and Safety Measurements

The safety functions of the KBS-3 repository system can be divided into containment safety function and retardation safety function, as described below.

(1) Containment safety function: adopt multiple barrier concept to prevent radionuclides' release from the spent nuclear fuels. In addition to the containment safety function of the zirconium alloy sheath of the spent nuclear fuel itself, the multiple barrier also includes a canister, buffer and backfill, which are often referred to as engineered barrier systems.
(2) Retardation safety function: when disposed for a long time, the containment safety function fails to allow the radionuclides to be released. There are still multiple barrier systems that can delay or block the radionuclides' transport after radionuclides are released into the engineered barrier system.

The safety measurements based on the above safety function are the placement of spent nuclear fuel in the corrosion-resistant canister with mechanical strength cast iron lining. The canister is surrounded by bentonite and placed in a deposition hole at a depth of more than 300 m above the surface as required by regulations in section 1.4.3. Under the safety measurement mentioned above, bentonite can reduce the effect of shear force caused by fractures on deposition holes and the effect of the isostatic load caused by the surrounding environment. Bentonite can also prevent corrosive agents from contacting the surface of the canister and reduce the canister corrosion. The host rock provides a long-term chemical, mechanical, thermal and hydrological stable environment. As a result, the buffer and host rock provide the canister with a long-term containment barrier.

As if the canister fails, the retardation safety function provided by the KBS-3 disposal system becomes functional. The safety measurements considered for the retardation safety function are that fuel, canister, buffer and host rock can retard the radionuclides release. The cast iron lining and copper shell of canisters can prevent an inflow of groundwater. The buffer can limit the groundwater from flowing into canisters and limit the release of radionuclides by sorption of bentonite. Groundwater would slowly flow in the rock fracture near the canister, so numerous kinds of radionuclides would tend to transport by diffusion and are likely to be adsorbed by host rock.

This report refers to the Swedish KBS-3 disposal concept, and the disposal system provides an effective containment safety function and retardation safety function. The safety functions provided by each system component in the disposal system are detailed in Chapter 7 of this report. The safety functions provided by each component of the disposal system are established based on the research results of Swedish SKB and the possible evolution of engineering design and geological environment, and the safety function indicators and criteria of individual components of the disposal system are set. Demonstrating that the barrier meets these safety function indicators and criteria in safety assessment provides arguments for the safety case that the barrier will function as expected as the repository evolution. If the barrier violates the safety function criteria, further assessment of the impact of the safety function on the overall disposal system performance is required, but this does not mean that the disposal system cannot maintain long-term safety.

If the safety function indicators criteria cannot be met, the condition can be developed into scenarios to assess the safety of the repository, and the results are compared with the safety indicators of Taiwan to confirm that the repository still meets the requirements of regulations of Taiwan even if the safety function indicators criteria are not fulfilled.

2.6. Expert Judgments

As the disposal site has not been decided, this report collects historical researches to establish the reference case for study. The use of some analysis methods and data is based on the recommendations of IAEA SSG-14, referring to common international practices and using expert judgment mechanisms to simplify and make assumptions so as to accelerate the promotion of research and development work and to establish the safety confidence of the disposal concept.

There are various forms of expert judgment. For instance, directly interpret experimental results or judge the impact of anthropogenic greenhouse effects on future climate evolution to assess possible impacts on the repository. The process of expert judgment includes expert qualification identification, expert invitation, convening discussion meetings and meeting records, which are all made into paper records to facilitate inquiries and traceability. The documents of expert judgment include review reports, data lists and meeting records, etc.

2.7. Information/Uncertainty Management

2.7.1. Definition of the Uncertainty

This report refers to international practice methods (NEA, 1997a; NEA, 2005; POSIVA, 2018-02; NDA/RWM/153, 2017) and considers the classification and property of the uncertainties. In general, the uncertainties can be divided into three categories: (1) system/scenario uncertainty, (2) concept/model uncertainty, and (3) data uncertainty (Figure 2-4). The source of uncertainty can be divided into epistemic uncertainty caused by lack of background knowledge and aleatory uncertainty caused by natural variations.

(1) System/scenario uncertainty

It is a comprehensive uncertainty. The main sources include (a) system evolution, (b) recognition of FEPs and their functions, and (c) the degree of understanding of the system. The uncertainty of the system is affected by the factors of FEPs related to the system and the capacity to describe the system. The uncertainty of the scenario is mainly caused by the setting of the scenario, which is not able to fully represent the future evolution. Therefore, whether the system description and scenario setting include the identified factors and processes of FEPs plays an important rolein reducing the uncertainty of the scenario. In practice, different evaluation cases can be set, and the possible future evolution of the repository can be fully considered to reduce the impact of the uncertainty of the scenario.

(2) Concept/model uncertainty

The main sources of uncertainty in this part are (a) the degree of understanding of the system and (b) the assumptions, simplifications, and limitations of the model. The degree of understanding of the evolution of the repository system will affect the uncertainty of the assessment. In addition, the model describing the evolution of the repository system and related effects also plays a very important role. The classification of models can be divided into the following three types according to the description of the repository system:

(a) Conceptual model:

The model is composed of a qualitative description of the repository system. The uncertainty may come from whether the understanding of the conceptual model is correct and whether all related FEPs are included in the model.

(b) Mathematical model:

Mathematical model describes the repository system by presenting parts of conceptual models with mathematical equations. The uncertainty mainly comes from the process of model simplification.

(c) Computational model:

Computational model describes the repository system all by mathematical model calculation. The uncertainty may come from potential errors in the model calculation process or time/space and numerical errors.

In the process of modelling, it is inevitable that a certain of uncertainty may be involved in each step. The uncertainty of the model can be reduced through model identification, which is verified by comparing the same types of models with each other or through independent review by experts. Verifying and comparing the calculation results of the models with experimental results, natural analogue is also a common method for model identification.

Since it is impossible to verify the interaction of the future, the uncertainty of the model may increase or decrease with the coverage of the assessment timescale, which needs to be supplemented by natural analogue or other evidence (STUK, 2014a).

(3) Data uncertainty

This part of the uncertainty involves all the input parameters used in the assessment, and the main sources are (a) the applicability of the data itself, (b) different types of data, (c) lack of data, and (d) the variability in space or time. Since the input parameters of the model are established according to the model requirements, the uncertainty of the concept/model and the uncertainty of the data are closely related to some extent. The use of different types of data also creates uncertainty when calculating probabilities for different scenarios and cases. Model identification and data identification procedures help maintain the quality of the data used in the evaluation model and can effectively reduce data uncertainty. In addition, the data uncertainty can be quantitatively evaluated by deterministic or probabilistic analysis or by combining the above two to deepen the confidence of the evaluation results (NEA, 2012b).

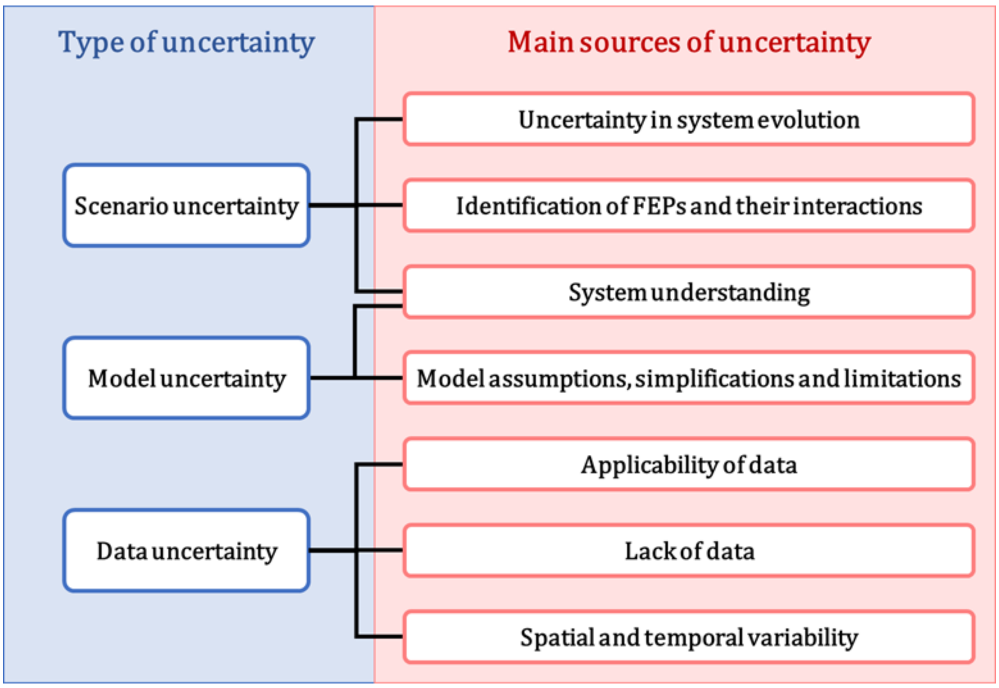

Figure 2-4: Classification of uncertainty.

2.7.2. Stylised Requirements of the Evolution Case

In the process of safety assessment, FEPs will be screened through FEPs, and a database of FEPs will be built to explore the impact of interactions. Analysis parameters will be set, and quantitative assessment models will be established to completely deal with the various uncertainties that affect the safety functions of the repository system. Biosphere and other external factors will be simplified in a "stylised" way of conservative assumptions. When evaluating the biosphere or external factors with high uncertainty, representative cases with a high probability or possibility of occurrence are used to describe the related evolutionary situation.

The biosphere surrounding the repository is located in the boundary of the repository system, which belongs to a part of the repository system. As a result, the uncertainty of the biosphere shall be discussed by the same method as the repository system. However, there are many processes that determine the evolution of the biosphere, which occur extremely unevenly (including multiple biospheres composed of multiple biosphere objects). In addition, the biosphere may changes dramatically compared to the evolution of the repository system. Some uncertainties of the biosphere cannot be reduced either. Therefore, it is generally recommended to describe the biosphere in a stylised way when evaluating the biosphere.

On the other hand, a detailed analysis of the climate evolution processes is not within the scope of the safety assessment of the repository. In addition, climate evolution analysis is still a developing discipline, and some uncertainties cannot be reduced. Therefore, in the assessment of climate evolution, a reasonable description of possible future evolution will be done in a stylised way along with the development of this discipline, including the uncertainty. The extreme climatic conditions that may affect the safety of the repository (such as the greenhouse effect caused by global warming) will also be described in a stylised way in order to make the uncertainty considerations in the safety assessment of the repository more complete.

2.7.3. Management of the Uncertainty

Identifying uncertainty, avoiding or reducing uncertainty, and uncertainty assessment are the basic strategies for uncertainty management (Posiva, 2012, 2017). During the management of uncertainty in this report, parameter sensitivity analysis will be carried out to understand the importance and relevance of the uncertainty of each input parameter to the evaluation results. In addition, the repository system will maintain a sufficient safety redundancy during the design, and use conservative assumptions to deal with most of the uncertainties, and confirm that it can meet the requirements of relevant laws and regulations. Finally, for the uncertainty of identification, feedback is provided to the engineering design and site investigation by evaluating the effects qualitatively and quantitatively. Currently, data uncertainties (including random/systematic errors, sample variability, measurement method defects and other experimental errors, as well as uncertainties related to the interpretation of experimental data, and deviations caused by data selection) are initially fed back to the model and scenario uncertainty, in order to carry out preliminary uncertainty management.

2.8. Quality Assurance

Quality assurance of this program is based on 10 CFR 60 Subpart G quality assurance criteria of the United States Code of Federal Regulations, and refers to Nuclear Quality Assurance (NQA-1) "Quality Assurance Requirements for Nuclear Energy Facilities" published by the American Society of Mechanical Engineers (ASME). The content is based on the requirements of 10 CFR 60.151, 152, and the quality assurance criteria of 10 CFR 50 appendix B, which lists the main points of quality assurance, the division of powers and responsibilities, and the operating requirements in order. Quality assurance of this program also strengthens the safety requirements of IAEA SSR-5 and safety guidelines of SSG-23, and fully reflects the responsibility of the relevant personnel for quality assurance of the “Spent Nuclear Fuel Final Disposal Program.”

2.8.1. Overview

Generally, the quality assurance project for the long-term safety assessment of the SNF repository helps to ensure that all factors related to long-term safety have been appropriately included in the safety assessment. The main purpose of the safety assessment is to confirm the long-term safety of the repository over time. In principle, it is determined by comparing the assessment results and the related radiation dose with the standards.

During the safety assessment, the scientific evaluation of the repository evolution will be carried out with models. The coupled process and mathematical model will be simulated with the understanding of the phenomenon. The mathematical model will be converted into code and input data to perform calculations. These processes need to be recorded to ensure its quality. In addition, the safety assessment needs to deal with many FEPs that affect long-term safety. The database that collects FEPs should also be used as a tool to check quality. The database could elaborate on how the specific FEPs are included in safety assessment and why others are excluded. Therefore, the quality assurance project is closely related to the quantitative processing of the evolution of the FEPs database and the repository. A complete quality assurance project and quality assurance system can help plan executives conduct safety assessments in a structured and comprehensive manner and help reviewers judge the quality and comprehensiveness of the assessment results.

2.8.2. Objectives of Quality Assurance

The objective of quality assurance is to do the right thing and review the results in the right way, which ensures that the factors related to long-term safety are included in the safety assessment.

The design of the quality assurance project can specifically assist in achieving the following goals:

(1) The program has followed proper project management procedures, such as document control procedures.
(2) Previous version of the FEPs database of the program is considered in the safety assessment, and all factors related to long-term safety are in the international NEA FEPs database as well.
(3) The excluded factors have been approved by authoritative experts.
(4) The methodology used for exclusion factors has been approved by authoritative experts.
(5) The processing method of the mathematical model in quantitative evaluation and the method of quality assurance in this model are confirmed.
(6) The quantitative evaluations are properly evaluated by parameters that have passed quality assurance procedures.
(7) The content of the safety assessment report and the response to the review are completed.

2.8.3. Quality Assurance Project

The quality management system has been established, promoted, evaluated, and continuously improved in this program. According to the task requirements of the disposal program, each level of quality management documents shall be formulated respectively.

Regularly internal and external audits are also implemented to ensure the effectiveness and efficiency of the procedures in compliance with the quality management system.

2.9. Risk Assessment

2.9.1. Regulatory requirements

According to the requirements of the SNF repository in Taiwan, such as "Regulations on the Final Disposal of High-Level Radioactive Waste and Safety Management of the Facilities" Article 10 in Section 1.4.2, it is necessary to ensure that the repository shall be designed to limit the personal annual risk caused by the radiation to a person in the key groups outside the repository to less than 1/1,000,000. According to the dose to risk conversion factor of 0.057/Sv reported in ICRP103, the annual risk limit of one part per million is equivalent to the effective dose limit of 18 μSv/year. However, according to regulatory requirements in Taiwan, the dose limit used in this report is 13.7 μSv/year and is more conservative than 18 μSv/year.

2.9.2. Application

In addition to setting the safety assessment dose and risk targets by complying with the requirements of the aforementioned domestic laws and regulations, safety assessment operations are implemented by referring to international regulations. For example, IAEA SSG-14 indicated that, "Safety assessment is the process of using appropriate methods to systematically analyze the facility risk, the capacity of the site and the design of the facility to meet safety requirements. A safety assessment for a geological repository should include quantitative analysis of the overall performance, uncertainty analysis and comparison with the design requirements and safety standards. Any significant deficiencies in scientific understanding, data or analysis that might affect the results presented also have to be identified in the safety assessment." The safety assessment should also determine any significant deficiencies in scientific knowledge, data, or analysis that may affect the results.

In general, several issues involved in the post-closure safety assessment of the repository are defined as below:

(1) Timescale of safety assessment:

As mentioned in Section 2.4, although laws and regulations in Taiwan do not specify the timescale of post-closure safety assessment of high-level radioactive waste repository, this report defines 1,000,000 years post-closure as the timescale for the safety assessment based on domestic consensus and international experience.

(2) Definition of the critical groups:

By the requirements of post-closure safety assessment, the definition of key groups (such as dose recipients) is based on the analysis of living habits and environmental characteristics, which considers the release and transport of various nuclides and their migration and exposure paths in the biosphere. The release and transport path with the highest risk are temporarily selected to be a safety impact on the key groups.

(3) The definition of time evolution period:

For the long-term evolution of the repository post-closure, this report uses the glacial cycle as the basis for dividing the time evolution period.

2.9.3. Alternative Safety Indicators

Even though safety indicators of dose and risk can be used to assess the possible future radiation effects of the repository on humans, the biosphere evolution remains highly uncertain even on shorter timescales. In safety assessment, it is necessary to make many assumptions against these uncertainties. As such, alternative safety indicators that do not require detailed assumptions about the biosphere or future human actions will often help to supplement dose and risk safety indicators and possible impacts on the non-human biosphere.

According to the Swedish Radiation Safety Authority's regulations concerning safety in connection with the disposal of nuclear material and nuclear waste (SSMFS, 2008:21), radionuclide concentrations in groundwater or near surface water, radionuclide fluxes in the biosphere, etc., can be used as alternative safety indicators for supplementary instructions. These alternative safety indicators usually have no clear quantitative benchmark to follow. Although a comparison of the assessment results with the concentrations/fluxes of nuclides in nature may be considered, there may be a problem that artificial radionuclides have no benchmarks to refer to. At this time, it can be considered to compare the assessment results with the total concentrations/fluxes of the corresponding α/β radionuclides in nature or compare the dose caused by each unit intake to compare their overall radiotoxicity.

In addition to the aforementioned alternative safety indicators such as the concentrations/fluxes of radionuclides, the hydraulic, chemical or mechanical states of the repository barriers (for example, stress state or ionic strength, etc.), or natural analogies can be used as alternative safety indicators to supplement the radiation effects of the repository. The safety function indicators mentioned in Chapter 7 are also an alternative safety indicators related to the status of the barriers. The safety function indicators are quantified and compared with the safety function indicator criteria to confirm their possible impact and can be used to assess the performance of the overall system.

The important international literature on safety indicators and reference values is as follows:

(1) The SPIN project (Becker et al., 2002)

As recommended by the SPIN project, the following two alternative safety indicators can be used to supplement the dose impact of the repository:

(a) Radiotoxicity concentration in biosphere water: preference for medium time frames, i.e. several thousand to several tens of thousands of years.

(b) Radiotoxicity flux from the geosphere: preference for late time frames.

The project also reports on reference values that could tentatively be used for comparisons to calculated concentrations/fluxes of radionuclides from the repository.

(2) Finnish activity release constraints (STUK, 2001)

According to the regulations of the Finnish Radiation and Nuclear Safety Authority (STUK) on the release activity, the release rate of radionuclides should comply with the following limits:

(a) 0.03 GBq/y for the long-lived α-emitting isotopes of Ra, Th, Pa, Pu, Am and Cm,

(b) 0.1 GBq/y for Se-79, I-129, and Np-237,

(c) 0.3 GBq/y for C-14, Cl-36, Cs-135, and the long-lived isotopes of U,

(d) 1 GBq/y for Nb-94 and Sn-126,

(e) 3 GBq/y for Tc-99,

(f) 10 GBq/y for Zr-93,

(g) 30 GBq/y for Ni-59,

(h) 100 GBq/y for Pd-107 and Sm-151.

The above limits only list long half-life radionuclides. The potential impact of their short half-life daughter nuclei has been taken into account when setting the limits. These radionuclide limits can be used to assess the possible radionuclides release to the biosphere due to the repository evolution after repository closure for thousands of years.

It should be noted that, when deriving the limits, the Finnish regulatory authority took into account the possible future evolution of the biosphere at its candidate site (Olkiluoto). Therefore, further evaluation may be required before the limits can be used as a benchmark for comparison in this report.

(3) SR-site safety analysis reports (SKB, 2011)

In SR-site safety analysis reports, the following four indicators are used as alternative safety indicators for the safety assessment:

(a) The release activity limit in Finnish activity release constraints,

(b) Radiotoxicity flux from the geosphere in the SPIN project,

(c) Measured concentrations of naturally occurring radionuclides in ecosystems at the Forsmark site or other comparable sites,

(d) Naturally occurring fluxes of radionuclides at the Forsmark site.

(4) The report of the Nuclear Energy Agency of the Organization for Economic Cooperation and Development (NEA, 2012b).

According to relevant laws and regulations in Taiwan, dose and risk are currently used as indicators to evaluate the repository’s safety. The alternative safety indicators and their reference values currently adopted internationally can be used as a reference in the future to assist in explaining the doses and risks that may be caused by the repository.

3. Features/Events/Processes (FEPs)

3.1. Introduction

Inspecting and screening the Feature, Event, Process (FEPs) that may affect the function and safety of the disposal repository is an important preparatory work before the implementation of the safety assessment. Through extensive research on the interaction between various influencing factors and disposal repository, the safety function indicators of disposal repository components were determined under the engineering design premises and geological initial conditions. At the same time, the reference evolution of the disposal repository within the timescale of 1 million years safety assessment was constructed, and various possible scenarios and cases were developed to quantify the possible radiation dose impact of the disposal repository under individual scenarios and cases by means of assessment model flowchart. Finally, the conclusion of the safety assessment, including the degree of risk compliance hazard and uncertainty analysis, is obtained by analyzing the influence of various scenarios.

3.2. FEPs Database of the Reference Case

There are three ways to establish the FEPs list. The first is to gather people who have an overall concept of the repository system. These people would cooperate with experts in various fields to form a working group and list and display the factors after comparison, discussion and integration. The second option is to select a FEPs list of other plans as the basis and modify it according to the repository design and site characteristics of the program. The third option is to collect known FEPs lists of other countries, and re-integrate the FEPs lists suitable for the Taiwan disposal program.

The SNF Final Disposal Program in Taiwan is based on the Swedish KBS-3 disposal concept, with crystalline rock as the priority for disposal. The concept of safety function from the Swedish SR-Site has been introduced into the safety assessment methodology. Therefore, this report first refers to the FEPs inventory of the Sweden SR-Site program and then conducts a preliminary screening based on the disposal planning process, background, and reference case characteristics to select the appropriate FEPs. The FEPs of the external factors and the biosphere are closely related to the local environment. Therefore, the external factors were adjusted according to the geological environment of Taiwan. In addition to the local environment of Taiwan considered in the biosphere, the biosphere-related FEPs in the Japan H12 report were also referred to. With the above steps, the reference case FEPs list was established. Furthermore, this FEPs list would be compared to the International FEPs List (IFEP) in the NEA FEPs database to ensure that all relevant factors have been taken into account.

After the above steps and incorporating the recommendations of recent expert meetings, a total of 439 FEPs were included in the FEPs database of the reference case. Based on the treatment of the FEPs in the safety assessment report, the FEPs in the FEPs database of the reference case are divided into five categories: (1) initial state, (2) internal processes, (3) variables, (4) biosphere and (5) external factors (台電公司, 2019a). The classification implications are as follows:

(1) Initial state (18 FEPs in total)

This section describes the requirements of the design, manufacture and construction of the system components for containment and retardation safety functions, as well as possible deviations. It also describes the initial state of the canister, buffer, backfill, and underground facilities.

(2) Internal Processes (198 FEPs in total)

The safety of the disposal repository is discussed from a long-term perspective in view of the individual or coupling effects of thermal-hydro-mechanical-chemical (THMC) processes in the disposal repository system component. The content includes SNF, canisters, buffer, backfill, underground facilities and geosphere.

(3) Variables (99 FEPs in total)

The variables are mainly based on scientific demonstration of the internal processes or interaction model analysis and experimental design. In the integration analysis of variables, it is necessary to consider the change of all internal processes on barrier characteristics over a long time evolution as far as possible.

(4) Biosphere (90 FEPs in total)

Based on local climatic conditions, geographical conditions, hydrological characteristics, cultural and ecosystem in Taiwan, the biosphere is divided into seven categories, which are thermal, hydrology, physical-chemical, radiology, migration, evolution and disturbance.

(5) External factors (34 FEPs in total)

The external FEPs classification mainly includes climate issues, regional geological processes, future human actions and others.

3.3. FEPs List of the Reference Case

The FEPs data list of this report is based on the FEPs list of the SNFD2017, whose design concept is also based on crystalline rock and a deep geological repository (台電公司, 2019a). Furthermore, from the FEPs database established in section 3.2, FEPs suitable for the reference cases in this report were selected. The principle of factor selection for the FEPs list is as follows:

(1) Evaluate the long-term safety of the disposal system, including FEPs related to the internal processes and variables of SNF, canister, buffer, backfill and geosphere.

(2) Select FEPs list associated with external conditions and biosphere based on geological and environmental characteristics of reference cases. For example, the FEPs about estimating the ancient climate of reference case, sea level variation caused by global ice age, and coastline migration could be studied. The FEPs about extreme regional climate, regional crust movement, and future human actions post-closure can also be included and discussed. The related factors of regional influence directly caused by the ice age are excluded.

(3) According to the current level of research and technology development, the related FEPs list is screened to explore its impact on the safety of the repository.

According to the above screening principles, this report establishes the FEPs data list of reference cases, with a total of 152 factors, as shown in Table 3-1.

Table 3-1: FEPs List of the Reference Case

Initial state (10 FEPs in total)		
Number	**FEP name**	**Definition**
TWISGen01	Major mishaps/ accidents/ intentional destruction	This FEPs are major mishaps/accidents that occur in the operation and transportation of packaging plants and repositories, such as fires, explosions, earthquakes and floods. Intentional destruction (chemically and physically) and improper management are included in this FEPs, accompanied by decontamination processes after the accidents occur.
TWISGen02	Effects of repository operation	Repository operation will mainly affect the following development of the lithosphere and overall repository. The hydrogeological condition of the bedrock will be disturbed while the repository is excavated. Different parts of the repository may complete at different times, which may encounter different hydrogeological conditions and affect the saturation of the buffer and the backfill. All these issues are parts of the expected evolution of the repository, but they are not available in the automatic process of repository evolution through time. Therefore, it needs to be properly discussed in the evolution of the repository.
TWISGen03	Incomplete closure	The impact of the unclosed and abandoned repository is considered
TWISGen04	Monitoring activities	The purpose of monitoring activities is to maintain long-term safety, including underground borehole monitoring.
TWISC01	Defective canister	The improper management and damage of the canister during manufacture, sealing and transportation. Although there is quality control in manufacturing and sealing, random defects are still considered for some common factors.
TWISC02	Design deviations - canister	Welding or material defects (caused by geometry or material composition), such as loss of ductility due to impurities in copper materials or poor manufacturing methods, or "cold cracking" due to poor manufacturing methods. Although the manufacturing and sealing are under quality control, some random defects are still under consideration.
TWISBu01	Mishaps – buffer	The installation failure or deviation of the buffer caused by the inflow of groundwater and the remote control of the suspension caused the unevenness of the buffer and/or reduced the density.
TWISBu02	Design deviations – buffer	Although there is quality control, there are still deviations in the properties of the buffer.
TWISBfT01	Mishaps - backfill in tunnels	The inflow of water or errors or deviations in the backfill placement caused uneven backfill.
TWISBfT02	Design deviations - backfill in tunnels	Although there is quality control, there are still deviations in the properties of backfill.
Internal Processes (58 FEPs in total)		

Number	FEP name	Definition
TWF01	Radioactive decay	Metamorphosis of the radioactive species in the fuel caused by radioactive decay.
TWF02	Radiation attenuation/heat generation	Energy is transferred to the fuel or cavity of the canister through radiation.
TWF03	Induced fission (criticality)	The possibility of nuclear fission and criticality induced in the canister.
TWF04	Heat transport	Heat is transferred from the fuel and cavity of the canisters to the canisters through conduction and radiation.
TWF05	Water and gas transport in cavity of the canisters	The transport of water, steam and other gases in the failed canister.
TWF08	Advection and diffusion	Solute flows in and out of the canister through advection and diffusion.
TWF09	Residual gas radiolysis/ acid formation	The air and water in the intact canister may be decomposed by radiation exposure, and then the product may be converted into corrosive gas, such as nitric acid or nitrous acid.
TWF11	Metal corrosion	The activated substances are released from the metal caused by corrosion of the fuel jacket and other system components in the fuel.
TWF12	Fuel dissolution	If water flows into the cavity of the canisters, the fuel may dissolve/transform, causing the release of uranium and other radionuclides in the fuel matrix.
TWF13	Dissolution of gap inventory	If water enters the canister, the material that has been isolated in the gap between the fuel and the sheath will release radionuclides.
TWF17	Radionuclide transport	The radionuclides dissolved in the canister are transported by advection and diffusion, while the gaseous nuclides (C-14, Rn-222, and Kr-85) may be transported in the gas phase.
TWC02	Heat transport	The heat transport of metal in the cast iron lining and the copper canister is transferred by conduction. If the gap between the cast iron lining and the copper shell is vacuum, heat will be transferred by radiation.
TWC03	Deformation of cast iron lining	When the canister is mechanically loaded, such as buffer expansion, the initial stress will make the canister material elastically deform. However, if the stress is large enough, plastic deformation will occur.
TWC04	Deformation of copper canister from external pressure	Copper canisters are mainly used to prevent corrosion. The mechanical strength of the copper canister is of secondary importance, but the canister must withstand the loads of manipulating, transportation and disposal. Copper must have sufficient ductility to allow the cast iron lining to deform caused by external loads, regardless of plastic or creep strain. In addition, the copper canister must withstand the load caused by the deformation of the cast iron lining caused by external pressure.
TWC09	Galvanic corrosion	If the copper shell is broken and groundwater flows in and contacts the cast iron lining, the

		electrochemical reaction on the copper surface will affect the corrosion of the cast iron lining.
TWC11	Corrosion of copper canister	Corrosion of copper canisters under the conditions of the repository.
TWC12	Stress corrosion cracking of the copper canister	Under the conditions of the repository, the possibility of stress corrosion cracking of copper canisters.
TWC15	Radionuclide transport	See TWF17 radionuclide transport.
TWBu02	Heat transport	After the canister is set up, the heat enters the buffer from the surface of the canister by conduction or radiation.
TWBu04	Water uptake and transport for unsaturated conditions	Under unsaturated conditions, the negative capillary pressure in the buffer absorbs and transmits water in the rock around the deposition hole.
TWBu05	Water transport for saturated conditions	The flow of water in the buffer under saturated conditions.
TWBu06	Gas transport/dissolution	The process of gas transport from the buffer. This gas includes the air existing between the pores in the unsaturated stage and the hydrogen produced by the anaerobic corrosion of the cast iron lining in the failed canister in the saturated stage. Depending on the state of the buffer and the rate of gas generation, the gas will be transported by means of dissolution and diffusion, capillary two-phase flow, and expansion channels.
TWBu07	Piping/erosion	The pipe flow forms channels and continuous water flow in the bentonite and erodes the hydrated bentonite colloid.
TWBu08	Swelling/mass redistribution	The expansion of the buffer and other stress-strain related effects that will cause the redistribution of the buffer quality, such as thermal expansion, creep, and the interaction of many buffers with canisters, near-field host rock and backfill.
TWBu10	Advective transport of species	The flow caused by pressure in the buffer causes the solute and colloid to be transported in the pore water.
TWBu11	Diffusive transport of species	The solute in the buffer is transported by diffusion, including enhanced cation diffusion and anion repulsion.
TWBu12	Sorption (including exchange of major ions)	The solute in the buffer is absorbed by ion exchange and surface complexation.
TWBu13	Alterations of impurities	Except for montmorillonite, the dissolution and secondary precipitation of accessory minerals and impurities in the buffer.
TWBu14	Aqueous speciation and reactions	The chemical reaction of the liquid phase includes thermodynamics and kinetics.
TWBu15	Osmosis	The impact on the properties of the bentonite buffer (swelling pressure and hydraulic conductivity) due to the difference in the mobility of ions flowing through the bentonite-rock interface.
TWBu16	Montmorillonite transformation	The deterioration of montmorillonite that occurs in the buffer.
TWBu18	Montmorillonite colloid release	The buffer is squeezed into the cracks of the rock mass around the deposition hole due to

		the expansion effect, which may cause the separation of individual montmorillonite layers or small groups of mineral layers.
TWBu22	Cementation	Cementation mainly refers to the change of the rheological behavior and swelling properties of the buffer due to different chemical or mechanical effects.
TWBu23	Colloid transport	The formation, concentration, stability and transport of colloids in the buffer, including the aggregation of radionuclides and the radionuclides adsorbed by colloidal particles. In particular, it refers to the transfer of the colloid in the buffer from the inside of the canister to the host rock of the deposition hole.
TWBu25	Transport of radionuclides in the water phase	The radionuclides in the buffer are transported by advection, diffusion, seeding, adsorption, colloidal transport, and radioactive decay.
TWBfT03	Water uptake and transport for unsaturated conditions	Under unsaturated conditions, because the internal pores of the backfill are under negative capillary pressure, water is drawn from the surrounding rock mass and forms water transport.
TWBfT04	Water transport for saturated conditions	Under saturated conditions, the transport of water in the tunnel backfill is mainly caused by hydraulic gradients.
TWBfT06	Piping/erosion	Due to the water pressure generated at the junction of the rock mass cracks around the tunnel and the backfill, the backfill in this area produces pipe flow and erosion.
TWBfT07	Swelling/mass redistribution	The mass redistribution and expansion of the backfill in the tunnel, including thermal expansion, creep, and the interaction of the backfill with buffer, rocks, and tunnel plugging.
TWBfT09	Substances advective transport	Advection of solutes (dissolved substances) and colloids in water caused by pressure.
TWBfT10	Substances diffusive transport	The diffusion and transport of the solute in the tunnel backfill, including enhanced significant cation diffusion and anion mutual repulsion.
TWBfT11	Sorption (including exchange of major ions)	The solute of the backfill in the tunnel is adsorbed by ion exchange and surface complexation.
TWBfT12	Alterations of backfill impurities	Dissolution and secondary precipitation of accessory minerals and impurities other than montmorillonite in the backfill.
TWBfT13	Aqueous speciation and reactions	See TWBu14: Seeding and reaction of aqueous solutions.
TWBfT14	Osmosis	The effect of osmosis on the properties of the backfill (swelling pressure and hydraulic conductivity).
TWBfT15	Montmorillonite transformation	The metamorphism of montmorillonite in the tunnel backfill and the corresponding metamorphic effect.
TWBfT16	Backfill colloid release	The mechanism of the colloid release of the tunnel backfill.

TWBfT21	Transport of radionuclides in the water phase	The process of movement of radionuclides in the backfill by advection, diffusion, speciation, adsorption, colloidal migration, and radioactive decay.
TWGe03	Groundwater flow	The groundwater flow in the surrounding host rock during the excavation, operation and closure of the repository.
TWGe05	Displacements in intact rock	The phenomenon of rock displacement around the repository due to mechanical or thermodynamic loads.
TWGe06	Reactivation - Displacement along existing discontinuities	The normal and shear displacements of the discontinuous surface of the rock mass under different loading conditions.
TWGe07	Fracturing	Bedrock rupture caused by high tension or stress concentration.
TWGe11	Advective transport/mixing of dissolved species	The solute is transported by the groundwater flow in the connecting fractures of the rock. These flow paths will intersect in some places, leading mixing of water from different conduction cracks. Advection results in the substitution and/or mixing of different types of water.
TWGe12	Diffusive transport of dissolved substances in fractures and rock matrix	The diffusion and transport of groundwater flow in fractures, at this time, the advection of groundwater is small. Diffusion in the pores of the rock matrix includes anion repulsion and surface diffusion.
TWGe13	Formation and sorption of substances	The water in the water-bearing fractures in the rock mass and the micro-cracks in the rock matrix are stagnant in some places, and there will be solute seeding and adsorption on the surface.
TWGe14	Reactions of groundwater/rock matrix	The chemical interaction between immobile groundwater and minerals in the rock matrix.
TWGe15	Dissolution/precipitation of fracture-filling minerals	The dissolution of minerals on the surface of the fracture and the precipitation of groundwater dissolved substances on the surface of the fracture, including co-precipitation of radionuclides.
TWGe24	Transport of radionuclides in the water phase	The integrated appearance of the transport-related effects of radionuclides in the water phase, that is, advection and dispersion (mixing), diffusion and rock matrix diffusion, adsorption and species formation, colloidal transport, and radioactive decay.
External Factors (30 FEPs in total)		
Number	**FEP name**	**Definition**
TWCli01	Climate system - Components of the climate system	The Earth's climate system is composed of five major parts, including the atmosphere, hydrosphere, cryosphere, surface and biosphere.
TWCli02	Climate system - Climate forcing	There are three types of natural climate drivers: (1) Changes in the radiation emitted by the sun. (2) The earth's orbit changes. (3) Geological structure. In addition, human drive can be added, although strictly speaking, human influence is not a part or component of the climate system.

TWCli03	Climate system - Physical process and interaction	The description of climate system processes and interactions is non-linear, covering energy budget, radiation balance, hydrological cycle, carbon cycle, and feedback mechanism. The feedback mechanism-related process is the enhancement (positive feedback) or weakening (negative feedback) of the initial change of external processes.
TWCli09	Climate- related issues - Shoreline migration	The relative sea-level changes associated with the adjustment of the glacial equilibrium have caused coastline migration.
TWCli11	Climate- related issues - Denudation	Describing the effects of combining all weathering and erosion processes, that is, denudation is the sum of the processes of abrasion or the gradual reduction of topographic unevenness.
TWCli12	Climate- related issues - Sea-level change	FEPs related to sea-level changes may undergo global (sea-level rise and fall) changes and regional geological changes, such as balanced movement of the crust.
TWCli13	Climate change	The effects of global warming, extreme climates, glacial cycles and monsoon changes.
TWCli14	Climate- related issues- Hydrological/hydrogeological response to climate changes	FEPs related to hydrology and hydrogeology, such as the response of climate change to groundwater replenishment in a certain area, sediment load and seasonality.
TWCli15	Climate system - Climate in Taiwan	Taiwan's current climate and future climate evolution.
TWLSGe02	Earthquakes	The distribution of earthquakes in Taiwan today, and the catalogue of earthquakes in Taiwan and the genesis mechanism of earthquakes.
TWLSGe03	Earthquake/ active faulting	The impact of earthquakes caused by fault activity on the repository, including current distribution and activity analysis of faults in Taiwan.
TWLSGe04	Volcanism/ Magmatic activity	"Magma" refers to the high-temperature molten fluid generated inside the earth. And the so-called volcanic activity refers to the activity of magma erupting to the surface and various geological phenomena caused by this activity. The safety-related factors are the range distribution, activity frequency and characteristics of volcanic/magma activities.
TWLSGe05	Uplift/ Subsidence	Terrain uplift and subsidence caused by orogenic movement and plate movement, rock-making bodies or terrain uplift and subsidence influence.
TWLSGe06	Diapirism/(mud diapir)	This refers to the argillaceous rock deep underground. Because of its low density and high plasticity, it arches upwards when squeezed by the stratum, causing it to penetrate into the overlying rock.
TWLSGe07	Hydrothermal activity	FEPs related to high-temperature groundwater include hydrothermal alteration of rocks and minerals, such as density-driven groundwater flow and high-temperature groundwater flow. The safety-related factor

		is the influence of hydrothermal activities on ground hydrology, underground chemistry and microbial activities.
TWLSGe08	Mechanical evolution plate	The evolution of past and present mechanics has an impact on the current mechanical conditions of the plate.
TWOth01	Meteorite impact	The consequences of meteorite impact on the safety of the repository.
TWOth02	special event - landslide	The phenomenon in which a large piece of rock or soil suddenly falls and moves down a long mountain slope is called a landslide. The falling soil, rock and cuttings are extremely unstable, and they often continue to collapse until the slope becomes slower, and then they will gradually stabilize. Landslides may include impacts such as falling rocks and landslides.
TWOth03	special event- mudflows	Earth-rock flow refers to the natural phenomenon of a mixture of materials such as mud, sand, gravel, boulders, and water, which is produced by gravity and flows from high to low along slopes or ditches.
TWOth04	special event-tsunami	A tsunami is triggered by a submarine earthquake and causes the sea to undulate violently, forming powerful waves.
TWOth05	Special events - extreme weather	Extreme weather includes the effects of floods, extreme precipitation, hailstorms and lightning. Its impact timescale is short, but it may have an important impact on the excavation operation period.
TWOth06	special event-erosion of seacoasts and rivers	Coast and river erosion refers to the interaction between sea water and the coast. As a result of long-term effects, in some places, the coastline will continue to recede and the beach width will be significantly reduced, or when the front edge of the beach and the slope of the sea bed become steep, coastal erosion might occur. Taiwan Island is surrounded by the sea with a coastline of more than 1,000 km. Coastal erosion has not only caused land loss but also the foundations of buildings in coastal areas may be hollowed out and collapsed. Coastal anti-wave facilities cannot even withstand violent tides and huge waves.
TWOth07	Disaster event-typhoon	A typhoon is a type of tropical cyclone, that is, a strong low pressure that occurs in the tropical ocean. When the maximum wind speed near the center of the tropical cyclone reaches or exceeds 17.2 m/s (about 62 km/hr), it is called a typhoon. According to statistics, on average, about 3 to 4 typhoons invade Taiwan per year. During the invasion, they often cause disasters such as strong winds, heavy rains, flooding, landslides, mudflows, storm surges, and seawater intrusion.
TWFHA01	General considerations	Overall consideration of future human actions involves waste management principles and generational responsibilities.

TWFHA02	Societal analysis, considered societal aspects	The occurrence of human actions in the future may affect important social issues of the repository.
TWFHA03	Technical analysis in general aspects	Human actions that need to be considered in the site selection and design of repository, economic aspects and technological development.
TWFHA04	Thermal impact and purpose of human action	The construction and technology that will affect the repository and functions, including the construction of heat storage, heat pump systems, extraction of geothermal heat, and construction of heating/cooling machines in the repository.
TWFHA05	Hydraulic impact and purpose of human action	The construction and technology that will affect the repository and its functions, including: sinking wells, constructing reservoirs, changing the direction of surface water (river, lake, sea), or connecting with other surface water.
TWFHA06	Mechanical impact and purpose of human action	The construction and technology that will affect the repository and its functions, including: drilling holes in rock formations, building caves, tunnels, building mines, and building garbage landfills.
TWFHA07	Chemical impact and purpose of human action	The construction and technology that will affect the repository and its functions, including: storing hazardous wastes in rocks, establishing sanitary landfills, acidizing or polluting the air, water, soil or rock pans, and disinfecting the soil.
Biosphere (54 FEPs in total)		
Number	**FEP name**	**Definition**
TWBioHY01	Groundwater release	The release of radionuclides from the geosphere to the biosphere in connection with the discharge or abstraction of groundwater.
TWBioHY02.1	Groundwater flow	Part of streamflow that has infiltrated the ground, entered the phreatic zone, and discharged into a stream channel, via springs or seepage water.
TWBioHY02.2	Surface runoff	The flow of water that occurs when excess storm water, meltwater or other sources flows over the earth's surface.
TWBioHY02.3	River flow	The amount of flow in rivers affects erosion and deposition.
TWBioHY02.5	Marine currents	A continuous, directed movement of seawater generated by forces acting upon this mean flow, such as breaking waves, wind, the Coriolis effect, densification, temperature and salinity differences.
TWBioHY02.6	Sea spray	Aerosol particles that are formed directly from the ocean, mostly by ejection into the atmosphere by bursting bubbles at the air-sea interface.
TWBioHY02.7	Flooding	An overflow of water that submerges land which is usually dry. Flooding will affect the area over which infiltration takes place.

TWBioHY03	Aquifer recharge	The addition of water to the aquifer either directly from surface waters or via another formation.
TWBioHY04	Precipitation	Precipitation is any product of the condensation of atmospheric water vapor that falls under gravity.
TWBioHY06	Evapotranspiration	Transfer of water from the soil to the atmosphere by evaporation from the soil and transpiration in plants.
TWBioMC01	Erosion(wind, water, floods)	Relatively continuous change in the landform due to the action of wind or water. Water erosion is produced by rainfall, surface runoff, river water and occasional floods that remove surface soil material or plants.
TWBioMC02	Soil conversion	Natural evolution of some environmental media could result in the formation or loss of soil. Natural processes like the ageing of lakes or changes in river courses may lead to lake or river sediments becoming land, and a lowering of the water level can have the same effect.
TWBioMC4.2	Adsorption/Desorption	Sorption or adhesion onto the solid surface of a layer of ions from an aqueous solution and the reverse process. Parameters like chemical form, Eh, pH and the presence of other chemical species influence the retardation processes, including ion exchange and complexation processes.
TWBioMC05	Weathering	Weathering is the disintegration and decomposition of rock and regolith into smaller pieces. Weathering can be chemical or mechanical.
TWBioRA01	External irradiation processes	Potential exposures to contaminated sources resulting in an external irradiation of the human critical group considered in the assessment.
TWBioRA02.1	Inhalation exposure processes	Incorporation of radioactivity into the body due to breathing air, including aerosols of resuspended dust and gases.
TWBioRA02.2	Ingestion exposure processes	Incorporation of radioactivity in water or contaminated substances via ingestion.
TWBioRA03	Resource usage	Human habits in the natural and agricultural contaminated resources usage could lead to a source for human exposure.
TWBioRA05	Water filtration	Filtration of water for drinking purposes or for other purposes.
TWBioRA06	Air filtration	Filtration of air by natural or artificial mechanisms.
TWBioRA07	Ventilation	Active ventilation of houses or rooms within houses.
TWBioRA08	Food processing	Preparation of food which may modify contaminant concentration in the final material consumed.
TWBioRA09	Location/shielding factors	Shielding and other reduction factors for calculation of external radiation doses.
TWBioRA10	Diet	Consumption rates of different products.
TWBioRA11	Ploughing	Ploughing is an agricultural practice which turns over the soil.

TWBioRA12	Soil fertilization	Fertilization with contaminated crop residues, ashes, green manure or cattle manure could add activity to the soil.
TWBioMI01.1	Transport processes between surface waters and porous media	Natural processes leading to the transport of contaminated water to the porous media or vice versa.
TWBioMI01.1.1	Percolation	Movement of contaminated water through the soil layers into the water table.
TWBioMI01.1.2	Capillary rise	Upwards transfer of water through soil layers above the water table due to capillary forces caused by evapotranspiration.
TWBioMI01.1.4	Infiltration	The flow of contaminated water from the surface to soil layers. The amount of water entering the unsaturated zone controls groundwater recharge.
TWBioMI01.2	Transport of suspended sediments	Transport of suspended sediments with flowing water.
TWBioMI02.2	Rock falls	Transport of solid material by rock falls.
TWBioMI02.3	Resuspension/ deposition	The resuspension of material into the atmosphere and subsequent deposition.
TWBioMI02.4	Sediment resuspension	Resuspension of sediments due to flowing water.
TWBioMI02.5	Sedimentation	The gravitational settling and deposition of suspended particles within water bodies to form sediments.
TWBioMI02.7	Bed-load transport	Transport of particles in a flowing fluid along the bed. Bed load moves by rolling, sliding and hopping.
TWBioMI03.1	Gas transport	Transport of gases and volatile material in the atmosphere.
TWBioMI04.1	Plant uptake	Uptake of radionuclides by absorption and biological processes of plants from surface media.
TWBioMI04.2	Translocation	The internal movement of material from one part of a plant to another.
TWBioMI04.3	Senescence/litterfall/excretion	Organic material of organism that falls to the ground.
TWBioMI04.4	Interception	Interception is the fraction of wet and dry deposition of elements that is retained on vegetation and does not immediately infiltrate into the ground.
TWBioMI04.6	Intake by animals	Consumption and inhalation by animals.
TWBioMI04.7	Internal transfer within animals	The transfer of material from animal feed to tissues which may be consumed by other biota and humans.
TWBioMI04.8	Intrusion	Intrusion is defined here as the process whereby organisms (including humans) enter the repository by, for example, locomotion, drilling or growth.
TWBioMI04.9	Bioturbation	The redistribution and mixing of soil or sediments by the activities of plants and burrowing animals.
TWBioMI05.1	Irrigation	The use of contaminated water from surface water bodies or a well to irrigate crops.
TWBioMI05.2	Well supply	Extraction of water from an aquifer.
TWBioMI05.3	Recycling of solid materials	Recycling of solid materials.

TWBioMI05.6	Dredging of sediments for soil	Human actions may cause significant movements of solid materials: dredging of sediments from lakes, rivers and placement on soil.
TWBioMI05.7	Earth work	Human action may cause significant movements of solid materials. These actions are exclusively building activities.
TWBioMI06	Import/export	Import/export is the process whereby something is transported into/out of the model domain.
TWBioEV01	Sea-level changes	Alteration in the level of the sea relative to the land. Sea-level change would affect coastal aquifers.
TWBioEV02	Topography changes	The change of topography involves the three-dimensional change of terrain, surface, and landforms.
TWBioEV04	Agriculture and aquaculture changes	Agriculture and aquaculture are the main food supply of human, and will be the most important pathways to estimate human exposure in the future.

3.4. Comprehensive Analyses

In this report, the treatment and related safety function of FEPs considered in the reference case will be elaborated in Chapters 4 to Chapter 7. The contents are briefly shown as below:

(1) Initial state and variations (Chapter 4):

Description of the initial state of the disposal repository, and details of radiation source items (SNF), and engineered barriers are described in Section 4.2. The geosphere and biosphere are described in Section 4.3. The disposal repository layout is described in Section 4.4. Monitoring is described in Section 4.5.

(2) External factors (Chapter 5):

For climate-related issues, the impact of the glacial period on the repository is considered, as described in Section 5.2. The issues related to tectonic evolution are described in Section 5.3. Future human actions which consider the impact of unintentional human intrusion are described in Section 5.4.

(3) Internal processes (Chapter 6):

The safety of the disposal repository is discussed from a long-term perspective based on individual or T-H-M-C coupling effects in the disposal system. The contents include the design of components of the disposal repository such as SNF, canister, buffer, backfill and geosphere, and the mechanism of T-H-M-C coupling in the geosphere. The internal processes are described in Chapter 6.

(4) Safety functions and safety function indicators (Chapter 7):

In the safety assessment, the safety function of each system component should be demonstrated to maintain isolation, containment and retardation of the repository, and to ensure that the exposed population will not be significantly affected by radioactivity. The safety functions are described in Section 7.2. Containment safety function indicators are described in Section 7.3. Retardation safety function indicators are described in Section 7.4. Key issues of evolution over time are described in Section 7.5.

Influencing factors of the evolution of safety function indicators over time are described in Section 7.6.

4. Initial State of the Repository

4.1. Introduction

The comprehensive description of the initial state of the repository system is one of the main bases for the safety assessment. In general, the initial states of the geosphere and biosphere are defined before the excavation period. Through site investigations, the initial state of the geosphere and biosphere can be obtained, and a reference case can be established for the following performance assessment of the engineering facility and safety assessment after closure. For an engineered barrier system, the initial state is defined at the time of completion of deposition/installation for an individual deposition hole.

The initial state of the engineered barrier system is largely obtained from the design specifications of the repository, including allowable tolerances or deviations. Besides, the manufacturing, excavation and control methods have to be described in order to adequately discuss and handle issues of the initial state caused by the incomplete design specifications.

This chapter briefly describes the initial state of the engineered barrier system, geosphere and biosphere, and layout of the repository. Understanding of initial state of the repository is the basis for the safety assessment.

4.1.1. Overview of the System

As mentioned in Section 2.5, the final disposal concept is based on an international recognized deep geological repository. By referring to the disposal concept of advanced countries, crystalline rocks are adopted as the host rock. The SNF would be vertically disposed at approximately 500 m depth underground in a stable stratum (natural barrier). The release of radionuclides would be contained and migration would be retarded by the multiple-barrier system, which is built with a natural barrier and engineered barrier (canister, buffer and backfill) to reduce the radiation influence on human.

As mentioned in Section 1.1, 4,913 MTU of SNF (corresponding to 2,571 canisters in the repository) needs to be disposed. The disposal facility has been sub-divided into a number of components or sub-systems, which are shown as below:

(1) Source term (SNF).
(2) Cast iron lining and copper shell canister.
(3) Buffer in the deposition holes.
(4) Disposal tunnels and backfill.
(5) Other underground space and backfill (e.g. transport tunnel, shaft, central area, etc.)
(6) Plug.
(7) Investigation boreholes and sealing materials.
(8) Host rock.
(9) Biosphere.

4.1.2. Initial State FEPs

The understanding of the initial state of the repository system is one of the main bases for the safety assessment. The initial state of the engineered barrier system is described according to variables of the FEPs database in Section 3.2 and the FEPs list of the reference case in Section 3.3.

4.2. Source Term and Initial State

4.2.1. Initial State related to Long-Term Safety of the Repository

At the point of safety assessment in the early stage post-closure, the considerations of the initial state of the repository system are as below:

(1) Influence from SNF decay heat in the canister on the short-term thermal evolution of the repository.
(2) Quality of welding/sealing canister.
(3) Strength of cast iron lining.
(4) Influence on density of buffer after installation.
(5) Influence on density of backfill after installation.

4.2.2. Format for Descriptions of the Initial State

The initial state of different components of the repository is described in this section. Firstly, the safety functions of each component and its design functions will be considered, and the corresponding specifications for each design function will be proposed. Finally, the design specifications of each component are produced, which are regarded as the initial states.

The following subsections will quantitatively explain the initial state of the source term, canister, buffer and backfill; meanwhile, backfilling of shafts and ramps, grouting materials and plug will be described by referring to relevant studies.

4.2.3. Source Term

BWR fuel assemblies of Taiwan are mainly designed by manufacturers such as GE, ANF, SPC, and Areva, with initial uranium enrichment ranging from 0.71 wt% to 4.064 wt%. PWR fuel assemblies of Taiwan are mainly designed by Westinghouse, with initial uranium enrichment ranging from 1.603 wt% to 4.75 wt%. The amount of SNF used in this report until the end of 2019 is based on the "Final Disposal Plan for Spent Nuclear Fuel (2018 Revision)" (Taipower Company, 2019c) for the related analysis and technical advancements, as shown in(Table 1-1).

After the SNF assemblies are discharged from the core, they are expected to be stored for 50 years (wet and dry storage) for cooling and decay before disposal, and the disposal operation is planned to start after 2055, and 50 canisters per year will be processed starting from the SNF of Chinshan nuclear power plant. Based on the conservative calculation method provided in NUREG RG 3.54 Revision 1 (US NRC, 1999) and CR-6999 (US NRC, 2010), the decay heat power generated by every bundle of SNF after 2055 is calculated. The average value of SNF decay heat power at the first year of SNF disposal in each power plant (including the expected SNF generated by Kuosheng and Maanshan power plants with the conservative assumption of decay heat power) and the average heat load of the canister are calculated. Taking the largest average heat load of canisters in the first year of disposal at each nuclear power plant and adding a conservative value of 50 W (SKB, 2010a), the decay heat source of all canisters during disposal is about 1,200 W.

The radioactivity of SNF is extremely high, and they emit large amounts of decay heat, including fission products/activation products (FP/AP) such as Tc-99, Cs-135, and I-129, and actinide (AC) such as Np-237, Pu-239, Am-243 and Cm-247. Some of these nuclides are alpha-emitting nuclides with half-lives of hundreds of thousands of years. SCALE/ORIGEN-S (ORNL, 2011) program developed by Oak Ridge National Laboratory (ORNL) was used in the assessment. Based on the operating history and fuel design information of the three Taiwan nuclear power plants, the burnup of SNF at each plant was evaluated, and the cooling time from the discharged date to the planned disposal date was taken into account to estimate the radionuclide inventory. In addition, the number of canisters was used as the weighting to calculate the weighted average of the inventory after considering the overall canister loading characteristics of the repository.

The radionuclides were identified primarily according to the following process (Figure 4-1):

(1) Fission/activation products:

The identification was mainly based on the radiotoxicity index (RI) and half-life of the fission/activation products. The radiotoxicity is calculated as follows:

$$RI(t)=A(t)\times DCF \tag{4- 1}$$

where,

RI(t): radiotoxicity index, [Sv].

A(t): activity of radionuclide in SNF, [Bq].

DCF: dose conversion factor, [Sv/Bq]. The dose conversion factors from ICRP 119 report (ICRP, 2012) were used in the calculation.

t: disposal time (yr).

According to radionuclide identification (SKB, 2010h) and the calculation results, firstly, the radionuclides with a radiotoxicity index greater than 0.1 Sv and a half-life greater than 10 years were selected; then the radionuclides with a radiotoxicity index lower than Cs-137 and Sr-90 within 1,000 years after disposal and those with radiotoxicity index close to zero within 10,000 years after disposal were excluded. There were 13 radionuclides identified including Sr-90, Cs-137, Tc-99, Zr-93, Pd-107, I-129, Cs-135, Sn-126, Se-79, C-14, Cl-36, Ni-59, and NB-94.

(2) Actinides and their daughter nuclides:

By excluding the radionuclides with a half-life of fewer than 10 years and no activity contribution among the actinides and their daughter nuclides, a total of 21 radionuclides, including the following nuclides, could be identified:

(a) 4N series: Pu-240→U-236→Th-232.

(b) 4N+1 series: Cm-245→Am-241→Np-237→U-233→Th-229.

(c) 4N+2 series: Cm-246→Pu-242→Pu-238→U-238→U-234→Th-230→Ra-226→Pb-210.

(d) 4N+3 series: Am-243→Pu-239→U-235→Pa-231→Ac-227.

The initial inventory of the 34 nuclides mentioned above (mole numbers of nuclides in each canister and the amount of SNF in each canister are shown in Section 4.2.4) is shown in Table 4-1.

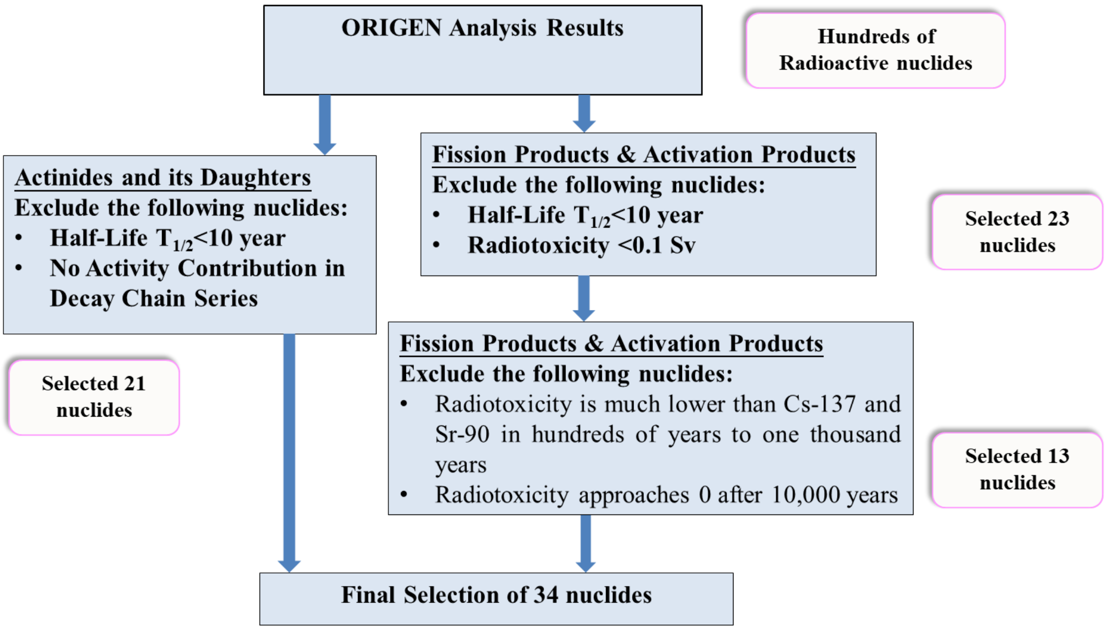

Figure 4-1: Screening process of the major radionuclides.

Reference: Tsai (2016)

Table 4-1: Initial inventory of the major radionuclides (34 in total).

	Nuclides	**mol/canister**
Fission / Activation product	C-14	3.25×10^{-2}
	Cl-36	7.00×10^{0}
	Ni-59	6.39×10^{2}
	Se-79	1.87×10^{-1}
	Sr-90	5.35×10^{0}
	Zr-93	2.37×10^{1}
	Nb-94	2.97×10^{-1}
	Tc-99	2.43×10^{1}
	Pd-107	6.93×10^{0}
	Sn-126	5.00×10^{-1}
	I-129	3.73×10^{0}
	Cs-135	9.83×10^{0}
	Cs-137	8.52×10^{0}
Actinide series	Pb-210	1.06×10^{-9}
	Ra-226	1.49×10^{-7}
	Ac-227	4.79×10^{-9}
	Th-229	5.28×10^{-8}
	Th-230	4.28×10^{-4}
	Pa-231	9.62×10^{-6}
	Th-232	1.30×10^{-4}
	U-233	1.50×10^{-4}
	U-234	2.55×10^{0}
	U-235	6.74×10^{1}
	U-236	5.20×10^{1}
	Np-237	6.60×10^{0}
	U-238	8.08×10^{3}
	Pu-238	1.75×10^{0}
	Pu-239	4.24×10^{1}
	Pu-240	2.65×10^{1}
	Am-241	1.12×10^{1}
	Pu-242	8.51×10^{0}
	Am-243	1.97×10^{0}
	Cm-245	4.40×10^{-2}
	Cm-246	7.66×10^{-3}

4.2.4. Canister

The canister is composed of a ductile copper shell on the outside and a high-strength cast iron insert, square channel tube and lid on the inside referring to the design concept of the Swedish KBS-3 disposal system. Basic safety functions are containment and retardation of radionuclides, so that the long-term safety of the repository can be maintained. In order to achieve the aforementioned goals, the canister must have the following design functions (POSIVA and SKB, 2017):

(1) Withstand corrosion: the copper shell of the canister is made of highly pure copper to avoid corrosion coupled to grain boundaries. Oxygen contents can only be allowed up to tens of ppm.

(2) Withstand isostatic load: the canister should be able to withstand pressures from buffer swelling pressure and groundwater pressure.

(3) Withstand uneven swelling pressure: the buffer could have different densities due to the non-uniform distributions of groundwater in the deposition hole during saturation. Therefore, the buffer could cause uneven swelling pressures to the canister, which the design of the canister needs to take into consideration.

(4) Withstand rock shear force: after the closure of the disposal tunnel, an earthquake might trigger shear movement of the rock fracture surrounding the deposition hole, and rock shear force could be imposed on the canister and the buffer. Thus, the canister design needs to consider this factor.

(5) Radiation dose: the canister should help meet the radiation-related regulations mentioned in Section 1.4. In addition, to avoid groundwater radiolysis and buffer bentonite material being influenced by radiation, the radiation dose rate at the surface of the canister must not exceed 1 Gy/h (POSIVA and SKB, 2017).

(6) Criticality: the canister must be designed to ensure the criticality safety (i.e., Effective Multiplication Factor, K_{eff} must not exceed 1). However, for conservative safety consideration reasons, a 5% deduction is further imposed, and therefore, the effective multiplication factor must not exceed 0.95 (SKB, 2010c; POSIVA and SKB).

The design requirements corresponding to the above design functions are shown in Table 4-2.

Insert and tube are the main components to resist external force based on their geometric shape and material strength. The ductile and corrosion-resistive copper shell on the outside can protect the SNF well even when large deformation is generated under shear displacement or uneven pressure. The copper shell is one of the important barriers to avoiding the release of radionuclides from the canister. The thickness of the copper shell is determined according to the corrosion resistance requirements of the disposal environment and the evaluation results of shielding effectiveness. The copper thickness of the canister is the same as the design concept of the Swedish KBS-3. Considering the deposition hole without suffering the erosion of the buffer, the thickness of the copper shell of 5 cm can resist corrosion for at least 1 million years. When the buffer is severely eroded, the thickness of the copper shell can still maintain sufficient safety functions of canisters for quiet a long time to reduce the radiotoxicity of radionuclides.

Because of the difference in component sizes between BWR and PWR, the canister will be loaded with 4 sets of PWR SNF assemblies or 12 sets of BWR SNF assemblies. Based on the estimated amount of SNF in Taiwan (Table 1-1), 2,571 canisters (1,491 for BWR and 1,080 for PWR) will be needed.

In addition, according to Section 4.2.3, the decay heat of each canister during disposal was estimated conservatively. The designed value of heat load of the canister and decay heat curve were formulated under consideration of 50 canisters being placed every year. The initial thermal power of the canister was set as 1,200 W. In addition, based on the maximum length of the fuel rod in Taiwan, and the necessary gap for installation, the canister specifications are as follows:

(1) The overall length: BWR canister is 4,905 mm, and the PWR canister is 4,835 mm.
(2) Outer diameter: 1,050 mm.
(3) Copper thickness: 50 mm.

(4) Insert length: BWR canister is 4,643 mm, PWR canister is 4,573 mm.

(5) Diameter of Insert: 949 mm.

(6) The relevant design specifications of the canister are summarized in Table 4-3 and shown in Figure 4-2 to Figure 4-6. The material specifications are shown in Table 4-4.

Table 4-2: Design functions and requirements of the canister.

Function of design	Character	Design requirements for long-term safety
Withstand even isostatic load	Containment	Withstand swelling pressure of the buffer (10 MPa) and groundwater pressure at the repository depth (5 MPa) (POSIVA and SKB, 2017).
Withstand uneven isostatic load	Containment	Withstand buffer swelling pressure between 3 MPa and 10 MPa (POSIVA and SKB, 2017).
Withstand shear force from the fracture	Containment	Withstand shear movement over deposition hole ≤ 5 cm at a velocity of 1 m/s for a buffer with the maximum allowed shear strength (POSIVA and SKB, 2017).
Radiation dose	Radiation effects	The repository shall be designed to ensure that the annual effective dose to a person outside the repository will not exceed 0.25mSv (Regulations for the Final Disposal of High- Level Radioactive Waste and Safety Management of the Facilities, Article 9).
Surface dose	Avoid the impact of radiation on the buffer, the radiative hydrolysis of groundwater, and the effects of SNF neutrons and gamma ray on the canisters.	Dose rate at the canister surface ≤ 1 Gy/h (POSIVA and SKB, 2017).
Criticality	Avoid excessive energy release that affects the engineered barrier and surrounding rocks. Substantial changes in the inventory of radioactive species may lead to an increase in nuclear species released from disposal sites.	It needs to be maintained in a subcritical state. The effective neutron multiplication factor needs to be less than 0.95 (POSIVA and SKB, 2017).

Table 4-3: Design specifications of the canister.

Common dimension for canister (mm)		
Copper shell		
Total length (A)	BWR	4,905
	PWR	4,835
Interior length	BWR	4,463
	PWR	4,443
Wall thickness (T)	50	
Outer diameter (B)	1,050	
Inner diameter (C)	850	
Inner diameter (E)	952	
Inner diameter (F)	821	
Inner diameter (G)	850	
Diameter, lid (H)	953	
Corner radius (I)	10	
Dimension (K)	35	

Dimension (L)	50		
Thickness, lid (M)	50		
Dimension (N)	60		
Dimension (P)	75		
Thickness, base (Q)	50		
Dimension (R)	50		
Insert			
Diameter (D)			949
BWR	Thickness of bottom (B)		60
	Interior length(C)		4,533
	Edge distance(H)		33.3
	Dimension (N)		Drill depth 90 mm
	Length (A)		4,643
PWR	Thickness of bottom (B)		80
	Interior length (C)		4,443
	Edge distance (H)		37.3
	Dimension (N)		Drill depth 100 mm
	Length (A)		4,573
Insert channel tubes			
BWR	Channel tube corner radius (I)		20
	Distance between channel tubes (K)		30
	Distance between compartments (J)		210
	Channel tube cross section (L)		160×160
	Channel tube thickness (M)		10
PWR	Channel tube corner radius (I)		20
	Distance between channel tubes (K)		110
	Distance between compartments (J)		370
	Channel tube cross section (L)		235×235
	Channel tube thickness (M)		12.5
Steel lids			
Diameter (E)			910
Lid thickness (F)			50
Dimension (G)			5°
Initial thermal load limit (W)			1,200

Table 4-4: Material specifications of the canister.

Weight of the canisters	Copper shell (BWR-canister)	7,500 kg
	Insert with lid (BWR-canister)	13,700 kg
	Canister with fuel (BWR-canister)	24,600 kg-24,700 kg
	Copper shell (PWR-canister)	7,500 kg
	Insert with lid (PWR-canister)	16,400 kg
	Canister with fuel (PWR-canister)	26,500 kg-26,800 kg
Copper shell	Elastic modulus	120 GPa
	Poisson's ratio	0.308
	Density	8.9×103 kg/m3
	Copper purity	>99.99%
	Elongation	>40%
	Creep ductility	>15%
	Average grain size	<800 μm
Insert	Elastic modulus	166 GPa
	Poisson's ratio	0.32
	Density	7.2×103 kg/m3
	Yielding strength	>267 MPa (tension) >270 MPa (compression)
	Ultimate strength	>480 MPa (tension)
	Fracture toughness in 0°C	J2mm > 88 kN/m J1c > 33 kN/m Klc > 78 MPa(m)1/2
	Elongation	>12.6 %
Steel lid	Elastic modulus	210 GPa
	Poisson's ratio	0.3
	Density	7.85×103 kg/m3
	Yielding strength	>335 MPa (tension)
	Ultimate strength	>470 MPa

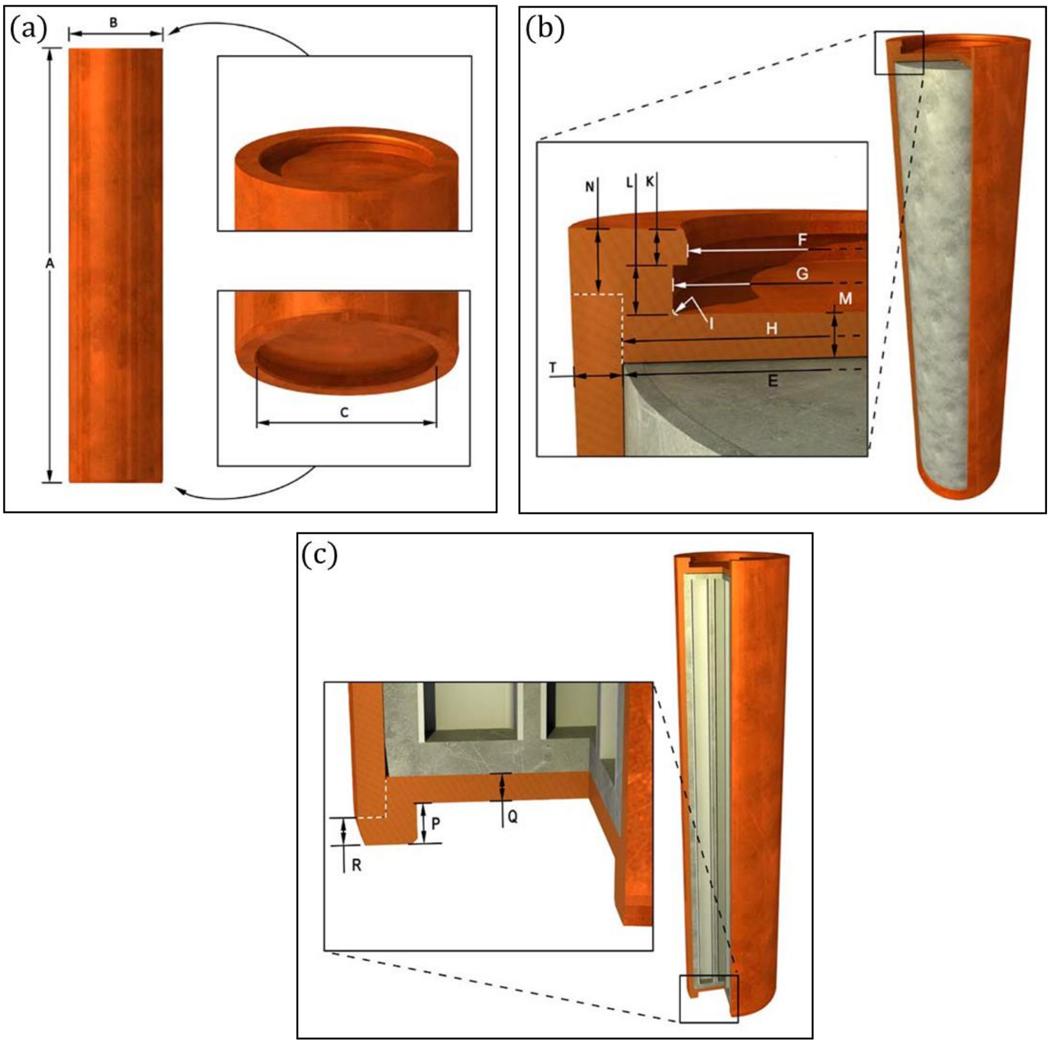

Figure 4-2: Specifications of copper shell of the canister.

Reference: SKB (2010l).

Note: the unit is mm. A=4,905; B=1,050; C=850; T=50; E=952; F=821; G=850; H=953; I=10; K=35; L= 50; M=50; N=60; P=75; Q=50; R=50.

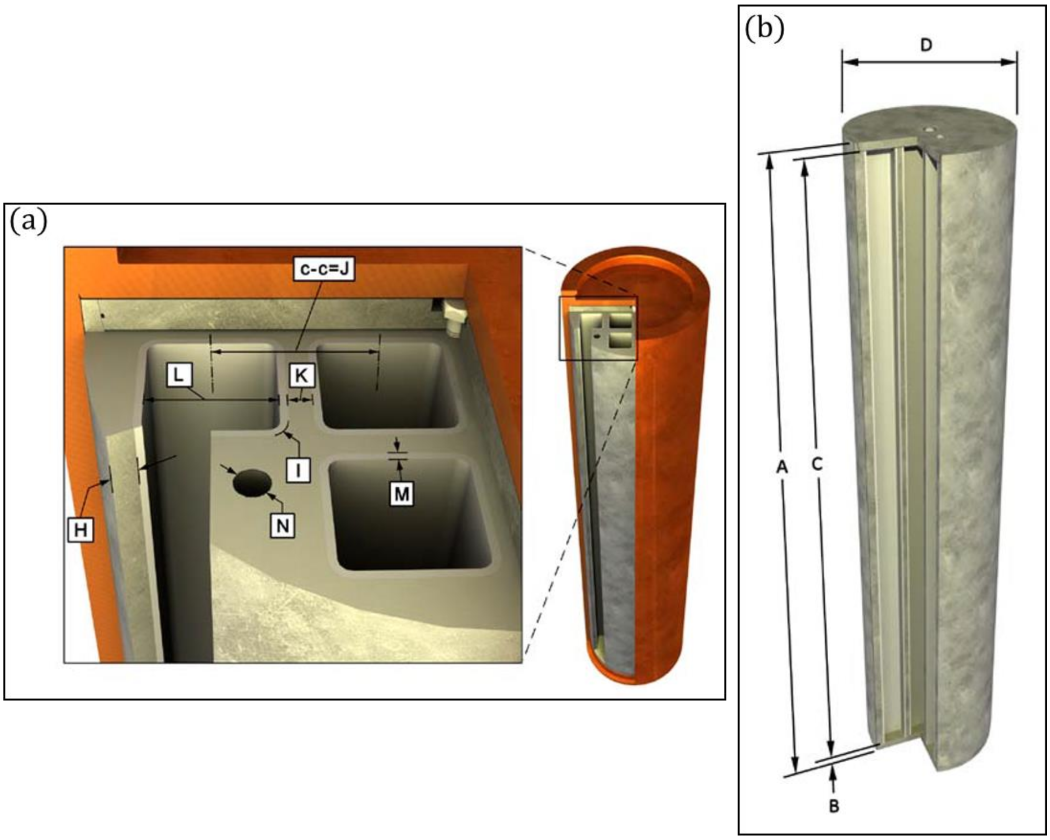

Figure 4-3: Specifications of cast iron lining of the canister.

Reference: SKB (2010l).

Note: the unit is mm. H=33.3; N=45; I=20; K=30; J=210; L=10; M=10; A=4,573; B=60; C=4,643; D=949.

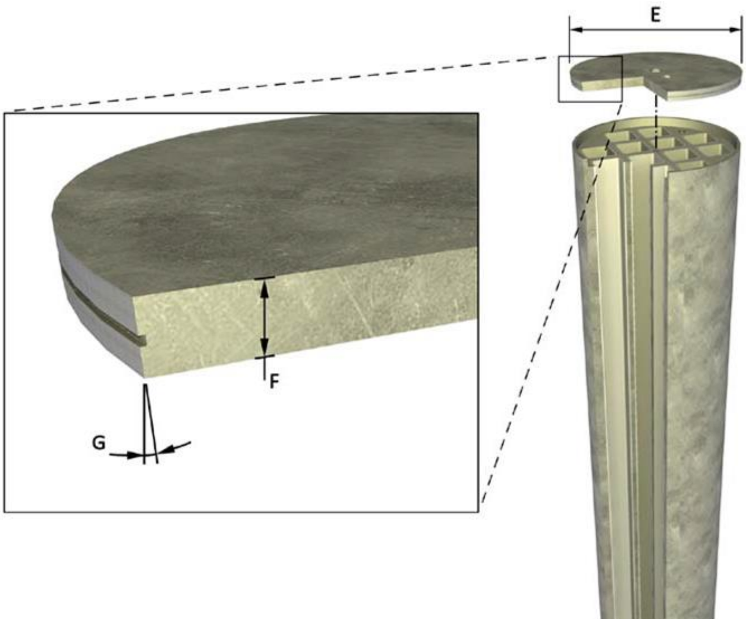

Figure 4-4: Specifications of steel lid of the canister.

Reference: SKB (2010l).
Note: the unit is mm. E=910; F=50; G=5°.

Figure 4-5: Specifications of copper shell and cast iron lining of the canister.
Note: the unit is mm. The A-A cross-section is shown as Figure 4-6.

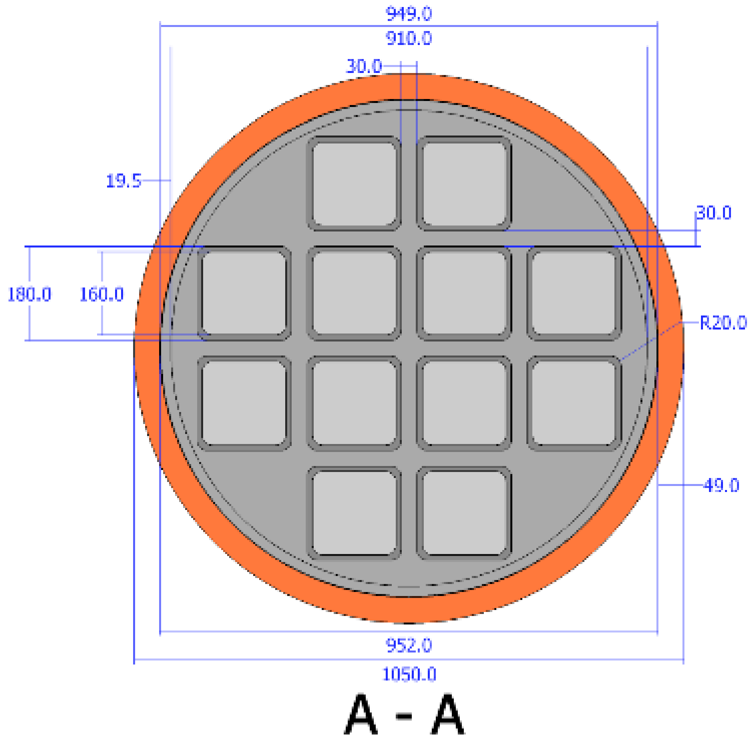

Figure 4-6: Cross-section of the canister
Note: the unit is mm.

4.2.5. Buffer

The buffer is one of the engineered barriers in the repository. The buffer is installed in the deposition holes and it will fill the space between the canisters and the host rock. The design functions of the buffer include the following items (SKB, 2010c):

(1) limit advective mass transport,

(2) limit microbial activity,

(3) filter colloids,

(4) keep the canister in position in the deposition hole,

(5) not significantly impair the barrier functions of the other barriers,

(6) maintain the barrier design function in a long-term perspective.

The design functions, properties, and design requirements of the buffer are shown in Table 4-5. The reference buffer is bentonite clay and its main composition is montmorillonite. Sufficient montmorillonite content of the bentonite can provide appropriate hydraulic conductivity and swelling pressure. In addition, the harmful substances content of bentonite should be limited, such as sulfide and sulfur, which may reduce the performance of the buffer or cause the canister to corrode.

MX-80 bentonite will be the raw material for the buffer, and its characteristics were investigated through experiments. Experiments on swelling pressure and hydraulic conductivity under different bentonite densities were carried out using distilled water and cation strength of 2.54 mM synthetic groundwater (the chemical composition and content are shown in Table 4-6, based on the groundwater composition in Section 4.3.2). The experiment results are shown in Figure 4-10 and Figure 4-11 to provide reference properties for design and to ensure that the designed specifications meet the design requirements. According to the experiment results, the dry density of MX-80 bentonite with a swelling pressure of 3 MPa is about 1,494 kg/m^3, which is equivalent to a saturated density of 1,950 kg/m^3. The dry density of the swelling pressure of 10 MPa is about 1,650 kg/m^3, which is equivalent to the saturated density of 2,050 kg/m^3. When the dry density of MX-80 bentonite is above 1,100 kg/m^3 (equivalent to the saturated density of 1,700 kg/m^3), it can satisfy the condition that the hydraulic conductivity is lower than 10^{-12} m/s. Therefore, the saturated density of the buffer is 1,950 kg/m^3 to 2,050 kg/m^3, which can meet the overall design requirements in Table 4-5.

The buffer installed in the deposition hole consists of compacted blocks and pellets with specific density. The specifications of each component of the buffer will be designed according to the specifications of the deposition hole and the design requirements of the thickness of the buffer (see Section 4.2.6), mainly including solid blocks above and below the canister, ring-shaped blocks around the canister, pellets filled in the gap between the buffer block and the deposition hole wall. The reference specifications of buffer blocks and pellets are presented in Table 4-7. The geometry specifications of buffer blocks are presented in Figure 4-7. And the design requirements for manufacturing and installation of the buffer are presented in Table 4-8.

A schematic of the canister and buffer installation in the deposition hole is shown in Figure 4-8 and as follows:

(1) Bottom of the canister: installed a solid block with a height of 575 mm and a diameter of 1,650 mm. The groove is designed according to the footing of the bottom of the canister to facilitate the installation and positioning of the canister (see Figure 4-5).

(2) Around the canister: ring-shaped blocks are designed to surround the canister according to the dimensions of the canister and deposition hole. The ring-shaped block has an inner diameter of 1,070 mm and an outer diameter of 1,650 mm. And consider the height of the canister, one ring-shaped block with height of 830 mm and 5 ring shaped blocks with a height of 800 mm will be used which will be stacked from the bottom to the top.

(3) Above the canister: the block above the canister is designed to fill the hollow in the canister lid (see Figure 4-5). On top of it, 2 solid blocks with a height of 500 mm will be used.

(4) Upper part with connecting bevel: filled with solid blocks and pellets.

According to the design requirements, the saturated density of each part of the buffer in the deposition hole should be between 1,950 and 2,050 kg/m^3 after installation and saturation. The saturation density of the buffer in each part of the deposition hole was calculated according to the reference specifications of buffer blocks and pellets, which are shown in Figure 4-9. The average saturated density is 2,019 kg/m^3 (average dry density is 1,590 kg/m^3), which fulfills the density of the relevant design requirements in Table 4-5. Figure 4-10 shows the relation between MX-80 bentonite dry density and swelling pressure, and Figure 4-11 shows the relation between MX-80 bentonite dry density and hydraulic conductivity. It can be seen that under the saturated density condition after buffer installation and saturation, the swelling pressure is larger than 2 MPa and the hydraulic conductivity is lower than 10^{-12} m/s, which fulfills the relevant design requirements in Table 4-5.

Table 4-5: Design functions, properties, and design requirements of the buffer

Design function	Properties	Design requirements for long-term safety
Limit advective mass transport	Properties that affect swelling pressure and hydraulic conductivity.	According to the safety function indicator for limit advective mass transport, the hydraulic conductivity of the buffer should be less than 10^{-12} m/s and the swelling pressure should exceed 1 MPa. Fulfilled for the swelling pressure required with respect to the capability to eliminate microbes and not damage the canister for expected shear movements.
Limit microbial activity	Properties that affect swelling pressure.	According to the safety function indicator for limit microbial activity, the swelling pressure shall exceed 2 MPa. Fulfilled for the swelling pressure required with respect to the capability to eliminate microbes and not damage the canister for expected shear movements.
Filter colloids	Properties that affect tortuosity and size of pores.	According to the safety function indicator for filter colloid, the dry buffer density shall exceed 1,000 kg/m^3. Fulfilled for the swelling pressure required with respect to the capability to eliminate microbes and not damage the canister for expected shear movements.
Keep the canister in position in the deposition hole	Properties that affect swelling pressure.	According to the safety function indicator for preventing canister sinking, the swelling pressure shall exceed 0.2 MPa. Fulfilled for the swelling pressure required with respect to the capability to eliminate microbes and not damage the canister for expected shear movements.
Not significantly impair the barrier functions of the other barriers	Properties that affect swelling pressure and its distribution, stiffness and shear strength.	The swelling pressure of the buffer shall be less than 10 MPa to fulfill the safety function indicator limiting the pressure applied to the canisters and rock. The swelling pressure of the buffer after installation and saturation should be less than 10 MPa, to prevent too high shear impact on the canister.
	Properties that affect the chemical conditions around the canister.	The content of organic carbon should be less than 1 wt%. The sulfide content should not exceed 0.5 wt% of the total mass, corresponding to approximately 1% of pyrite. The total sulfur content (including the sulfide) should not exceed 1 wt%.
Maintain barrier design function and its long-term durability	Properties that affect the ability of the buffer to uphold and maintain the minimum swelling pressure, maximum hydraulic conductivity, acceptable stiffness and shear strength, tortuosity and size of pores and chemical composition.	The design requirements should follow the geometric requirements of the buffer and other requirements that may affect the geometry of the buffer and the deposition hole (i.e. initial installed mass and saturated density).
	Properties that affect the ability of the buffer to	After swelling, the buffer should uphold the minimum swelling pressure 2 MPa and the

	uphold and maintain the minimum swelling pressure, maximum hydraulic conductivity, acceptable stiffness and shear strength, tortuosity and size of pores and chemical composition.	hydraulic conductivity should not exceed 10^{-12} m/s independently of dominating cation and for chloride concentration up to 1 M. After swelling, the shear strength of the buffer must not exceed the strength used in the verifying analysis of the canister's resistance against shear force.
	Properties that affect the heat transport through the buffer.	According to the safety function indicator for resist buffer transformation, the temperature of the buffer should be less than 100 °C. The buffer geometry, water content and distances between deposition holes should be selected such that the temperature in the buffer is less than 100°C.

References：SKB (2010c); Posiva and SKB (2017).

Table 4-6: Chemical composition of the synthetic groundwater.

Component	**Molecular mass**	**Weight (g) ($1L \cdot H_2O$)**
NaCl	58.44	0.0572
$NaNO_3$	84.99	0.0504
K_2SO_4	174.27	0.008
$MgSO_4 \cdot 7H_2O$	246.48	0.0145
$Mg(NO_3)_2 \cdot 6H_2O$	256.41	0.0013

Table 4-7: Reference specifications of the buffer blocks and pellets.

Parameter		**Reference specification**	**Accepted variation**
Solid blocks	Dry density (kg/m^3)	1,710	+/- 20
	Water content (%)	17	-
	Dimensions (mm)	H: 500	
Ring shaped blocks	Dry density (kg/m^3)	1,770	+/- 20
	Water content (%)	17	-
	Dimensions (mm)	H: 800 / bottom H: 830	
Pellets	Dry density loose filling (kg/m^3)	1,000	+/-40
	Water content (%)	17	-
	Dimensions (mm)	16×6×8	-

Table 4-8: Design requirements for manufacturing and installation of the buffer.

Design consideration	Require property	Design requirements
The bentonite of buffer and methods for manufacturing, installation, testing, and inspection shall be based on well-tired or tested techniques. Buffer must be manufactured and installed to the designed specifications with a high-reliability technique.	The buffer can be compact to required density.	-
	The dimensions, weight and water content of the buffer must be designed so that it can be manufactured, transported, and installed with high reliability.	The reference sequence for deposition of the canister. The reference sequence of installation of the buffer and backfill. The reference design of deposition holes.

Reference: SKB (2010c)

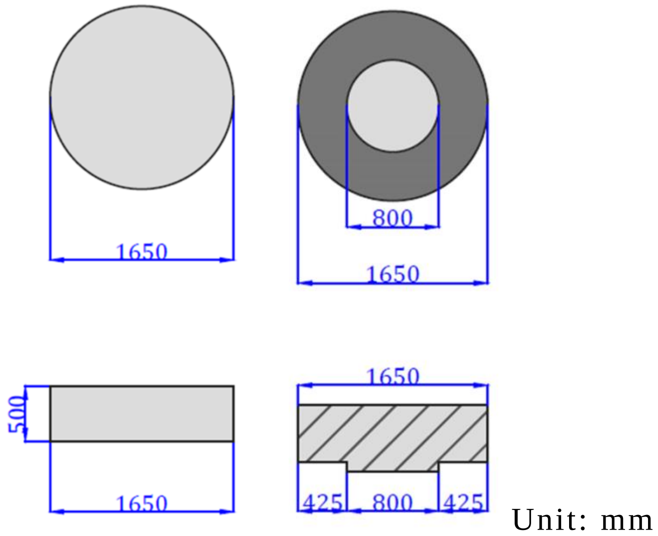

(a) Specifications of buffer blocks in the upper part of the deposition hole (left) and above the canister (right).

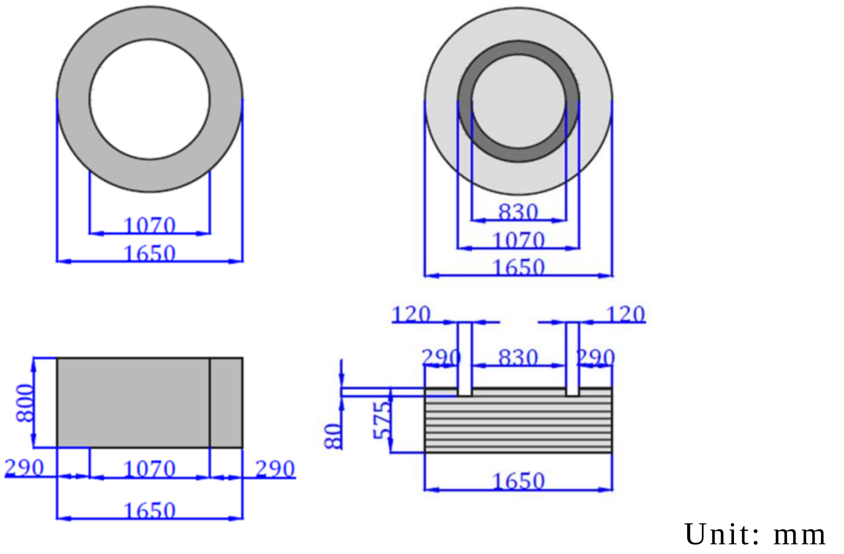

(b) Specifications of buffer rings around the canister (left) and under the canister (right).

Figure 4-7: Geometry specifications of the buffer blocks and rings.

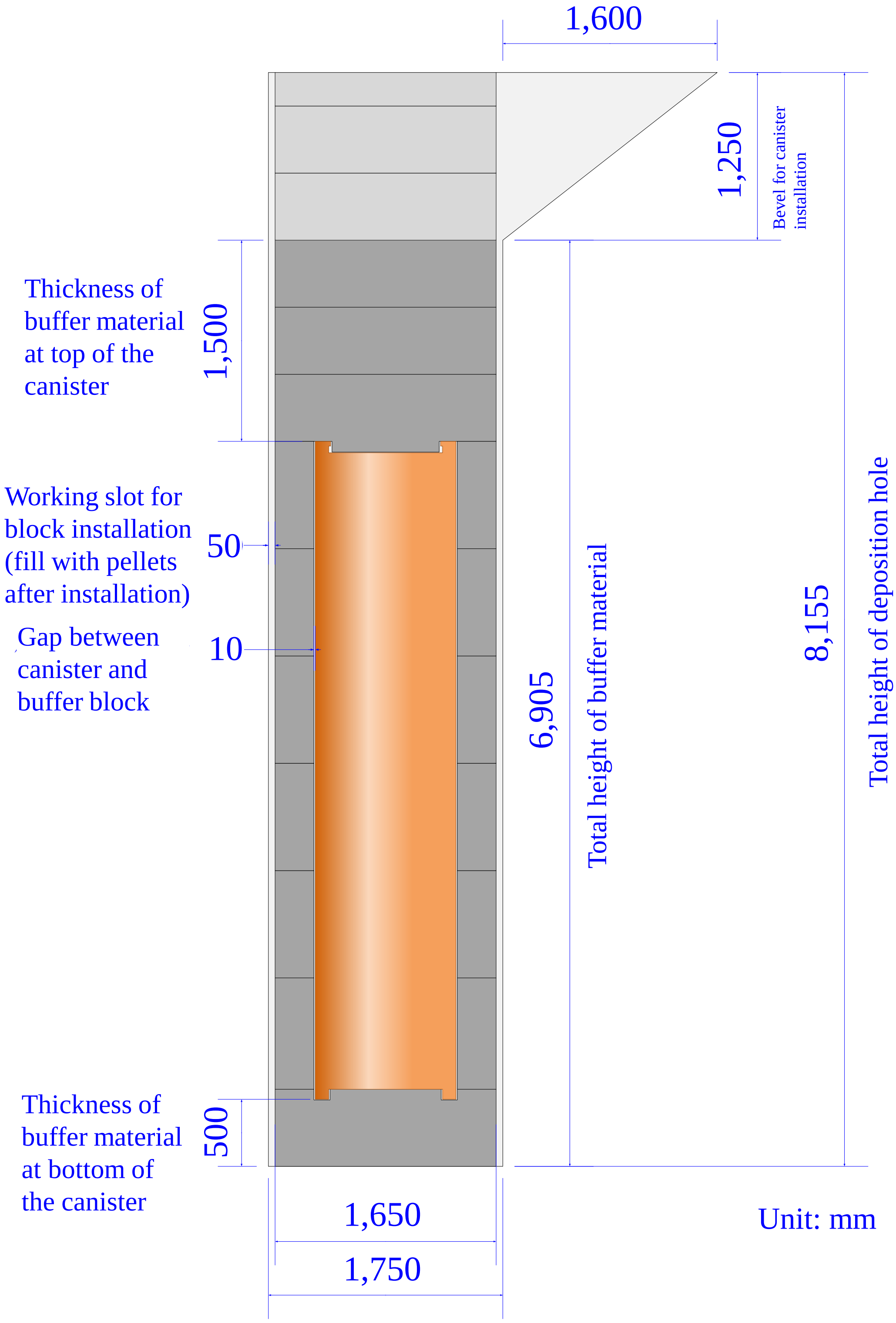

Figure 4-8: Installation of canister and buffer in the deposition hole.

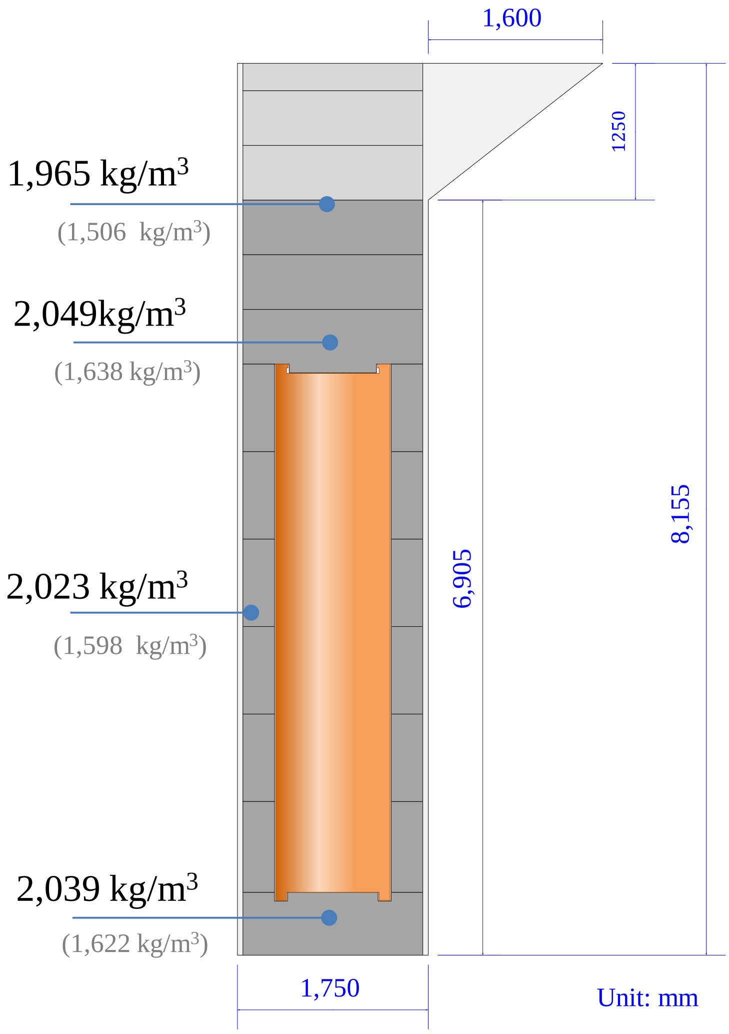

Figure 4-9: Saturated densities of buffer in the deposition hole.

Note: the numbers in the brackets refer to dry densities.

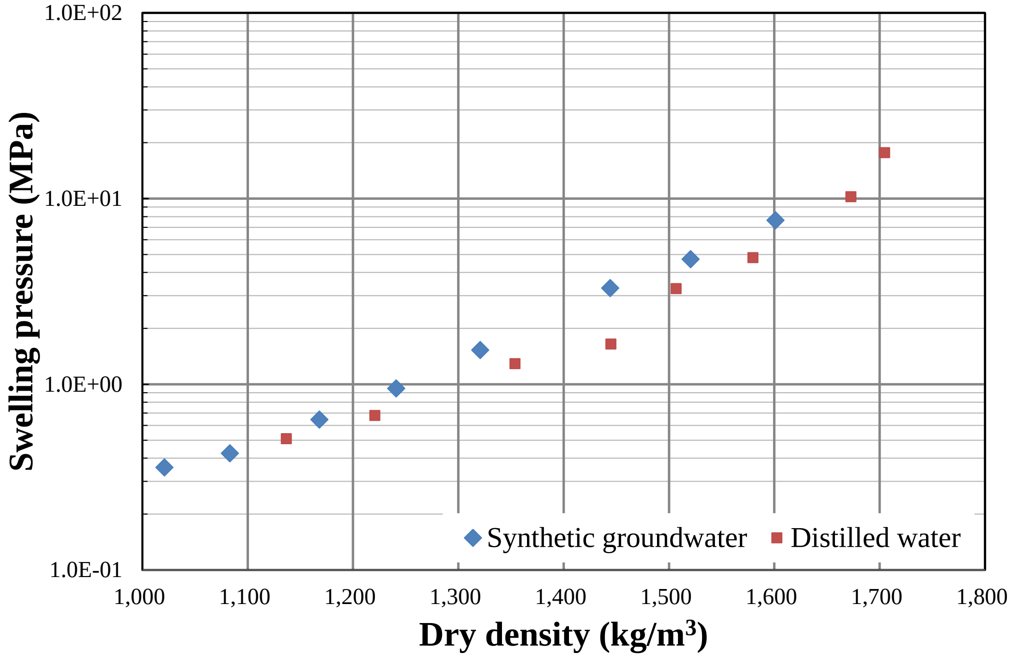

Figure 4-10: Swelling pressure versus bentonite dry density for different water solutions.

Reference: 台電公司 (2018a).

Note: MX-80 bentonite in distilled water and synthetic groundwater conditions.

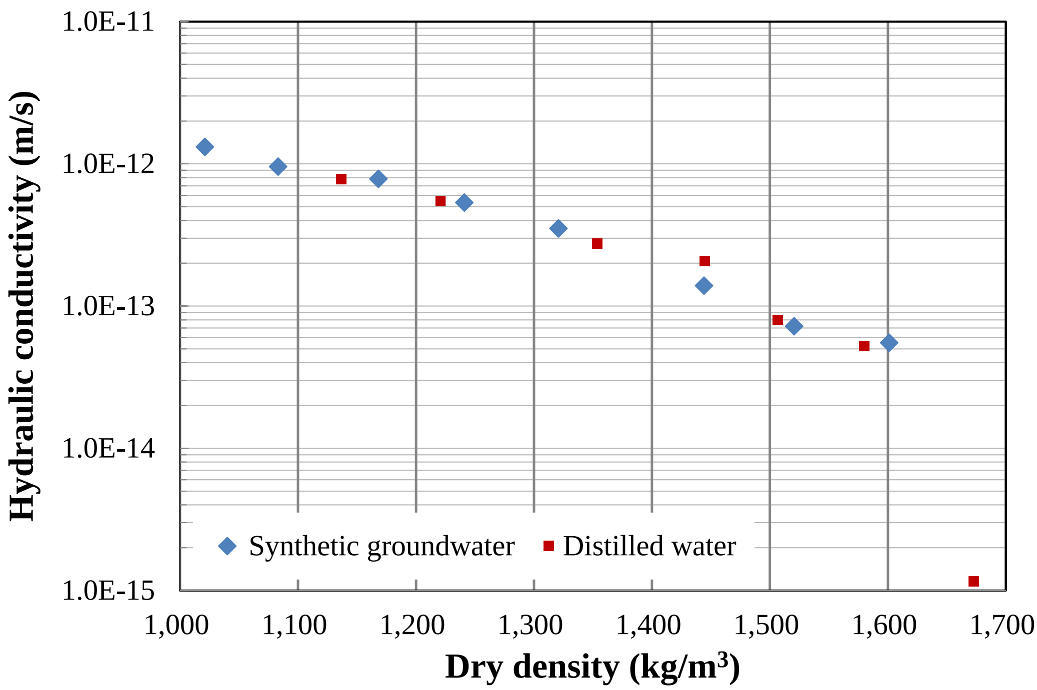

Figure 4-11: Hydraulic conductivity versus bentonite dry density for different water solutions.

Reference: 台電公司 (2018a).

Note: MX-80 bentonite in distilled water and synthetic groundwater conditions.

4.2.6. Deposition Hole

The design requirements of the deposition hole are listed in Table 4-9, and the geometry design requirements of the deposition hole are illustrated in Figure 4-12. The design of the deposition hole needs to limit the dimension and geometry, so that the installed buffer component can reach the expected design condition. The inflow rate of the deposition hole should be less than 0.1 L/min to avoid buffer loss due to piping erosion. The connected effective transmissivity integrated along the full length of the deposition hole wall and as averaged around the hole, should be less than 10^{-10} m^2/s (SKB, 2010j). According to the design requirements related to the deposition hole and the designed diameter of the canister (see Section 4.2.4), the diameter of the deposition hole is 1,750 mm, and the height is 8,155 mm.

The upper part of the deposition hole is designed with a bevel to allow the canister to turn into an upright position over the deposition hole. According to the height of the disposal tunnel (see Section 4.2.7), the rotation space for installing the canister, and the height of the construction equipment for installing canister, the height from the top of the canister with construction equipment to the bottom of the disposal tunnel should be less than 4,100 mm (Figure 4-13). Therefore, it is expected that when the canister is installed, the center of the canister is inclined at an angle of 38° above the center of the deposition hole, and the bottom of the canister is 500 mm away from the bevel for rotation space. And the height from the top of the canister to the bottom of the disposal tunnel is about 4,069 mm (Figure 4-13), which meets the aforementioned 4,100 mm requirements.

Table 4-9: Design requirements of the deposition hole.

Design consideration	Require property	Design requirements
Sufficient thickness of the buffer around and at upper and lower parts of the canister to provide the function of protecting the canister.	The diameter and height of the deposition hole shall have enough space to accommodate the buffer and canister.	Design thickness of the buffer: around the canister 350 mm below the canister 500 mm above the canister 1,500 mm Dimensions of the canister refer to the "Design of the canister" report and Section 4.2.4 of this report.
The level of the bottom of the deposition hole is required to ensure that the buffer blocks and the canister be effectively installed in a central position.	Inclination of the deposition hole bottom should be able to allow installation of buffer and deposition of the canister.	If the bottom of the deposition hole is tilted, the buffer block will not be effectively installed in the center position of the deposition hole, which will affect the canister installation in position. The inclination over the part of the cross-section where the Bottom buffer block placed shall be less than 1/1,750.
Limit the dimension of the deposition hole to ensure that the density of the designed buffer component after installation can be maintained within the design requirements.	The dimension variations of the deposition hole must not be larger than to allow deposition of the buffer according to specification.	Each horizontal cross section must not exceed the designed cross- section by more than 7%. According to the diameter of the canister (1,050 mm) and the thickness of the buffer around the canister (350 mm), the deposition hole where the buffer is going to be installed the design diameter is 1,750 mm, and shall be at least 1,745 mm.

Reference: SKB (2010c).

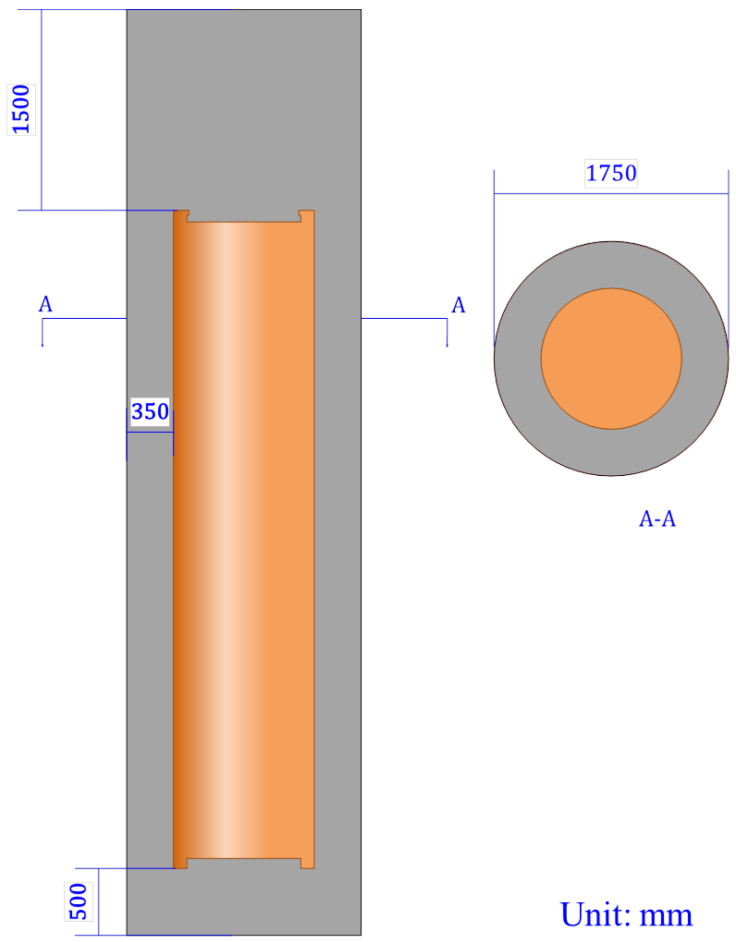

Figure 4-12: Geometry design requirements of the deposition hole.

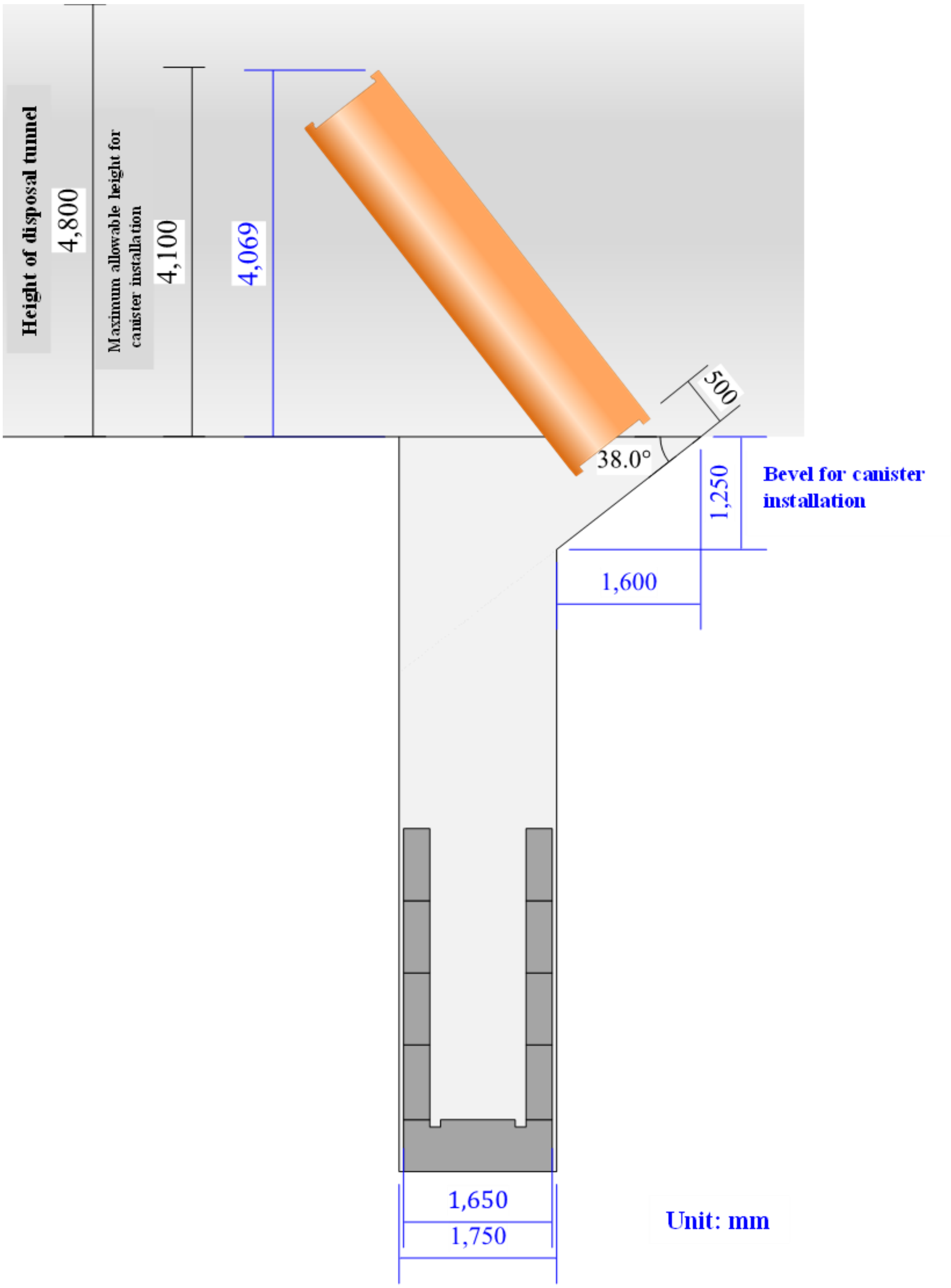

Figure 4-13: Bevel design of the deposition hole and demonstration of the installation of the canister.

4.2.7. Backfill

The design of the disposal tunnel and the backfill is to ensure that backfill after installation reaches the expected density, so the geometry and dimension of the disposal tunnel must be limited in order to control the excavation volume. The acceptable dimension and geometry of the disposal tunnels are illustrated in Figure 4-14. The design requirements related to the disposal tunnel are given in Table 4-10. The requirements comprise acceptable dimensions and geometry, and acceptable inflow to the disposal tunnel.

The backfill is the material installed in the disposal tunnels to fill the empty space. It is also one of the engineered barriers in the repository. The design functions of the backfill include the following items:

(1) limit flow of water (advective transport) in disposal tunnels to decrease the harm of water flow to engineered barriers.

(2) restrict buffer upward swelling/expansion to provide mechanical support and maintain its volume in the deposition hole, preventing the buffer from swelling outside the deposition hole and decreasing its density.

(3) not significantly impair the barrier function of the other barriers.

(4) maintain its barrier functions and long-term durability in the environment expected in the repository.

The design functions, properties, and design requirements of the backfill are presented in Table 4-11, in which bentonite is manufactured as backfill blocks and pellets with specific sizes and densities. The design requirements for manufacturing and installation of the backfill are presented in Table 4-12. Moreover, the interaction between the backfill and disposal tunnel should be seriously considered to ensure technical feasibility.

The backfill will be made of bentonite whose main composition is montmorillonite. Sufficient montmorillonite content of the bentonite can provide appropriate hydraulic conductivity and swelling pressure to fulfill the design requirements of backfill. The montmorillonite content will also affect the compressibility of the material and the capability of the backfill to restrict upward swelling/expansion of the buffer. In addition, the harmful substances content of bentonite should be limited, such as sulfide, sulfur, and organic carbon which reduce the performance of the other barriers.

MX-80 bentonite will be the raw material for the backfill, and its characteristics were investigated through experiments. Experiments on swelling pressure and hydraulic conductivity under different bentonite densities were carried out using distilled water and cation strength of 2.54 mM synthetic groundwater (the chemical composition and content are shown in Table 4-6 based on groundwater composition in Section 4.3.2) to provide reference properties for the design.

The backfill is composed of bentonite blocks and pellets to a specific density and filled in the disposal tunnel with the maximum filling amount according to the dimension and geometry of the disposal tunnel. The geometry specifications of backfill blocks are presented in Figure 4-15. The reference specifications of backfill blocks and pellets are presented in Table 4-13. The backfilling will mainly use machinery control and automatic installation to reduce the radiation dose of personnel. Schematic of the backfill installed in the disposal tunnel and reference design of the installed backfill are presented in Figure 4-16 and Table 4-14. The description of each component installed in the disposal tunnel is as follows:

(1) Bottom bed of the disposal tunnel: the bottom bed is installed with pellets and compacted to a flat layer with a thickness of 10 cm. To achieve a reliable installation, the bottom bed needs to be compacted so that the density is high enough to yield sufficient bearing capacity for the blocks and flat enough to yield a symmetric block.

(2) Disposal tunnel: the dimension of the block is 70 cm long, 66 cm in width, and 52 cm in height. There are 6 blocks stacked horizontally for each tunnel cross-section, and the width after stacking is 396 cm, leaving about 10 cm gaps between the blocks and the tunnel wall, which facilitates the dry spraying equipment to eject the pellets to

fill the gap. There are 7 blocks stacked vertically for each tunnel section, and the height after stacking is about 364 cm (excluding the bottom bed).

(3) Upper part of the disposal tunnel: the dimension of the block is 70 cm long, 60 cm in width, and 25 cm in height, arranged by the upper part of the tunnel, as shown in Figure 4-16. There are 17 blocks in total.

(4) Gap between blocks and the tunnel wall: the gap between blocks and the top/side of the tunnel wall will be filled with pellets.

The calculated dry density of the backfill after installation in the tunnel is presented in Table 4-15. Under the nominal block part of the cross-section and largest acceptable tunnel volume, the average dry density of a tunnel section is 1,461 kg/m^3. According to Table 4-14, at least 60% of the tunnel volume needs to be filled with blocks. Under this condition, the lowest dry density is 1,408 kg/m^3. According to Figure 4-10 and Figure 4-11, for the properties of the swelling pressure and hydraulic conductivity of MX-80 bentonite, the swelling pressure of the installed backfill is greater than 0.1 MPa, and the hydraulic conductivity of the installed backfill is lower than 10^{-10} m/s, which fulfill the relevant design requirements shown in Table 4-11.

The density of the designed backfill needs to be considered as below: (1) to limit the groundwater flow in the disposal tunnel, (2) having enough mechanical support to maintain the volume of buffer in the deposition hole, and (3) to keep the swelling pressure of buffer larger than 2 MPa, which can be achieved by the dry density of backfill being larger than 1,240 kg/m^3 according to the evaluation of buffer swelling property and backfill compressibility (SKB, 2010e).

Table 4-10: Design requirements of the disposal tunnel.

Require property	Design requirements
Limit the deviations of the floor and wall surfaces in disposal tunnels from the nominal in order to allow backfill installation according to designed specifications.	For each tunnel blast round, the actual blasted total volume must not exceed 30% of the designed excavation volume. The maximum cross-sectional area of the tunnel shall not exceed 35% of the designed tunnel cross-section. The disposal tunnel floor must be even enough for the installation equipment to drive on it to achieve a dependable backfill installation. Underbreak is not accepted, to ensure that the design, manufacture and installation of the backfill can fulfill the designed density conditions.
The floor and wall surfaces in disposal tunnels shall consist of rock surfaces so that the backfill will be indirect contact with the rock surface.	Limit the area of construction materials covering the disposal tunnel and must not extend over the full tunnel width.
During backfill installation and saturation process, groundwater seepage into disposal tunnels must not significantly impair the backfill barrier function.	The total water inflow into every disposal tunnel shall be determined to ensure the stability of the backfill installation. If tunnels with total inflow less than 0.5 L/min, no further actions are needed. If tunnels with total inflow between 0.5 L/min to 1 L/min, and there are any fracture zones with inflow rates more than 0.5 L/min, relevant water handling methods are required. If tunnels with total inflow more than 1 L/min, and there are any fracture zones with inflow rates more than 0.25 L/min, relevant water handling methods are required. (Sandén , T. et al., 2018a) The transmissivity of EDZ (Excavation Damaged Zone) should be less than 10^{-8} m^2/s (SKB, 2010j)

Reference: SKB (2010e)

Table 4-11: Design functions, properties, and design requirements of the backfill

Design function	Properties	Design requirements for long-term safety
Limit flow of water (advective transport) in the disposal tunnels.	Properties that affects swelling and hydraulic conductivity under saturated conditions.	Hydraulic conductivity less than 10^{-10} m/s. Swelling pressure more than 0.1 MPa.
Restrict upwards buffer swelling/expansion.	Properties that affect compatibility during saturation and after saturation.	The designed dry density of the backfill blocks and pellets shall maintain the designed buffer density during saturation and after saturation. Backfill deformation shall be sufficiently limited to keep the buffer swelling pressure larger than 2 MPa in average over the buffer volume.
Not significantly impair the barrier function of the other barriers.	Limit the content of harmful substances in bentonite. Properties that affect the chemical conditions around the buffer and canister.	Impurities in the backfill shall not provide a significant source of sulfide, as this may corrode the copper canister.
Maintain its barrier functions and long-term durability in the environment expected in the repository.	Maintain its design condition in the long-term impact of the repository environment.	-

Reference: SKB (2010e), Posiva and SKB (2017).

Table 4-12: The design requirements for manufacturing and installation of the backfill.

Design consideration	Require property	Design requirements
The design and methods for preparation, installation, testing and inspection shall be based on well-tried or tested techniques. Backfill with specified properties shall be possible to prepare and install with high reliability.	The backfill must be possible to compact to the required density.	-
	The backfill components shall be designed so that installation can be performed with high reliability.	The reference sequence for deposition of the canister. The reference sequence of installation of the buffer and backfill.
	The combination of the geometrical configuration of the backfill and the installation technique shall be such that the seepage into the disposal tunnels and the resulting hydraulic processes that take place during installation do not impair the barrier functions of the backfill.	The design of the backfill must consider the allowable inflow from the tunnel and plug.

Reference: SKB (2010e).

Table 4-13: Reference specifications of the backfill blocks and pellets.

Parameters		Reference specification	Accepted variation
Blocks	Dry density (**kg**/m^3)	1,700	+/- 50
	Dimensions (cm)	70× 66×52	+/- 2
		(upper part of the tunnel) 70× 60×25	
Pellets	Pellet dry density (**kg**/m^3)	1,700	-
	Pellet dimensions (cm)	-	The pellets' dimensions and geometry will be determined by the filling test.
	Dry density loose filling (**kg**/m^3)	1,000	+/- 100

Reference: 台電公司 (2018a).

Table 4-14: Design parameters, specifications, and installation requirements of the backfill.

Design parameters		Design specifications	Installation requirements
Blocks	Volume of blocks filling in disposal tunnel	Arranged as shown in Figure 4-16, number of stacked blocks per cross-section. Block dimension 70×66×52: 7× 6 blocks, total 42 blocks. Dimension 70×60×25: total 17 blocks (arranged by the upper part of the tunnel).	> 60% block filling. Blocks and tunnel wall reserve > 10 cm of free space to facilitate the pellet filling construction.
Pellets	Volume of pellet filling in the gap between blocks and tunnel wall	Depends on the actual volume between blocks and tunnel wall.	Record the weight of pellets according to actual filling volume.
	Bottom bed	Thickness 10 cm	Record the weight of pellets according to actual filling volume.
	Dry density (kg/m^3)	> 1,000	-

Reference: 台電公司 (2018a).

Table 4-15: The estimated dry density of backfill after installation.

-	Nominal block part of cross-section	Acceptable block part of cross-section (60% filled with blocks)
Block dry density (kg/m^3)	1,700	1,700
Dry density after pellet filling (kg/m^3)	1,000	1,000
Tunnel cross-section (m^3/m) (Set to the largest acceptable)	25	25
Volume fraction of slots between blocks	2 %	2%
Volume of pellet filling (include bottom bed) (m^3/m)	$25 - 16.96 \times (1 + 0.02)$= 7.7	$25 - 25 \times 0.60 \times (1 + 0.02)$=9.7
Calculated installed dry density (kg/m^3)	1,461	1,408

Reference: 台電公司 (2018a).

Note: volume of block filling per meter of tunnel using dimension 70 cm ×66 cm ×52 cm blocks; $1 \times 0.66 \times 0.52 \times 42(\text{blocks}) = 14.41\ (\text{m}^3/\text{m})$; volume of block filling per meter of tunnel using dimension 70 cm ×60 cm ×25 cm blocks; $1 \times 0.6 \times 0.25 \times 17\text{(blocks)} = 2.55$ (m^3/m); total volume of block filling per meter of tunnel; $14.41 + 2.55 = 16.96$ (m^3/m).

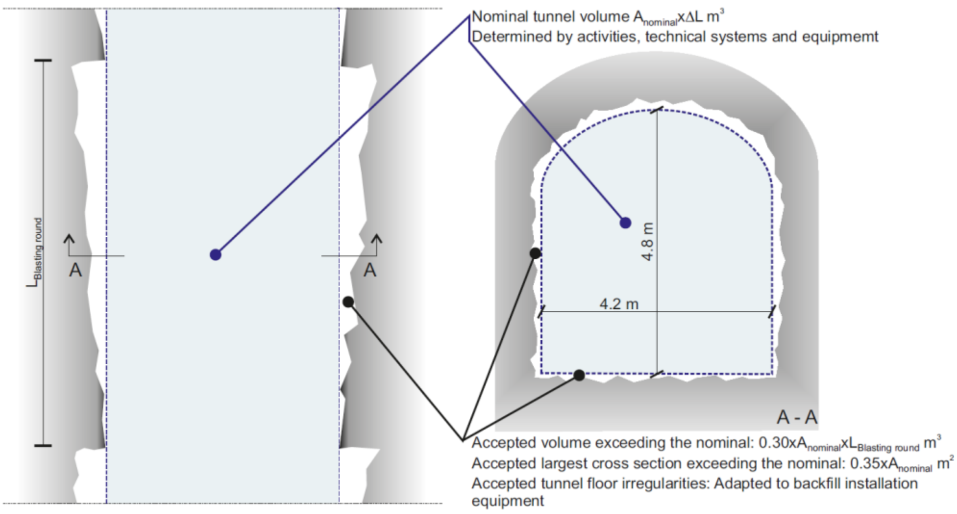

Figure 4-14: Specifications of the disposal tunnel.

Reference: SKB (2010e)

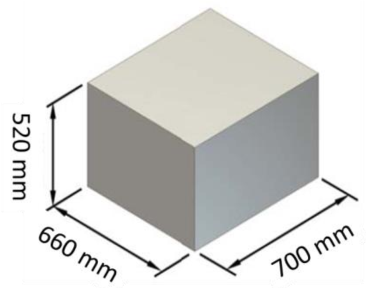

(a) Backfill block

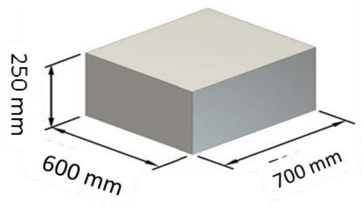

(b) Backfill block (upper part of the tunnel)

Figure 4-15: Geometry specifications of the backfill blocks.

Reference: 台電公司 (2018a)

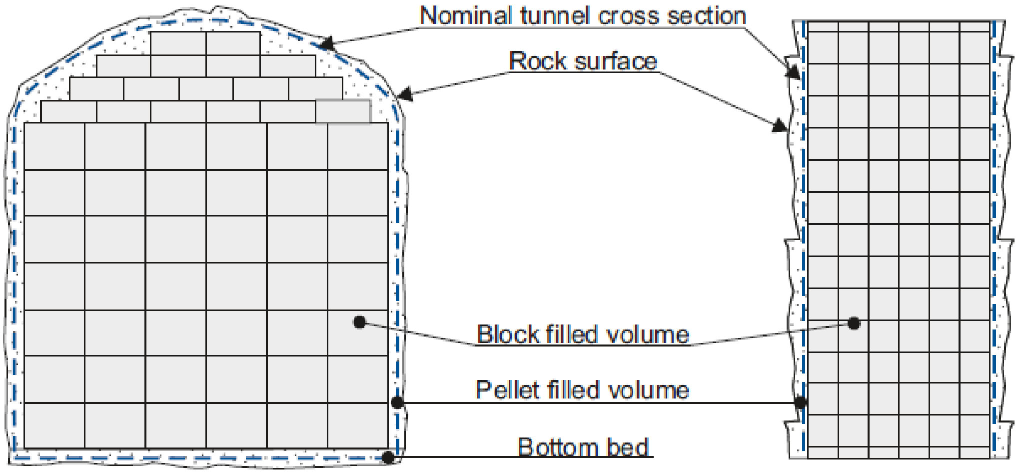

Figure 4-16: Installation of backfill in the disposal tunnel.

Reference: SKB (2010e).

4.2.8. Characteristics of the Buffer and Backfill

The swelling pressure and the hydraulic conductivity of the buffer and backfill will depend on density, the content of montmorillonite, adsorbed ionic species and the ionic strength of the surrounding groundwater. In particular, the ionic strength of the groundwater will affect the most (SKB, 2006b).

The density of the buffer and backfill are usually expressed as dry density. The criterion for the buffer density in the deposition hole is expressed as saturated density. And saturated density can be expressed as the following:

$$\rho_{sat} = \frac{\rho_{water} \times V_p + W_{solid}}{V} \tag{4- 2}$$

Where,

ρ_{sat}=saturated density, [kg/m^3].

ρ_{water}=density of water, 1000 [kg/m^3].

V_p=pore volume, [m^3].

W_{solid}=dry mass of bentonite, [kg].

V=total volume, [m^3].

The relation between dry density and swelling pressure and the relation between dry density and hydraulic conductivity of MX-80 bentonite for distilled water and synthetic groundwater are presented in Figure 4-10 and Figure 4-11. As discussed in Section 4.2.5 and Section 4.2.7, the reference buffer and the reference backfill specifications can fulfill the relevant design requirements, such as providing sufficient swelling pressure and maintaining low enough hydraulic conductivity.

4.2.9. Backfilling of Shafts and Ramps

The repository is divided into deposition holes, disposal tunnels, main tunnels, central area tunnels, vertical shafts and ramps based on their functions. These tunnels also need to be backfilled when the repository is closed to maintain the closure of the repository.

Before backfilling the shaft and ramp, it is necessary to remove the relevant internal construction equipment and the pavement foundation for transportation, but shotcrete, rock bolt and grout materials will be retained. The backfill for shafts and ramps will be backfilled with clay materials in the range from 500 m underground to 200 m underground. From 200 m underground to 50 m underground, gravel with a maximum particle size of 200 mm is used for backfilling. The coarse aggregate material is used at 50 m near the ground surface, and they are well compacted to avoid unintentional intrusion. (SKB, 2010q)

At present, only the design concepts of shafts and ramps are described, and the conditions of shafts and ramps are not considered in the analysis model. Model establishment can be referred to in Section 4.4.2. When detailed site and geological survey data are obtained in the future, shafts and ramps will be considered in the analysis.

4.2.10. Shotcrete and Grout Materials

During the excavation process, the structure may be unstable due to stress released from the rock mass. Supporting structure constructed with shotcrete and grouting materials will be used to improve stability.

Since the concrete and mortar commonly used for shotcreting and grouting materials have a highly alkaline pore solution, the highly alkaline pore solution will diffuse into the groundwater and affect the volume stability of bentonite in buffer (the chemical properties of bentonite in an environment with a pH value > 11 may be unstable leading to the dissolution of montmorillonite) and influence the safety function of the buffer. Therefore, low-pH concrete is planned to be used for the purpose of decreasing the pH value < 11, reducing the hydraulic conductivity < 10^{-8} m/s and increasing the compressive strength > 280 kg/cm^2. This can prevent high pH in the porewater of the concrete and maintain the stability of the buffer (SKB, 2010j).

4.2.11. Plugs

The function of the plug is to ensure that the buffer and backfill stay in their original positions, and to prevent groundwater in the disposal tunnels from flowing into the main tunnel. In addition, flowing out of the backfill from the disposal tunnels can be reduced; therefore, water sealing is the main function of the plug.

The front end of the plug will be provided with a filter layer and a sealing layer to block water. The geometry of the side is close to the arch shape, which sustains the swelling pressure and thermal stress. It can transfer stress to the upper and lower bedrock and provide good support and stability. The geometric dimensions of the plug are shown in Figure 4-17 (SKB, 2010e), and the relevant position diagram after installation at the entrance of the disposal tunnel is shown in Figure 4-18. In order to maintain the density of the backfill in the disposal tunnel, each disposal tunnel will be sealed with a plug immediately after backfilling.

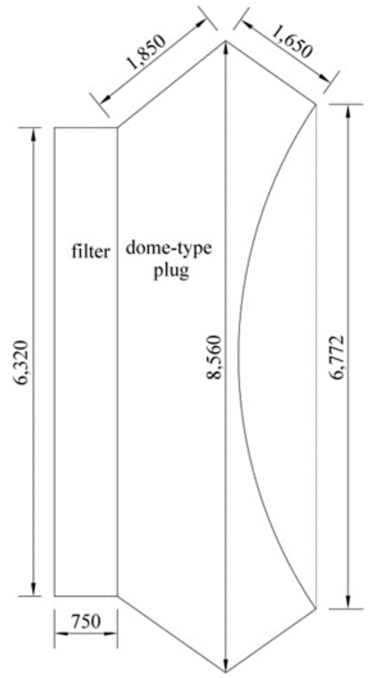

Figure 4-17: Geometry specifications of the plug.

Note: the unit is in mm.

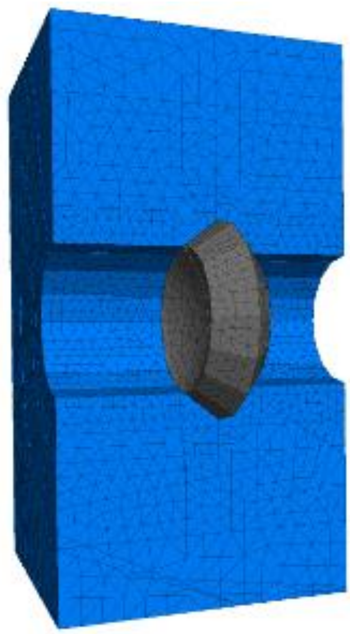

Figure 4-18: Profile of the plug.

Note: the plug is demonstrated in black and the surrounding rock mass is demonstrated in blue.

4.2.12. Borehole Seals

In order to obtain data on the properties of the host rock, a series of boreholes may be drilled during the site investigation period. These boreholes shall be sealed before the closure of the repository in order to avoid potential release paths. Boreholes will also be drilled from the disposal tunnels to the host rocks during the construction phase implying that horizontal and upwards-directed holes also have to be sealed.

Considering nuclear safety and radiation protection, the hydraulic conductivity of the sealing should not significantly change the natural groundwater flow. The design requirements stipulate that the hydraulic conductivity of the sealing material at the intersection with the water-containing fracture should be 10^{-6} m/s or lower (Luterkort et al., 2012; Sandén et al., 2018b). The borehole seals which are in hydraulic connection with the repository should be mechanical stable during the lifetime of the repository. Borehole seals should prevent surface water flowing down in the borehole and contaminating the groundwater. Different water-bearing regolith layers shall not have contact with each other via the sealed borehole (Sandén et al., 2018b).

The design concept of borehole seals refers to The Sandwich-concept from Swedish SKB, as shown in Figure 4-19 (Sandén et al., 2018b). The borehole with water-bearing fractures section is filled with a permeable material such as sand which will not significantly change the natural groundwater flow. The parts without water-bearing fractures are sealed with bentonite. To prevent interaction between the different materials, quartz-based concrete (quartz sand and low pH cement) is positioned at a certain length in the transition zones between bentonite and sand. In addition, copper plugs are installed between the materials to facilitate construction and prevent mixing between different materials. Borehole survey and characterization can be carried out before sealing to classify the borehole sections and, after that, perform a detailed design of the closure material. The uppermost part of the borehole is filled with bentonite pellets and has a top seal which a larger diameter than the borehole, to ensure that no surface water is transported via the borehole down to water-bearing zones (Sandén et al., 2018b).

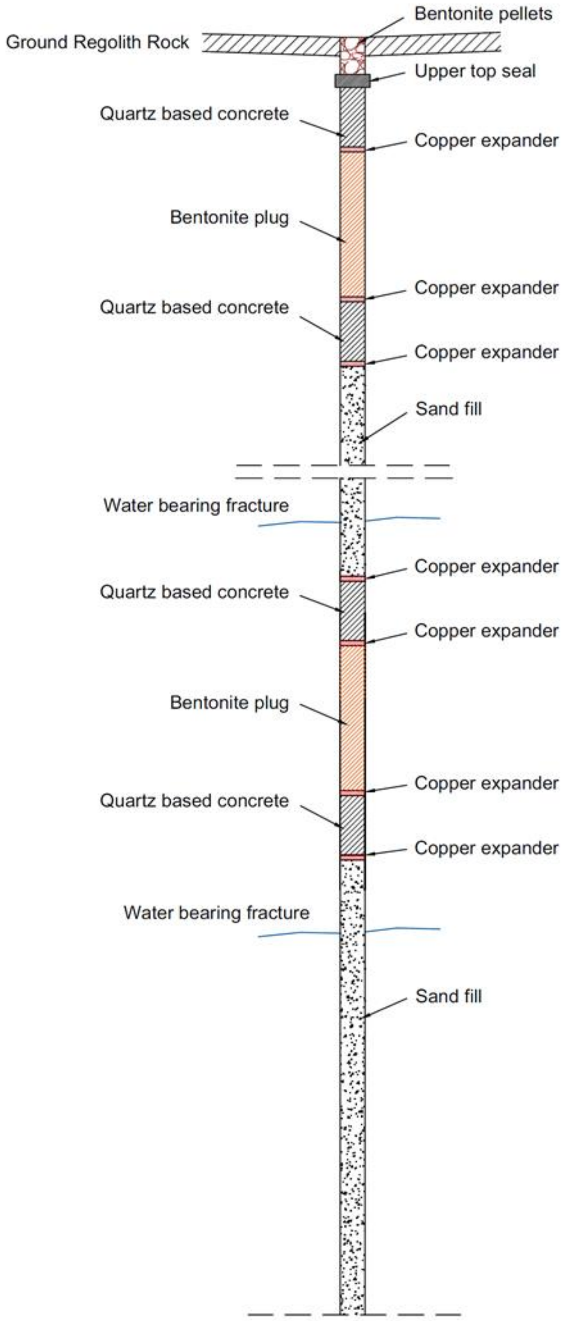

Figure 4-19: Schematic view of the borehole seal.

Reference: Sandén et al. (2018b).

4.3. Initial State of Geosphere and Biosphere

4.3.1. Data Corresponding

According to Section 1.2, the candidate site in Taiwan has not been selected yet. By referring to the international experience, the geological data and biosphere information from survey data in Taiwan were applied. Without a specific disposal site, the "reference case" was established for the following application of engineering design and safety assessment in this report.

The geological data of the reference case includes the distribution of geologic units, thermal-hydrological-mechanical-chemical properties and overall information about the environment. The geological information of the reference case is based on the survey data from Spent Nuclear Fuel Final Disposal Plan in crystalline rock areas in Taiwan (台電公司, 2006-2019). Field surveys such as ground-surface survey, gravity and magnetic survey, electrical resistivity survey, satellite images analysis, hydrological investigation, geological drilling, fracture survey and hydrogeological survey were implemented. Laboratory works such as thermal and mechanical tests of rocks, hydraulic conductivity tests, mineral composition analysis and groundwater chemical composition analysis were also conducted. The results of the field survey and laboratory works were applied to establish the reference case with crystalline rock characteristics and localized parameters.

The biosphere data of the reference case includes radionuclide-dependent and ecosystem-related parameters. The radionuclide-dependent parameters were mainly referred to BIOMASS-6 Report (IAEA, 2003), Handbook of Parameter Values for the Prediction of Radionuclide Transfer (IAEA, 2010b) and JAEA Report (Kato and Suzuki, 2008). The parameters related to the ecosystem were mainly referred to the statistic information of Taiwan, such as the National Food Consumption Database (Taiwan Food and Drug Administration, 2017), Kinmen Monthly Statistics Report (Accounting and Statistics Department, Kinmen County Government, 2017), water statistics (Water

Resources Agency, 2017), labor statistics (Ministry of Labor, 2017), forest resource survey (Chu et al., 2015), Summary Report of the National Important Wetland Carbon Sink Research Project (Green Engineering Technology Research Center, 2011), Carbon Flux Research Project of Coastal Wetland in Kinmen National Park (Lin and Lee, 2011) and relevant research data (Huang et al., 2006). For the lack of some parameters, international researches were referred to, such as BIOMASS-6 Report, JAEA Report, POSIVA Biosphere Parameter Report (POSIVA, 2014), SKB limnic ecosystems report TR-10-02 (Andersson, 2010), Irrigation Water Management Report (Brouwer, 1986) and Biosphere Modelling and Dose Assessment for Yucca Mountain (Smith et al., 1996).

Sweden experience and classification method (Andersson et al., 2013) were referred to for data integration and assessment, which is classified into geology, thermal and mechanical properties of rock, hydrology and hydrogeology, hydrochemistry, transport properties of rock, and biosphere. The reference case in Taiwan is presented in these six categories for the following application of safety assessment.

4.3.2. Reference Case

4.3.2.1. Geology

4.3.2.1.1. Geologic Units

The range, geometry and classification of geologic units are the basis of the reference case. The geologic units in this report are based on the ground-surface survey, geological drilling, gravity and magnetic survey and inversion, and electrical resistivity survey through the years in one of the crystalline rock area in Taiwan (Figure 4-21). According to SNFD 2017 Report, granite is the main rock type in this investigated crystalline rock area in Taiwan. As a result, granite is set as the disposal host rock in the reference case in this report. There are main water-conducting structures around the disposal host rock which might affect the groundwater flow. Regolith generated by weathering of host rock surface is also considered. In summary, geologic units consist of granitic host rock (R), regolith (R0) and main water-conducting structure (F#). The three-dimensional distribution is shown in Figure 4-22. Detail parameters are shown in Table 4-16.

(1) Granitic host rock (R):

Except for regolith and water-conducting structure, the granitic rock mass is defined as the host rock.

(2) Regolith (R0):

While granite bedrock is denudated and approaches to the ground surface, weathering and decompression generate denuded joints and form fractured regolith, which becomes the main shallow aquifer in the granitic area. In this report, the regolith depth of the reference case is set as 70 m.

(3) Main water-conducting structure (F#):

The setting of the main water-conducting structure in this report refers to SNFD2017 Report. There are two main water-conducting structures named F1 and F2. The attitude of the F1 structure is N64°E, 70°N. The attitude of the F2 structure is N80°W, 50°S, which might be the conjugated fractured zone of F1. The width of F1 is 200 m, and the width of F2 is 20 m in the reference case.

4.3.2.1.2. Fracture

Generally, the granitic host rock is hard and firm with low porosity and a certain number of fractures. The same fracture distribution data as the SNFD2017 report is adopted to establish the discrete fracture network (DFN) parameter database in this report (台電公司, 2019a). The parameters in the DFN parameter database are presented in Table 4-17 and elaborated as below.

(1) Fracture domain:

With the setting of the reference case, it is divided into two fracture domain with a boundary of 70 m depth. The upper layer is regolith, and the bottom layer is granitic host rock. The fracture strength and characteristics are recorded individually by in-hole photography and are summarized as below.

(a) Fracture domain above 70 m depth is called FDMA, and the fracture strength value (P_{32}) is 2.4 m^{-1}.

(b) Fracture domain below 70 m depth is called FDMB, and the fracture strength value (P_{32}) is 0.3 m^{-1}.

(2) Fracture cluster:

(a) FDMA: there are 4 fracture clusters. The pole trend, pole plunge, Fisher distribution (κ) and proportion of fracture strength ($\mathbf{P_{32,real}}$) of each cluster are listed below:

(i) Cluster 1: 198°/18°/18/26%.

(ii) Cluster 2: 155°/4°/15/24%.

(iii) Cluster 3: 264°/23°/16/18%.

(iv) Cluster 4: 98°/81°/11/32%.

(b) FDMB: there are 5 fracture clusters. The pole trend, pole plunge, Fisher distribution (κ) and proportion of fracture strength ($\mathbf{P_{32,real}}$) of each cluster are listed below:

(i) Cluster 1: 65°/17°/20/15%.

(ii) Cluster 2: 344°/38°/18/24%.

(iii) Cluster 3: 281°/29°/16/30%.

(iv) Cluster 4: 174°/22°/17/10%.

(v) Cluster 5: 175°/75°/19/21%.

(3) Fracture location: stationary random (Poisson) process is adopted to generate the center location of each set of fracture.

(4) Fracture size (radius): it is described by a power function statistical distribution model.

(a) $\boldsymbol{k_r}$: the exponent of fractal dimension, or the so-called fracture radius scaling exponent. $\boldsymbol{k_r}$ is set to be 2.6.

(b) $\boldsymbol{r_0}$: the minimum radius value. $\boldsymbol{r_0}$ is set as 0.1 m to create more large fracture surface, and increase fracture connectivity, and reduce the computational burden of DFN simulation.

(c) Assuming that the maximum fracture surface is a rectangle of 1000 m×1000 m, the upper threshold of fracture radius is set to be 564 m.

(5) Fracture transmissivity (T):

(a) FDMA: $\boldsymbol{T = 1.51 \times 10^{-7} \times (\frac{L_f}{100})^{0.7}}$

(b) FDMB: $\boldsymbol{T = 3.98 \times 10^{-10} \times (\frac{L_f}{100})^{0.5}}$

Where L_f is the physical length (m) of an intersecting fracture in the orthogonal direction.

(6) Fracture aperture: it is calculated by the equation of $e=0.5\times\sqrt{T}$, with T being fracture transmissivity (m^2/s) and e being fracture aperture.

4.3.2.1.3. Mineral composition

The mineral composition of the reference case is determined by the result of field survey, mineral identification, composition analysis and geochemical analysis.

Mineral composition of the granitic host rock in the reference case consists of coarse and gray to pink granitic gneiss. Major minerals of fresh rock samples include quartz, potassium feldspar, plagioclase, biotite, and seldom amphibolite, orthite, zircon, apatite, garnet and opaque minerals. Secondary minerals such as sericite and chlorite occasionally appear between major minerals with fine quartz veins. Rocks in the fractured zone are ruptured and rough with strong alterations. High argillization and chloritization generate white-yellow green cryptocrystalline secondary minerals covered above. Most minerals have turned to alteration minerals with some weathered rusts.

4.3.2.2. Thermal Properties and Mechanical Properties of the Rock

4.3.2.2.1. Thermal Properties

The ground temperature of the reference case is 23.8 ℃, and the temperature gradient is 0.015 ℃/m to 0.019 ℃/m, with an average of 0.017 ℃/m (台電公司, 2007, 2008, 2009, 2017, 2019a).

The average thermal conductivity of granitic host rock is 2.3 W/mK to 3.0 W/mK. Considering that the density of the rest geologic units (R0 and F#) is relatively low, the thermal conductivity value of the rest geologic units should be lower than that of host rock and diabase dike.

As a result, the thermal conductivity value of the rest geologic units was set as 2.0 W/mK (Table 4-18).

The specific heat of the granitic host rock is 730 J/kg·K to 903 J/kg·K, and the rest of geologic units is 800 J/kg·K. The coefficient of thermal expansion was set to be 8×10^{-6} (1/K) (台電公司, 2017).

4.3.2.2.2. Mechanical Properties

Rock mechanical properties of the reference case are summarized in Table 4-18, including strength property, deformation property and in-situ stress. All the parameters are referred to the results of rock mechanics analysis and in-situ investigation conducted in crystalline rock areas over the years. The basic physical property of rocks includes unit weight, moisture content, specific gravity, saturated density, dry density, water absorption and porosity. Strength property includes uniaxial compressive strength, tensile strength and shear strength (cohesion C and internal friction angle ϕ). Deformation property includes static elastic module (E_s), static poisson's ratio (ν_s), dynamic elastic module (E_d), dynamic shear module (G_d) and dynamic poisson's ratio (ν_d) (台電公司，2006；2014；2015；2016). The in-situ stress data were collected from the measurement data in the KMBH01 well, including the hydraulic fracturing method and the existing fissure hydraulic method (台電公司, 2006; 2013).

4.3.2.3. Hydrology and Hydrogeology

According to the classification of geologic units (Section 4.3.2.1.1), the hydrogeologic units of the reference case can be classified as granitic host rock (R), regolith (R0), and main water-conducting structure (F#).

The hydrologic characteristics of granitic host rock are referred to the indoor hydraulic test (台電公司, 2007) and in-situ double packer test (台電公司, 2006-2010). The hydraulic conductivity of R is 4.1×10^{-12} m/s to 1×10^{-9} m/s. The hydraulic conductivity of F# is 3.0×10^{-8} m/s to 10^{-4} m/s, with an average of 5.0×10^{-6} m/s, which is referrd to the double packer test conducted in water-conducting fracture zone in the drill. The corresponding hydraulic properties are presented in Table 4-19 (台電公司, 2006, 2016, 2017, 2019a).

4.3.2.4. Hydrogeochemistry

The groundwater data of the reference case were acquired by groundwater sampling and analysis in Taiwan granite areas (台電公司, 2007, 2008, 2013, 2019a). Detailed information is listed in Table 4-20.

(1) pH scale

The pH of shallow groundwater (<50m depth) is 4.6 to 7.1 (Liu et al., 2008), and deep groundwater (50m to 500m depth) is 6.29 to 9.76. Due to the large range of pH variation, the buffering capacity is limited.

(2) Eh scale

The Eh of deep groundwater is -0.48 volts to +0.35 volts. In general, the groundwater is in a reducing environment (Eh<0) where the depth is deeper than 400 m.

(3) The groundwater is much lighter than sea water at a depth of 500 m.

4.3.2.5. Transport Properties

The retardation of radionuclide migration of host rock depends on transport properties such as groundwater flow characteristic, nuclide adsorption capacity of the host rock, and nuclide diffusion in host rock.

The groundwater flow characteristic is affected by the transport path of groundwater and connected water-conducting structure. For hydraulic parameter and fracture characteristic, please refer to Section 4.3.2.

The nuclide adsorption capacity of host rock and nuclide diffusion in host rock are two major factors that affect transport properties. For a nuclide of low adsorption capacity, it will diffuse deeper than a nuclide of high adsorption capacity (JNC, 2000, ch.3.2.4.3). These two parameters are closely related to host rock characteristic and environment. As a result, the range of transport properties (such as diffusion coefficient and partition coefficient (K_d)) can be confirmed till the phase of the site characteristic survey. In order to evaluate the influence of parameter uncertainty, international data with similar disposal condition is adopted for nuclide-related parameters in this report.

4.3.2.6. Biosphere

(1) Surface ecosystem

The reference case is set on a sub-tropical island with hills in the center and is flat at the edge. According to the meteorological observation data of Taiwan's offshore island from 1991 to 2019, the annual rainfall is between 649.20 mm and 1,873.10 mm, and the evaporation is between 856.8 mm and 1,650.90 mm. The average annual rainfall and evaporation are set to be 1,116.83 mm and 1,277.39 mm in this report. In the reference case, there is no orographic rain, and the streams are short and ephemeral resulting that river flow directly responds to the rainfall. In order to store the water, plenty of reservoirs, farm ponds, and small water dams were constructed. The total water area is about 14.3 ha for the maximum water level.

In addition, the groundwater recharge could be estimated according to the annual rainfall and evaporation mentioned above by the water budget balance method (Shu et al., 1991). The result shows that the annual groundwater recharge is between -145 mm and 336.64 mm from 1991 to 2019, as shown in Figure 4-23, and the average recharge is 66.8 mm (台電公司, 2020).

(2) Aquatic Landscape

The reference case is an island, some parts of the coast are an extension of the granite bedrock, and the other parts are sandy or muddy coast. The reference case is famous for the oyster farming industry, and there are also related farming industries of grass shrimp and white shrimp. Marine species and biomass can be obtained from the Carbon Flux Research Project of Coastal Wetland in Kinmen National Park (Lin and Lee, 2011).

With the flat topography and high evaporation of the reference case, there is little capacity to keep the precipitation, leading to a water shortage issue. Most daily usage, drinking, and irrigation water are supplied from reservoirs, farm ponds dug by inhabitants, small water dams, and well. The amount of well water pumped is assumed according to the water rights statistics of the Water Resources Agency (Water Resources Agency, 2017). The alluviation effect on the catchment area causes the sedimentation of the sand and pebble gravel at the bottom of the freshwater, and green algae, water weeds are covering above. Several benthic organisms, such as mollusks and arthropoda, and different kinds of fish occur in the freshwater. The benthic organisms that grow in the lake include molluscs (such as clams and snails), arthropods (such as shrimps and crabs), as well as various fishes. In consideration of future environmental evolution, rivers and lakes may appear after the sea level drops. The future biomass parameters related to rivers are temporarily referred to the relevant research data of Taiwan’s main island (Huang, 2006; Green Engineering Technology Research Center, Kao Yuan University, 2011).

(3) Land Use

The terrestrial ecosystem in the reference case includes forest and agricultural land. The forest here is a semi-natural system, accounting for 45.8% of the total terrestrial area with less human action affection (Chu et al., 2015). The agricultural land area accounts for 28.3% of the total terrestrial area according to Kinmen Monthly Statistics Report (Accounting and Statistics Department, Kinmen County Government, 2017). Since lateritic soil is degenerating in the reference case, soil has been moved to the reference case from other places to improve soil quality. The total area of forest and agricultural land accounts for almost 80% of the reference case, and the rest is the city, industrial area, and traffic construction of the human living environment.

The main crops in the reference case are sorghum, wheat, and a small number of vegetables, sweet potatoes and fruits. In addition to human ingestion, the crops are also used to feed livestock. Animal agriculture in the reference case is prevalent, and the livestock production is enough for the annual requirement for most people. Although there is a large area of forest in the reference case, hunting activity is illegal in Taiwan. Sometimes people may dig the bamboo shoot in the forest. The main fish farms in the reference case are freshwater fish and oyster farming. Most of the industries are the construction industry, with only a few manufacturing industries. For business activities, the merchants of accommodation and catering are more than retail merchants due to the flourishing development of tourism in the reference case.

Human habit settings of the reference case are mainly referred to National Food Consumption Database (Taiwan Food and Drug Administration, 2017) for all kinds of human food ingestion. Human actions in different areas (such as agricultural land and water area) are set by referring to labor statistics (Ministry of Labor, 2017).

Table 4-16: Parameters of geologic units of the reference case.

Geologic unit	SNFD2021 parameter
R0	Regolith Thickness: 5-90 m 70m is recommended in simulation.
R	Granite host rock
F#	Main water-conducting structure
F1	Attitude: N64°E/70°N; width > 150 m 200 m width is recommended in simulation.
F2	Attitude: N80°W/50°S; width 8-15 m 20 m width is recommended in simulation.
R0	Regolith Thickness: 5-90 m 70m is recommended in simulation.

Table 4-17: DFN parameters of the reference case.

Name	SNFD2021 parameter	
Fracture Domain	FDMA	FDMB
	Elevation (depth below surface, m) < 70 m	Elevation (depth below surface, m) > 70 m
Fracture clusters (Pole_Trend, Pole_Plunge)	Cluster 1 = (198, 18), Fish distribution $(\theta, \kappa = 18)$, $P_{32,rel}$=26%	Cluster 1 = (65, 17) , Fish distribution $(\theta, \kappa = 20)$, $P_{32,rel}$=15%
	Cluster 2 = (155, 4), Fish distribution $(\theta, \kappa = 15)$, $P_{32,rel}$=24%	Cluster 2 = (344, 38) , Fish distribution $(\theta, \kappa = 18)$, $P_{32,rel}$=24%
	Cluster 3 = (264, 23), Fish distribution $(\theta, \kappa = 16)$, $P_{32,rel}$=18%	Cluster 3 = (281, 29) , Fish distribution $(\theta, \kappa = 16)$, $P_{32,rel}$=30%
	Cluster 4 = (98, 81), Fish distribution $(\theta, \kappa = 11)$, $P_{32,rel}$=32%	Cluster 4 = (174, 22) , Fish distribution $(\theta, \kappa = 17)$, $P_{32,rel}$=10%
		Cluster 5 = (175, 75) , Fish distribution $(\theta, \kappa = 19)$, $P_{32,rel}$=21%
	Fisher distribution $f(\theta,\ \kappa) = \frac{\kappa sin\theta e^{\kappa cos\vartheta}}{e^{\kappa}-e^{-\kappa}}$; θ is the angular displacement form the mean pole vector κ is a concentration parameter of Fisher distribution	
Fracture intensity	$P_{32} = 2.4$	$P_{32} = 0.3$
	P_{32} =Area of fractures per unit volume of rock mass (volumetric intensity, m^{-1})	
Fracture size	Power law : $k_r = 2.6$, $r_0 = 0.1\ m$, $r_{min} = 4.5\ m$, $r_{max} = 564\ m$	Power law : $k_r = 2.6$, $r_0 = 0.1\ m$, $r_{min} = 4.5\ m$, $r_{max} = 564\ m$
	$P\ (R \geq r) = \left(\frac{r_0}{r}\right)^{k_r}$, $P_{32}(r_{min}, r_{max}) = \frac{[{r_{min}}^{kr-2} - {r_{max}}^{kr-2}]}{{r_0}^{kr-2}} P_{32}(r_0, \infty)$ R is the fracture radius r_0 is the minimum radius value r is any fracture radius between r_0 and ∞ k_r is the exponent of fractal dimension, or the “fracture radius scaling exponent” (La Pointe, 2002). $P\ (R \geq r)$ is the probability that a circular-shape fracture with a radius greater than or equal to r $P_{32}(r_{min}, r_{max})$ is the volumetric fracture intensity corrected with determined fracture radius between r_{min} and r_{max}	
Fracture location	Stationary random (Poisson) process	Stationary random (Poisson) process
Fracture Transmissivity $(T, m^2/s)$	$T = 1.51 \times 10^{-7} \times (L^{0.7})$; $L = \sqrt{(\pi r^2)}$	$T = 3.98 \times 10^{-10} \times (L^{0.5})$; $L = \sqrt{(\pi r^2)}$

Name	SNFD2021 parameter	
	L is the equivalent size (m) of a square fracture.	L is the equivalent size (m) of a square fracture.
Fracture Aperture (e, m)	$e = 0.5\sqrt{T}$	$e = 0.5\sqrt{T}$
Source	SNFD-SKBI-PL2015-1023; Vidstrand et al., 2010	SNFD-SKBI-PL2015-1023; Vidstrand et al., 2010

Table 4-18: Thermal properties and mechanical properties of the reference case.

Name	SNFD2021 parameter				
Unit ID	R0	R	F1	F2	D
Heat conductivity $(W/(m \cdot K))$	2.0	2.3-3.0	2.0	2.0	2.3-3.0
Specific heat $(J/(kg \cdot K))$	800	730-903	800	800	730-903
Thermal expansion coefficient $(1/K)$	8.0e-06	8.0e-06	8.0e-06	8.0e-06	8.0e-06
Dry density (kg/m^3)	2000	2610-2770	2600	2600	2740-2750
Specific gravity	-	2.63-2.79	-	-	2.76
Saturated density (kg/m^3)	-	2620-2780	-	-	2750
Porosity (%)	-	0.34-0.77	-	-	0.60-0.77
Water adsorption (%)	-	0.12-0.28	-	-	0.22-0.28
Uniaxial compressive strength (MPa)	-	75.68-168.66	-	-	51.51to 92.47
Cohesion (MPa)	-	17.99-29.51	-	-	22.75
Friction angle (degree)	-	47.90-59.08	-	-	56
Tensile strength (MPa)	-	6.91-14.06	-	-	7.37
Secant Young's modulus (GPa)	-	31.70-51.77	-	-	25.52
Secant Poisson's ratio	-	0.11-0.27	-	-	0.15
Dynamic shear modulus (GPa)	-	12.99-29.24	-	-	
Dynamic Young's modulus (GPa)	-	30.28-73.60	-	-	26.50 - 33.10
Dynamic Poisson's ratio	-	0.10-0.27	-	-	0.14 - 0.24
In-situ stress (MPa) (HF@306m)	-	σ_v=8.11	-	-	-
	-	σ_H=10.68	-	-	-
	-	σ_h=5.75	-	-	-
In-situ stress (MPa) (HF@430m)	-	σ_v=11.40	-	-	-
	-	σ_H=14.43	-	-	-
	-	σ_h=9.38	-	-	-
In-situ stress (MPa) (HTPF@300m)	-	σ_1=10.29-12.34	-	-	-
	-	σ_2=6.66-8.62	-	-	-
	-	σ_3=0.76-2.14	-	-	-

Table 4-19: Hydraulic characteristics of the reference case.

Name		SNFD2021 parameter
Hydraulic conductivity (m/s)	R0	5.0×10^{-6}-1.0$\times 10^{-4}$
	R	4.1×10^{-12}-1.0$\times 10^{-9}$
	F1	3.0×10^{-8}-1.0$\times 10^{-4}$
	F2	3.0×10^{-8}-1.0 $\times 10^{-4}$
	D	4.1×10^{-12}-1.0 $\times 10^{-9}$

Effective porosity (%)	F1	0.01
	F2	0.007-0.015
Effective velocity (m/s)	F1	2.0×10^{-5}
	F2	1.3×10^{-4}-2.9×10^{-4}
Mechanic dispersion coefficient (m^2/s)	F1	2.0×10^{3}
	F2	2.9×10^{-5}-1.0×10^{-2}
Hydraulic dispersivity (m)	F1	100
	F2	0.1-75
Peclet number (P_e)	F1	10
	F2	8-1,350
Tortuosity (travel length/distance)	F1	6
	F2	35

Table 4-20: Composition of groundwater of the reference case.

Name	**SNFD2021 parameter**				
Average Groundwater Quality				**Average Surface Water**	
	Reference Case			**River (global)**	**Sea (global)**
Depth (m)	300 to 400m*	400 to 500m**	300 to 500m***	surface	surface
pH	7.67	8.98	8.60		7.5~(8.2)~8.4
pe	-3.10	-6.79	-5.73		
T(℃)	28.80	31.70	30.87	25	15
EC (mS/cm)	0.407	0.320	0.345	~0.1	~42.9
Cl_tot (mol/L)	1.29e-03	8.55e-04	9.77e-04	2.20e-04	5.46e-01
C_tot (mol/L)	1.32e-03	1.15e-03	1.21e-03	8.52e-04	2.33e-03
S_tot (mol/L)	1.30e-04	9.59e-05	1.05e-04	1.15e-04	2.82e-02
N_tot (mol/L)	2.12e-05	4.03e-05	3.35e-05		1.07e-02
P_tot (mol/L)	1.63e-06	2.05e-06	1.88e-06	6.46e-07	2.00e-06
B_tot (mol/L)				9.25e-07	4.16e-04
Si_tot (mol/L)	1.18e-03	6.90e-04	8.31e-04	2.31e-04	7.94e-05
F_tot (mol/L)	1.19e-04	2.11e-04	1.85e-04	5.26e-08	6.84e-05
Br_tot (mol/L)				2.50e-07	8.42e-04
I_tot (mol/L)				5.51e-08	5.01e-07
Na_tot (mol/L)	1.29e-03	1.68e-03	1.57e-03	2.74e-04	4.68e-01
K_tot (mol/L)	1.48e-04	6.98e-05	9.22e-05	5.88e-05	1.02e-02
Ca_tot (mol/L)	6.18e-04	2.79e-04	3.76e-04	3.74e-04	1.03e-02
Mg_tot (mol/L)	1.30e-04	2.00e-05	6.38e-05	1.69e-04	5.31e-02
Al_tot (mol/L)				1.85e-06	7.94e-08
Fe_tot (mol/L)	1.37e-05	5.18e-06	7.62e-06	7.16e-07	3.16e-08
Cu_tot (mol/L)	1.18e-07	2.76e-07	2.37e-07	1.10e-07	7.94e-09
Mn_tot (mol/L)	3.90e-06	9.60e-07	1.94e-06	1.27e-07	3.98e-09
Zn_tot (mol/L)	7.22e-06	1.17e-06	2.90e-06	3.06e-07	
Cd_tot (mol/L)	ND	3.11e-08	3.11e-08	8.89e-11	
Cr_tot (mol/L)	1.92e-08	2.50e-07	1.35e-07	1.92e-08	6.31e-09
Ni_tot (mol/L)	5.59e-05	3.30e-05	4.07e-05	5.11e-09	2.51e-08
Pb_tot (mol/L)	1.25e-07	1.57e-07	1.46e-07		
As_tot (mol/L)	ND	1.00e-08	1.00e-08	2.67e-08	5.01e-08
U_tot (mol/L)				1.68e-10	1.99e-10
Salinity (‰)	0.279	0.208	0.228		
Ionic strength (mol/L)	8.24e-03	5.92e-03	6.64e-03	3.77e-03	7.06e-01

Note:* Average data from KMBH01-W2 and KMBH04-W3.
** Average data from KMBH01-W3, KMBH01-W4, KMBH04-W4, KMBH06-W3 and KMBH06-W3A.

*** Average data from KMBH01-W2, KMBH01-W3, KMBH01-W4, KMBH04-W3, KMBH04-W4, KMBH06-W3and KMBH06-W3A.

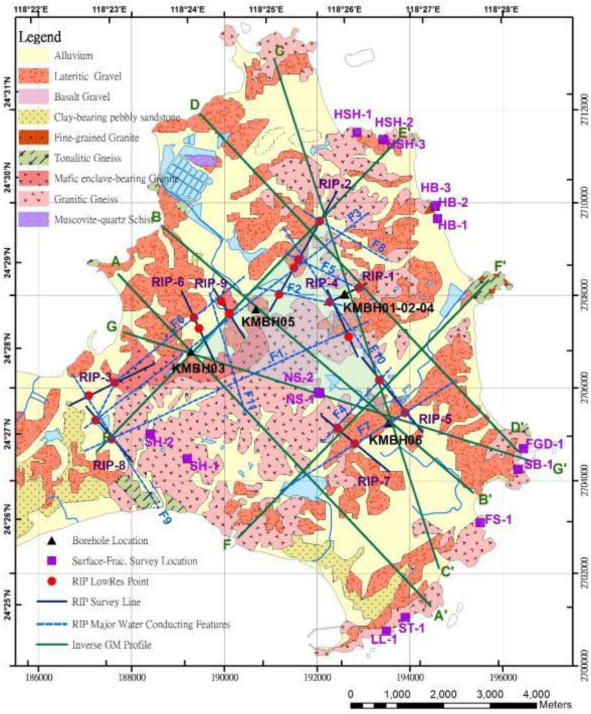

Figure 4-20: The geological map and borehole location in one of the granitic area in Taiwan.

Reference: 台灣電力公司 (2017).

Note: The black triangles represent the borehole locations. The purple squares represent the ground-surface fracture survey locations. The blue lines represent the resistivity inversion profile. The green lines represent gravity and magnetic inversion profile.

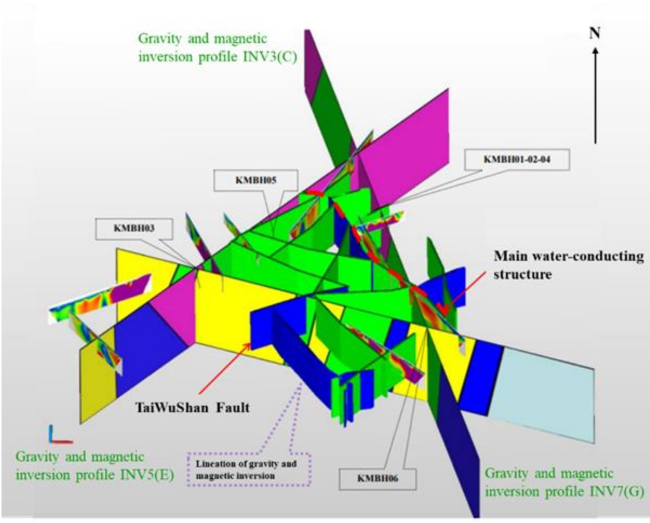

Figure 4-21: Comprehensive analysis map of geophysical survey in one of the granitic area in Taiwan.

Reference: 台電公司 (2011).

Note: KMBH represents the location of drilling. Shallow profiles are the results of electrical resistivity survey (500 m deep). Other profiles are the results of gravity and magnetic inversion (2 km deep).

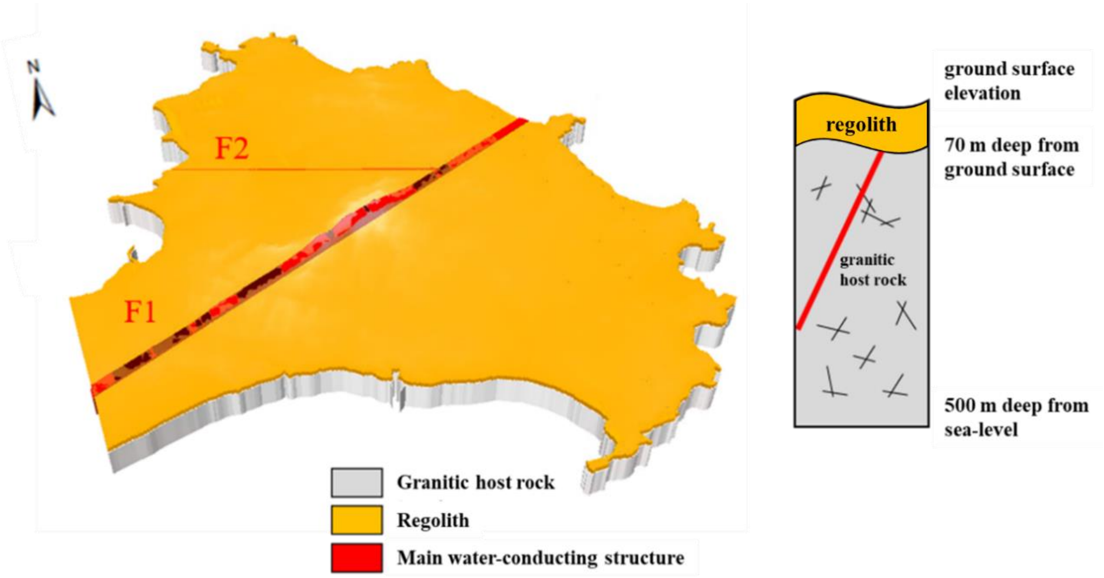

Figure 4-22: Three dimensional distribution of geologic units in the reference case and schematic profile.

Note: F1 and F2 structure are not active faults.

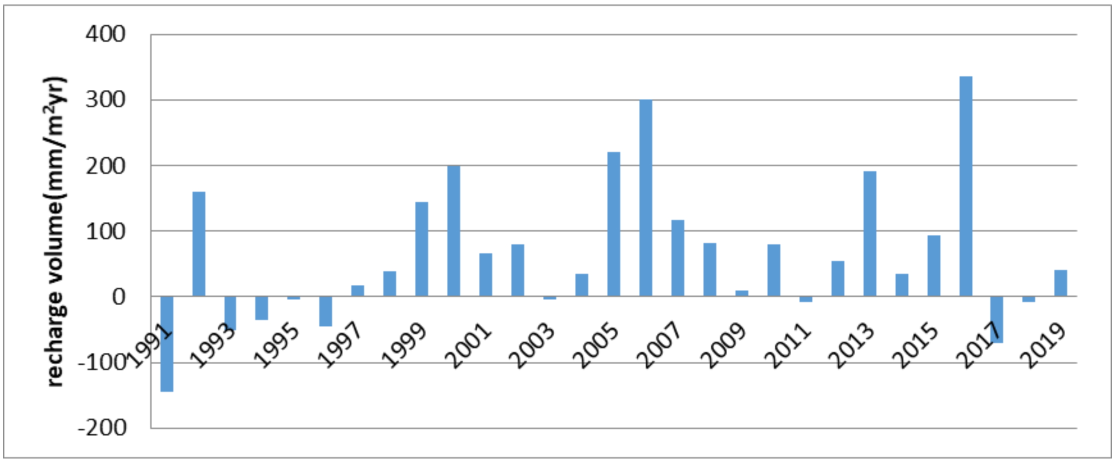

Figure 4-23: Recharge volume from 1991 to 2019 of the reference case.

4.4. Layout of the Repository

4.4.1. Methodology

The repository layout should adapt to the characteristics of the reference case, such as geological structure, rock volume, in situ stress and groundwater flow field, etc. Also, the design layout should incorporate the number of canisters, repository depth, thermal dimensioning, extended full perimeter criterion and required rock volume. Besides, the feasibility and economic efficiency of construction should take into account as well. In other words, the design layout has to integrate the complex adaptation issues between overall requirements and site condition. Therefore, an iterative and stepwise process is proposed. For the preliminary repository layout, the consideration of each factors is illustrated as follows:

(1) Geological structure:

No deposition holes would be located within 100 m from the deformation zones which have trace lengths larger than 3 km (SKB, 2009b).

(2) In situ stress:

The disposal tunnels should be aligned parallel or sub-parallel (±30°) to the maximum horizontal stress to minimize the stress magnitude concentration on the disposal tunnels and deposition holes (SKB, 2009b).

(3) Thermal dimensioning:

Thermal dimensioning is the distance between centers of two deposition holes. Temperature of the buffer needs to be less than 100 °C to meet the requirements of the engineered barriers (Section 4.2.5). Note that the criteria is valid from the present Swedish situation, but there is definitely room for other perspectives. Allowing higher temperatures could have significant economic and technical value. According to the assumption of homogeneous heat transport properties of rock, and parameters of initial power, thermal conductivity and heat capacity, host rock temperature at mid-height of canister in specific thermal dimensioning caused by decay heat was calculated with proper temperature surplus (SKB, 2009c). The temperature changes of the bentonite on the top of the canister were also calculated (SKB, 2009c). Then the highest bentonite temperature on the top of the canister can be calculated with the information. Since the top of the canister directly contacts the bentonite, the highest temperature tends to distribute in this area (SKB, 2009c). (Figure 4-24).

Thermal dimensioning should be well arranged to meet the requirements of temperature under 100° C.

(4) Intersected deposition hole rejection criteria:

In order to prevent shear failure of the canister caused by the intersection of fracture, the intersected deposition hole rejection criteria was taken into account. In addition, in the stage of repository design, the space of the host rock for the repository needs to be assessed by referring to the number of intersected deposition hole. In this report, whether the place of the deposition hole is suitable for placing the canister is assessed by numerical modelling. 3DEC software is used to implement the relevant assessment of the deposition hole intersected by fracture. In the assessment, the fracture is assumed as an extremely thin circle plane. The intersected logic is assumed within the timescale of safety assessment. Even if the shear displacement occurs on the fracture, the radius of the fracture will not grow longer (Hicks, 2005; Barton, 2013; Kana et al., 1991).

The intersected deposition hole rejection criteria of the assessment are as follows:

(a) FPC (full perimeter criterion):

If a fracture intersects the wall of the disposal tunnel and penetrates the tunnel perimeter completely, and the linear extension of the fracture intersects the canister, the deposition hole will be rejected.

(b) EFPC (extend full perimeter criterion):

Deposition positions being intersected by five continuous fractures are rejected (Figure 4-25).

(5) Hydrogeological conditions:

If the inflow into the deposition hole is too large, the buffer will be lost due to pipe flow erosion, which may affect the long-term safety function of the buffer post-closure. Additionally, the excessive inflow may cause difficulty in tunnel excavation and buffer/backfill placement.

The favorable hydrological condition of the deposition hole is the inflow lower than 0.1 L/min and 1% of the total inflow to the disposal tunnel to reduce the initially deposited buffer is lost due to piping/erosion (SKB, 2010g). The inflow of the deposition hole is modelled in FracMan with a hybrid DFN/ECPM model, see Figure 4-26.

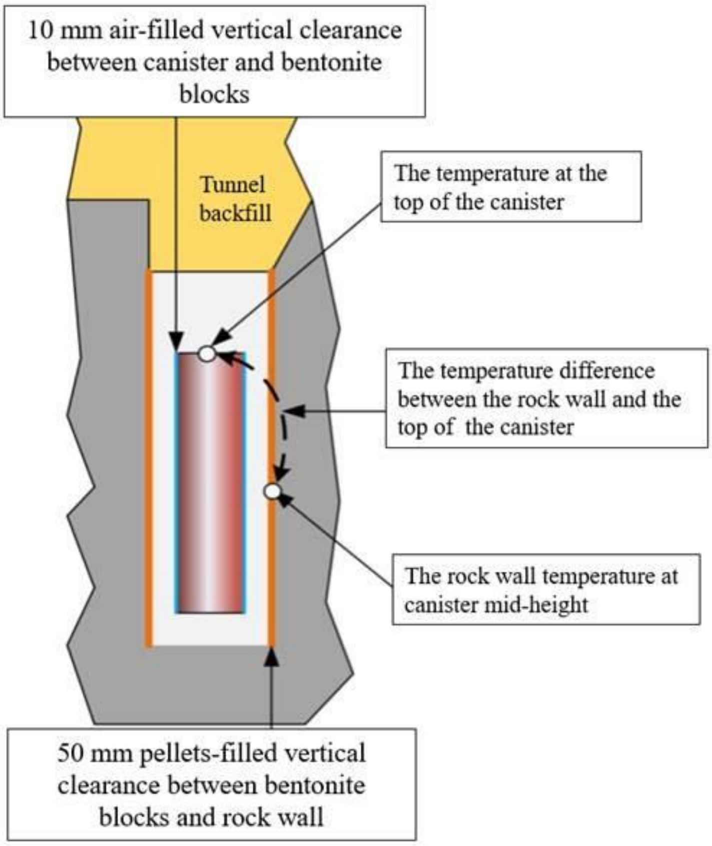

Figure 4-24: Estimation steps of thermal dimensioning.

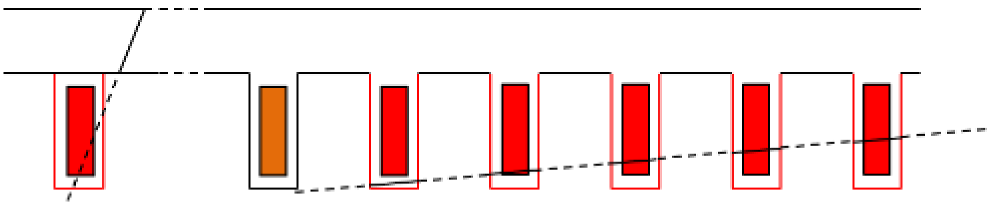

Figure 4-25: Extended Full Perimeter InterSection Criterion (EFPC).

Note: canisters shown in red mean the deposition position rejected. Left hand side shows a deposition position rejected due to FPC prior to excavation. Right hand side shows 5 deposition positions being intersected by a fracture intersecting in a row are rejected post excavation.

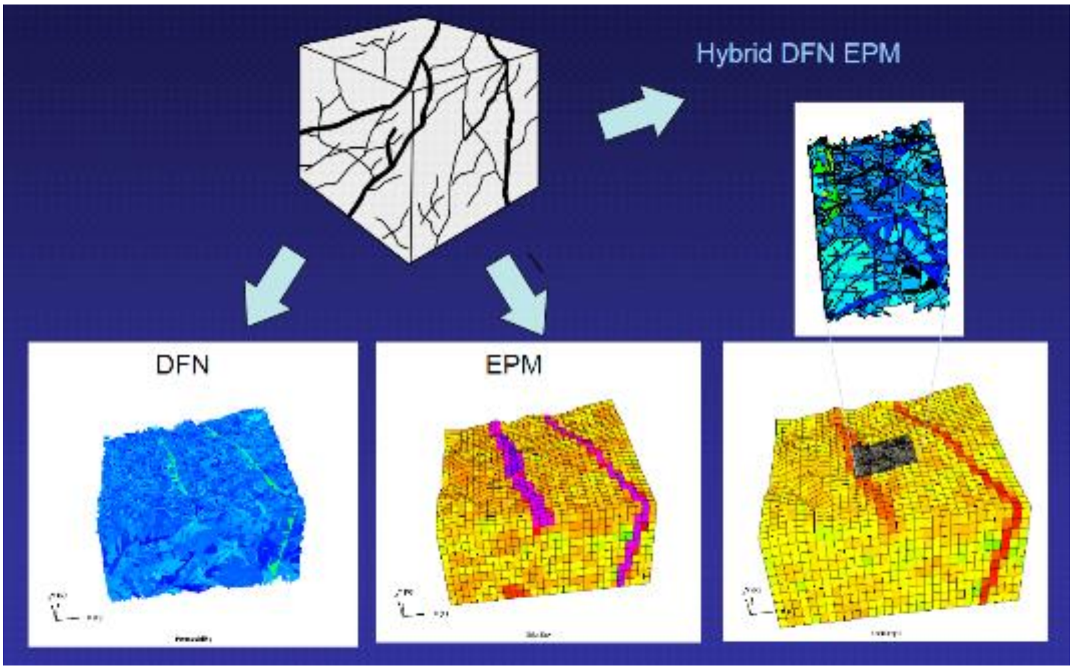

Figure 4-26: Hybrid DFN/ECPM model.
Reference: Golder Associates Inc. (2009).

4.4.2. Layout in the Reference Case

According to the methodology in Section 4.4.1, repository layout is configured as follows:

(1) According to in situ stress of the reference case (Table 4-21), the acceptable trend of disposal tunnels should be aligned within azimuth 74° to 134°, hence the trend of disposal tunnels is aligned to azimuth 120°.

(2) The relation between bentonite maximum temperature at the canister top and thermal dimensioning is shown in Figure 4-27 with surface temperature 23.8 °C, thermal gradient 0.019 °C/m, initial power of canister 1,200 W, thermal conductivity of rock 2.3 $W/(m \cdot K)$, heat capacity of rock $2.152 \times 10^6 J/(m^3 \cdot K)$ and 8 °C margin (SKB, 2009c).

The center-to-center spacing for the disposal tunnels was set to 40 m, and the center-to-center spacing for the deposition holes was set to 9 m.

Considering the issues mentioned above, a reference design layout was developed; see Figure 4-28 and Figure 4-29. The repository depth of 500 m established for the reference design is based on thermal and chemical conditions (for the most part of the area, deep groundwater in the reference case is in a reducing environment (Eh <0 mV) as the depth is below 400 m). The diameter of the deposition hole is 1,750 mm and the height is 8,155 mm. The height of the disposal tunnel is 4,800 mm and the width is 4,200 mm. The height of the main tunnel is 7 m and the width is 10 m. The first deposition-hole position is at least 20.6 m from the entrance of the disposal tunnel and the last deposition-hole position will be located at 10 m from the end of the disposal tunnel. There are two panels with 150 m distance (no specific requirements but refer to Posiva (2012) and SKB (2009b)). Each panel contains 52 disposal tunnels. The length of the disposal tunnel is 250 m with 25 deposition holes capacity in the western panel. The length of the disposal tunnel is

300 m with 30 deposition holes capacity in the eastern panel. The layout has a gross capacity of 2,860 deposition-hole positions, which provides approximately 11% for a loss of deposition-hole positions with respect to the 2,571 canisters required.

Based on the resampling of 2,000 DFN realizations of EFPC analysis for the single disposal tunnel model, the mean value of loss of deposition-hole positions is 4.2% and the standard deviation is 0.7% for 104 disposal tunnels. Also, the distribution approximates Gaussian distribution. The design of deposition hole capacity is expected to be sufficient to accommodate the canisters needed.

The required footprint area of the repository is around 1 km^2 using the following formula (SKB, 2004):

$$A = N_d \times A_s \tag{4- 3}$$

where,

A=Footprint area of repository [m^2]

N_d=Number of canisters

A_s= Preliminary specific area required for each deposition hole [m^2]

The design of repository access consists of a ramp and four shafts. The shafts are vertical underground openings with diameters of 3.5 m to 5.5 m. The skip shaft is the shaft that connects the skip hall of the central area with the inner operation area of the surface facility. The elevator shaft provides space for elevators for transport between the surface facility and the central area. The basic function of the central area is to supply openings for the operation and maintenance of the deposition work and the rockwork activities. Also, there are one supply airshaft and one exhaust airshaft.

The ramp, a 6 m high 5.5 m wide tunnel, is to provide a transport route for machines or waste. Two alternative designs of the ramp system are considered currently.

(1) Bypass Layout: According to the plan, ramps with slopes of 5% as the slope ratio are to be added. The slope of the turning lane is to be horizontal to provide the buffer space for the deceleration of transportation vehicles, so the risk of transportation of machinery will be reduced. The safety shoulders can be potentially added to the tunnels. The total length of the ramp tunnel is about 14 km and reaches a disposal depth of 500 m.

(2) Local Layout: The second design aims mainly to lower the total excavated volume. The slope ratio of the ramps is increased to 8%. The total length of the tunnel can be reduced, but as it certainly saves on the construction cost, the risks associated with vehicle transportation increase as the ramp slope becomes steeper.

Table 4-21: In-situ stress of the reference case.

KMBH01 Depth(m)	σ_v (MPa)	σ_h (MPa)	σ_H (MPa)	σ_H direction	$\frac{\sigma_{Ha}}{\sigma_v}$
175	4.64	4.58	8.29	N55.9°W	1.39
238	6.31	4.54	8.41	N58.2°W	1.03
306	8.11	5.73	10.68	N53.6°W	1.01
430	11.40	9.38	14.43	N76.4°W	1.04

Reference: Yang et al. (2003).
Note: σ_V is vertical stress: σ_H is maximum horizontal stress. σ_h is minimum horizontal stress. σ_{Ha} is the average of σ_H and σ_h.

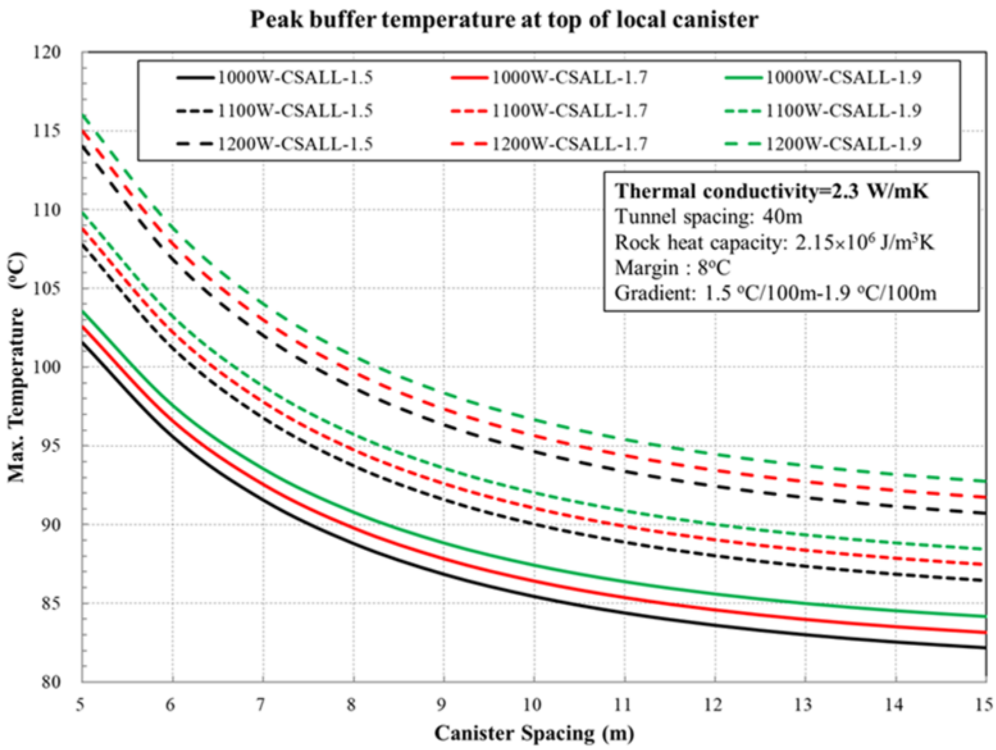

Figure 4-27: Maximum temperature in the buffer versus canister spacing under different geothermal gradient and different initial power output.

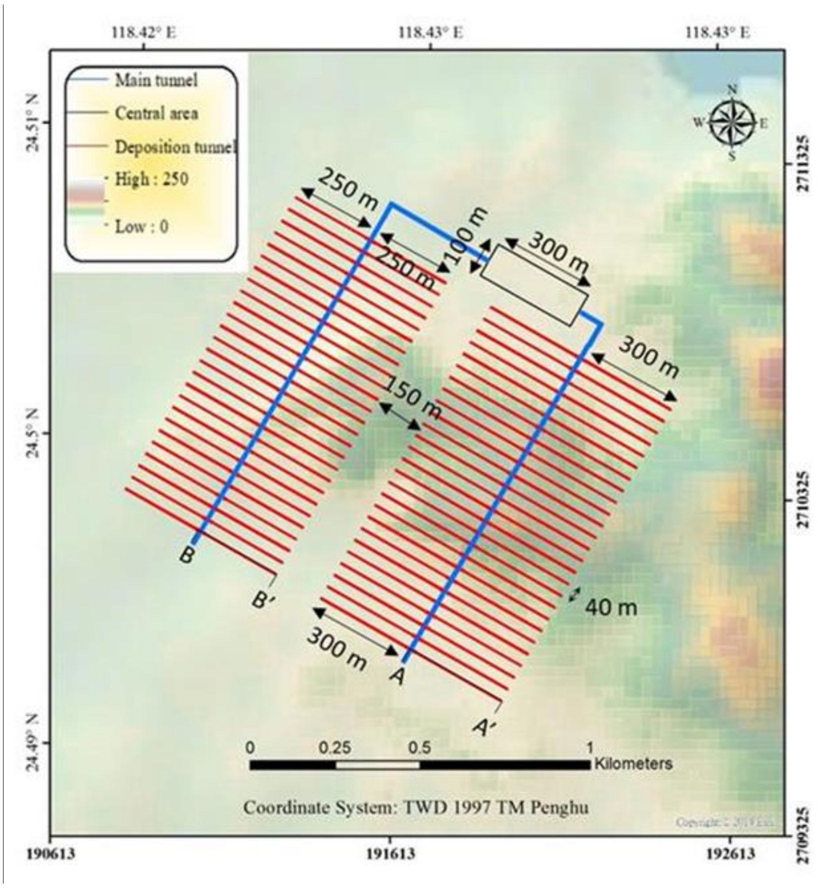

Figure 4-28: Layout of the underground facility.

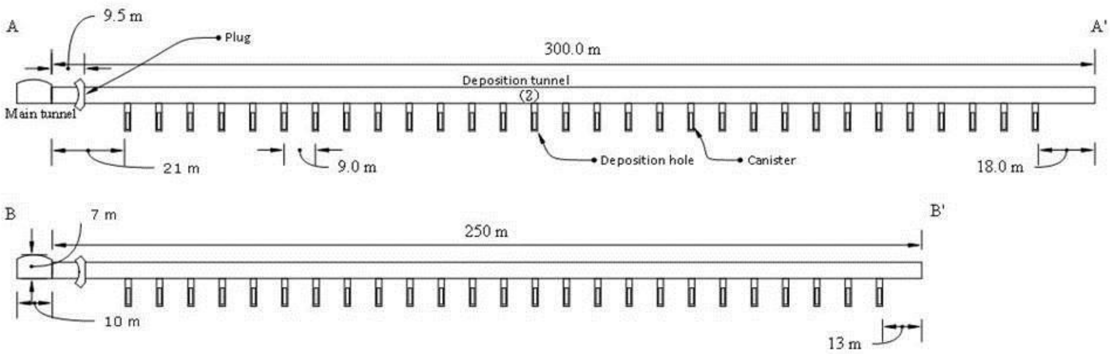

Figure 4-29: Layout of deposition holes in the disposal tunnel.

4.5. Monitoring

The excavation, construction, operation, and closure of the repository will disturb and affect its surroundings, and the safety of the repository needs monitoring. According to the results of the implementation and monitoring of all stages, monitoring measures are adjusted if necessary. In addition, the monitoring plan should be included as part of the management plan, and regular technical reviews should also be conducted.

The monitoring items of each stage are shown in Table 4-22.

Table 4-22: Main monitoring items at each stage.

Management component		**Characteristics of the study area**	**Construction**	**Operation**		**Closure**	**Closed**
				Engineered barrier system setting	**Disposal main tunnel backfill**	**Connecting tunnel and entrance tunnel backfill**	
(1) Quality control: design, manufacture, installation, construction of the engineered barrier system and the repository	Design factor	Design status of engineered barrier system Buffers phenomenon Saturation of Buffers Corrosion of waste canister	Rock behavior Rock deformation	Rock behavior Rock deformation		Rock behavior Rock deformation	Land control Logo Fence Storage records
			Tunnel support integrity Stress and strain of support and lining, etc.	Tunnel support integrity Stress and strain of support and lining, etc.		Tunnel support integrity Stress and strain of support and lining, etc.	
	Manufacturing, installation and construction	Relevant information and technology of manufacturing, installation and construction required for quality control of engineered barrier system (obtained by verification and experiment)	Grouting Material control, etc.	Grouting Material control, etc.	Tunnel backfill Backfill density, etc.	Tunnel backfill Backfill density, etc.	
		-	Tunnel excavation Quality control of support materials, etc.	Engineered barrier system manufacturing Buffer density, etc.	Plug Material quality control, etc.	Plug Material quality control, etc.	
(2) Monitoring of geological conditions around the engineered	Disposal of tunnel surroundings	Hydrogeology Groundwater Grouting pressure, etc.	Hydrogeology Groundwater Grouting pressure, etc.	Hydrogeology Groundwater Grouting pressure, etc.		Hydrogeology Groundwater Grouting pressure, etc.	

barrier system and the repository		Geochemistry pH value, Eh value, etc.	Geochemistry pH value, Eh value, etc.	Geochemistry pH value, Eh value, etc.	Geochemistry pH value, Eh value, etc.	
		Geology Geothermal gradient, etc.	Geology Geothermal gradient, etc.	Geology Geothermal gradient, etc.	Geology Geothermal gradient, etc.	
(3) Environmental management of the repository	Surface water quality Environmental radiation, etc.	Surface water quality Environmental radiation, etc.	Surface water quality Environmental radiation, etc.	Surface water quality Environmental radiation, etc.	Surface water quality Environmental radiation, etc.	
(4) Staff protection surveillance	Temperature, humidity, gas, etc.	Temperature, humidity, gas, etc.	Temperature, humidity, gas, etc.	Temperature, humidity, gas, etc.	Temperature, humidity, gas, etc.	
(5) Nuclear protection of the repository	Human actions	-	-	Human actions	Plug, fences, etc.	-

5. External Factors

5.1. Introduction

In order to evaluate the safety of the repository under long-term evolution, it is necessary to consider the impact of external factors on the long-term function of the repository. External factors are classified into three issues, which are climate, tectonic evolution, and future human actions.

The following statement will discuss the possible evolution of these three topics. The possible impact of the evolution of external factors on the repository will be evaluated based on relevant references, research results and interpretations in the expert conference.

5.2. Climate

5.2.1. Climate Evolution

From the Last Glacial Maximum (LGM) to the present, relevant climate evolution of the reference case is described below:

(1) LGM period :

Taiwan is located in a subtropical region. However, during the LGM glacial period, glaciers may cover mountains with an altitude of more than 3,300 m, while the low-altitude surface will not be affected.

The dry and cold air caused the surface seawater temperature to be 3.5 ℃ to 6 ℃ lower than the current level (Hsieh et al., 1996), and the ground temperature was 8 ℃ to 9 ℃ lower than the current level, and the annual rainfall was about half of current level (Liu, 2003). In addition, the global sea-level was about 120 m lower than it is today (Rohling et al., 1998). The shallow sea shelf of the Taiwan Strait had become a land bridge connecting the Asian continent, and the coastline near Taiwan may move south to the south of Penghu (Murray-Wallace and Woodroffe, 2014).

(2) After LGM :

After LGM, rising global temperatures caused sea-levels to rise, and the coastline moved towards the land, and the land bridge that originally connected the Asian continent was gradually submerged by the sea. As follow:

(a) From 20,000 years ago to 15,000 years ago: the sea-level rose at a rate of about 6 m per thousand years, which is relatively slow.

(b) From 15,000 years ago to 10,000 years ago: the sea-level rose at a rate of approximately 10 m per thousand years (台電公司, 2019a).

(c) About 10,000 years ago: the topography of the strait was the same as today. The glaciers in the high mountains of Taiwan's main island disappeared, leaving the remains of the glaciers (Siame et al., 2007).

(d) From 10,000 years ago to 6,000 years ago: the climate gradually stabilized, and the sea-level reached its highest point, which was about 10 m higher than today (IPCC, 2013). The coastal plains around Taiwan Island were submerged by sea water, and the coastline was located at the front edge of the foothills and hilly land today.

(e) From 6,000 years ago to the present: the sea-level no longer rose, and rivers carried a large amount of sediment and accumulate on the coast, gradually expanding into the western coastal plain.

Climate evolution is a periodic cycle. Based on the last ice age and the Holocene glacial period (from 120,000 years ago to the present), a glacial period is 120,000 years, and the cycle is repeated. By referring to related research (TraCE-21ka, 2011), the basic climate evolution under the million years safety assessment scale is presented below (Figure 5-1):

(1) Present: it belongs to a subtropical climate, with an average temperature of 23.8°C, and an average annual rainfall of 1,100 mm.

(2) After 16,700 years: it can be corresponded to the climate condition 8,550 years ago. The average temperature will be 18.96℃, and the average annual rainfall will be 1,200 mm. The climate type will still be a subtropical climate. The sea-level will be about 20 m lower than the present.

(3) After 33,300 years: it can be corresponded to the climate condition 11,000 years ago. The average temperature will be 19.21℃, and the average annual rainfall will be 800 mm. The climate pattern will change to a temperate climate. The sea-level will be about 40 m lower than the present.

(4) After 50,000 years: it can be corresponded to the climate condition 11,700 years ago. The average temperature will be 18.76℃, and the average annual rainfall will be 800 mm. The climate pattern will be temperate. The sea-level will be about 60 m lower than the present.

(5) After 66,700 years: it can be corresponded to the climate condition 15,300 years ago. The average temperature will be 17.86℃, and the average annual rainfall will be 984.23 mm. The climate pattern will be temperate. The sea-level will be about 80 m lower than the present.

(6) After 83,300 years: it can be corresponded to the climate condition 19,991 years ago. The average temperature will be 17.88℃, and the average annual rainfall will be 962.29 mm. The climate pattern will be temperate. The sea-level will be about 100 m lower than the present.

(7) After 100,000 years: it can be corresponded to the climate condition 22,000 years ago. The average temperature will be 17.72℃, and the average annual rainfall will be 974.28 mm. The climate pattern will be temperate. The sea-level will be about 120 m lower than the present.

(8) After 120,000 years: it can be corresponded to the present climate condition.The average temperature will be 23.8℃, and the average annual rainfall will be 1,645.43 mm. The climate pattern will revert to a subtropical climate. The sea-level will be the same as the current height.

Due to the low latitude of the reference case, there will still be a temperate climate during the glacial period, and there should be no long-term frozen glaciers on the surface.

According to the long-term average temperature observation data of the Intergovernmental Panel on Climate Change 5th assessment report, the global surface temperature increased by 0.85°C between 1880 and 2012 (IPCC, 2013). In addition, it was affected in 2014 and 2016. In 2014 and 2015, the global surface temperature also increased significantly due to the influence of the El Niño phenomenon. IPCC's 5th assessment report will use the representative concentration pathway (RCP) to evaluate the possible degree of global climate warming in the future. The results show that under the most severe warming situation (RCP 8.5), the global surface temperature at the end of the 21st century may be 3.7°C higher than that between 1986 and 2005. In the case of moderate emissions of warming (RCP 4.5), the global surface temperature at the end of the 21st century may increase by 1.8°C from 1986 to 2005 (Figure 5-2) (IPCC, 2013).

The IPCC s published the latest 6th assessment report in 2021 (IPCC, 2021), which indicated that global temperature in the first two decades of the 21st century (2001-2020) was 0.99℃ higher than 1850-1900. In addition, under the affection of the El Niño phenomenon from 2014 to 2016, global temperature increased dramatically in 2014 and 2015. The IPCC 6th assessment report combined Shared Socioeconomic Pathway (SSP) and RCP. The results showed that compared to 1850-1990, the global surface temperature averaged over 2081-2100 is very likely to be higher by 3.3℃ to 5.7℃ under the very high Greenhouse Gas (GHG) emissions scenario (SSP5-8.5) and by 2.1℃ to 3.5℃ in the intermediate GHG emissions scenario (SSP2-4.5) (IPCC, 2021).

According to data from the Central Weather Bureau, the annual temperature in Taiwan has risen by about 1.3 ℃ in the past 100 years (from 1900 to 2017). The temperature rise has accelerated in the past 50 years. This phenomenon of temperature increase has shown a stage with the changes over the years, and there has been a larger increase since 1980 (Figure 5-3).

Therefore, climate warming is also one of the important factors that must be considered in evaluating the climate evolution of the repository. The evolution analysis for possible warming of the repository will be included in the following development of the program.

The evolution of the repository under two different climate evolutions is discussed in Chapter 9:

(1) Basic evolution: in which future climate conditions will evolve according to 120,000-year glacial cycle is described in Section 9.2.

(2) Global warming evolution: in which impact on climate evolution and the repository from greenhouse gases will be discussed is described in Section 9.6.

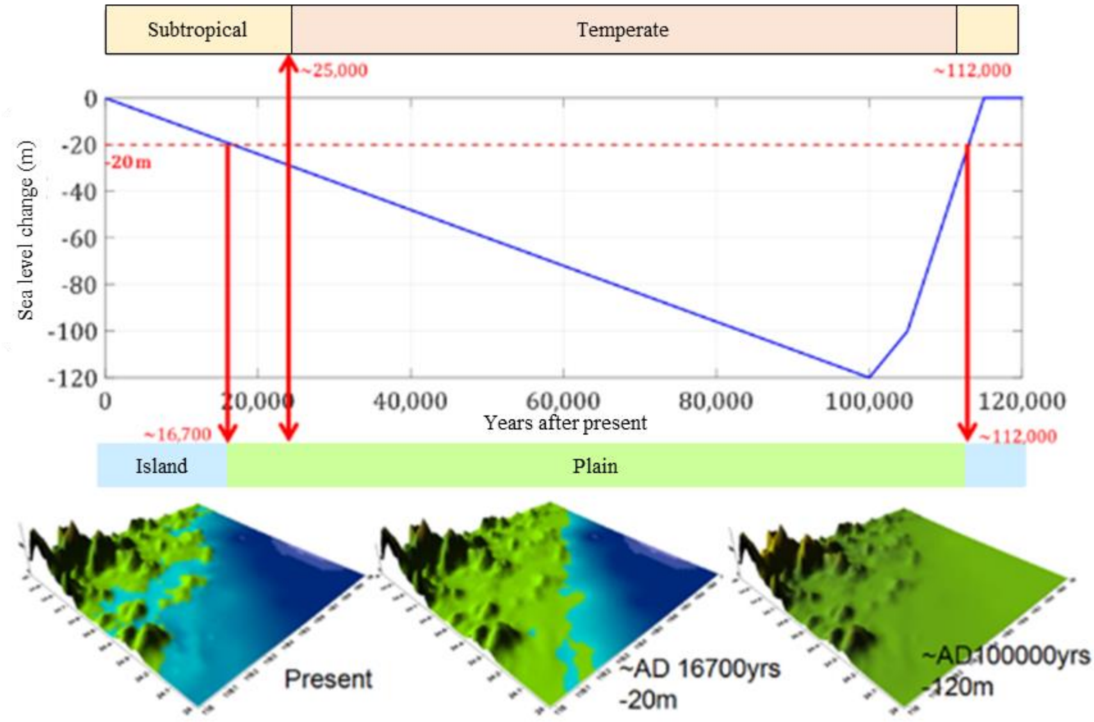

Figure 5-1: Estimated climate evolution and sea-level changes.
Reference: INER (2017b).

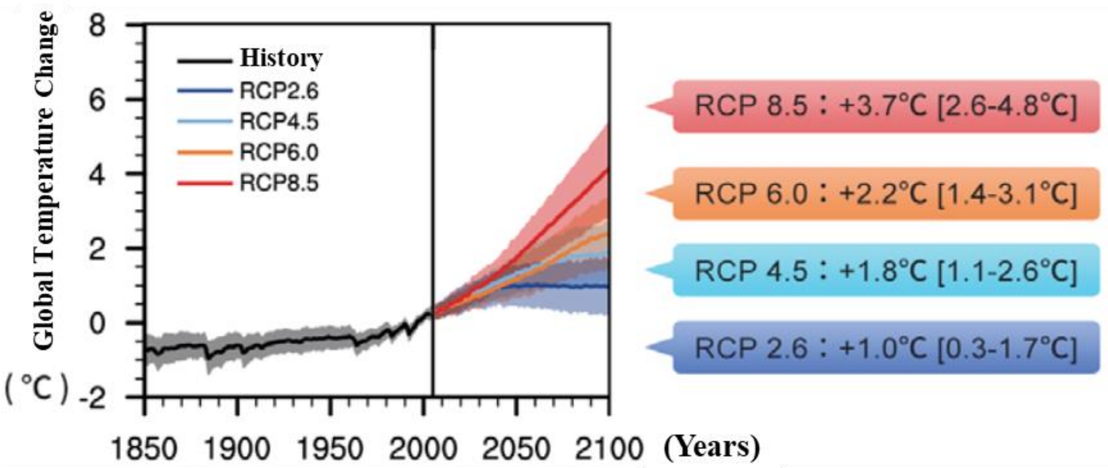

Figure 5-2: Global temperature changes in different RCP scenarios.
Reference: Chen et al. (2018) and Zhou et al. (2017).

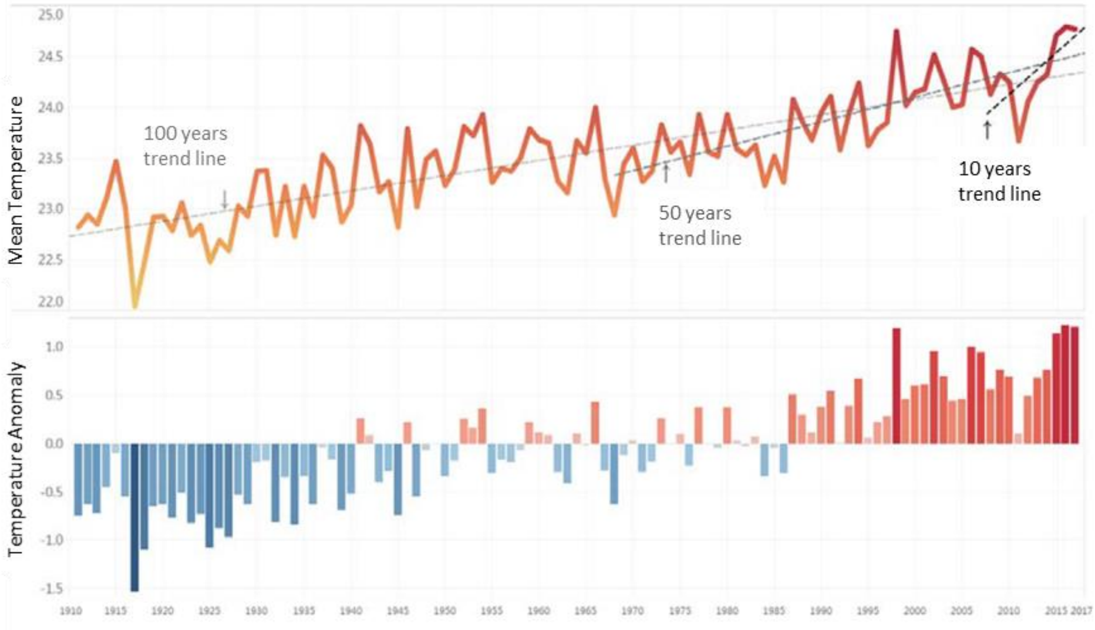

Figure 5-3: Observation data of temperature changes of Taiwan (from 1900 to 2017).
Reference: Chen et al. (2018) and Zhou et al. (2017).

5.2.2. Impact on Safety of the Repository

From the assessment results in Section 5.2.1, for the next 1 million years post-closure, the climate of the reference case will change from subtropical climate to temperate climate and then back to subtropical climate with the glacial cycle. During the glacial cycle, the sea-level will slowly decrease and then rise. The reference case will gradually evolve from an outlying island to a coastal land and then return to an outlying island environment.

The main impact of climate on the safety of the repository is coastline migration. Coastline migration will not only change the surface conditions but also change the underground conditions, resulting in changes in permeability, groundwater pressure, groundwater flow and composition. For the safety of the repository, it is necessary to evaluate the changes in groundwater salinity at the depth of the repository, as well as high groundwater flow and other factors that affect the retardation safety function of the geosphere. In addition, the migration of the coastline may also have an impact on the locations and development of the biosphere objects, which needs to be considered when assessing radionuclide transport in the environmental medium of the landscape .

5.2.3. Uncertainties related to the Long-Term Evolution of the Climate

The long-term climate evolution is complicated and difficult to predict, and the time and extent of the evolution are uncertain. Moreover, the greenhouse gas emissions caused by humans, the duration and the impact on the climate also form uncertainties for climate evolution.

As mentioned in Section 2.7, uncertainty can be divided into: (1) system/scenario uncertainty, (2) concept/model uncertainty, and (3) data uncertainty. The analysis and assessment of long-term climate evolution can be handled in the following ways:

(1) System/scenario uncertainty:

The climate and environmental changes within a reasonable range in the future are considered. For example, future climate change and landscape evolution caused by the total release of different greenhouse gases in the future are under consideration. Relevant uncertainties are combined to define a normal evolution scenario (or so-called expected evolution scenario) as a reference point to develop a conceptual model of quantitative evaluation.

(2) Concept/model uncertainty:

The uncertainty of the climate model itself comes from the equations used in the model. Even though the theoretical basis for describing atmospheric motion is considered mature, many high-order and complex calculations would be ignored in model analysis due to the limitation of computation resources. In addition, the climate model and earth system model are idealized states of the actual climate system. The interactions and feedback mechanisms cannot be reproduced completely. In the process of model integration over time, the errors caused by incomplete calculation will gradually accumulate, and finally, the deviation of the simulation results will be formed, leading to the generation of uncertainty. Different models and observation data can be adopted to verify the result. Meanwhile, assessment models can be developed by multiple people to establish a consensus which may reduce errors caused by the design defects of a single model.

(3) Data uncertainty:

Generally, the data can be analyzed through probability calculation or a combination of variability determination alternative parameter. Some boundary conditions are easily predicted, such as changes in the earth's orbit over time. Some have high uncertainties, such as changes in atmospheric carbon dioxide concentration in the future. Reasonable assumptions are needed in consideration of research in various fields. The long-term evolution of climate focuses on the development of trends rather than decisive forecasts, so the boundary conditions are set within reasonable assumptions.

5.2.4. Documentation

The following are the relevant documentary records of sea-level variations, which can be used as supporting evidence for the analysis of the climate evolution of the repository.

The Antarctic Deep Ice Core of Dome Fuji and Vostok provides information on glacial-interglacial climate change and atmospheric composition (Kawamura et al., 2007), reconstructing the northern hemisphere climate cycle and presenting a table of climate changes over the past 360,000 years. Based on the ratio of oxygen to nitrogen molecules in Antarctica's ice cores, the annual climate change is reconstructed. In line with Milankovitch's climate change theory, the glacial-interglacial cycle is driven by changes in the summer sunshine in the high latitudes of the northern latitude. The change of summer sunshine in the northern hemisphere can examine the climate change in the southern hemisphere during the transition between glacial and interglacial periods.

The sea-level data shows that during the last ice age, about 20,000 years ago, the sea-level dropped by about 120 m (Rohling et al., 1998). In addition, the study of Antarctic ice core data shows that the global sea-level during the last ice age was about 100 m lower than the current one, and the reduction of 120 m to 135 m is a reasonable range (SKB TR-10-49; Yokoyama et al., 2000).

Hsieh et al. (2006) used 29 core data from the western coastal plain in Taiwan. The core contained radiocarbon dating to determine the sea-level of Taiwan from 10,000 years ago to 5,000 years ago. All dates were obtained from coastal sediments, and the deposition location was assumed to be ±3 m at sea-level. The sinking rate of a given sea-level height was calculated with the dating date. The results are as below:

(1) Rapidly ascending from 11,000 years ago to 10,000 years ago (the ascent rate is greater than 13 m ky^{-1}).
(2) About 10,000 years ago to 6,500 years ago, the ascent rate was about 8 m ky^{-1} to 9 m ky^{-1}.
(3) 6,500 years ago or 66,000 years ago, the sea-level approached the current sea-level, and the ascent rate has slowed down.

5.3. Tectonic Evolution

According to the FEPs list of the reference case in Section 3.3, three factors relevant to tectonic evolution could affect the long-term safety of the repository. These factors, including earthquakes, volcanism, and uplift, subsidence and denudation of rocks, will be stated in the following chapters.

5.3.1. Earthquakes

An earthquake is the shaking of the ground induced by the energy released through seismic waves from rock failure. Nature phenomena, such as tectonic and volcanic activities, and meteor impact or human actions (nuclear testing, retaining of reservoir, etc.) could also be the cause of earthquake. Disasters accompanied by earthquakes can be a serious threat to the lives of humankind.

Two factors are considered crucial while evaluating the impact of earthquakes on the long-term safety of the repository. One is the effects of shear displacement, and the other is the effects of ground motions (ground acceleration) caused by seismic wave propagation.

(1) Risk from shear displacement:

(a) When shear displacement occurs within the site, the fracture plane could intersect the repository damaging the engineered barrier system and lowering its safety functions.

(b) While shear failure is adjacent to the site, it could activate the faults and fracture near the repository, and induce displacement or change the flow of the groundwater and the chemical environment.

(2) Risk from ground acceleration:

(a) Ground acceleration could damage the repository in the pre-closure phase while it exceeds the design basis of the facility.

(b) In the post-closure phase, the underground facility of the repository will not have any free surfaces. The scale of the facility is in very small dimensions (meter scale) compared with seismic wavelengths (kilometer scale), and thus the shaking will not have any impact on it (SKB, 2010n).

Since the ground acceleration may deal less risk to the underground facility, and it can be evaluated by seismic hazard analysis, a well-developed procedure has been applied to the nuclear facilities in Taiwan (NCREE, 2018). The main focus will lie on the risk of shear displacement.

IAEA has divided seismic sources into two categories (IAEA, 2010). One is sources with obvious geological structures such as fault sources and subduction interfaces. The other is sources with unknown geological structures, called diffuse seismicity, based on the geological survey nowadays. As mentioned in Section 1.4, active faults (faults with evidence of activity over the last 100,000 years and signs of reactivating in the near future by the definition of the Central Geological Survey) and adjacent geologically sensitive area (GSA) will be avoided while choosing suitable locations for the repository lowering the chances of shear displacement occurred within the site. As for the impact from adjacent shear displacement, it is evaluated by earthquake simulation.

When conducting earthquake simulation, three major parameters, including the geometry, maximum magnitude, and seismicity rate of seismic sources, are considered. According to the geological evolution, the tectonic settings in the reference case will be invariant within 1,000,000 years from now (台電公司, 2018b). The parameters will be derived from current geological and seismic data. And the uncertainties of these parameters will be considered through a logic tree. The geometry, maximum magnitude, and seismicity rate for different types of seismic sources in the reference case are shown as follow:

(1) Fault source:

The active fault near the reference case is Binhai fault (Figure 5-4). Based on the data from previous studies and workshops, the Binhai fault can be divided into two rupture models (Figure 5-5).

(a) Model 1:

The length of the fault is 71 km (Chang et al., 2010), and the dip of the fault plane is 54 degrees toward the east (Cheng et al., 2011; Chu et al., 2005). The seismogenic depth in this region is around 25 km (Zhang, 2020). The maximum magnitude of the Binhai fault can reach Mw 7.3 (Wells and Coppersmith, 1994; Yen and Ma, 2011). Slip rates are 0.02, 0.2, and 0.5 mm/yr.

(b) Model 2:

The length and dip of the fault are 450 km and 60 degrees toward the west, respectively. Three possible seismogenic depths are 10, 15, and 20 km (台電公司, 2018b). The maximum magnitudes evaluated from in-situ stress are Mw 7.93, 8.27, and 8.51. Slip rates are 0.02, 0.2, and 0.5 mm/yr.

(2) Diffuse seismicity:

There are no definite geometries for the rupture plane of diffuse seismicity (or called area sources in probabilistic seismic hazard analysis, PSHA). A boundary where earthquakes within it share similar focal mechanisms, for diffuse seismicity can be defined through geophysical and geological surveys, thus narrowing down the uncertainties of rupture planes. Three boundaries of diffuse seismicity referring to previous studies nearby reference cases are listed below:

(a) A circle with a 200 km radius from the reference case (200 km_radius):

The length of the radius is determined by the distance from the reference case to the deformation front in the Taiwan region. The edge of the circle also coincided with the front of Peikang High and the seismicity distribution in Taiwan (Yu, 1997; Wu and Zhao, 2013; 台電公司, 2017).

(b) AS_K01 and DS_K01:

AK_K01 and DS_K01 are the area sources that cover the Taiwan Strait region. Their boundaries are modified from areal sources proposed in previous seismic hazard analysis for nuclear power plants in the Taiwan (Wen et al., 2011), and the study of design earthquakes in Taiwan Strait region (Chang, 2010).

These boundaries of diffuse seismicity are shown in Figure 5-6. The upper and lower depths of diffuse seismicity are 2 km and 35 km, referring to the depths of areal sources in the past PSHA studies in Taiwan. Since this diffuse seismicity cannot be linked to any known geological structure, a non-surface rupture model is assumed. Based on the assumption and the study from Shimazaki (1986), the maximum magnitude for the diffuse seismicity is set as 6.5. A maximum magnitude of 6.5 also coincided with the observed seismic data within this region after eliminating events related to the Binhai fault (Xu et al., 2006). The seismicity rate of diffuse seismicity in this research is derived by the truncated exponential model (Cornell and Van Marke, 1969). The truncated exponential model (equation 5-1) is based on Gutenberg-Richter's law (Gutenberg and Richter, 1944) by substituting $\dot{N}(m)$, which represents the counts of cumulative annual numbers of earthquakes in certain magnitude, for $N(m)$ and adding an upper limit of magnitude in the original equation.

$$\dot{N}(m) = \dot{N}(m_0)\frac{\exp\left(-\beta(m-m_0)\right) - \exp\left(-\beta(m_u-m_0)\right)}{1.0 - \exp\left(-\beta(m_u-m_0)\right)} \qquad (5\text{-}1)$$

where,

$\beta = b \cdot ln10$. And b is the same as b-value in the Gutenberg-Richter's law. [-].

m_0 is the lower limit of magnitude, [-].

m_u is the upper limit of magnitude, [-].

$\dot{N}(m_0)$ is the seismicity rate for lower magnitude, [-].

Based on the result from the sensitivity study, m_0 will be 3.5. And m_u will be 6.5 as mentioned above. The b-value and $\dot{N}(m_0)$ is derived by the maximum likelihood method using an earthquake catalogue in each boundary of diffuse seismicity, then used to calculate the relationship between cumulative annual earthquake number and magnitude. Based on the results of calculations, the estimated numbers of earthquakes with moment magnitudes of 6.5 in one million years in 200km_radius, AS_K01 and DS_K01 diffuse seismicity boundary are 145 (Figure 5-7), 14 (Figure 5-8) and 6 (Figure 5-9).

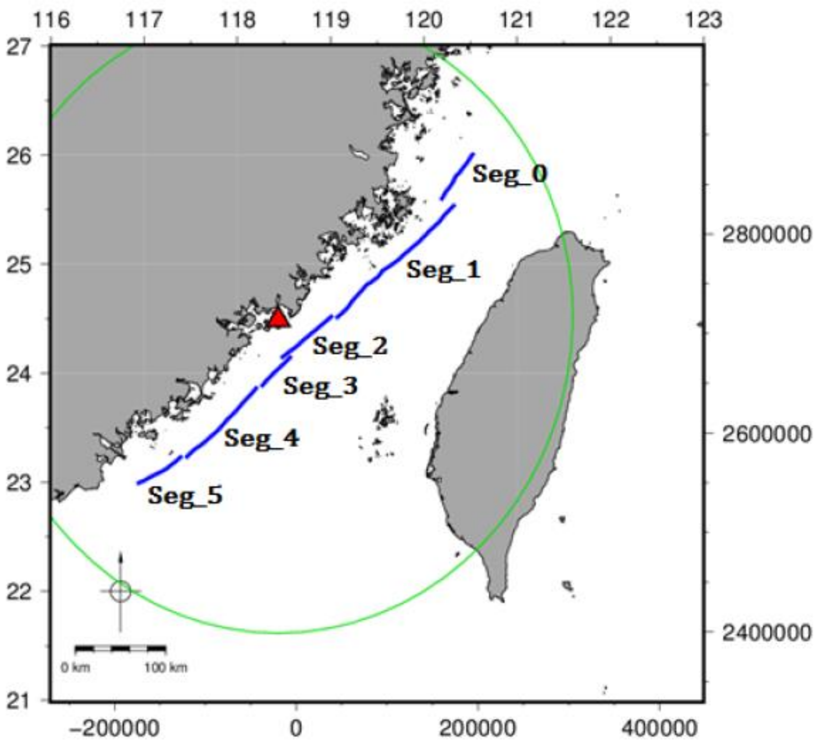

Figure 5-4: Location of Binhai fault (blue line) and reference case (red triangle)

Reference: Pan (2016)

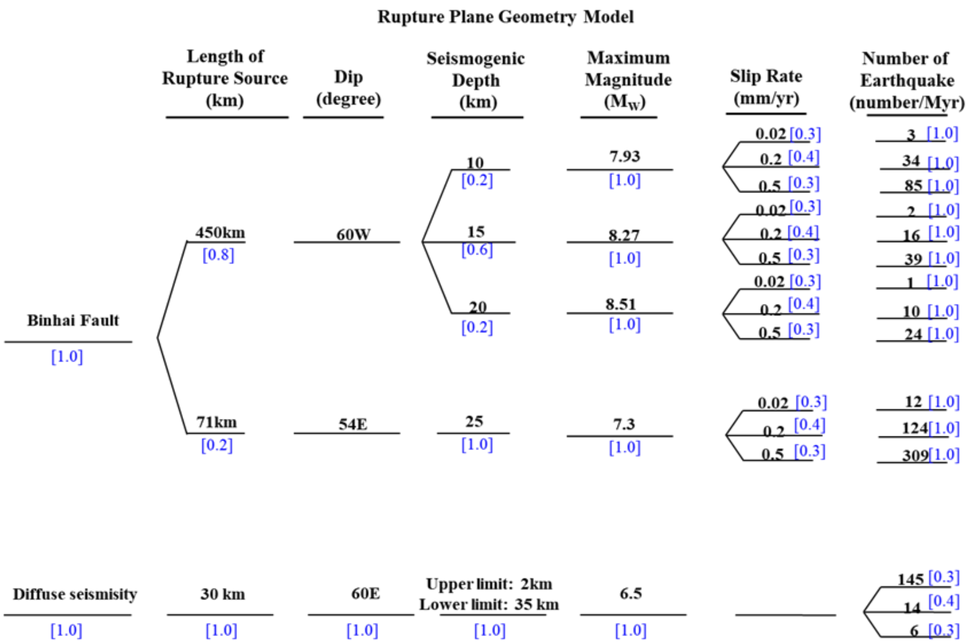

Figure 5-5: Logic tree for seismic hazard analysis.

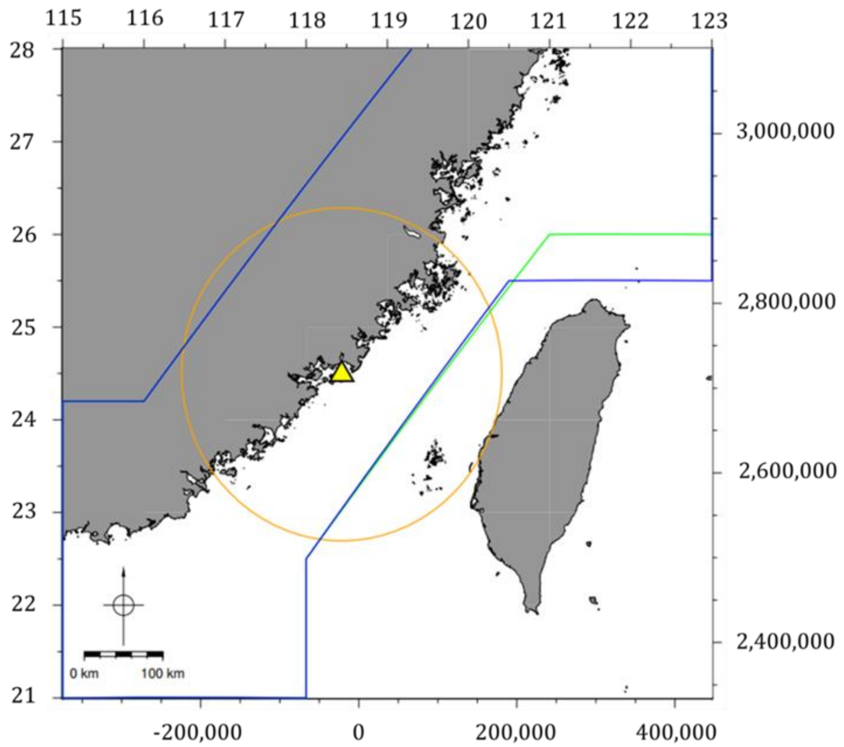

Figure 5-6: Boundaries of the three diffuse seismicity.

Note: the yellow triangle is the location of reference case, the orange circle is the range of 200 km radius from the reference case, the blue line indicates the area of AS_K01, and the green line indicates the area of DS_K01.

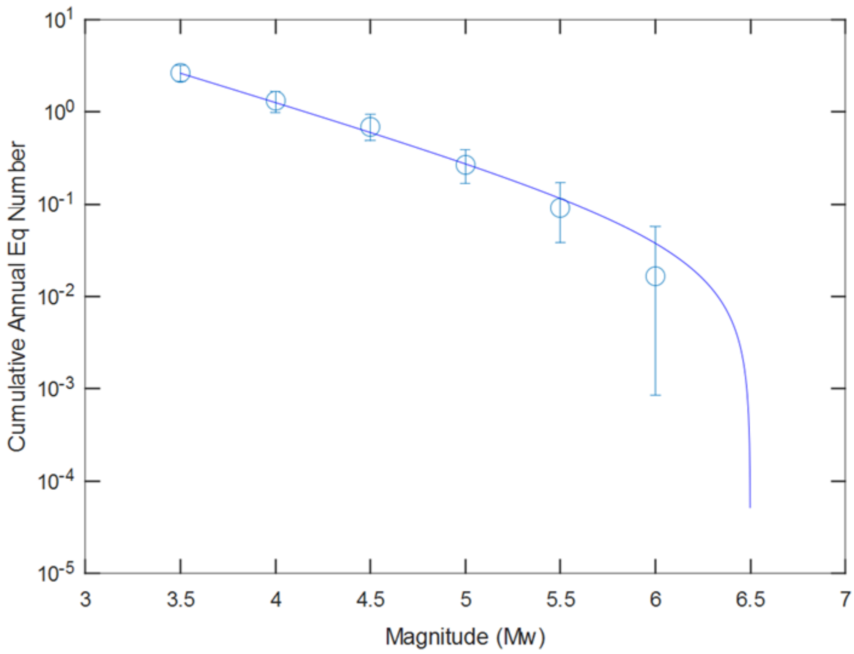

Figure 5-7: Accumulated seismicity rate versus earthquake magnitude within the range of 200 km radius from the reference case.

Note: solid line indicates the estimation results from the truncated exponential model, and circle indicates the observation results. The number of earthquakes in one million year for magnitude 6.5 is 145.

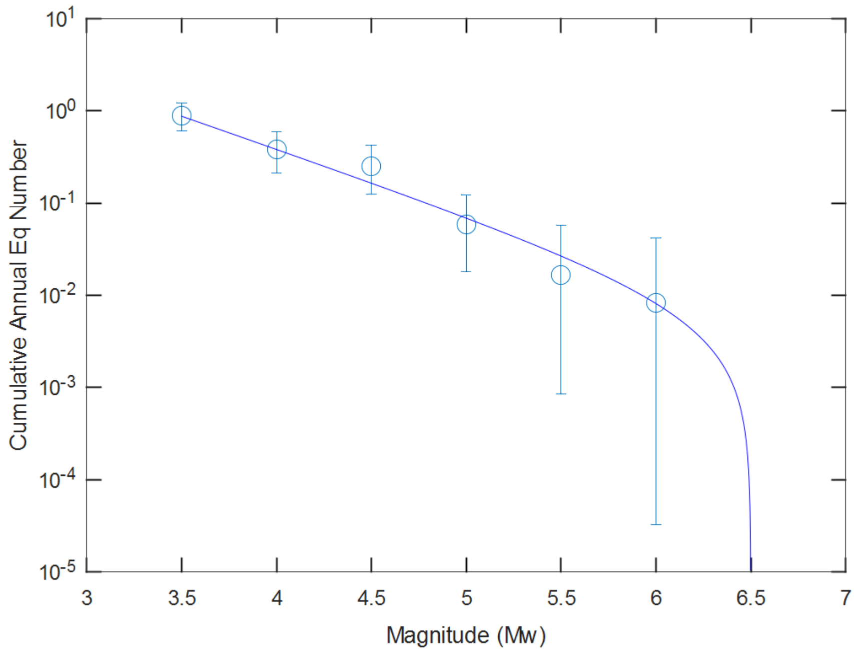

Figure 5-8: Accumulated seismicity rate versus earthquake magnitude within AS_K01 region.

Note: solid line indicates the estimation results from the truncated exponential model, and circle indicates the observation results. The number of earthquakes in one million year for magnitude 6.5 is 14.

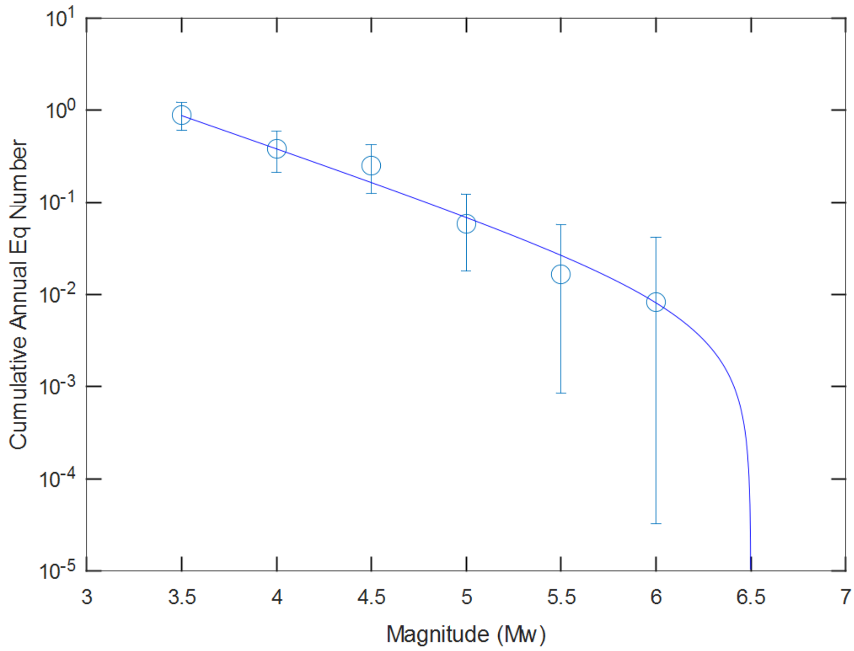

Figure 5-9: Accumulated seismicity rate versus earthquake magnitude within DS_K01 region.

Note: solid line indicates the estimation results from the truncated exponential model, and circle indicates the observation results. The number of earthquakes in one million year for magnitude 6.5 is 6.

5.3.2. Uplifting/Subsidence and Denudation

The uplifting/subsidence and denudation of a rock are determined by the characteristics of the local geological frame and evolution. Taking sea-level as a relative base level, the uplifting or denudation will reduce the disposal depths of radioactive waste, thus shortening the safe distance from it to human habitat and lowering the safety functions, such as isolation, containment, and retardation of the geosphere (Figure 5-10). The uplifting/subsidence and denudation of a rock can also change the characteristics of the flow field and chemical properties of groundwater around the repository, affecting its safety functions and long-term stability. On the other hand, subsidence accompanied by sedimentation will increase the disposal depths of radioactive waste, keeping it away from human habitat.

Taiwan is situated on the edges of the Philippine Sea and the Eurasian plate. The former converges toward the northwest at a rate of 8.2 cm/yr, inducing an uplift rate of 2 cm/yr in the Taiwan mountain belt. Taiwan, located in the path of typhoons in the west Pacific Ocean region, also bears high denudation rates, due to high precipitation (Chang, 2016). According to the results from the geodetic survey, topography, evolution of plate tectonics, and thermochronology, the reference case is in a relatively stable tectonic environment, located far from the tectonic boundary and deformation zone, with no obvious uplift or subsidence. The stability could last for the next couple of 10 million years.

The results from rock samples and low-temperature thermochronology show a slow uplift rate between 0.01 mm/yr and 0.1 mm/yr in the reference case (SNFD-ITRI-2015-0001-c3.4.2). Since there is no specific thermal event within 76 MaBP for the reference case, and it’s in anorogenic period with a very stable geological environment, the uplift and denudation rates are assumed to be the same for the reference case in the safety assessment timescale.

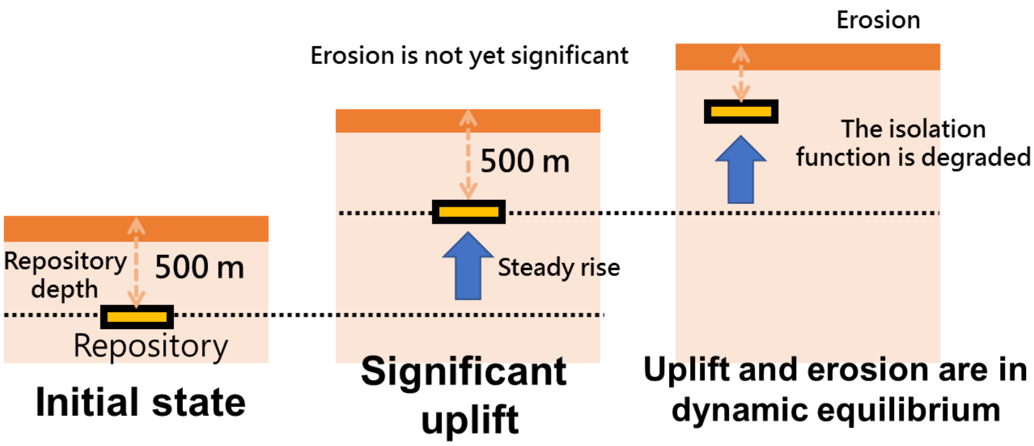

Figure 5-10: Impact on long-term safety of the repository due to uplifting and denudation.

5.3.3. Volcanism

Volcanism is one of the igneous activities induced by the process of magma intruding from the mantle or lower crust, forming igneous rocks after cooling. It can be categorized into intrusive type in depth or extrusive type near the surface (台電公司, 2017). Volcanic activities in Cenozoic in the Taiwan region was associated with the extension in the southeast margin of mainland China, and the subduction of the Philippine Sea plate. After the late Miocene, volcanism was related to the subduction between Philippine Sea plate and the Eurasian plate. Volcanism in Cenozoic in Taiwan region is divided into the western, eastern, and northern parts of Taiwan (Juan, 1985; Chen, 1990) (Figure 5-11).

(1) Volcanism in the western part of Taiwan:

Beginning in the early Paleocene (65 MaBP to 38 MaBP), the intraplate volcanism in the western part of Taiwan was related to the extensional tectonics in the eastern margin of the Eurasian plate, and was most active in Miocene (23 MaBP to 8 MaBP). The locations of magma activity were separated in Penghu island, Taiwan strait, central north of Taiwan (Guanxi–Zhudong, Jiaoban Mountai, and Gongguan), and central south of Taiwan (Alishan, Nanzixianxi, Laonong river, Muzha, and Jianshi). The volcanism is considered to have ceased (Chung et al., 1994; Chung et al., 1995; Chen et al., 2016b).

(2) Volcanism in the eastern part of Taiwan:

It was active from Miocene to Pliocene (16 MaBP to 2.2 MaBP). The associated igneous rocks constitute the backbone of the North Luzon Arc (Chen, 1990; Chen et al., 2016b).

(3) Volcanism in the northern part of Taiwan:

The relatively late (from late Pliocene to Quaternary) and short-lived magmatism (Chuang, 1988) in the northern part of Taiwan was initiated by the westward propagation of the Ryukyu Arc system and post-orogenic extension (Wang et al., 2004; Lallemand et al., 2013; Chen et al., 2016b).

Figure 5-12 shows six potential erupting locations (Konstantinou, 2014). Although Taiwan is located in the Pacific Ring of Fire, the volcanic areas are restricted to specific regions located in the eastern and northern parts of Taiwan.

Volcanism could bring impact on the repository. A high geothermal gradient will accelerate the velocity of groundwater flow and, therefore, increase the migration rate of radionuclides. The direct intrusion of magma, magma mixing, and volcanic gas mixing could change groundwater chemical properties lowering the safety functions of the multiple barriers system (MBS) (JNC, 2000).

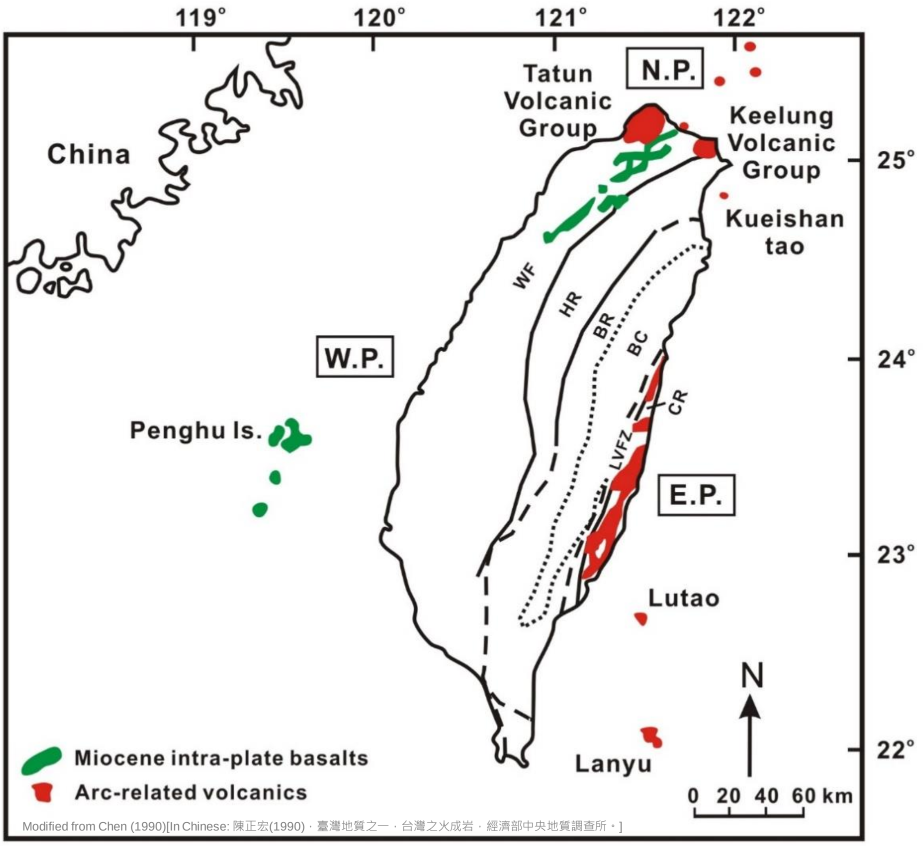

Figure 5-11: Volcanism distribution in Taiwan.

Reference: Chen (1990)

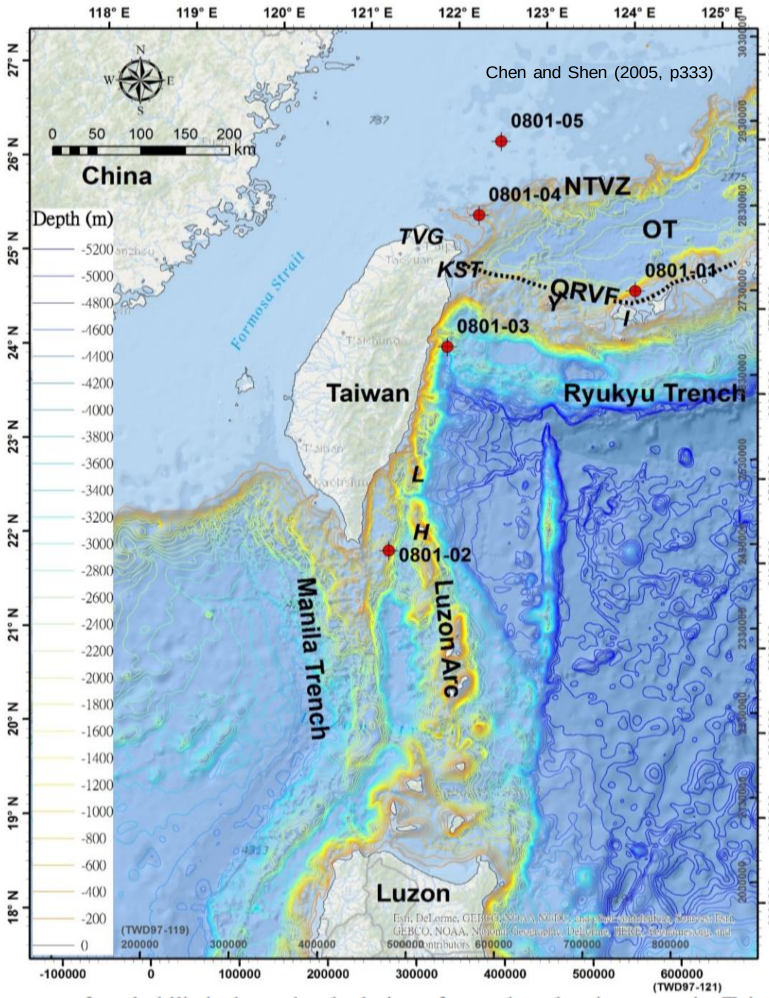

Table 1 Summary of probabilistic hazard calculations for each volcanic center in Taiwan based on the repose interval T of the last eruption

Konstantinou (2014, p9/19)

Volcanic center	T (years)	$P(+1\sigma)$	$P(-1\sigma)$	$H(+1\sigma)$	$H(-1\sigma)$
TVG	6,000	0.018	0.036	6.41×10^{-5}	3.63×10^{-5}
KST	7,000	0.016	0.032	5.50×10^{-5}	3.12×10^{-5}
0802-01	90	0.365	0.434	0.0027	0.0014
0801-05	98	0.349	0.419	0.0026	0.0013
0801-04	147	0.278	0.350	0.0019	1×10^{-4}
0801-03	161	0.264	0.335	0.0017	9.32×10^{-4}

P signifies the probability of exceedance of the repose interval, while H is the hazard rate. σ refers to the standard error of the α, β parameters (see text for more details). The numbers 0802-01, -05, -04 and -03 refer to confirmed submarine eruptions offshore Taiwan

Figure 5-12: Distribution and eruption probability for volcanoes in Taiwan.

Reference: Konstantinou, K.I. (2014)

5.4. Future Human Actions

5.4.1. Human Actions affecting Long-Term Safety of the Repository

Current human actions that may affect the long-term safety of repository are shown in Table 5-1. It is generally accepted that "drilling in rock formations" is the only human activity which is technically feasible and can directly lead to penetration of the canisters, allowing radionuclides released from the canister to further affect human and the environment. Although the repository site will be selected through strict selection procedures, it is difficult to predict what resources may become valuable resources in the future. Therefore, when the repository is no longer under supervision and the relevant information is lost, the repository may be artificially invaded due to the exploration of minerals or water resources or drilling for research purposes.

Table 5-2 shows the possible causes and depths of drilling operations in rock formations, which mainly include operations for mining, geothermal energy/oil and gas exploration and development, scientific research, and geological surveys for special structures. Although the site of the repository is usually set in a deep stratum without economic resources, it could not be ruled out that there may be changes in the characteristics of rock, or a new economic benefit in the future. Even so, the repository is often located in large rock masses, and the possibility of unintentionally intruding a repository for investigation is still low.

Table 5-1: Human actions that may affect long-term safety of the repository.

Category	Activity
Thermal impact	T1: Building heat store*
	T2: Building heat pump system*
	T3: Extracting geothermal energy (geothermics)*
	T4: Building plant that generates heating/cooling on the surface above the repository
Hydrological impact	H1: Constructing well*
	H2: Building dam
	H3: Changing the course or extent of surface water bodies (streams, lakes, sea) and their connections with other surface water bodies
	H4: Building hydropower plant*
	H5: Building drainage system
	H6: Building infiltration system
	H7: Building irrigation system*
	H8: Changing conditions for groundwater recharge by changes in land use
Mechanical impact	M1: Drilling in the rock*
	M2: Building rock cavern, tunnel, shaft, etc.*
	M3: Excavating open-cast mine or quarry*
	M4: Constructing dump or landfill
	M5: Bombing or blasting on the surface above the repository
	M6: Subsurface bombing or blasting*
Chemical impact	C1: Storing/disposing hazardous waste in the rock*
	C2: Construct sanitary landfill (refuse tip)
	C3: Acidifying air, water, soil and bedrock
	C4: Sterilizing soil
	C5: Causing accident resulting in chemical contamination

Note: * includes or may include drilling and/or construction of rock cavern.
Reference: SKB (2010n)

Table 5-2: Purposes, depth, and targeted formations of drilling.

Human actions	Depth	Formations to drill
Mining exploration / exploitation	Shallow and deep	Crystalline rock or sedimentary environments
Water supply	Normally only up to about 100 m	Fractured rocks or porous rocks/formations
Geothermal energy exploration/ exploitation	Deep	Sedimentary and crystalline rock (fractured or not)
Hydrocarbon exploration	Deep	Fractured or porous rock formations with lower permeability formations (reservoirs)
Future waste disposals location (toxics and/or radioactive)	Shallow and deep	Not fractured crystalline rock and sedimentary formations with low permeability.
Oil/gas exploration and exploitation	Shallow and deep	Rock formations
Oil/gas underground storage	Shallow and deep	Sedimentary formations (mainly old caverns in evaporates) and crystalline rock
CO_2 storage	Deep	Sedimentary formations
Scientific research	Shallow and deep	General

Building and construction	Generally, less than 50 m, apart from very exceptional examples, such as deep tunnels and secure facilities	General
Brine injection wells (mining industry)	Shallow to intermediate. Generally, less than 100 m	Fractured Rocks or porous rocks/formations

Reference: POSIVA (2013, Table 1)

5.4.2. Impact on Safety of the Repository

Among current human actions, drilling operations are the only direct result of the penetration of the canister, allowing the radionuclides to further affect humans. Table 5-2 summarizes the purpose, impact depth and target formation of drilling operations (POSIVA, 2013). According to Table 5-2, some of the targeting formations of drilling operations are less suitable as candidate sites for the repository, such as salt wells and CO_2 sequestration. Drilling typically does not exceed 50 m. Due to the high cost of deep drilling, non-invasive investigations, such as geophysical prospecting, are usually conducted before execution, thus alerting the investigator to the presence of the repository prior to the actual drilling operation. In addition, deep drilling usually requires skilled drillers who are likely to follow good procedures during the drilling process and are more likely to detect anomalies during the drilling process. Therefore, the probability of affecting the safety of the repository due to drilling operations is actually not high.

Future human actions involve social and technological development, with high uncertainty and unpredictable impact. In order to provide a complementary argument for the long-term safety impact of future human actions on the repository, a scenario analysis of future human actions will be conducted in Chapter 13.

6. Internal Processes

6.1. Introduction

Assessing the safety of a repository over a long period of time requires a comprehensive understanding of the internal processes of the disposal system. Based on relevant domestic and foreign literature, long-term research results of disposal plans, and interpretation of expert meetings, long-term safety-related functions of the engineered barriers and host rock of the repository can be identified. The following describes processes handling, document format of internal processes, process mapping/process tables and assessment model flow chart (AMF) of assessment models.

6.1.1. Identification of the Internal Processes

The internal processes consider the five main system components of the disposal repository (source term (SNF), canister, buffer, backfill and geosphere), which evolve over time and are affected by different variables, such as radiation, temperature, mechanical, chemical and microbial, and their relationship with the variables.

6.2. Coupling of the Internal Processes

The internal processes of the repository system are comprehensively considered through the coupling of (1) THMC processes, (2) variables, and (3) system components.

In order to present the large amount of information coupled with the internal processes in an easy manner, the process diagram of each system component can be used to illustrate the relationship between variables, processes and their interdependence. The process diagram is usually derived from the analysis and evaluation of the FEPs list. From the process diagram, the variables that affect each process, and impact of a specific process on the variables can be presented. In addition, it also describes the interactive processes of the adjacent system components. The process diagram can help analysts to identify the role, barrier characteristics, and their interdependence in a structured way.

Figure 6-1 elaborates the process impact between buffer, backfill, copper shell, cast iron lining and geosphere. The arrows represent the impact direction between variables and processes. Each process in Figure 6-1 can be organized as the corresponding influence table (Table 6-1). Table 6-2 to Table 6-6 are process mapping/process tables developed by SKB (SKB, 2006b). Among them, the green fields in the tables are irrelevant or negligible functions. The red fields are the functions that need to be simulated and quantified in the safety assessment, and the orange fields are the functions that can be neglected under certain conditions. As the basic concept, the corresponding fields of these tables can elaborate the developing technology in Taiwan.

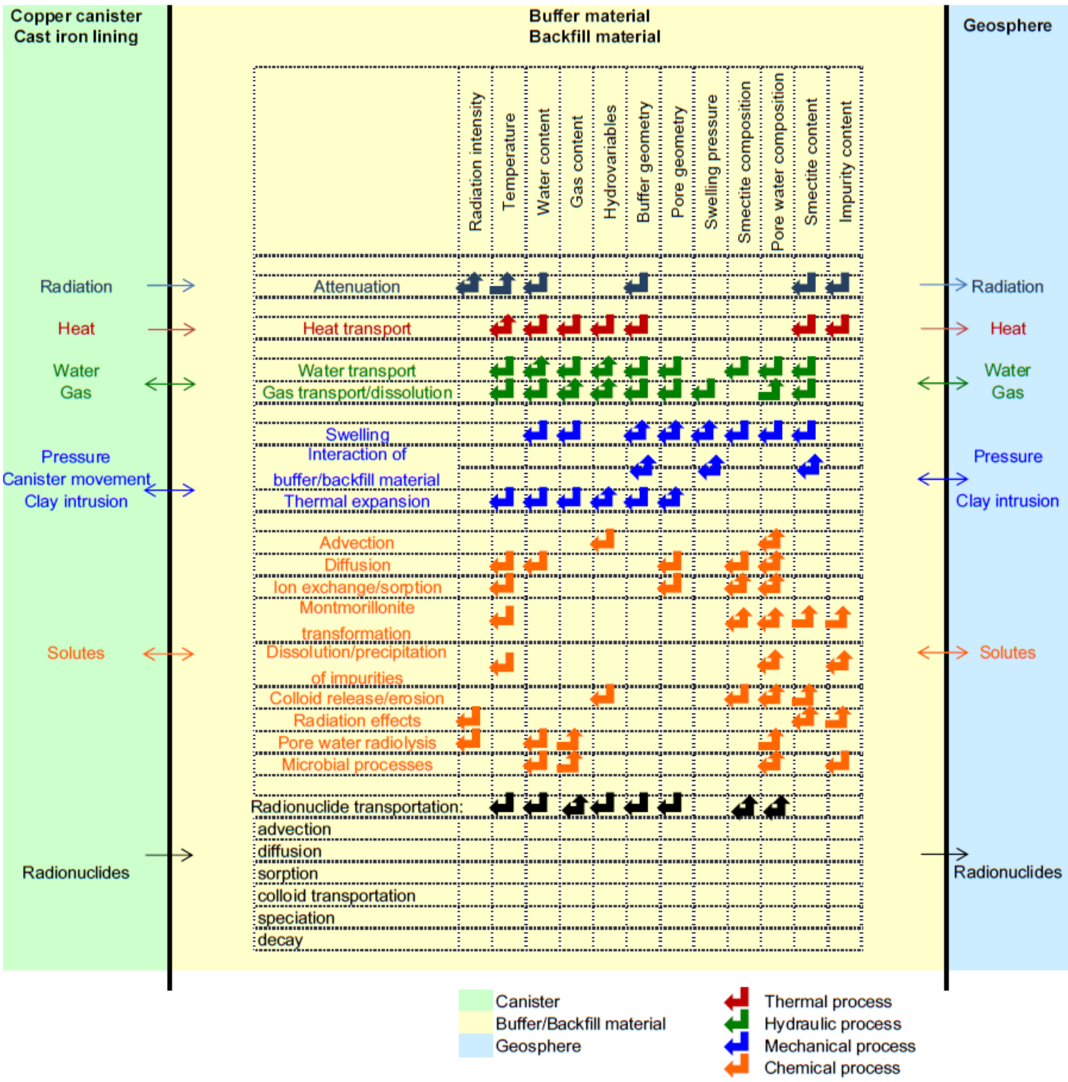

Figure 6-1: Concept of process diagram (buffer/backfill).

Note: the upper part of the table indicates variable, whereas the left part of the table indicates internal process.

Table 6-1: Concept of influence table of the internal processes of the geosphere.

Variable	Variable influence on process			Process influence on variable		
	Influence or not	Time period/ Climate domain	Handling of influence	Influence or not	Time period/ Climate domain	Handling of influence
Temperature in host rock	Yes. Temperature in host rock influences flow, viscosity, and density, which may cause buoyancy force.	Excavation/operation/resaturation	Compared with the influence of flowing into the repository, this can be neglected.	Yes, but the influence is little. In principle, heat is transferred through the conduction of flowing groundwater and rocks. However, the former is only meaningful in highly permeable rocks.	Excavation/operation/resaturation	Little influence, neglected.
		Temperate	The influence of geothermal gradient on density and viscosity is considered in the main calculation. SR Can/Hartley et al. solved the influence of SNF thermal effect in the scope calculation. The effect is negligible, so it is not considered in this report.		Temperate	The effect is small and can be neglected in the main calculation. In the scope calculation, the influence of the heat generated by the SNF is taken into account, but the influence can be neglected.
		Periglacial	The influence of geothermal gradient is considered. The temperature distribution over time is constant, because the process of periglacial will change with time.		Periglacial	Little influence, ignorable.

Variable	Variable influence on process			Process influence on variable		
	Influence or not	Time period/ Climate domain	Handling of influence	Influence or not	Time period/ Climate domain	Handling of influence
		Glacial	Processes smaller than the ice sheet can be neglected.		Glacial	Little influence, ignorable.
Groundwater pressure	Yes. The pressure gradient is a driving force for groundwater flow.	All	Included in the model	Yes. Pressure and flow are coupled.	All	Determined by calculation of groundwater flow.
Gas phase flow	Yes. Groundwater and natural gas are coupled.	Excavation/operation/resaturation	Using a model that expresses the groundwater level through a free surface, the influence of the gas phase is implicitly considered for the excavation/operation phase. This can produce drawdown and inflow. It is noted that during this period, the repository will not produce any gas. The simplified gas and water phase flow models are used to explicitly consider the influence of the gas	Yes. Groundwater and natural gas are coupled.	Excavation/operation/resaturation	Modeling is not clear, which is because the water level and water inflow can be determined based on a model that treats the groundwater level as a free surface. A simplified model for gas-phase flows that are not explicitly represented in the resaturation calculation is used.

Variable	Variable influence on process			Process influence on variable		
	Influence or not	Time period/ Climate domain	Handling of influence	Influence or not	Time period/ Climate domain	Handling of influence
			phase in the resaturation calculation.			
		Temperate	It is neglected in the mainstream calculation. The amount of gas generated is small, and the influence is localized. The gas influence is evaluated by the range calculation of SR-Can/Hartley et al.		Temperate	It is considered in the estimation of the dissolved gas transport capacity carried out by SR-Can/Hartley et al.
		Periglacial	Influence is less than the effect of permafrost and can be neglected.		Periglacial	Gas phase flow is a relatively small process and can be neglected.
		Glacial	Processes smaller than the ice sheet can be neglected.		Glacial	Gas phase flow is a relatively small process and can be neglected.
Repository geometry	Yes. The geometry of the repository affects the distribution and characteristic	Excavation/operation/resaturation	Detailed representation of the repository tunnel is included in the model.	No. The geometry of the repository will not be affected.	--	--
		Temperate	A detailed representation of the repository tunnel is included			

Variable	Variable influence on process			Process influence on variable		
	Influence or not	Time period/ Climate domain	Handling of influence	Influence or not	Time period/ Climate domain	Handling of influence
	s of the flow path		in the local flow model.			
		Periglacial	Influence is smaller than other effects and can be neglected.			
		Glacial	Influence is smaller than other effects and can be neglected.			
Fracture geometry	Yes. The pore size, geometry and connectivity of the fracture determine the permeability of the rock. The geometry of the pore space in the matrix will affect the diffusion of the rock matrix, which may	Excavation/operation/resaturatio n	Site-specific description of the geometry of cracks and crack areas.	No influence. However, it is generated indirectly through changes in the composition of the groundwater through the influence of the interaction of groundwater and rocks.	--	The indirect changes due to precipitation/dissolutio n are expected to be long-term and relatively small, and therefore, have not been resolved. Since the groundwater flow is very small, the change of the fracture aperture is not considered. The influence of possible high pore pressure and fracture "hydraulic jacking" under the ice sheet has been solved.
		Temperate	Site-specific description of the geometry of cracks and crack areas. The influence of EDZ is solved by distributing the increased hydraulic conductivity relative to the host rock. Changes over time can be neglected. The influence is small and within uncertainty.	It is also indirectly affected due to changes in the pore size of the fractures caused by changes in groundwater pressure related to		

Variable	Variable influence on process			Process influence on variable		
	Influence or not	**Time period/ Climate domain**	**Handling of influence**	**Influence or not**	**Time period/ Climate domain**	**Handling of influence**
	affect the composition of groundwater (especially salinity) and the flow.	Periglacial/Glacial	Continuous mode description of site characteristics based on the geometry of fractures and fracture areas.	groundwater flow and possible glacier processes.		
Rock stresses	No. But indirectly through the change of fracture geometry.		Ignorable. However, the EDZ modeling considers the influence of rock stress changes on the nature of fractures near the repository during the excavation, operation and resaturation of the repository. Except for the heat flux generated by the construction of the repository, fuel, ice load, structural changes over a long period of time, and changes caused by earthquakes, the stress changes are expected to be relatively small.	No. However, groundwater flow indirectly affects rock stress through the contribution of groundwater pressure to effective stress. The change in groundwater pressure is usually small that the influence on rock stress is negligible, except for desaturation and resaturation of the repository and possible ice loads.		Little influence, ignorable.

Variable	Variable influence on process			Process influence on variable		
	Influence or not	Time period/ Climate domain	Handling of influence	Influence or not	Time period/ Climate domain	Handling of influence
Matrix minerals	No. But indirectly through the composition and diffusion of groundwater through the rock matrix.		Compared with other influences considered, it is of little significance and can be neglected.	No. But it diffuses indirectly through the matrix in the flowing groundwater.	--	Refer to the chemical process in the buffer.
Fracture minerals	No. But indirectly affects the fracture geometry.		Compared with other influences considered, it is of little significance and can be neglected.	No. But it is formed indirectly through groundwater.	--	Refer to the chemical process in the buffer
Groundwater composition	Yes. The salinity of groundwater will affect its density and viscosity.	Excavation/operation/resaturation	The influence of salinity in a specific location is considered.	Yes. Also impacted by dispersion/diffusion and matrix diffusion.	Excavation/operation/resaturation	The transport of salt was modeled through advection and matrix diffusion.
		Temperate	The model illustrates the location-specific differences and distribution of salinity and reference water.		Temperate	The transport of salinity water and reference water is simulated by advection and matrix diffusion.
		Periglacial	The influence of salinity in a specific location is considered.		Periglacial	The transport of salt was modeled through advection and matrix diffusion.
Gas composition	No.	--	--	Yes.	All	The concentration of dissolved gas is

Variable	Variable influence on process			Process influence on variable		
	Influence or not	Time period/ Climate domain	Handling of influence	Influence or not	Time period/ Climate domain	Handling of influence
				Dissolved gases transported by flowing groundwater may escape from the solution when the pressure drops.		usually low and can be neglected.
Structural and stray materials	Yes. Grouting may affect the flow rate.	Excavation/operation/resaturation	Reduce the permeability of adjacent rocks to simulate the sensitivity study of different grouting levels.	Yes. Flow will affect the local degradation of cement slurry.	Excavation/operation/resaturation	See degradation of grouting, which can be neglected.
		Temperate	Conservative, the grout is not showing up.		Temperate	Ignorable.
		Periglacial	Ignorable.		Periglacial	Ignorable.
Saturation	Yes. Affect the effective permeability and the flow rate.	Excavation/operation/resaturation	The influence of saturation changes is considered by simplifying the model, and the unsaturated flow is treated in a simplified manner in the model, and the free surface is expressed in the area above the water level. Solve the near surface	Yes. May change the saturation.	Excavation/operation/resaturation	Saturated ground or non-existent water level is used as a model. Model is built in near-surface flow calculation.

Variable	Variable influence on process			Process influence on variable		
	Influence or not	Time period/ Climate domain	Handling of influence	Influence or not	Time period/ Climate domain	Handling of influence
			area in the calculation of the flow.			
		Temperate	Ignorable. The unsaturated zone near the surface has very little flow influence on saturated deep rocks. The unsaturated zone is considered in the MIKE SHE calculation to determine the maximum potential recharge (precipitation minus evapotranspiration).		Temperate	Ignorable. The unsaturated zone near the surface has almost no flow to saturated deep rock. The unsaturated zone is considered in the MIKE SHE calculation to determine the maximum potential recharge (precipitation reduces evapotranspiration).
		Periglacial	Ignorable. Under permafrost, the ground is usually saturated (unless large enough bubbles are formed).		Periglacial	Ignorable. Under permafrost, the ground is usually saturated (unless large enough bubbles are formed).
		Glacial	Ignorable.		Glacial	Ignorable.

Table 6-2: Concept of process mapping/process table of the source term and relevant development status in Taiwan.

Processes	SKB		Current status of Taiwan's technological development
	Intact canister	**Failed canister**	
TWF01 Radioactive decay	Thermal model (MATLAB and Fluent are currently used in the program)	COMP23	SNF decay heat analysis: radionuclide inventory and decay heat assessment are performed based on the actual operating burnup of the fuel bundles of each power plant and the cooling time from the exit of the furnace core to disposal. The curve of decay heat change with time: total decay heat of SNF in Chinshan Nuclear Power Plant from 2055 to 2105 is analyzed. The data is normalized to 1,200 W based on the total decay heat of 2055. At present, analyzed by MATLAB and Fluent when the canister is completed; and analyzed by GoldSim after the canister is failed.
TWF02 Radiation attenuation/heat generation	Thermal model	Neglected when the canister failure occurs after a period of elevated temperatures.	SNF decay heat analysis: radionuclide inventory and decay heat evaluation are performed based on the actual operating burnup of the fuel bundles of each power plant and the cooling time from the exit of the furnace core to disposal. The curve of decay heat change with time: total decay heat of SNF in Chinshan Nuclear Power Plant from 2055 to 2105 is analyzed. The data is normalized to 1,200 W based on the total decay heat of 2055. At present, analyzed by MATLAB and Fluent when the canister is completed; and analyzed by GoldSim after the canister is failed.
TWF03 Induced fission (criticality)	Neglected. There will be insufficient amounts of moderators inside the canister prior to failure.	Neglected. The probability is negligibly small if credit is taken for the burn-up of the fuel. .	The criticality analysis of the SNFD2017 report uses an indirect comparison method. By comparing the effective multiplication factor of SNF in Taiwan with SKB, it is preliminary determined that the acceptable loading standard established by the fine-tuned SKB can be applied to the SNF in Taiwan.

Processes	SKB		Current status of Taiwan's technological development
	Intact canister	Failed canister	
			The reactivity sensitivity of canister composition and parameter are analyzed, and the combination of canister parameters is summarized. At present, analyzed by MCNP when the canister is completed and failed. The probability is negligibly small if credit is taken for the burn-up of the fuel under the failure of the canister, as discussed in Ch12.3. If a criticality event has occurred hypothetically, the fission reaction would generate power and increase in temperature, which may damage the container and cause the radioactive isotopes to release. However, the chain reaction will terminate until negative feedback mechanisms, such as a decrease in moderator density associated with heating or depletion of the fissile material.
TWF04 Heat transport	Thermal model	Neglected when the canister failure occur after a period of elevated temperatures.	Canister heat transfer analysis technology (numerical solution): the heat transfer mode of the canister is a 1/4 symmetric model, and only the total calorific value of the canister can be set. Thermal spacing analysis technology of deposition holes (analytical solution): the temperature at the center point of the top surface of the canister copper shell is produced. It is assumed that this temperature is also the temperature of the bentonite which contacts the canister. At present, analyzed by MATLAB and Fluent when the canister is completed.
TWF05 Water and gas transport in canister cavity, boiling/ condensation	Not relevant.	Integrated with other relevant processes	It is set according to the groundwater transmission conditions in the buffer around the canister.

Processes	SKB		Current status of Taiwan's technological development
	Intact canister	Failed canister	
TWF08 Advection and diffusion	Not relevant.	Integrated with other relevant processes	It is set according to the groundwater transmission conditions in the buffer around the canister.
TWF09 Residual gas radiolysis/acid formation	Neglected. The amount of produced corrodents is negligible.	Not relevant.	
TWF11 Metal corrosion	Not relevant.	Pessimistic handling: a) No barrier function, all radionuclides instantaneously released upon water contact in COMP23. b) 1,000 years for complete corrosion if advective conditions in the buffer.	The metal parts will be completely corroded within a short time after the groundwater enters the canister, and the radionuclide will be released. At present, analyzed by GoldSim after the canister is failed.
TWF12 Fuel dissolution	Not relevant.	Modelled as constant, pessimistic dissolution rate in COMP23.	The dissolution rate is constant, with a relatively long dissolution time, and the radionuclide will be released during dissolution. At present, analyzed by GoldSim after the canister is failed.
TWF13 Dissolution of gap inventory	Not relevant.	Pessimistic, instantaneous	The fraction of radionuclide inventory in the gap will be released instantaneously when the groundwater enters, and the radionuclide will be released. At present, analyzed by GoldSim after the canister is failed.
TWF17 Radionuclides transport		COMP23	According to the containment and retardation safety functions,the integrity of the canister and surrounding buffer. At present, analyzed by GoldSim after the canister is failed.

Table 6-3: Concept of process mapping/process table of the canister and relevant development status in Taiwan.

Processes	**SKB**		**Current status of Taiwan's technological development**
	Intact canister	**Failed canister**	
TWC02 Heat transport	Thermal model.	Neglected when the canister failure occur after a period of elevated temperatures.	Canister heat transfer analysis technology (numerical solution): the canister heat transfer mode is a 1/4 symmetrical model, and only the total calorific value of the canister can be set. Canister spacing analysis (analytic solution): the temperature at the center point of the top surface of the canister copper shell is produced. It is assumed that this temperature is also the temperature of the bentonite which contacts the canister. At present, analyzed by MATLAB and Fluent when the canister is completed.
TWC03 Deformation of cast iron lining	Isostatic load: uniform external pressure on the stress change of the cast iron lining. Uneven expansion: the stress change of the non-uniform buffer's swelling pressure on the cast iron lining. Creeping changes in all the above cases: not included.	Not relevant.	Canister anti-isostatic load performance evaluation: ABAQUS is used to investigate the impact of the uneven and uniform expansion of the buffer during the unsaturated and saturated periods of the buffer. The canister is confirmed to meet the isostatic load design criteria. At present, analyzed by ABAQUS when the canister is completed.
TWC04 Deformation of copper canister from external pressure	The swelling pressure of the buffer and the action of external force (such as earthquakes) cause the canister to deform.	Not relevant.	Canister anti- isostatic load performance evaluation: by performing canister's anti- isostatic load performance evaluation, it is confirmed that the canister can meet the isostatic load design criteria Numerical analysis of canister affected by seismic crack displacement: using the integrated model of canister and buffer to analyze the seismic shear displacement Canister anti-shear displacement performance analysis technology: by performing the canister's shear resistance performance evaluation, the possibility of canister failure is evaluated.

Processes	SKB		Current status of Taiwan's technological development
	Intact canister	**Failed canister**	
			At present, analyzed by ABAQUS when the canister is completed.
TWC09 Galvanic corrosion	Not relevant.	Integrated with other relevant processes.	
TWC11 Corrosion of copper canister	The nitric acid decomposed by air radiation and the oxygen in the atmosphere before closure are classified as limited corrosion due to their limited reaction time. Radiation-hydrolyzed oxidant, initially restricted oxygen and pyrite sulfide after closure are classified as limited corrosive effects due to the limited total amount of corrosive produced by them. Sulfides in groundwater are long-term corrosion.	Not relevant.	Canister metal material corrosion resistance test verification: confirm that the thickness of the copper shell is not 0 cm through the corrosion test results.
TWC12 Stress corrosion cracking, copper canister	The stress corrosion cracking medium is not easy to reach the copper surface through diffusion, so there is not enough medium for stress corrosion cracking. In addition, the corrosion potential and pH value are not higher than the Cu_2O/CuO reaction line, so the stress corrosion cracking will not happen.	Not relevant.	
TWC15 Radionuclide transport	Not relevant.	COMP23.	Near-field radionuclide transport analysis technology: By performing the evaluation of the anti- isostatic load performance of the canister, it is confirmed that the canister can meet the isostatic load design criteria. At present, analyzed by GoldSim after the canister is failed.

Table 6-4: Concept of process mapping/process table of the buffer and relevant development status in Taiwan.

Processes	**SKB**			**Current status of Taiwan's technological development**
	Resaturation/“thermal” period	**Long-term after saturation and “thermal” period**	**Earthquakes**	
Intact canister				
TWBu02 Heat transport	Thermal model.	Thermal model.	Not relevant.	Research on the basic properties of buffer /backfill and thermal conductivity of buffer and backfill Canister heat transfer analysis technology (numerical solution): the heat transfer mode of the canister is a 1/4 symmetric model, and only the total calorific value of the canister can be set. Thermal spacing analysis technology of deposition holes (analytical solution): the temperature at the center point of the top surface of the canister copper shell is produced. It is assumed that this temperature is also the temperature of the bentonite which contacts the canister. At present, MATLAB is used to analyze the resaturation/thermal period, the long-term after saturation and the thermal period.
TWBu04 Water uptake and transport for unsaturated conditions	THM model.	Not relevant by definition.	Not relevant.	At present, FLAC3D is used to analyze the resaturation/thermal period, the long-term after saturation and the thermal period.
TWBu05 Water transport for saturated conditions	Neglected under unsaturated conditions. For the saturated conditions, the treatment is the same as for “Long-term”.	Neglected if hydraulic conductivity $<10^{-12}$ m/s since diffusion would then dominate.		Research on the basic properties of buffer/backfill and the hydraulic conductivity of buffer and backfill. At present, FLAC3D is used to analyze the long-term after saturation and the thermal period.

Processes	SKB			Current status of Taiwan's technological development
	Resaturation/“thermal” period	Long-term after saturation and “thermal” period	Earthquakes	
TWBu06 Gas transport/dissolution	The gas is transported by diffusion or dissolution.	All gases are assumed to dissolve in the pore water.	All gases are assumed to dissolve in the pore water.	Research on the corrosion rate of corrosive gas on the buffer.
TWBu07 Piping/erosion	Through empirical calculation.	Not relevant.	Not relevant.	At present, the resaturation/thermal period is analyzed by referring to SKB empirical formula and verifying its applicability through experiments.
TWBu08 Swelling/Mass redistribution	Analytical modelling of interaction buffer/backfill.	Integrated evaluation of relevant processes.	Part of integrated assessment of buffer/canister/rock.	Research on the basic properties of buffer/backfill and the swelling pressure of buffer and backfill. Analysis of characteristics of unsaturated bentonite. Analysis of the properties of buffer and backfill: based on the water-absorbing and re-expanding characteristics of the buffer, the swelling pressure is calculated when the buffer reaches saturation, and the impact of the buffer and backfill is explored after the buffer is lifted up and pushing the upper backfill. At present, FLAC3D is used to analyze the resaturation/thermal period, and ABAQUS is used to analyze the long-term after saturation and thermal period and earthquake.
TWBu10 Material advection transport	Simplified assumptions of mass transport of dissolved species during saturation.	Neglected if hydraulic conductivity< 10^{-12} m/s.		
TWBu11 Material Diffusion transport	PHAST (thermal, saturated phase; unsaturated phase disregarded).	PHAST		At present, PHREEQC technology continues to develop the resaturation/thermal period, the long-term after saturation and the thermal period.

Processes	SKB			Current status of Taiwan's technological development
	Resaturation/“thermal” period	Long-term after saturation and “thermal” period	Earthquakes	
TWBu12 Sorption (including ion exchange)	PHAST (thermal, saturated phase; unsaturated phase disregarded).	PHAST		Taking the chemical composition of K-areas groundwater as experimental conditions, using radionuclides such as Cs, U and Th to establish a batch adsorption experiment technology for radionuclide in buffer and backfill. At present, PHREEQC technology continues to develop the resaturation/thermal period, the long-term after saturation and the thermal period.
TWBu13 Alterations of impurities	PHAST (thermal, saturated phase; unsaturated phase disregarded).	PHAST		
TWBu14 Speciation and reaction of aqueous solutions	PHAST (thermal, saturated phase; unsaturated phase disregarded).	PHAST		At present, PHREEQC technology continues to develop the resaturation/thermal period, the long-term after saturation and the thermal period.
TWBu15 Osmosis	SR-CAN: Simulation of buffer/backfill interactions under extreme conditions. SR-SITE: Evaluated by comparison with empirical data.	SR-CAN/SR-SITE: Evaluated by comparison with empirical data.		At present, relevant experimental studies are continuously developed for the resaturation/thermal period, the long-term after saturation and the thermal period.
TWBu16 Montmorillonite transformation	Model calculation (only for thermal and saturated phase; unsaturated phase is not considered).	Evaluate based on evidence from nature.		
TWBu18 Release of montmorillonite colloid	Neglected if $[M^{2+}] > 8$ mM. Otherwise, analysis should be implemented.	Neglected if $[M^{2+}] > 8$ mM. Otherwise, analysis should be implemented.		At present, MATLAB and experimental studies are used to analyze the

Processes	SKB			Current status of Taiwan's technological development
	Resaturation/“thermal” period	**Long-term after saturation and “thermal” period**	**Earthquakes**	
				resaturation/thermal period, the long-term after saturation and the thermal period.
Failed canister				
TWBu06 Gas transport/dissolution	Quantitative estimation based on empirical data (no failures are expected during this period).	Quantitative estimation based on empirical data.		Research on the corrosion rate of corrosive gas on buffer At present, the long-term after saturation and thermal period analysis is carried out by developmental experimental studies.
TWBu23 Colloid transport	Neglected if density at saturation > 1,650 kg/m^3, otherwise bounding calculation (no failures are expected in this period).	Neglected if density at saturation > 1,650 kg/m^3, otherwise bounding calculation.		
TWBu25 Transport of radionuclides in water phase	COMP23 Analytic (no failures are expected during this period).	COMP23 Analytic	COMP23 Analytic Reduced diffusion path.	According to the retardation safety functions integrity of the buffer. At present, GoldSim is used to analyze the long-term after saturation, thermal period and earthquake.

Table 6-5: Concept of process mapping/process table of the backfill and relevant development status in Taiwan.

Processes	**SKB**		**Current status of Taiwan's technological development**
	Resaturation/“thermal” period	**Long-term after saturation and “thermal” period**	
Intact canister			
TWBfT03 Water uptake and transport for unsaturated conditions	THM model.	Not relevant by definition.	At present, FLAC3D is used to analyze the resaturation/thermal period.
TWBfT04 Water transport for saturated conditions	It can be neglected under unsaturated conditions. Under saturated conditions, the treatment method is the same as the "long period and heating phase after saturation".	Geosphere model conditions should be included for evaluation.	Research on the basic properties of buffer/backfill and the hydraulic conductivity of buffer and backfill. At present, FLAC3D is used to analyze the long-term after saturation and the thermal period.
TWBfT06 Piping/erosion	Through empirical calculation.	Not relevant.	At present, the resaturation/thermal period is analyzed by referring to SKB empirical formula and verifying its applicability through experiments.
TWBfT07 Swelling/Mass redistribution	SR-CAN: Analytical modeling of buffer/backfill interactions. SR-SITE: THM model analysis of buffer and backfill, including buffer/backfill interaction and uniform conditions in the disposal tunnel.	Integrated evaluation of relevant processes.	Analysis of the properties of buffer and backfill: based on the water-absorbing and re-expanding characteristics of the buffer, the swelling pressure is calculated when the buffer reaches saturation, and the impact of the buffer and the backfill is explored after the buffer is lifted up and pushing the upper backfill. At present, FLAC3D is used to analyze the resaturation/thermal period, and ABAQUS is used to analyze the long-term after saturation and thermal period and earthquake.
TWBfT09 Material advection transport	Simplifying assumes mass transfer of dissolved material during saturation.	Geosphere model conditions needs to be included for evaluation.	

Processes	SKB		Current status of Taiwan's technological development
	Resaturation/“thermal” period	**Long-term after saturation and “thermal” period**	
TWBfT10 Material Diffusion transport	Because the conditions in the backfill are roughly the same in the long-term evolution, no specific research has been conducted on the initial state after closure.	PHAST	At present, PHREEQC technology continues to develop the long-term evolution after saturation and thermal period.
TWBfT11 Sorption (including ion exchange)	Because the conditions in the backfill are roughly the same in the long-term evolution, no specific research has been conducted on the initial state after closure.	PHAST	Reference groundwater chemical composition is used as experimental conditions. Cs, U and Th and other radionuclides are used to establish a batch adsorption experiment technology for radionuclide in buffer and backfill. At present, PHREEQC technology continues to develop the long-term evolution after saturation and thermal period.
TWBfT12 Impurity alteration of backfill	The effect of inorganic reduction on oxygen is simulated.	PHAST	
TWBfT13 Speciation and reaction of aqueous solutions	Because the conditions in the backfill are roughly the same in the long-term evolution, no specific research has been conducted on the initial state post-closure.	PHAST	At present, PHREEQC technology continues to develop the long-term evolution after saturation and thermal period.
TWBfT14 Osmosis	In the THM model, hydraulic conductivity coefficients of different salinities are selected to evaluate the influence of osmosis.	Evaluation through comparison with empirical data.	At present, PHREEQC technology continues to develop the resaturation/thermal period, the long-term evolution after saturation and the thermal period.
TWBfT15 Montmorillonite transformation	SR-CAN: Neglected because the temperature increases only slightly.	SR-CAN: Neglected because the temperature increases only slightly.	
TWBfT16 Release of backfill colloid	SR-SITE: model calculation (considering only reactions in heating and saturated phases; not considered in the unsaturated phase).	SR-SITE: indicates mode calculation.	
Failed canister			

Processes	SKB		Current status of Taiwan's technological development
	Resaturation/“thermal” period	Long-term after saturation and “thermal” period	
TWBfT21 Transport of radionuclides in water phase	COMP23 Analytic (no failures are expected in this period).	COMP23 Analytic.	Included when considering the Q2 transport path. At present, GoldSim is used to analyze the long-term evolution after saturation, thermal period.

Table 6-6: Concept of process mapping/process table of geosphere and relevant development status in Taiwan.

Processes	SKB					Current status of Taiwan's technological development
	Excavation/operation	Temperate	Permafrost	Glaciation	Earthquakes	
TWGe03 Groundwater flow	The inflow of assumed saturated groundwater flow is modeled with water upconing. MIKE-SHE is used to simulate near-surface effects.	Modelling of resaturation (DarcyTools) and saturated flow (CONNECTFLOW) at different scales.	Modelling of flow pattern with Darcy Tools.	Modelling of groundwater flow pattern during advance and retreat of an ice sheet.		Groundwater flow field evaluation model and interface integration, and groundwater flow field evolution analysis. The analysis of each period is as follows: Excavation/operation: FracMan was used to analyze the groundwater inflow in the nearby field and calculate the inflow of the disposal tunnel and deposition hole at different excavation times. Temperate: a site-scale groundwater flow field simulation of salinity was performed using DarcyTools to obtain groundwater pressure and salinity distribution. Glaciation: Using DarcyTools to establish hydrogeological conceptual models at different regional scales according to

Processes	SKB					Current status of Taiwan's technological development
	Excavation/operation	**Temperate**	**Permafrost**	**Glaciation**	**Earthquakes**	
						different time segments, and according to the corresponding boundary conditions, the groundwater flow field simulation is performed to obtain groundwater pressure distribution.
TWGe05 Rock displacement	3DEC stress modelling of nearfield effects of excavation of tunnels and deposition holes.	3DEC modelling of thermal stresses and deformations.	Thermal effects neglected provided that only marginal changes in mechanical state occur.	3DEC stress modelling of near field.	Included in the modelling of shear movements.	3DEC is currently used in the program to analyze stability during excavation and perform seismic analyses of the disposal tunnels.
TWGe06 Reactivation – displacement along existing discontinuities	3DEC modelling of construction-induced reactivation. Construction-induced seismicity neglected since construction-induced stresses are too limited and expected to be relaxed at the time of deposition.	3DEC modelling of reactivation due to thermal load. Estimation of earthquake probability (consequence analysis, see Earthquake).	Thermal effects neglected provided that only marginal changes in mechanical state occur. Estimation of seismic probability. (consequence analysis, see Earthquake).	3DEC modelling of ice-load induced reactivation. Assessment of MH effects of hydraulic jacking. Estimation of seismic probability. (consequence analysis, see Earthquake).	Design rules (respect distance and canister distance) are applied. The probability of canister failure due to fracture shear displacement is evaluated.	Fracture shear displacement induced by fault sources and diffuse seismicity was evaluated using 3DEC. Relevant results and the geometrical rejection criteria were applied to the repository layout, to assess the shear failure rate of the canisters. (1) seismic hazard analysis and (2) historical disastrous earthquake source model and relevant sensitivity study have been established in the assessment of seismic probability.

Processes	SKB					Current status of Taiwan's technological development
	Excavation/operation	Temperate	Permafrost	Glaciation	Earthquakes	
TWGe07 Fracturing	Assessment of EDZ. Modelling (3DEC) and observations (APSE) of fracturing around deposition holes (spalling).	Modelling (3DEC) of potential for fracturing induced by thermal stresses. Estimations of effects of gas overpressure.	Thermal effects neglected provided that only marginal changes in mechanical state occur.	Modelling (3DEC) of potential for fracturing induced by ice load. Assessment of risk for hydraulic fracturing.	Neglected based on observations of earthquake-induced damage around open tunnels at shallow depth.	Analysis of spalling of deposition hole wall caused by near field thermal load using 3DEC. The analysis of each period is as follows: Excavation/operation: 3DEC; Evaluation of excavation disturbance zone. Spalling of deposition hole wall after simulated construction. Temperate: system to 3DEC; Spalling of deposition hole wall caused by the simulated thermal load. Glaciation: rupture caused by 3DEC thermal simulation. Earthquake: rupture of adjacent disposal facility caused by earthquake has been executed.
TWGe11 Advection transport and mixing of dissolved species	Salt advection is included in the hydrogeological model. The composition of the mixture from hydrogeological modeling and site is analyzed.	Salt advection is included in the hydrogeological model. The composition of the mixture from hydrogeological modeling and site is analyzed.	Modelling of transport of outfrozen salt.	Modelling of up-coning of saline water and transport of glacial meltwater to repository depth.	Not relevant.	The Darcy flow simulation and salinity distribution were carried out, and the concentration was calculated by PHREEQC. The analysis of each period is as follows: Excavation/operation: Flow simulation and salinity distribution are carried out by Darcy and concentration calculation is carried out by PHREEQC.

Processes	SKB					Current status of Taiwan's technological development
	Excavation/operation	Temperate	Permafrost	Glaciation	Earthquakes	
						Temperate: Flow simulation and salinity distribution are carried out by Darcy and concentration is calculated by PHREEQC. Glaciation: Analysis of salt advection included in hydrogeological models. Understanding the composition of the assessment mixture from hydrogeological modelling and sites.
TWGe12 Fracture and diffusion of dissolved species in rock matrix	Diffusion of salt between mobile and immobile groundwater is included in hydrogeological modelling.	Diffusion of salt between mobile and immobile groundwater is included in hydrogeological modelling.	Diffusion of salt between mobile and immobile groundwater included in modelling of transport of out-frozen salt.	Diffusion of salt included in modelling of groundwater flow pattern during advance and retreat of an ice sheet. Included in modelling of oxygen consumption.	Not relevant.	
TWGe13 Speciation and sorption	Not relevant.	Simplified K_d-approach for modelling sorption of radionuclides. Speciation considered in the selection of K_d.	Simplified K_d-approach for modelling sorption of radionuclides. Speciation considered in the selection of K_d.	Simplified K_d-approach for modelling sorption of radionuclides. Speciation considered in the selection of K_d.	Not relevant.	Taking the chemical composition of the groundwater in the K-areas area as the experimental conditions, using Tc, Cs, and I and other nuclide species to establish the batch adsorption experiment and penetration diffusion experiment technology of radionuclide on crushed granite, and the internal diffusion

Processes	SKB					Current status of Taiwan's technological development
	Excavation/operation	Temperate	Permafrost	Glaciation	Earthquakes	
						experiment technology using granite flakes. At present, dynamic K_d is developed for warm systems and the solubility limit of nuclear species is calculated.
TWGe14 Reactions groundwater/rock matrix	Neglected. Reactions are considered to take place at fracture surfaces only.	Neglected. The impact on groundwater composition and matrix porosity is insignificant.		A simulation of the reaction between water transfer and rock must be established on a long-term scale.	Not relevant.	
TWGe15 Dissolution/precipitation of fracture-filling minerals	Modelling of mixing (M3) and of reactions (PHREEQC).	Modelling of mixing (M3) and of reactions (PHREEQC).		Included in modelling of oxygen consumption. Assessment of impact on flow paths of calcite dissolution/precipitation.	Not relevant.	At present, PHREEQC modeling technology is developed for excavation/operation and temperate system.
TWGe24 Transport of radionuclides in the water phase	Not relevant. Engineered barriers are intact.	Advection, dispersion, matrix diffusion, sorption, and radioactive decay are included in integrated modelling (FARF31).	Advection, dispersion, matrix diffusion, sorption, and radioactive decay are included in integrated modelling (FARF31).	Advection, dispersion, matrix diffusion, sorption, and radioactive decay are included in integrated modelling (FARF31).	No credit taken for radionuclide retention in the geosphere.	At present, GoldSim is used for the ananalysis of temperate and glaciation systems.

6.3. Assessment Model Flowchart (AMF)

For the description of how different models are connected to each other, an assessment modelling flow chart (AMF) is used to provide an overall description of the assessment models of various system components of the repository. Correlation between the assessment models under the long-term evolution is also demonstrated using AMF. In addition, the parameters used in each assessment model (including input parameters and output parameters) can also be recorded according to AMF to ensure traceability of the evaluation process.

AMF is shown in Figure 6-2. The graphics and symbols used in AMF represent the following meanings:

(1) Yellow oval: represents the assessment model used.

(2) Blue square: represents the input parameters of the assessment model or the output parameters calculated by the assessment model.

(3) White diamond: represents performing further evaluation based on the output of the assessment model for the following assessment.

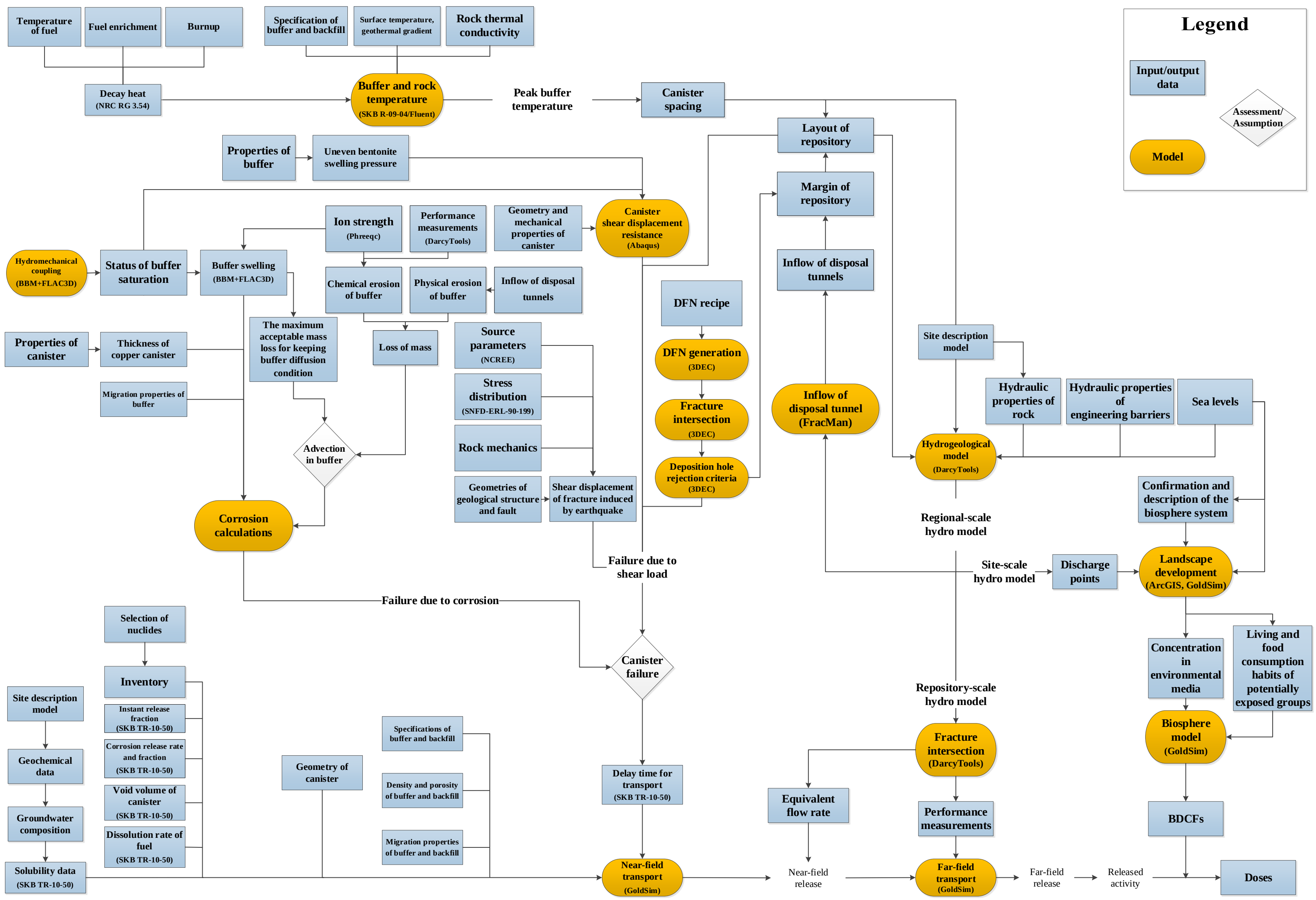

Figure 6-2: Assessment model flowchart (AMF).

7. Safety Functions and Safety Function Indicators

7.1. Introduction

In safety assessment, safety functions (isolation, containment, and retardation) of the repository should be proven to ensure that the safety functions of each system component of the multiple barriers system can be maintained and that the biosphere will not be significantly affected by the SNF. As isolation safety functions of the repository, whose safety function indicator is the depth of the repository, can be identified through proper site selection procedures, containment (Section 7.3) and retardation (Section 7.4) safety functions of the repository will mainly be considered in this chapter. And quantitative safety function indicators have also been established for total-system safety assessment.

Although the geological conditions of Taiwan are different from those of Sweden and Finland, similar granite rocks have certain characteristic ranges. Therefore, in the SNFD2017 report, safety functions and safety function indicators of each system component in crystalline rock had been established based on the geological characteristics of Taiwan and the design concept of Swedish KBS-3. These safety functions and safety function indicators and the criteria co-edited by SKB and Posiva (Posiva and SKB, 2017) have been taken as the basis for the update of the safety function indicator criteria. Besides that, existing knowledge and research results have also been taken into account. The criteria can be further modified according to the conditions and characteristics of Taiwan.

7.1.1. Dose Dilution

Dose dilution can have a huge influence on the results of the final dose assessment. If the repository is located in a coastal area, the dose can be significantly reduced through potential dose dilution of the sea because of its large volume. And the associated radiation risk can be reduced thereby. However, the amount of dose dilution cannot be controlled through engineering design; it can only be modified through site selection. Besides, although the dose can be reduced by the sea initially, for the following 1 million years after closure, the site might evolve from a coastal area to an inland area. Also, the estimation of climate-related parameters may contain differences of several orders of magnitude when taking uncertainties of climate evolution into account, and this could have a huge effect on the estimation of hydrogeology evolution. Therefore, the results of dose dilution could vary significantly over time.

Dose dilution can be regarded as spatial redistribution of the released radionuclides, and must be included in the quantitative assessment of the radionuclides released (SKB, 2011). For the reasons described above, spatial redistribution of the radionuclides should not be directly defined as a positive or negative effect because of the uncertainties of climate evolution. And because dose dilution cannot be simply controlled by engineering design, when discussing the safety functions of the barrier in this chapter, the impact of dose dilution will not be included.

7.2. Safety Functions, Safety Function Indicators, and Safety Function Indicator Criteria

(1) Safety function:

In order to quantify and evaluate the safety of the repository, it is necessary to understand how system components of the repository maintain the primary safety functions (isolation, containment, and retardation). Safety functions can be defined as the contribution of each system component of the repository to safety. For example, the canisters should be able to provide a barrier against corrosion so that the containment safety functions will not be degraded by corrosion. Therefore, “the canisters should be able to provide a barrier against corrosion” will be one of the required safety functions.

(2) Safety function indicator:

In order to evaluate the safety of the repository specifically, measurable or calculable indicators, which are the "safety function indicator," have been used to clearly verify the degree of fulfillment of the safety functions. For example, "the canisters should be able to withstand an isostatic load." Since isostatic load comes from swelling pressure of the buffer and groundwater pressure, these two can be calculated by quantitative evaluation and be quantified as the safety function indicator of "withstanding isostatic load." In other words, safety function indicators are indicators that can be measured or calculated to show clearly whether the safety functions of the system components can be satisfied so that the safety functions can be easily quantified.

(3) Safety function indicator criteria:

In order to confirm whether the safety functions of each system component are maintained over the timescale of safety assessment, a numerical range (i.e., "safety function indicator criteria") is set for safety function indicators. In other words, safety function indicator criteria are quantitative limits of safety function indicators. It is assumed that when safety function indicator criteria are satisfied, the corresponding safety functions can be maintained. Safety function indicator criteria are different from the "design requirements" mentioned in Chapter 4. Safety function indicator criteria are there to ensure that the long-term safety of the repository can be maintained when the criteria of each component are met for at least 1 million years. On the other hand, design requirements describe the initial state of each component of the disposal system. When specifying design requirements, a sufficient margin should be kept to ensure that although the performance of the disposal system may degrade during one million years, the safety function indicator criteria of each component can still be met. For example, the design requirements of the canister is that thickness of the canister should be greater than 5 cm of the copper shell to cope with impact from copper shell corrosion. When specifying safety function indicator criteria of the canister, the thickness of the canister copper shell should be greater than 0 cm to ensure the containment safety functions of the canister can be maintained through 1 million years and canister failure will not occur because of copper shell corrosion. Therefore, 0 cm is used as the safety function indicator criterion for “providing a barrier against corrosion.”

7.3. Containment Safety Function Indicators

This section describes the safety functions, safety function indicators, and safety function indicator criteria of the system components (canister, buffer, backfill, and geosphere) related to the containment safety function. The containment safety functions of each system component are summarized in Table 7-1.

Table 7-1: Containment safety functions, containment safety function indicators, and containment safety function indicator criteria.

Containment safety functions, containment safety function indicators, and containment safety function indicator criteria			
System components	**Safety function**	**Containment safety function indicator and criteria**	**References and instructions**
canister	Can1: provide barrier against corrosion	copper shell thickness > 0 cm	SKB, 2011
	Can2: withstand isostatic load	isostatic load < 50 MPa	Posiva and SKB, 2017
	Can3: withstand shear force	shear displacement < 5 cm and velocity of shear displacement < 1 m/s	SKB, 2011
buffer	Buff1: limit advection	(a) hydraulic conductivity of buffer < 1×10^{-12} m/s (b) swelling pressure of buffer > 1 MPa	SKB, 2011
	Buff2: limit microbial activity	swelling pressure of buffer > 2 MPa	Posiva and SKB, 2017
	Buff3: damp rock shear force	buffer density < 2,050 kg/m^3	SKB, 2011
	Buff4: resist transformation	buffer temperature < 100 ℃	SKB, 2011
	Buff5: prevent canister sinking	swelling pressure of buffer > 0.2 MPa	SKB, 2011
	Buff6: limit pressure applied to the canisters and rock	(a) swelling pressure of buffer < 10 MPa (b) buffer temperature > -2.5 ℃	Posiva and SKB, 2017
backfill	BF1: limit buffer expansion	swelling pressure of backfill should not be too low	Posiva and SKB, 2017
geosphere	R1: provide preferred chemical conditions	(a) redox state: limit Eh value (b) ionic strength, salinity: $\Sigma q[M^{q+}] > 8$ mM; TDS < 35 g/L (instant total dissolved solids < 70 g/L) (c) limit concentration of harmful substances: $[NO_2^-] < 10^{-3}$ M; $[HS^-] < 3$ mg/L$\approx 10^{-4}$ M; $[K^+] < 0.1$ M (d) pH value of groundwater should be between 5 and 11 (e) avoid chlorides from corrosion: pH value > 4 and $[Cl^-] < 2$ M	Posiva and SKB, 2017
	R2: provide preferred hydrogeologic and transport conditions	(a) flow-related transport resistance in the fracture (F) > 10,000 yr/m (b) equivalent flow rate < 1×10^{-4} m^3/yr	SKB, 2011
	R3: provide mechanically stable environment	limit groundwater pressure shear displacement < 5 cm and velocity of shear displacement < 1 m/s	SKB, 2011
	R4: provide preferred thermal environment	host rock temperature should be between -2.5 ℃ and 100 ℃	Posiva and SKB, 2017

Note: SKB and POSIVA reports were referred to for the specification of the safety function indicators and criteria, and research results of SKB and POSIVA were referred to for the specification of quantitative values of the safety function indicator criteria. However, some of the safety function indicators could have various impact factors, and a single value for the safety function indicator criteria might be difficult to specify. In these circumstances, no quantitative value was used.

7.3.1. Canister

The canisters will be placed at a depth of 500 m underground. Primarily, canisters should be able to resist impact from hydrostatic pressure from groundwater, swelling pressure from water absorption of the buffer, shear displacement from earthquakes, and corrosion.

(1) Can1: provide barrier against corrosion

In order to maintain the integrity of the canister, the copper shell must not be penetrated. That is, the minimum thickness of the copper shell should be greater than 0 cm. Therefore, the safety function indicator is “copper thickness,” and the safety function indicator criterion is “copper shell thickness > 0 cm.”

(2) Can2: withstand isostatic load

Isostatic load to the canister at the repository depth is the sum of hydrostatic pressure and swelling pressure. Therefore, the safety function indicator is “isostatic load,” and the safety function indicator criterion is “isostatic load < 50 MPa.”

Although the safety function indicator criterion is set to be “isostatic load < 50 MPa,” it has to be noticed that it does not mean that the canister will be damaged when the isostatic load exceeds 50 MPa.

(3) Can3: withstand shear force

In order to maintain the integrity of the canister, the canister should be able to withstand fractures intersecting the canister having shear displacement. The canister should retain its integrity and maintain its ability to withstand uniform load after a 5 cm fracture displacement at a velocity of 1 m/s for fractures of any angles or locations intersecting the deposition hole. Therefore, the safety function indicator is set to be “shear displacement” and “velocity of shear displacement,” and the safety function indicator criteria are set to be “shear displacement < 5 cm” and “velocity of shear displacement < 1 m/s.”

7.3.2. Buffer

Buffer will be installed in the deposition holes between the canisters and the host rock. It is one of the important system components of the engineered barrier system.

(1) Buff1: limit advection

Buffer should be able to limit contact of the canisters with corrosive substances and contain nuclides released from the canisters. Therefore, the buffer should prevent substances from transport by advection. The safety function indicator is set to be "hydraulic conductivity of buffer" and "swelling pressure of buffer" due to expansion of the buffer. The safety function indicator criteria are "hydraulic conductivity of buffer < 1×10^{-12} m/s" and "swelling pressure of buffer > 1 MPa."

(2) Buff2: limit microbial activity

Microorganisms (sulfate-reducing bacteria) in the buffer will reduce sulfates in the bentonite and the groundwater, which can produce sulfide and induce corrosion of the copper shell. The prerequisites for maintaining the activity of the microorganisms require sufficient free water, nutrients, and space for microorganisms to grow. On the other hand, the pressure of the bentonite, low hydraulic conductivity, and low pore space in the bentonite can reduce the activity of the microorganisms (Motamedi et al., 1996; Pedersen et al., 2000a, Pedersen et al., 2000b, Masurat et al., 2010b); therefore, the safety function indicator is set to be "swelling pressure," and the safety function indicator criterion is "swelling pressure > 2 MPa" which can suppress sulfide produced by the microorganisms and avoid serious copper corrosion.

(3) Buff3: damp rock shear force

The buffer should be able to assist the canisters from being damaged by shear force (Can3). If the deformation capacity of the buffer in the deposition hole is small, the stress transferred to the canister when receiving shear force would be high. The deformation capacity of the buffer can be modified by buffer density. Therefore, the safety function indicator is set to be "buffer density," and the safety function indicator criterion is "buffer density < 2,050 kg/m^3." The canisters are not supposed to be impacted by shear force with 5 cm displacement at a velocity of 1 m/s under such conditions (SKB, 2011).

(4) Buff4: resist transformation

In order to prevent montmorillonite in the buffer from transferring into non-expandable minerals such as illite under high temperature, thereby reducing its swelling pressure, the safety function indicator is set to be “buffer temperature,” and the safety function indicator criterion is “buffer temperature < 100 ℃.”

(5) Buff5: prevent canister sinking

The buffer around the canisters must have sufficient swelling pressure to provide sufficient support to prevent the canisters from sinking or tilting. Therefore, the safety function indicator is set to be “swelling pressure,” and the safety function indicator criterion is “swelling pressure > 0.2 MPa.”

(6) Buff6: limit pressure applied to the canisters and rock

For the canisters to withstand uniform load, the sum of buffer swelling pressure and groundwater pressure should not exceed 15 MPa. Therefore, according to the analysis results, the safety function indicator is set to be “swelling pressure,” and the safety function criterion is “swelling pressure <10 MPa.”

In addition, if groundwater freezes, the volume of pore water in the buffer will increase, generating additional pressure on the canisters. Meanwhile, the buffer can also lose its swelling ability under low temperature (Birgersson et al., 2010). Although Taiwan is located in a subtropical zone, a freeze of the buffer is not likely to occur; the safety function indicator “buffer temperature” is still conservatively set for the repository. And the safety function indicator criterion is “buffer temperature > -2.5 ℃,” so the buffer can maintain sufficient swelling pressure.

7.3.3. Backfill

Backfill is used to backfill the disposal tunnels. The safety function of the backfill is described as follows:

(1) BF1: limit buffer expansion

The backfill must be able to resist the swelling pressure of the buffer, maintain the volume of the buffer in the deposition holes, and keep the swelling pressure of the buffer to be greater than 2 MPa; therefore, the backfill must have sufficient swelling pressure to offset buffer swelling. However, there are many influencing factors such as the flow rate of the groundwater and saturation time and sequence of the buffer and the backfill, and the safety function indicator is difficult to be defined as a specific value. Hence, the safety function indicator is set to be "swelling pressure of backfill," and the safety function indicator criterion is "swelling pressure of backfill should not be too low."

7.3.4. Geosphere

Safety functions of the host rock involve many factors and their interactions. These factors are difficult to be determined directly by simple standards. The effect of these factors and their interactions should be analyzed comprehensively. The safety functions of the host rock relating to its chemical, mechanical, hydrogeological and thermal conditions are described as follows:

(1) R1: provide preferred chemical conditions

The composition and characteristics of groundwater are important factors for determining the chemical conditions of the repository. The redox-oxidation state of groundwater, ionic strength, salinity, concentration of harmful substances, pH value, and chlorides are explained below:

(a) Redox state

The most basic requirement related to chemical conditions is the redox state, which can ensure that the canister will not be affected by oxidation. The solubility of fuel and radionuclides are low under a reduced state, and radionuclide adsorption of the buffer, backfill, and the host rock is also better. Also, because oxidation occurs when oxygen is present, another basic requirement for the host rock is it should be in an oxygen-free environment. The safety function indicator is set to be “redox oxidation state,” and the safety function indicator criterion is “limit Eh value.”

(b) Ionic strength and salinity

When the ionic strength of groundwater is high enough, the formation of colloids can be inhibited and stability can thereby be increased. One of the main sources of colloids in groundwater is chemical erosion in the interface of buffer and host rock. And chemical erosion requires a low ionic strength environment. Therefore, the safety function indicator is set to be “charge concentration of cations in water,” and the safety function indicator criterion is “charge concentration of cations in water > 8 mM.”

Groundwater with high salinity will have a negative impact on swelling pressure and hydraulic conductivity of the buffer and the backfill. Therefore, the safety function indicator is set to be “total dissolved solids (TDS),” and the safety function indicator criterion is “TDS < 35 g/L (instant total dissolved solids < 70 g/L).”

(c) Limit concentration of harmful substances

In an oxygen-deficient environment, sulfide is the main factor in the corrosion of the canisters. Sulfides exist in the groundwater and can be generated through microbial activities in groundwater, buffer, and backfill. Therefore, in addition to limiting the concentration of sulfides in groundwater, concentrations of methane and dissolved hydrogen gas should also be limited, so that the activity of microorganisms can be inhibited. Besides, pH value, chloride ion, sulfate, bicarbonate ion, and stress corrosion cracking (SCC) enhancing factors (including nitrogenous compounds such as nitrite, ammonium, and acetate) will all affect the corrosion of the canisters. In order to improve the long-term stability of the montmorillonite, the concentration of potassium and iron in groundwater should also be limited.

The safety function indicator is set to be "concentration of harmful substances in groundwater should be limited ([NO_2^-] < 10^{-3} M, [HS^-] < 3 mg/L≈10^{-4} M, and [K^+] < 0.1 M)."

(d) pH value

During construction, grouting materials and plug materials may produce high alkaline pore water because of chemical degradation. If the abovementioned pore water is in contact with the bentonite, the montmorillonite can become chemically unstable and the montmorillonite may dissolve. Therefore, the safety function indicator is set to be "pH value of the groundwater," and the safety function indicator criterion is "pH value of the groundwater should be between 5 and 11" (Posiva and SKB, 2017).

(e) Avoid chlorides from corrosion

In an oxygen-deficient environment, only when the pH value is lower than 4 and chloride concentration is high ([Cl^-]> 2 M), chloride corrosion of canisters will occur (Masurat et al., 2010). Therefore, the safety function indicator is set to be "acid-base value of groundwater" and "chloride concentration," and the safety function indicator criteria are "pH value in groundwater > 4" and "chloride concentration < 2 M."

(2) R2: provide preferred hydrogeologic and transport conditions

Host rock needs to provide preferred hydrogeologic and transport conditions for the repository. Such conditions include high flow-related transport resistance (F) of flow paths to limit groundwater transport and low equivalent flow rate (Q_{eq}) of the interface between the buffer and the host rock to limit solute exchange. Therefore, the safety function indicator is set to be "flow-related transport resistance of fracture" and "equivalent flow rate." The safety function indicator criteria are "flow-related transport resistance of fracture (intersecting with deposition holes) > 10,000 yr/m" and "equivalent flow rate < 1×10^{-4} m^3/yr."

(3) R3: provide mechanically stable environment

Two potential mechanical factors that could induce destruction of the canisters are destruction induced by isostatic load and destruction induced by shear displacement of fractures intersecting deposition holes. Therefore, the safety function indicator is set to be “groundwater pressure,” and the safety function indicator criterion is “limit groundwater pressure.” Shear displacement of fractures intersecting deposition holes can be evaluated based on a series of mechanical models. According to the design requirements of the canisters, the safety function indicator criteria are “shear displacement < 5 cm and velocity of shear displacement < 1 m/s.”

(4) R4: provide preferred thermal environment

If clay materials of the bentonite freeze, pressure in the deposition holes will increase and the canisters or the surrounding host rock may be damaged. According to safety functions Buff4 and Buff6, buffer temperature should be between -2.5 ℃ and 100 ℃. Therefore, the safety function indicator is set to be “host rock temperature,” and the safety function indicator criterion is “host rock temperature should be between -2.5 ℃ and 100 ℃.”

7.4. Retardation Safety Function Indicators

This section describes the safety functions, safety function indicators, and safety function indicator criteria of the system components (spent nuclear fuel, canister, buffer, backfill, and geosphere) related to retardation safety function. The retardation safety functions of each system component are summarized in Table 7-2.

Table 7-2: Retardation safety functions, containment safety function indicators, and containment safety function indicator criteria.

Retardation safety functions, retardation safety function indicators, and retardation safety function indicator criteria			
System components	**Safety function**	**Containment safety function indicator and criteria**	**References and instructions**
SNF	F1: constraint radionuclides	(a) fuel matrix conversion rate: low (b) metal corrosion rate $<10^{-3}$ /year	Posiva and SKB, 2017
	F2: precipitation	nuclides solubility: low	SKB, 2011
	F3: avoid criticality	effective multiplication factor (k_{eff}) < 0.95, when the canister is filled with water	SKB, 2011
canister	Can4: resist transportation	(a) delay time (t_{delay}):long (b) the time for the canister to lose its ability to reduce the transmission rate (t_{large}):long	SKB, 2011
	Can5: avoid criticality	(a) suitable geometric characteristics of the canister (b) suitable material characteristics of the canister	SKB, 2011
buffer	Buff1: limit advection	(a) hydraulic conductivity of buffer $<1\times10^{-12}$ m/s (b) swelling pressure of buffer >1 MPa	SKB, 2011
	Buff4: resist transformation	buffer temperature < 100 ℃	SKB, 2011
	Buff5: prevent canister sinking	swelling pressure of buffer > 0.2 MPa	SKB, 2011
	Buff7: filter colloid	buffer dry density >1,000 kg/m^3	Posiva and SKB, 2017
	Buff8: absorb radionuclides	distribution coefficient (K_d): high	Posiva and SKB, 2017
	Buff9: allow gas transmission	swelling pressure of buffer: low	Posiva and SKB, 2017
backfill	BF2: limit advection	(a) hydraulic conductivity of backfill $<10^{-10}$ m/s (b) swelling pressure of backfill >0.1 MPa	SKB, 2011
	BF3: absorb radionuclides	distribution coefficient (K_d): high	SKB, 2011
geosphere	R1: provide preferred chemical conditions	(a) redox-oxidation state: limited Eh value (b) ionic strength and salinity: charge concentration of cations in groundwater > 8 mM and TDS < 35 g/L(instant total dissolved solids < 70 g/L) (c)limit concentration of harmful substances: $[NO_2^-] < 10^{-3}$ M; $[HS^-] < 3$ mg/L$\approx10^{-4}$ M; $[K^+] < 0.1$ M (d) pH value of groundwater should be between 5 and 11	Posiva and SKB, 2017
	R2: provide preferred hydrogeologic and transport conditions	(a) flow-related transport resistance in the fracture (F) > 10,000 yr/m (b) equivalent flow rate $< 1\times10^{-4}$ m^3/yr (c) effective diffusion coefficient (D_e): high; distribution coefficient (K_d): high (d) colloid concentration: low	Posiva and SKB, 2017

Note: SKB and POSIVA reports were referred to for the specification of the safety function indicators and criteria, and research results of SKB and POSIVA were referred to for the specification of quantitative values of the safety function indicator criteria. However, some of the safety function indicators could have various impact factors, and a single value for the safety function indicator criteria might be difficult to specify. In this circumstances, no quantitative value was used.

(1) Spent Nuclear Fuel

(a) F1: constraint radionuclides

SNF needs to have a complete crystal lattice structure so that it can maintain stability in the repository and the radionuclides can be confined in the fuel. Radionuclides may be released through fuel conversion effects such as chemical dissolution and oxidative dissolution of the fuel matrix. Therefore, the safety function indicator is set to be “fuel matrix conversion rate,” and the safety function indicator criterion is “low fuel matrix conversion rate.”

In addition, because the metal of the fuel assembly also has the function of restricting the radionuclide species, the safety function indicator is set as the "metal corrosion rate of the fuel assembly," and the safety function indicator criterion is set as the "metal corrosion rate of the fuel assembly per year."

In addition, the metal of the fuel assembly can also constrain radionuclides. Therefore, the safety function indicator is set to be “metal corrosion rate of the fuel assembly,” and the safety function indicator criterion is “metal corrosion rate of fuel assembly < 10^{-3}/year.”

(b) F2: precipitation

Release of the radionuclides will be constrained by the solubility limit. Therefore, the safety function indicator is set to be “nuclide solubility,” and the safety function indicator criterion is “low nuclide solubility.”

(c) F3: avoid criticality

In order to maintain sub-criticality within the canisters (neutron effective multiplication factor < 1) to avoid criticality, the safety function indicator is set to be “effective multiplication factor,” and the safety function indicator criterion is “effective multiplication factor (k_{eff}) < 0.95, when the canister is filled with water.”

(2) Canister

(a) Can4: resist transportation

Groundwater will infiltrate into the canister and contact with the fuel when the canister is damaged. And radionuclides may be released along with the water flow. Although the design of the canister is not used to reduce the transport rate, certain restrictions to the transport rate can be provided within a limited amount of time after the canister is damaged. Therefore, the safety function indicators are set to be "the time from the canister is damaged to the radionuclides are released (delay time, t_{delay})" and "the time for the canister to lose its ability to reduce the transmission rate (t_{large})." The safety function indicator criteria are "the delay time (t_{delay}) should be long" and "the time for the canister to lose its ability to reduce the transmission rate (t_{large}) should be long".

(b) Can5: avoid criticality

The geometry and material properties of the canisters should be able to avoid criticality. Therefore, the safety function indicator is set to be "the geometric and material characteristics of the canister," and the safety function indicator criterion is "suitable geometric and material characteristics of the canister."

(3) Buffer

(a) Buff1: limit advection

The buffer should be able to limit contact between the canisters and possible corrosive substances and confine radionuclides released from the canisters. That is, the buffer should be able to help avoid materials transport rapidly through advection. Therefore, the safety function indicator is set to be "hydraulic conductivity of buffer" and "swelling pressure of buffer." The safety function indicator criteria are "hydraulic conductivity of buffer < 1×10^{-12} m/s" and "swelling pressure > 1 MPa."

(b) Buff4: resist transformation

In order to prevent montmorillonite in the buffer from transferring into non-expandable minerals such as illite under high temperature, thereby reducing its swelling pressure, the safety function indicator is set to be "buffer temperature," and the safety function indicator criterion is “buffer temperature < 100 ℃.”

(c) Buff5: prevent canister sinking

Buffer around the canisters must have sufficient swelling pressure to provide sufficient support for the prevention of the canisters from sinking or tilting. Therefore, the safety function indicator is set to be “swelling pressure,” and the safety function indicator criterion is “swelling pressure > 0.2 MPa.”

(d) Buff7: filter colloids

The buffer should be sufficiently compact to avoid colloids from getting through. The particle size of colloids is around 10^{-9} to 10^{-6} m, fuel colloids can be constrained if the buffer has sufficient density when the canister is damaged. According to the results of metal colloids experiments (Kurosawa et al., 1997; Holmboe et al., 2010), colloid transport can be blocked when the dry density of the bentonite is greater than 1,000 kg/m^3. Therefore, the safety function indicator is set to be “buffer dry density,” and the safety function indicator criterion is “buffer dry density > 1,000 kg/m^3.”

(e) Buff8: absorb radionuclides

The buffer can constrain the release of radionuclides through sorption. Therefore, the ability to absorb radionuclides is one of the important functions of the buffer. The safety function indicator is set to be the “distribution coefficient (K_d),” and the safety function indicator criterion is “high distribution coefficient (K_d).”

(f) Buff9: allow gas transmission

When the canister is damaged, groundwater intrusion may lead to anaerobic corrosion of the cast iron lining, and hydrogen gas may thereby be generated. The buffer needs to have sufficient transmissibility for gas so that the generated gas can be released and will not accumulate between the canister and the buffer. When the pressure of the gas is high, a gas passage will be formed in the buffer, and the gas will be released from it. Meanwhile, the passage can compromise the retardation safety function of the buffer. Gas transmissibility is related to swelling pressure of the buffer. Lower swelling pressure can be beneficial to the transmission of the gas. Therefore, the safety function indicator is set to be “swelling pressure,” and the safety function indicator criterion is “swelling pressure should be low.”

(4) Backfill

(a) BF2: limit advection

The ability to restrict advection of the backfill can keep the buffer and the canisters from being damaged by potentially harmful substances in the groundwater. By limiting the hydraulic conductivity of backfill to near or lower than the one of the surrounding host rock, radionuclides transport through advection can also be avoided, thereby achieving the retardation safety function. The safety function indicator is set to be “hydraulic conductivity of backfill,” and the safety function indicator criterion is “hydraulic conductivity of backfill $< 1 \times 10^{-10}$ m/s.”

In addition, the swelling pressure of the backfill should be adequate to backfill uniformly and completely, so that the safety functions of the buffer can be maintained. Therefore, the safety function indicator is set to be “swelling pressure of backfill,” and the safety function indicator criterion is “swelling pressure of backfill > 0.1 MPa.”

(b) BF3: absorb radionuclides

The ability of the backfill to absorb radionuclides can limit radionuclides outward transport, which is one of the important factors related to the transport of radionuclides. The safety function indicator is set to be the “distribution coefficient (K_d),” and the safety function indicator criterion is “high distribution coefficient (K_d).”

(5) Geosphere

The retardation safety functions that the geosphere should have a focues on the suitability of chemical, hydrogeologic, and transport characteristics. Most safety function indicators are the same as the containment safety functions, which include: providing preferred chemical conditions (R1) and providing preferred hydrogeologic and transport conditions (R2):

(a) R1: provide preferred chemical conditions

(i) Redox state

The basic requirement of chemical conditions for the repository is a redox state. Canisters can be protected from oxidation, the solubility of fuel matrix and radionuclides will be lower, and sorption of the buffer, backfill, and the host rock will be better in the redox state. Since oxidation occurs in an aerobic environment, the requirement for the host rock will be without dissolved oxygen. The safety function indicator is set to be “redox-oxidation state,” and the safety function indicator criterion is “limited Eh value.”

(ii) Ionic strength and salinity

Formation of colloids can be suppressed and stability can be improved when the ionic strength of groundwater is high enough. Colloids produced by chemical erosion in the interface of buffer and host rock are one of the main sources of colloids in groundwater. Since chemical erosion requires low ionic strength, the safety function indicator is set to be “charge concentration of cations in groundwater,” and the safety function indicator criterion is “charge concentration of cations in groundwater > 8 mM.”

Besides, high salinity groundwater will have a negative impact on swelling pressure and hydraulic conductivity of the buffer and the backfill. Therefore, the safety function indicator is set to be “total dissolved solids,” and the safety function indicator criterion is “TDS < 35 g/L (instant TDS < 70 g/L).”

(iii) Concentration of harmful substances

Sulfide is one of the main corrosive factors of the copper shell in an anaerobic environment. Sulfides can be generated through microbial activities in groundwater, buffer, and backfill, and exist in the groundwater. In order to inhibit microbial activity, besides the concentration of sulfides in groundwater, the concentration of methane and dissolved hydrogen should also be limited. Other factors like pH value, chloride ions, sulfate ions, bicarbonate ions, and stress corrosion cracking (SCC) enhancing factors (including nitrogenous compounds such as nitrite, ammonium, and acetate) will also affect the corrosion of the canisters. Also, other than improving the long-term stability of the montmorillonite, the concentration of potassium and iron in groundwater should be constrained.

The safety function indicator is set to be "concentration of harmful substances in groundwater should be limited ($[NO_2^-] < 10^{-3}$ M, $[HS^-] < 3$ mg/L$\approx 10^{-4}$ M, and $[K^+] < 0.1$ M)."

(iv) pH value

During construction, grouting materials and plug materials may produce high alkaline pore water because of chemical degradation. If the abovementioned pore water is in contact with the bentonite, the montmorillonite can become chemically unstable and the montmorillonite may dissolve. Therefore, the safety function indicator is set to be "pH value of the groundwater," and the safety function indicator criterion is "pH value of the groundwater should be between 5 and 11" (Posiva and SKB, 2017).

(b) R2: provide preferred hydrogeologic and transport conditions

Host rock needs to provide preferred hydrogeologic and transport conditions for the repository. Such conditions include high flow-related transport resistance (F) of flow paths to limit groundwater transport, and low equivalent flow rate (Q_{eq}) of the interface between the buffer and the host rock to limit solute exchange. Therefore, the safety function indicator is set to be “flow-related transport resistance of fracture” and “equivalent flow rate.” The safety function indicator criteria are “flow-related transport resistance of fracture (intersecting with deposition holes) > 10,000 yr/m” and “equivalent flow rate < 1×10^{-4} m^3/yr.”

In addition, the following safety functions are also required:

(i) Matrix diffusion and sorption of the host rock

Radionuclides can be retarded by matrix diffusion and sorption of the host rock. Therefore, the safety function indicator is set to be the “effective diffusion coefficient (D_e)” and “distribution coefficient (K_d),” and the safety function indicator criteria are “high effective diffusion coefficient (D_e)” and “high distribution coefficient (K_d).”

(ii) Colloid concentration

The concentration of the natural colloids should be limited to avoid radionuclides transport through groundwater in the fractures by attaching to the colloids. Therefore, the safety function indicator is set to be “colloid concentration,” and the safety function indicator criterion is “low colloid concentration.”

7.5. Key Issues of Evolution over Time

The purpose of defining the safety functions of the repository system is to compare the evolution of multiple barriers at different times to safety function indicator criteria so that quantitative evaluation of barrier performance can be conducted and long-term safety of the repository can be assured by the system components.

After evolution analyses, those against the safety function indicator criteria should be the key issues for the safety assessment. Further evaluation and analysis are required to ensure that possible consequences will not jeopardize the long-term safety of the repository.

Table 7-1 and Table 7-2 show the key issues that should be further analyzed in the following assessment.

7.6. Factors affecting Safety Function Indicators over Time

The safety of the repository is judged by whether the safety functions of the repository are maintained. The evolution of the repository is mainly controlled by initial state, coupling of internal processes, and external factors. And these will affect the measurement and calculation of the safety function indicators.

The correlation of these factors, how these factors relate to the measurement and calculation of the safety function indicators, and how the safety functions of the repository will be affected will depend on key issues considered in the safety assessment. Relevant analysis results are in Chapter 11.

8. Compilation of Input Data and Data Uncertainty

8.1. Introduction

In order to complete the evaluation of safety functions of containment and retardation, multiple assessment models were correlated in the safety assessment.

In safety assessment, the assessment results of models are transferred to radionuclide transport models. The data used in radionuclide transport models are directly influenced to the resulting dose consequences. Therefore, input parameters in the assessment models for radionuclide transport (Figure 8-1) are compiled in this chapter, and the uncertainties are shown by tables and graphs as the basis for subsequent deterministic or probabilistic analyses. The input parameters that have substantial influences can also be identified. Detailed assessment, research, and investigations can also be planned according to this information.

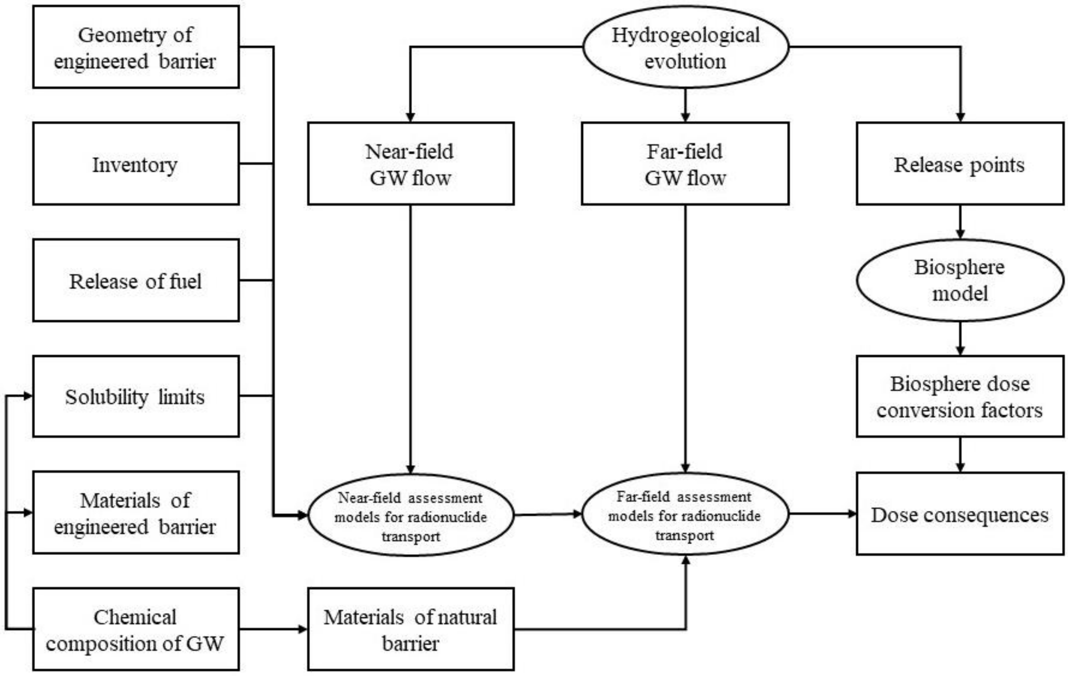

Figure 8-1: Input data parameters for radionuclide transport in safety assessment.

Note: The ovals represent the models and the rectangles represent the input/output data.

8.2. Reference Requirements and Criteria for Judgment

Input data parameters can have certain uncertainties because of the large temporal and spatial scale in the assessment. Deviations of the repository and the system units between design and manufacturing/installation were also taken into consideration in the assessment. The suitability of input data parameters was discussed by the suppliers and the applicants, and data improvements will be continued in the future. The above-mentioned uncertainties would be passed on to total-system safety assessment eventually through assessment models in each step. Multiple assessment cases and sensitivity analyses were performed in the safety assessment to identify key issues and parameters, and to clarify what should be focused on in detailed assessment, research, and investigations in the future.

8.3. Inventory of Data

The models and parameters used in safety assessment have been shown in the assessment model flow chart. Except for the near and far-field radionuclide transport models, the main parameters for other assessment models and sources are described in the respective sections. The main input parameters for the radionuclide transport model are shown in Figure 8-1, and the geometry parameters of the engineered barrier are covered in Section 4.2. The hydrogeological evolution of the repository is covered in Sections 9.3.6 and 9.4.6, groundwater flow assessment for near-field and far-field radionuclide transport model are covered in Sections 12.4.1 and 12.4.2, and the biosphere dose conversion factors will be covered in Section 12.2. The other input parameters are summarized as follows:

(1) Fuel and initial inventory of the interested radionuclides:

The initial inventory of the interested radionuclides of the SNF is listed in Table 4-1. If a canister fails, groundwater will enter the void of the canister, and the fuel matrix or corroded metal assemblies of the fuel will dissolve into the groundwater. The fuel dissolution rate and its uncertainties were adopted from the SKB report (SKB, 2010i) and can be found in Table 8-1 (SKB, 2010i). Uncertainties of two orders of magnitude were considered for the dissolution rate. The release duration of the corroded metal assemblies of the fuel is specified in Table 8-2 and they were also adopted from the SKB report (SKB, 2010i). The range of fully corroded time was estimated using the corrosion rate of relatively fast corroded material (stainless steel) and the thickness of the thinnest part of fuel (Inconel spacers) by SKB. The most conservative fully-corroded time was adopted for the other metal parts. The corrosion release fraction (CRF) of the radionuclides is in Table 8-3 (SKB, 2010i; SKB, 2010i), and the instant release fraction (IRF) of the radionuclides which are instantly released to the groundwater is listed in Table 8-4 (SKB, 2010h; SKB, 2010i).

(2) Material parameters of the repository:

Barriers such as buffer, backfill and host rock were included in the radionuclide transport calculation models. Dry densities and porosities of the materials should be put into the models. Dry densities and porosities of the buffer and backfill were adopted from the SKB report (SKB, 2010h; SKB, 2010i). The values used in the deterministic and stochastic analyses are listed in Table 8-5, and they were estimated based on spatial variability. On the other hand, the dry densities and porosities of the host rock were adopted from the previous research (台電公司, 2019a). And the values are listed in Table 8-5 as well.

(3) Properties of the radionuclides:

Radionuclides will transport through an engineered barrier system of different materials. The properties of radionuclides will be affected by the composition of groundwater, and the composition of groundwater will then be influenced by climate evolution and sea-level fluctuations. Two sets of deterministic parameters were assumed for the assessment of the influence mentioned previously: (i) current sea-level and (ii) sea-level falls to -120 m. SKB reports were mainly referred to for the setting of the parameters in the set of current sea-level. The values are the median values of the probability distributions (for instance, effective diffusion coefficient and available porosity) or suggested values (for instance, partition coefficients for fresh/saline groundwater)/median values (for instance, solubility limits for groundwater composition in a temperate climate) in the probability distributions for a specific groundwater composition. POSIVA reports were mainly referred to for the setting of the parameters in the set of sea-level falls to -120 m. Suggested values for fresh water in glacial periods were used. To carry out the probabilistic calculation, SKB reports were referred to for the setting of uncertainty parameter set. Suggested values based on different internal and external conditions of the repository were used.

The element-specific effective diffusion coefficients (De) for different barrier materials can be found in Table 8-6. These values were suggested by SKB by taking groundwater composition and sources of uncertainties into consideration.

The diffusion-available porosity of buffer, backfill and rock matrix can be found in Table 8-7. The diffusion-available porosity of the rock matrix is equal to its physical porosity.

The solubility limits are in Table 8-8, and Figure 8-2 to Figure 8-5, and the partition coefficients (K_d) are shown in Table 8-9 to Table 8-11.

Table 8-1: Fuel dissolution rate.

Deterministic analysis			
Fuel dissolution rate [yr^{-1}]			
			10^{-7}
Probabilistic analysis			
Fuel dissolution rate [yr^{-1}]			
Lower limit	**Best estimation**	**Upper limit**	**Distribution**
10^{-8}	10^{-7}	10^{-6}	Triangular distribution in the $\log_{10}$ space.

Table 8-2: Release duration of the metal assemblies of corroded fuel.

Deterministic analysis			
Release duration of the metal assemblies of fuel [yr]			
			10^{3}
Probabilistic analysis			
Release duration of the metal assemblies of fuel [yr]			
Lower limit	**Best estimate**	**Upper limit**	**Distribution**
10^{2}	10^{3}	10^{4}	Triangular distribution in the $\log_{10}$ space.

Table 8-3: Corrosion release fraction (CRF).

Deterministic analysis				
Radionuclide	**Corrosion release fraction [-]**			
C-14				6.40×10^{-1}
Cl-36				1.50×10^{-2}
Ni-59				9.60×10^{-1}
Se-79				1.30×10^{-4}
Zr-93				1.30×10^{-1}
Nb-94				9.82×10^{-1}
Tc-99				6.10×10^{-5}
U-233				2.50×10^{-1}
Probabilistic analysis				
Radionuclide	**Corrosion release fraction [-]**			
	Lower limit	**Best estimation**	**Upper limit**	**Distribution**
C-14	5.70×10^{-1}	6.40×10^{-1}	6.80×10^{-1}	Double triangular distribution in normal space (the probability of each triangular is 50%).
Cl-36	1.40×10^{-2}	1.50×10^{-2}	1.80×10^{-2}	
Ni-59	9.00×10^{-1}	9.60×10^{-1}	9.90×10^{-1}	
Se-79	0	1.30×10^{-4}	5.50×10^{-4}	
Zr-93	9.30×10^{-2}	1.25×10^{-1}	1.40×10^{-1}	
Nb-94	-	1	-	
Tc-99	4.00×10^{-5}	6.10×10^{-5}	1.30×10^{-4}	
U-233	1.26×10^{-1}	2.50×10^{-1}	2.90×10^{-1}	

Table 8-4: Instant release fraction (IRF).

Deterministic analysis	
Radionuclide	**Instant release fraction [-]**
C-14	9.20×10^{-2}
Cl-36	8.60×10^{-2}
Ni-59	1.20×10^{-2}
Se-79	4.20×10^{-3}
Sr-90	2.50×10^{-3}
Zr-93	9.20×10^{-6}

Deterministic analysis	
Nb-94	1.80×10^{-2}
Tc-99	2.00×10^{-3}
Pd-107	2.00×10^{-3}
Sn-126	3.00×10^{-4}
I-129	2.90×10^{-2}
Cs-135	2.90×10^{-2}
Cs-137	2.90×10^{-2}

Probabilistic analysis				
Radionuclide	**Instant release fraction [-]**			
	Lower limit	**Best estimate**	**Upper limit**	**Distribution**
C-14	8.50×10^{-2}	9.20×10^{-2}	1.10×10^{-1}	Double triangular distribution in normal space (the probability of each triangular is 50%)..
Ni-59	1.60×10^{-3}	1.20×10^{-2}	1.70×10^{-2}	
Sr-90	0	2.50×10^{-3}	1.00×10^{-2}	
Zr-93	6.30×10^{-8}	9.20×10^{-6}	1.40×10^{-5}	
Nb-94	6.40×10^{-7}	1.80×10^{-2}	2.70×10^{-2}	
Tc-99	0	2.00×10^{-3}	1.00×10^{-2}	
Pd-107	0	2.00×10^{-3}	1.00×10^{-2}	
Sn-126	0	3.00×10^{-4}	1.00×10^{-3}	
	Mean value	**Standard deviation**		**Distribution**
Cl-36	7.60×10^{-2}	6.40×10^{-2}		Normal distribution.
Se-79	3.80×10^{-3}	3.20×10^{-3}		
I-129	2.50×10^{-2}	2.10×10^{-2}		
Cs-135	2.50×10^{-2}	2.10×10^{-2}		
Cs-137	2.50×10^{-2}	2.10×10^{-2}		

※For those which are not listed in the table are not released to groundwater instantly.

Table 8-5: The material parameters of the disposal system.

Deterministic analysis						
System unit	**Dry density [kg/m³]**			**Porosity [%]**		
Buffer	1,562.00			45.00		
Backfill	1,504.00			46.00		
Host rock	2,750.00			0.53		
Probabilistic analysis						
System unit	**Dry density [kg/m³]**			**Porosity [%]**		
	Lower limit	**Peak value**	**Upper limit**	**Lower limit**	**Peak value**	**Upper limit**
Buffer	1,484	1,562	1,640	41.00	43.50	46.00
Backfill	1,458	1,504	1,535	44.00	46.00	48.00
Distribution	The dry density distribution of backfill is the double triangular distribution in normal space (the probability of each triangular is 50%). The distribution of the other parameters is the triangular distribution in normal space.					

Table 8-6: Element specific effective diffusion coefficients.

Deterministic analysis			
System unit	**Buffer**	**Backfill**	**Host rock**
Current sea-level			
Effective diffusion coefficients [m²/yr]	4.20×10^{-3} 8.40×10^{-3} (Cs) 2.50×10^{-4} (Cl, I, and Se)	5.00×10^{-3} 9.90×10^{-3} (Cs) 3.10×10^{-4} (Cl, I, and Se)	6.30×10^{-7} 2.00×10^{-7} (Cl, I, and Se)
Sea-level falls to -120 m			

Effective diffusion coefficients [m^2/yr]	4.10×10^{-3} 7.38×10^{-3} (Cs) 2.38×10^{-2} (Ra and Sr) 8.81×10^{-7} (Cl, I, and Se)		1.43×10^{-7}
Note	The effective diffusion coefficients of Pb and Ac in buffer in fresh water were not mentioned in the references, thus were assumed to have the same values as the other cation elements.		
Probabilistic analysis			
System unit	**Effective diffusion coefficient [m^2/yr]**		
	Lower limit	**Best estimate**	**Upper limit**
	In $\log_{10}$ space		
Buffer	-2.53	-2.36	-2.18
Distribution	The triangular distribution in $\log_{10}$ space.		
Cs	-2.52	-1.88	-1.88
Distribution	Right triangular distribution in $\log_{10}$ space.		
Cl, I, and Se	-4.72	-3.46	-2.72
Distribution	Double triangular distribution in $\log_{10}$ space.		
Backfill	-2.46	-2.30	-2.12
Distribution	The triangular distribution in $\log_{10}$ space.		
Cs	-2.46	-1.82	-1.82
Distribution	Right triangular distribution in $\log_{10}$ space.		
Cl, I, and Se	-4.50	-3.43	-2.66
Distribution	Double triangular distribution in $\log_{10}$ space (the probability of each triangular is 50%).		
	Mean value	**Standard deviation**	
	In $\log_{10}$ space		
Host rock	-6.18	2.5×10^{-1}	
Cl, I, and Se	-6.68	2.5×10^{-1}	
Distribution	Normal distribution in $\log_{10}$ space.		

Table 8-7: Diffusion-available porosity of the system units.

Deterministic analysis			
	System unit		
	Buffer	**Backfill**	**Host rock**
Current sea-level			
Diffusion-available porosity [%]	45.00 18.00 (Cl, I, and Se)	46.00 19.00 (Cl, I, and Se)	0.53
Sea-level falls to -120 m			
Diffusion-available porosity [%]	45.00 1.00 (Cl, I, and Se)	46.00 1.00 (Cl, I, and Se)	0.53
Probabilistic analysis			
System unit	**Diffusion-available porosity [%]**		
	Upper limit	**Upper limit**	**Upper limit**
Buffer	4.60×10^{1}	4.60×10^{1}	4.60×10^{1}
Distribution	The triangular distribution in normal space.		
Cl, I, and Se	2.41×10^{1}	2.41×10^{1}	2.41×10^{1}
Distribution	Double triangular distribution in normal space (the probability of each triangular is 50%).		
Backfill	4.80×10^{1}	4.80×10^{1}	4.80×10^{1}
Distribution	Double triangular distribution in normal space (the probability of each triangular is 50%).		
Cl, I, and Se	2.56×10^{1}	2.56×10^{1}	2.56×10^{1}
Distribution	The triangular distribution in normal space.		

Table 8-8: Solubility limits for each element.

Deterministic analysis		
Element	**Current sea-level**	**Sea-level falls to -120 m**
	Solubility limits [mol/m^3]	
Ac	Totally dissolved.	
Am	2.50×10^{-3}	3.30×10^{-5}
C	Totally dissolved.	
Cl	Totally dissolved.	
Cm	2.60×10^{-3}	3.30×10^{-5}
Cs	Totally dissolved.	
I	Totally dissolved.	
Nb	4.90×10^{-2}	2.10×10^{-1}
Ni	3.00×10^{-1}	1.40×10^{-4}
Np	1.00×10^{-6}	1.00×10^{-5}
Pa	3.30×10^{-4}	1.00×10^{-5}
Pb	1.70×10^{-3}	1.70×10^{-3}
Pd	3.90×10^{-3}	4.00×10^{-3}
Pu	4.80×10^{-3}	1.40×10^{-8}
Ra	9.10×10^{-4}	4.20×10^{-7}
Se	6.70×10^{-6}	5.90×10^{-6}
Sn	9.00×10^{-5}	4.20×10^{-3}
Sr	3.70	2.00×10^{-2}
Tc	3.80×10^{-6}	4.40×10^{-6}
Th	2.60×10^{-6}	2.10×10^{-6}
U	9.50×10^{-7}	8.70×10^{-6}
Zr	1.80×10^{-5}	1.80×10^{-5}

Probabilistic analysis			
Element	**Solubility limits [mol/m^3]**		
	5% percentile	**Mean value**	**95% percentile**
Ac	Totally dissolved.		
Am	1.18×10^{-4}	2.56×10^{-3}	9.14×10^{-3}
C	Totally dissolved.		
Cl	Totally dissolved.		
Cm	1.28×10^{-4}	3.16×10^{-3}	1.18×10^{-2}
Cs	Totally dissolved.		
I	Totally dissolved.		
Nb	1.92×10^{-2}	9.78×10^{-2}	3.17×10^{-1}
Ni	1.36×10^{-3}	2.36	1.28×10^{1}
Np	1.66×10^{-7}	2.93×10^{-6}	1.08×10^{-5}
Pa	1.18×10^{-4}	3.92×10^{-4}	8.93×10^{-4}
Pb	1.70×10^{-4}	1.16×10^{-3}	3.55×10^{-3}
Pd	4.03×10^{-4}	1.02×10^{-2}	3.96×10^{-2}
Pu	2.13×10^{-5}	6.15×10^{9}	1.99×10^{3}
Ra	2.07×10^{-4}	5.99×10^{-3}	2.35×10^{-2}
Se	3.28×10^{-7}	3.06×10^{-5}	1.22×10^{-4}
Sn	1.47×10^{-5}	2.15×10^{-4}	7.55×10^{-4}
Sr	2.28×10^{-1}	1.82	5.48
Tc	1.65×10^{-6}	5.33×10^{-6}	1.22×10^{-5}
Th	4.52×10^{-7}	2.14×10^{-5}	8.70×10^{-5}
U	8.75×10^{-11}	1.33×10^{-5}	4.67×10^{-5}
Zr	7.09×10^{-7}	1.25×10^{-4}	4.51×10^{-4}
Distribution	As shown in Figure 8-2.		

Table 8-9: Partition coefficients for each element of the system units (deterministic analysis).

Element	System unit			
	Buffer and backfill		**Host rock**	
	Current sea-level	**Sea-level falls to -120 m**	**Current sea-level**	**Sea-level falls to -120 m**
	Partition coefficient [m^3/kg]			
Ac	8.00	8.00	1.48×10^{-2}	1.48×10^{-2}
Am	6.10×10^{1}	1.35×10^{2}	1.48×10^{-2}	1.50×10^{-1}
C	0	0	0	0
Cl	0	0	0	0
Cm	6.10×10^{1}	1.35×10^{2}	1.48×10^{-2}	1.50×10^{-1}
Cs	9.30×10^{-2}	4.10×10^{-1}	3.49×10^{-4}	1.40
I	0	0	0	0
Nb	3.00	1.81	1.98×10^{-2}	4.20×10^{-1}
Ni	3.00×10^{-1}	3.15	1.10×10^{-3}	3.00×10^{-1}
Np	2.00×10^{-2}	6.30×10^{1}	4.13×10^{-4}	4.00×10^{-1}
Pa	3.00	8.10×10^{1}	5.92×10^{-2}	3.60×10^{-1}
Pb	7.40×10^{1}	7.40×10^{1}	2.52×10^{-2}	2.52×10^{-2}
Pd	5.00	3.14	5.20×10^{-2}	3.00×10^{-1}
Pu	2.00×10^{-2}	2.40×10^{1}	9.14×10^{-3}	6.00×10^{-1}
Ra	4.50×10^{-3}	1.06×10^{-1}	2.42×10^{-4}	1.80×10^{-2}
Se	0	0	2.95×10^{-4}	0
Sn	6.30×10^{1}	1.14	1.59×10^{-1}	1.80×10^{-3}
Sr	4.50×10^{-3}	1.06×10^{-1}	3.42×10^{-6}	8.00×10^{-4}
Tc	0	2.00	0	4.00×10^{-1}
Th	6.30×10^{1}	6.30×10^{1}	5.29×10^{-2}	4.00×10^{-1}
U	3.00	5.60×10^{-3}	1.06×10^{-4}	1.60
Zr	4.00	6.30×10^{1}	2.13×10^{-2}	4.00×10^{-1}

Table 8-10: Partition coefficients for each element of buffer and backfill (probabilistic analysis).

Element	**Lower limit [m^3/kg]**	**Most probable value [m^3/kg]**	**Upper limit [m^3/kg]**
Ac	3.00×10^{-1}	8	2.33×10^{2}
Am	1.00×10^{1}	6.10×10^{1}	3.78×10^{2}
C	0	0	0
Cl	0	0	0
Cm	1.00×10^{1}	6.10×10^{01}	3.78×10^{2}
Cs	1.50×10^{-2}	9.30×10^{-2}	5.60×10^{-1}
I	0	0	0
Nb	2.00×10^{-1}	3	4.50×10^{1}
Ni	3.00×10^{-2}	3.00×10^{-1}	3.30
Np	4.00×10^{-3}	2.00×10^{-2}	2.00×10^{-1}
Pa	2.00×10^{-1}	3	4.50×10^{1}
Pb	1.20×10^{1}	7.40×10^{1}	4.57×10^{2}
Pd	3.00×10^{-1}	5	7.50×10^{1}
Pu	2.00×10^{-3}	2.00×10^{-2}	2.00×10^{-1}
Ra	7.50×10^{-4}	4.50×10^{-3}	2.70×10^{-2}
Se	0	0	0
Sn	2.30	6.30×10^{1}	1.76×10^{3}
Sr	7.50×10^{-4}	4.50×10^{-3}	2.70×10^{-2}

Tc	0	0	0
Th	6	6.30×10^{1}	7.00×10^{2}
U	5.00×10^{-1}	3.00	1.80×10^{1}
Zr	1.00×10^{-1}	4	1.03×10^{2}
Distribution	The triangular distribution in $\log_{10}$ space.		

Table 8-11: Partition coefficients for each element of host rock (probabilistic analysis).

Element	**Mean value [m^3/kg]**	**Standard deviation**	**Lower limit [m^3/kg]**	**Upper limit [m^3/kg]**
	In $\log_{10}$ space			
Ac	-1.83	7.20×10^{-1}	-3.24	-4.17×10^{-1}
Am	-1.83	7.20×10^{-1}	-3.24	-4.17×10^{-1}
C	0	0	0	0
Cl	0	0	0	0
Cm	-1.83	7.20×10^{-1}	-3.24	-4.17×10^{-1}
Cs	-3.46	5.10×10^{-1}	-4.46	-2.45
I	0	0	0	0
Nb	-1.70	6.40×10^{-1}	-2.96	-4.52×10^{-1}
Ni	-2.96	6.50×10^{-1}	-4.22	-1.69
Np	-1.28	6.50×10^{-1}	-2.55	-7.00×10^{-3}
Pa	-1.23	4.80×10^{-1}	-2.17	-2.86×10^{-1}
Pb	-1.60	5.60×10^{-1}	-2.69	-5.09×10^{-1}
Pd	-1.28	8.30×10^{-1}	-2.91	3.44×10^{-1}
Pu	-1.83	7.20×10^{-1}	-3.24	-4.17×10^{-1}
Ra	-3.62	4.10×10^{-1}	-4.41	-2.82
Se	-3.53	5.50×10^{-1}	-4.60	-2.46
Sn	-8.00×10^{-1}	2.80×10^{-1}	-1.35	-2.53×10^{-1}
Sr	-5.47	9.90×10^{-1}	-7.42	-3.46
Tc	-1.28	6.50×10^{-1}	-2.55	-7.00×10^{-3}
Th	-1.28	6.50×10^{-1}	-2.55	-7.00×10^{-3}
U	-1.28	6.50×10^{-1}	-2.55	-7.00×10^{-3}
Zr	-1.67	3.50×10^{-1}	-2.35	-9.91×10^{-1}
Distribution	The normal distribution in $\log_{10}$ space.			

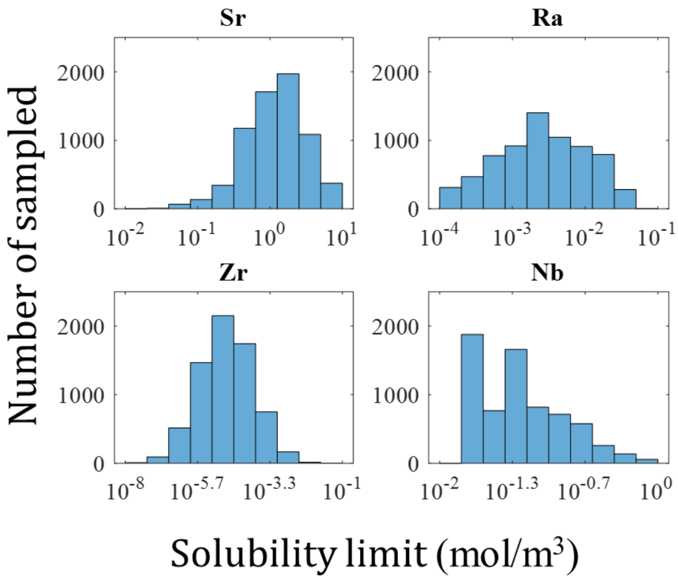

Figure 8-2: The distributions of solubility limits for strontium, radium, zirconium, and niobium in probabilistic analyses.

Note: The sample size of the solubility for each element is 6,916.

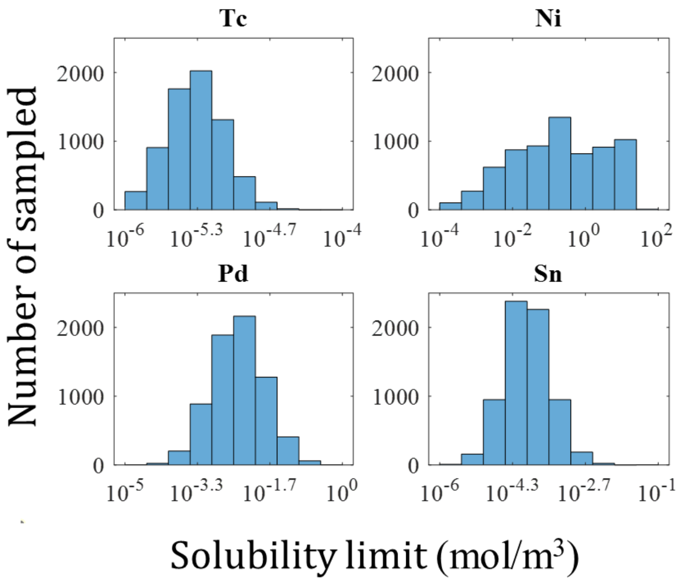

Figure 8-3: The distributions of solubility limits for technetium, nickel, palladium, and tin in probabilistic analyses.

Note: The sample size of the solubility for each element is 6,916.

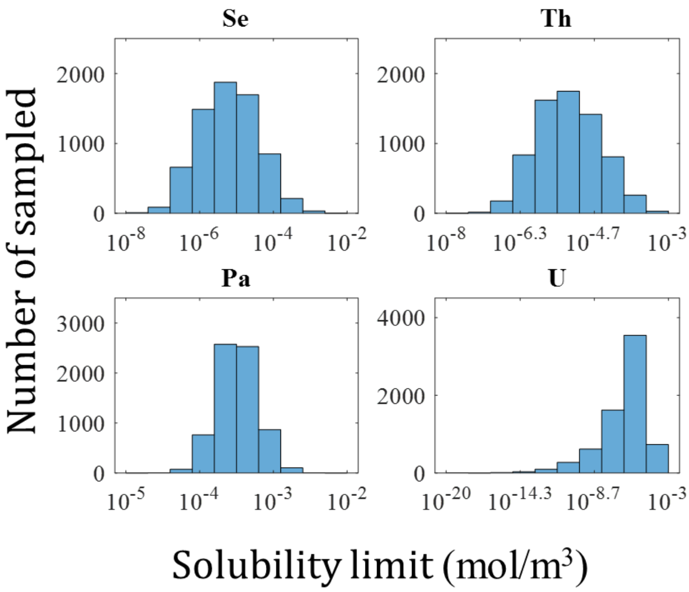

Figure 8-4: The distributions of solubility limits for selenium, thorium, protactinium and uranium in probabilistic analyses.

Note: The sample size of the solubility for each element is 6,916.

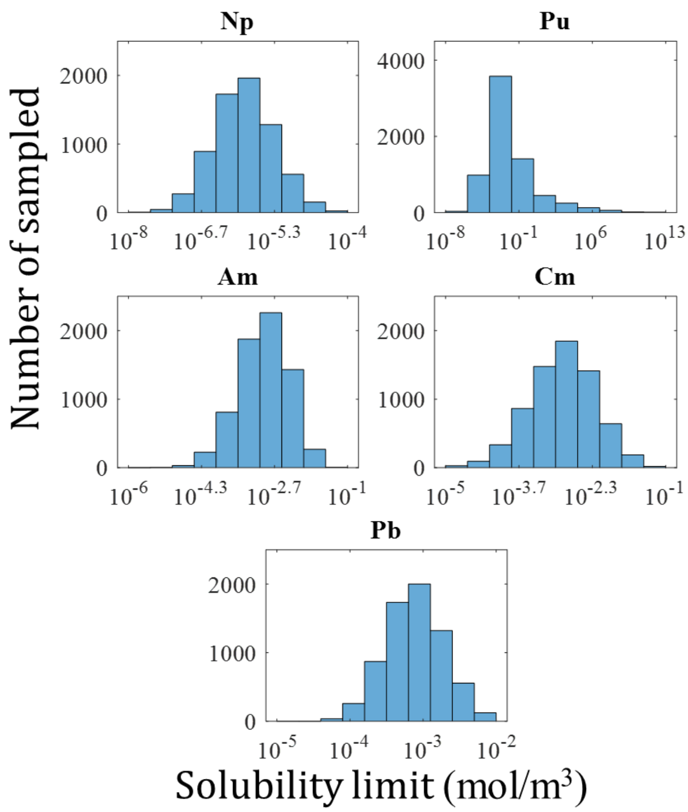

Figure 8-5: The distributions of solubility limits for neptunium, plutonium, americium, curium and lead in probabilistic analyses.

Note: The sample size of the solubility for each element is 6,916.

8.4. Procedure for Assigning Values

The input data parameters used in the models of safety assessment were mainly specified based on past research, i.e. Table I to Table III of the SNFD2017 reference case (台電公司, 2019). If the design was modified or new evidence and evaluation data were acquired, internal experts would discuss the influence and applicability. Meanwhile, a conference with external experts was also held to review how input data parameters would be used in models. The values and their uncertainties in the safety assessment were determined according to the procedures stated above.

For proper management of uncertainties of input data parameters, a standardized protocol (SKB, 2006b) will be introduced in the future according to relevant references to determine the values of input data parameters and evaluate uncertainties.

9. Evolution Analyses of the Repository

9.1. Introduction

The overall evolution of the repository, which is the basis for establishing scenarios of safety assessment, will be mainly described in this chapter. Besides, the rationality of the repository evolution will also affect the definition process of the main scenarios.

The discussion of this chapter will mainly focus on the containment safety functions of the repository. Through evaluation of relevant safety functions over the assessment period, whether the containment safety functions can be maintained or not will be further discussed. Based on the evaluation results of this chapter and the development of assessment scenarios in Chapter 10, overall analyses for the failure of containment safety functions will be discussed in Chapter 11. Finally, a relevant assessment of the release of radionuclide is described in Chapter 12.

In this report, repository evolution under two different kinds of climate evolution will be discussed:

(1) Basic evolution: in which future climate conditions will evolve according to 120,000-year glacial cycle.

(2) Global warming evolution: in which impact on climate evolution and the repository from greenhouse gases will be discussed.

The initial state of the repository for the two evolution is based on the description in Chapter 4, and the management of relevant internal processes is described in Chapter 6.

9.1.1. Prerequisites

The foundation of the evolution analysis of the repository is based on the description of Chapter 4 to Chapter 6, and it is summarized as follows:

(1) Initial state of the engineered barrier:

Tolerance of each component of the repository should be included in consideration of the initial state. For example, the design requirement for the saturation density of the buffer is 2,000 kg/m^3.

However, the allowable saturation density is 2,000±50 kg/m^3 in the preliminary design. When discussing the evolution of the repository, the above-mentioned range of the saturation density should be taken into account.

The initial state of the engineered barrier system is described in Section 4.2. And the tolerance for each component has been considered in the design concept. For example, welding defect is included in the initial state of the canister; geometry defect of the deposition hole, the composition of the bentonite, and flaws in the manufacturing are included in the initial state of buffer density.

Please note that, currently, not all of the defects or deviations between design and manufacturing can be taken into account in the repository evolution analyses; however, possible deviations from the initial state of the components will be discussed in Chapter 10.

(2) The initial state of the geosphere and biosphere:

The initial state of the geosphere and biosphere are described in Section 4.3.2, and the repository layout is described in Section 4.4.2.

(3) Internal processes:

The internal processes of the repository dominate the evolution of the whole system. These processes are described in Chapter 6, categorized as SNF/canister, buffer/backfill, geosphere and biosphere. And the uncertainties for these processes will be evaluated based on relevant measures described in Chapter 8.

(4) Basic evolution:

Future climate evolution and the probability of a specific climate evolution are difficult to be estimated. Assuming that climate evolution follows the same evolution cycle from the past is a more feasible way. Hence, the climate evolution of the repository is assumed to follow the climate evolution cycle described in Chapter 5. The repository will go through subtropical climate and temperate climate (including the sea-level evolution under this climate change) in a 120,000-year cycle. And the climate evolution cycle will repeat to the end of the safety assessment timescale (please refer to Table 5-1 and Figure 5-1).

This climate evolution is one of the evolution that is more likely to happen during the glacial period. Please note that it is not a prediction of future climate evolution but a reasonable estimation for the safety assessment of the repository based on scientific evidence. For the robustness of the assessment, extreme climate evolution will also be taken into account.

(5) Global warming evolution:

The greenhouse effect is another important factor influencing future climate evolution. Global warming caused by the greenhouse effect may induce a relatively warm climate over a long period, as described in Section 5.2.1 (IPCC, 2017). Currently, the assessment of global warming evolution has not been yet completed, and this will be one of the research objectives in the future.

9.1.2. Structure of the Assessment

The basic evolution can be divided into four periods as follows:

(1) The excavation and operation period: the research targets of this period are mainly focused on the state of the underground facility of the repository, which includes the disposal tunnels and the canisters. During this period, the climate and the sea-level are assumed to be the same as nowadays (Table 5-1 and Figure 5-1). Relevant evolution analyses are described in Section 9.2.

(2) The initial period after closure (post-closure 1,000 years): the research targets of this period are mainly focused on the state of the repository from the time that the repository is closed to post-closure 1,000 years. During this period, the climate and the sea-level will be similar to nowadays (Table 5-1 and Figure 5-1). Relevant evolution analyses are described in Section 9.3.

(3) The remaining glacial period after closure (post-closure 120,000 years): the research targets of this period are mainly focused on the state of the repository from post-closure 1,000 years to the end of a

glacial period. The climate is assumed to evolve from the current climate (subtropical climate) to a temperate climate then go back to the subtropical climate (Table 5-1 and Figure 5-1). And the sea-level will fall to -120 m from the current sea-level and then rise back to the same as the current sea-level. Relevant evolution analyses are described in Section 9.4.

(4) The subsequent glacial cycles: the research targets of this period are mainly focused on the state of the repository after the end of the first glacial period to the end of a one million-year safety assessment timescale. Relevant evolution analyses are described in Section 9.5.

Discussion related to global warming evolution is described in Section 9.6. The possible impact of the repository under global warming evolution will be included in the section.

In every section of this chapter, analyses of climate, biosphere, THMC evolution of the geosphere, THMC evolution of the engineered barrier system, and the state of the safety function indicators in each period are discussed, respectively.

9.1.3. Conceptual Hydrogeological Model

Based on the reference case shown in Section 4.3.2, regolith (R0), rock mass (R), and major water-conducting zone (F#) are included in the hydrogeological conceptual model. And the fault zone (F1) and fracture zone (F2) are assumed to only reveal on the island.

For the evaluation of hydrogeological evolution, different model domains based on different sea-level conditions should be created. The DEM, which includes coastal areas of mainland China, Taiwan Straits, and Taiwan Island, is included in the estimation of different scale domains. The regional scale domains and their natural boundaries are chosen to define a natural-topography-based water divide and water shield.

Based on the estimated climate and sea-level evolution in Section 5.2, in the period of one glacial cycle, the topography of the reference case is likely to evolve from island to plain gradually while the sea-level changes from 0 m to -120 m. After that, the topography will evolve from plain to island while the sea-level changes from -120 m back to 0 m. When the sea-level descends to -20 m, the topography will evolve from island to coastal area, and there will be a huge impact on the groundwater flow field. In addition, when the topography becomes plain while the sea-level descends to -120 m, there will also be an impact on the groundwater flow field. Therefore, four specific time points were selected to develop model domains for the evaluation of hydrogeological evolution in one glacial cycle:

(1) the site scale model (the sea-level is the same as nowadays);
(2) the regional scale model (post-closure 16,700 years, the sea-level will drop to -20 m, and the topography of the reference case will become a coastal area);
(3) the regional scale model (post-closure 100,000 years, the sea-level will drop to -120 m, and the topography of the reference case will become plain);
(4) the site scale model (post-closure 120,000 years and the sea-level will regain to the same as nowadays).

The above-mentioned model domains are shown in Figure 9-1 to Figure 9-3.

The infiltration rate and recharge rate of the reference case are calculated by empirical functions using the meteorological data in Section 4.3.2.6. The annual average infiltration rate of the reference case was calculated to be 66.8 mm/yr.

The parameters for hydrogeological models are shown in Table 9-1. During the excavation and operation period and the initial period after closure (post-closure 1,000 years), the climate and the sea-level will be the same as nowadays, and the site scale model with salinity equal to sea water (3.2%) was used in the calculation. On the other hand, in the remaining glacial period after closure, the sea-level will gradually decrease from 0 m to -120 m, and regional scale models with salinity equal to freshwater were used in the calculation.

For the purpose of subsequent safety assessment, performance measures including flow-related transport resistance (F) and equivalent flow rate (Q_{eq}) were calculated using DarcyTools.

Flow-related transport resistance (F) is a parameter describing the retention and retardation of radionuclides within rock mass:

$$F = \left(\frac{a_r L}{q}\right)_i \tag{9- 1}$$

where,

F=flow related transport resistance, [s/m].

a_r=the flow wetted surface per unit volume of rock, [m^2/m^3].

L=path lengths, [m].

q=Darcy flux, [m/s].

The hydraulic conductivity in the deposition hole was assigned to be 1.0×10^{-12} m/s, which was based on the design requirements of hydraulic properties of buffer in Section 4.2.6. The equivalent flow rate is a fictitious flow rate of water that carries a concentration equal to the one at the compartment interface (Romero et al., 1995):

$$Q_{eq} = 2UH\sqrt{4D_w t_{DH}/2} \tag{9- 2}$$

where,

Q_{eq}=equivalent flow rate, [m^3/s].

U=equivalent initial flux in the fracture system averaged over the rock volume adjacent to the deposition hole, [m/s].

H=height of the deposition hole, [m].

D_w=diffusivity in the water, [m^2/s].

t_{DH}=the time that the water is in contact with the deposition hole within each fracture, [s].

In summary, the hydrogeological models can be categorized into repository scale, site scale, and regional scale:

(1) Repository scale model: this model was used to analyze the groundwater inflow rate of the disposal tunnels and deposition holes during the excavation and operation period. The model is scaled in a range from a few meters to hundreds of meters.

(2) Site scale model: this model was used to analyze the steady-state groundwater flow field and salinity distribution of the repository and the adjacent area in the initial period after closure (post-closure 1,000 years). The model is scaled in a range from hundreds of meters to a few kilometers, including the repository geometry, adjacent hydrogeological units and structures, and topology of the reference case and the adjacent sea area.

(3) Regional scale model: this model was used to analyze the evolution of the groundwater flow field of the repository in the remaining glacial period after closure (post-closure 120,000 years). The model is scaled in a range from tens of kilometers to hundreds of kilometers including coastal areas of mainland China and Taiwan Strait.

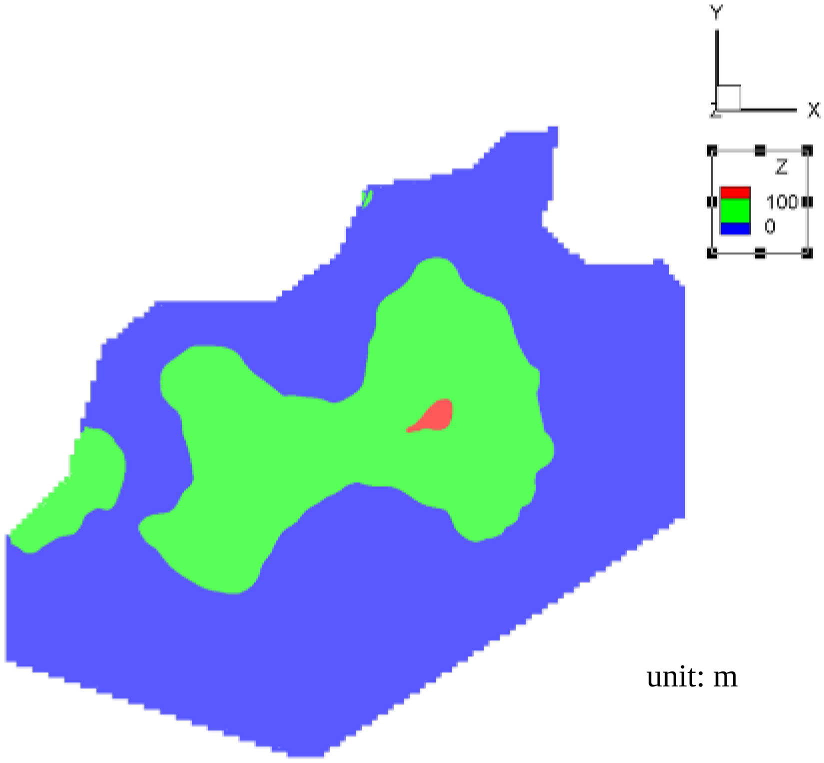

Figure 9-1: Hydrogeological model with sea-level equals to 0 m.

Note: the model domain includes land and the adjacent sea areas.

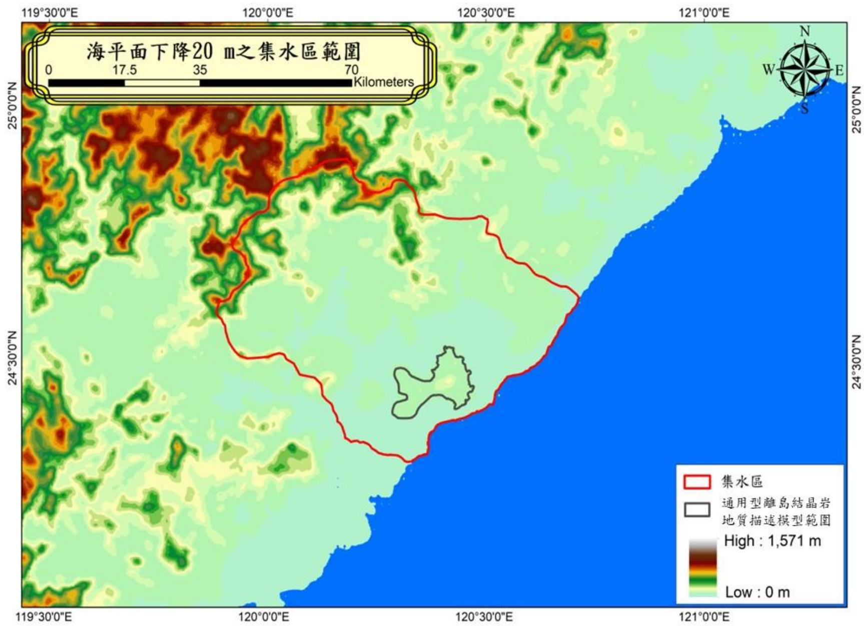

Figure 9-2: Hydrogeological model with sea-level dropping to -20 m.

Note: red line indicates the catchment area when sea-level drops 20 m, which also indicates the simulation area.

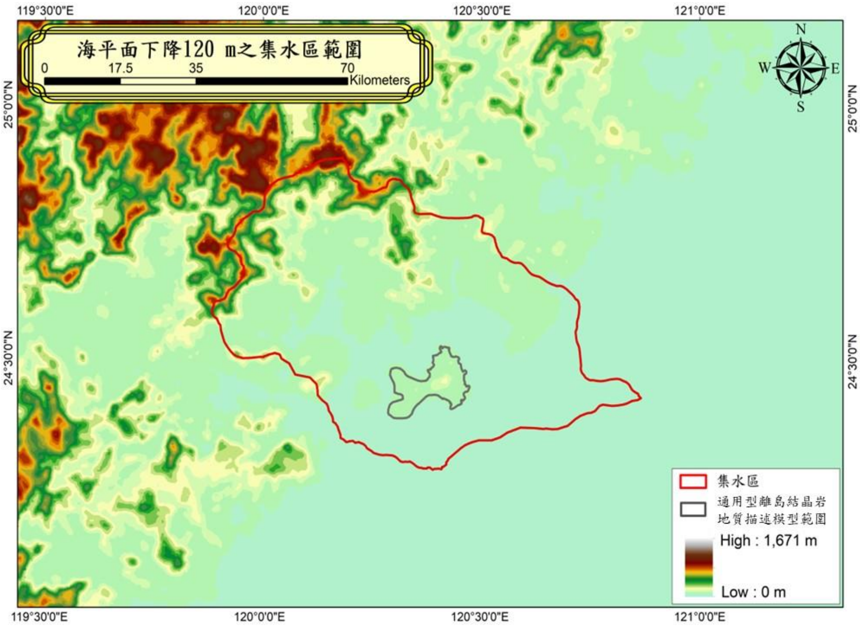

Figure 9-3: Hydrogeological model with sea-level dropping to -120 m.

Note: red line indicates the catchment area when the sea-level drops 120 m, which also indicates the simulation area.

Table 9-1: Parameters of the hydrogeological model at different evolution periods.

Period	Climate pattern	Sea-level	Hydrogeological model	Salinity
The excavation and operation period	Subtropical	0 m	Repository scale	Sea (3.2 %)
The initial period after closure	Subtropical	0 m	Site scale	Sea (3.2 %)
The remaining glacial period	Subtropical→temperature	-20 m→-120 m	Regional scale	Fresh water (0.0105 %)
The subsequent glacial cycle	The initial cycle of 0.12 million years is repeated.			

9.2. Excavation and Operation Period

The hydrological, mechanical, and chemical evolution of the repository during the excavation and operation period (this period takes about tens to a hundred years depending on the number of canisters that need to be disposed and the schedule of excavation and operation activities) is described in this chapter. According to Chapter 5, the climate during this period will be very similar to the present; hence the sea-level would most likely be the same, too.

9.2.1. Near-Field Thermal Evolution

Based on the parameters of the reference case (i.e. the surface temperature is 23.8 ℃ and the geothermal gradient is 0.019 ℃/m), the estimated ambient temperature at 500 m underground will be 9.5 ℃ higher than the surface temperature, which will be about 33.3 ℃. This temperature will be affected by ventilation design during the excavation period, but is supposed to be negligible compared to the influence from the decay heat of SNF. Since influence from the decay heat can last thousands of years, a detailed discussion is included in Section 9.3.

When considering the safety of the repository, the most important factor is the change in maximum temperature in the repository over time. As excavation activities and operation activities are done step-by-step, the activity of radionuclides can have a greater impact on thermal evolution. In addition, the disposal operation pattern (e.g,. simultaneous disposal or sequential disposal) will also affect the change in maximum temperature.

9.2.2. Near-Field Rock Mechanical Evolution

During the excavation and operation period, the main impact on near-field rock mechanics is shown below:

(1) The development of excavation damaged zone (EDZ) and other impacts on rock hydraulic characteristics (safety function R2):

A relevant assessment has not been done yet. But excavation of the deposition holes is supposed to cause very little disturbance to the surrounding host rock, and the impact on the transmissivity is less than $10^{-10}\,m^2/s$ (SKB, 2011). Therefore, if the drilling and blasting method is used for the excavation of tunnels, it is assumed that the transmissivity of EDZ will be $10^{-8}\,m^2/s$ (SKB, 2008; Bäckblom, 2008; SKB, 2010i).

(2) Spalling (safety function R2, buffer density will also be directly or indirectly affected, thereby affecting the safety functions of buffer):

If in-situ stress is high before excavation, spalling may occur due to decompression after excavation. Spalling of the disposal tunnels can be effectively reduced by making long axes of the tunnels parallel to the maximum horizontal stress direction when designing the disposal tunnels.

In addition, spalling can also be reduced by incorporating appropriate construction techniques, such as strengthening the support structure during excavation. When spalling occurs in the deposition hole before disposing the canister, and the spalling depth is within 5 cm and has no impact on the density of the buffer after filling, this deposition hole will remain effective; otherwise, it will be discarded (SKB, 2011).

3DEC(3D Finite Difference Method Computational Mechanics Mode) numerical analysis model was used to analyze tunnel stability after excavation and during an earthquake by taking the influence of in-situ stress direction into account. The rock mass is assumed to be homogeneous, isotropic and without fractures, and the Mohr-Coulomb constitution law is adopted to quantitatively calculate the safety factor of the rock mass. Table 2 of the SNFD2017 reference case (台電公司, 2019a) is referred to for relevant mechanical parameters. And the parameters are summarized in Table 9-2. In order to avoid the boundary effect of the numerical model, size of the model must be at least 5 times the tunnel’s cross-section. While the tunnel’s cross-section is 4.20 m wide and 4.80 m high, the size of the model would be 21 m × 24 m. In-situ stress in 500 m depth was adopted as the boundary condition of the model, and the absorption boundary was set to avoid wave rebound during the earthquake. Finally, safety was confirmed by stability analysis of the tunnel’s cross-section. The analysis results are shown as follows:

(a) Excavation stability of the disposal tunnel:

Rock mass will gradually decompress when excavating the disposal tunnel and affect the stability of the disposal tunnel. Principal stress distribution around the disposal tunnel was analyzed using the 3DEC numerical analysis model, and the safety factor was calculated based on the Mohr-Coulomb failure criterion. The results show that the minimum safety factor after excavation is 1.61, mainly located at the edge of the bottom of the disposal tunnel (as shown in Figure 9-4).

(b) Seismic analysis of the disposal tunnel:

Earthquake acceleration duration of the granite outcrop was obtained by seismic hazard analysis. The maximum acceleration is 0.288 g. And refer to the procedures required by U.S. nuclear energy regulation R.G 1.208 (US NRC, 2007) to carry out the ground response analysis. The ground response analysis to calculate the seismic waveform was performed, and transmit the outcrop earthquake (at 70 m underground) obtained by the seismic hazard to the depth of 500 m where the repository will be located.

The site response analysis is performed by Strata which is one-dimensional wave propagation analysis software. The concept is to consider both the seismic wave propagation characteristics and the site vibration characteristics (including shear wave velocity, shear modulus, damping ratio versus shear strain, etc.) An earthquake will be amplified or decayed after the interaction of these parameters. The designed earthquake in the analysis was located in the outcrop of the rock base. And the location of the rock base of the reference case is 70 m underground, where shear wave velocity will be 3,000 m/s. Input earthquake of the tunnel stability analysis was generated through site response from 70 m underground to 500 m underground, and the maximum acceleration is 0.206 g.

Then, the principal stress distribution around the tunnel at the time of maximum acceleration was analyzed using the 3DEC numerical analysis model. The safety factor was also calculated based on Mohr-Coulomb’s failure criterion. The results show that the minimum safety factor during the earthquake is 1.57, mainly located at the edge of the bottom of the disposal tunnel (as shown in Figure 9-5).

From the results of excavation stability and seismic analysis of the disposal tunnel, it can be seen that the safety factor when encountering an earthquake will only be slightly lower than the safety factor after excavation. It is speculated that the induced stress increment has relatively little effect on stability because of the high in-situ stress deep underground. In addition, influence from an earthquake has also been considered, and additional stress from the remaining external load should be very small; therefore, the safety factor should be conservatively sufficient.

(3) Recovery of fracture reactivation (safety functions R2 and R3):

A relevant assessment has not been done yet. However, redistribution of stress during the excavation and operation period may cause the existing near-field cracks to reactivate.

According to the assessment results (SKB, 2011), this could be covered by assuming the transmissivity of the EDZ to be 10^{-8} m^2/s.

Table 9-2：Material parameters of the rock.

Rock mass classification	Unit Weight (kg/m^3)	Cohesion (MPa)	Friction angle (°)	Elastic modulus (GPa)	Poisson's ratio
Granite gneiss	2,750	27.46	51.05	44.18	0.17

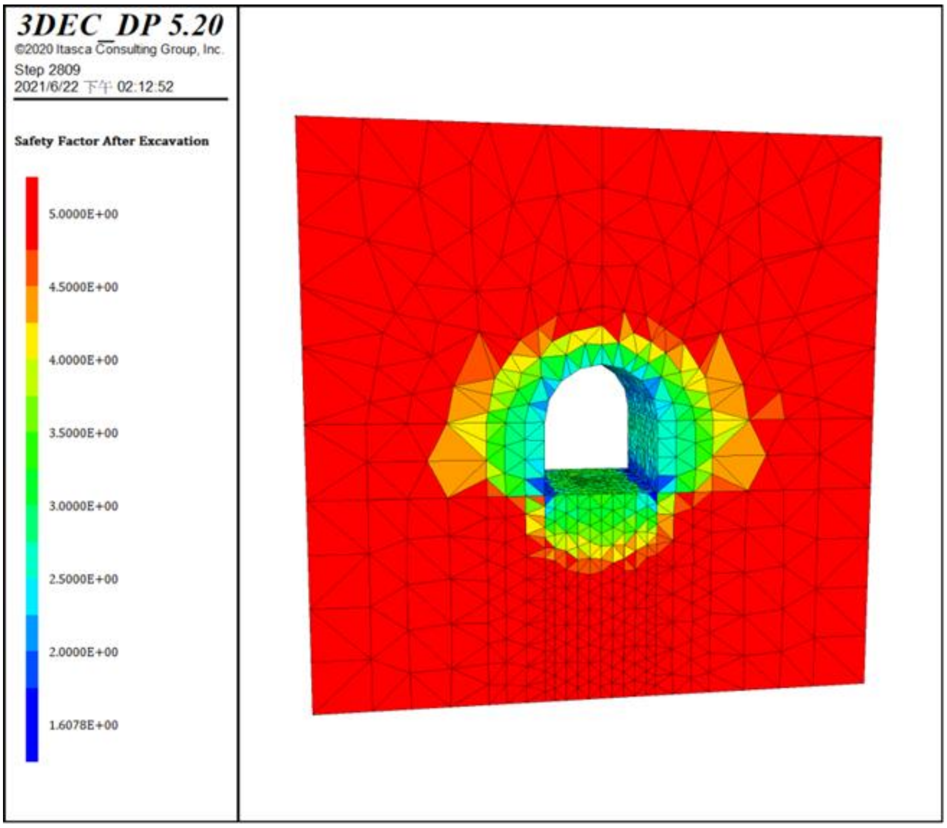

Figure 9-4: Safety factors of the disposal tunnel after excavation.

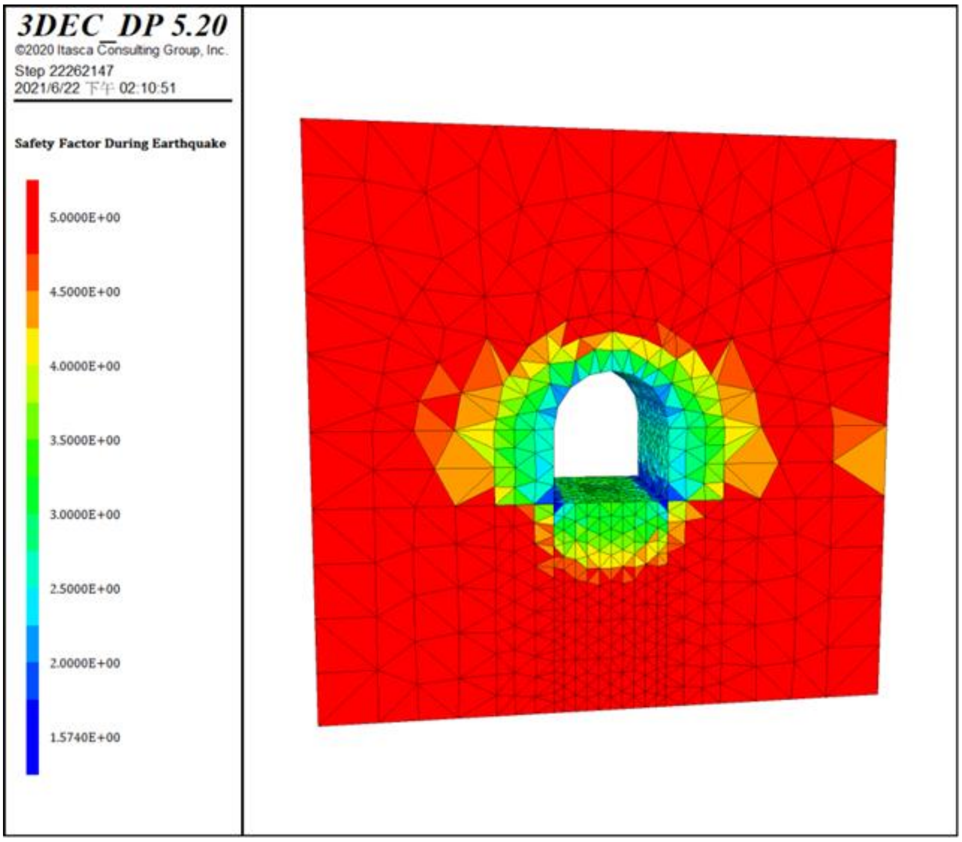

Figure 9-5: Safety factors of the disposal tunnel during an earthquake.

9.2.3. Hydrogeological Evolution

During the excavation and operation period, the pressure of the repository is equivalent to the atmospheric pressure. The inflow of groundwater flowing into the repository depends on the hydraulic characteristics of water-conducting fractures. The possible impact of groundwater flow into the repository is shown as follows (SKB, 2010k):

(1) Upconing of saline water from deep area.

(2) Drawdown of groundwater table.

(3) Infiltration of near-surface groundwater into deeper parts of the bedrock.

(4) Guiding seawater into the repository.

(5) Guiding organic matter and oxides into the repository.

(6) Interfering with excavation and operation of the repository.

The hydrogeological evolution analysis model includes the near-field region, which contains the repository. X and y dimensions of the model are both 2,000 m, and the z dimension of the model is 300 m from the center of the repository, which the z-coordinate direction is the region from the depth of 350 m to the depth of 650 m. In order to make the whole consistent, the FracMan program imports the fracture model and regional flow field of the near-field which is outputted by the DarcyTools program. The hydraulic boundary condition is the repository-scale flow field extracted from the site-scale flow field calculation results of the DarcyTools program. The pressure at the disposal facility is equivalent to atmospheric pressure during the excavation and operation period. The DarcyTools program analyzes the regional-scale flow field of the equivalent continuous porous medium model and exports the fractures and flow field to the FracMan program, and the FracMan program analyzes the inflow of disposal facilities in the near-field during the excavation and operation period (Figure 9-6). After importing the fractures in the near-field, which are exported from the DarcyTools program, the FracMan program analyzes the fractures connected to the disposal facilities (Figure 9-7), constructs the triangular finite element grids for all connected fractures, and the total water pressure of each node at fractures are interpolated by the total water pressure in the near-field which outputed from the DarcyTools program. Because the FracMan program calculates the water flow by the total head, the total water pressure in the near-field is converted into the total head (Figure 9-8). Then the FracMan program is used to calculate the repository inflow in the fractured section under steady-state conditions.

In order to maintain high spatial resolution, the DFN model is used to describe the distribution of the fractures, connectivity of the fractures, and groundwater flow in a detailed fashion of fracture regions around the tunnels. The analysis results of deposition hole DH-61 are shown as an example to illustrate the inflow of the disposal hole during the excavation and operation period. Figure 9-9 shows the geometry of the fracture intersecting the deposition hole. According to the analysis results, the hydrostatic pressure of the fracture is between 4.9 MPa and 5.2 MPa (Figure 9-10), the velocity of flow in the fracture is between 1.31×10^{-5} m/s and 9.18×10^{-5} m/s (Figure 9-11), and the inflow rate from the fracture into the deposition hole is about 1.03×10^{-5} L/min to 4.29×10^{-5} L/min (Figure 9-12).

The results show that the inflow of the repository will be relatively large at the beginning of the excavation, and then it will decrease over time; finally the inflow will tend to a stable value. This is because the pressure difference of the groundwater in the fracture is an important factor in driving the groundwater flow. At the beginning of the excavation, the pressure difference of the groundwater in the fracture would be large; therefore, the inflow of groundwater into the tunnel surface would be large. As time goes by, the pressure difference of the groundwater in the fracture would decrease, and the inflow would also decrease correspondingly.

According to the Cubic Law, flow in the fracture is proportional to the third power of the fracture aperture. One of the factors that affect the difference in inflow by up to 6 orders of magnitude is the fracture aperture in the near-field region which is between the magnitude of 10^{-6} to 10^{-4}. The other factor is the difference in the regional groundwater flow.

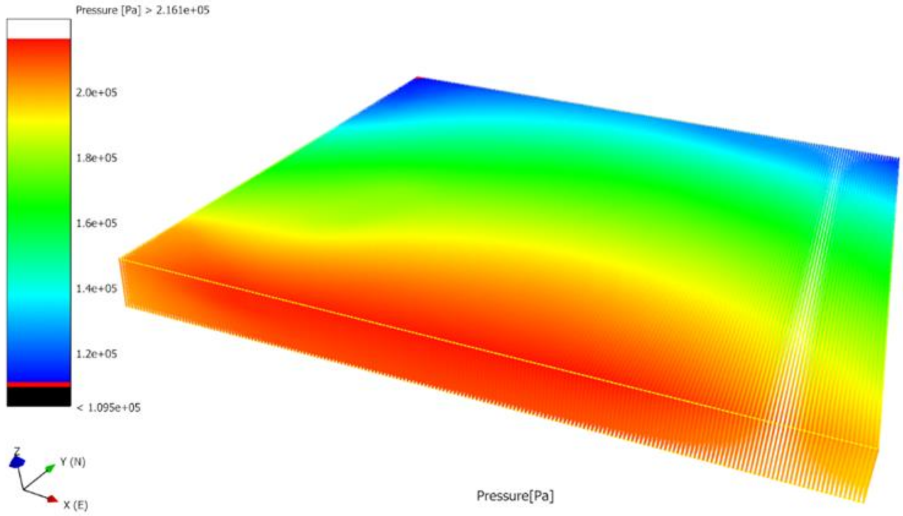

Figure 9-6: Total water pressure results in near-field outputted by DarcyTools.

Figure 9-7: FracMan imports the near-field fractures exported by DarcyTools and analyzes the fracture connectivity.

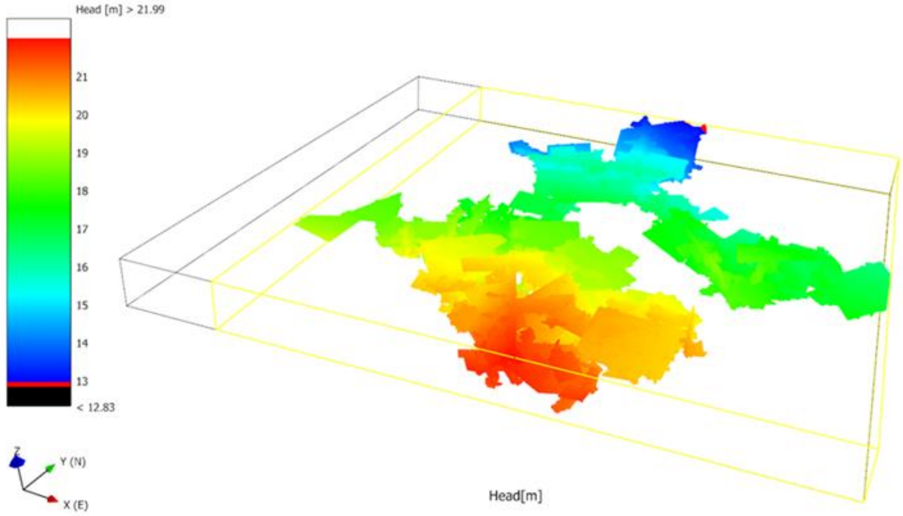

Figure 9-8: Total head for each node on the fractures of FracMan.

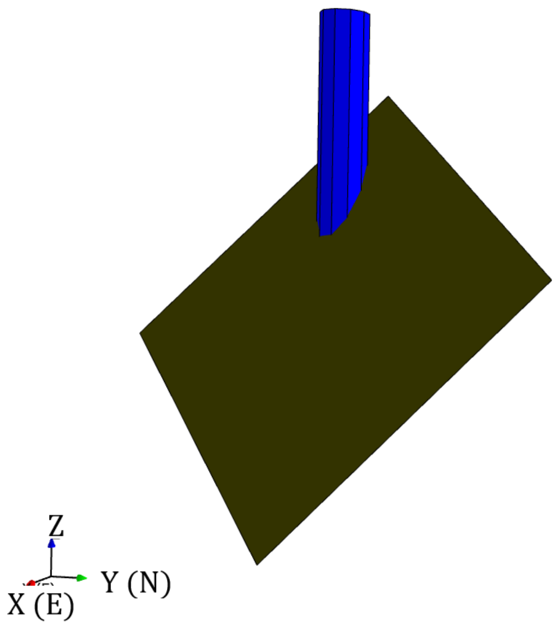

Figure 9-9: Deposition hole DH-61 and the intersecting fracture.

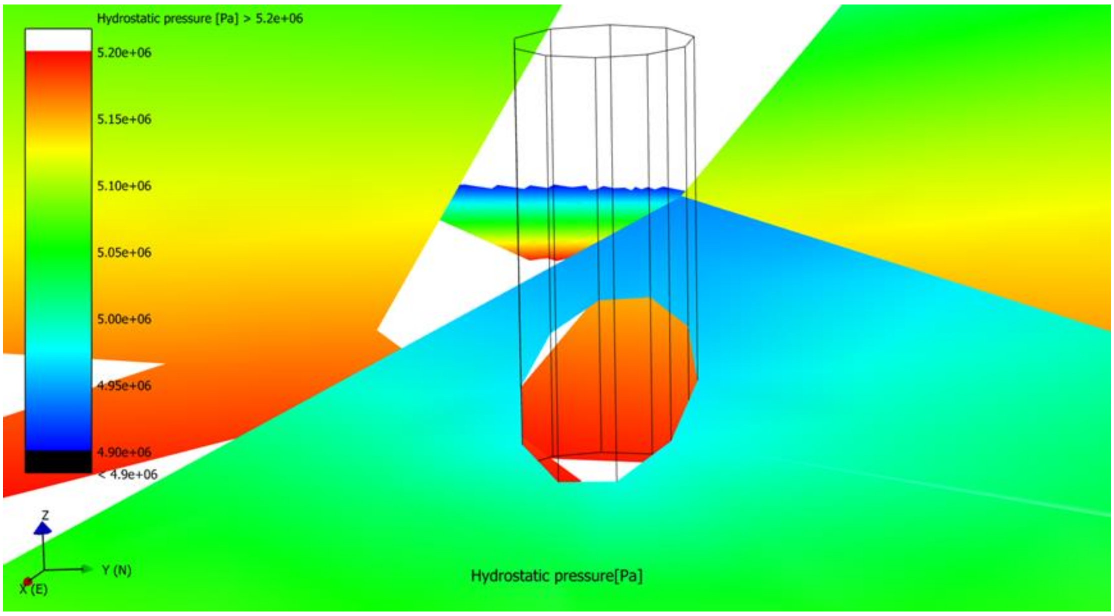

Figure 9-10: Hydrostatic pressure of DH-61 deposition hole and the fracture.

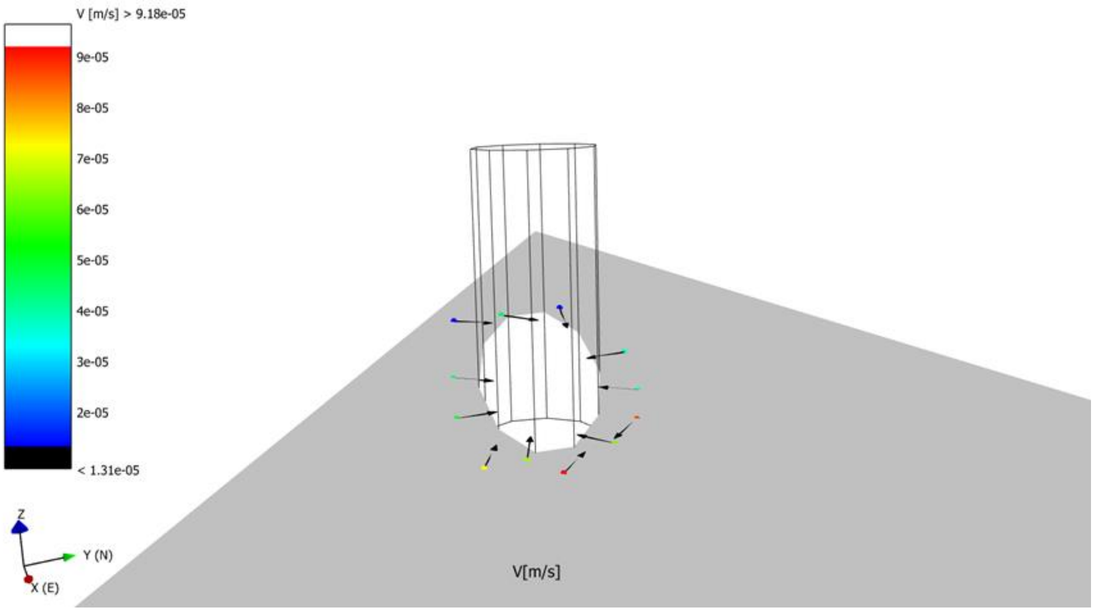

Figure 9-11: Velocity and direction of flow in the fracture.

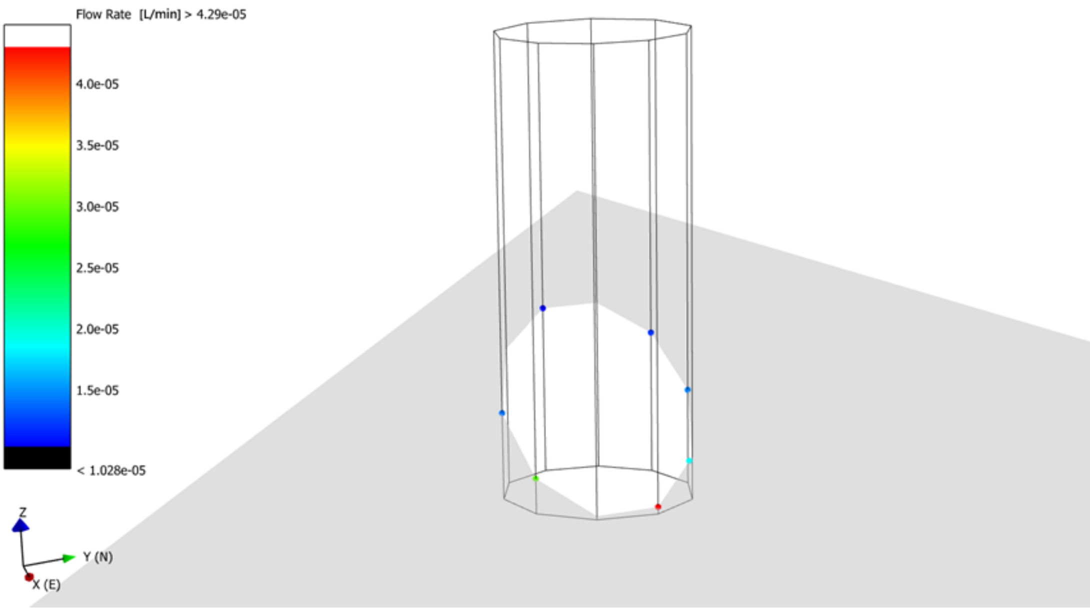

Figure 9-12: Flow rate in the fracture.

9.2.4. Evolution of Buffer and Backfill

During the excavation and operation period, bentonite clay will still be unsaturated. Groundwater will gradually flow into the deposition holes and the disposal tunnels from the fractures in the rock mass. Firstly, groundwater inflow will contact the bentonite filling (pellets) and fill the gaps in between. And then, groundwater inflow will contact the bentonite blocks and gradually wet the bentonite blocks. When the bentonite blocks are wet, the bentonite will expand due to its water absorbing and swelling properties; thereby, the space in the deposition holes and the disposal tunnels will be filled (Figure 9-13). Before the buffer or the backfill is saturated, if the amount of local inflow exceeds the one that the bentonite can absorb, the water pressure generated may result in the formation of connected piping inside the bentonite, causing erosion of bentonite particles at the interface between the bentonite and water by water flow, hence the loss of mass.

In order to assess this phenomenon, piping and erosion tests were developed to confirm that the bentonite erosion empirical formula was applicable to the evaluation of piping and erosion of the bentonite in the reference case.

The tests have been developed based on similar tests conducted in Sweden. Relations between inflow rate and erosion (SKB, 2006) and relevant engineering design requirements (SKB, 2010j) were analyzed in the tests. And inflow rate into the deposition holes was set to be less than 0.1 L/min to avoid loss of buffer in the deposition holes due to piping and erosion (as described in Section 4.4.1).

A series of piping and erosion tests were also performed in Sweden, by applying various geometry settings, bentonite block types, solution conditions, and so on, to assess the impact of piping and erosion during the excavation and operation period. The test results were compiled in double logarithmic charts (Figure 9-14 and Figure 9-15), and an empirical equation was established as follows (Sandén et al., 2008):

$$m_s = \beta \times (m_w)^{\alpha} \quad (9\text{- }3)$$

where,

m_s= accumulated mass of eroded bentonite, [g].

m_w= accumulated mass of eroding water, [g].

α= parameter defined by the inclination of the straight line relation, [·].

β= parameter defined by the level of erosion at a certain accumulated water flow, [·].

The horizontal piping and erosion test was used to represent erosion of the disposal tunnels, and the vertical piping and erosion test was used to represent the erosion of the deposition holes, so that different inflow directions could be taken into account. As shown in Figure 9-14 and Figure 9-15, α which is the slope of the linear relation is 0.65, and β which is the level of erosion at a certain accumulated water flow is between 0.02 and 2 in horizontal piping and erosion tests and between 0.02 and 0.2 in vertical piping and erosion tests.

Tests were conducted using a similar setting (Sandén and Börgesson, 2008; Sandén et al., 2008) to verify the applicability of equation (9- 3). Bentonite particles were uniformly filled into a 1 m long horizontal tubular container. The dry density of the bentonite after filling was about 1,600 kg/m^3. Then, deionized water and synthetic groundwater (Section 4.3.2) were injected into the container at two fixed injection rates, 0.0025 L/min and 0.01 L/min, separately to observe the erosion of the bentonite. The test results are shown in Figure 9-16. The trends of accumulated eroded material versus accumulated water flow fall within the interval of the empirical equation (9- 3), and the slopes are also similar; therefore, equation (9- 3) was assumed to be applicable for the evaluation of erosion in the reference case.

The eroded amount of the bentonite in the excavation and operation period was estimated according to the results of the piping and erosion test mentioned above. A few assumptions were made for the evaluation as follows. Inflow water coming from fractures in the surroundings of the disposal tunnels and the deposition holes will first fill the larger space between bentonite particles. Also, the volume of the gap between backfill blocks in the disposal tunnels was assumed to be around 2% of the volume of the blocks, and it will be filled with groundwater. Besides, the bentonite blocks are assumed to absorb 20% of additional water due to their compactness and impermeability.

The evaluation results of the east disposal area are taken as an example. 30 deposition holes are there in a 300 m long disposal tunnel (Section 4.4.2). The gap between the bentonite filling in the deposition holes and the disposal tunnel, and the gap between the backfill blocks in the disposal tunnel will have a total volume of 1,562 m^3. This was considered the inflow volume that may induce piping and erosion.

Assuming that all of the inflow water will run through a particular water-conducting fracture in the deposition hole. Through estimation from equation (9-5) (α was 0.65, β was between 0.02 and 0.2), the mass loss of the bentonite in the deposition hole would be between 21.30 kg to 213.01 kg. Under this condition, the average dry density of the buffer in the deposition hole would be between 1,589 kg/m^3 to 1,573 kg/m^3 after saturation (the saturated density would be between 2,011 kg/m^3 to 2,001 kg/m^3). According to Figure 4-10 and Figure 4-11, the corresponding swelling pressure would be more than 3 MPa, and the corresponding hydraulic conductivity would be below 1×10^{-12} m/s. Hence, the requirements of safety functions Buff1, Buff2, and Buff5, and the design requirements of the saturated density in Chapter 4 can be met.

On the other hand, the total amount of backfill bentonite in a single disposal tunnel would be around 10,560 tonnes. If the inflow water that goes into the disposal tunnel is also assumed to be 1,562 m^3, from equation (9-5) (α was 0.65, β was between 0.02 and 0.2), mass loss of the backfill bentonite in the disposal tunnel would be 21.30 kg to 2130.12 kg, which is very small compared with the total amount of the backfill in the disposal tunnel. Under this condition, the average dry density of the backfill would be 1,408 kg/m^3 after saturation. Almost nothing would be changed in the density of the backfill, and the safety functions of the backfill will not be affected.

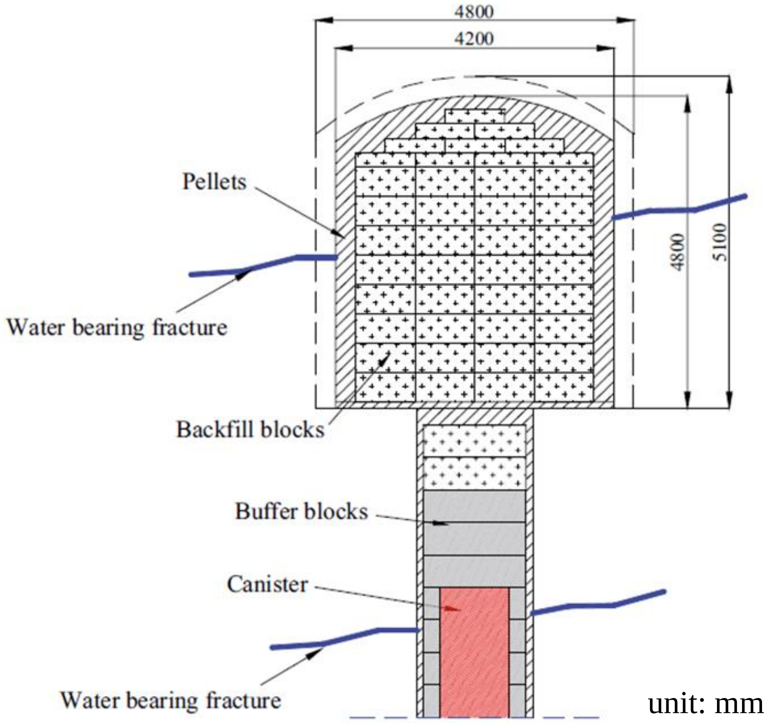

Figure 9-13: Demonstration of water flow into the disposal tunnel and deposition hole through fracture.

Reference: Sandén and Börgesson (2010).

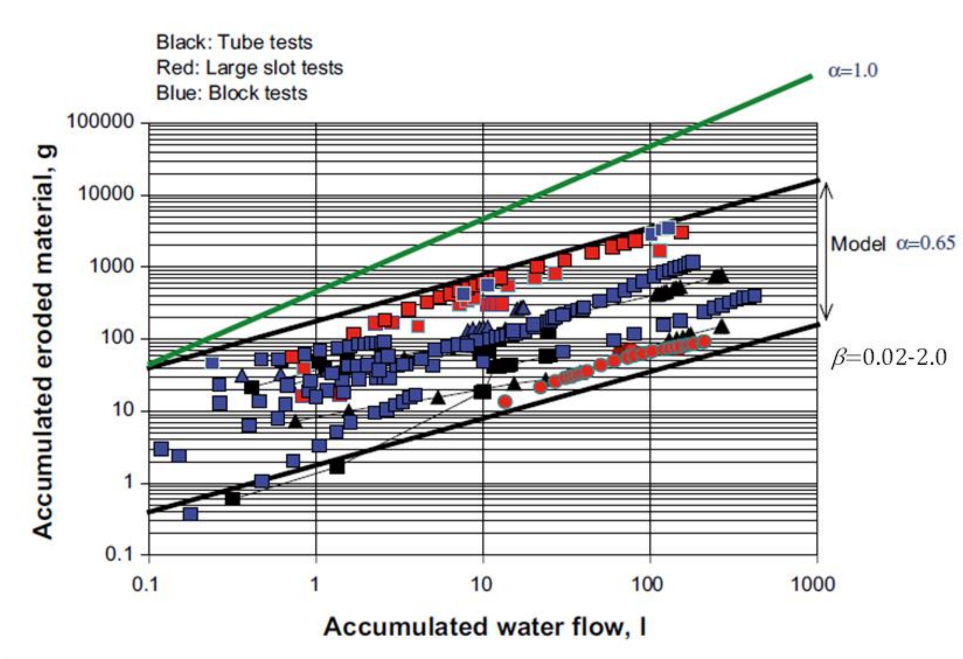

Figure 9-14: Accumulated eroded material versus accumulated water flow of horizontal erosion test.

Reference: Sandén and Börgesson (2010).

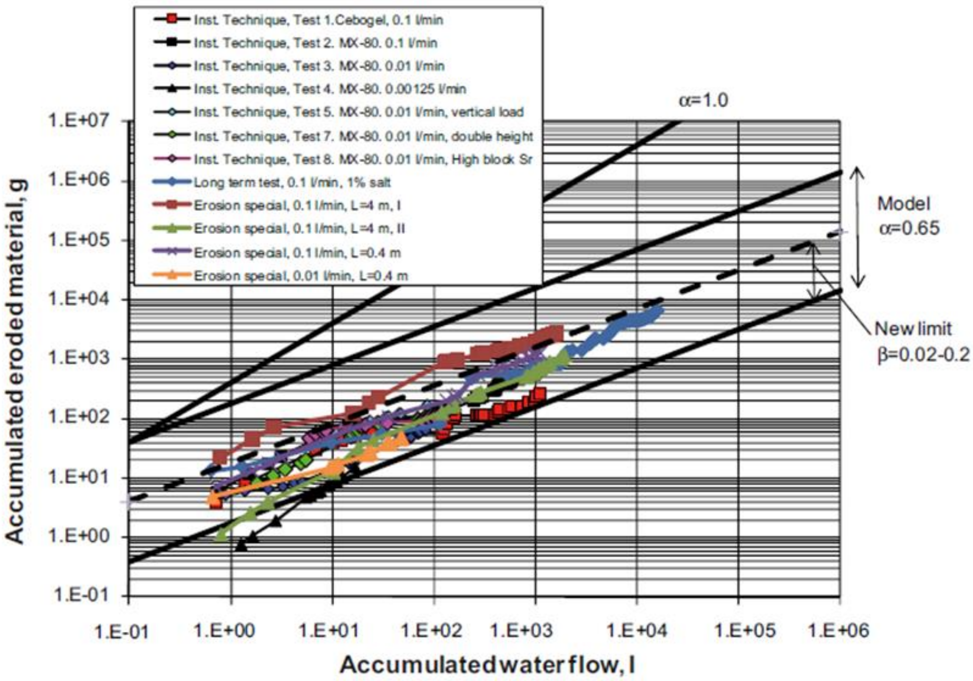

Figure 9-15: Accumulated eroded material versus accumulated water flow of vertical erosion test.

Reference: Sandén and Börgesson (2010).

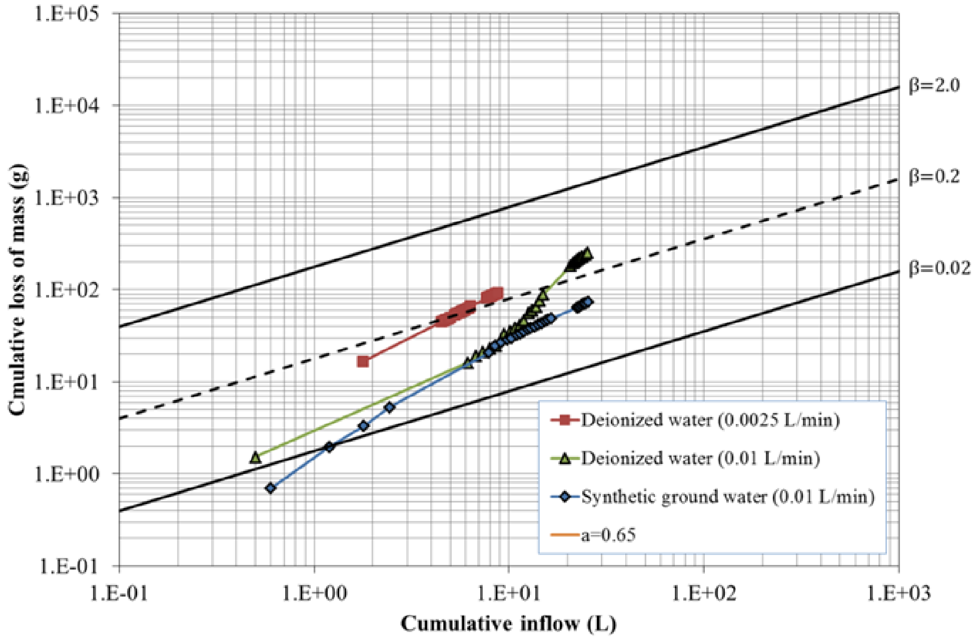

Figure 9-16: Accumulated eroded material versus accumulated water flow.

Reference: 李思偉 etc. (2018).

9.2.5. Chemical Evolution of the Surrounding Environment

A relevant assessment has not been done yet. However, the groundwater flow field in the surroundings of the repository will be changing along with the groundwater inflow to the disposal tunnels in this period based on the reference (SKB, 2011). Upconing of the high salinity groundwater might follow. After the repository is closed, saline water is supposed to sink back to deeper strata because of the high density it has. And the salinity of groundwater might recover to its initial state.

The relevant impact has not been evaluated yet. The chemical evolution model of the repository will be one of the research objectives in the future.

9.2.6. Impact of Operation on the Completed Parts of Repository

A relevant assessment has not been done yet. However, excavation of the repository is supposed to only affect local areas based on the reference (SKB, 2011). Backfill and plug will be installed immediately after the disposal activities to maintain the safety functions of the buffer and backfill. Therefore, it is not expected to have harmful effects on the completed part of the repository from excavation and operation in other parts of the repository. For the purpose of evaluating the safety of the repository and establishing appropriate excavation and operation procedures, detailed evaluation of the impact will be one of the research objectives in the future.

9.2.7. Summary

The excavation and operation period will take several decades depending on the operation method of the excavation and operation, the number of canisters, and so on. The state of the repository during the excavation and operation period is described in Chapter 4. This state could be affected by the activities during the excavation and operation period, which are different from the evolution of the repository after closure driven by natural processes. A summary of the possible impact on the repository in the excavation and operation period based on the assessment results from Section 9.2.1 to 9.2.6 is listed below:

(1) Thermal evolution:

The thermal evolution of the repository during the exaction and operation period will mainly be dominated by the decay heat of SNF in the canisters. Some of the system components may reach their highest temperature during the excavation and operation period, but none of them exceed 100 ℃.

(2) Mechanical evolution:

The mechanical evolution of the repository during the excavation and operation period will mainly be dominated by the excavation activities. According to Section 9.2.2, no huge impact is expected to be seen on the transmissivity of the host rock during excavation. The transmissivity of EDZ was thereby assumed to be $10^{-8}\ m^2/s$ in accordance with the reference (SKB, 2011). The impact of fracture reactivation would also be negligible and can be covered by the impact of EDZ.

The possibility of spalling can be reduced by making long axes of the disposal tunnels parallel to the maximum horizontal stress direction when designing the disposal tunnels and by strengthening the supporting structure during excavation. If spalling with a depth larger than 5 cm does occur, the deposition hole shall be discarded. According to the analysis results of excavation stability and seismicity, the bottom of the disposal tunnel would be slightly unstable. But the stability of disposal tunnels is maintained to a certain degree, and that relevant safety functions are not supposed to be affected.

(3) Hydrogeological evolution:

The hydrogeological evolution of the repository during the excavation and operation period is described in Section 9.2.3. In general, groundwater flows into the disposal tunnels and the deposition holes would be relatively more at the beginning of the excavation. The inflow will decrease gradually and converge to a constant over time. According to the analysis results, the inflow is expected to be between 10^{-9} L/min to 10^{-2} L/min, and the flow velocity is expected to be between 10^{-9} m/s to 10^{-7} m/s.

(4) Evolution of buffer and backfill:

Buffer and backfill will not be saturated during the exaction and operation period, and piping and erosion of the bentonite might occur in this period. The analysis results show that an amount of 21.30 kg to 213.01 kg buffer bentonite might be lost inside one single deposition hole due to piping and erosion; meanwhile, the dry density of the remaining buffer would be between 1,589 kg/m^3 to 1,573 kg/m^3 (the saturated density would be between 1,950 kg/m^3 to 2,050 kg/m^3). On the other hand, an amount of 21.30 kg to 2,130.12 kg of backfill bentonite might be lost in one single disposal tunnel but is expected to have no influence on the backfill density.

(5) Chemical evolution:

The chemical evolution of the repository during the excavation and operation period will mainly be dominated by upconing and dropping of the groundwater level. Except for a few areas where the salinity would increase due to upconing, the salinity of most of the areas would decrease owing to a drop in the groundwater level.

(6) Impact of operation on the completed parts of the repository:

The excavation activities will only affect parts of the repository; besides, the disposal tunnels will be backfilled and plugged immediately after the disposal activities are completed. No harmful effects on the repository are expected to be seen.

9.3. The Initial Period after Closure (post-closure 1,000 years)

9.3.1. Introduction

The subtropical climate is expected to be lasted for at least 25 thousand years after the repository is closed (Figure 5-1). Since most of the initial and transient phenomena of the repository are expected to occur in the first one thousand years after the repository is closed, detailed analyses of the first one thousand years will be discussed in this section.

9.3.2. External Factors

According to Chapter 5, climate evolution over the safety assessment timescale of the reference case will follow a 120,000 years glacial cycle. According to the assessment result, climatic conditions such as temperature and annual rainfall are not expected to change a lot in the first 1,000 years after the repository is closed. The climate of the reference case will still be a subtropical climate. The reference case will still be under the influence of the East Asia Continent and the Northwest Pacific monsoon system, and the climate change of the reference case will be dominated by monsoon. The annual temperature of the reference case will be above 0 ℃. In summer, the reference case will be affected by southwest currents and typhoons, and there will be strong convection and heavy rainfall. On the other hand, in winter, dry and cold northeast monsoons will prevail, and evaporation will be high.

As a result, the climatic conditions of the reference case are assumed to be similar to the present. The annual average surface temperature will be about 23.8 ℃, annual rainfall will be about 1,100 mm, and the sea-level and catchment will be similar to the present.

9.3.3. Biosphere

The main driving force of the biosphere evolution in the reference case would be changes in the climate conditions and the corresponding sea-level changes. Landscapes and human actions will be different along with the topography, which will be influenced by changes in the sea-level. In addition, the impact on humans from the radionuclides released from the repository will vary with different topography and release locations. Biosphere evolution of the reference case is discussed according to the topography, the ecosystem, and the release location of radionuclides:

(1) Surface topography

The reference case will still be an island in the initial period after closure (post-closure 1,000 years). Temperature and precipitation will not be very different from nowadays. Besides, the altitude of the sea-level will not be very different, so the coastline displacement is small and no significant changes in the topography. Therefore, they are assumed to be the same as nowadays.

(2) Ecosystem

As mentioned earlier, the surface environment of the reference case will not change much in this period. Therefore, ecosystems including the marine and terrestrial ecosystems, will remain similar to nowadays. There will be agricultural, livestock, and oyster farming activities with high yields in the reference case.

(3) Release location of radionuclides

According to the analysis results of radionuclide release, most of the radionuclides will release into the ocean in the initial period after closure (post-closure 1,000 years); therefore, humans might receive doses through activities related to the sea.

Besides, the radionuclides might attach to sea aerosol and float to the surrounding land by sea spray. Hence, those living near the coast or those participating in the marine-related industry will be the main objectives of the assessment of the biosphere.

9.3.4. Near-Field Thermal Evolution

The assessment of near-field thermal evolution was performed assuming that all of the deposition holes were disposed with canisters. The temperature effect of the engineered barrier due to the thermal evolution of the decay heat was also calculated.

The maximum temperature is often found on the top of the canisters for this area is directly contacted with bentonite (SKB, 2009c). In accordance with the analytical steps described in Section 4.4.1, the initial thermal power of the canisters was conservatively set to the limit of the initial heat load (1,200 W). The canister spacing was 9 m. The heat transfer properties of the host rock were assumed to be uniform.

And the thermal conductivity was between 2.3 W/mK and 3.0 W/mK. According to thermal conductivity and other relevant parameters, the temperature of the host rock at half-height of the canister due to decay heat was calculated (SKB, 2009c). The temperature change of the bentonite at the top of the canister due to heat transfer via the air gap in the buffer was also calculated (SKB, 2009c). A summation of the two would give maximum temperature of the bentonite at the top of the canister (SKB, 2009c).

The peak buffer temperature at the top of the canister over time is shown in Figure 9-17 and Figure 9-18. The analysis results show that the maximum temperature of the bentonite can be found around 15 years after the canister was disposed. The higher the thermal conductivity of the host rock (3.0 W/mK), the easier it is to dissipate the heat from each heat source; therefore, the change in temperature of the bentonite at the top of the canister would be smaller.

It can be seen that in the initial period after closure (post-closure 1,000 years), the temperature of the bentonite at the top of the canister will increase gradually. When the thermal conductivity of the host rock is 2.3 W/mK, the temperature will reach its highest value in about 10 years after closure (approximately 90.3 ℃). When the thermal conductivity of the host rock is 3.0 W/mK, the temperature will reach its highest value in about 10 years after closure (approximately 83.9 ℃). The temperature of the bentonite at the top of the canister will decrease gradually after reaching the maximum value. In the 25th year after the repository is closed, the maximum temperature of the bentonite at the top of the canister will be about 88.46 ℃ and 82.12 ℃, respectively. The temperature is expected to decrease over time due to the decrease of the decay heat. Temperature requirements related to safety functions Buff4 and Buff6 can be met when 8 ℃ of temperature margin is taken into account.

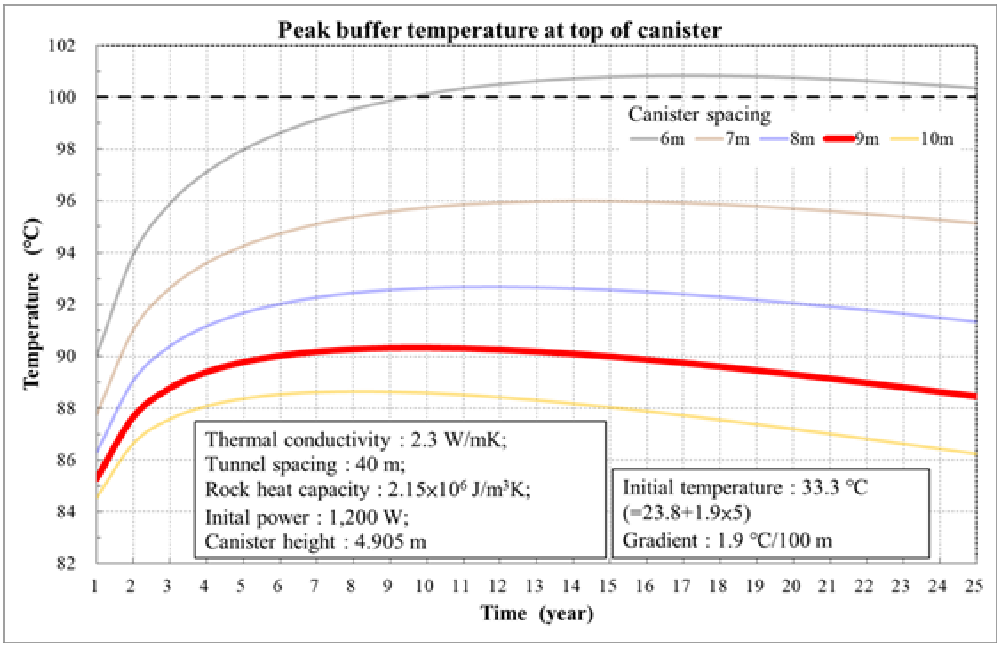

Figure 9-17: Peak buffer temperature at the top of the canister over time with different canister spacing (thermal conductivity of the host rock: 2.3 W/mK).

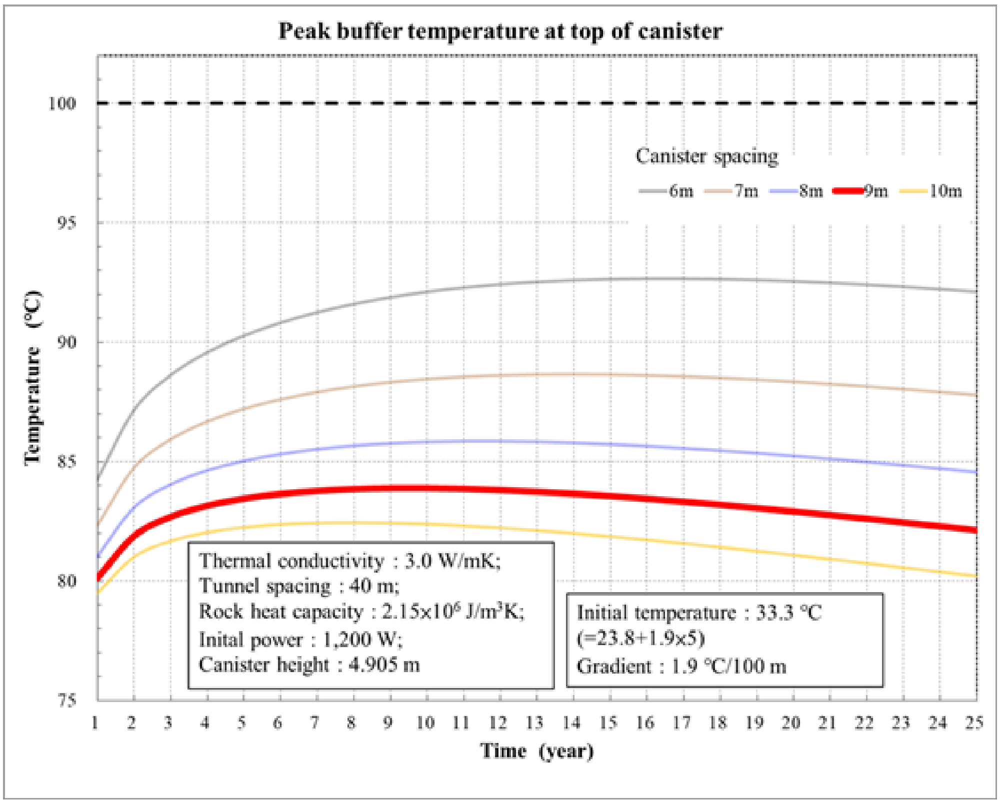

Figure 9-18: Peak buffer temperature at the top of the canister over time with different canister spacing (thermal conductivity of the host rock: 3.0 W/mK).

9.3.5. Rock Mechanical Evolution

In the initial period after closure (post-closure 1,000 years), the main impact on mechanics is shown below:

(1) Reactivation of fractures in the near-field due to thermal load:

The temperature will rise due to the decay heat of the SNF in the canisters. This will lead to the expansion of rock that causes aperture closure or fracture displacement. Safety function R3 and fracture transmissivity could thereby be affected. However, the changes in near-field fracture transmissivity would be local and limited (SKB, 2011). According to the reference from SKB (SKB, 2011), part of the fractures might be closed under the influence of thermal load. On the other hand, fracture apertures near the excavation plane might increase locally. This would be taken into account when evaluating the effect of EDZ.

(2) Reactivation of fractures in the far-field due to thermal load:

As mentioned earlier, the simulation of fracture with 150 m radius at 450 m depth shows that the maximum thermal-induced shear displacement of fracture will be less than 7 mm. And the increasing normal stress on the fracture will reduce rather than increase the fracture transmissivity. Thus changes in fracture transmissivity from the influence of thermal load are very small and do not need to be considered in far-field hydrogeology analysis.

(3) Spalling might occur and change the geometry of the deposition holes, which affects radionuclide transportation between the rock and the buffer (safety function Buff1):

Thermal load in the initial period after closure (post-closure 1,000 years) might lead to spalling of the host rock around the deposition holes. Spalling strength is expected to be around 50% of the uniaxial compressive strength (SKB, 2011). And this can be reduced by analyzing thermal load distribution and optimizing the canister disposing sequence during the excavation and operation period.

(4) Fracture reactivation is caused by the deformation of rock due to plate movement, which can affect the mechanical stability of the deposition holes (safety function R3):

According to the geological records, structural activities, including ductile shearing, were active between 129 Ma and 76 Ma. On the other hand, faulting was active between 76 Ma and 58 Ma, and there were no obvious structural activities after 58 Ma (台電公司, 2019a). Thus, fracture reactivation due to plate movement will mainly be induced by an earthquake in the reference case.

After the repository is closed, the shear displacement of fractures in the host rock can accumulate because of an earthquake. If the fracture intersect a canister, the canister is likely to suffer from the shear force, which might lead to failure of the canister. Earthquake-induced shear displacement of fractures in a single seismic event was analyzed using 3DEC. And the accumulation of shear displacement of fractures after multiple seismic events over the safety assessment timescale was also estimated under cautious assumption. Please refer to Section 9.4.4 for detailed analysis results.

9.3.6. Hydrogeological Evolution

The assessment of hydrogeological evolution in the initial period after closure (post-closure 1,000 years) can be divided into three parts, including the analyses of the groundwater flow field, release paths, and performance measures. These analyses are described as follows:

(1) Groundwater flow field:

Based on the conceptual hydrogeological model described in Section 9.1.3, the groundwater flow field in the initial period after closure (post-closure 1,000 years) was evaluated. The model domain is shown in Figure 9-1, which is a site scale model. The parameters of the conceptual model are shown as follows:

(a) Hydrogeological model: the model includes regolith (R0), rock mass (R), and major water conducting structure (F#). And the fault structure (F1) and fracture structure (F2) only exist on the island.

(b) Sea-level: same as nowadays (0 m).

(c) Salinity: river water average (0.0105 %) and sea 3.2 %.

(d) Computational grid:

(i) The whole domain and structures: the cell size applied in the domain was 256 m×256 m×256 m, and the refinement was applied by setting a cell size of 32 m×32 m×32 m in fault structure (F1) and fracture structure (F2) where permeability is higher than the rock mass.

(ii) The top of the domain: refinement was applied by setting a cell size of 32 m×32 m×32 m at the top of the domain.

(iii) The repository: first of all, the rock mass close to the repository was refined to 64 m×64 m×64 m; then the grid was globally refined to 8 m×8 m×8 m in the repository zone. In addition, the main tunnels, disposal tunnels, and deposition holes were refined to 1 m×1 m×1 m, EDZ was refined to 1 m×1 m×0.125 m, and walls of the deposition holes were refined to 0.25 m×0.25 m×0.5 m.

The successive refinement led to around 18 million cells, and the grids of the site scale model are shown in Figure 9-19.

The DFNs were generated based on the DFN recipe of the reference case. And for the purpose of involving the stochastic process in fracture generation, a coefficient that determines the spread of the generated random deviates using a uniform distribution of the relationship between fracture transmissivity and fracture size was added. Finally, connectivity analysis that removed all isolated single fractures or isolated clusters of fractures was conducted to generate an effective fracture system for effective hydraulic properties transformation because the flow will be the main focus. Regarding the hydraulic properties of EDZ, the transmissivity was set to be 10^{-8} m^2/s (Bäckblom, 2008; SKB, 2008; SKB, 2010i) according to Section 9.3.5. In addition, We assume the buffer and backfill are all saturated after closure when we consider the hydraulic properties of the buffer and backfill involved in the groundwater flow and release path simulation in this section.

The module used to perform effective hydraulic transformation in DarcyTools was GEHYCO (GEneral Hydraulic COnditions) which is a finite volume code. The directional properties would be calculated using GEHYCO based on the effective fracture system (Svensson, 2010; Svensson and Ferry, 2010; Svensson et al., 2010). Aneffective hydraulic transformation would be done according to the effective fracture system. The result can be seen in Figure 9-20.

Regarding the setting of the boundary conditions, prescribed hydrostatic pressure and salinity were assigned on all lateral boundaries. An infiltration rate of 66.8 mm/yr with a salinity of 0.0105% was assigned on the top boundary, and the bottom boundary was assigned to be a no-flow boundary.

The analysis result of the pressure field is shown in Figure 9-21. The result shows that the pressure of the central area is likely to be higher, and the pressure will decrease gradually to the coastline. This indicates that the groundwater would flow from the central area to the coastline. The analytical result of the salinity field is shown in Figure 9-22. The result shows that there will be an obvious seawater and freshwater interface beneath the island, and flow paths might be affected accordingly.

(2) Release paths:

Based on the results of groundwater flow field analysis, the particle tracking method was used to model potential release paths (Figure 9-23) of (a) particles released from the intersection between fracture and deposition hole (Q1 path) and (b) particles released from EDZ (Q2 path).

(a) The particles released from the intersection between fracture and deposition hole (Q1 path):

Particle release number is highly related to repository layout, fracture system, and geometrical rejection criteria. According to the setting of these parameters, a total of 148 potential release locations were there in the Q1 path.

The results of particle tracking of the Q1 path are shown in Figure 9-24. The results show that the paths would be strongly influenced by the groundwater pressure field and salinity field. The results also show that particles are likely to move towards the north, the northeast, and the northwest due to the gradient caused by the central area. The seawater and freshwater interface will also affect flow paths in the coastline area. That is, the downward flow paths will turn upward at the interface, which will lead to most of the particles released near the coastline.

(b) Particles released from EDZ (Q2 path):

As described above, the particle release number is highly related to repository layout, fracture system, and geometrical rejection criteria. According to the setting of these parameters, a total of 2,643 potential release locations were there in the Q2 path.

The results of particle tracking of the Q2 path are shown in Figure 9-25. The results indicate that the EDZ dominates the Q2 paths in the repository area. The results also show that the flow paths of Q2 would be very similar to Q1; that is, particles are likely to move towards the north, the northeast, and the northwest. The seawater and freshwater interface will still play an important role in affecting flow paths. Therefore, the salinity field and the seawater and freshwater interface are important to the assessment of the hydrogeological evolution of the repository.

(3) Performance measures:

In order to evaluate engineered barrier performance, such as buffer erosion and copper corrosion, performance measures are important parameters that need to be obtained. Performance measures include equivalent initial flux, flow-related transport resistance (F), equivalent flow rate (Q_{eq}), and so on. Based on the requirements of safety function R2, the evaluation was mainly focused on flow related transport resistance and equivalent flow rate.

According to the requirements of safety function R2, flow-related transport resistance of the Q1 path should be larger than 10,000 yr/m and the equivalent flow rate of Q1 path should be smaller than 1.0×10^{-4} m^3/yr (SKB, 2011).

(a) Flow-related transport resistance (F): the cumulative distribution function of flow related transport resistance (F) is shown in Figure 9-26. The results indicate that the minimum flow related transport resistance of the Q1 path would be 1.60×10^6 yr/m, which fulfills the requirements of safety function R2. And the minimum flow-related transport resistance of the Q2 path would be 9.21×10^5 yr/m. The distribution is very similar to the one of the Q1 path.

(b) Equivalent flow rate (Q_{eq}): the cumulative distribution function of equivalent flow rate is shown in Figure 9-27. The results indicate that the maximum value of the Q1 path would be 7.46×10^{-6} m^3/yr, which fulfills the requirements of safety function R2. And the maximum equivalent flow rate of the Q2 path would be 3.3×10^{-5} m^3/yr. The maximum equivalent flow rate of the Q2 path would be smaller than the maximum equivalent flow rate of the Q1 path.

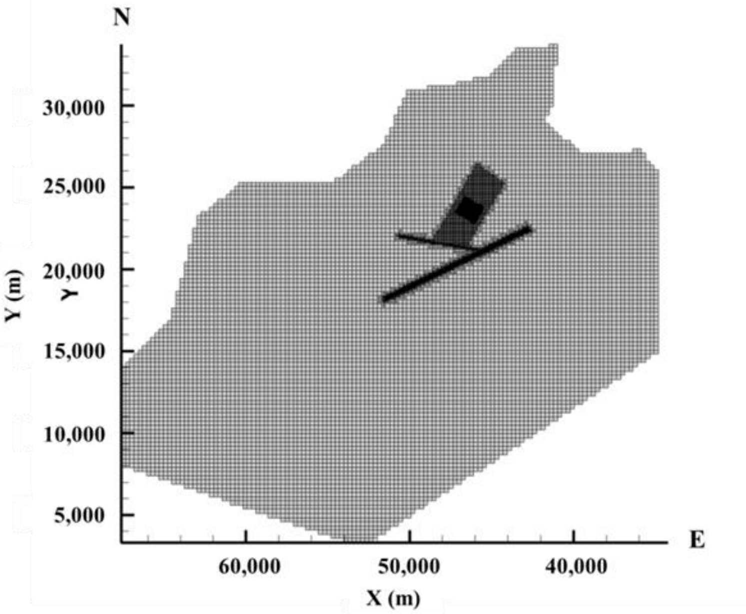

Figure 9-19: Grids of the site scale model.

Note: the horizontal cut plane at z=-504 m.

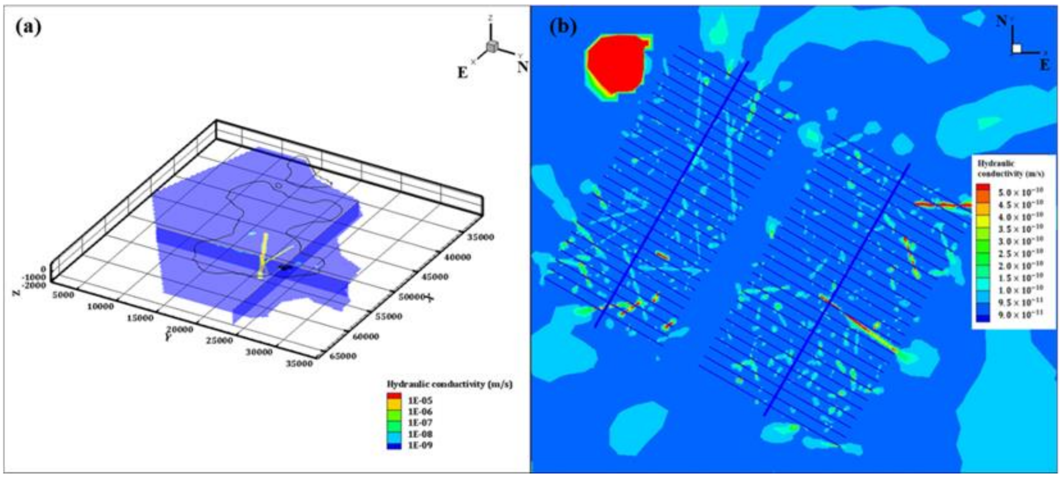

Figure 9-20: Effective hydraulic conductivity values of the site scale model.

Note: (a) the horizontal cut plane at z=-504 m, and vertical planes at x=53,625 m and y=23,650 m; (b) plane of the effective hydraulic conductivity near the repository at z=-504 m.

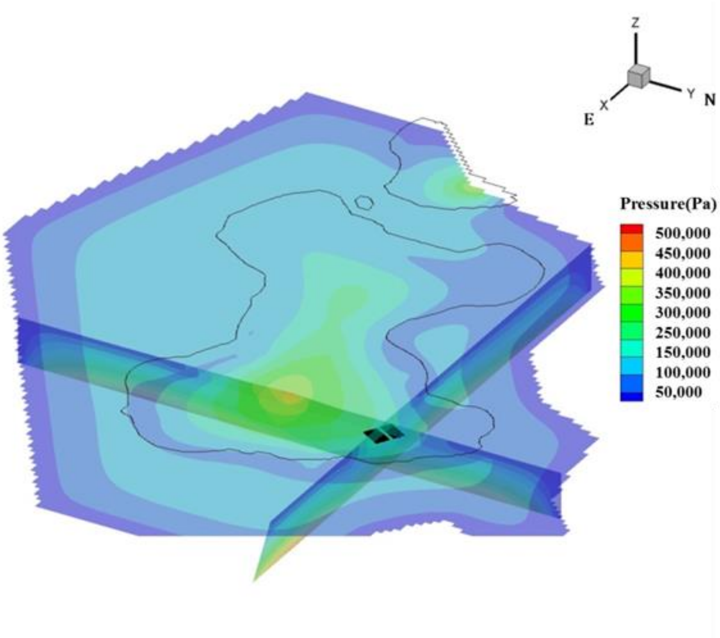

Figure 9-21: Dynamic pressure of the site scale model.
Note: the horizontal cut plane at z=-504 m, and vertical planes at x=53,625 m and y=23,650 m.

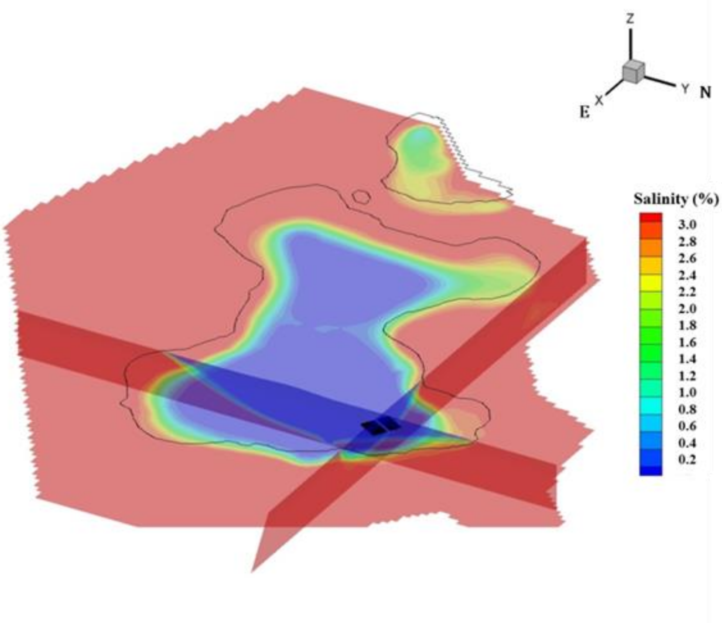

Figure 9-22: Salinity of the site scale model.
Note: the horizontal cut plane at z=-504 m, and vertical planes at x=53,625 m and y=23,650 m.

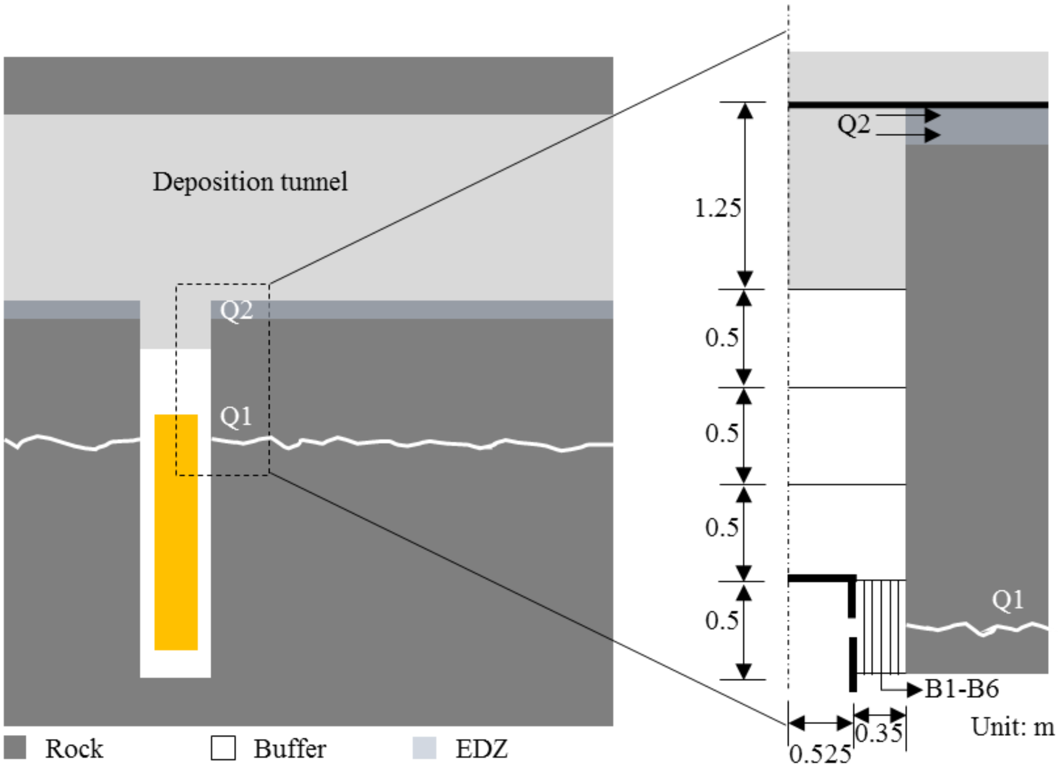

Figure 9-23: Concept of Q1 and Q2 release paths.

Reference: Joyce et al. (2010).

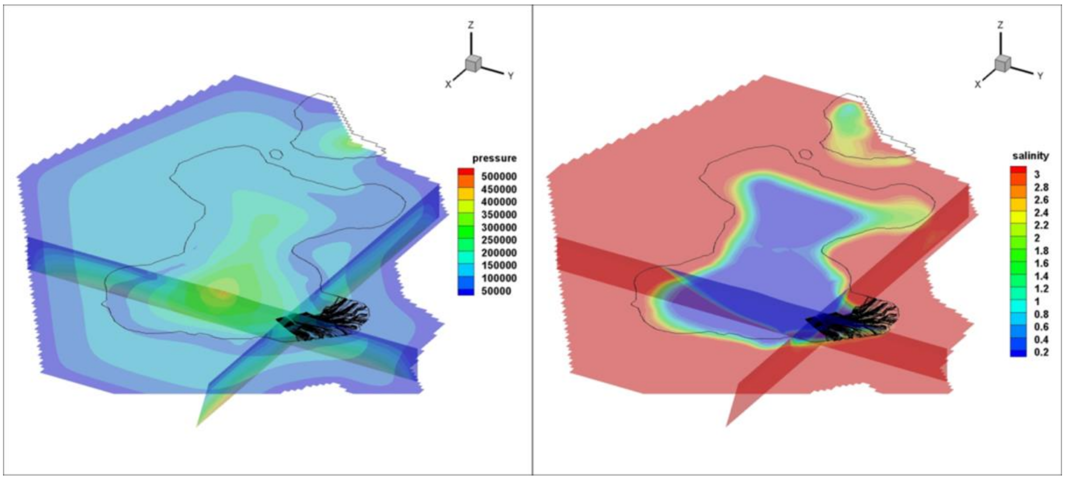

Figure 9-24: Dynamic pressure and salinity of Q1 release paths of the site scale model.

Note: the horizontal cut plane at z=-504 m, and vertical planes at x=53,625 m and y=23,650 m.

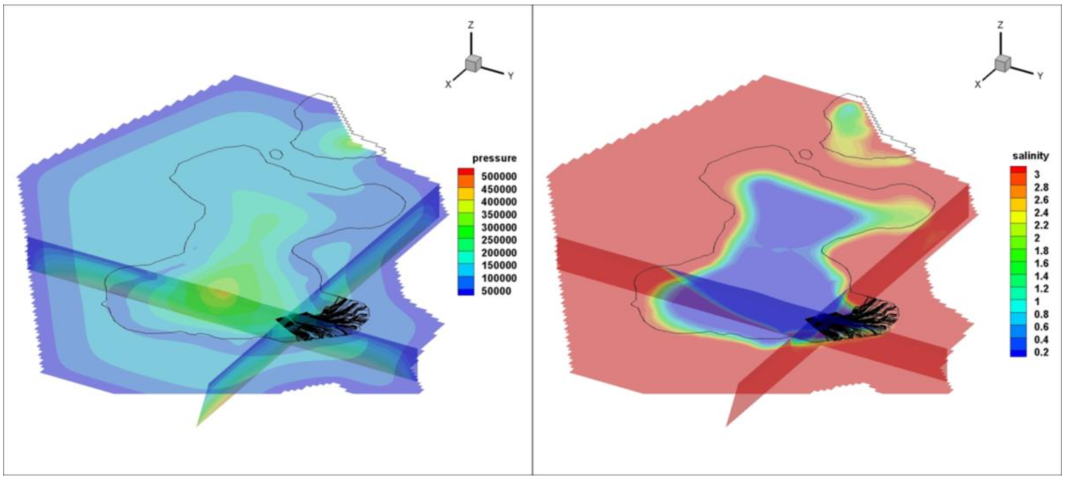

Figure 9-25: Dynamic pressure and salinity of Q2 release paths of the site scale model.

Note: the horizontal cut plane at z=-504 m, and vertical planes at x=53,625 m and y=23,650 m.

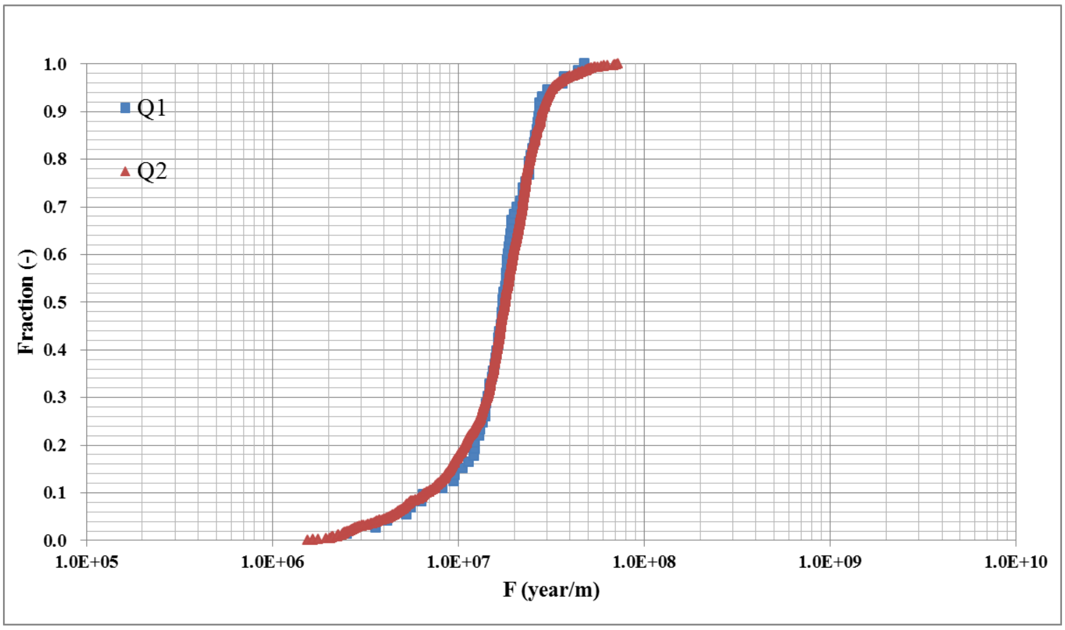

Figure 9-26: Cumulative distribution functions of flow related transport resistance for Q1 and Q2 paths of the site scale model.

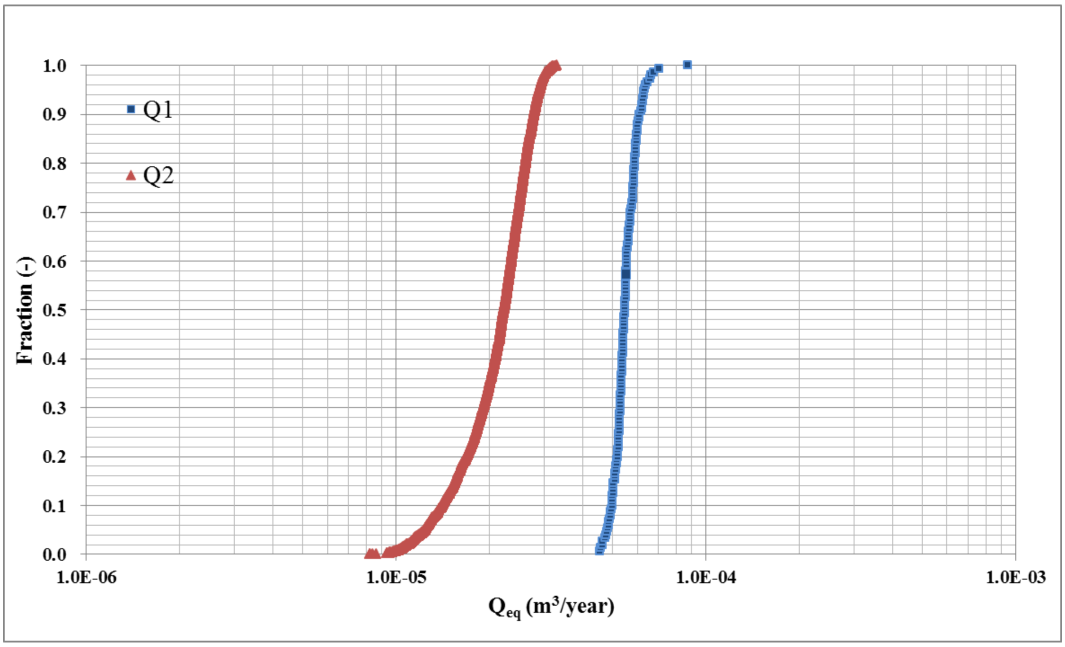

Figure 9-27: Cumulative distribution functions of equivalent flow rate for Q1 and Q2 paths of the site scale model.

9.3.7. Chemical Evolution of the Surrounding Environment

The hydrogeology condition of the repository will be affected by groundwater inflow and precipitation, which will affect the hydrochemistry condition of the repository including redox-oxidation potential, salinity, ionic strength, pH, and chemical species such as potassium, sulfide and iron that may affect safety functions of the buffer and the canister. Therefore, safety function R1 should be maintained to provide favorable chemical conditions.

According to Section 9.3.5, the steady-state salinity distribution of the repository in the initial period after closure is shown in Figure 9-22, and the steady state salinity distribution at the depth of center of gravity for canisters (z=-504) is shown in Figure 9-28. The results show that the salinity will be between 0.002% and 0.013% with obvious freshwater and seawater interface. This interface might allow particle transport, thus influencing the assessment results of particle tracking.

Currently, the hydrochemical model for the assessment has not been well established yet. Based on groundwater salinity, PHREEQC was used to analyze chemical species distribution, TDS, ionic strength, pH, and concentration of potassium, sulfide, and iron. The corrosion rate for all of the deposition holes (i.e., 2,860) has been calculated by combining the hydrogeological and geochemical conditions together, i.e., by considering the Q_{eq} value and the geochemical parameters of each hole. Then five deposition holes with the top five corrosion depths were selected for the following safety assessment. According to calculation results of corrosion rate, five deposition holes with the highest corrosion depth (DH-216, DH-812, DH-2110, DH-2632, and DH-2633) were taken as an example to evaluate chemical species distribution in groundwater conservatively (the detailed information will be elaborated in Section 9.3.13). The assessment results of ionic strength, pH, and concentration of sulfide and iron are shown in Table 9-3.

The assessment results show that TDS in the surrounding environment of the repository will be between 1.33 g/L and 1.18 g/L, the salinity will be between 0.0133% and 0.0118%, and the pH value will be between 7.07 and 7.10. These indicate that the requirements related to pH value and TDS (safety function R1) can be fulfilled in this period.

However, the results also show that the ionic strength in the surrounding environment of the repository is likely to be low (below 8 mM), and the concentration of hydrogen sulfide ion is likely to be slightly over the requirements of safety function (slightly over 10^{-4} M). These may lead to colloid release of the buffer and the backfill, and the canisters may thereby be corroded. A detailed assessment of these phenomena is shown in Sections 9.3.10 and 9.3.12.

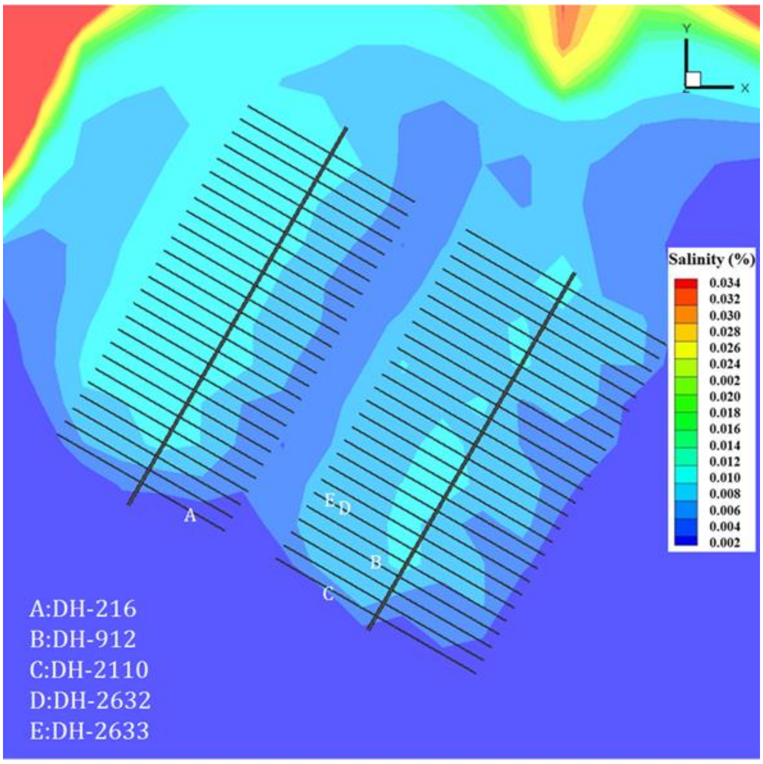

Figure 9-28: Salinity distribution at the depth of canisters.

Note: depth at z=-504 m. A to E are the locations and numbers of the deposition holes with the top five highest corrosion depths.

Table 9-3: Evaluation results of chemical evolution of the five deposition holes.

Deposition hole NO.	**TDS (g/L)**	**Ionic strength (mM)**	**pH**	**[HS^-] (mole/L, M)**	**[Fe^{+2}] (mole/L, M)**	**[Fe^{+3}] (mole/L, M)**
DH-216	1.24	2.34	7.08	1.74×10^{-4}	1.25×10^{-7}	2.13×10^{-7}
DH-812	1.33	2.51	7.10	1.80×10^{-4}	1.14×10^{-7}	1.89×10^{-7}
DH-2110	1.18	2.23	7.07	1.71×10^{-4}	1.34×10^{-7}	2.31×10^{-7}
DH-2632	1.33	2.51	7.10	1.80×10^{-4}	1.14×10^{-7}	1.89×10^{-7}
DH-2633	1.33	2.51	7.10	1.80×10^{-4}	1.14×10^{-7}	1.90×10^{-7}

9.3.8. Saturation of the Buffer and Backfill

During the initial period after closure (post-closure 1,000 years), the buffer and the backfill will still be unsaturated. And groundwater inflow will gradually increase the degree of saturation of the buffer and the backfill.

A numerical model was established using the FLAC3D program. The dimensions of the disposal tunnels and deposition holes in the numerical model were established based on the designed dimensions of the buffer in Section 4.2.5 (Figure 4-8), as shown in Figure 9-29. The initial dry density of the buffer and backfill was set according to the designed density in Section 4.2.5 (Figure 4-9), as the initial dry density was $1{,}590\,\mathrm{kg/m^3}$ and $1{,}461\,\mathrm{kg/m^3}$ of the buffer and the backfill respectively (Figure 9-30).

The hydraulic conductivity of the buffer and backfill was set according to the experimental results of the buffer in Section 4.2.5 (Figure 4-11), as the hydraulic conductivity of the buffer and the backfill was $3.21 \times 10^{-12}\,\mathrm{m/s}$ and $2.92 \times 10^{-12}\,\mathrm{m/s}$ respectively. Boundary conditions were set according to the groundwater flow field and the groundwater pressure distribution in Section 9.3.6. And the attitude of the fracture was based on the analysis results of Section 9.3.5.

It was assumed that after installation of buffer and backfill, fracture of the host rock would generate subsequently, and a gap would be created around the intersection of buffer and backfill. Fracture-intersected repository, buffer and backfill were of full-face inflow, indicating that the groundwater would flow through the intersection and gap.

FLAC3D model was employed to simulate the average saturation of the buffer and backfill in the disposal tunnels and the deposition holes after groundwater inflow through the fractures.

According to Section 9.3.5, two main types of fracture intersection occur most frequently: (1) both the disposal tunnel and the deposition hole are intersected, and (2) only the deposition hole is intersected. There were 2 situations that were modelled. Case 1 was when the disposal tunnel and the deposition hole were both intersected by fractures (Figure 9-31). The relationship between average saturation and time is shown in Figure 9-32. From the results, it will take about 200 years for the disposal tunnel and deposition hole to reach full saturation. Case 2 was when only the deposition hole was intersected by fractures (Figure 9-33). The relationship between average saturation and time is shown in Figure 9-34. From the results, it will take about 9,300 years for the disposal tunnel and deposition hole to reach full saturation. And the saturation time would be much longer. This is because the intersected area in Case 2 is smaller, and the inflow of groundwater will be relatively small compared to Case 1. In addition, groundwater in Case 2 traveled upwards from the fracture area to the disposal tunnel. In this case, the groundwater would also need to resist the influence of gravity, which resulted in a longer saturation time for the disposal tunnel.

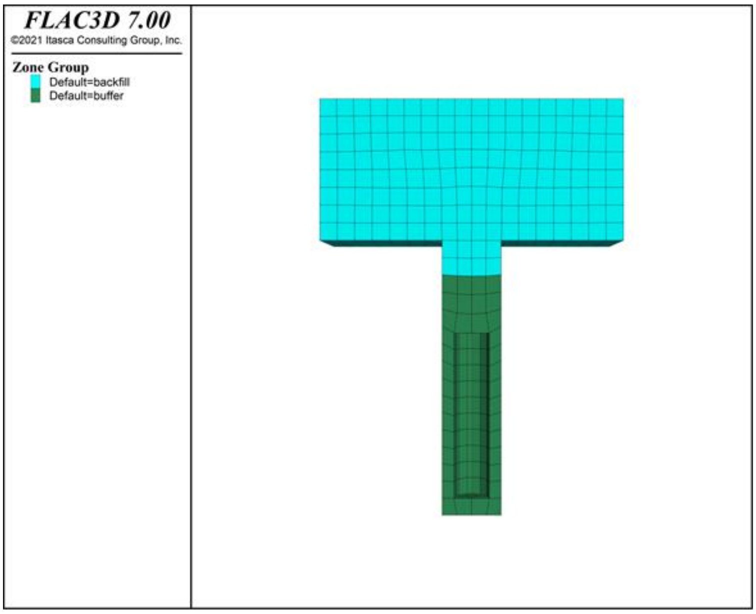

Figure 9-29: The 3D numerical model.

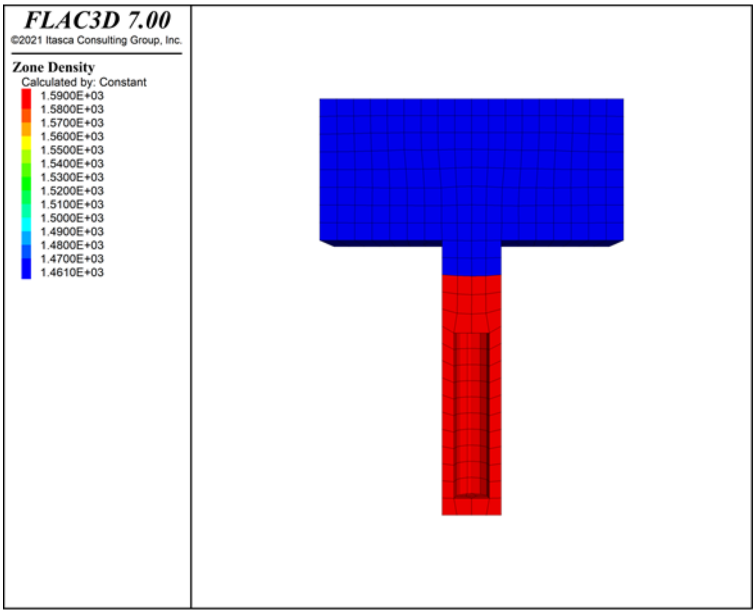

Figure 9-30: Initial dry density of the buffer and backfill.

Note: the unit of density is kg/m^3.

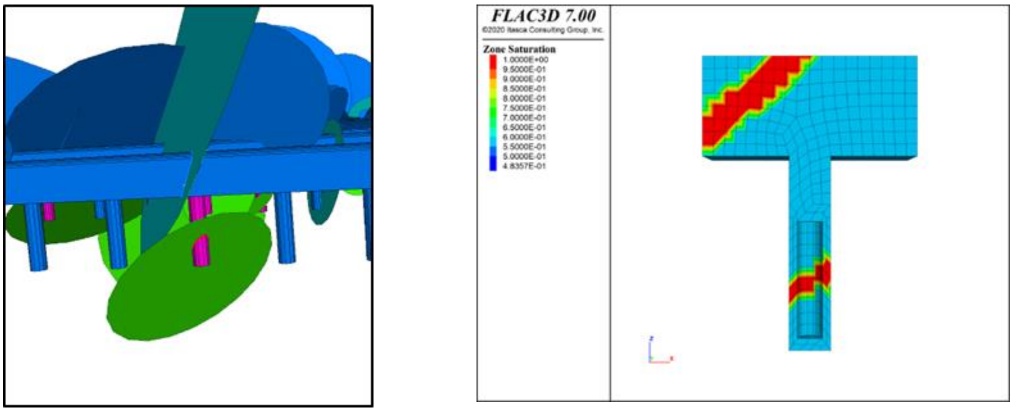

(a) Positions of fractures (b) Initial state of saturation

Figure 9-31: Fracture positions and initial state of saturation (the fractures intersect with both the disposal tunnel and the deposition hole).

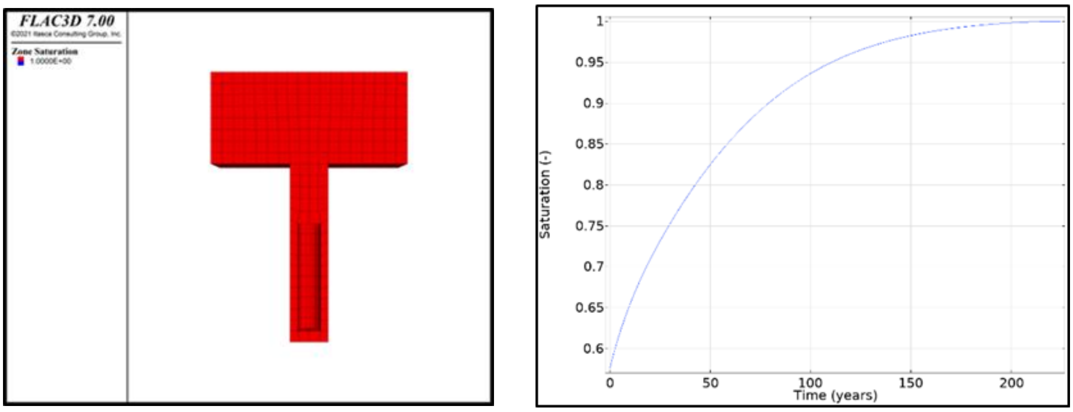

(a) Distribution of saturation around 200 years (b) Average saturation vs. time

Figure 9-32: Average saturation versus time (when fractures intersect with both the disposal tunnel and the deposition hole).

Note: Y-axis refers to average saturation and X-axis refers to time (year) in (b).

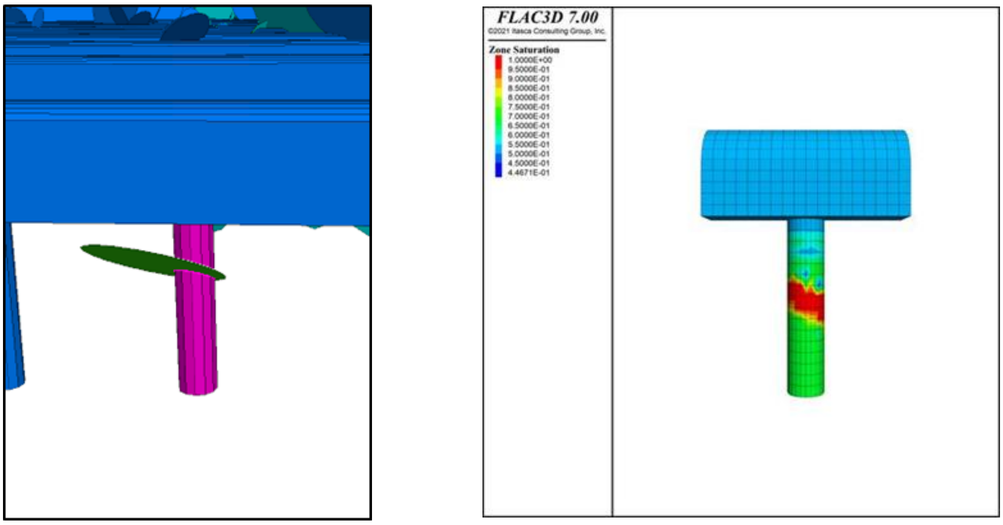

(a) Position of fracture (b) Initial state of saturation

Figure 9-33: Fracture position and initial state of saturation (the fracture only intersects with the deposition hole).

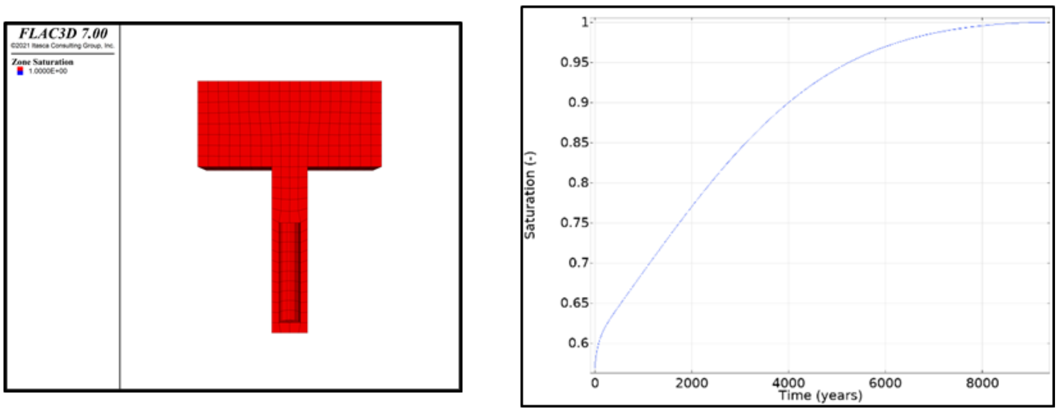

(a) Distribution of saturation around 9,300 years

(b) Average saturation vs. time

Figure 9-34: Average saturation versus time (when fracture only intersects with the deposition hole).

Note: Y-axis refers to average saturation and X-axis refers to time (year) in (b).

9.3.9. Swelling and Swelling Pressure

The main function of the buffer is to ensure that substances transported between the canisters and the host rock are mainly by diffusion (safety function Buff1). For this purpose, the bentonite needs to maintain sufficient swelling pressure to fill the gaps in the deposition holes (such as working joints, block joints, rock mass cracks around the deposition hole, and so on). Also, the buffer needs to be tightly connected with the host rock to avoid additional transmission channels in the deposition holes.

Besides requirements of the above-mentioned safety function Buff1, there are certain requirements of safety function Buff1, Buff2, Buff5, and Buff6 for swelling pressure of the buffer as well. The swelling pressure of the buffer should be between 2 MPa and 10 MPa to fulfill the requirements. Additionally, the density of backfill should be high enough to resist up-swelling of the buffer so that the buffer will not squeeze into the disposal tunnels due to swelling, and the swelling pressure of the buffer can be maintained above 2 MPa (safety function BF1). And the swelling pressure of backfill should be above 0.1 MPa to limit advection (safety function BF2).

Impact on the bentonite and its swelling pressure due to (1) saturation, (2) sinking of the canisters, and (3) redistribution of the bentonite mass was evaluated as the following:

(1) Saturation of the bentonite:

When bentonite absorbs water, the water fills its pores, and makes the bentonite swell. This produces swelling pressure, and swelling of the bentonite thus occurs. The abovementioned characteristic is related to the hydraulic conditions of the area.

Similar to the analysis setting in Section 9.3.8, in Case 1, the disposal tunnel and the deposition hole were both intersected by fractures, and groundwater flows into the disposal tunnel and deposition hole through fractures in the host rock. The initial swelling pressure of the disposal tunnel and deposition hole is shown in Figure 9-35. As groundwater flows into the disposal tunnel and the deposition holes, the buffer and the backfill will gradually reach saturation and generate swelling pressure. When they reach full saturation, the swelling pressure generated by the backfill will be about 1.5 MPa, and the one generated by the buffer will be about 5 MPa, as shown in Figure 9-37. In Case 2, only the deposition hole was intersected by fractures. Groundwater will flow into the deposition hole through a fracture in the host rock, and it will gradually flow upwards from the fracture. The initial swelling pressure of the deposition hole is shown in Figure 9-36. As groundwater flows into the disposal tunnel and the deposition holes, the buffer and the backfill will gradually reach saturation and generate swelling pressure. When they reach full saturation, the swelling pressure generated by the backfill will be about 1.5 MPa, and the one generated by the buffer will be about 5 MPa, as shown in Figure 9-37.

From Figure 9-37, one can see that the swelling pressure is the same in Cases 1 and 2 when fully saturated. The reason is that the initial conditions (such as the initial dry density, the initial saturation, etc.) of the two cases are the same. The position of the intersection only affects distribution of the swelling pressure in the transient state of the saturated and unsaturated periods. When the buffer and backfill are saturated and the pressure is balanced, backfill with an initial dry density of $1{,}461\ \mathrm{kg/m^3}$ will produce a swelling pressure of approximately 1.5 MPa; on the other hand, buffer with an initial dry density of $1{,}590\ \mathrm{kg/m^3}$ will produce a swelling pressure of about 5.0 MPa.

In addition, Figure 9-37 shows that a small portion of the buffer located at the bottom of the deposition hole has swelling pressure of about 8.23 MPa. This is because swelling materials at the bottom of the deposition hole bear the weight of the canister above, making its density slightly larger than other areas. Therefore, higher swelling pressure will be generated. But it is still within the requirements of the safety function indicator.

According to the analysis results, when backfill is saturated, the swelling pressure will be 1.5 MPa. This satisfies the requirements of safety function indicator BF2, which states that the swelling pressure of the backfill should at least be 0.1 MPa to avoid advection. When the buffer is saturated, the swelling pressure will be 5 MPa. This satisfies the requirements of safety function indicators Buff1, Buff2, Buff5, and Buff6, which state that the swelling pressure of the buffer should be between 2 MPa and 10 MPa.

(2) Sinking of the canisters:

The swelling pressure of the buffer should be greater than 0.2 MPa to meet the requirements of safety function Buff5 and prevent the canister from sinking because of its weight. To avoid sinking of the canister, the buffer must have a certain thickness and density. If the density of the buffer is too low, it will be deformed by the weight of the canister. And this will further cause the canister to sink or tilt, reduce the thickness of the surrounding buffer or cause the canister to contact the wall or bottom of the deposition hole. If so, the buffer can no longer cover the canister completely, and the safety function Buff1 cannot be fulfilled.

According to Chapter 7, the swelling pressure of the buffer should be greater than 0.2 MPa to meet the requirements of safety function Buff5. In order to estimate the degree of deformation of the buffer below the canister after bearing the weight of the canister and the backfill above, a numerical simulation using FLAC3D was implemented.

The design of the canister in Section 4.2.4 can be referred to for the geometric dimensions of the canister. And design dimensions of the buffer in Section 4.2.5 can be referred to for the dimensions and the geometric dimensions of the buffer. Generally speaking, the deformation of the canister is relatively small compared to the deformation of the buffer. Therefore, currently, only the deformation of the buffer was taken into account in the simulation. And the canister was regarded as a rigid body. The overall weight would be the weight of the canister and the SNF inside. The designed weight of the canister in Section 4.2.4 was referred to, and the weight of the PWR fuel bundle, which is heavier than the BWR fuel bundle, was assumed as the boundary condition. The total weight of the canister and the PWR fuel would be 26,800 kg.

As for the initial conditions of the simulation, the designed density of the buffer (Figure 4-9) in Section 4.2.5 was referred to for the initial dry density of the buffer and backfill. The initial dry density would be $1{,}590\ kg/m^3$, as shown in Figure 9-38. Under the influence of the weight of the canister (26,800 kg), the vertical displacement of the buffer at the bottom of the canister would be about 0.024 cm, as shown in Figure 9-39. This value would be the sinking volume of the canister. The density distribution of the buffer is shown in Figure 9-40. The density of the buffer at the bottom of the canister would rise slightly due to mechanical action, and the density of the buffer at the top would decrease slightly. However, these would have little impact on the swelling pressure after saturation. The requirements of safety function Buff5 can still be fulfilled.

(3) Redistribution of the bentonite mass:

The hydraulic conductivity of the buffer should be lower than 1×10^{-12} m/s, and the swelling pressure should be greater than 2 MPa according to the requirements of safety function Buff1, Buff2, and Buff5.

When the dry density of the bentonite is greater than 1,100 kg/m^3, the hydraulic conductivity will be lower than 1×10^{-12} m/s according to Figure 4-11. And when the dry density of the bentonite is greater than 1,420 kg/m^3, the swelling pressure will be greater than 2 MPa, according to Figure 4-10. Based on the specifications of the deposition hole and buffer in Section 4.2.5, the dry density of the buffer around the canister will be 1,598 kg/m^3 (Figure 4-9). If the buffer loses more than 1,324.5 kg of bentonite, the dry density will reduce to 1,420 kg/m^3. Redistribution after 1,200 kg and 2,400 kg of bentonite were lost due to erosion was evaluated using

ABAQUS software. The swelling pressure distribution after redistribution was also evaluated to see the possible impact on the safety functions of the buffer.

Figure 9-41 shows the redistribution at different times after 1,200 kg of bentonite was lost due to erosion. The results show that the missing parts can be completely refilled in about 3.5 years; meanwhile, the swelling pressure of most of the areas will be around 4 MPa.

From the analysis results described above, the buffer is expected to maintain safety function Buff1 when the mass loss of the bentonite does not exceed 1,200 kg. Please refer to Section 9.3.11 and Section 9.4.8 for a more detailed discussion of bentonite erosion caused by colloid release.

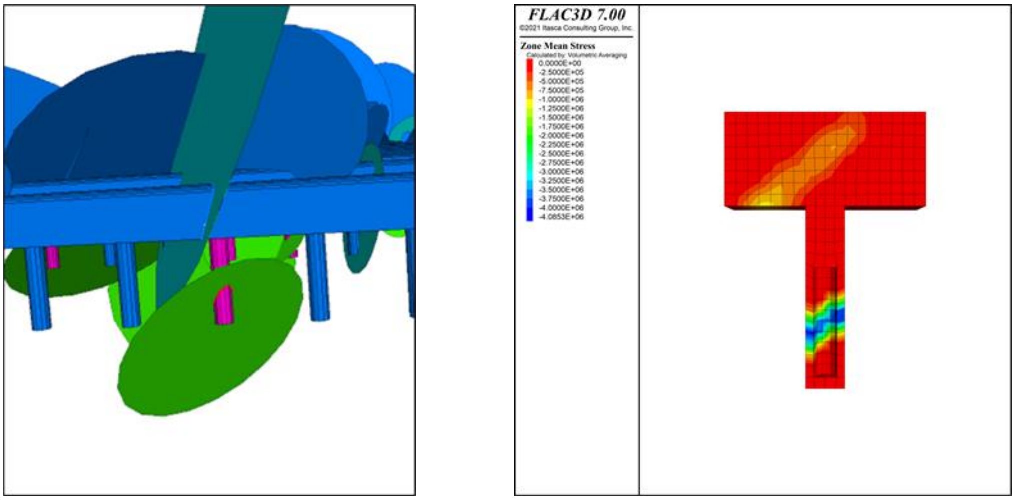

(a) Positions of fractures (b) Swelling pressure at saturate state

Figure 9-35: Fracture positions and swelling pressure when saturated (the fractures intersect with both the disposal tunnel and the deposition hole).

Note: the unit of stress is Pa in (b).

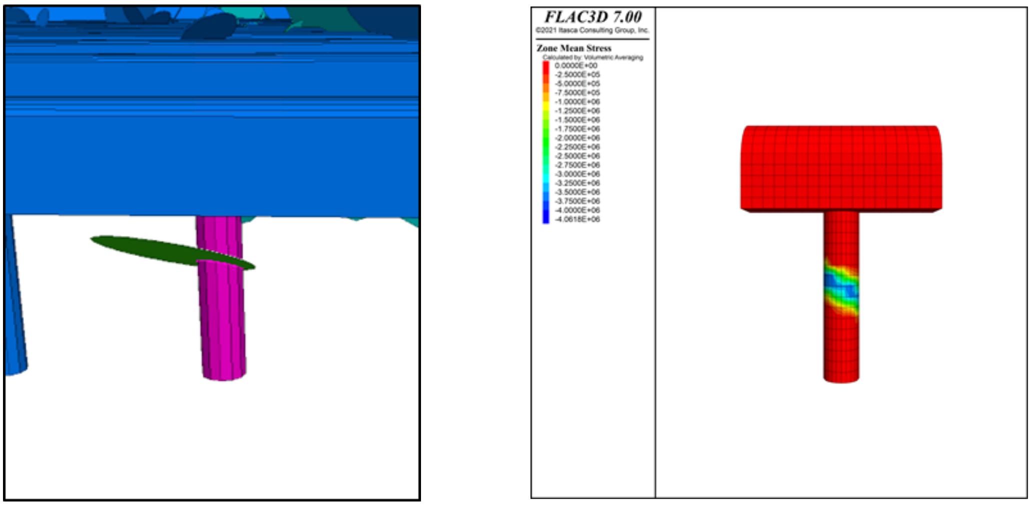

(a) Positions of fractures (b) Swelling pressure at saturate state

Figure 9-36: Fracture positions and swelling pressure when saturated (the fracture only intersects with the deposition hole).

Note: the unit of stress is Pa in (b).

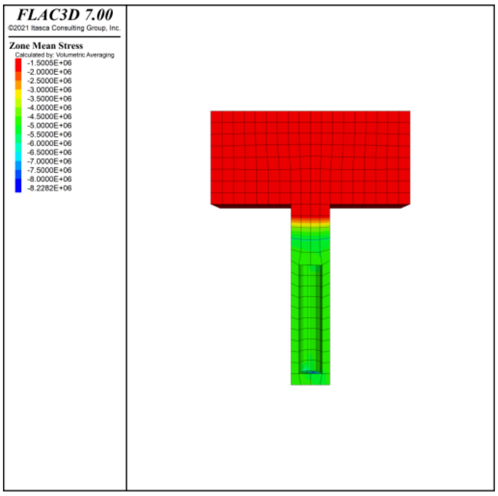

(a) Case 1 (the fractures intersect with both the disposal tunnel and the deposition hole)

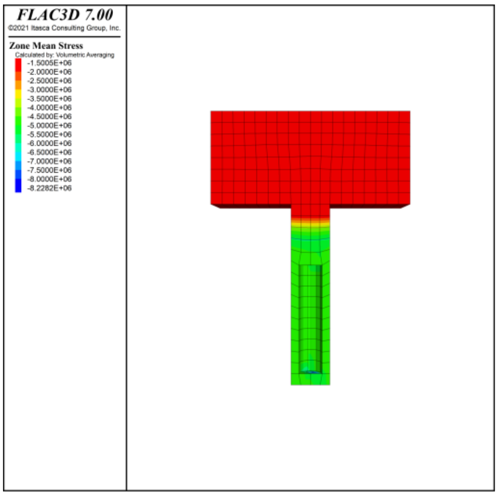

(b) Case 2 (the fracture only intersects with the deposition hole)

Figure 9-37: Swelling pressure distribution when saturated.

Note: the unit of stress is Pa.

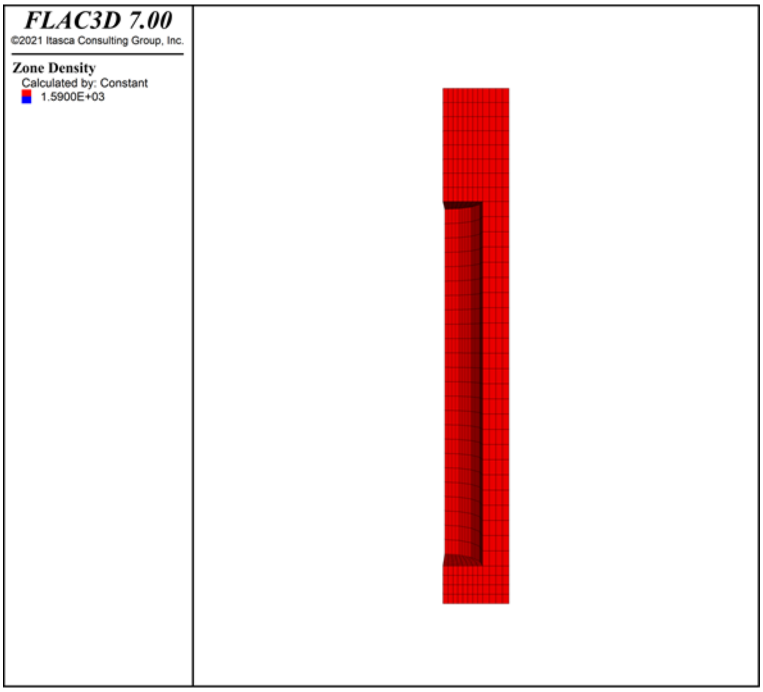

Figure 9-38: Initial dry density distribution.

Note: the unit of dry density is kg/m^3.

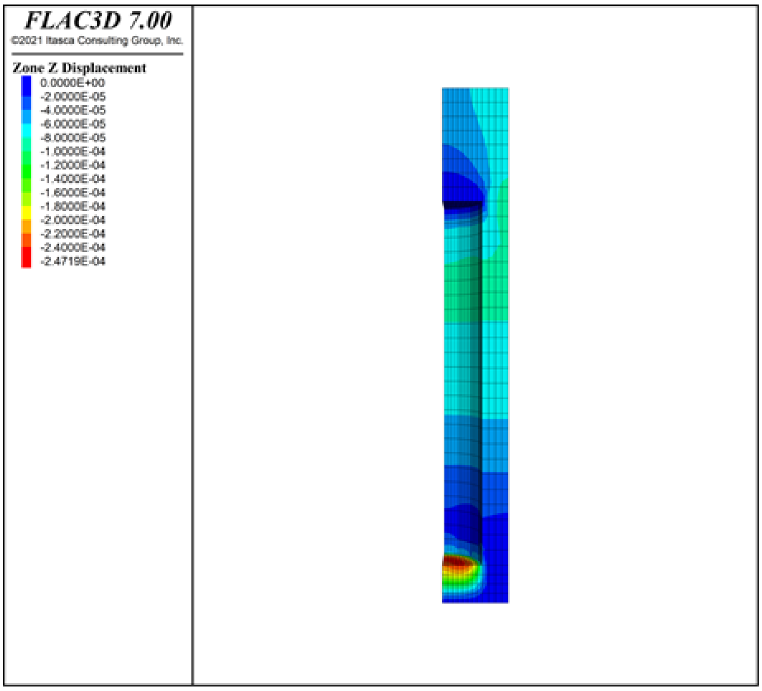

Figure 9-39: Distribution of vertical displacement after canister sinking.

Note: the unit of dry displacement is meter.

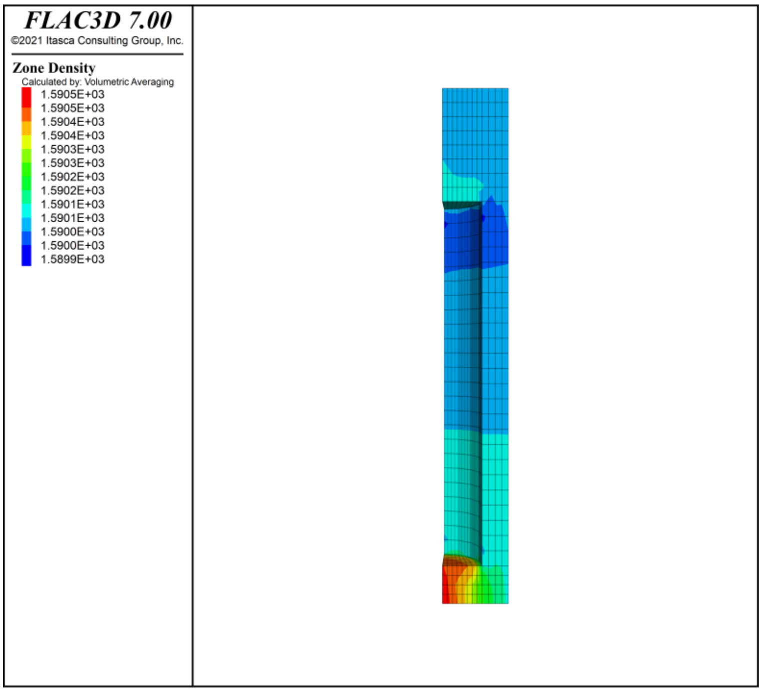

Figure 9-40: Distribution of dry density after canister sinking.

Note: the unit of dry density is kg/m^3

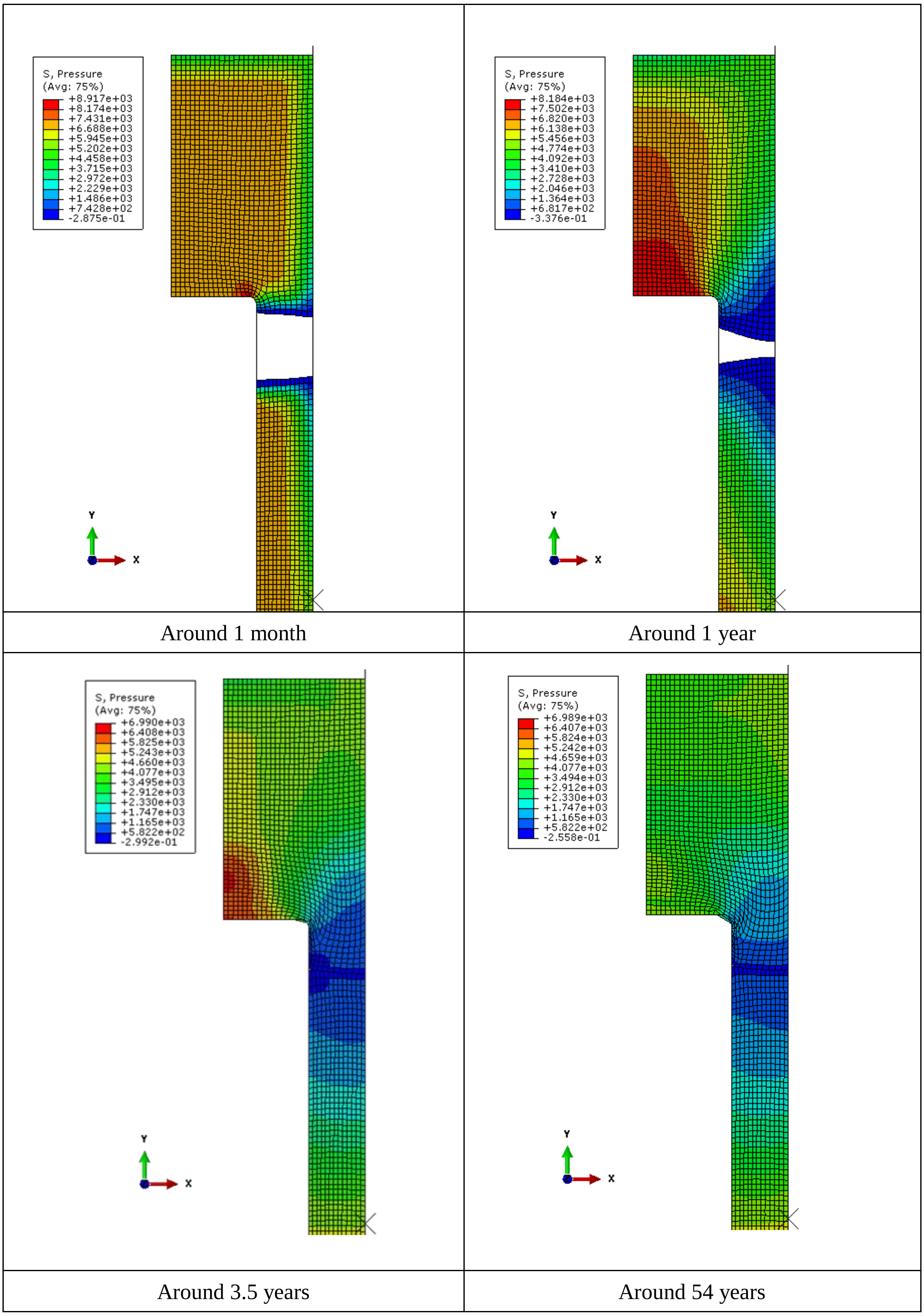

Figure 9-41: Redistribution of bentonite at different times after loss of 1,200 kg bentonite.

Note: the unit of pressure is Pa.

9.3.10. Chemical Evolution of Buffer and Backfill

The buffer will evolve after the repository is closed due to changes in decay heat, hydraulic gradient generated when saturation occurs, and hydrostatic pressure of the surrounding rock. When the near-field is saturated, and the ambient temperature is cooled down, the interaction between groundwater and bentonite can force the solute in porewater to change or force the accessory minerals and cations to redistribute.

The bentonite porewater will evolve along with the mixing process with groundwater during saturation. When the buffer and the backfill are saturated, solute in the porewater will transmit mainly through diffusion. Accessory minerals in the bentonite will dissolve or precipitate because of the groundwater. This might lead to cementation of the bentonite, alteration of the composition of the montmorillonite, or alteration of cations in the porewater, which will change the swelling properties of the bentonite. Besides, carbonate and sulfate generated from the interaction between the minerals in the bentonite and the groundwater might precipitate in between the surface of buffer and canisters, forming a porous area. When the repository is saturated and cooled down, the precipitates will dissolve again under certain temperature conditions. These materials will diffuse through the buffer in ionic form. In addition to all these, the carbonate and pyrite in the bentonite might also affect pH value, oxidation-redox potential, and alkalinity in the near-field.

The bentonite of the buffer and the backfill includes about 85% of montmorillonite, and other minerals, including quartz (~3%), feldspars (~3%), gypsum (~0.7%), calcite (~0.1%), etc. (Karnland et al., 2006). During saturation, calcium sulfates and amorphous SiO_2 will dissolve and precipitate. But the impact will be small, so the swelling properties of the buffer will not be altered and the canisters will not be corroded because of that (SKB, 2011). Moreover, the pyrite in the bentonite might generate a corroding agent, which may induce corrosion of the canisters. However, MX-80 bentonite contains very little pyrite (about 0.07%) and the buffer also contains very little oxygen; the impact from pyrite in the bentonite should be limited (please refer to Section 9.3.13 for more discussion).

9.3.11. Colloid Release

When groundwater enters the deposition holes, the buffer will absorb water and expand. The expansion will be limited by the size of the deposition hole. If there is a fracture intersecting the deposition hole, the buffer can expand freely into the fracture and be carried away by groundwater. This will lead to loss of the buffer, and interfere with safety functions Buff1, Buff2, and Buff5.

The maximum expansion capacity of the bentonite will be affected by ionic value and concentration in the montmorillonite layers of the bentonite. If the solute concentration in groundwater is low, the distance between the montmorillonite layers will increase, and the bentonite will act like “sol” which results in individual colloidal particles formed by a single montmorillonite layer or a small group of montmorillonite layer. These colloidal particles will be carried away by groundwater easily; therefore, the bentonite is more likely to be lost when the ionic strength in groundwater is low.

The reasons why the buffer will be lost are buffer expanding into fractures, buffer eroded by seeping water, and sedimentation (SKB, 2016). The stability of montmorillonite particles in bentonite is related to critical coagulation concentration (CCC). When the ionic strength in groundwater is greater than 8 mM, the colloid release of the bentonite can be avoided (Hedström et al., 2015); therefore, if the ionic strength in groundwater is greater than CCC when the bentonite squeezes into fractures because of the swelling pressure, montmorillonite particles or colloid will not be released, the bentonite will only be lost because of expansion. On the contrary, if the ionic strength in groundwater is lower than CCC when the bentonite squeezes into fractures, erosion by seeping water and sedimentation will contribute to the loss of the bentonite.

Based on the description above, the loss of the bentonite can be estimated by the following methods (SKB, 2016):

(1) Buffer expanding into fractures:

Mass loss of bentonite caused by expansion can be expressed as a function of fracture aperture and time:

$$M(t) = \delta(93.74t - 0.0004521t^2 + 2.236 \times 10^{-9}t^3) \qquad (9\text{- }4)$$

where,

M(t) = accumulated mass loss, [kg].

δ = fracture aperture, [m].

t = time, [s].

(2) Buffer eroded by seeping water:

Bentonite loss rate due to erosion by seeping water can be expressed as a function of water velocity, fracture aperture, ion strength, and distance to the rim of the buffer, which can be calculated by the following equation:

$$N_{erosion} = \rho_s \delta \emptyset_R 4\sqrt{D_R(C_{ion})\pi r_R u_0} \qquad (9\text{- }5)$$

where,

ρ_S = density of smectite, [kg/m^3].

$N_{erosion}$ = erosion rate, [kg/s].

δ = fracture aperture, [m].

u_0 = water velocity, [m/s].

$\emptyset_R$ = smectite volume fraction at the rim of the buffer, [-].

r_R = distance to the rim of the buffer, [m].

Interaction between buffer expanding into fractures and buffer eroded by seeping water should be taken into account when evaluating the distance to the rim of the buffer (r_R). A pseudo-steady-state (PSS) assumption was applied in the evaluation (SKB, 2016):

$$r_{RSS} = r_i \left(\frac{G/2}{ProductLog\left(\frac{G}{2}\right)} \right)^2 \quad (9\text{- }6)$$

$$\mathrm{G} = \frac{D_i \pi (\emptyset_i - \emptyset_R)}{2\emptyset_R \sqrt{D_R(C_{ion}) r_i u_0}} \quad (9\text{- }7)$$

where,

ProductLog(z) = Lambert W function.

r_i = radius of the deposition hole, [m].

D_i = smectite diffusion coefficient in the deposition hole, [m^2/s].

$\emptyset_i$ = smectite volume fraction in the deposition hole, [-].

$\emptyset_R$ = smectite volume fraction at the rim, [-].

u_0 = water velocity, [m/s].

Also, $D_R(C_{ion})$ indicates the smectite diffusion coefficient at the rim:

$$D_R(C_{ion}) = 10^{-9.42911 - 1.5309x - 1.88737x^2 - 0.783596x^3} \quad (9\text{- }8)$$

where,

C_{ion}= ion concentration, [mM].

x = $\log_{10}(C_{ion})$, [mM].

(3) Sedimentation:

Bentonite loss rate due to sedimentation ($N_{Sedimentation}$) can be obtained by calculating the experimental value (N_{Exp}, kg/s) and the theoretical value (N_{Sed}, kg/yr) of maximum bentonite loss rate:

$$N_{Sedimentation} = \min(N_{Exp}, N_{Sed}) \quad (9\text{- }9)$$

$$N_{Sed} = \frac{\delta^3}{12\mu_{agg}} (\rho_{agg} - \rho_W) g \emptyset_R \rho_S 2 r_{RSS} \quad (9\text{- }10)$$

$$N_{Exp} = J_{Exp}\delta 2\pi r_{RSS} sin(\alpha) \tag{9- 11}$$

$$r_{RSS} = \frac{F_{Exp}}{ProductLog\left(\frac{F_{Exp}}{r_i}\right)} \tag{9- 12}$$

$$F_{Exp} = \frac{D_i \rho_s (\emptyset_i - \emptyset_R)}{J_{Exp} sin(\alpha)} t_y \tag{9- 13}$$

where,

N_{Sed}= maximum sedimentation theoretical value, [kg/yr].

N_{Exp}= maximum sedimentation experimental value, [kg/s]

r_{RSS}= distance to the rim at steady state, [m].

δ = fracture aperture, [m].

J_{Exp} = flux of released sediments, [kg/m^2/yr].

α = angle between the fracture and the horizontal plane, [rad].

t_y = time coefficient, [s/yr].

μ_{agg} = viscosity of the agglomerate fluid, [Pa-s].

ρ_{agg} = density of the agglomerate fluid, [kg/m^3].

ρ_W = density of the water, [kg/m^3].

ρ_S = density of the smectite, [kg/m^3].

g = acceleration of gravity, [m/s^2].

The overall bentonite loss rate can be obtained by summing the calculation results of (1), (2), and (3). Accumulated mass loss curve can also be obtained by calculating bentonite loss rate over different time periods according to their hydrogeological evolution. Based on the velocity of seeping water in Section 9.3.5 and the ionic strength of groundwater in Section 9.3.6 (Table 9-4), assuming angle α is 45°, bentonite loss of the five deposition holes (DH-216, DH-812, DH-2110, DH-2632, and DH-2633) was evaluated.

From the evaluation results in Table 9-5, the loss of bentonite would be less than 1,200 kg; therefore, the safety functions of the buffer will not be interfered with. Note that the results were calculated based on current hydrogeological conceptual model of the reference case, not all aspects of the hydrogeological units and DFN model were taken into account in the assessment. All of the calculations should be revised while the hydrogeological conceptual model of the reference case changes.

Table 9-4: Relevant parameters in the evaluation of mass loss of the bentonite.

Deposition hole No.	**Seeping water velocity (m/sec)**	**Ionic strength (mM)**	**Fracture aperture (m)**
DH-216	3.55×10^{-7}	2.34	7.18×10^{-6}
DH-812	2.80×10^{-7}	2.51	1.16×10^{-5}
DH-2110	2.64×10^{-7}	2.23	1.21×10^{-5}
DH-2632	1.36×10^{-7}	2.51	2.09×10^{-5}
DH-2633	1.32×10^{-7}	2.51	2.25×10^{-5}

Table 9-5: Mass loss of bentonite during the initial period after closure.

Deposition hole No.	**DH-216**	**DH-812**	**DH-2110**	**DH-2632**	**DH-2633**
Mass loss(kg)	14.23	52.99	55.08	94.9	102.19

9.3.12. Evolution of the Plug

In the initial period after closure (post-closure 1,000 years), the main concern of the evolution of the plug will be its impact on safety function BF1. The concrete in the plug may deteriorate over time and produce alkaline fluid. The reaction transmission between the alkaline fluid and the backfill was evaluated (SKB, 2011), and the distribution of porewater, porosity, and pH values of the plug and the backfill at post-closure 1 year and 100 years are shown in Figure 9-42 and Figure 9-43. The results show that deterioration of the concrete might produce alkaline fluid (pH > 11) that will infiltrate into the backfill. However, the pH value will get back to neutral in about 10 years, hence the impact time will be relatively short, and the impact can be seen as negligible.

In addition, cement and other substances in the concrete may dissolve and lose over time, which may greatly reduce the structural strength and rigidity. The plug might be squeezed and deformed when it cannot sustain the swelling pressure of the backfill, and further reduces the density and swelling pressure of the backfill. Density loss of the backfill will be more obvious near the plug and decreases over distance because of friction of the rock surface. According to the analysis results, when the distance from the plug increases, it decreases, as shown in Figure 9-44. And according to the analysis results, the backfill closest to the plug only produces an axial displacement of 7 cm, and the displacement decreases with distance. There is no significant impact found on the backfill of the first deposition hole by disintegration and deformation of the plug.

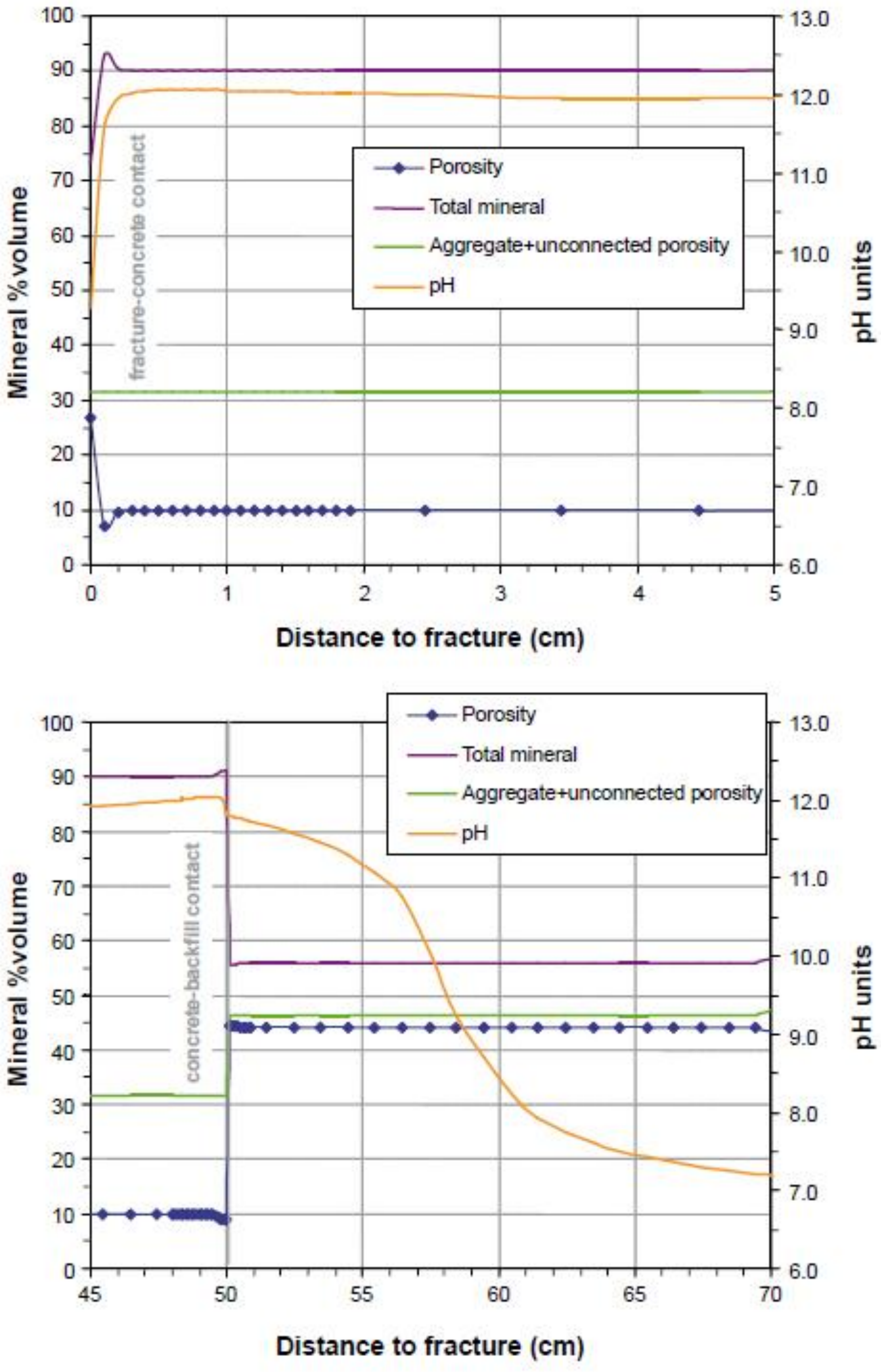

Figure 9-42: Distribution of pore water, porosity, and pH value of the plug and backfill after 1 year of closure.

Reference: SKB (2011).

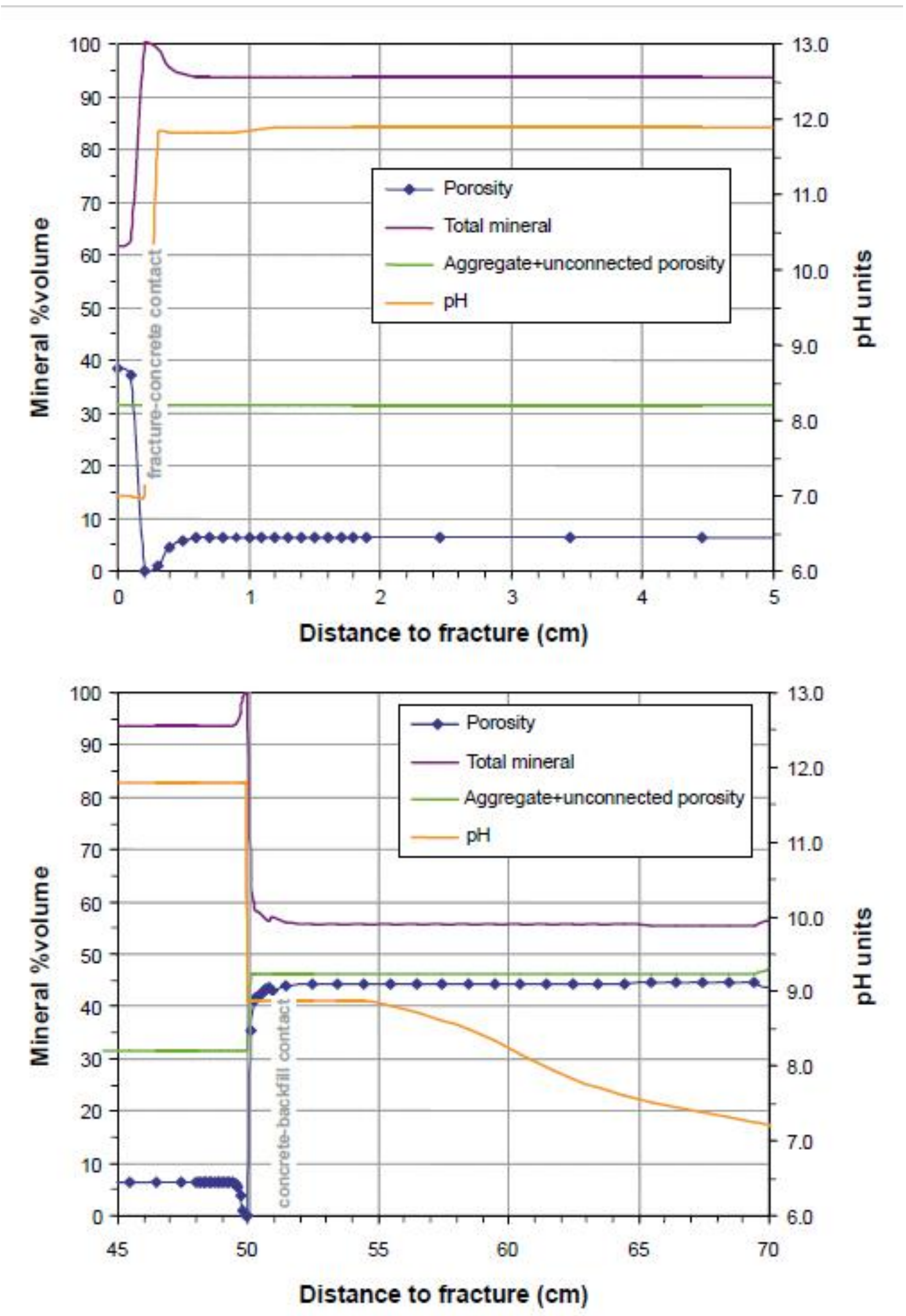

Figure 9-43: Distribution of pore water, porosity, and pH value of the plug and backfill after 100 years of closure.

Reference: SKB (2011).

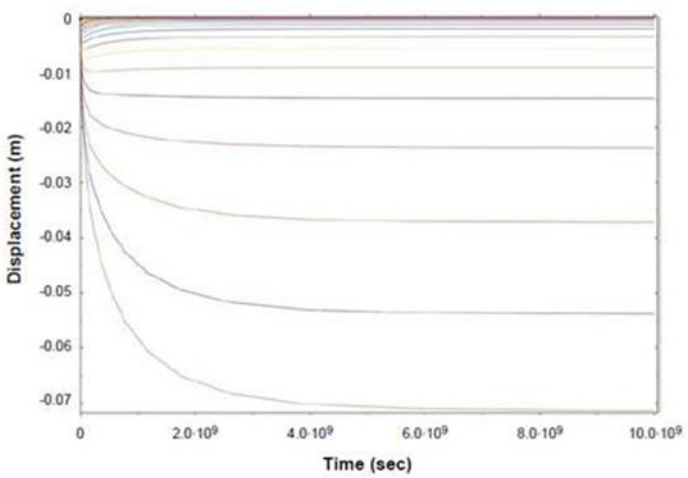

Figure 9-44: Relationship between axial displacement of the backfill behind the plug and time

Reference: SKB (2011).

Note: the curves from bottom to top are 10 cm, 20 cm, 30 cm from the plug, and so on.

9.3.13. Evolution of the Canister

Two main safety functions of the canisters: Can1 and Can2 are there to prevent the copper shell from being penetrated and to maintain the integrity of the canisters. During the initial period after closure (post-closure 1,000 years), the canister evolution that might affect these safety functions are: (1) thermal evolution, (2) mechanical influence due to buffer expansion, and (3) copper shell corrosion. The evolution is described as follows:

(1) Thermal evolution:

According to Section 9.3.4, the temperature of the buffer will not exceed 100 ℃ during the initial period after closure (post-closure 1,000 years). During saturation of the buffer, the maximum temperature on the surface of the canisters and at half-height of the canisters will be about 2 ℃ higher than the maximum temperature of the buffer (that is the maximum temperature will be lower than 102 ℃) (SKB, 2009c). After the buffer is fully saturated, the buffer will be closely contacted with the canisters, and the temperature on the surface of the canisters and at half-height of the canisters will be even lower (about 20 ℃ lower than the temperature during saturation). Under conservative assumptions, the maximum temperature on the outer surface of the copper shell and on the cast iron lining will not exceed 117 ℃. This indicates that the maximum temperature of the cast iron lining will be lower than the design requirement of 125 ℃, and the integrity of the canisters will not be compromised.

(2) Mechanical influence due to buffer expansion:

After the canisters and buffer are placed in the deposition holes, groundwater will enter the deposition holes through water-conducting fractures or through diffusion. The groundwater will be absorbed by the buffer which leads to buffer expansion subsequently that causes external load on the canisters. Since cast iron lining and square pipes of the canisters will be responsible for withstanding external force, the mechanical influence due to buffer expansion was evaluated according to the mechanical damage criterion which was defined by the material properties of the cast iron lining. According to Table 4-4, the yielding tensile stress of the cast iron lining is 267 MPa. When maximum tensile stress is lower than 267 MPa, the cast iron lining is still an elastic material and will not be affected by uneven confining pressure.

From the analysis results of buffer and backfill saturation in Section 9.3.8, after the repository is closed, groundwater will flow in gradually, buffer and backfill saturation will also increase, and finally reach full saturation. Therefore, the influence from the swelling pressure of the buffer on the canister when the buffer and backfill are unsaturated and saturated has been examined.

(a) In the unsaturated period:

When the buffer is saturating, it might encounter the following situations: (i) non-uniform swelling pressure distribution of the buffer due to uneven water absorption when groundwater flows into the deposition holes; (ii) non-uniform swelling pressure distribution of the buffer due to non-uniform buffer density distribution caused by depressions or protrusions from collapse or peeling of the rock surface; (iii) non-uniform swelling pressure distribution of the buffer due to other environmental impacts. The non-uniform swelling pressure distribution of the buffer may have a mechanical impact, such as shear force and bending moment on the canisters, thereby affecting the safety function Can2.

In the evaluation, groundwater was assumed to infiltrate the deposition hole according to Figure 9-45. The groundwater infiltrated into the deposition hole through fracture and diffused outwards, resulting in higher saturation and higher swelling pressure near the fracture. The swelling pressure generated by infiltration of the groundwater is shown in Figure 9-45 (the blue arcs). They distribute triangularly, and the pressure decreases with the distance to the fracture increases. The stress distribution of cast iron lining and copper shell of the following two cases were evaluated based on the following assumptions. One of them was that the deposition hole was cylindrical and was subjected to a 6.59 MPa non-uniform isostatic load due to uneven saturation. The other one was that the deposition hole was banana-shape (as shown in Figure 9-46, δ_1=8 mm and δ_2=0 mm) due to over-excavation or collapse of rocks during excavation. The canister was subjected to a 7.82 MPa stress additionally (SKB, 2010b).

The stress distribution of cast iron lining and copper shell analyzed by ABAQUS are shown in Figure 9-47, Figure 9-48, and Table 9-6. The results show that, when the deposition hole was cylindrical, the maximum tensile stress of the cast iron lining caused by the non-uniformly distributed swelling pressure would be 92.04 MPa. When the deposition hole was banana-shaped, the maximum tensile stress of the cast iron lining caused by the non-uniformly distributed swelling pressure would be 112.4 MPa. The damage criterion would not be exceeded.

(b) In the saturated period:

When the canister was assumed to be non-uniformly affected by swelling pressure, as stated in Figure 9-45, the following cases were evaluated for the stress distribution of cast iron lining and copper shell. (i) the deposition hole was cylindrical (δ_1= 0 mm and the stress was 7.50 MPa, δ_2= 0 mm and the stress was 5.83 MPa as shown in Figure 9-46), and the canister was subjected to non-uniform isostatic load due to uneven saturation; (ii) the deposition hole was banana-shape due to over-excavation or collapse of rocks during excavation (δ_1= 8 mm and the stress was 6.86 MPa, δ_2= 0 mm and the stress was 4.12 MPa as shown in Figure 9-46), and the canister was subjected to non-uniform isostatic load due to uneven saturation; (iii) the deposition hole was banana-shape due to over-excavation or collapse of rocks and even collapse of the inner wall of the deposition hole during excavation (δ_1= 8 mm and the stress was 7.82 MPa, δ_2= 33 mm and the stress was 3.73 MPa as shown in Figure 9-46), and the canister was subjected to non-uniform isostatic load due to uneven saturation (SKB, 2009d).

The stress distribution of cast iron lining and copper shell are shown in Figure 9-49 to Figure 9-51 and Table 9-7. From the results, it can be seen that when the deposition hole was cylindrical, the maximum tensile stress of the cast iron lining caused by uneven saturation would be 43.52 MPa; when the deposition hole was banana-shaped, the maximum tensile stress of the cast iron lining caused by uneven saturation would be 69.86 MPa (δ_1= 8 mm and δ_2= 0 mm) and 106.7 MPa (δ_1= 8 mm and δ_2= 33 mm). The damage criterion would not be exceeded.

(3) Copper shell corrosion:

A geological environment with fresh water condition of the reference case was selected for assessment of copper shell corrosion. All of the corrosion processes were covered in the assessment. Through qualitative evaluation and screening, the general corrosion process is considered the most important one for canister copper shell corrosion (Hung et al., 2017).

Corrosion of the copper shell will have different influence factors in different evolution time periods. The evolution periods of copper shell corrosion could be further subdivided into: (a) aerobic environment in excavation and operation period, (b) aerobic environment in the initial period after closure and (c) anaerobic environment in the initial period after closure, to ensure that the requirements of safety function Can1 can be maintained throughout the period.

(a) Aerobic environment in excavation and operation period:

After SNF is placed and encapsulated in the canisters, the canisters will be disposed in the deposition holes according to the planned schedule. There will be a period of time that the canisters are exposed to the atmosphere before the disposal tunnel is closed. This might lead to corrosion of the copper shell. Since the reaction time is limited, it belongs to a limited corrosion source. It was conservatively assumed that the canisters would be exposed to the atmosphere for 3 years before the disposal tunnel is closed. And according to the empirical function of the atmospheric corrosion rate, a maximum corrosion depth of 0.0015 mm of the copper shell is expected in this period of time. The main corrosion product will be copper oxide.

(b) Aerobic environment in the initial period after closure :

When the disposal tunnel is closed, the repository will be in an aerobic environment initially. The primary corrosive agent will be oxygen, and its main origin will be the air in the pores of the buffer and backfill. Since the amount of trapped oxygen is limited, it belongs to a limited corrosion source. The amount of oxygen can be deduced by calculating the pore volume of backfill and buffer. Assuming that the oxygen in the backfill and buffer will diffuse to the surface of the canister and corrode the copper shell subsequently, based on the principle of mass balance, the maximum corrosion depth would be 0.1034 mm.

In addition to corrosion caused by oxygen, corrosive agents can also be generated by radiation reactions caused by radioisotopes in the SNF. When the disposal tunnel is closed and the bentonite is not yet saturated, humid air might exist between the buffer and the canister. The humid air might generate nitric acid under gamma ray (mainly from Cs-137 in the SNF) exposure. The nitric acid will dissolve in pore water and induce corrosion of the copper shell subsequently. In the repository, nitrogen-oxygen-water can be regarded as in the same system, the amount of nitric acid will thereby be proportional to the amount of radiation absorbed by the humid air. Assuming that the corrosion induced by nitric acid will be uniformly distributed on the surface of the canisters, based on the principle of mass balance, the maximum corrosion depth is estimated to be 1.3×10^{-6} mm.

After the disposal tunnel is closed and the bentonite is fully saturated, groundwater around the canisters will generate hydrogen and oxidant under the irradiation of gamma-rays (mainly from Cs-137 in the SNF) and induce corrosion of the canisters subsequently. Assuming that the corrosion will be uniformly distributed, based on the principle of mass balance, the maximum corrosion depth (which is estimated to be 0.011 mm) can be deduced from the volume of pore water.

The radioactivity of Cs-137 (half-lives are both about 30 years) which causes the radiolysis of air and water mentioned above, is expected to drop below one-thousandth of the initial radioactivity post-closure 300 years. The gamma dose rate will greatly reduce, and the degree of corrosion caused by products of radiolysis will greatly reduce as well. Since the reaction time is limited, it belongs to a limited corrosion source. The maximum corrosion depth will be in the degree of nanometer. As a result, the corrosion caused by radiolysis products should be able to be negligible after 300 years of closure.

(c) Anaerobic environment after closure:

After the oxygen in the pores of the buffer and backfill is consumed, the repository will enter an oxygen-free environment. Meanwhile, the bentonite is fully saturated. The primary corrosive agent in the repository will be sulfide, and the main corrosion products will be copper sulfide and hydrogen.

Possible sources of sulfide include: (i) pyrite in the buffer and the backfill, (ii) reduction reaction of sulfate-reducing bacteria (SRB), and (iii) the existing sulfide in groundwater. The corrosion of these sources is described below:

(i) Pyrite in the buffer and the backfill:

After the buffer and the backfill are fully saturated, the pyrite in them might dissolve and release sulfide ions. Corrosion of the canisters might occur if the sulfide ions diffuse to the surface of the canisters. Since the amount of pyrite is limited, it belongs to a limited corrosion source. The maximum corrosion depth can be deduced from the amount of pyrite, solubility of pyrite, and diffusion coefficient of sulfur in the buffer based on the principle of mass balance. The maximum corrosion depth caused by pyrite in the buffer and the backfill is expected to be 0.115 mm.

(ii) Reduction reaction of sulfate-reducing bacteria:

SRB exists in the repository and can reduce sulfate in the buffer, the backfill, or groundwater into sulfide ions. Corrosion of the canister might be induced subsequently by the sulfide ions dissolved in the water. Most sulfate will adhere to the bentonite tightly, so when the buffer is fully saturated, only a small amount of sulfate will dissolve in groundwater. Since the amount of sulfate in the compacted bentonite is limited, it belongs to a limited corrosion source.

When the bentonite is fully saturated (saturated density 2,000 kg/m^3), the formation rate of copper sulfide can be estimated through test results in the reference (Masurat et al., 2010). The estimated formation rate of copper sulfide would be 3.4×10^{-14} $mol/mm^2/day$, and the corresponding maximum corrosion depth would be 0.177 mm.

(iii) The existing sulfide in groundwater:

The existing sulfide in groundwater is also one of the possible factors that cause the corrosion of canisters. The concentration of sulfide in groundwater will be affected by the groundwater flow field, underground facility layout, and erosion of the buffer and the backfill. Based on the conceptual model of buffer transmission and the principle of mass balance, and assuming that the corrosion on the copper shell will react quickly, completely, and irreversibly, the corrosion rate of the copper shell in different evolution periods was evaluated according to groundwater composition, the erosion rate of the buffer, and diffusion or advection transmission speed of sulfide ions. The evaluation concept is as follows (Neretnieks et al., 2010):

$$v_{corr} = Q_{eq} \cdot [HS^-] \frac{f_{HS}\ M_{Cu}}{\rho_{Cu}\ A_{corr}} \qquad (9\text{- }14)$$

where,

v_{corr} = corrosion rate, [m/yr].

Q_{eq} = equivalent flow rate, [m^3/yr].

$[HS^-]$ = sulfide concentration, [M].

f_{HS} = sulfide stoichiometry, [-].

M_{Cu} = molar mass of copper, [g/mol].

ρ_{Cu} = density of copper, [kg/m^3].

A_{corr} = corrosion area, [m^2].

According to the calculation of the equivalent flow rate (Q_{eq}), the impact on corrosion of the copper shell from an increase of groundwater flow rate after buffer erosion was taken into account. The groundwater flow rate (q_{eb}) after the buffer is eroded is:

$$q_{eb} = f_{conc} U_0 2 r_h h_{can} \tag{9- 15}$$

where,

q_{eb} = groundwater flow rate after the buffer is eroded, [m^3/yr].

f_{conc} = concentration coefficient of water flow for buffer erosion, [−].

U_0 = equivalent initial flux, [m/yr].

r_h = radius of the deposition hole, [m].

h_{can} = height of the canister, [m].

If the concentration is reduced due to diffusion, the flow rate can be expressed as:

$$q_{lim} = 1.13^2 \frac{V_{zone} D_w}{d_{buffer}^2} \tag{9- 16}$$

where,

q_{lim} = equivalent flow rate, [m^3/yr].

V_{zone} = erosion volume of the buffer, [m^3].

D_w = diffusion coefficient of water, [m^2/yr].

d_{buffer}^2 = thickness of the buffer, [m].

The equivalent flow rate is determined through the following equations:

$$\text{when } q_{eb} \leq q_{lim}, Q_{eq} = q_{eb} \tag{9- 17}$$

$$\text{when } q_{eb} > q_{lim},$$

$$Q_{eq} = \sqrt{q_{lim}}\sqrt{q_{eb}} = 1.13 \frac{\sqrt{q_{eb} D_w V_{zone}}}{d_{buffer}} \tag{9- 18}$$

where,

q_{eb} = groundwater flow rate after the buffer is corroded, $[m^3/yr]$.

q_{lim} = equivalent flow rate, $[m^3/yr]$.

Q_{eq} = equivalent flow rate, $[m^3/yr]$.

V_{zone} = erosion volume of the buffer, $[m^3]$.

D_w = diffusion coefficient of water, $[m^2/yr]$.

d_{buffer} = thickness of the buffer, [m].

When the groundwater flow rate (q_{eb}) of the eroded buffer is small, the equivalent flow rate will be the flow rate of the eroded buffer; but when the groundwater flow rate (q_{eb}) of the eroded buffer is large, the equivalent flow rate will be a function ($\sqrt{q_{eb}}$) of the square root of the groundwater flow rate after the buffer is eroded.

The corrosion rate for all of the deposition holes (i.e., 2,860) was calculated, and then five deposition holes with the top five corrosion depths (DH-216, DH-812, DH-2110, DH-2632, and DH-2633) were selected for the following safety assessment. The hydrogeological input parameters in different periods are shown in Table 9-8, Table 9-9 and Table 9-10. The concentration of sulfide and iron in the groundwater (Section 9.3.7 and Section 9.4.7) and erosion of the buffer (Section 9.3.9 and Section 9.4.8) were also used in the evaluation. When the erosion of buffer is less than 1,200 kg, substances are expected to be transported mainly by diffusion; and the corrosion rate of the copper shell is expected to be low. When the erosion of buffer is more than 1,200 kg, substances are expected to be transported mainly by advection; and the corrosion rate of the copper shell is expected to be high. Besides, different sea-levels could have different groundwater compositions, which will affect the erosion rate of the buffer and subsequently affect the corrosion rate of the copper shell.

Based on the aforementioned description, the corrosion rate of the copper shell in different evolution periods, including the present, about 16,700 years after closure (sea-level: -20 m), about 100,000 years after closure (sea-level: -120 m), about 112,000 years after closure (sea-level: -20 m), and about 120,000 years after closure (sea-level: 0 m) was evaluated.

The results of deposition hole DH-2110 are shown as follows:

(*) The corrosion rate will rise from 5.75×10^{-8} mm/yr to 2.45×10^{-7} mm/yr during 16,700 years.

(*) About 21,400 years after closure, substances transported in the buffer will become mainly through advection. The corrosion rate will rise from 2.45×10^{-7} mm/yr to 1.25×10^{-5} mm/yr during post-closure 16,700 years to post-closure 21,400 years.

(*) The corrosion rate will decrease from 1.25×10^{-5} mm/yr to 7.44×10^{-6} mm/yr during post-closure 21,400 years to post-closure 100,000 years.

(*) The corrosion rate will rise from 7.44×10^{-6} mm/yr to 1.25×10^{-5} mm/yr during post-closure 100,000 years to post-closure 112,000 years, and then decrease to 3.33×10^{-6} mm/yr during post-closure 112,000 years to post-closure 120,000 years.

The above-mentioned results are shown in Table 9-11 and Table 9-12. The relation between the corrosion depth of the copper shell and time is shown in Figure 9-52.

It can be seen from the results that if substances are mainly transported through advection, the corrosion depth will increase significantly. The evaluation results of deposition hole DH-2110 (which is expected to have the highest corrosion rate and deepest corrosion depth) show that the maximum corrosion depth would be 10.20 mm after the safety assessment timescale.

The interaction time of air radiation decomposition and water radiation decomposition will be about 300 years after the closure, and the interaction time of oxygen in the atmosphere will be 3 years before the closure. Corrosion by oxygen in the atmosphere can be regarded as a limited source of corrosion because the interaction time is limited. In addition, oxygen trapped in the repository during the initial period after closure is limited, sulfide generated is limited because the amount of pyrite is small, and sulfide generated by sulfate-reducing bacteria is also limited. Therefore, these are also regarded as limited sources of corrosion. On the other hand, the long-term corrosion source will be the corrodent in groundwater during the anaerobic period, which will reach the surface of the canister through diffusion or advection over time, resulting in long-term corrosion of the canister. In summary, the maximum corrosion depth of all the above corrosive agents is shown in Table 9-13 and Table 9-14. The results show that corrosion caused by corrosive agents in an aerobic environment, and pyrite, SRB, and other corrosive agents in an anaerobic environment have a maximum corrosion depth of approximately 0.408 mm in general corrosion.

In addition, local corrosion might occur in an aerobic environment (oxygen trapped in the repository after closure will be the primary corrosive agent). The additional corrosion depth caused by local corrosion is expected to be 4 times the depth of general corrosion (King and Litke, 1992; King et al., 2001). Therefore, the maximum corrosion depth caused by local corrosion is estimated to be about 0.4136 mm.

As mentioned in Section 4.2.3, the initial thickness of the copper shell will be 5 cm. The possible uncertainty during manufacturing, general corrosion and local corrosion caused by limited corrosion sources, and corrosion caused by the existing sulfide in groundwater were all taken into account, and the canisters are expected to remain about 36.8 mm thickness of copper shell 1 million years after the closure. Hence, the requirements of safety function Can 1 should be able to maintain, and the integrity of the canisters will not be jeopardized.

Table 9-6: Maximum tensile stress of the cast iron lining due to uneven swelling pressure when the buffer is not yet saturated.

		BWR type canister	PWR type canister
Maximum stress (MPa)	Normal condition(cylinder shape deposition hole)	92.04	89.48
	Banana-shape deposition hole (δ_1=8 mm, δ_2=0 mm)	112.4	108.7

Table 9-7: Maximum tensile stress of the cast iron lining due to uneven swelling pressure when the buffer is saturated.

		BWR type canister	PWR type canister
Maximum stress (MPa)	Normal condition (cylinder shape deposition hole)	43.52	42.28
	Banana-shape deposition hole (δ_1=8 mm, δ_2=0 mm)	69.86	67.84
	Banana-shape deposition hole (δ_1=8 mm, δ_2=33 mm)	106.70	103.10

Table 9-8: Hydrogeological input parameters of sea-level 0 m.

Name	Transmissivity [m^2/s]	U [m/year]	Velocity (DFN) [m/year]	F [year/m]	Qeq for corrosion [m^3/year]	HS- in buffer [M]
DH-2110	5.82×10^{-10}	1.23×10^{-5}	83.2	2.23×10^{7}	2.11×10^{-4}	6.38×10^{-4}
DH-812	5.41×10^{-10}	1.26×10^{-5}	88.3		2.16×10^{-4}	7.09×10^{-4}
DH-2632	1.75×10^{-9}	1.10×10^{-5}	42.9		1.89×10^{-4}	7.09×10^{-4}
DH-2633	2.03×10^{-9}	1.15×10^{-5}	41.6		1.97×10^{-4}	7.07×10^{-4}
DH-216	2.06×10^{-10}	9.83×10^{-6}	11.2	2.27×10^{7}	1.69×10^{-4}	6.65×10^{-4}

Table 9-9: Hydrogeological input parameters of sea-level -20 m.

Name	Transmissivity [m^2/s]	U [m/year]	Velocity (DFN) [m/year]	F [year/m]	Qeq for corrosion [m^3/year]	HS- in buffer [M]
DH-2110	5.82×10^{-10}	5.94×10^{-5}	40.2	2.13×10^{7}	1.02×10^{-3}	4.98×10^{-4}
DH-812	5.41×10^{-10}	5.58×10^{-5}	39.1	2.41×10^{7}	9.57×10^{-4}	4.98×10^{-4}
DH-2632	1.75×10^{-9}	4.61×10^{-5}	18.0	2.55×10^{7}	7.91×10^{-4}	4.98×10^{-4}
DH-2633	2.03×10^{-9}	4.60×10^{-5}	16.7		7.90×10^{-4}	4.98×10^{-4}
DH-216	2.06×10^{-10}	5.11×10^{-5}	58.2	2.71×10^{7}	8.78×10^{-4}	4.98×10^{-4}

Table 9-10: Hydrogeological input parameters of sea-level -120 m.

Name	Transmissivity [m^2/s]	U [m/year]	Velocity (DFN) [m/year]	F [year/m]	Qeq for corrosion [m^3/year]	HS- in buffer [M]
DH-2110	5.82×10^{-10}	3.52×10^{-5}	23.8	1.65×10^{7}	6.05×10^{-4}	4.98×10^{-4}
DH-812	5.41×10^{-10}	3.08×10^{-5}	21.6	1.07×10^{7}	5.29×10^{-4}	4.98×10^{-4}

DH-2632	1.75× 10^{-9}	3.46× 10^{-5}	13.5	7.00× 10^{6}	5.94× 10^{-4}	4.98× 10^{-4}
DH-2633	2.03× 10^{-9}	3.28× 10^{-5}	11.9	7.79× 10^{6}	5.62× 10^{-4}	4.98× 10^{-4}
DH-216	2.06× 10^{-10}	3.22× 10^{-5}	36.6	3.39× 10^{6}	5.53× 10^{-4}	4.98× 10^{-4}

Table 9-11: Corrosion rate of the copper canister due to the existing sulfides in groundwater (when the buffer is intact).

Deposition hole No.	**Corrosion rate (mm/yr)**		
-	0 m	-20 m	-120 m
DH-216	4.63× 10^{-8}	2.15× 10^{-7}	1.42× 10^{-7}
DH-812	5.89 × 10^{-8}	2.32× 10^{-7}	1.37× 10^{-7}
DH-2110	5.75 × 10^{-8}	2.45× 10^{-7}	1.55× 10^{-7}
DH-2632	5.16 × 10^{-8}	1.96× 10^{-7}	1.52× 10^{-7}
DH-2633	5.39× 10^{-8}	1.96× 10^{-7}	1.45× 10^{-7}

Table 9-12: Corrosion rate of the copper canister due to the existing sulfides in groundwater (when substances transport through advection in the buffer).

Deposition hole No.	**Corrosion rate (mm/yr)**		
-	0 m	-20 m	-120 m
DH-216	2.77× 10^{-6}	1.08× 10^{-5}	6.80× 10^{-6}
DH-812	3.79× 10^{-6}	1.18× 10^{-5}	6.51× 10^{-6}
DH-2110	3.33× 10^{-6}	1.25× 10^{-5}	7.44× 10^{-6}
DH-2632	3.31× 10^{-6}	9.72× 10^{-6}	7.31× 10^{-6}
DH-2633	3.45× 10^{-6}	9.71× 10^{-6}	6.91× 10^{-6}

Table 9-13: Maximum corrosion depth of the copper canister in the initial aerobic environment after closure.

	Operating period	**After closure**			
			Bentonite is unsaturated	**Bentonite is saturated(closure for 300 years)**	**Bentonite is saturated(closure after 300 years)**
Main corrosive	Oxygen in the atmosphere	Oxygen in the pores	Nitric acid produced by air radiation decomposition	Oxidant produced by radiation decomposition of pore water	Oxidant produced by radiation decomposition of pore water
Maximum corrosion depth	0.0015 mm	0.1034 mm	1.3 × 10^{-6}mm	0.011 mm	Nanoscale (Ignorable)

Table 9-14: Maximum corrosion depth of the copper canister in the anaerobic environment after closure.

Source of sulfide	**Pyrite in buffer and backfill**	**Reduction reaction of sulfate-reducing bacteria**	**Existing sulfides in groundwater**

Maximum corrosion depth	0.115 mm	0.177 mm	About 10.20 mm (1 million years after the closure).

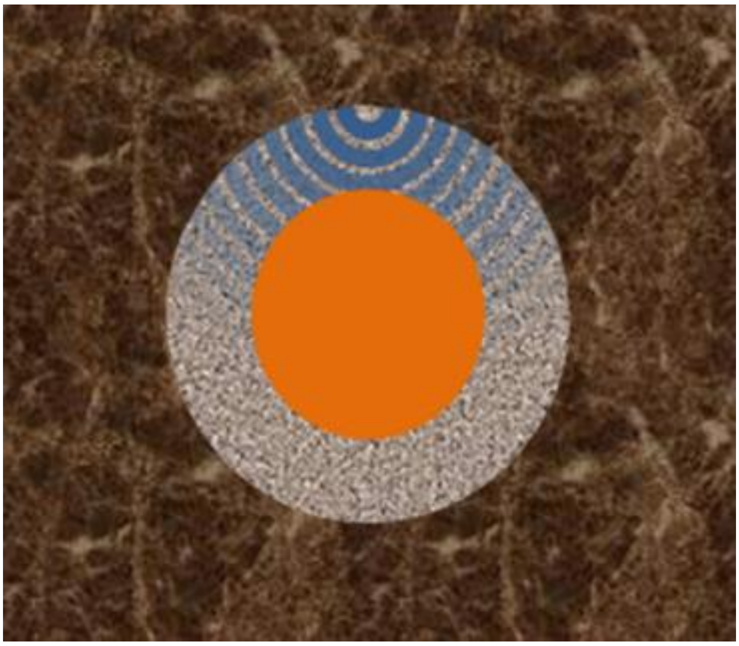

Figure 9-45: Groundwater infiltrates into the deposition hole through water-conducting fracture.

Reference: SKB (2009d).
Note: the blue indicates GW infiltration, the orange indicates the canister, the grey indicates the buffer, and the brown indicates the host rock.

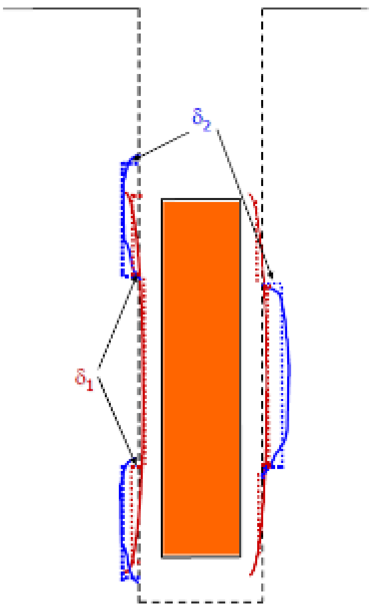

Figure 9-46: Banana shape deposition hole due to over-excavation or collapse of rock.
Reference: SKB (2010b).

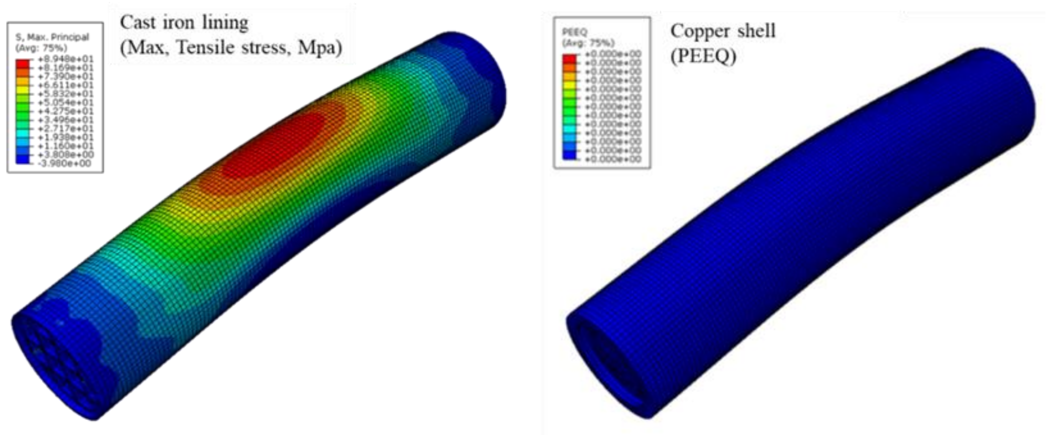

Figure 9-47: Stress distribution of cast iron lining and copper shell due to uneven swelling pressure when the buffer is not saturated (cylindrical deposition hole, δ_1=0 mm, δ_2=0 mm).

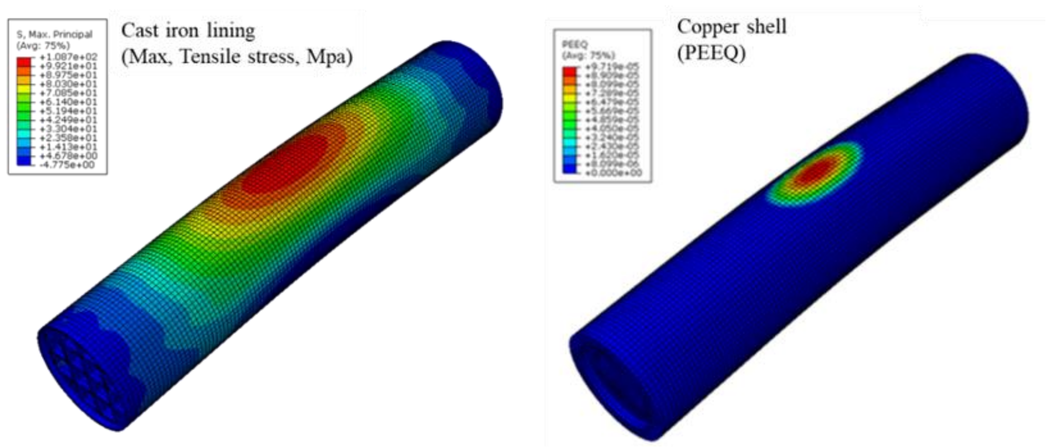

Figure 9-48: Stress distribution of cast iron lining and copper shell due to uneven swelling pressure when the buffer is not saturated (banana shape deposition hole, δ_1=8 mm, δ_2=0 mm).

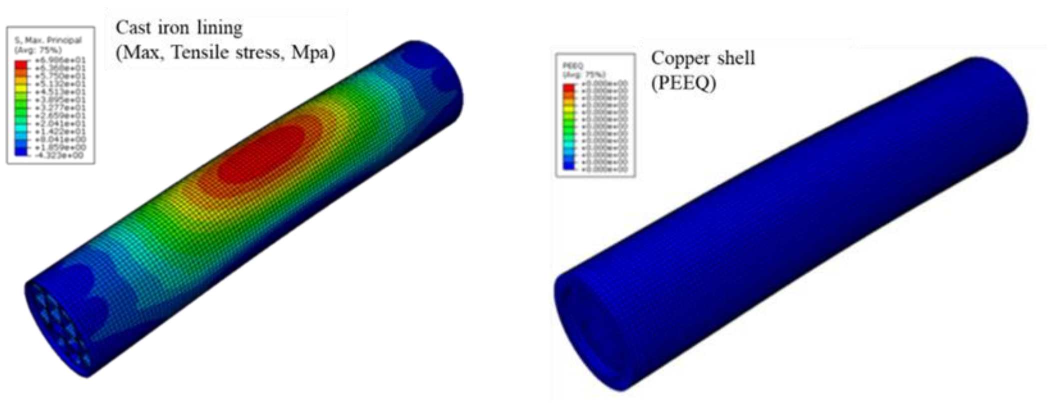

Figure 9-49: Stress distribution of cast iron lining and copper shell due to uneven swelling pressure when the buffer is saturated (cylindrical deposition hole, δ_1=0 mm, δ_2=0 mm).

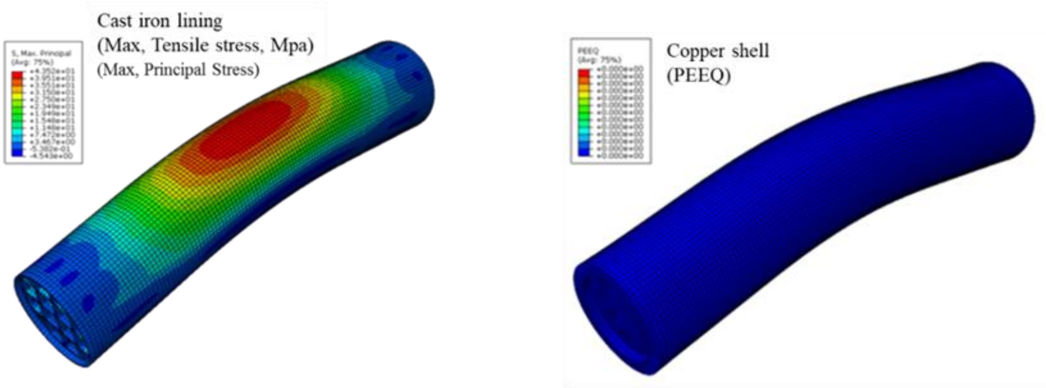

Figure 9-50: Stress distribution of cast iron lining and copper shell due to uneven swelling pressure when the buffer is saturated (banana shape deposition hole, δ_1=8 mm, δ_2=0 mm).

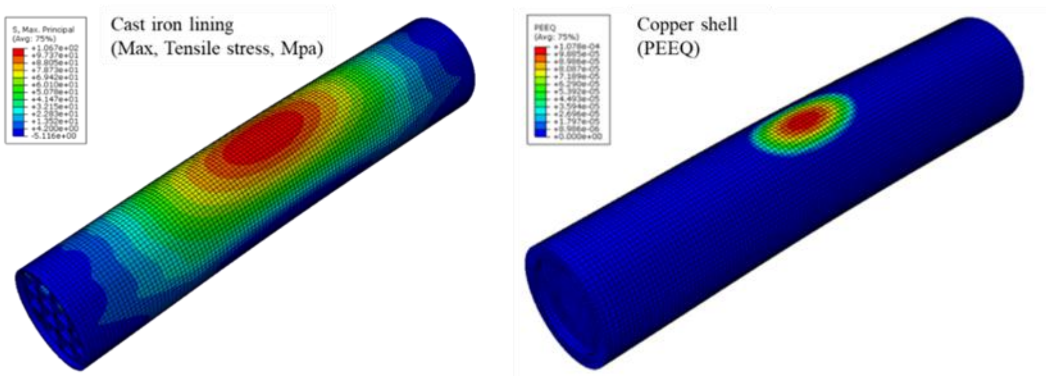

Figure 9-51: Stress distribution of cast iron lining and copper shell due to uneven swelling pressure when the buffer is saturated (banana shape deposition hole, δ_1=8 mm, δ_2=33 mm).

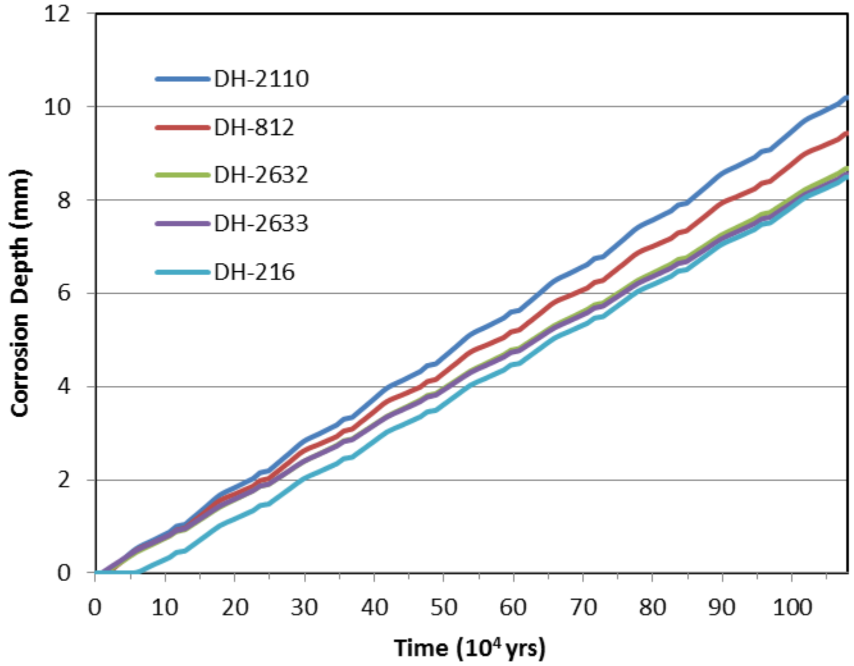

Figure 9-52: Corrosion depth of the copper canister versus time due to the existing sulfides in groundwater.

9.3.14. Evolution of the Central Area and Borehole Seals

As described in Section 4.2.9, the central area, the ramp, and the upper part of the vertical shafts will be backfilled and closed. The backfill of the central area is to prevent aggregation and subsidence of the surrounding rock; on the other hand, the backfill of the ramp and upper part of the shafts is to avoid human intrusion and to maintain the location of the backfill in the central area. The backfill used in the above-mentioned areas is rock debris which has higher hydraulic conductivity than the buffer and the backfill in the disposal tunnels.

In order to prevent investigation boreholes from forming groundwater flow paths and jeopardizing the safety functions, these boreholes will also be sealed according to Section 4.2.11. When sealing the boreholes, MX-80 bentonite will be used to seal to wells and silica cement (using low-alkali concrete) will be used to solidify water-conducting fracture zones.

Currently, the assessment of the central area, wells, and other relevant areas has not been established. The central area will take about 150 years to be saturated, and the ramp will take about 20 years to be saturated.

In terms of the evolution of the borehole seal, interaction between the concrete and the bentonite should be taken into account. The concentration of chloride ion should be below 0.4 $kmol/m^3$ to ensure safety functions of the bentonite will not be affected.

9.3.15. Summary

The following is a summary of the possible evolution of the repository during the initial period after closure (post-closure 1,000 years) based on the results of Section 9.3.1 to Section 9.3.14.

(1) Thermal evolution:

Decay heat of the SNF will cause the temperature of the buffer to rise. From the assessment results, peak temperature will appear 5 to 15 years after disposal. As decay heat decreases over time, the temperature will also decrease gradually. The maximum temperature of the buffer will have a certain margin from its temperature limit during the initial period after closure (post-closure 1,000 years) under 9 m-canister spacing, when thermal properties of the host rock are taken into account. Therefore, relevant safety functions: Buff4 and Buff6 are expected not to be jeopardized. For detailed analysis results, please refer to Section 9.3.4.

(2) Mechanical evolution:

The mechanical evolution of the host rock during the initial period after closure (post-closure 1,000 years) will be mainly dominated by the thermal load of the canister. Besides, other factors like swelling pressure of the buffer and the backfill and long-term changes of the stress field in the host rock will also affect the mechanical evolution of the host rock.

According to Section 9.3.5, the thermal load of the canisters has little effect on the hydraulic conductivity of fractures in the near-field and far-field; and the impact will be limited to the region near the disposal tunnels. As a result, relevant safety functions can still be maintained. In addition, spalling caused by thermal load around the deposition holes can also be reduced by suitable planning of the disposal schedule.

In terms of influence caused by plate movement, most structural and fault activities related to plate movement frequently occurred before 58 Ma. No obvious structural activities were seen afterwards. Therefore, fracture reactivation in this period will be mainly due to fracture displacement caused by earthquakes. The time-span of the initial period after closure is only 1,000 years, so the cumulative fracture displacement during this period will be extremely low. Relevant safety functions will hardly be affected.

(3) Hydrogeological evolution:

According to Section 9.3.6, groundwater will flow into the repository after closure, but the inflow will decrease over time. In order to assess the safety of the repository, flow characteristics of the reference case, including flow-related transport resistance (F) and equivalent flow rate (Q_{eq}) were calculated according to groundwater flow analysis results of regional scale and repository scale of the saturated host rock.

Through the analysis results, it is found that at least 70% of the deposition holes will not be connected to water-containing fractures, and diffusion will be the main transport method between the deposition holes, EDZ, and the disposal tunnels. In terms of steady-state groundwater pressure distribution, groundwater pressure will be dominated by the central area, and the flow field will be radially outward and downward. The groundwater pressure distribution will also affect the transport paths of released particles. The trend of release paths of the Q1 path and Q2 path is consistent, which is northward at first affected by groundwater pressure of the central area, then because of the seawater and freshwater interface, particles will be released on the surface of the coastline area.

In the analysis of performance measures, the minimum flow-related transport resistance of the Q1 path and Q2 path are both greater than 10^6 yr/m which complies with safety function indicator criterion R2 (flow-related transport resistance should be higher than 10,000 yr/m), and the maximum equivalent flow rate of Q1 path is slightly higher than 10^{-5} m^3/yr indicates that few paths do not have equivalent flow rate satisfying safety function indicator criterion R2 (equivalent flow rate should be lower than 1×10^{-4} m^3/yr). Since safety function R2 will be compromised, this should be taken into account in the development of scenarios.

Regarding the salinity distribution, the salinity in the depth of the repository is stable. The salinity will range from 0.2% to 1.3%. And there will be an obvious seawater and freshwater interface which can affect the transport of the particles.

(4) Chemical evolution:

Salinity distribution of the repository was assessed using chemical conditions of the synthetic water to deduce salinity and groundwater composition of the deposition holes for initial/boundary conditions that may be used in the assessment of corrosion of the canisters subsequently.

(5) Evolution of the buffer and the backfill:

According to Section 9.3.8 and Section 9.3.9, the repository will be gradually saturated by an average of 5 MPa of inflow. When the buffer and the backfill are fully saturated, the maximum swelling pressure will be 8.23 MPa, which will be located near the bottom of the deposition hole. The swelling pressure of the backfill will be around 1.5 MPa which can fulfill the requirements of the safety function indicator Buff6.

The buffer will be lost because of the combination effect of intrusion, inflow water erosion, and sedimentation. According to Section 9.3.10, the buffer in a single deposition hole may lose up to 102 kg of bentonite during the initial period after closure (post-closure 1,000 years). However, hydraulic conductivity and swelling pressure of the buffer will still comply with the requirements of safety functions Buff1 and the others. Meanwhile, substances will transport in the buffer mainly through diffusion.

Moreover, when the buffer is eroded, the eroded part can be refilled by other parts through swelling. According to Section 9.3.9, if the buffer loses 1,200 kg of the bentonite, the missing part will be completely refilled in about 3.5 years, and swelling pressure can be re-established. Meanwhile, swelling pressure in most of the areas will be about 4 MPa. The minimum swelling pressure will be located near the refilled area, and the swelling pressure on the remaining area will be around 4 MPa.

In addition, the maximum sinking volume of the canisters will be around 2.4×10^{-2} cm. The sinking of the canisters will only make the buffer under the canisters to be slightly compacted but will not affect relevant safety functions.

(6) Evolution of the Canister:

According to Section 9.3.12, the canisters will have higher decay heat during the unsaturated period, and temperature will be relatively easy to accumulate. From the analysis results, the maximum temperature will not exceed 117 ℃, which is lower than the design requirements (125 ℃). The integrity of the canisters will not be affected by the rise in temperature.

Besides, through mechanical analyses, the safety function of Can2 can be maintained when conservatively assuming that the canisters will be subjected to maximum swelling pressure of the buffer (15 MPa) and groundwater pressure uniformly. Meanwhile, certain safety factors and the integrity of the canisters can be maintained when the canisters are subjected to non-uniform isostatic load caused by over-excavation or collapse of rock.

During the entire safety assessment timescale, the copper shell of the canisters will gradually be corroded in the initial aerobic environment and the subsequent anaerobic environment. When the uncertainty of the manufacturing of copper shell and the impact from general corrosion and local corrosion are taken into account, the copper shell will still have a thickness of about 36.8 mm after 1 million years after the closure. Safety function Can1 can be maintained.

9.3.16. Safety Functions for the Initial Period after Closure

The evolution of safety functions of the repository during the initial period after closure (post-closure 1,000 years) is shown in Table 9-15 to Table 9-17, which are organized according to the analysis results of Section 9.3.4 to Section 9.3.14.

Table 9-15: Safety functions of the canister during the initial period after closure.

Safety function	**Safety function indicator**	**Safety function indicator criteria**	**Summary of evolution during the initial period after closure**
Can1. provide barrier against corrosion	Copper shell thickness	> 0 cm	The analysis results show that the copper shell thickness of the canisters still has 36.8 mm and this safety function can be maintained under long-term corrosion over the safety assessment timescale. Therefore, the safety function can also be maintained in the initial period after closure.
Can2. withstand isostatic load	Isostatic load	< 50 MPa	The maximum uniform isostatic load of the canister would be 13.23 MPa, and the safety function can be maintained. In addition, if the canisters are subjected to non-uniform isostatic load caused by over-excavation or rock collapse, the stress on the cast iron lining will not reach the yield stress, and the integrity of the canisters can be maintained.
Can3. withstand shear force	Shear displacement	> 5 cm	The maximum displacements are only within 7 mm due to fractures re-activation by the thermal load. Therefore, this safety function can be maintained during this period.

Table 9-16: Safety functions of the buffer and the backfill during the initial period after closure.

Safety function	**Safety function indicator**	**Safety function indicator criteria**	**Summary of evolution during the initial period after closure**
Buff1. limit advection	(a) hydraulic conductivity	$<10^{-12}$ m/s	After conservative analysis, the loss of buffer will be about 102 kg. The safety function can be maintained.
	(b) swelling pressure	> 1 MPa	The buffer may be eroded by groundwater flow during this period, but it can redistribute by its swelling characteristics, and the eroded part can thereby be healed. The average swelling pressure will be about 4 MPa after the buffer is refilled, and the safety function can be maintained.
Buff2. limit microbial activity	swelling pressure	> 2 MPa	The buffer eroded by groundwater flow during the initial period after closure will be less than 1,200 kg. Although the dry density of the bentonite will decrease, it will still be above 1,420 kg/m^3, and the swelling pressure will be greater than 2 MPa. The safety function can be maintained.
Buff3. damp rock shear force	density	< 2,050 kg/m^3	Creeping of the host rock may affect the geometry of the deposition holes, which may cause the buffer to squeeze and increase its density. Detailed assessment has not been done yet.
Buff4. resist transformation	temperature	< 100 ℃	The canister spacing is set to 9 m and the disposal tunnel spacing is set to 40 m currently. According to the layout, the maximum temperature of the buffer will be lower than 100 ℃ around the first ten years after the closure. And the temperature will continue to drop. The safety function can be maintained.

Buff5. prevent canister sinking	swelling pressure	> 0.2 MPa	According to the analysis results, the buffer can provide a swelling pressure of more than 2 MPa. The safety function can be maintained. Sinking of the canister due to its own weight might slightly compact the buffer under the canister, but the amount will be around 2.4×10^{-2} cm.
Buff6. limit pressure applied to the canisters and rock	(a) swelling pressure	< 10 MPa	According to the analysis results, the average swelling pressure of the buffer will be around 5 MPa and the maximum swelling pressure near the bottom region will be about 8.23 MPa. Safety function Buff6 can be maintained.
	(b) temperature	> -2.5 ℃	According to the analysis results, the maximum temperature of the buffer will not exceed 100 ℃. As decay heat in the canister continues to decrease, the temperature of the buffer will gradually approach the temperature of the host rock (about 33.3 ℃) after hundreds of years. The safety function can be maintained.
BF1. limit buffer expansion	swelling pressure of backfill	Not too low	According to the analysis results, the swelling pressure of the backfill will be around 1.5 MPa. The safety function can be maintained.

Table 9-17: Safety functions of the geosphere during the initial period after closure.

Safety function	Safety function indicator	Safety function indicator criteria	Summary of evolution during the initial period after closure
R1. provide preferred chemical conditions	(a) redox state; Eh	Limit Eh value	Chemical conditions around the repository were evaluated, and the results show that pH value will be slightly higher than 7, cation strength will be lower than 8 mM, and concentration of hazardous substances will be slightly higher than 10^{-4} M. Safety function R1 might be compromised.
	(b) salinity; TDS	TDS<35 g/L	
	(c) ionic strength; $\Sigma q[Mq^{+}]GW$	Cation charge concentration > 8 mM	
	(d)concentration of hazardous substance	$[NO_2^{-}]<10^{-3}$ mol/L $[HS^{-}]<3$ mg/L≈10^{-4} M $[K^{+}]<0.1$ mol/L	
	(e) pH	The pH needs to be 5 to 11	
	(f) avoid chlorides to promote corrosion; pH and $[Cl^{-}]$	pH > 4; $[Cl^{-}]$ < 2M	
R2. provide preferred hydrogeologic and transport conditions	(a) transport resistance (F)	>10,000 yr/m	The analysis results show that the transport resistance of Q1 and Q2 will be higher than 10^{6} yr/m, and the equivalent flow rate will be lower than 10^{-4} m^2/yr. The safety function can be maintained.
	(b) equivalent flow rate (Q_{eq})	$<1 \times 10^{-4}$ m^3/yr	
R3. provide mechanically stable environment	groundwater pressure	Limit	Groundwater pressure of the repository will be slightly higher than 5 MPa. A stable mechanical environment can be provided.

R4. provide preferred thermal environmen t	temperature	-2.5℃ to 100℃	Temperature of the host rock will be about 33.3 ℃. The safety function can be maintained.

9.4. The Remaining Glacial Period after Closure (post-closure 120,000 years)

9.4.1. Long-Term Evolution of the Climate

Climate evolution over the safety assessment timescale of the reference case will follow the 120,000 years glacial cycle. The reference case is located in the subtropical area. Therefore, the climate type of the reference case will gradually transfer from subtropical climate to temperate climate, then return to subtropical climate (Figure 5-1).

As described in Section 9.3.2, climate change of the reference case will be dominated by monsoon under the influence of the East Asian Continent and Northwest Pacific monsoon system in the subtropical climate. Under the subtropical climate, the annual temperature of the reference case will be above 0 ℃. In summer, the southwesterly air flow and typhoon will bring more rain; and in winter, the dry and cold northeast monsoon will prevail, and the evaporation will be high. When the climate type changes to temperate climate, rainfall conditions in summer and winter will remain the same under the influence of the Asian monsoon, but the temperature will become lower. The main difference will be the distribution of temperature.

From the analysis results in Section 5.2.1, the annual average surface temperature will decrease from 23.8 ℃ to 17 ℃-18 ℃ gradually (post-closure 10,000 years), and then return to 23.8 ℃ (post-closure 120,000 years). Annual rainfall will be between 500 mm and 1,700 mm. Normally, there will not be snowfall or glacier on the surface. During the glacial cycle, sea-level will gradually decline along with the evolution of climate, then gradually rise back to the original sea-level.

9.4.2. Biosphere

As mentioned in Section 9.3.3, biosphere evolution is driven by the sea-level change caused by climate change. Release locations and potentially exposed groups are affected by the changing topography and ecosystem. The biosphere evolution of the reference case will be discussed according to the topography, the ecosystem, and the release location of radionuclides:

(1) Surface topography

According to Section 9.4.1, the climate evolution of the reference case over a million-year safety assessment timescale will repeat every 120,000 years. The reference case will change from subtropical climate to temperate climate, then back to subtropical climate. According to Section 5.2.1, the annual surface average temperature will decrease from 23.8 ℃ to 17 ℃ ~ 18 ℃ gradually (post-closure 10,000 years), and then return to 23.8 ℃ (post-closure 120,000 years). Annual rainfall will be between 500 mm and 1,700 mm.

During the glacial cycle, the sea-level will gradually decrease and return to the original sea-level, along with climate change. When the sea-level falls to -20 m, most catchments in the reference case will be connected to mainland China except for the southern area because the topography of the sea bottom is relatively flat and will emerge faster except for the southern area (Figure 9-2). When the sea-level falls to -120 m, all catchment will be located in an inland region away from the ocean. The reference case will change from an ocean-monsoon climate affected by the marine current to an inland temperate climate.

(2) Ecosystem

During the 120,000-year glacial cycle, the ecosystem will gradually turn from marine to terrestrial and finally return to the marine ecosystem. When the sea-level gradually falls, an estuary or bay area where the topography is flat may become lagoon or wetland because of sedimentation of sand coming from the tidal current or bed-load transport process. Besides, lakes may also form in basin area where water flow gathers. After a long period of sedimentation, these lakes may be filled with sediment, leaving only main river courses, and the ecosystem will become a terrestrial and river ecosystem.

Human actions may be changed along with the ecosystem. Currently, agriculture, livestock farming, and oyster farming are widespread in the reference case. When a lagoon or wetland is formed, farming of freshwater fish may appear. The marine ecosystem will be replaced by limnic and river ecosystem gradually, and oyster farming will be replaced by freshwater fish farming correspondingly.

(3) Release location of radionuclides

According to the results of particle tracking, the conditions of the initial period of the remaining glacial period will be very similar to the initial period after closure (post-closure 1,000 years). The reference case will remain an island, and radionuclides will be released into the ocean. People may be exposed through sea-related exposure pathways. Besides, radionuclides may attach to sea aerosol and be transported to the surrounding land by sea spray. The main assessment point will be the impact on the groups who live near the coast or engage in the sea-related industry.

Lagoon, lake, or river ecosystems might appear when the sea-level falls gradually. Different considerations should be taken into account for release locations of these ecosystems:

(a) Lagoon: radionuclides may be released into lagoons near the ocean. People might be exposed to radionuclides through lagoon and sea simultaneously. Meanwhile, radionuclides might attach to the soil through irrigation of the lagoon water. The groups engaging in farming or animal husbandry near the lagoons should be put into the assessment.

(b) Lake: radionuclides may be released into low-lying lakes. People might be exposed to radionuclides through irrigation, ingestion of well water, or other lake-related industry. The groups engaging in farming, animal husbandry, or freshwater fish farming near the lakes should be put into the assessment.

(c) River: radionuclides may be released into rivers when lakes are filled with sediment and only main river courses are left. People might be exposed to radionuclides through irrigation or ingestion of well water. The groups engaging in farming or animal husbandry near the rivers would be put into the assessment since rivers do not have enough space for freshwater fish farming.

In each case, the capillary rise process, which causes the transport of the radionuclides from groundwater to agricultural lands near the waterbody, is considered.

9.4.3. Thermal Evolution

According to the analysis of near-field thermal evolution during the initial period after closure (post-closure 1,000 years) in Section 9.3.4, it is shown that the maximum temperature of the buffer will appear on top of the canisters. This will occur about 15 years after the disposal. After the buffer reaches the maximum temperature, the temperature will gradually decrease along with time and decrease of the decay heat. Besides, based on the analysis in Section 5.2.1, the climate of the reference case over the safety assessment timescale will be subtropical climate or temperate climate. The temperature of the surface or the rock will not be much varied. On the other hand, the temperature will not be affected by glaciers, and there is no possibility for the buffer to be frozen.

9.4.4. Rock Mechanical Evolution

For repository in the remaining glacial period after closure (post-closure 120,000 years), the rock mechanical factors that have potential safety impact are listed below:

(1) Fracture reactivation in the near-field due to thermal load:

Because of the decay heat of SNF in the canisters,the temperature will rise and lead to expansion of the rocks, which causes aperture closure or fracture displacement. This phenomenon may affect the mechanical stability (safety function R3) of the disposal system and also the transmissivity of the fracture.

According to Section 9.3.4 and 9.4.3, the temperature will reach its maximum in about ten years after the closure of the repository. Then rising of the temperature will slow down along with time and decrease of the decay heat. It is estimated to have less impact compared to the initial period after closure.

(2) Fracture reactivation in the far-field due to thermal load:

As previously mentioned, the rising temperature may also affect fracture transmissivity (safety function R2) and induce shear displacement on fractures in the far-field. However, in the remaining glacial period after closure (post-closure 120,000 years), because the temperature will reach its maximum in about ten years after the closure, and the temperature will then gradually decrease with time due to a decrease of the decay heat, fracture reactivation in the far-field due to thermal load is estimated to be much limited comparing to the initial period after closure.

(3) Creep of the host rock, which may affect the geometry of the deposition holes (safety functions Buff3 and Buff6):

Creep is an effect that host rock gradually accumulates permanent strain over time. The creep of the host rock may affect the geometry of the deposition holes and further impact safety functions Buff3 and Buff6 of the buffer. Currently, the creep of the rock during the remaining glacial period after closure (post-closure 120,000 years) has not been evaluated yet. The potential impact of creep is expected to be evaluated through numerical modelling in the future.

(4) Fracture reactivation is caused by the deformation of the rocks due to plate movement, which might affect the mechanical stability of the deposition holes (safety function R3):

As described in Section 9.3.5, there were no obvious structural activities after 58 Ma. Thus, deformation of the host rock in the reference case will be mainly caused by the earthquake-induced shear displacement of fractures. After the repository is closed, shear displacement of fractures in the host rock could be accumulated because of an earthquake. If a fracture intersects a canister, the canister is likely to suffer from the shear force and lead to failure of the canister. For the evaluation of the probability of canister failure due to shearing, 3DEC was used to analyze earthquake-induced shear displacement of fractures in a single earthquake. And the accumulation of shear displacement of fractures after multiple seismic events over the safety assessment timescale was calculated, applying weighting and conservative assumptions. Fractures used in this evaluation were based on the DFN recipe for depth greater than 70 m in Section 4.3.2 (Table 4-17, FDMB). The mechanical parameters of fractures are referenced from SKB's work (SKB, 2010p). The cohesion of fractures is 0.5 MPa. The friction angle is 34°. The dilation angle is 0°. The residual cohesion is 0 MPa. The residual friction angle and dilation angle is 0°. The normal and shear stiffness is 10 GPa/m.

Illustrations of maximum shear displacement and max. The permanent shear displacement of fractures induced by one earthquake is shown in Figure 9-53. The average of shear displacement and permanent shear displacement of each fracture cluster (Table 4-17, FDMB) were also calculated. Shear displacement of each fracture cluster induced by fault source and diffuse seismicity are listed in Table 9-18.

According to the logic tree and the following assumptions, the accumulation of shear displacement induced by multi-earthquakes over the safety assessment timescale was estimated:

(a) Only earthquakes coincide with the source model in the logic tree will occur.

(b) Fractures will not propagate with the accumulation of shear displacement.

(c) Fractures will not accumulate interseismic shear displacement.

(d) Strength of fractures will remain consistent.

(e) Faults in the reference case will not dislocate during earthquakes.

(f) Directions of shear displacement triggered by every source model are consistent.

(g) Shear displacement of fractures is regarded as permanent displacement whether the fractures fail.

In the remaining glacial period after closure (post-closure 120,000 years), the shear displacement of each fracture cluster induced by multiple fault source earthquakes and diffuse seismicity are listed in Table 9-19. Results of the whole safety assessment timescale are listed in Table 9-20. Accumulation of maximum shear displacement and average shear displacement over time are shown in Figure 9-54 and Figure 9-55.

According to safety function R3 in Chapter 7, the shear displacement of the deposition holes should be less than 5 cm with a shear velocity of less than 1 m/s to fulfill the design requirements of the canister. Based on the evaluation results, fault source earthquakes, diffuse seismicity, and summation of both will not induce shear displacement larger than 50 mm in the remaining glacial period after closure (post-closure 120,000 years). However, cluster 1 and 4 have an accumulation of fault-source-earthquake-induced maximum shear displacement larger than 50 mm over the safety assessment timescale while all the other clusters have an accumulation of average shear displacement less than 30 mm. As for shear displacement induced by diffuse seismicity, clusters 1, 2, and 4 can accumulate more shear displacement than cluster 3s and 5. Besides, the summation of the accumulation of maximum shear displacement triggered by fault source earthquakes and diffuse seismicity indicates that all the clusters can accumulate maximum shear displacement of more than 50 mm. Accumulation of average shear displacement for clusters 1, 2, and 4 will be larger than 50 mm as well. Nevertheless, the simulation of diffuse seismicity in the evaluation had a 200 km radius area as the diffuse seismicity boundary, the difference of the geological areas was not taken into account, and the number of earthquakes might be over-estimated in the evaluation.

Table 9-18: Earthquake-induced shear displacement of fracture clusters by fault source and diffuse seismicity in a single earthquake event.

Fracture cluster	Shear displacement of fracture	Fault source earthquake				Diffuse seismicity
		Mw 7.3	Mw 7.93	Mw 8.27	Mw 8.51	
1	Max. shear displacement (mm)	0.04	0.31	2.36	28.18	2.70
	Avg. shear displacement (mm)	0.03	0.26	0.5	10.92	1.60
	Max. permanent shear displacement (mm)	0.0083	0.16	2.27	24.04	2.40
	Avg. permanent shear displacement (mm)	0.0058	0.13	0.46	10.08	1.40
2	Max. shear displacement (mm)	0.04	0.91	3.7	7.59	3.60
	Avg. shear displacement (mm)	0.03	0.19	0.69	1.87	2.00
	Max. permanent shear displacement (mm)	0.011	0.52	3.36	6.32	3.50
	Avg. permanent shear displacement (mm)	0.01	0.1	0.61	1.43	1.90
3	Max. shear displacement (mm)	0.04	0.21	0.31	18.13	1.30
	Avg. shear displacement (mm)	0.03	0.17	0.25	5.72	0.13
	Max. permanent shear displacement (mm)	0.011	0.07	0.24	18.04	0.94
	Avg. permanent shear displacement (mm)	0.01	0.06	0.19	5.23	0.10
4	Max. shear displacement (mm)	0.05	1.58	3.71	10.29	2.70
	Avg. shear displacement (mm)	0.04	0.16	0.81	2.16	2.00
	Max. permanent shear displacement (mm)	0.049	1.42	3.37	6.04	2.40

	Avg. permanent shear displacement (mm)	0.033	0.1	0.71	1.68	1.77
5	**Max. shear displacement (mm)**	0.02	0.15	0.36	6.24	1.00
	Avg. shear displacement (mm)	0.015	0.07	0.13	0.87	0.59
	Max. permanent shear displacement (mm)	0.006	0.08	0.28	5.56	0.89
	Avg. permanent shear displacement (mm)	0.003	0.03	0.1	0.74	0.44

Table 9-19: Earthquake-induced accumulated shear displacement of fracture clusters by fault source and diffuse seismicity in the remaining glacial period after closure.

Fracture cluster	**Accumulation of shear displacement**	**Fault source**	**Diffuse seismicity**	**Total**
1	**Max. accumulation of shear displacement (mm)**	5.735	13.200	18.936
	Avg. accumulation of shear displacement (mm)	2.081	7.700	7.781
2	**Max. accumulation of shear displacement (mm)**	4.008	19.250	23.258
	Avg. accumulation of shear displacement (mm)	0.800	10.450	11.250
3	**Max. accumulation of shear displacement (mm)**	3.160	5.170	8.330
	Avg. accumulation of shear displacement (mm)	1.061	0.550	1.611
4	**Max. accumulation of shear displacement (mm)**	4.766	13.200	17.966
	Avg. accumulation of shear displacement (mm)	1.000	9.735	10.735
5	**Max. accumulation of shear displacement (mm)**	1.184	4.895	6.079
	Avg. accumulation of shear displacement (mm)	0.227	2.420	2.647

Table 9-20: Earthquake-induced accumulated shear displacement of fracture clusters by fault source and diffuse seismicity over the safety assessment timescale.

Fracture cluster	Accumulation of shear displacement	Fault source	Diffuse seismicity	Total
1	Max. accumulation of shear displacement (mm)	65.88	122.16	188.04
	Avg. accumulation of shear displacement (mm)	23.68	71.26	94.94
2	Max. accumulation of shear displacement (mm)	45.40	178.15	223.55
	Avg. accumulation of shear displacement (mm)	9.00	96.71	105.71
3	Max. accumulation of shear displacement (mm)	36.11	47.85	83.96
	Avg. accumulation of shear displacement (mm)	12.00	5.09	17.09
4	Max. accumulation of shear displacement (mm)	51.87	122.16	174.03
	Avg. accumulation of shear displacement (mm)	11.07	90.09	101.16
5	Max. accumulation of shear displacement (mm)	13.44	45.30	58.74
	Avg. accumulation of shear displacement (mm)	2.54	22.40	24.94

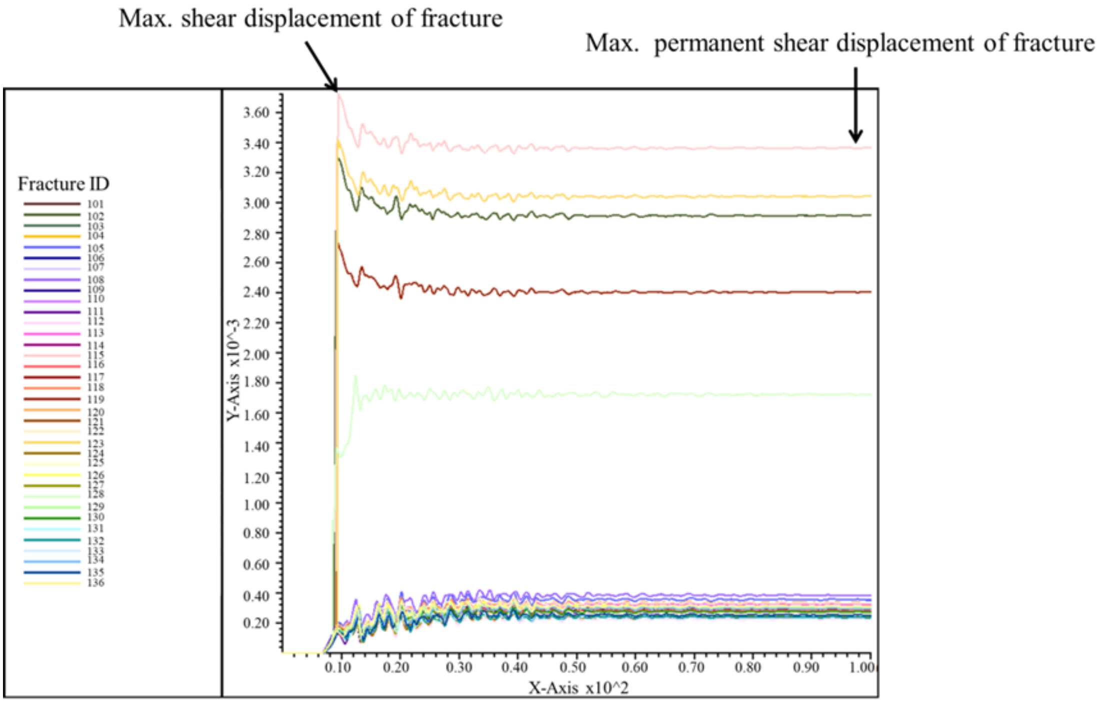

Figure 9-53: Maximum shear displacement and max. Permanent shear displacement of fracture induced by fault source and diffuse seismicity of a single earthquake event.
Note: X-axis indicates time (s) and Y-axis indicates shear displacement (m).

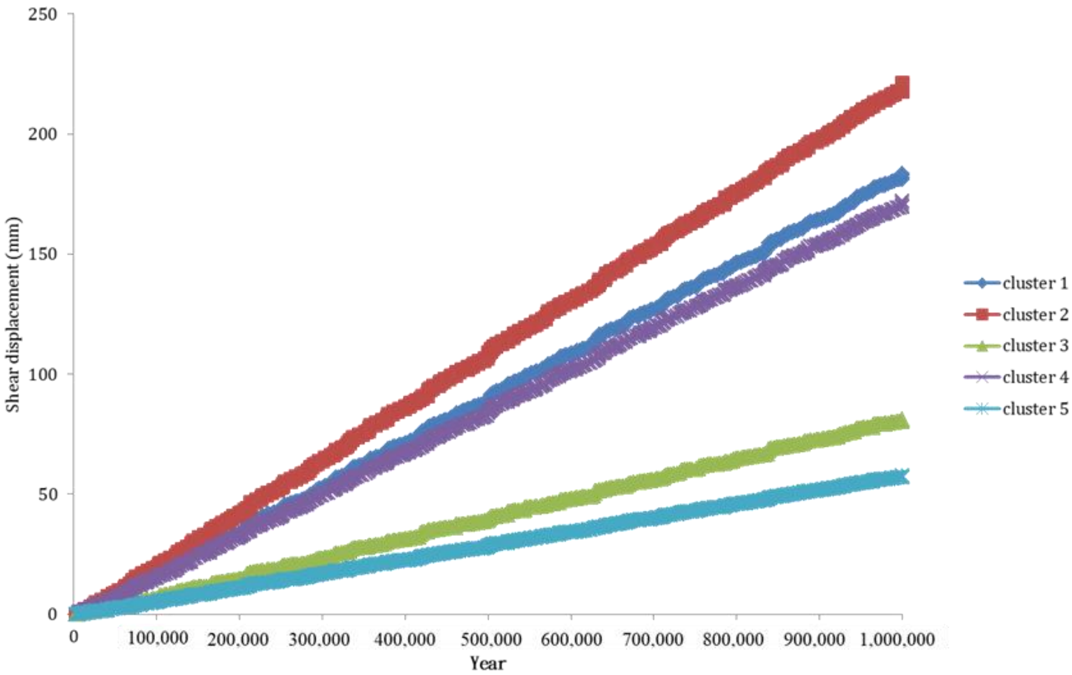

Figure 9-54: Maximum accumulated shear displacement of each fracture cluster over the safety assessment timescale under conservative assumptions.

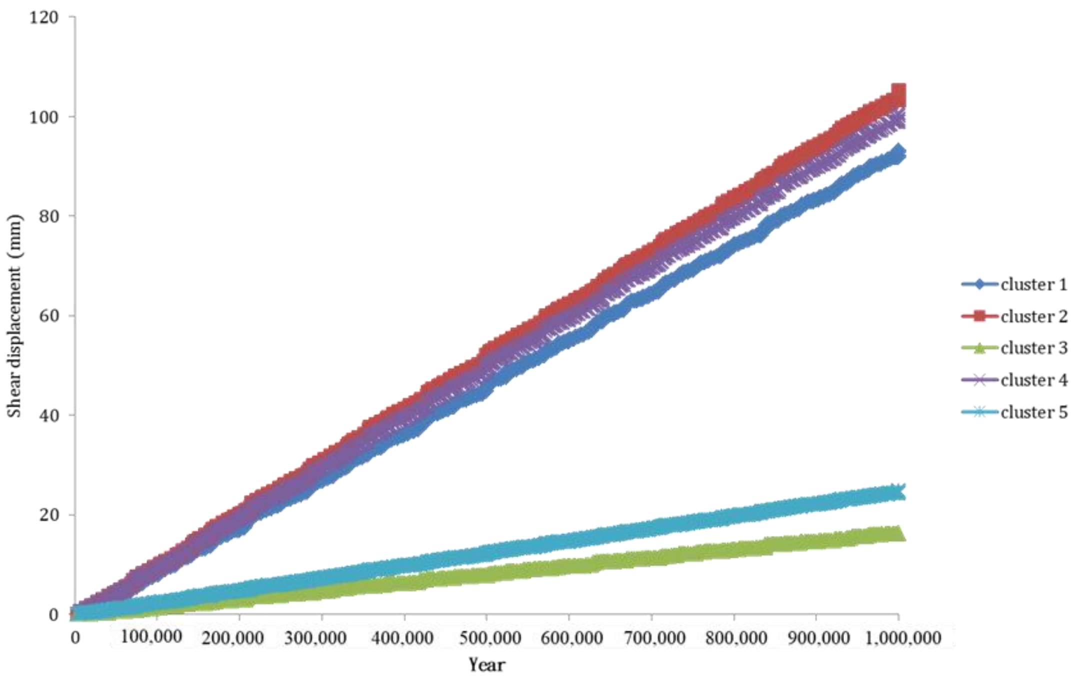

Figure 9-55: Average accumulated shear displacement of each fracture cluster over the safety assessment timescale under conservative assumptions.

9.4.5. Canister Failure due to Shear Displacement of Fractures

Fracture shear displacement across a deposition hole is one of the primary reasons that a canister would fail over the safety assessment timescale. Fracture shear displacement is expected to be mainly induced by earthquakes in the reference case, especially since Taiwan is located at the junction of the Eurasian Plate and the Philippine Sea Plate along the Circum-Pacific seismic and volcanic zone. Once a fracture intersecting the canister has a displacement that exceeds safety function indicator criterion Can3, the integrity of the canister could be jeopardized and should be assessed.

Based on the repository layout, EFPC (Section 4.4), and fracture shear displacement (Section 9.4.4), the canister failure rate was evaluated by applying 50,000 DFN realizations over the safety assessment timescale (see Figure 9-56). It was assumed that fracture size would be constant throughout the safety assessment timescale. The minimum fracture radius was set to the equivalent tunnel radius (2.88 m), the maximum fracture radius was set to 250 m (SKB, 2010f), and the shape of the fracture was set to be a circle plane.

As shown in Figure 9-56, the earliest possible time for canister failure due to shear displacement (accumulated shear displacement exceeds 5 cm) would be around 230 thousand years after the closure. The probability of failure would be around 10^{-6}.

This indicates that there will be no canister failure in the remaining glacial period. As time goes on, fractures continuously accumulate shear displacement up to 22 cm by the earthquake and the canister failure rate increases to 3×10^{-4} at the end of the assessment period. Table 9-21 shows 5 cases among 50,000 DFN realizations which have shear displacement exceeding safety function indicator criterion Can3.

Possible reasons for the canister failure rate to change over time are inferred as the following:

(1) Fracture shear displacement induced by earthquakes depends on fracture size in the evaluation model, i.e., the larger the fracture, the earlier the displacement exceeds 5 cm.

(2) Distribution of shear displacement for a fracture depends on the distance from the intersecting position to the fracture center, i.e., the shorter the distance, the larger the displacement can be.
(3) Fractures with a small radius will induce smaller shear displacement. However, as time goes by, shear displacement could be accumulated to a certain degree over repeated earthquakes, which might cause the canister to fail. Therefore, fracture size that could induce canister failure can become smaller.

Three possible canister failure cases obtained from the analyses were provided for the subsequent assessment. The parameters of the three fracture sets are shown in Table 9-22 and Figure 9-57.

Table 9-21: Five cases of canister failure due to shear displacement in 50,000 DFN realizations.

Shear displacement of fracture at the end of the assessment period (cm)	Timing of shear displacement exceed 5 cm (thousand years)	Fracture cluster
22.1	23	2
13.9	36	3
8.2	61	5
5.4	92	4
5.0	100	1

Table 9-22: Parameters of the three fracture sets leading to canister failure.

<table>
<tr><th>Fracture case</th><th>Dip direction</th><th>Dip angle</th><th>Fracture radius(m)</th><th>x</th><th>y</th><th>z</th><th>Failure time(yr)</th></tr>
<tr><td>1</td><td>249.6</td><td rowspan="3">38.6</td><td rowspan="3">249.4</td><td>-1161.5</td><td>593.8</td><td>-599.7</td><td rowspan="3">230,000</td></tr>
<tr><td>2</td><td rowspan="2">9.6</td><td>101.1</td><td>111.8</td><td>-599.7</td></tr>
<tr><td>3</td><td>600.7</td><td>978.0</td><td>-599.7</td></tr>
</table>

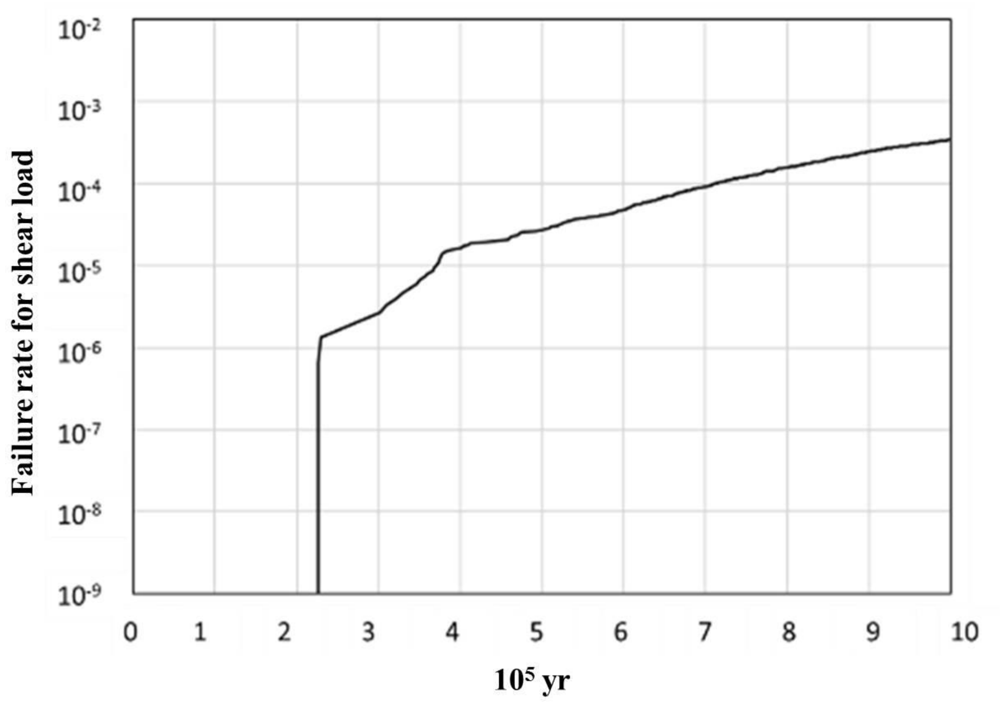

Figure 9-56: Canister failure rate due to shear displacement over the safety assessment timescale.

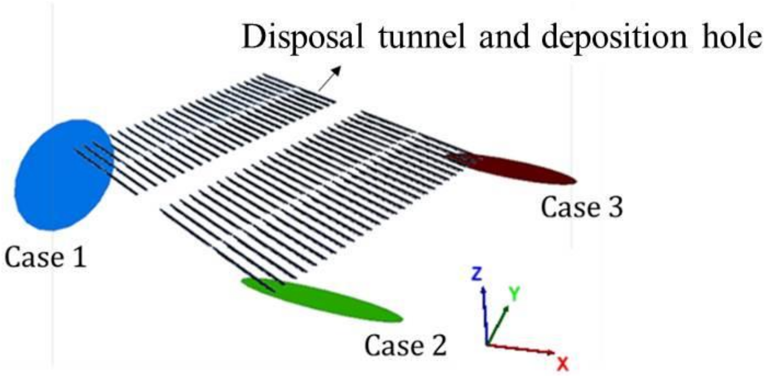

Figure 9-57: Relative position of the three fracture sets.

9.4.6. Hydrogeological Evolution

The assessment of hydrogeological evolution in the remaining glacial period after closure (post-closure 120,000 years) can be divided into three parts, including the analyses of the groundwater flow field, release paths, and performance measures. These analyses are described as follows:

(1) Groundwater flow field:

Simulation of the groundwater flow field in the remaining glacial period was conducted. According to Section 5.2 and Section 9.4.1, the sea-level will gradually decrease over time, and the reference case will change from an island to a plain correspondingly. Based on Section 9.1.3, two specific time points were selected to develop model domains for the evaluation of hydrogeological evolution:

(a) Regional scale model with the reference case changing to a coastal area (post-closure 16,700 years and the sea-level will drop to -20 m):

The model domain, which is a regional scale model (Section 9.1.3), is shown in Figure 9-2. The repository layout and fracture system were set as the same as the one in the initial period after closure (post-closure 1,000 years) in Section 9.3.6.

(i) Hydrogeological model: the model includes regolith (R0), rock mass (R), and major water conducting structure (F#). The fault structure (F1) and fracture structure (F2) only exist on the island, and there are only regolith (R0) and rock mass (R) outside the island.

(ii) Salinity: river water average (0.0105 %).

(iii) Computational grid:

(*) The whole domain and structures: the cell size applied in the domain was 512 m×512 m×512 m, and the refinement was applied by setting a cell size of 256 m×256 m×256 m in the area of the site scale domain.

(*) Fault structure (F1) and fracture structure (F2): the cell size applied in fault structure (F1) and fracture structure (F2) which has higher permeability than the rock mass was 32 m×32 m×32 m.

(*) The top of the domain: refinement was applied by setting a cell size of 32 m×32 m×32 m at the top of the domain.

(*) The repository: first of all, the rock mass close to the repository was refined to 64 m×64 m×64 m; then the grid was globally refined to 8 m×8 m×8 m in the repository zone. In addition, the main tunnels, disposal tunnels, and deposition holes were refined to 1 m×1 m×1 m, EDZ was refined to 1 m×1 m×0.125 m, and walls of the deposition holes were refined to 0.25 m×0.25 m×0.5 m.

The successive refinement led to a total amount of 17,840,457 cells, and the grids of the regional scale model is shown in Figure 9-58.

(b) The regional scale model with the reference case changing to a plain (post-closure 100,000 years and the sea-level will drop to -120 m):

The model domain, which is a regional scale model (Section 9.1.3), is shown in Figure 9-3. The repository layout and fracture system were set as the same as the one in the initial period after closure (post-closure 1,000 years) in Section 9.3.6.

(i) Hydrogeological model: the model includes regolith (R0), rock mass (R), and major water conducting structure (F#). The fault structure (F1) and fracture structure (F2) only exist on the island, and there are only regolith (R0) and rock mass (R) outside the island.

(ii) Salinity: river water average (0.0105 %).

(iii) Computational grid:

(*) The whole domain and structures: the cell size applied in the domain was 512 m×512 m×512 m, and the refinement was applied by setting a cell size of 256 m×256 m×256 m in the area of the site scale domain.

(*) Fault structure (F1) and fracture structure (F2): the cell size applied in fault structure (F1) and fracture structure (F2) which has higher permeability than the rock mass was 32 m×32 m×32 m.

(*) The top of the domain: the refinement was applied by setting a cell size of 32 m×32 m×32 m at the top of the domain.

(*) The repository: first of all, the rock mass close to the repository was refined to 64 m×64 m×64 m; then the grid was globally refined to 8 m×8 m×8 m in the repository zone. In addition, the main tunnels, disposal tunnels, and deposition holes were refined to 1 m×1 m×1 m, EDZ was refined to 1 m×1 m×0.125 m, and walls of the deposition holes were refined to 0.25 m×0.25 m×0.5 m.

The successive refinement led to a total amount of 18,619,161 cells, and the grids of the regional scale model are shown in Figure 9-59.

Analyses of groundwater flow field were performed as described in Section 9.3.6. The DFNs were generated based on the DFN recipe of the reference case. And a connectivity analysis that removed all isolated single fractures or isolated clusters of fractures was conducted to generate an effective fracture system for effective hydraulic properties transformation using GEHYCO of DarcyTools (Svensson, 2010; Svensson and Ferry, 2010; Svensson et al., 2010). The effective fracture system was the same as the one in Section 9.3.6. The effective hydraulic fields of the two model domains are shown in Figure 9-60 and Figure 9-61, respectively. The following settings of boundary conditions were applied for the two regional scale models:

(a) The regional scale model with the reference case changing to a coastal area (post-closure 16,700 years and the sea-level will drop to -20 m):

The bottom boundary and all watersheds were assigned to be no-flow boundaries. A specific head was assigned at rivers, and a specified recharge equal to 66.8 mm/yr (with salinity of 0.0105%) was assigned at the top boundary. Originally, the specific hydrostatic head of seawater should be assigned to the eastern coastline; however, because of the following reasons, the coastline would be assigned to a no-flow boundary: first, no further studies have been done for salinity distribution when the sea-level drops to -20 m; second, the regional flow would flow from the northwest to the southeast, the repository would be far from the coastline, and seawater and freshwater interface could be simulated using a no-flow boundary. Therefore, salinity is expected not to have an impact on the repository much; third, if mass-salt coupled simulation is performed, enormous time and resources will be needed.

(b) The regional scale model with the reference case changing to a plain (post-closure 100,000 years and the sea-level will drop to -120 m):

The bottom boundary and all watershed were assigned to be no-flow boundaries. A specific head was assigned at rivers, and a specified recharge equal to 66.8 mm/yr (with salinity of 0.0105%) was assigned at the top boundary.

The groundwater flow simulation results of the two regional scale model domains are described as follows:

(a) The regional scale model with the reference case changing to a coastal area (post-closure 16,700 years and the sea-level will drop to -20 m):

The resulting pressure field is shown in Figure 9-62. The results show that the regional flow direction would move toward the southeast. And the regional flow field is expected to play an important role in controlling the movement of the particles. If particles are released from the repository, they are expected to transport along the regional flow and transport toward the bottom boundary and the southeast.

(b) The regional scale model with the reference case changing to a plain (post-closure 100,000 years, the sea-level will drop to -120 m, and the top boundary was set to be recharge):

The resulting pressure field is shown in Figure 9-63. The results show that the regional flow direction would move toward the southeast. The regional flow field would play an important role in controlling the movement of the particles. If particles are released from the repository, they are expected to transport along the regional flow and transport toward the bottom boundary and the southeast.

(c) The regional scale model with the reference case changing to a plain (post-closure 100,000 years, the sea-level will drop to -120 m, and the top boundary was set to be the specific head):

According to the above-mentioned results, there may not be particles released on the surface over the safety assessment timescale because the travel time and trace length are expected to be extremely long. In order to conservatively assess the possible impact on the biosphere, the top boundary was assigned to be a specific head as the topography (implying that a freshwater head equaled the elevation of the ground surface). This setting could force the particles to transport to the top boundary, and the performance measurement of these traces could be calculated. The resulting pressure field is shown in Figure 9-64. The results show that the regional flow direction would move toward the southeast, and the site scale flow field near the repository would play an important role in controlling particle movements. If particles are released from the repository, the transportation of most of the particles will be affected by the site scale flow field toward the north, northwest, and northeast. On the other hand, a small portion of the particles will be affected by both the regional flow field and site scale flow field concurrently. In this case, there might be release points on the surface within one million years.

(2) Release paths:

Based on the results of groundwater flow field analyses, the particle tracking method was used to model potential release paths (Figure 9-23) of (a) particles released from the intersection between fracture and deposition hole (Q1 path), and (b) particles released from EDZ (Q2 path). Since the effective fracture system is the same as those in section 9.3.6, the release number of the Q1 and Q2 paths is also the same as those in section 9.3.6. A total of 148 potential release locations were there in the Q1 path, and a total of 2,643 potential release locations were there in the Q2 path.

(a) The regional scale model with the reference case changing to a coastal area (post-closure 16,700 years and sea-level will drop to -20 m):

The results of particle tracking of Q1 and Q2 paths are shown in Figure 9-65 and Figure 9-66, respectively. The results indicate that the paths will be strongly influenced by the topography of the southeast part of mainland China, and the particles will move toward the southeast. In addition, the force of the regional hydraulic gradient would be greater than the recharge rate, so the particles will first move to the lateral side and slightly downwards, then move upwards under the influence of F1. When particles leave F1, they will move to the lateral side and eventually be released near the boundaries.

(b) The regional scale model with the reference case changing to plain (post-closure 100,000 years, sea-level will drop to -120 m, and the top boundary was set to be recharge):

Particle tracking of Q1 and Q2 paths are shown in Figure 9-67 and Figure 9-68, respectively. The results indicate that the paths will be strongly influenced by the topography of the southeast part of mainland China, and particles will move toward the southeast. In addition, owing to the increase of the model domain in the southeast, the hydraulic gradient of the regional flow will be reduced. Therefore, particles will move at an extremely slow pace. During one million years, the particles are expected to only travel a short distance.

(c) The regional scale model with the reference case changing to a plain (post-closure 100,000 years, sea-level will drop to -120 m, and the top boundary was set to be the specific head):

Particle tracking of Q1 and Q2 paths are shown in Figure 9-69 and Figure 9-70, respectively. The results show that the paths will be affected by the site scale flow field in the central mountain area of the reference case, and the paths will direct toward the coastline. Most of the particles will then be affected by the regional gradient and move toward the southeast. A small portion of the particles which are influenced by the site scale regional flow will move to the west. However, all of the particles will be released on land.

(3) Performance measures:

In order to evaluate engineered barrier performance, such as buffer erosion and copper corrosion, performance measures are important parameters that need to be obtained. According to requirements of safety function R2 (Section 7.3.4), preferred hydrogeologic conditions should be provided by the geosphere in order to limit the transport of solutes. Therefore, the evaluation was mainly focused on flow related transport resistance (F) and equivalent flow rate (Q_{eq}).

According to the requirements of safety function R2, the flow-related transport resistance of the Q1 path should be larger than 10,000 yr/m, and the equivalent flow rate of the Q1 path should be smaller than 1.0×10^{-4} m^3/yr (SKB, 2011).

(a) The regional scale model with the reference case changing to a coastal area (post-closure 16,700 years and the sea-level will drop to -20 m):

(i) Flow-related transport resistance (F): the cumulative distribution function of the flow-related transport resistance (F) is shown in Figure 9-71. The results indicate that the minimum flow related transport resistance of the Q1 path would be 5.29×10^5 yr/m, which fulfills the requirements of safety function R2. However, compared to the results in section 9.3.6, the distribution has changed, having a jump at around a fraction of 0.6-0.7. And the minimum flow-related transport resistance of the Q2 path would be 5.46×10^5 yr/m. The distribution is very similar to the one of the Q1 path.

(ii) Equivalent flow rate (Q_{eq}): the cumulative distribution function of equivalent flow rate (Q_{eq}) is shown in Figure 9-72. The results indicate that the maximum value of the Q1 path would be 1.32×10^{-4} m^3/yr, which is slightly larger than the requirements of safety function R2. However, the break of the safety function indicator for a safety function doesn't mean the repository is not safe; it reflects that the detailed safety assessment should be needed via safety assessment to make sure the safety of the repository.

The maximum equivalent flow rate (Q_{eq}) of Q2 path would be 7.38×10^{-5} m^3/yr. The maximum equivalent flow rate of the Q2 path would be smaller than the maximum equivalent flow rate of the Q1 path.

(b) The regional scale model with the reference case changing to a plain (post-closure 100,000 years, the sea-level will drop to -120 m, and the top boundary is recharge):

(i) Flow-related transport resistance (F): since no particles will be released on the land and no particles will reach the boundaries, there is no flow related transport resistance in this case. Particle tracking simulation for the period after post-closure of 1 million years will be performed in the future to study the path, flow-related transport resistance, release time, and release position of this path.

(ii) Equivalent flow rate (Q_{eq}): the cumulative distribution function of the equivalent flow rate (Q_{eq}) is shown in Figure 9-73. The results indicate that the maximum value of the Q1 path would be 9.42×10^{-5} m^3/yr, which fulfills the requirements of safety function R2. However, compare to the results in section 9.3.6, the distribution has changed, having a jump at around a fraction of 0.6-0.7. The maximum equivalent flow rate (Q_{eq}) of the Q2 path would be 6.00×10^{-5} m^3/yr. The maximum equivalent flow rate of the Q2 path would be smaller than the maximum equivalent flow rate of the Q1 path.

(c) The regional scale model with the reference case changing to a plain (post-closure 100,000 years, the sea-level will drop to -120 m, and the top boundary is specific head):

(i) Flow-related transport resistance (F): the cumulative distribution function of the flow-related transport resistance (F) is shown in Figure 9-74. The results indicate that the minimum flow related transport resistance of the Q1 path would be 1.23×10^{6} yr/m, which fulfills the requirements of safety function R2. The minimum flow-related transport resistance of the Q2 path would be 9.16×10^{5} yr/m and the distribution is very similar to the one of the Q1 path.

(ii) Equivalent flow rate (Q_{eq}): the cumulative distribution function of the equivalent flow rate (Q_{eq}) is shown in Figure 9-75. The results indicate that the maximum value of the Q1 path would be 1.02×10^{-5} m^3/yr, which fulfills the requirements of safety function R2. The maximum equivalent flow rate (Q_{eq}) of the Q2 path would be 6.21×10^{-5} m^3/yr. The maximum equivalent flow rate of

Q2 path would be smaller than the maximum equivalent flow rate of the Q1 path.

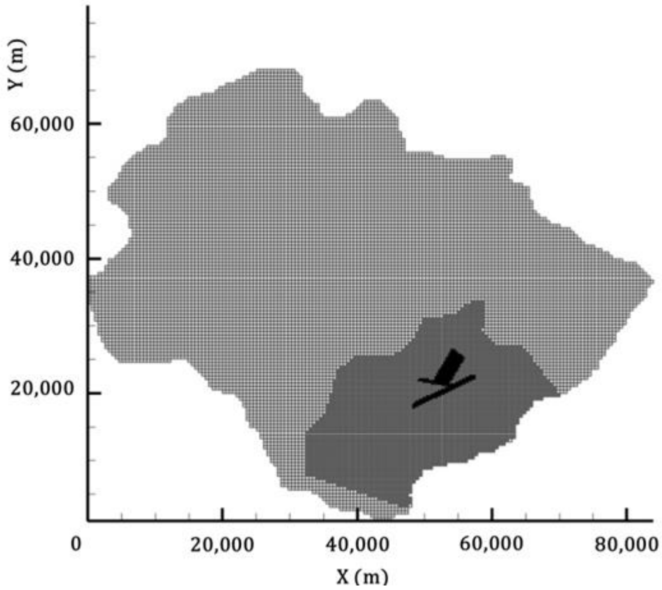

Figure 9-58: Grids of the regional model with sea-level equal to -20 m.
Note: this is the horizontal cut plane z=-504 m.

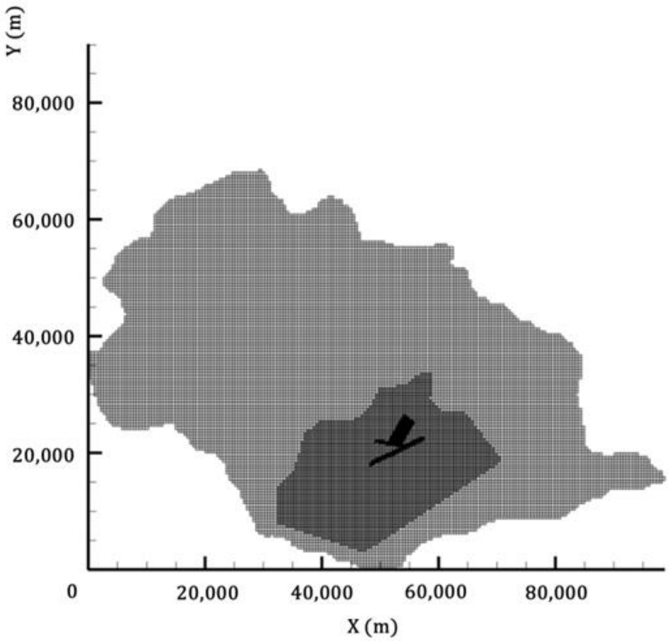

Figure 9-59: Grids of the regional model with sea-level equal to -120 m.
Note: this is the horizontal cut plane at z=-504 m.

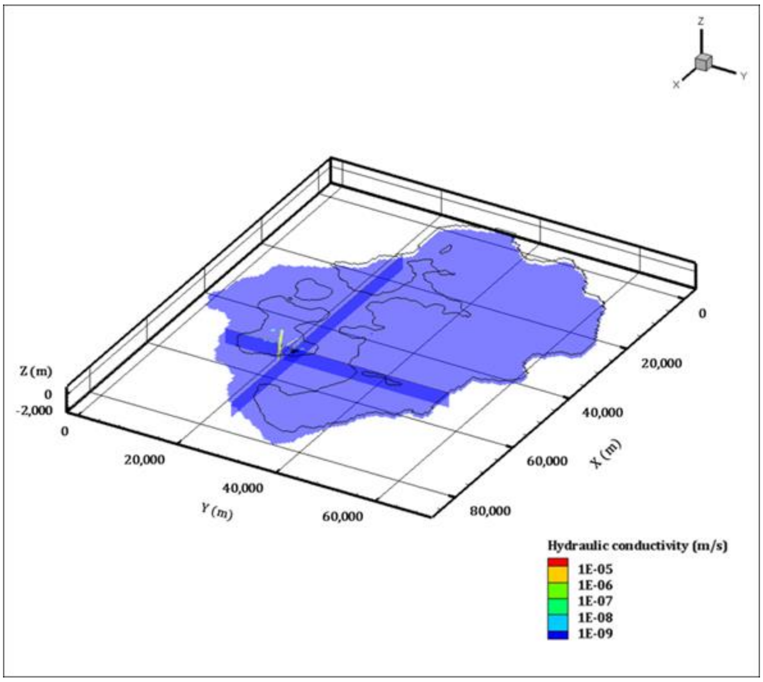

Figure 9-60: Effective hydraulic conductivity values of the regional model with sea-level equal to -20m.

Note: this is the cross-section of x=53,625 m, y=23,650 m, and z=-504 m.

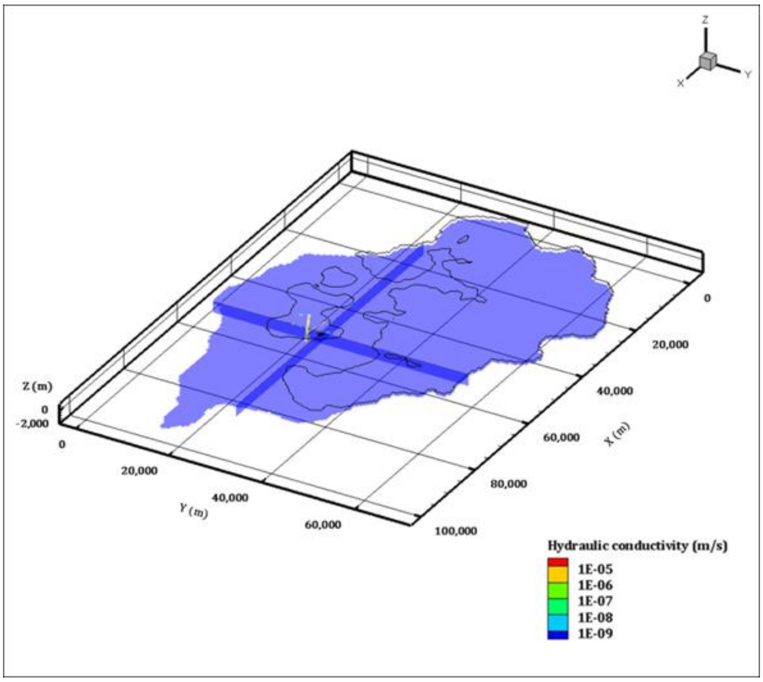

Figure 9-61: Effective hydraulic conductivity values of the regional model with sea-level equal to -120m.

Note: this is the cross-section of x=53,625 m, y=23,650 m, and z=-504 m.

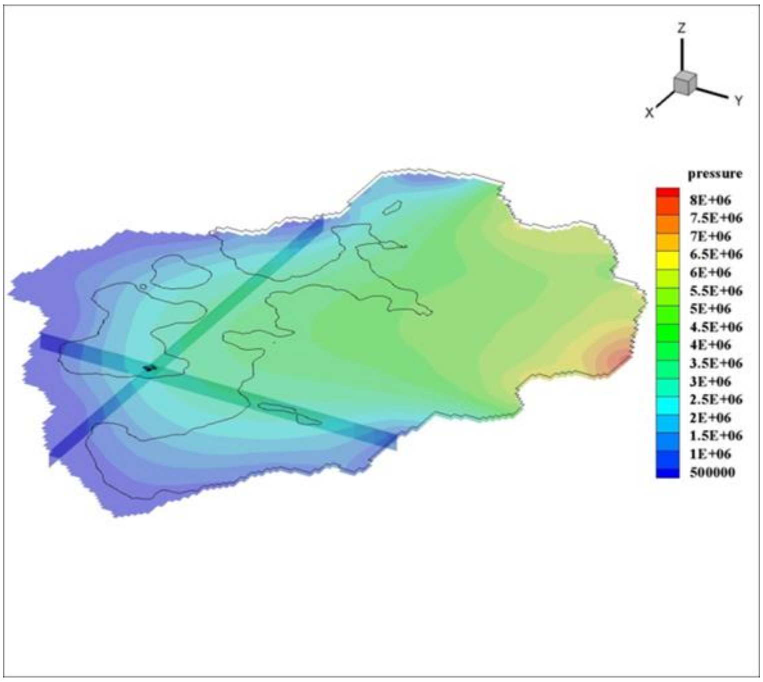

Figure 9-62: Dynamic pressure of the regional model with sea-level equal to -20 m.
Note: this is the cross-section of x=53,625 m, y=23,650 m, and z=-504 m.

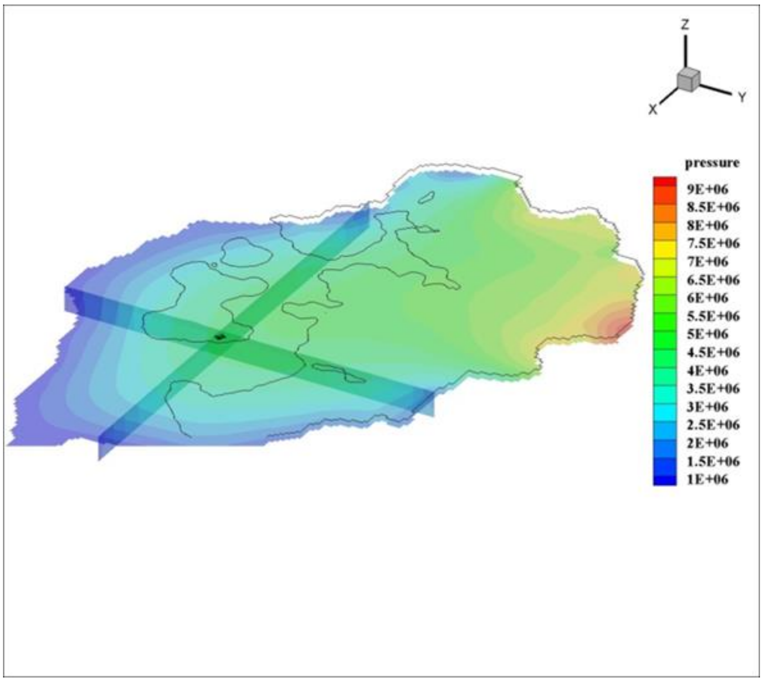

Figure 9-63: Dynamic pressure of the regional model with sea-level equal to -120 m.
Note: this is the cross-section of x=53,625 m, y=23,650 m, and z=-504 m.

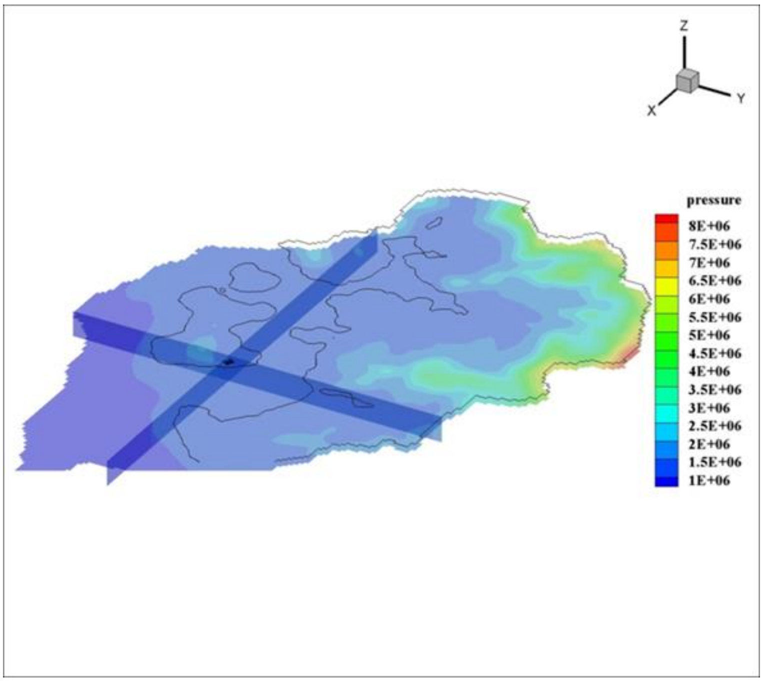

Figure 9-64: Dynamic pressure of the regional model with sea-level equal to -120 m.

Note: this is the cross-section of x=53,625 m, y=23,650 m, and z=-504 m. The top boundary is assigned to a specific head.

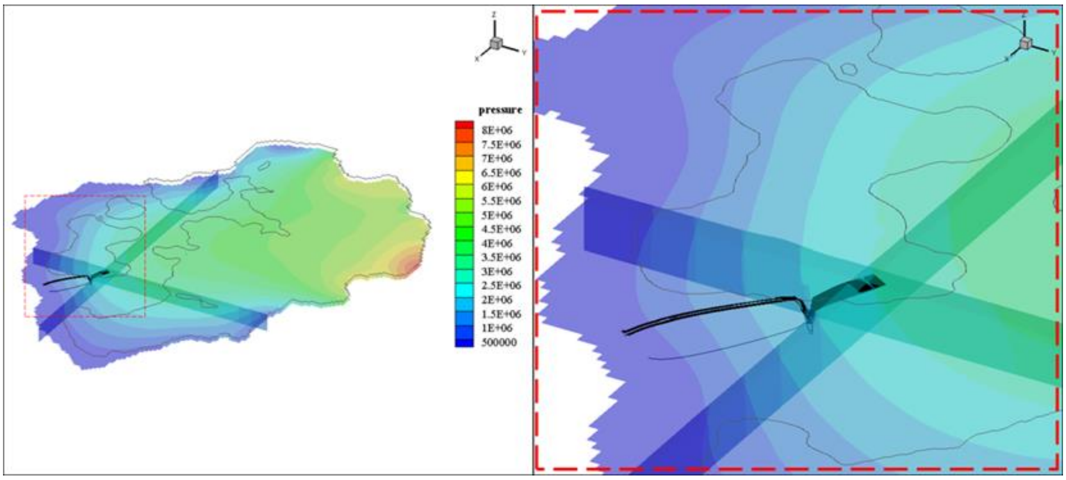

Figure 9-65: Dynamic pressure and Q1 paths from the repository of the regional model with sea-level equal to -20 m.

Note: this is the horizontal cut plane at z=-504 m and two vertical planes at x=53,625 m and y=23,650 m.

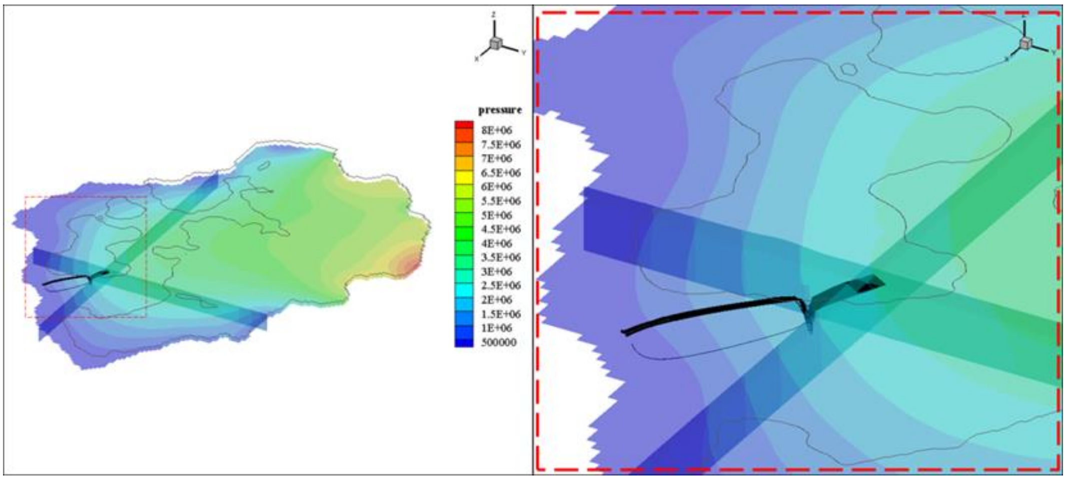

Figure 9-66: Dynamic pressure and Q2 paths from the repository of the regional model with sea-level equal to -20 m.

Note: this is the horizontal cut plane at z=-504 m and two vertical planes at x=53,625 m and y=23,650 m.

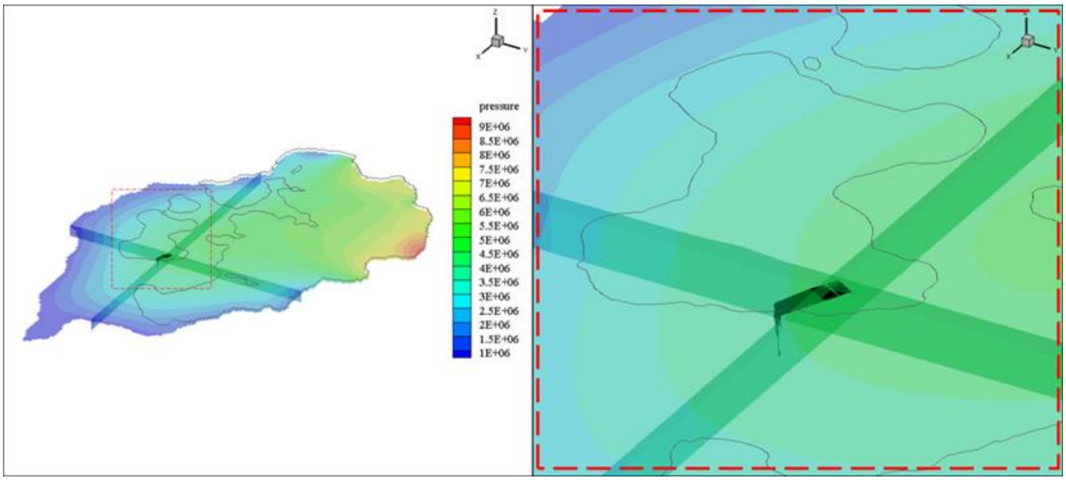

Figure 9-67: Dynamic pressure and Q1 paths from the repository of the regional model with sea-level equal to -120 m.

Note: this is the horizontal cut plane at z=-504 m and two vertical planes at x=53,625 m and y=23,650 m.

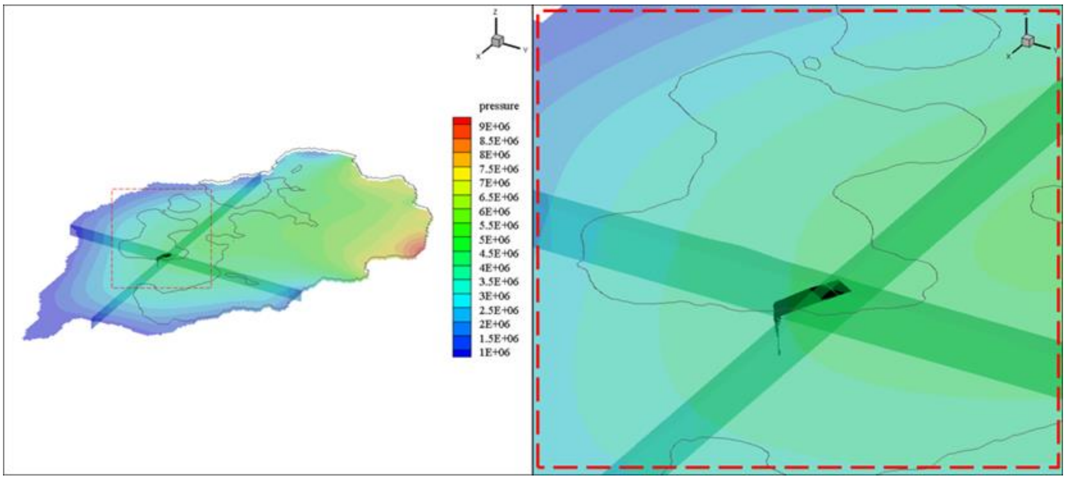

Figure 9-68: Dynamic pressure and Q2 paths from the repository of the regional model with sea-level equal to -120 m.

Note: this is the horizontal cut plane at z=-504 m and two vertical planes at x=53,625 m and y=23,650 m.

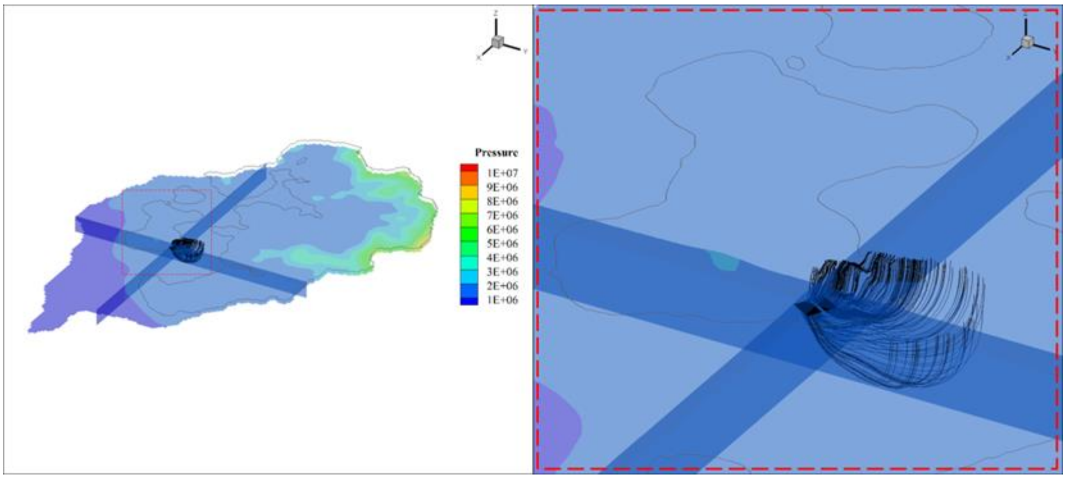

Figure 9-69: Dynamic pressure and Q1 paths from the repository of the regional model with sea-level equal to -120 m.

Note: this is the horizontal cut plane at z=-504 m and two vertical planes at x=53,625 m and y=23,650 m. The top boundary is assigned to a specific head.

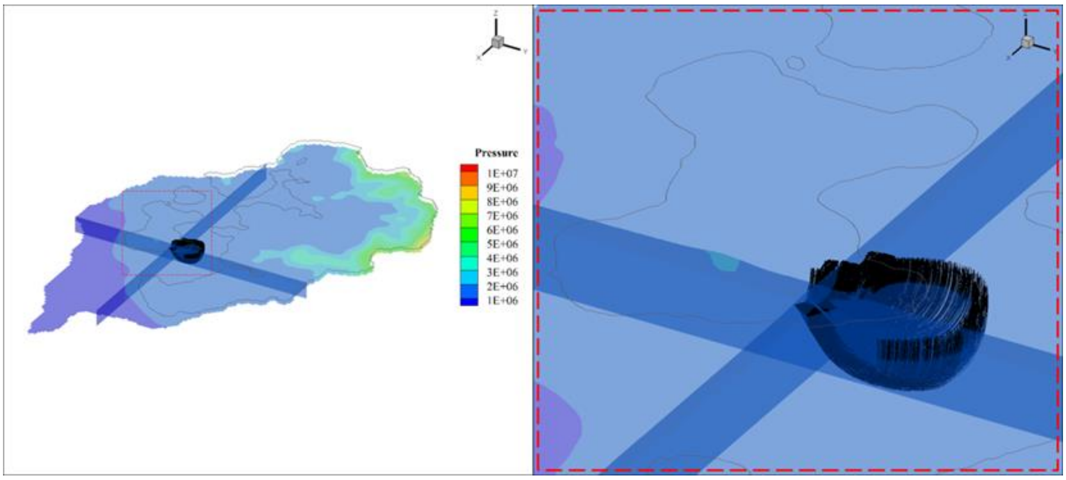

Figure 9-70: Dynamic pressure and Q2 paths from the repository of the regional model with sea-level equal to -120 m.

Note: this is the horizontal cut plane at z=-504 m and two vertical planes at x=53,625 m and y=23,650 m. The top boundary is assigned to a specific head.

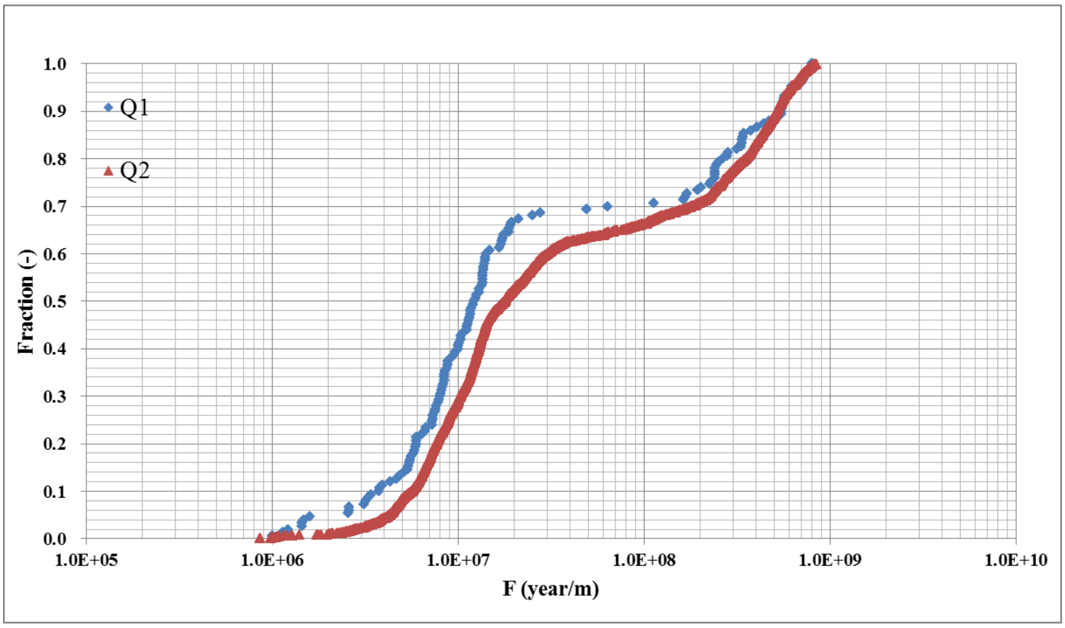

Figure 9-71: Cumulative distribution functions of flow related transport resistance for Q1 and Q2 paths of the regional model with sea-level -20 m.

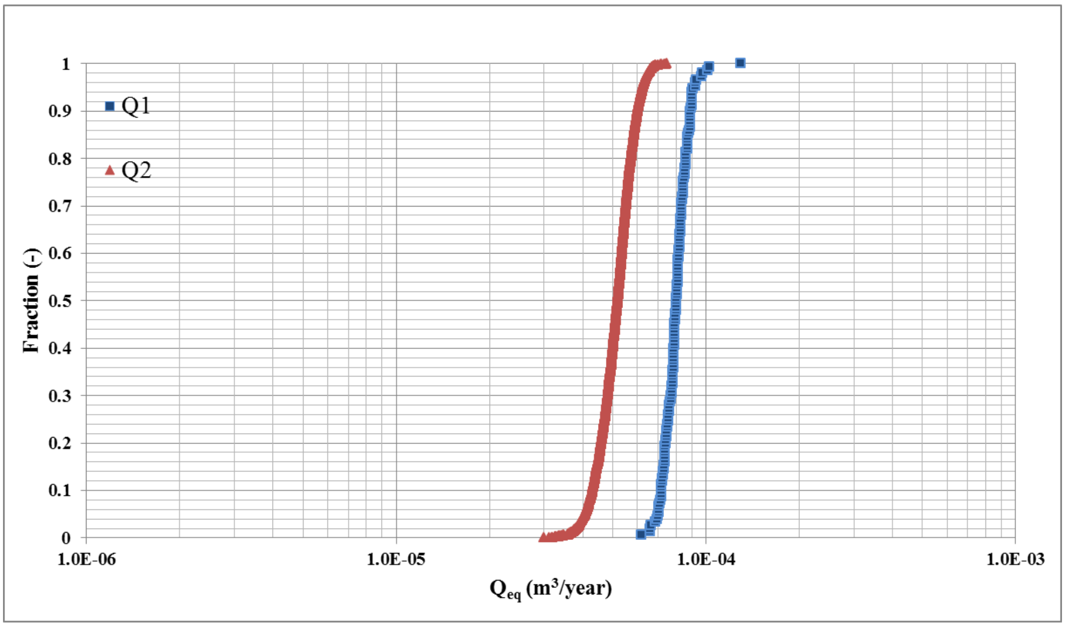

Figure 9-72: Cumulative distribution functions of equivalent flow rate for Q1 and Q2 paths of the regional model with sea-level -20 m.

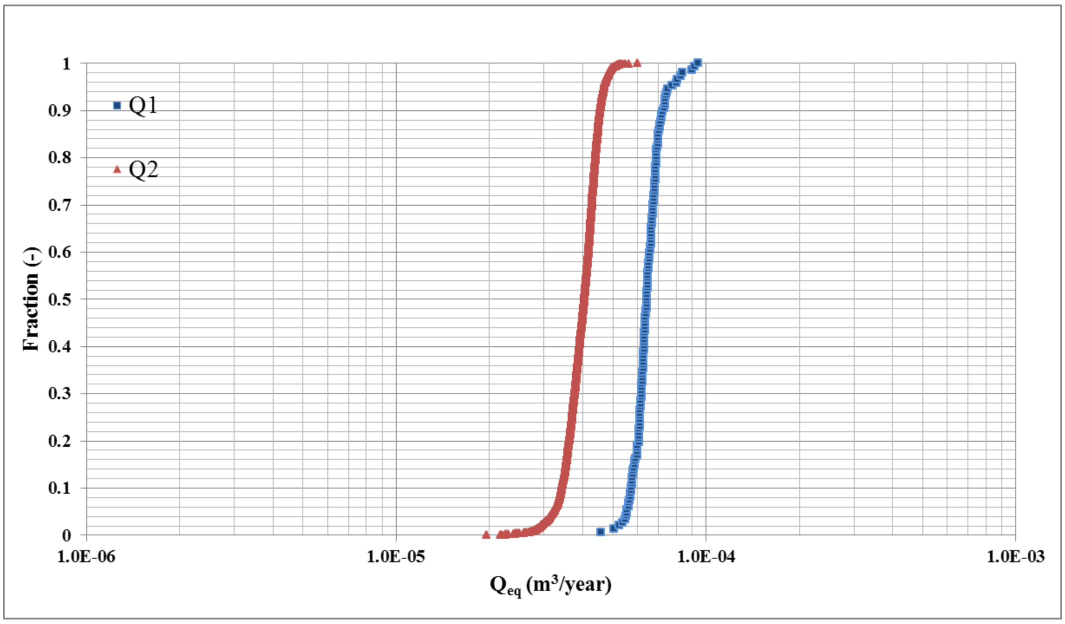

Figure 9-73: Cumulative distribution functions of equivalent flow rate for Q1 and Q2 paths of the regional model with sea-level -120 m.

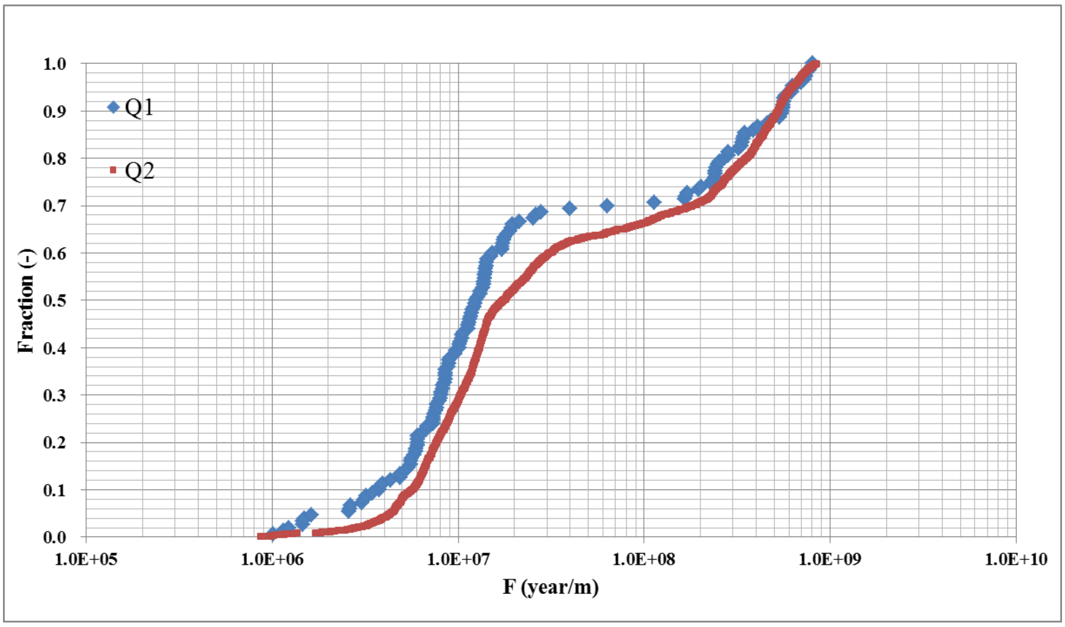

Figure 9-74: Cumulative distribution functions of flow related transport resistance for Q1 and Q2 paths of the regional model with sea-level -120 m.

Note: the top boundary is assigned to a specific head.

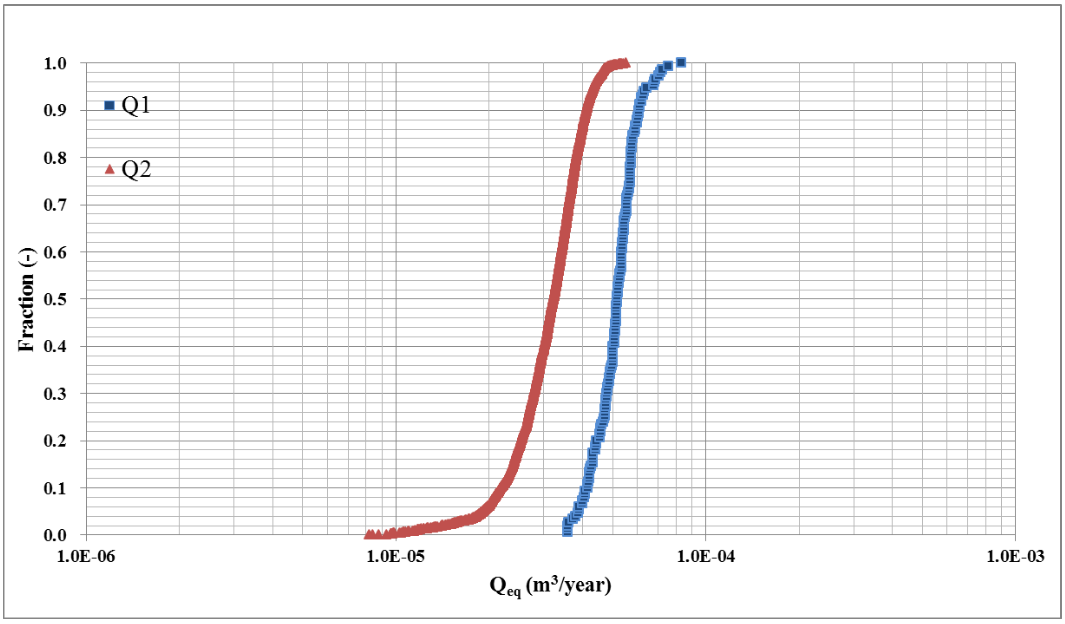

Figure 9-75: Cumulative distribution functions of equivalent flow rate for Q1 and Q2 paths of the regional model with sea-level -120 m.

Note: the top boundary is assigned to a specific head.

9.4.7. Geochemical Evolution

In the remaining glacial period (after post-closure 120000 years), the geochemistry condition of the repository including salinity distribution, groundwater composition, and ionic concentration, will be influenced by climate evolution and the corresponding sea-level changes.

According to Section 9.4.6, the reference case will transfer from this island to coastal land in the remaining glacial period (after post-closure 120,000 years), and the impact from seawater will be weaker. After post-closure 16,700 years (sea-level -20 m), seawater and freshwater interface will be far from the repository, and the impact from seawater will be insignificant. It can be assumed that after post-closure 16,700 years, the repository will be mainly surrounded by freshwater in the remaining cycle.

Currently, a hydrochemical model for the assessment has not been well established yet. According to the assumption of hydrogeological evolution in Section 9.4.6, the characteristics of groundwater were assumed to be the same as the average of characteristics of global rivers. PHREEQC was used to analyze chemical species distribution, TDS, ionic strength, pH, and concentration of potassium, sulfide, and iron. The assessment results are shown in Table 9-23.

The assessment results show that TDS in the surrounding environment of the repository will be around 1.05 g/L, the salinity will be about 0.0105%, and the pH value will be 7. These indicate that the requirements related to pH value and TDS (safety function R1) can be fulfilled in this period. Also, the results show that the concentration of hydrogen sulfide ion will be lower than 10^{-4} M, which meets the requirements of safety function R1 ($[HS^{-}] < 3$ mg/L$\approx 10^{-4}$ M); but the ionic strength is likely to be low (below 8 mM) which might lead to colloid release of the buffer and the backfill. For a detailed assessment of the impact, please refer to Section 9.4.8.

Table 9-23: Evaluation results of TDS, ionic strength, pH, and the concentration of sulfide and iron.

	TDS (g/L)	**Ionic strength (mM)**	**pH**	**$[HS^{-}]$ (mole/L, M)**	**$[Fe^{+2}]$ (mole/L, M)**	**$[Fe^{+3}]$ (mole/L, M)**
River water average	1.05	1.40	7	6.05×10^{-5}	2.01×10^{-7}	3.77×10^{-27}

9.4.8. Impact on the Buffer and Backfill

According to Section 9.3.8 and Section 9.3.9, during the remaining glacial period after closure (post-closure 120,000 years), the buffer and the backfill should be fully saturated. The average swelling pressure in the disposal tunnels and deposition holes will be around 5 MPa and 1.5 MPa, respectively.

The saturated bentonite may be affected by expansion, erosion by seeping water, and settlement when fractures intersect the deposition holes. Presently, according to groundwater velocity (Section 9.4.6) and ionic strength (Section 9.4.7), when the sea-level is at 0 m, -20 m, and -120 m (Table 9-4, Table 9-24, and Table 9-25), assuming that the angle between the fracture and the horizontal is $\alpha = 45°$, estimation method in Section 9.3.9 was used to evaluate bentonite mass loss over time of the five deposition holes (DH-216, DH-812, DH-2110, DH-2632, DH-2633). The results are shown in Figure 9-76.

The results show that it takes 78,547 years (DH-216), 22,158 years (DH-812), 21,358 years (DH-2110), 12,537 years (DH-2632), and 11,661 years (DH-2633) to lose 1,200 kg of bentonite mass for each deposition hole, respectively. Among all, the bentonite loss rate of DH-2633 would be the largest, followed by DH-2632, DH-2110, DH-812, and DH-216. Advection will dominate the internal flow field of the deposition hole once the bentonite loses more than 1,200 kg. And this will also affect the erosion rate of the canister.

Table 9-24: Parameters used to evaluate mass loss of the bentonite at sea-level -20 m.

Deposition hole No.	Seeping water velocity (m/sec)	Ionic strength (mM)	Fracture aperture (m)
DH-216	1.84E-06	1.40	7.19E-06
DH-812	1.24E-06	1.40	1.16E-05
DH-2110	1.27E-06	1.40	1.21E-05
DH-2632	5.70E-07	1.40	2.09E-05
DH-2633	5.29E-07	1.40	2.25E-05

Table 9-25: Parameters used to evaluate mass loss of the bentonite at sea-level -120 m.

Deposition hole No.	Seeping water velocity (m/sec)	Ionic strength (mM)	Fracture aperture (m)
DH-216	1.16E-06	1.40	7.17E-06
DH-812	6.85E-07	1.40	1.16E-05
DH-2110	7.556E-07	1.40	1.21E-05
DH-2632	4.28E-07	1.40	2.09E-05
DH-2633	3.76E-07	1.40	2.25E-05

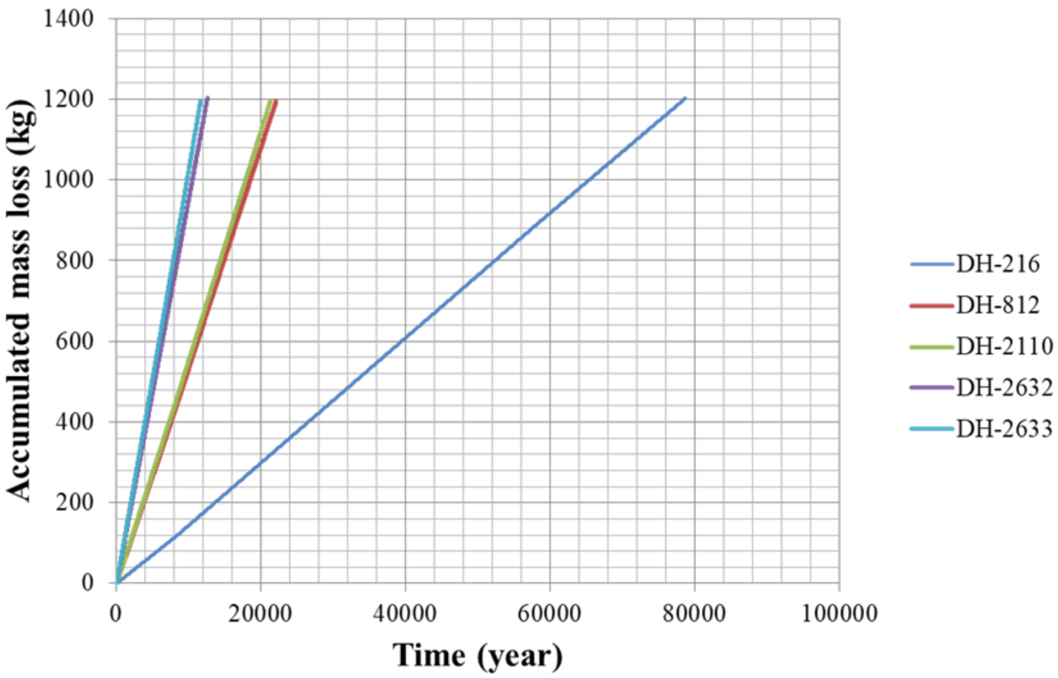

Figure 9-76: Mass loss of the bentonite versus time after closure.

9.4.9. Impact on the Canister

Containment safety functions of the canisters include providing a barrier against corrosion (Can1), withstanding isostatic load (Can2), and withstanding shear force (Can3), as described in Section 7.3. During the remaining glacial period after closure (post-closure 120,000 years), thermal, hydrological, mechanical, and chemical conditions of the repository continue to evolve, which may affect the containment safety functions of the canisters. The following evaluation was implemented for the assessment of the possible impact on the canisters: (1) the canister is subjected to uneven isostatic load after the buffer is saturated, (2) shear failure of the canister, and (3) corrosion of the canister.

(1) The canister is subjected to uneven isostatic load after the buffer is saturated:

As mentioned in Section 9.3.13, the swelling pressure of the saturated buffer may have a mechanical impact on the canister in a uniform manner. Other mechanical impacts on the canister may also occur due to the following reasons: (i) groundwater seeps into the deposition hole causing uneven water absorption. Therefore, the swelling pressure of the buffer is distributed unevenly. (ii) Density of the buffer is unevenly distributed because of the squeezing of depressions or protrusions from collapse or peeling of the porous rock layer surface. (iii) Other environmental factors causing the density of the buffer to distribute unevenly, therefore inducing an unevenly distributed swelling pressure.

If the canister is affected by uneven swelling pressure due to the aforementioned factors, the following three cases were analyzed: (i) the deposition hole was cylindrical (as shown in Figure 9-46, δ_1=0 mm and stress value was 7.50 MPa, and δ_2=0 mm and stress value was 5.83 MPa) and subjected to uneven isostatic load due to uneven saturation. (ii) The deposition hole was banana-shape (as shown in Figure 9-46, δ_1=8 mm and stress value was 6.86 MPa, and δ_2=0 mm and stress value was 4.12 MPa) due to over-excavation or collapse of rocks during excavation. The canister was subjected to uneven isostatic load caused by uneven saturation. (iii) The deposition hole was banana-shaped (as shown in Figure 9-46, δ_1=8 mm and stress value was 7.82 MPa, and δ_2=33 mm and stress value was 3.73 MPa) due to over-excavation or collapse of rocks during excavation and also rock formation of the inner wall of the deposition hole. The canister was subjected to uneven isostatic load caused by uneven saturation.

The stress distribution of the cast iron lining and copper shell of the canister are shown in Figure 9-49 to Figure 9-51 and Table 9-7. The maximum stress caused by uneven saturation on the cast iron lining would be 106.7 MPa which does not exceed the failure criterion of the material.

(2) Canister failure due to shear displacement:

The canister may be affected by rock shear displacement during the remaining glacial period after closure (post-closure 120,000 years). Relevant discussion on the failure of the canister due to shear displacement can be found in Section 9.4.5. According to the analysis results, the relation between the shear failure rate of the canister caused by fault source and diffuse seismicity earthquakes and the time after closure is shown in Figure 9-56. Among them, the earliest possible time for canister failure due to shear displacement will be about 230,000 years after closure, and the occurrence rate will be about 1 in a million. That is, during the remaining glacial period after closure (post-closure 120,000 years), the probability of canister failure due to shear displacement will be extremely low. At the time of one million years after closure, the total probability of canister failure due to shear displacement will be about one in three thousandth.

(3) Corrosion of the canister:

As described in Section 9.3.13, during the remaining glacial period after closure (post-closure 120,000 years), oxygen in the pores of buffer and backfill will all be consumed, and the repository will be an oxygen-free environment. At the same time, the bentonite will be fully saturated. The main corrosive agent in the repository will be sulfide, and the possible source of sulfide will be sulfide ions in groundwater. Primary corrosion products of the corrosion will be copper sulfide and hydrogen.

According to the analysis results, maximum corrosion depths of the copper shell of the canisters due to the corrosive agents in aerobic and anaerobic environments are shown in Table 9-13 and Table 9-14, respectively. From the analysis results, it can be seen that the maximum corrosion depth caused by corrosive agents such as pyrite and sulfate-reducing bacteria will be about 0.408 mm in the aerobic environment.

When possible uncertainties in the manufacturing process, general corrosion and local corrosion caused by limited corrosion sources, and corrosion caused by existing sulfides in the groundwater are taken into account, the copper shell of the canisters is expected to have a thickness of about 36.8 mm after post-closure 1,000,000 years. The safety function of Can1 and the integrity of the canisters can therefore be maintained.

9.4.10. Evolution of Other Parts of the Repository

The analyses of evolution in this report have been mainly focused on those directly related to safety functions (such as canister, buffer, backfill, and geosphere). Assessment of the evolution of other parts of the repository will be performed in the future based on international literature (SKB, 2011).

9.4.11. Safety Functions at the End of the Remaining Glacial Period

According to Section 9.4.1 to Section 9.4.10, canister, buffer, backfill, and geosphere safety function evolution is compiled in Table 9-26 to Table 9-28.

Can3 and R1 might be compromised during evolution. Therefore, the impact on containment safety functions is discussed in Chapter 11 and is regarded as the basis for the subsequent retardation safety functions evaluation. However, detailed research on Buff3 has not been done yet.

Table 9-26: Safety functions of the canister during the remaining glacial period.

Safety function	Safety function indicator	Safety function indicator criteria	Evolution during the remaining glacial period
Can1. provide barrier against corrosion	Copper shell thickness	> 0 cm	The analysis results show that the copper shell thickness of the canisters still has 36.8 mm and this safety function can be maintained under long-term corrosion over the safety assessment timescale. Therefore, the safety function can also be maintained.
Can2. withstand isostatic load	Isostatic load	< 50 MPa	The maximum uniform isostatic load of the canister would be 13.23 MPa, and the safety function can be maintained. In addition, if the canisters are subjected to non-uniform isostatic load caused by over-excavation or rock collapse, the stress on the cast iron lining will not reach the yield stress, and the integrity of the canisters can be maintained.
Can3. withstand shear force	Shear displacement	> 5 cm	The analysis results show that possible sources of earthquakes are fault sources and diffuse seismicity over the safety assessment timescale. The cumulative fracture shear displacement may exceed 5 cm, and the safety function will not be maintained (which might cause the canister to fail). The earliest possible time for cumulative fracture shear displacement to exceed 5 cm will be about 230,000 years after the closure. Over the safety assessment timescale, the failure probability of the canisters due to shear force will be about 1/3000.

Table 9-27: Safety functions of the buffer/backfill during the remaining glacial period.

Safety function	Safety function indicator	Safety function indicator criteria	Evolution during the remaining glacial period
Buff1. limit advection	**(a) Hydraulic conductivity**	**<10^{-12} m/s**	The earliest time that the buffer will lose more than 1,200 kg will be around 11,600 years after closure. As a consequence, the hydraulic conductivity will increase, and the safety function cannot be guaranteed.
	(b) Swelling pressure	**> 1 MPa**	The buffer may be eroded by groundwater flow during this period, but it can redistribute by its swelling characteristics, and the eroded part can thereby be healed. The average swelling pressure will be about 4 MPa after the buffer is refilled, and the safety function can be maintained.
Buff2. limit microbial activity	**Swelling pressure**	**> 2 MPa**	The earliest time that the buffer will lose more than 1,200 kg will be around 11,600 years after closure. Local swelling pressure will be lower than 2 MPa, and the safety function cannot be guaranteed.
Buff3. damp rock shear force	**Density**	**< 2,050 kg/m^3**	Creeping of the host rock may affect the geometry of the deposition holes, which may cause the buffer to squeeze and increase its density. Detailed assessment has not been done yet.
Buff4. resist transformation	**Temperature**	**< 100 ℃**	The canister spacing is set to 9 m and the disposal tunnel spacing is set to 40 m currently. According to the layout, buffer temperature will reach its peak value around ten years after the closure (lower than 100 ℃). And the temperature will continue to drop to the natural rock temperature (33.3 ℃). The safety function can be maintained.
Buff5. prevent canister sinking	**Swelling pressure**	**> 0.2 MPa**	According to the analysis results, the buffer can provide a swelling pressure of more than 2 MPa. The safety function can be maintained. Sinking of the canister due to its own weight might slightly compact the buffer under the canister, but the amount will not exceed 2.4×10^{-2} cm.
Buff6. limit pressure applied to the canisters and rock	**(a) Swelling pressure**	**< 10 MPa**	According to the analysis results, the maximum swelling pressure of the buffer will be 8.23 MPa. Safety function Buff6 can be maintained.

	(b) Temperature	**> -2.5 ℃**	According to the analysis results, the maximum temperature of the buffer will not exceed 100 ℃. As decay heat in the canister continues to decrease, the temperature of the buffer will gradually approach the temperature of the host rock (about 33.3 ℃) after hundreds of years. The safety function can be maintained.
BF1. limit buffer expansion	**Swelling pressure of backfill**	**Not too low**	The backfill can counteract buffer expansion. The average swelling pressure will be about 5 MPa. And the safety function can be maintained.

Table 9-28: Safety functions of the geosphere during the remaining glacial period.

Safety function	**Safety function indicator**	**Safety function indicator criteria**	**Evolution during the remaining glacial period**
R1. provide preferred chemically conditions	(a) Reducing conditions	Eh limited	According to the analysis results, the surrounding groundwater will be mainly composed of freshwater (pH: 7) under different sea-levels. Generally, the ionic strength will be lower than 8 mM and the concentration of HS^{-} will be lower than 10^{-4} M. In general, the safety function cannot be maintained.
	(b)Salinity	TDS<35 g/L	
	(c)Ionic strength	$\Sigma q[Mq^{+}]GW > 8$ mM	
	(d) Concentrations	$[NO_2^{-}]<10^{-3}$ mol/L $[HS^{-}]<3$ mg/L≈10^{-4} M $[K^{+}]<0.1$ mol/L	
	(e) pH	5<pH< 11	
	(f) Avoid chloride-assisted corrosion	pH > 4; $[Cl^{-}] < 2M$	
R2. provide preferred hydrogeologic and transport conditions	(a) Transport resistance in fractures (F)	>10,000 yr/m	Minimum transport resistance of Q1 will be around 10^{6} yr/m, and the equivalent flow rate will be 0.084 L/m. The safety function can be fulfilled.
	(b) Equivalent flow rate (Q_{eq})	$<\mathbf{1 \times 10^{-4}}$ m^3/yr	
R3. provide mechanically stable environment	GW pressure	Limited	The groundwater will flow from the north-west to the south-east on a regional scale; besides, the flow field will also be affected by the neighboring mountain area on a relatively small scale.
R4. provide preferred thermal environment	Temperature	-2.5℃ to 100℃	Temperature of the host rock will be about 33.3 ℃. The safety function can be maintained.

9.5. The Subsequent Glacial Cycles

The climatic evolution of the reference site is simply assumed that the first glacial cycle will repeat until the end of the safety assessment timescale. A single glacial cycle takes about 120,000 years, therefore, there will be about eight cycles over the entire assessment period.

Reversible processes like thermal, hydrogeological and geochemical evolution of the bedrock will also change periodically along with the dominant external factors. Among these, thermal evolution for the subsequent glacial cycles in the near-field will be affected by natural processes instead of decay heat.

On the other hand, impact from irreversible processes such as buffer erosion, canister corrosion and possible earthquake-induced effects is expected to accumulate over the cycles. At the end of the safety assessment timescale, the possible impact might be eight times greater than the initial. The relevant impact is listed as the following:

(1) For buffer erosion, eight times erosion of the erosion in the first glacial cycle is expected at the end of the safety assessment timescale.

(2) The evaluation results of canister corrosion (Table 9-13 and Table 9-14) show that under the influence of buffer erosion, the copper thickness can maintain its function (copper thickness around 36.8 mm). And the canisters will not fail due to corrosion over the safety assessment timescale.

(3) According to Section 9.4.5 (Figure 9-56), the canister failure rate due to multiple earthquakes emerge at 230 thousand years post-closure and increase to 3×10^{-4} at the end of the safety assessment timescale.

9.5.1. Safety Functions at the End of the Assessment Timescale

The compilation of canister, buffer, backfill, and geosphere safety functions evolution until the end of the safety assessment timescale is shown in Table 9-29 to Table 9-31.

Table 9-29: Safety functions of the canister during the remaining glacial period.

Safety function	Safety function indicator	Safety function indicator criteria	Evolution during the subsequent glacial cycles
Can1. provide barrier against corrosion	**Copper thickness**	**> 0 cm**	The analysis results show that the copper shell thickness of the canisters still has 36.8 mm and this safety function can be maintained under long-term corrosion over the safety assessment timescale. Therefore, the safety function can also be maintained.
Can2. withstand isostatic load	**Isostatic load**	**< 50 MPa**	The maximum uniform isostatic load of the canister would be about 13.23 MPa, and the safety function can be maintained. In addition, if the canisters are subjected to non-uniform isostatic load caused by over-excavation or rock collapse, the stress on the cast iron lining will not reach the yield stress, and the integrity of the canisters can be maintained.
Can3. withstand shear force	**Shear displacement**	> **5 cm**	The analysis results show that possible sources of earthquakes are fault sources and diffuse seismicity over the safety assessment timescale. The cumulative fracture shear displacement may exceed 5 cm, and the safety function will not be maintained (which might cause the canister to fail). The earliest possible time for cumulative fracture shear displacement to exceed 5 cm will be about 230,000 years after the closure. Over the safety assessment timescale, the failure probability of the canisters due to shear force will be about 1/3000.

Table 9-30: Safety functions of the buffer/backfill during the remaining glacial period.

Safety function	Safety function indicator	Safety function indicator criteria	Evolution during the subsequent glacial cycles
Buff1. limit advection	**(a) Hydraulic conductivity**	**<10^{-12} m/s**	The earliest time that the buffer will lose more than 1,200 kg will be around 11,600 years after closure. As a consequence, the hydraulic conductivity will increase, and the safety function cannot be guaranteed.
	(b) Swelling pressure	**> 1 MPa**	The buffer may be eroded by groundwater flow during this period, but it can redistribute by its swelling characteristics, and the eroded part can thereby be healed. The average swelling pressure will be around 4 MPa after the buffer is refilled, and the safety function can be maintained.
Buff2. limit microbial activity	**Swelling pressure**	**> 2 MPa**	The earliest time that the buffer will lose more than 1,200 kg will be around 11,600 years after closure. Local swelling pressure will be lower than 2 MPa, and the safety function cannot be guaranteed.
Buff3. damp rock shear force	**Density**	**< 2,050 kg/m^3**	Creeping of the host rock may affect the geometry of the deposition holes, which may cause the buffer to squeeze and increase its density. Detailed assessment has not been done yet.
Buff4. resist transformation	**Temperature**	**< 100 ℃**	The canister spacing is set to 9 m and the disposal tunnel spacing is set to 40 m currently. According to the layout, buffer temperature will reach its peak value around ten years after the closure (lower than 100 ℃). And the temperature will continue to drop to the natural rock temperature (33.3 ℃). The safety function can be maintained.
Buff5. prevent canister sinking	**Swelling pressure**	**> 0.2 MPa**	According to the analysis results, the buffer can provide a swelling pressure of more than 2 MPa. The safety function can be maintained. Sinking of the canister due to its own weight might slightly compact the buffer under the canister, but the amount will not exceed 2.4×10^{-2} cm.
Buff6. limit pressure applied to the canisters and rock	**(a) Swelling pressure**	**< 10 MPa**	According to the analysis results, the maximum swelling pressure of the buffer will be 8.23 MPa. Safety function Buff6 might be compromised.

Safety function	Safety function indicator	Safety function indicator criteria	Evolution during the subsequent glacial cycles
	(b) Temperature	**> -2.5 ℃**	According to the analysis results, the maximum temperature of the buffer will not exceed 100 ℃. As decay heat in the canister continues to decrease, the temperature of the buffer will gradually approach the temperature of the host rock (about 33.3 ℃) after hundreds of years. The safety function can be maintained.
BF1. limit buffer expansion	**Swelling pressure**	**Not too low**	The average swelling pressure of the buffer will be about 1.5 MPa. And the safety function can be maintained.

Table 9-31: Safety functions of the geosphere during the remaining glacial period.

Safety function	Safety function indicator	Safety function indicator criteria	Evolution during the subsequent glacial cycles
R1. provide preferred chemically conditions	**(a) Reducing conditions**	**Eh limited**	According to the analysis results, the surrounding groundwater will be mainly composed of freshwater (pH: 7) under different sea-levels. Generally, the ionic strength will be lower than 8 mM and the concentration of HS^{-} will be lower than 10^{-4} M. In general, the safety function cannot be maintained.
	(b)Salinity	**TDS<35 g/L**	
	(c)Ionic strength	**$\Sigma q[Mq^{+}]GW > 8$ mM**	
	(d) Concentrations	**$[NO_2^{-}]<10^{-3}$ mol/L $[HS^{-}]<3$ mg/L$\approx 10^{-4}$ M $[K^{+}]<0.1$ mol/L**	
	(e) pH	**5<pH< 11**	
	(f) Avoid chloride assisted corrosion	**pH > 4; $[Cl^{-}] < 2$M**	
R2. provide preferred hydrogeologic and transport conditions	**(a) Transport resistance in fractures (F)**	**>10,000 yr/m**	Minimum transport resistance of Q1 will be around 10^{6} yr/m, and the equivalent flow rate will be 0.084 L/m. The safety function can be fulfilled.
	(b) Equivalent flow rate (Q_{eq})	**$<1 \times 10^{-4}$ m^3/yr**	
R3. provide mechanically stable environment	**GW pressure**	**Limited**	The groundwater will flow from the north-west to the south-east on a regional scale; besides, the flow field will also be affected by the neighboring mountain area on a relatively small scale.
R4. provide preferred thermal environment	**Temperature**	**-2.5°C to 100°C**	Temperature of the host rock will be about 33.3 °C. The safety function can be maintained.

9.6. Global Warming

9.6.1. External Factors

Natural-driven force and man-made driven forces will cause various possible development for future climate. According to the model evaluation of future climate evolution (IPCC, 2007; Kjellstrom, T. et al., 2009), it can be seen that increase in greenhouse gases (mainly CO_2) may cause future global temperature rise and aggravate impact from global warming.

According to the IPCC 5th assessment report, it is estimated that global average rainfall change and global temperature change under global warming are roughly linearly related. The rainfall will increase by 1% to 3% in every 1 ℃ increase in the temperature (Figure 9-77). RCP8.5 has the highest degree of global warming among all, and the increase in rainfall is also the largest. If the climate evolution of the reference case follows global warming evolution, the rainfall may increase along with the increase in global average temperature.

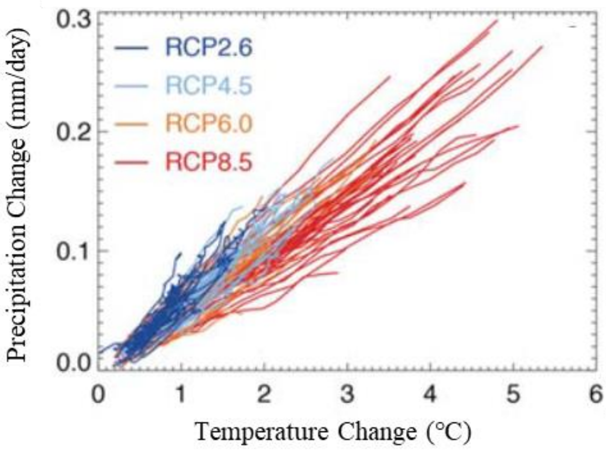

Figure 9-77: Rainfall versus temperature changes under global warming.
Reference: Chen et al. (2018) and Zhou et al. (2017).

9.6.2. Biosphere

According to the Intergovernmental Panel on Climate Change 4th assessment report (IPCC, 2007), the global average temperature might increase about 4℃ (2.4℃ to 6.4℃) before 2100 under the conservative assumption of the CO_2 concentration.

Global warming mainly affects the surface system. Although the deep geological repository system will not be affected directly, the variation of the external factors will indirectly affect the safety functions of the repository system.

Under the effect of global warming, the rising of sea-level causes a decrease in land area, so the probability of the radionuclides released to the terrace is reduced. Therefore, it is assumed that the radionuclides will release into the ocean as same as the initial period after closure.

9.6.3. Evolution of the Repository

The following describes the geochemical evolution, buffer and backfill evolution, and canister evolution of the repository under global warming evolution:

(1) Geochemical evolution

The geochemical evolution around the repository is mainly related to coastline migration of the reference site and changes in groundwater flow caused by rainfall. However, since it is assumed that only surface temperature will increase under global warming evolution and other conditions will remain the same as the ones of the initial period after closure (post-closure 1,000 years), it is expected that groundwater flow will not change significantly, and chemical conditions around the repository will not be affected.

(2) Buffer and backfill evolution

As mentioned earlier, since only the surface temperature of the repository is expected to increase during global warming evolution and other conditions remain the same as the ones of the initial period after closure (post-closure 1,000 years), the evolution of the buffer and the backfill is also presumed to be similar to the one of basic evolution.

(3) Canister evolution

The corrosion rate of canisters is expected to be the same as the one during the initial period after closure (post-closure 1,000 years). Therefore, it is expected that during the prolonged subtropical climate period in global warming evolution, the impact on corrosion of the canisters is very small and can be ignored.

The probability of canister failure due to shear displacement caused by earthquakes is proportional to the evolution time of the repository. Therefore, it is expected that there will be no additional impact on shear displacement caused by earthquakes during prolonged subtropical climate period in global warming evolution. During this period, the probability of canister failure due to shear displacement caused by earthquakes will be the same as the failure probability of basic evolution.

9.6.4. Safety Function Indicators under the Influence of Global Warming

From the analyses in Section 9.6.3, it can be inferred that the safety function indicators at the end of prolonged subtropical climate (50,000 years) in global warming evolution will be very similar to the ones of the initial period after closure (post-closure 1,000 years) described in Section 9.3. Therefore, it will not be described further.

9.7. Conclusion of the Evolution Analysis

According to the evaluation results, the safety functions can be maintained during the initial period after closure (post-closure 1,000 years). However, in the remaining glacial period after closure (post-closure 120,000 years), Can3 might be jeopardized due to earthquake-induced shear displacement and the canister might fail, and Buff1 might also be jeopardized due to buffer loss from erosion and the transport mechanism changes from diffusion to advection in the buffer. Moreover, the requirements of R1 for water chemistry might not be fulfilled too.

The overall impact on the repository from a failure of the safety functions will be quantified in Chapter 11. And in the subsequent glacial cycles, it is assumed that no other safety functions will be jeopardized.

10. Selection of Scenarios

10.1. Introduction

Scenario development is the key issue of safety assessment because it can capture uncertainty and quantify its impact, verify the maintenance of the safety functions over the safety assessment timescale, and quantify possible radiation impact on the repository (PAMINA, 2011). In the development of scenarios, the uncertainty of scenarios and evolution needs to be considered. The repository might have various evolution throughout 1 million years. In safety assessment, a set of scenarios that is appropriate to represent the evolution of the repository should be developed. It can constitute key elements in the safety case, and be the basis for the assessment of post-closure safety and management of uncertainty.

In the safety assessment in which the long-term safety of the repository is discussed, scenarios are divided into four categories according to the NEA report (NEA, 2016) as the following:

(1) Design-basis evolution scenarios: assess the radiological impact of the most likely evolution in the following 1 million years after closure based on the design of the repository and characteristics of the host rock.

(2) Non-design-basis evolution scenarios: events/processes that are listed in the reference case FEPs list but are not considered in the design of the repository. Once these FEPs occur or under their continuous influence, the long-term safety of the repository might be jeopardized. Therefore, non-design-basis evolution scenarios are developed based on these FEPs for the evaluation of the potential impact on the long-term safety of the repository and possible radiation influence over 1 million years.

(3) Future human action scenarios: social and technological development of human beings in the future is difficult to predict. Therefore, a stylised method is used, and representative cases are selected for the assessment.

(4) What-if scenarios: extremely unreasonable or impossible assumptions are used for the evaluation. The safety functions of the

remaining barriers are assessed, assuming the safety functions of one or more barriers are jeopardized to illustrate the robustness of the disposal system.

10.2. Design-Basis Evolution Scenarios

According to the ICRP-122 report (ICRP, 2013), design-basis evolution is developed based on the possible evolution of the repository over 1 million years according to the engineering design and the host rock condition. Design-basis evolution can be used to evaluate potential exposure dose under normal conditions. This kind of exposure can be regarded as planned exposure and can be regulated by risk constraints or dose constraints according to the suggestion of ICRP. Therefore, the definition of design-basis evolution in the ICRP-122 report was referred to for the development of the design-basis evolution scenarios in this report. The exposure in design-basis evolution scenarios is regarded as planned exposure, and the assessment results should be lower than the dose limits of the regulations.

Design-basis evolution scenarios can also demonstrate the uncertainty of expected behavior/situation and evolution of the repository over a long period of time. The purpose of developing design-basis evolution scenarios is to reasonably demonstrate that possible scenarios of the repository over a long period of time are taken into account when designing the repository and implementing the safety assessment. Therefore, the potential radiation impact on humans and the biosphere from the long-term evolution of the repository can be evaluated. Adjustments to the engineering design of the repository can also be made according to the evaluation results of design-basis evolution scenarios.

In the safety assessment of this report, the development of the design-basis evolution scenarios was implemented using mainly the safety function analysis method (top-down approach) and also the FEPs analysis method (bottom-up approach). Since the safety functions of each component of the repository are important indicators for the performance of the repository, the design of the repository should be able to maintain safety functions for over 1 million years. Therefore, the design-basis evolution scenarios were developed according to the following steps. First, key issues that might affect the safety of the repository were identified based on the safety functions of the canister. Then, a set of FEPs that might have an impact on the safety function (key issue) was identified from the reference case FEPs list. Interaction between the set of FEPs and other FEPs or safety functions was analyzed. Finally, scenarios were developed by correlating the FEPs and safety functions. The flowchart of the development is shown in Figure 10-1.

A systematic scenario development flowchart was also used to illustrate the thoroughness of the scenarios in safety assessment, so that scenarios and assessment cases could be developed thoroughly, important impact factors would not be missed, and communication with relevant personnel or stakeholders would be facilitated.

According to the containment safety functions of the canister in Section 7.3 and the analysis results of canister evolution in Chapter 9: under the conditions of the reference case, the canister has a large margin to resist isostatic load (Can3). In the following 1 million years after closure, the canister is most likely to be damaged by the impact from corrosion and shear force. Therefore, the key issues of the design-basis evolution scenarios, which are canister failure due to corrosion and canister failure due to shear force. were identified according to safety functions Can1 and Can3.

10.2.1. Canister Failure due to Corrosion

Canister corrosion is one of the important issues in the evolution of the repository. The reason for corrosion of the canister might be the corrosive agent in groundwater, which contacts the surface of the copper shell of the canister for a long time resulting in long-term corrosion. Another possible reason for canister corrosion is that the surrounding environment of the repository might transform from a reduction environment to an oxidation environment due to disturbances, resulting in rapid corrosion of the copper shell of the canister. However, when the depth of the repository remains at the designed depth and is over 400 m, the surrounding groundwater environment will be unlikely to transform into an oxidation environment. Therefore, corrosion is not considered in the design-basis evolution scenario of this report and will be discussed in the non-design-basis evolution scenario.

The scenario development process of the canister corrosion failure issue is shown as follows:

(1) Climate evolution issues are first taken into account: evaluate whether hydrogeological conditions of the host rock and safety functions of the host rock and the buffer will be affected by the climate conditions of the scenario. For example, when the sea level changes and the fracture in the far-field is filled with groundwater, several variables of the geosphere might influence the safety functions of the geosphere and have an impact on the safety functions of the buffer subsequently.

    (a) Groundwater flow: if the groundwater flow rate is too high, piping erosion of the unsaturated buffer might occur after the repository is closed. This will lead to a decrease in buffer density, and the safety functions of the buffer might be jeopardized.

    (b) Groundwater salinity: if cation strength is less than the safety function indicator criteria for ionic strength of the geosphere, bentonite erosion might occur.

    (c) Groundwater composition: if there are harmful substances in the groundwater, the long-term stability of the buffer and the backfill will be significantly jeopardized.

(2) Assess whether the buffer can maintain its containment safety functions when the hydrogeological conditions are changed. If the buffer is eroded due to the above-mentioned reasons, the buffer will lose its ability to limit advection. Hence, groundwater will contact the canister more easily, and corrosion of the canister will be facilitated.

(3) Assess whether the canister can maintain safety function Can1 when the above-designed condition occur.
(4) If the canister is failed because of corrosion, evaluate the impact from retardation safety functions of the SNF and the buffer on radionuclide transport.
(5) When evaluating the safety functions of the barrier, the influence of relevant FEPs on the safety functions will be considered.

The whole scenario development process, including the interaction between the relevant FEPs and the safety functions, can be drawn as a scenario development flowchart (Figure 10-2). A simplified storyboard can also be seen in Figure 10-3. For the evaluation and calculation results of containment safety functions of the barrier, please refer to Chapter 11, and for the analysis of radionuclide transport after the canister fails because of corrosion, please refer to Chapter 12.

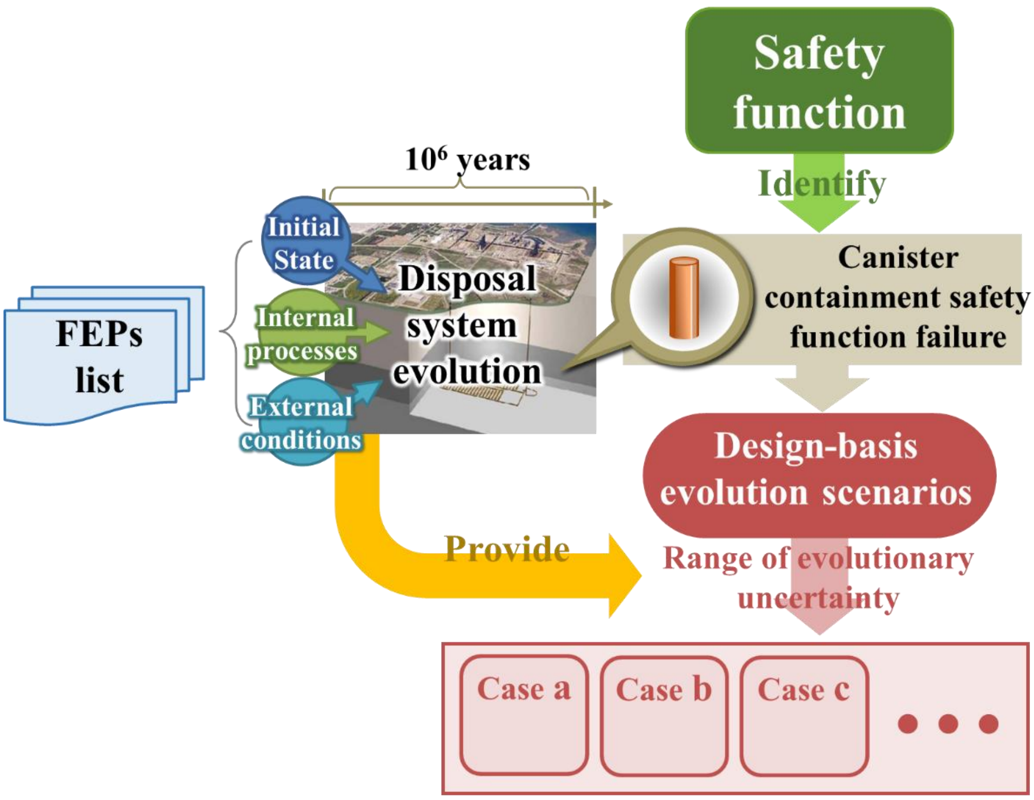

Figure 10-1: Establishment of design-basis evolution scenarios.

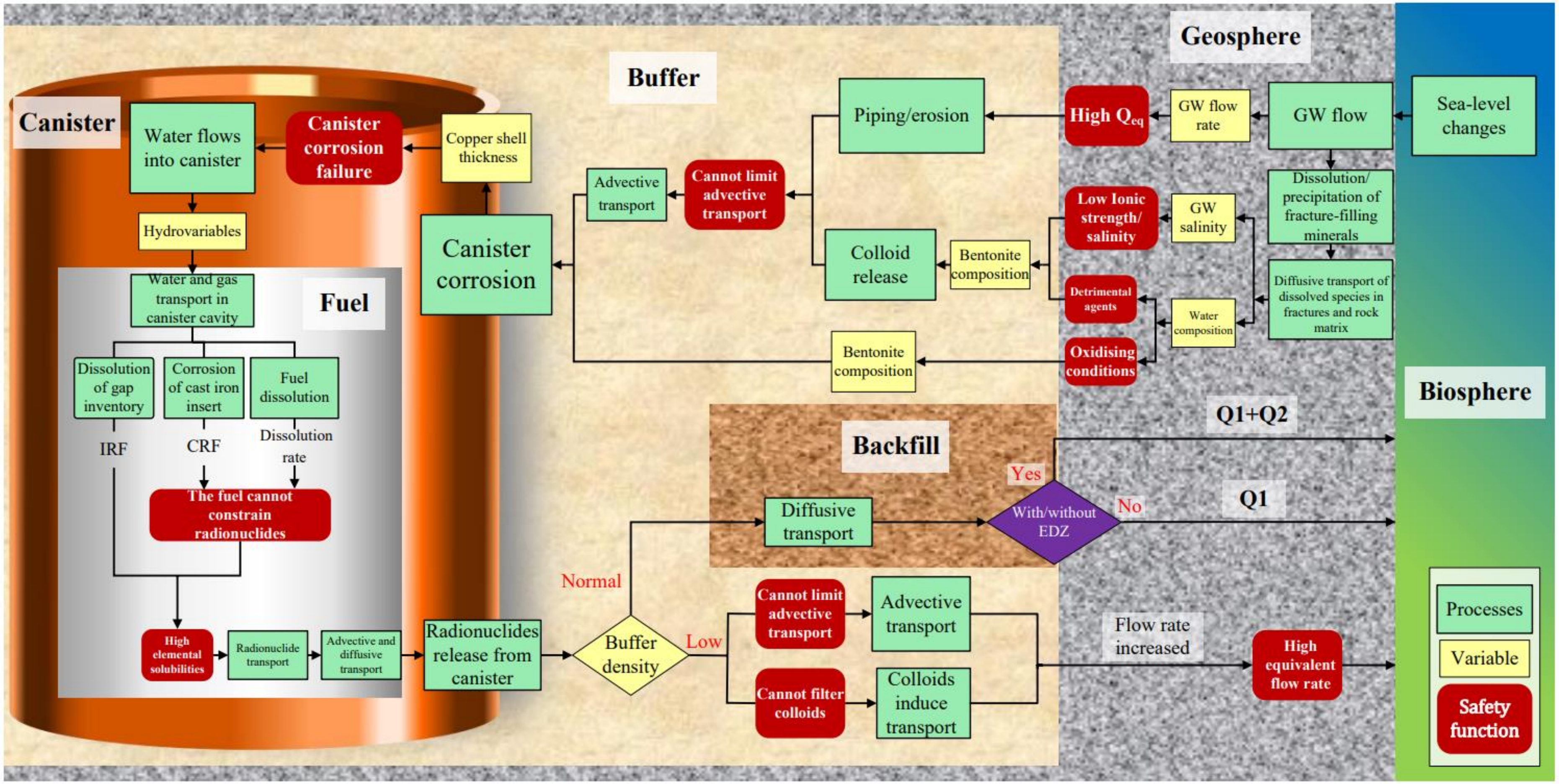

Figure 10-2: Flowchart of the development of canister failure due to corrosion.

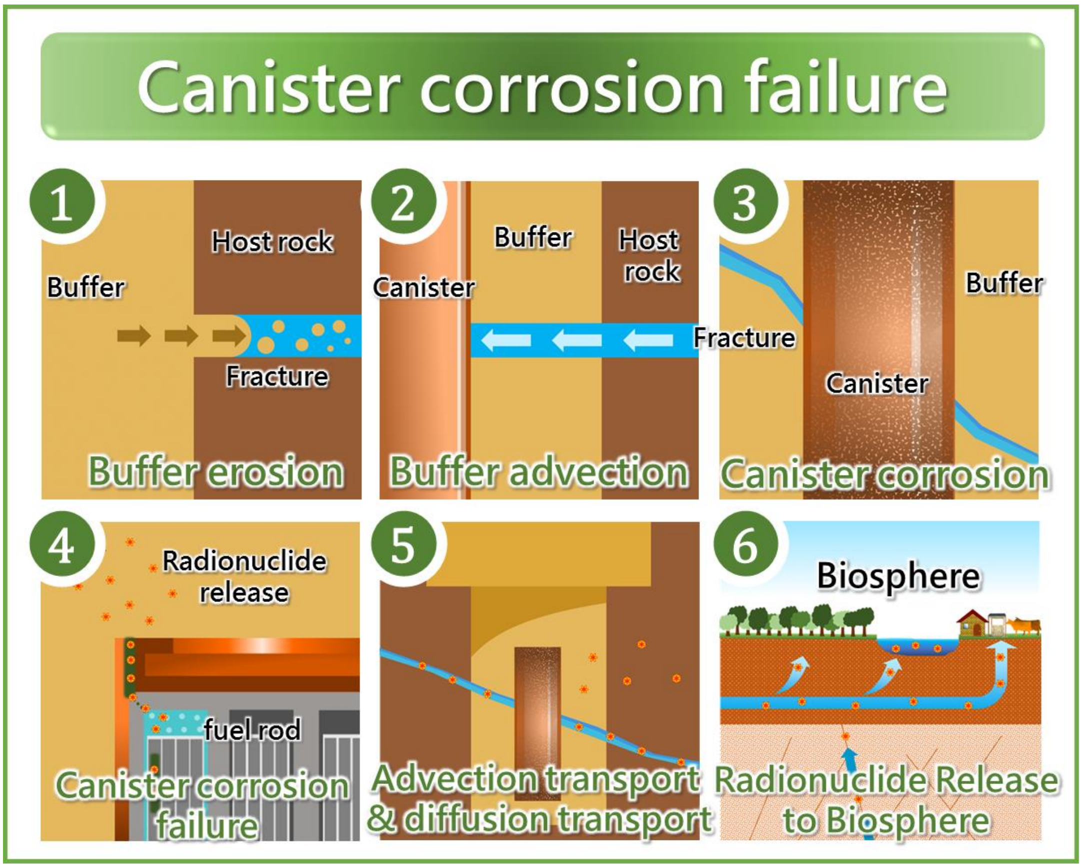

Figure 10-3: Storyboard of canister failure due to corrosion.

10.2.2. Canister Failure due to Shear Force

Taiwan is located at the junction of the Eurasian plate and the Philippine Sea plate. And earthquakes occur frequently. Earthquakes are one of the main reasons for shear force on the canister. In order to understand whether the design of the canister can resist shear force, so that radiological impact on humans from canister failure due to the shear force can remain under the requirements of the regulations, shear force issue was included in the design-basis evolution scenarios for evaluation. The assessment results of the shear force issue can also be fed back to the engineering design for better resistance of the canister against shear force.

The scenario development process of the canister shear force failure issue is shown as follows:

(1) Changes in hydrological conditions after fracture displacement are first taken into account: containment safety functions of the buffer might be influenced by the hydrological conditions of the host rock.

(2) When the fracture intersecting the canister has a displacement that exceeds 5 cm, and the safety function indicator criterion Can3 cannot be fulfilled, the canister would fail due to the influence of shear force. Evaluate the impact from retardation safety functions of the SNF and the buffer on radionuclide transport.

(3) When evaluating the safety functions of the barrier, the influence of relevant FEPs on the safety functions will be considered.

The whole scenario development process, including the interaction between the relevant FEPs and the safety functions, can be drawn as a scenario development flowchart (Figure 10-4). A simplified storyboard can also be seen in Figure 10-5. For the evaluation and calculation results of containment safety functions of the barrier, please refer to Section 11.7, and for the analysis of radionuclide transport after the canister is failed because of shear force, please refer to Section 12.6.

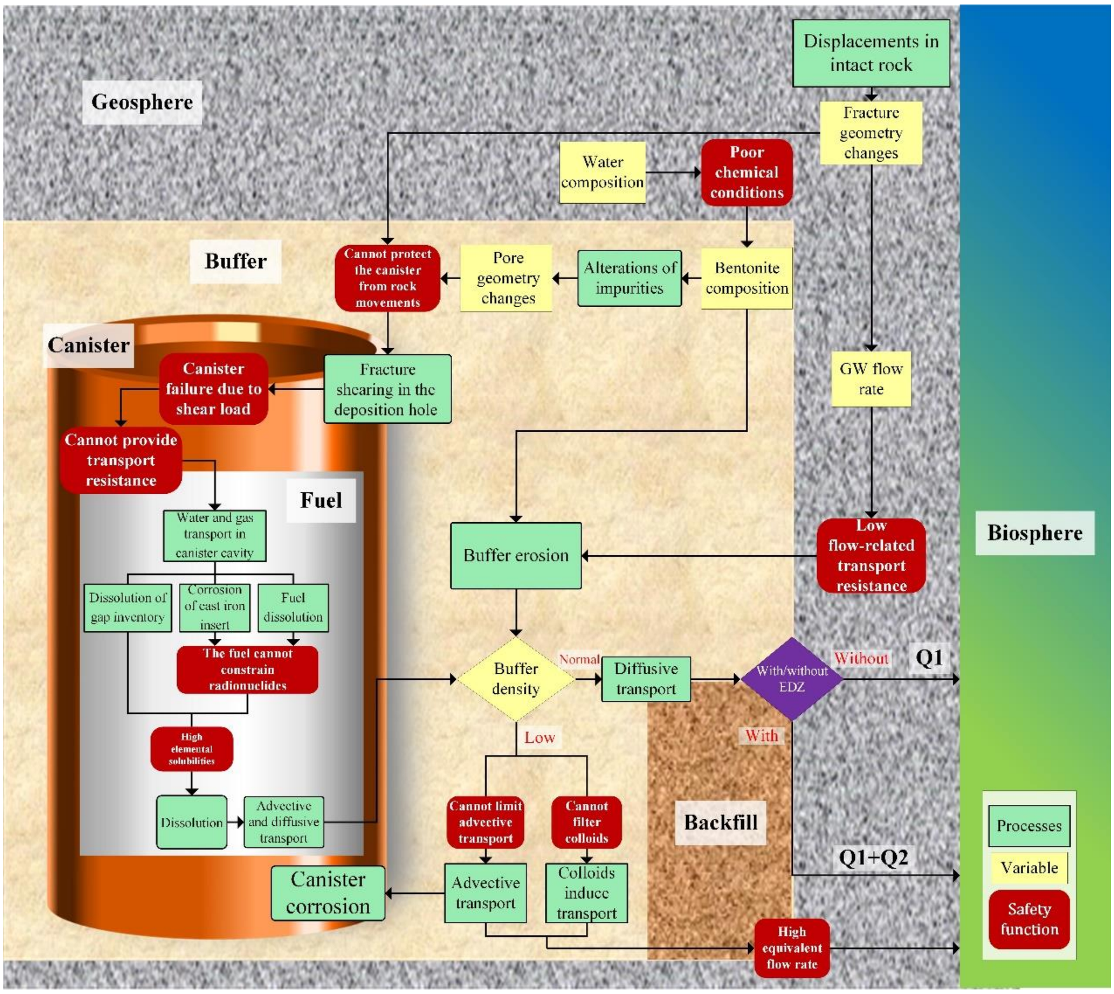

Figure 10-4: Flowchart of the development of canister failure due to shear force.

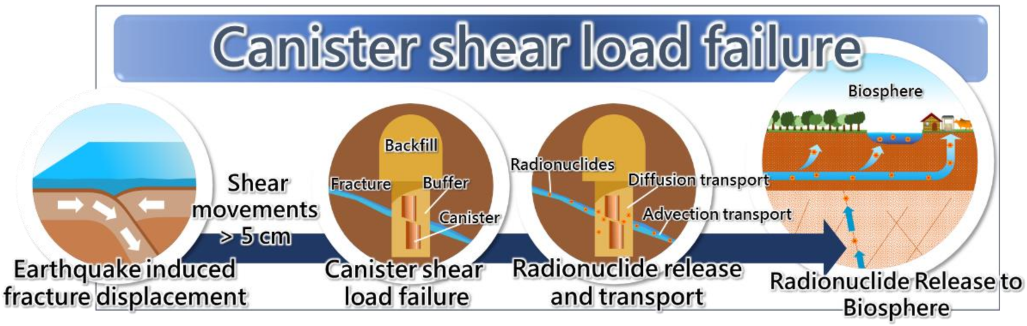

Figure 10-5: Storyboard of canister failure due to shear force.

10.3. Non-Design-Basis Evolution Scenarios

According to the ICRP-122 report, non-design-basis evolution is when a highly unlikely or extreme natural event results in significant exposure to humans or the environment over 1 million years after the repository is closed. Serious natural damage events that are not included in the design-basis evolution can be seen as emergency exposure and existing exposure. The impact of these events can be evaluated through typical or simplified methods during the design of the facility (ICRP, 2013).

Based on the definition of non-design-basis evolution in ICRP-122, FEPs that may have a potential impact on the safety of the repository were identified for the development of non-design-basis evolution scenarios and the assessment cases. According to the FEPs list of the reference case, large-scale geological processes, including strata uplift/subsidence and volcanic activity, are those that may affect the long-term safety of the repository. Therefore, non-design-basis evolution scenarios and relevant assessment cases were developed according to these FEPs, to evaluate their impact on the repository.

10.3.1. Uplifting and Denudation

Uplifting/denudation (TWLSGe05) is one of the processes that may affect the reference case in the FEPs list of the reference case. According to Section 5.3.2, disposal depth and safe distance from the biosphere might decrease under the influence of uplifting and denudation, and the isolation safety function provided by the designed depth of the repository might also be jeopardized. In addition, the long-term stability of the repository might also be jeopardized because of changes in the groundwater flow field and chemical properties around the repository. Therefore, uplifting/denudation was developed as one of the analysis cases of the non-design basis evolution scenario for further quantitative analysis.

10.3.2. Volcanism

As described in Section 5.3.3, if the repository is affected by volcanic activity, the groundwater flow rate might increase due to excessive earth temperature, thereby increasing the radionuclide transport rate. In addition, if magma associated with volcanic activity might intrude on the repository, groundwater might mix with magma or volcanic gases, thereby changing the chemical properties of the groundwater, and jeopardizing the safety functions of the multiple barriers system. Besides, the canister might fail because of the intruding magma. If the canister fails, radionuclides might mix with the eruptive materials and spread in the surface environment along with the eruption. This will eventually result in radiation impact on the potentially exposed group.

In accordance with the “Regulations on the Final Disposal of High-Level Radioactive Waste and Safety Management of the Facilities,” “Regulations on Siting of High-level Radioactive Waste Final Disposal,” and other relevant regulations (please refer to Section 1.4), areas with potential volcanic activity should be avoided for high-level radioactive waste repository sites. Therefore, the potential risk caused by volcanic activity is excluded in this report. However, Taiwan is located next to the Pacific Rim seismic belt; if newly-born volcanoes can be avoided is unknown, although existing volcanoes can be avoided by siting. Also, the impact of volcanic activity on the long-term safety of the repository cannot be ruled out completely. Hence, volcanism was developed as one of the analysis cases of the non-design basis evolution scenario for further analysis. And the possible radiological impact is discussed in Section 13.2.

10.4. Future Human Actions (FHA)

When evaluating the possible impact of future human actions on the repository, for it is difficult to predict future human behaviors and actions, a “stylised” approach (NEA, 2016) is usually adopted. No attempt is made to cover all possible scenarios, and no probability of occurrence is assigned to these scenarios. Instead, a representative set of cases will be evaluated based on current knowledge and experience and results of communication with the regulatory agency or between the regulatory agency and the facility applicant. In addition, due to the large uncertainty of future technology and social development, scenario assumptions are often made based on present knowledge, experience, and patterns of human actions (NEA, 1995; SSM, 2008).

According to Section 5.4, drilling is the only activity that may lead to penetration of the canister directly, and have an impact on humans and the environment furtherly. Therefore, drilling was developed as the analysis case of future human actions according to the “stylised” approach for assessment. It is assumed that all relevant data of the repository have been lost after the repository is closed for 300 years. Also, the drilling technique is assumed to be the same as the present. The analysis case was developed as the following:

(1) A canister in the repository is assumed to be penetrated during drilling; meanwhile, the drilling operator finds out the abnormality and stops the operation.
(2) SNF in the canister is carried to the surface along with the drilling water, resulting in a circular contaminated area on the ground, which causes external exposure to the drilling operator.
(3) A family is assumed to move to the contaminated area one month after the drilling operation has been ceased. The family use the contaminated water from the drilled hole for drinking and farming and receive radiation dose from the contaminated area.
(4) For Detailed analysis results please refer to Section 13.2.

10.5. What-If Scenarios

According to the NEA report, what-if scenarios are widely used in investigating or demonstrating the robustness of the disposal system and illustrating the functions of specific barriers. When developing what-if scenarios, one or more than one barrier are assumed to have poor performance or even fail so that role and related safety functions of the barriers can be studied (NEA, 2016). What-if scenarios are those that are very unlikely to happen. Irrational or impossible assumptions are used to test the robustness of the repository and assess the relative importance of each system component and safety function.

According to the purpose and definition of what-if scenarios, three cases were developed as the following:

(1) Initial defect of the canister:

According to the design requirements, the initial state of the canister is assumed that the perforated defect does not exist in the copper shell of the canister. However, in order to explore the retardation capability of the buffer and geosphere, perforated defect when it is made is assumed in the canister, groundwater is able to enter the canister at the initial period after closure, and radionuclides in the canister might transport through groundwater. Meanwhile, the retardation capability of buffer, geosphere, and other system components is complete so that the annual effective dose to the biosphere under different transport conditions can be assessed. For relevant cases and e assessment results, please refer to Section 12.6.1.

(2) Colloid facilitated transport:

In this case, retardation of colloid and buffer is ignored.The bentonite barrier can be seen as having poor performance or even having no function. In addition, the colloid concentration would be a conservative value referred to SKB (2010m) to test the robustness of the system when the buffer safety function is having poor performance. For relevant cases and assessment results, please refer to Section 12.6.2.

(3) Radionuclide transport in gas phase:

If the canister is damaged, groundwater will be able to enter the canister and the cast iron lining of the canister might be corroded anaerobically. This produces hydrogen gas which will leak from the damaged canister. Because the buffer is intact, the gas containing gaseous radionuclides will accumulate continuously. Eventually, the pressure pulse will be generated. In this case, the retardation capability of the buffer and geosphere will be ignored, and the gas channel which allows the gas to pass through the buffer and the geosphere to the biosphere is assumed to be produced by a pressure pulse. Some of the gaseous radionuclides (C-14 and Rn-222) can thereby transport to the biosphere faster than transportation through water. For relevant cases and the assessment results, please refer to Section 12.6.3.

Different safety function failure of the barriers is assumed in the what-if scenarios, such as (1) in the case of an initial defect of the canister, thecontainment safety function of the canister is assumed to fail at the beginning; (2) in the case of colloid facilitated transport, the retardation safety function of the buffer is assumed to be jeopardized, and radionuclide transport will be accelerated by the erosion-generated colloid; (3) in the case of radionuclide transport in the gas phase, it is assumed that there is no retardation safety function of the buffer and the geosphere. The remaining retardation capability of the system components and barriers will be evaluated through the assessment of the abovementioned cases. Also, the impact on the robustness of the repository, and importance of each system component and the relevant safety function when the performance of the barriers is jeopardized can be shown by the assessment results. For cases of what-if scenarios and the assessment results, please refer to Chapter 12.

10.6. Conclusion

The scenarios of the report are classified into (1) design-basis evolution scenarios, (2) non-design-basis evolution scenarios, (3) future human actions scenarios, and (4) what-if scenarios according to different evaluation purposes. All of the scenarios and assessment cases are listed in Table 10-1.

(1) Design-basis evolution scenarios:

The design-basis evolution scenarios are developed based on the safety functions of the canister. The most probable evolution of the

KBS-3 concept repository is chosen for the development of the design-basis evolution scenarios. Corrosion issues and shear force issue are defined in accordance with the safety functions of the canister. For relevant cases and analysis results, please refer to Chapter 11 and Chapter 12.

(2) Non-design-basis evolution scenarios:

Extreme external conditions in the FEPs list are chosen for the development of the non-design-basis evolution scenarios. These external conditions are unlikely to happen, but will jeopardize the long-term safety of the repository if they occur. The events related to the extreme external conditions belong to boundary cases and are still within the range of variation of the evolution. The assessment cases of the report are uplift/denudation and volcanism. For further discussion, please refer to Section 13.1.

(3) Future human actions scenarios:

Future human actions are difficult to predict reasonably, and according to international experience, they are treated in a "stylised" approach and categorized in an independent scenario category. The assessment case for future human action scenarios in this report is drilling. For further discussion, please refer to Section 13.2.

(4) What-if scenarios:

What-if scenarios are developed based on highly unreasonable assumptions, to conceptually examine the robustness of the repository and evaluate the relative importance of system components and safety functions. The what-if scenarios in this report include the following three cases: initial defect of the canister, colloid facilitated transport, and radionuclide transport in the gas phase. For further discussion, please refer to Section 12.7.

Table 10-1: List of the scenarios.

Scenario classification	Cases	Instruction
Design-basis evolution scenarios	(1) Canister corrosion failure (2) Canister shear force failure	See Chapters 11 and 12 for further discussion.

Non-design-basis evolution scenarios	(1) Uplift/denudation (2) Volcanism	See Section 13.1 for further discussion.
Future human actions scenarios	Drilling	See Section 13.2 for further discussion.
What-if scenarios	(1) Initial defect of the canister (2) Colloid facilitated transport (3) Radionuclide transport in gas phase	See Section 12.7 for further discussion.

11. Containment safety function Analyses of the Selected Scenarios

11.1. Introduction

11.1.1. Overview

Following the procedures of the methodology for the safety case, the evolution analyses are executed. Results show that some containment safety functions provided by components may not be maintained during the reference evolution. In this chapter, their quantitative results are carried out with cases defined in scenario development. Those are the basement to develop subsequent cases for retardation safety function failure.

When the containment safety functions of the canister fail, groundwater intrudes the canister and the radionuclides dissolve in it, causing the radionuclides to migrate into the engineered and natural barriers.

According to the reference evolution analysis, the containment safety functions of the repository components are gradually affected by the long-term evolution of external factors. The canister and the buffer in the deposition hole are the crucial components that provide the containment safety functions. For corrosion and shear force issues in design basis evolution, the corresponding containment safety functions Can1 and Can3, and their mutual interactions with the FEPs are discussed in Chapter 10. The purpose of this section is to confirm the containment safety functions and the impact after those functions failed based on the research of Chapter 9 and Chapter 10.

Therefore, the analyses of the containment safety function scenario are performed separately for the advection condition and transformation of the buffer and various failure modes of the canister. Those will be the basis for further discussion of retardation safety functions. This section describes issues as below:

(1) Section 11.2 describes buffer advection and its analysis mode.

(2) Section 11.3 describes buffer transformation.

(3) Section 11.4 summarizes the conclusions of the buffer scenario analyses

(4) Section 11.5 describes the modes of the canister fail due to corrosion and their impact.

(5) Section 11.6 describes the modes of the canister fail due to isostatic load.

(6) Section 11.7 describes the modes of the canister fail due to shear force and their impact.

(7) Section 11.8 describes a comprehensivey discussion of possible failure modes and their mutual impact.

11.1.2. Definition of the Scenarios

This chapter discusses the design-basis scenarios under reference evolution conditions, including basic cases and variant cases. The basic case is set based on the analysis results of the evolution of the repository in Chapter 9. Therefore, the basic cases include the relevant prerequisites regarding the evolution of the repository in Section 9.1.1 and provide a reasonable description of the repository evolution. Some effects cannot be completely ruled out at present and may have a certain degree of impact on the consequences. So, those are regarded as variant cases and their consequences are evaluated.

For example, it has been evaluated that the containment safety function of the canister is jeopardized by corrosion under the reference evolution conditions. However, the hydrogeological conditions and geochemical conditions around the repository are different in different sites. Therefore, for corrosion issues in this report, one canister failed is set up as a variant case. And related evaluation techniques were developed for radiological impact evaluation of the corrosion issue.

11.1.3. Climate Evolution in the Analyses

In the design-basis evolution scenario, the impacts of the long-term safety of components from changes in environmental conditions and related process accumulation after several glacial cycles are mainly discussed.

During the glacial cycle, the long-term climate evolution mainly causes significant sea-level rise and fall as well as changes in the external factors of the repository, such as alterations in surface temperatures and ecosystems, which in turn affect the safety functions of the repository. In chapter 9, the safety assessment timescale is divided into 4 periods to perform the components' evolutions and exam their safety functions under the reference evolution.

11.2. Buffer Advection

11.2.1. Introduction

The important safety function of the buffer is to protect the canister from contacting the groundwater flow directly and to reduce the hydraulic conductivity by enveloping the canister with bentonite.

Depending on its initial state and the evolving conditions during the safety assessment timescale, containment and retardation safety functions of the buffer in the deposition hole may be kept or not. In order to achieve the safety function of restricting advection, the hydraulic conductivity of the buffer must be low enough. The factors that affect the hydraulic conductivity include the buffer density and the types of cations in the buffer. The buffer density is the most critical factor for this. These factors and the strength of the cations in the groundwater will also affect the swelling pressure of the buffer. Therefore, in addition to safety function Buff1 where the hydraulic conductivity of the buffer should not exceed 1×10^{-12} m/s, the following safety function indicator criteria can also be regarded as standards related to safety function Buff1:

(1) The swelling pressure of the buffer >1 MPa.

(2) The cationic strength of groundwater >8 mM.

(3) Total dissolved solids <35 g/L (instant total dissolved solids <70 g/L).

(4) The temperature of the buffer is less than 100 ℃.

(5) The pH value for groundwater should be between 5 and 11

There are two main ways that affect the hydraulic conductivity of the buffer:

(1) The buffer lost due to erosion, resulting in a decline in its dry density and a rise in its hydraulic conductivity. Then, the main transport mechanism in the buffer changes from diffusion to advection. At the same time, the swelling pressure of the buffer is too low for self-recovery.

(2) The transformation of Montmorillonite in the buffer makes hydraulic conductivity change (discussed in Section 11.4).

The aforementioned may also lead to canister sinking. And this will be discussed in Section 11.2.3.

According to the analysis results in Chapter 9, the strength of cation in the groundwater in the reference case will be lower than the safety function indicator criteria and will affect safety function Buff1.

In order to include the uncertainty of the parameters that may affect the transport mechanism of the buffer for buffer advection, three cases are assumed:

(1) Basic evolution advection case: According to the analysis result of the basic evolution, the parameters related to the transportation of the buffer are set.

(2) Initial advection case: The transport mechanism of buffer in all deposition holes is advection over the safety assessment timescale (Bounding case).

(3) No advection case: The transport mechanism of buffer in all deposition holes is diffusion over the safety assessment timescale (Bounding case).

11.2.2. Quantitative Assessment of Buffer Advection

Associated assessment methods for long-term evolution have been described in Chapter 9. Current geochemical conditions indicate that the cationic strength in groundwater is less than 1.4 mM. Even if the cationic strength increased to 2.5 mM after bentonite loss, it is still below the safety function indicator criteria R1 (8 mM). Therefore, this will lead to chemical and physical corrosion of the buffer and cause the loss of the buffer.

According to Chapter 9, when a relatively conservative estimate of buffer loss is greater than 1,200 kg, the safety function Buff1 is violated and changes from diffusion to advection. During the unsaturated phase of the buffer, the buffer loss due to piping erosion is only from 16.4 kg to 164 kg under the extreme condition. It is not supposed to affect the safety function Buff1.

After the buffer is saturated completely, the buffer loss of up to 1,200 kg is achieved circa 11,661 years after the repository is closed by extrusion, inflow erosion and precipitation. Safety function Buff1 will be lost, and substances transported in the buffer will be transferred from diffusion to advection. Among the deposition holes with significant corrosion, the earliest advective condition occurred about 2,200 years after closure, and the slowest one are achieved around 985,000 years. Therefore, the average advection time is about 226,000 years and the median advection time is around 7,000 years. This is the base of further evaluation of erosion and transportation.

11.2.3. Case Study of Canister Sinking

The safety function of Buff5 is to prevent the buff thickness around the canisters from decreasing, so the canister will not directly contact the bottom or the wall of the deposition hole. Its safety function indicator criterion is swelling pressure of the buffer > 0.2 MPa. In accordance with the assessment results of Section 9.3.8, the swelling pressure of the buffer is about 5 MPa at an early stage after saturation.

As mentioned in Section 9.3.9, the primary safety function of the buffer is to limit advection (Buff1). To ensure this safety function, the density of the buffer should be kept to a certain degree. If the buffer density is too low, the buffer will deform by loading the canister. This may cause the canister to sink or incline (Buff5), resulting in reducing the thickness of the buffer surrounding the canister or the canister contacting the bottom or the wall of the deposition hole. The canister is no longer covered by the buffer fully and lost its restricting advection safety function.

FLAC3D was used to evaluate the degree of deformation of the buffer under the canister after loading the weight of the canister and the backfill. Based on the results of the reference evolution analysis in Chapter 9, the maximum sink is approximately 0.024 cm in depth for bentonites with different water content. The density of the buffer under the canister is slightly higher than the initial value after compacting. But its value is close to the initial value. After saturation, the average swelling pressure is about 5 MPa. It is still higher than 0.2 MPa, and relevant safety functions can thus be maintained.

11.2.4. Summary

Because the sink process will not affect safety functions, the discussion will focus on factors related to the advection of the buffer. Uncertainties of the factors related to buffer advection in the evolution are covered in the aforementioned three cases (basic evolution advection case, initial advection case, and no advection case). Therefore, the impact on the canister from three buffer advection cases will be discussed in the following discussion.

11.3. Buffer Transformation

The montmorillonite contained in the buffer may transform into minerals without swelling property such as illite or change its property due to accumulation of impurities. If the buffer transforms, it will lose its swelling pressure, resulting in the loss of the safety functions of containment. Furthermore, it can increase the groundwater flow and boost the corrosion rate of the canister. It also may lead to the increased production of sulfide from sulfate-reducing bacteria and accelerate the corrosion rate of the canister. Besides, it may also decrease swelling pressure in the buffer, increase conductivity, and accumulate impurities in the buffer. Then, the pore space might be filled and hydraulic conditions might be changed.

In order to keep safety function Buff4, the relevant safety function indicator criteria are as follows:

(1) The temperature of the buffer is less than 100 ℃.

(2) pH value of groundwater should be between 5 and 11.

According to the analysis results in Chapter 9, the temperature of the buffer on top of the canister will reach the highest temperature (90.30 ℃) around 10 years after the closure under the basic evolution situation. Then decay heat continues to drop with time. Considering the temperature margin (8 ℃), the peak temperature of the buffer will not exceed 100 ℃ over the safety assessment timescale. Therefore, safety function Buff4 can be maintained.

11.4. Conclusion for Buffer Scenarios

Based on the aforementioned analysis of buffer advection and buffer transformation, the conclusions are:

(1) The factors related to buffer advection and the influence of their uncertainties on the evolution can be included in the three cases described in Section 11.2 (basic evolution advection case, initial advection case, and no advection case). Therefore, the impact on the canister from three buffer advection cases will be discussed in the following discussion.

(2) Based on the assessment results, it is assumed that the possibility of buffer transformation could be avoided under the current repository layout. So, no further discussion will be followed about the impact of buffer transformation on canisters.

11.5. Canister Failure due to Corrosion

11.5.1. Introduction

The containment safety function of the canisters Can1 considers the resistance of corrosion for the canister during the safety assessment timescale. In order to maintain this safety function of the canister, its safety function indicator criteria is set as "copper shell thickness > 0 cm."

Only when buffer advection happens, the canister might fail due to corrosion. Thus, the integrity of the buffer is an important factor for the canister corrosion assessment. This section follows the results from Section 11.4; the assessments are implemented mainly based on the hydro-geological evolution of the reference evolution, the geochemical condition evolution around the repository, and the chemical evolution of the buffer and the backfill. The assessment of the impact on the integrity of safety functions of the buffer and the canister (Buff1 and Can1) under three different sea-levels (current sea level, sea level falls to -20m, and sea-level falls to -120m with the corresponding groundwater flow fields and groundwater composition) was implemented. Based on the erosion time of the buffer and the corrosion rate of the canister, the corrosion depth of each canister is evaluated over the safety assessment timescale. Finally, the specific degree of corrosion impact was evaluated from Section 9.3.13 and abstracted in Section 11.5.2.

11.5.2. Quantitative Assessment of Corrosion

Based on the analysis results of the basic evolution, relevant cases of the corrosion of the canisters are set up, and quantitative assessments of the corrosion of the canisters are carried out.

As mentioned before, the canister may fail due to corrosion only occurring during buffer advection. According to Section 11.2, under the reference evolutionary conditions, the buffer reaches advection conditions around 2,200 years after the repository is closed. Then, the advection starts to accelerate corrosion of the canisters.

Actually, this situation only occurs in certain deposition holes with large inflows and fracture apertures. According to the analysis results in Chapter 9, there are different impact factors for the corrosion effect of the copper shell at different evolution time frames. Those factors can be mainly divided into:

(1) Initial aerobic environment after closure (excavation and operation period is included):

    (a) Aerobic corrosion.

    (b) The corrosive effect of the oxidant produced after the radiolysis of air and water.

(2) Oxygen-free environment after closure:

    (c) Corrosion effect of sulfide dissolved from pyrite in the buffer and the backfill.

    (d) Corrosion caused by sulfide produced by the reduction reaction of sulfate-reducing bacteria.

    (e) Corrosion caused by existing sulfides in groundwater.

Among them, the corrosive effect of the initial aerobic environment (the excavation and operation period of the repository are included) after closure, and the corrosion caused by the sulfide produced by the reduction reaction of pyrite and sulfate-reducing bacteria in the anaerobic environment after closure are limited corrosion. The corrosive depths caused by the above effects are listed in Table 9-13 and Table 9-14. The maximum corrosive depth is about 0.408 mm. Further considering the possible impact of the local corrosion, it is estimated that the maximum corrosive depth is around 0.414 mm.

On the other hand, the corrosive effect caused by the sulfide in groundwater is not limited. It varies with the amount of groundwater contact with the canister and the concentration of the sulfide in groundwater. The erosion status of the buffer based on the information of the hydraulic conditions in different time frames after the closure was estimated, and the changes of corrosive agents in each time frame were also calculated. Therefore, the corrosion rates of the canister copper shell caused by sulfide in groundwater are evaluated. It is estimated that the maximum corrosion depth caused by existing sulfides in groundwater is approximately 10.20 mm within the safety assessment timescale.

The initial thickness of the copper shell of the canister is 5 cm, and for conservative evaluation, buffer erosion rate and canister corrosion rate are assumed to be the same with the highest estimated value at different deposition holes. The thickness of the copper shell can still maintain about 36.8 mm after the repository has been closed for 1 million years.

11.5.3. Summary

The canister will only fail when advection happens in the buffer. Therefore, the analysis results of buffer advection in Section 11.2 are further discussed. Their evaluation results are for (1) The basic evolution advection case and (2) the initial advection case are summarized below.

(1) Cases of corrosion of canisters under buffer advection in the basic evolution:

According to the analysis results in Section 11. 5.2, under buffer advection condition in the basic evolution, the corrosion of the copper shell in an aerobic and anaerobic environment will cause about 11.02 mm in depth after being closed for 1 million years. The thickness of the copper shell is conservatively estimated at about 36.8 mm at this time, which means the canister will not fail because of corrosion. Therefore, the containment safety function can be maintained.

(2) Corrosion case of canister under the initial advection of buffer:

Uncertainties of characteristics for potential sites which might affect the hydraulic condition and geochemical condition dramatically. In order to take those impacts into consideration, the variant case, initial advection of buffer, is carried out as below. Hence, after the repository closed for about 100,000 years, one canister is assumed to lose its containment safety function due to corrosion.

11.6. Canister Failure due to Isostatic Load

11.6.1. Introduction

The most important safety function of the canisters related to isostatic load is to withstand isostatic load (Can2). This safety function is directly related to the containment safety function of the canister. In order to achieve the safety function of the canister against the isostatic load, the safety function indicator criteria "isostatic load < 50 MPa" must be met.

The canister is affected by the isostatic load, which is mainly evaluated based on the hydrostatic pressure at the disposal depth, the swelling pressure of the buffer, and the strength of the canister. When the sum of the first two terms is greater than the last one, the canister may fail. The influence of the aforementioned factors on the isostatic load of the canister will be discussed in Section 11.6.2 and Section 11.6.3 separately.

With the conclusions of Section 11.4, this chapter analyzes the relevant effects on the isostatic load of the canister under the different buffer advection conditions. However, when buffer advection is reached, the mass loss of the buffer will be relatively large. At the same time, the swelling pressure and the isostatic load of the canister will also be low. Therefore, only when the buffer is not in advection condition (un-eroded) the cases of the isostatic load of the canister are evaluated.

11.6.2. Swelling Pressure of the Buffer

According to the reference evolution analysis in Chapter 9, the two situations in which both the disposal tunnel and the deposition hole are intersected by fracture (Case 1) and only the deposition hole intersected by fracture (Case 2) are considered. The analysis results are shown as shown Figure 9-35. When the buffer reaches a fully saturated state in Cases 1 and Case 2, the average swelling pressure is about 5 MPa, while the local area at the bottom of the canister has a larger swelling pressure, about 8.23 MPa. It is in line with the safety function indicator criteria of Buff1, Buff2, Buff5 and Buff6. Therefore, the safety functions of the buffer can be maintained.

11.6.3. Strength of the Canister

According to the analysis results of the reference evolution of the canister in Section 9.3.13, when the buffer is not saturated, the shape of the deposition hole is cylindrical under normal conditions, and the maximum stress caused by the uneven saturation state on the cast iron lining is 92.04 MPa. When the deposition hole has a displacement of 8 mm and is banana-shaped, the maximum stress value of the cast iron lining caused by the uneven saturation state is 112.40 MPa.

All of the above results show that during the unsaturated period of the buffer, the stress caused by different conditions will not exceed the yield stress of the cast iron lining, 267 MPa. The material can still maintain an elastic state and will not be damaged. Therefore, the mechanical integrity of the canister can be ensured.

When the buffer reaches saturation, it is assumed that the canisters are affected isotropically by the maximum buffer swelling pressure and the hydrostatic pressure of the design requirements. When the deposition hole loads uneven pressure under normal conditions, the maximum load on the cast iron lining is evaluated to be about 43.52 MPa. When the deposition hole deforms 8 mm and is banana-shaped, the maximum load on the cast iron lining by uneven saturated status is evaluated to be about 69.86 MPa. When the deposition hole deforms 8 mm and is banana-shaped with an extra 33 mm displacement, the maximum load on the cast iron lining by uneven saturated status is evaluated to be about 106.70 MPa. All of the above results show that during the saturated period of the buffer, the stress caused by different conditions will not exceed the yield stress of the cast iron lining (267 MPa). The materials can still maintain an elastic state and will not be damaged. Therefore, the mechanical integrity of the canister can be ensured.

11.6.4. Comprehensive Analyses

Based on previous analyses, it is concluded that the maximum swelling pressure of the buffer is 8.23 MPa and the maximum isostatic load of the canister is 13.23 MPa which is less than the safety function indicator criteria: 50 MPa. On the other hand, the canister might fail due to the cast iron lining collapsing. After the evaluation, the maximum mechanical load: 112.40 MPa will not exceed the yield stress of the cast iron lining under un-even saturation of the buffer. However, the cast iron lining won’t collapse and the canister won’t fail due to isostatic load.

In summary, considering the uncertainty of the factors related to the isostatic load of the canisters, it is believed that the current design of the canisters can provide enough margin to withstand the isostatic load within 50 MPa. Over the safety assessment timescale, the canister will not fail due to isostatic load.

11.7. Canister Failure due to Shear Force

11.7.1. Introduction

The most important safety function related to shear force is to withstand shear force (Can3). This safety function is directly related to the containment safety function of the canister. In order to achieve the safety function of the canister against the shear force, the safety function indicator criteria "shear displacement < 5 cm" and "shear displacement velocity < 1 m/s" must be met. This ability to resist shear force is mainly affected by the design, manufacturing quality, and non-destructive detecting quality of the canister.

Because buffer can damp shear force and reduce the direct impact on the canisters, safety functions Can3 and Buff3 should both be met to reduce the impact on the canisters.

With the conclusions of Section 11.4, this chapter analyzes the relevant effects on the shear effect of the canister under the different buffer advection conditions. However, in the basic evolution advection case and the initial advection case, the buffer is eroded, and its density is reduced. These reduce the impacts of surrounding shear force on canisters. Therefore, only when the buffer is not in advection condition (un-eroded and with relatively high density), the cases of the shear effect of the canister are evaluated. It is conservatively estimated that the canister is affected by shear force.

11.7.2. Quantitative Assessment of Canister Failure due to Shear Force

The reference case is located at the junction of the Philippine Sea plate and Eurasian plate. Earthquakes, fault sources, and diffuse seismicity are included, which is the main reason for the occurrence of shear force. After the repository is closed, if the fracture in the host rock accumulates shear displacement due to the earthquake and intersects the canister, the canister is subjected to shear force. When the fracture shear displacement exceeds the limit of the allowable displacement of the deposition hole, it is assumed that the canister is destroyed and invalids.

Shear displacement of fractures occurs periodically because of seismic disturbances induced by plate movement in the reference case. However, the prerequisites for shear displacement having an impact on the canister are that the canister needs to be intersected by fracture and that shear displacement of the fracture exceeds the allowable displacement limit of the deposition hole. Therefore, the layout of underground facilities must be considered. The DFN is used to analyze intersections of the fractures and underground facilities. It should also follow the FPC and EFPC.

Seismic simulation based on the collected source data was performed, and a logical tree of simulation parameters of fault source and diffuse seismicity was established. The accumulated fracture shear displacement of a single earthquake event was analyzed using the 3DEC numerical analysis model. The analysis results are shown in Table 9-18. In addition, in order to assess the cumulative impact of several earthquake events on the same fracture, the following conservative assumptions are also used to conduct the cumulative fracture shear displacement of several earthquakes over the safety assessment timescale:

(1) The earthquake is limited to the source model in the source logic tree.

(2) The fractures do not grow due to shear displacement.

(3) The fractures do not creep during the aseismic period.

(4) The strength of the fractures has not been affected by the geological process.

(5) Faults do not displace in the reference case.

(6) The direction of the fracture shear displacement caused by each source mode is the same.

(7) Regardless of the status of fractures, the shear displacement of the fracture is considered an irreversible permanent displacement.

The cumulative amount of displacements caused by several fault sources and diffuse source events for each fracture cluster are analyzed. The results are shown in Table 9-20.

Then, according to the analysis results of the maximum cumulative fracture shear displacement caused by earthquake-induced fracture shear displacement, DFN was used to analyze the correlation between fractures and the repository layout when the deposition hole rejection criteria were taken into account. Finally, the canister failure probability due to shear force was calculated based on the safety function indicator criterion Can3 (shear displacement < 5 cm). According to the analysis results in Chapter 9, the relation between the shear failure probability and time caused by fault sources and diffuse sources is shown in Figure 9-56. The earliest possible canister failed due to shear force is about 230,000 years after the repository is closed and its probability of occurrence is about one in a million. Over the safety assessment timescale, the probability of the canister failure due to shear force caused by the earthquake is about 1/3,000. The total number of canisters is 2,571 in the repository. Assuming that each canister failure event is independent and the binomial distribution is adopted, the expected value (E) corresponding to the number of canisters that failed due to shear force at 1 million years after the repository is closed is calculated as follows:

$$f(k,n,p) = \binom{n}{k} p^k (1-p)^{n-k} \quad (11\text{- }1)$$

$E = f \times k = n \times p$	(11- 2)

where,

f = the probability corresponding to the number of canisters failed due to shear force at 1 million years after the repository is closed, [-].

E = the expected value of the number of canisters failed due to shear force at 1 million years after the repository is closed, [canisters].

k = the number of canisters failed due to shear force at 1 million years after the repository is closed, [canisters].

n = the total number of canisters in the repository, [canisters].

p = a single canister failure probability due to shear force, [-].

The calculated results are shown in Figure 11-1. Therefore, the expected value is the failure of the number of the canisters multiplied by its corresponding probability at one million years after the repository is closed. Finally, the results, which show that about 0.87 canisters might fail, were obtained.

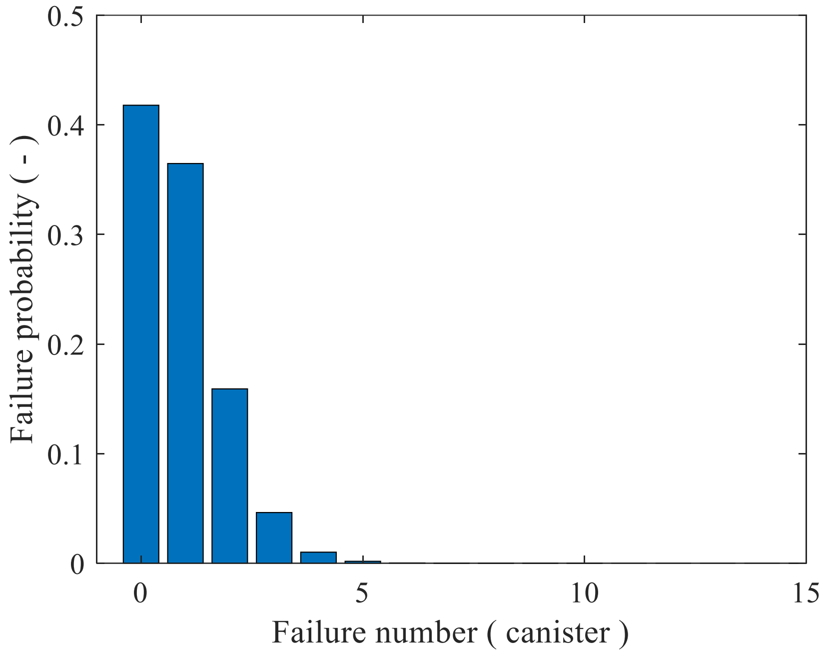

Figure 11-1: Number of canister failure due to shear force and its corresponding probability.

11.7.3. Conclusion

The aforementioned analysis concludes that the canister may fail due to the shear force caused by the earthquakes. Thus, continuing the results of buffer advection in Section 11.2, the impact from the shear force on the canister under the buffer is not in advection condition are evaluated. The earliest possible canister failed due to shear force is about 230,000 years after the repository is closed and its probability of occurrence is about one in a million. For the entire safety assessment timescale, the probability of canister failure due to shear force caused by an earthquake will be about 1/3,000. and the expected value of canister failure number will be around 0.87 canisters.

11.8. Scenarios Synthesizing Analysis

11.8.1. Summary of the Analysis Results

Based on the analysis results of Section 11.2 to Section 11.7, the conclusions of each case for the containment safety function analyses are summarized. Subsequent analyses are performed in Section 12.5 to Section 12.7.

(1) Buffer advection (Section 11.2):

According to the evaluation results of the uncertainty related to buffer advection, the possible advection transportation conditions are set. Then, the following three cases, the basic evolution advection case, the initial advection case and the no advection case, which causes the canister failure due to corrosion, are discussed. Therefore, under the basic evolution conditions, the advection time and conditions of all fracture-connected deposition holes are included in the subsequent evaluation. At the same time, for the more extreme boundary cases, advection (initial advection case) and diffusion (no advection case) are used to carry out the following evaluation.

(2) Buffer transformation (Section 11.3):

Considering the uncertainty related to the factors of buffer transformation, thermal analysis and chemical conditions related to those factors are evaluated. It is preliminarily supposed that there are sufficient margins to avoid buffer transformation. Therefore, the related subsequent impact researches for this case are suspended.

(3) Canister corrosion failure (Section 11.5):

From the previous analyses, buffer advection transport is the primary reason for the corrosion failure of the canister. After the buffer is eroded to a certain degree, the main transport mechanism of the substance in the buffer changes from diffusion to advection, and the canister may fail due to corrosion.

Therefore, the impact of corrosion failure of the canister in the three cases of buffer advection was discussed, and the initial advection case would be analyzed. The following analysis is performed in Section 12.5.

(4) Canister isostatic load failure (Section 11.6):

Considering the uncertainty of the factors related to the isostatic load of the canisters, it is supposed that the current canister design can provide sufficient margin to withstand isostatic load on the canister over the safety assessment timescale.

Therefore, the related subsequent impact researches for this case are suspended.

(5) Canister shear force failure (Section 11.7):

The canister may fail because of shear force and lose its containment safety function when the impact of diffuse source and fault source and uncertainty from the related factors are taken into account.

The earliest possible canister failed due to shear force is about 230,000 years after the repository is closed and its probability of occurrence is about one in a million. Over the safety assessment timescale, the probability of the canister failure due to shear force caused by the earthquake is about 1/3,000, and the expected value of the number of canister failures is around 0.87 canisters. The following analysis is performed in Section 12.6.

11.8.2. Assessment of the Containment Safety Function

According to the aforementioned analysis results, canisters will not fail from the impact of corrosion and isostatic load. Canisters only fail due to the shear force and lose their containment safety function under the reference evolution conditions in the design-basis scenario. Therefore, the main scenario will focus on this.

11.8.3. Combination of the Analyzed Scenarios

The various processes of the canister and the buffer may occur individually or combined at the same time during the reference evolution. In order to consider the circumstances comprehensively, the influences of one or multiple processes that occur simultaneously might have to be discussed.

From the foregoing analysis results, the buffer erosion and the copper shell of the canister corrosion (when the buffer is eroded to a certain degree, the substance transport mechanism in the buffer is to transfer from diffusion into advection) and shear displacements on the canister will affect the safety function of the engineered barrier system of the repository.

The following discussions are the combined effects of the four analysis scenarios occurring at the same time:

(1) Buffer loss due to erosion. (which is discussed in Chapter 9.4.8)

(2) After the buffer is eroded to a certain degree, the transport mechanism of the buffer transfers from diffusion to advection, and the copper shell of the canister begin to be corroded. (which is discussed in Chapter 9.3.13)

(3) The canisters fail due to shear force occurring at deposition holes intersected by fractures (which is discussed in Chapter 9.4.5).

(4) The canister suffers from the isostatic load. (which is discussed in Chapter 9.3.13 and Chapter 9.4.9)

(1) and (2) have been analyzed for the combined effects of canister failure due to the corrosion scenario.

(1) Synthesis of buffer erosion/canister copper shell corrosion with the shear force exerted on the canister.

(a) Impact of shear force exerted on canister under buffer erosion condition.

Buffer density would decrease when the buffer is eroded, and the failure probability of the canister due to shear force would dramatically drop (Buff3: buff density < 2,050 kg/m^3).

In addition, the impact of the shear force on the canister when the buffer is not eroded has been evaluated in the “no advection case” of the buffer. The probability of shear force impacted on the canister and buffer erosion is positively correlated with fracture size; therefore, the probability of occurrence of these effects is not mutually independent.

(b) The influence of the canister copper shell corrosion on the shear force on the canister

The cast iron lining is the main structure that provides mechanical support in the canister, and it will not be affected by the corrosion of the copper shell.

When the buffer is eroded, it will cause corrosion of the copper shell of the canister. Since the buffer density will reduce due to erosion, the canister failure probability caused by shear force will drop significantly. This should be able to compensate for the loss of the mechanical support via the canister corrosion.

If the canister fails due to shear force, it will no longer contain the radionuclides, in which the corrosion effect has no other negative influences on the shear load cases.

(c) The influence of shear force on the buffer erosion

The criteria of causing the canister failure due to the shear force criteria is shear displacement > 5 cm. When the canister does not fail due to shear yet (shear displacement < 5 cm), only a minor impact on the thickness of the buffer occurs. Therefore, it will not affect the erosion time for the buffer.

In addition, shear force may cause an increase of the flow in fractures, but the impact on the erosion of the buffer should not be significant (SKB, 2011). However, this effect cannot be completely ruled out based on current domestic research; the consequences will be evaluated in the retardation safety function analysis.

(d) The influence of the shear force on the corrosion of the canister copper shell

The shear force will stress on the canister copper shell. However, it can only have a further impact on canister corrosion (usually through stress corrosion cracking) when the cation concentration is high and the environment is in oxidation condition. However, this kind of environment will not be evolved in the reference case; it is supposed that the shear force should not have other additional impacts on the corrosion of the canister copper shell.

(2) Synthesis of buffer erosion/canister shell copper corrosion and the isostatic load of the canister

(a) The impact of the buffer erosion on the isostatic load of the canister

The buffer erosion will reduce its density, which in turn reduces its swelling pressure. Then, the isostatic load of the canister also drops. Therefore, it is regarded as a positive effect on maintaining the safety function of the canister against the isostatic load.

(b) The influence of the canister copper shell corrosion on the isostatic load of the canister

As mentioned previously, the cast iron lining is the main structure that provides mechanical support in the canister and it will not be affected by the corrosion of the copper shell. Therefore, the corrosion of the canister copper shell will not have a negative impact on the safety function of the canister against the isostatic load.

(c) The influence of the isostatic load of the canister on the buffer erosion / the corrosion of the canister copper shell

Isostatic load is composed of hydraulic pressure and swelling pressure. Under the relatively stable hydrogeology condition, the isostatic load will not dramatically change with hydraulic pressure. And hydraulic pressure has already been considered as the boundary condition in the analyses of basic evolution.

Hence, there is currently no relevant evidence suggesting that if the isostatic load of the canister increases, the buffer erosion and the corrosion of the canister will increase (SKB, 2011). But if the isostatic load is increasing caused by the hydrostatic pressure, it will lead to a negative effect on the buffer erosion and the corrosion of the canister (the swelling pressure will decline together with buffer erosion). Therefore, this situation has been evaluated in the analysis case of the buffer erosion / the corrosion of the canister copper shell.

(3) The synthesis of the canister shell copper corrosion and the isostatic load of the canister

(a) The influence of the isostatic load of the canister on the shear force of the canister

Isostatic load and shear force will affect the canister at the same time.

Based on the reference(SKB, 2011), the results should not be more severe than the case that only the shear force on the canister is considered even under the condition with a higher isostatic load. Actually, it can’t cause large-scale earthquakes and shear force under a high isostatic load environment. Therefore, impacts on the canister caused by isostatic load and shear load can be covered by the influence of shear load.

(b) The influence of the shear force of the canister on the isostatic load of the canister

The canister can still maintain its ability to resist the isostatic load after accumulating 5 cm of shear force displacement (SKB, 2011).

12. Retardation safety function Analyses of the Selected Scenarios

12.1. Introduction

The migration of radionuclides after they are released from the canister and their influence on the biosphere for the scenarios selected in Chapter 11 will be assessed in this chapter to ensure the retardation safety function of the repository over the safety assessment timescale.

The assessment models of radionuclide migration and dose evaluation in the biosphere are described in Section 12.2. Potential criticality for a failed canister is demonstrated in Section 12.3. The assessment models of radionuclides transport in the water phase and the radionuclides that should be considered are described in Section 12.4. The analyses of the retardation safety function of the selected scenarios: canister failure due to corrosion and canister failure due to shear force are demonstrated in Sections 12.5 and 12.6. The analyses results of “what-if” scenarios are in Section 12.7. Finally, summaries of risk and conclusions of the aforementioned analyses are stated in Sections 12.8 to 12.11.

12.2. Assessment of the Biosphere

The main assessment objective of biosphere assessment is the biosphere dose conversion factor (BDCF) of the potentially exposed groups in the reference case.

The BDCF is defined by the equilibrium annual individual effective dose (Sv/y) caused by the accumulated radionuclides in each environmental medium with a constant release rate of 1 Bq per year from groundwater. The annual individual effective dose will increase every year until equilibrium. The total annual individual effective dose of the potentially exposed groups could be estimated by multiplying the BDCF with the release rate of each radionuclide calculated by the safety assessment of the retardation safety function.

12.2.1. Approaches and Concepts for Biosphere Assessment

Currently, potentially exposed groups are defined according to the methodology suggested by the BIOMASS-6 report (IAEA, 2003). Human action is assumed according to the initial state of the reference case, as shown in section 4.3.2.6. In order to consider the biosphere evolution, the critical exposure pathways are identified from the landscape at different periods in the future, and the potentially exposed groups with different habits are defined according to these critical exposure pathways. Finally, the BDCFs of potentially exposed groups are figured out and transferred to the overall safety assessment group to estimate their annual individual effective dose. The critical group could be found and their dose and risk are compared with the regulatory constraints to demonstrate compliance. (Figure 12-1).

The results analyzed in Chapter 9 are considered to reflect the landscape evolution in the different periods in the future. It shows that the main driving factor of the biosphere evolution is the sea-level change, and it further causes the change of the landscape and the release locations. For example, if the radionuclides are released into the arable land, people may be exposed by the ingestion of the polluted crop and soil, the inhalation of the dust coming from polluted soil and the external exposure from the polluted soil. If the radionuclides are released into the sea, people may be exposed by the ingestion of polluted seafood or sediment ingestion or the external exposure from the polluted seawater or sediment. Nevertheless, the radioactive dose may be lower because of the dilution of the seawater.

The radionuclide transport modules of the different landscapes, including the land, river, lake, and sea, were built. These landscape modules are connected according to the different release types caused by sea-level change. The accumulated radionuclide activity concentration of each environmental media could be found, and then the BDCF could be figured out by implementing the habits of potentially exposed groups and connecting the corresponding exposure pathways to the polluted media. Finally, the maximum BDCF in different periods will be selected cautiously and then delivered to the following safety assessment.

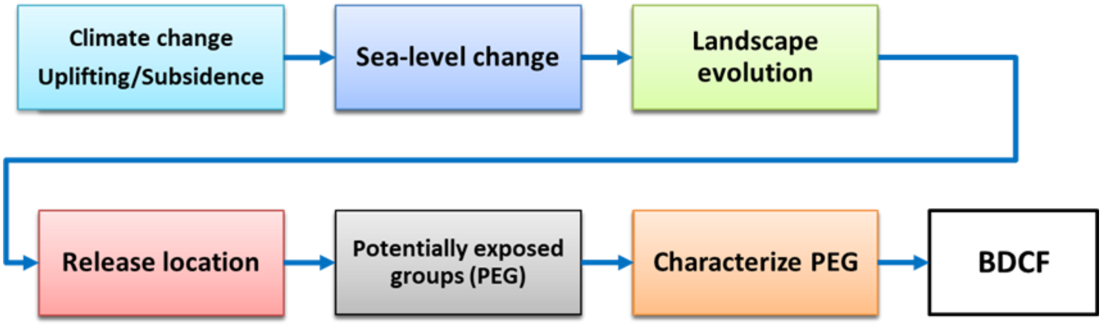

Figure 12-1: Approach and concept for biosphere assessment.

12.2.2. Location and Development of the Biosphere objects

The radionuclides are assumed to release from the repository to the biosphere by groundwater transporting in the safety assessment. The landscape on the release location of radionuclides may cause different exposure pathways for the potentially exposed group.

Different types of landscape radionuclides transport modules were built to consider the radioactive effect on the people caused by different release locations according to the conditions of reference evolution. The parameters required in the biosphere assessment are collected from the program from 2005 to 2020. When the data need to be supplemented, the related local data is adopted preferentially, and then the international reference. The landscape modules include terrestrial land, lake, river, and sea. The landscape modules could be connected according to the different assumptions of the release types. Besides, the well-water module is also built to consider the radioactive effect of using well-water as the drinking and irrigating water.

Furthermore, in order to model the landscape at different periods to consider the biosphere evolution, the sea-level change is assumed to be the main driving factor that causes the landscape evolution in the biosphere, according to the result shown in Chapter 9. The climate evolution in the whole safety assessment time frame is assumed that the glacial cycle will repeat continually. The first glacial cycle is about 120,000 years, so the glacial cycle will repeat about 8 times in the next 1 million years. As mentioned in Chapter 5, Taiwan is located in sub-tropical regions. During the 120,000-year glacial cycle, the climate will change from sub-tropical to temperate and then return to sub-tropical. The surface temperature gradually decreases from 23.8 ℃ to about 17℃ or 18℃, and then gradually returns to 23.8℃. The reference case is livable during the whole glacial cycle. Besides, sea-level fall will fall to -120 m when temperature decreases, and the land will expand. The radionuclides have much probability to release into the land. Therefore, the landscape evolution during the whole glacial cycle should be considered when the BDCFs are calculated.

Six kinds of landscape combinations (Table 12-1) may be during the glacial cycle:

(1) Release into sea (coastal period):

The reference case is an island where the radionuclides are easy to be released into the sea. The radionuclide transport model with the land and sea landscape modules was built to cover this circumstance.

(2) Release into lagoon (coastal period):

With the evolution of the glacial cycle, the sea-level falls gradually. The release location may become the lagoon caused by the sedimentation of sand that came from tidal currents and the bed-load transport process, and the residents may use the water of it. The radionuclide transport model with the land, lake, and sea landscape modules was built to cover this circumstance.

(3) Release into lake (inland period):

When the sea-level falls continuously, the depression on the land may become a lake. The radionuclides may be released to the lake far from the sea and then transported to the downstream area along with the river flow. The radionuclide transport model with upstream and downstream land and lake landscape modules was built to cover this circumstance.

(4) Release into river (inland period):

Besides the lake, the radionuclide may be released into the river when the site is far from the sea. It may be transported from the upstream to downstream catchment by river flow. The radionuclide transport model with upstream and downstream land and river landscape modules was built to cover this circumstance.

(5) Release into well (coastal period):

The impact of the contaminated well-water is considered. When the reference case is an island, the freshwater is not enough, so that the well-water is used as the drinking and irrigation water by potentially exposed groups. The radionuclide transport model with well and sea landscape modules was built to cover this circumstance.

(6) Release into well (inland period):

The impact of the contaminated well-water for the inland period is considered. When the released location is far from the sea, and the radionuclides are released into the river, the freshwater resources may not be enough for the resident. Therefore, the well-water may be used as the drinking and irrigation water by potentially exposed groups, and the radionuclide transport model with well and river landscape modules was built to cover this circumstance.

As mentioned in the ICRP publication 122 (ICRP, 2013), “in many cases, different scenarios, each associated with different representative persons, may be considered for the distant future.” Therefore, different potentially exposed groups are considered when the radionuclides are released into the different landscapes, , as shown in Table 12-2. Six potentially exposed groups corresponding to the terrestrial landscape, two potentially exposed groups corresponding to the aquatic landscape, and a reference group were taken into the assessment.

(1) The reference group (R.G.)
(2) Staple grower (terrestrial landscape) (Sta)
(3) Fruit and vegetable grower (terrestrial landscape) (F.V.)
(4) Cow farmer (terrestrial landscape) (Cow)
(5) Pig farmer (terrestrial landscape) (Pig)
(6) Poultry farmer (terrestrial landscape) (Pou.)
(7) Freshwater fish farmer (aquatic landscape) (F.F.)
(8) Oyster farmer (aquatic landscape) (O.F.)

As International Commission on Radiological Protection (ICRP) mentions (ICRP, 1999), the habits and characteristics of the critical group can only be assumed, and it is suggested that “the habits and characteristics assumed for the group should be chosen on the basis of reasonably conservative and plausible assumptions, considering current lifestyles as well as the available site or region specific information". Therefore, the living and food consumption habits of potentially exposed groups are assumed according to domestic information on current human habits. The consumption rate data came from the national food consumption database (Food and Drug Agency, 2017). The occupancy data of different groups came from labor statistics survey (Ministry of Labor, 2017). Besides the reference group, whose consumption rates are set to be the mean values, the higher consumption rates (three times the mean) of critical ingestion pathways are assumed for each group, and the occupancy values for different locations of each group are assigned (IAEA, 2003). The considered groups in each case of landscape evolution are shown in Table 12-2. The exposure pathways of each group are shown in Table 12-3. Also, ICRP states that "an adult representative person will adequately represent the exposure of a person representative of the more highly exposed individuals in the population" for geological disposal cases with levels of radionuclides in the environment that change slowly over the time scale of a human life time. Therefore, the corresponding data of adults is used for potentially exposed groups.

The related exposure pathways of the environmental media in the landscape module are shown in Figure 12-2. The mathematics models of exposure pathways are shown in Appendix C and D, and the corresponding parameters are listed in Appendix E.

Table 12-1: The radionuclide transport model of each release type.

Release type	Release location	Radionuclide transport model
Release into the sea (coastal period)	Sea	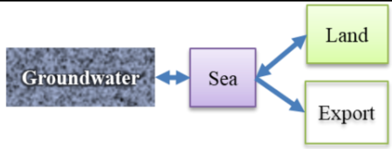
Release into the lagoon (coastal period)	Lagoon and surrounded land	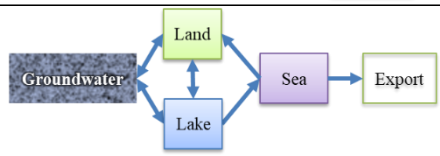
Release into the lake (inland period)	Lake and surrounded land	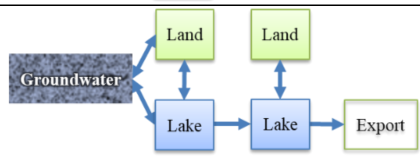
Release into the river (inland period)	River and surrounded land	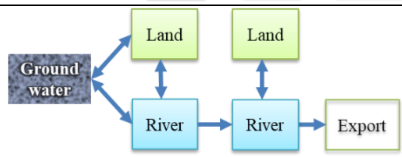
Release into the well (coastal period)	Well-water	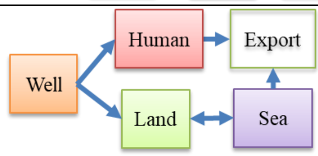
Release into the well (inland period)	Well-water	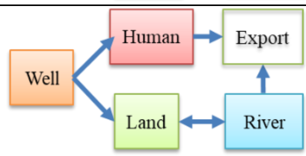

Table 12-2: Potentially exposed groups of each release type.

Release type	Considered potentially exposed groups							
	R.G.	Sta.	F.V.	Cow	Pig	Pou.	F.F.	O.F.
Sea (coastal)	※	※	※	※	※	※		※
Lagoon (coastal)	※	※	※	※	※	※	※	※
Lake (inland)	※	※	※	※	※	※	※	
River (inland)	※	※	※	※	※	※	※	
Well (coastal)	※	※	※	※	※	※		
Well (inland)	※	※	※	※	※	※		

Table 12-3: Exposure pathways of the potentially exposed groups.

Exposure mode	Exposure pathway	R.G.	Sta.	F.V.	Cow	Pig	Pou.	F.F.	O.F.
Ingestion	Water	Δ	Δ	Δ	Δ	Δ	Δ	Δ	Δ
	Liquor	Δ	Δ	Δ	Δ	Δ	Δ	Δ	Δ
	Root	Δ	◎	Δ	Δ	Δ	Δ	Δ	Δ
	Green vegetable	Δ	Δ	◎	Δ	Δ	Δ	Δ	Δ
	Grain	Δ	◎	Δ	Δ	Δ	Δ	Δ	Δ
	Fruit	Δ	Δ	◎	Δ	Δ	Δ	Δ	Δ
	Beef	Δ	Δ	Δ	◎	Δ	Δ	Δ	Δ
	Pork	Δ	Δ	Δ	Δ	◎	Δ	Δ	Δ
	Chicken	Δ	Δ	Δ	Δ	Δ	◎	Δ	Δ
	Milk	Δ	Δ	Δ	◎	Δ	Δ	Δ	Δ
	Offal	Δ	Δ	Δ	Δ	◎	Δ	Δ	Δ
	Egg	Δ	Δ	Δ	Δ	Δ	◎	Δ	Δ
	Freshwater fish	Δ	Δ	Δ	Δ	Δ	Δ	◎	Δ
	Oyster	Δ	Δ	Δ	Δ	Δ	Δ	Δ	◎
	Soil	X	Δ	Δ	Δ	Δ	Δ	X	X
	Sediment	X	X	X	X	X	X	X	Δ
Inhalation	Air_land (CO_2)	O	O	O	O	O	O	O	O
	Air_aquatic (CO_2)	X	X	X	X	X	X	O	O
	Dust (soil)	O	O	O	O	O	O	X	X
	Dust (grain)	X	X	X	X	X	X	O	O
	Dust (sediment)	X	X	X	X	X	X	O	O
External	Work on soil	O	O	O	O	O	O	X	X
	Live on soil	O	O	O	O	O	O	O	O
	Work on sediment	X	X	X	X	X	X	O	O

Note: Δ: average value, ◎: 3 times of the average value, X: not considered, O: considered.

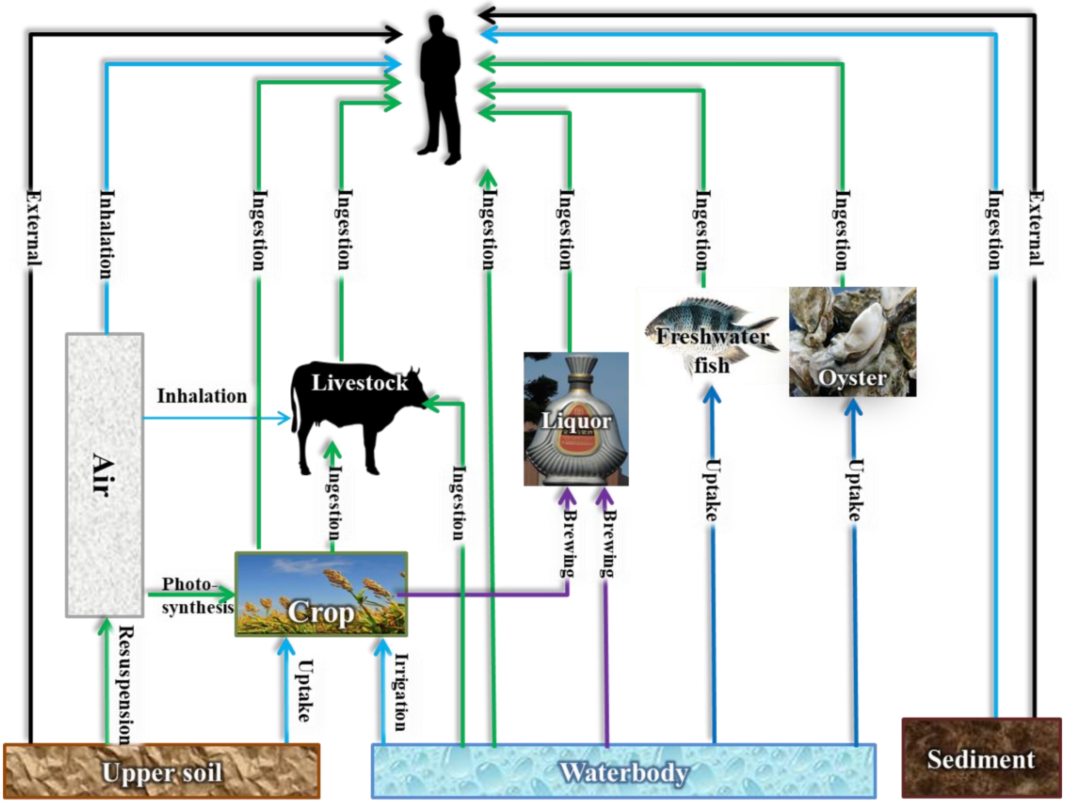

Figure 12-2: Relation between exposure pathways and environmental media.

12.2.3. Radionuclide Model for Biosphere

As mentioned in Section 12.2.2, the radionuclide transport model is built by the compartment model of the GoldSim program to calculate the radionuclide activity concentration of environmental media. The six kinds of landscape combinations, which represent the different release locations, are considered: (1) Release into the sea (coastal period), (2) Release into the lake (inland period), (3) Release into the lake (inland period), (4) Release into the river (inland period), (5) Release into the well (coastal period), and (6) Release into the well (inland period). The mathematical models of the processes considered in the model are shown in Appendix A and B, and the corresponding parameters are listed in Appendix E.

The landscape module is constructed by the environmental media compartments referencing the international examples (IAEA, 2003; POSIVA, 2014; Lindborg, 2010). The landscapes include land, lake (including lagoon), river, sea, and well-water, described as follow:

(1) Land:

The environmental media compartments built include lower soil, upper soil, crop, woods, and air.

(a) Soil: the soil is divided into two layers because of the radionuclide heterogeneity in the soil, which is caused by multiple radionuclide transport processes. The processes include percolation, capillary rise, root uptake, and bioturbation.

(b) Crop and woods: in the reference case, the terrestrial land is composed of cropland and forest. Therefore, some radionuclides are assumed to be up taken by the crops and woods when the radionuclides enter the terrestrial landscape.

(c) Air: the air compartment is added to consider the transport of C-14 in the biosphere. It will be up taken by the plant through the photosynthesis process from the air.

The conceptual model of the terrestrial landscape module is shown in Figure 12-3. The corresponding radionuclide transport process in the terrestrial module and their transport directions are shown in the figure.

(2) Lake:

The waterbody on the surface usually gathers in the local depression and becomes a lake, river or sea under different topography, and the groundwater usually discharges to these depressions, too. Therefore, the landscape modules of the lake, river, and sea were built for the biosphere assessment. The compartments of the lake module include the soil, sediment, waterbody, primary producer, and air, explained as follows:

(a) Soil and sediment: the lake bottom is covered by sand, pebble gravel, and organic matter. The sediment is divided into two layers, where the upper layer is disturbed by the sedimentation and the resuspension processes of the lake, and the net sedimentation process brings the radionuclides to the lower layer. Besides, the radionuclides in the sediment may be transported to the land by the sediment dredging process.

(b) Waterbody: the radionuclides in the waterbody may be transported to the land by the irrigation and flooding process.

(c) Primary producer: the radionuclides in the waterbody may be up-taken by the primary producer, whose biomass data came from the result of the national carbon sequestration survey of important wetland project (高苑科技大學綠工程技術研發中心, 2011).

(d) Air: the carbon dioxide will resolve into the waterbody and degas to the air from the waterbody. The carbon budget data is considered in the lake module and came from the result of the national carbon sequestration survey of important wetland projects (高苑科技大學綠工程技術研發中心, 2011).

The conceptual model of the lake landscape module is shown in Figure 12-4 (freshwater). The corresponding radionuclide transport process in the lake module and their transport directions are shown in the figure.

(3) River:

The structure of the river landscape module is almost the same as the lake module; the compartment of the lake module includes the soil, sediment, waterbody, primary producer, and air described below:

(a) Soil and sediment: compared with the lake, the volume of the river is small, and the flow rate is high, so the sedimentation and resuspension rates are faster than the lake. Besides, the radionuclides in the sediment are transported to the land and sea sediment by sediment dredging and bed-load transport processes.
(b) Waterbody: the radionuclides in the waterbody may be transported to the land by the irrigation and flooding process.
(c) Primary producer: biomass parameters were assumed according to the characteristics of the reference case (黃家勤等人, 2006). Total biomass in the river was set to be lower than in the lake.
(d) Air: the air compartment of the river is relatively small, and the water flow is fast, so there are a few of the carbon budget research on the river. Therefore, the carbon budget data for the river is assumed to be the same as the lake.

The conceptual model of the river landscape module is shown in Figure 12-4 (freshwater). The corresponding radionuclide transport process in the river module and their transport directions are shown in the figure.

(4) Sea:

When the release location is in the sea, the radionuclides will release to the sea bed, which is covered by soil and sediment, and then transported to the sea-water which will cause massive dilution. However, the radionuclides may be concentrated in a specific area by the sea current. Radionuclides are assumed to be concentrated in the tidal zone. The compartment of the sea module includes the soil, sediment, waterbody, primary producer, and air, explained as follows:

(a) Soil and sediment: The sea bottom of the tidal zone is covered by sand and organic matter. The sediment is divided into two layers, where the upper layer is disturbed by the sedimentation and the resuspension processes of the tide, and the net sedimentation process brings the radionuclides to the lower layer.

(b) Waterbody: The radionuclides in the seawater may be transported to the land by the sea-spray process. It will be taken out of the system by the ocean current.

(c) Primary producer: parameters were assumed according to the characteristics of the reference case (林幸助與李麗華, 2011).

(d) Air: The tidal zone research result of the national carbon sequestration survey of important wetland project (高苑科技大學綠工程技術研發中心, 2011) is used to set up the carbon budget data.

The conceptual model of the sea landscape module is shown in Figure 12-4 (sea). The corresponding radionuclide transport process in the river module and their transport directions are shown in the figure.

(5) Well-water:

The well-water module is a particular case that belongs to the terrestrial landscape module. The well water is available for any terrestrial landscape, and the radionuclides could be released along the well-water. Therefore, the well-water module is built combined with the terrestrial landscape.

The conceptual model well-water module (the same as the terrestrial landscape module) is shown in Figure 12-3. The only difference between the well-water landscape and terrestrial module is that the radionuclides are not released from the groundwater to the lower soil layer but are directly extracted along with the well-water (the 14 well irrigation in Figure 12-3). In this module, a part of the well-water will be drunk by humans, and the other part will be irrigated onto the upper soil layer and flowed into the different environmental media. The radionuclides are diluted by the well-water pumpage, whose data came from the water right data recorded by the Water Resources Agency (水利署, 2017).

When the well-water is used for irrigation, the conceptual model of the well-water module is the same as Figure 12-3. The corresponding radionuclide transport process in the well-water module and their transport directions are shown in the figure.

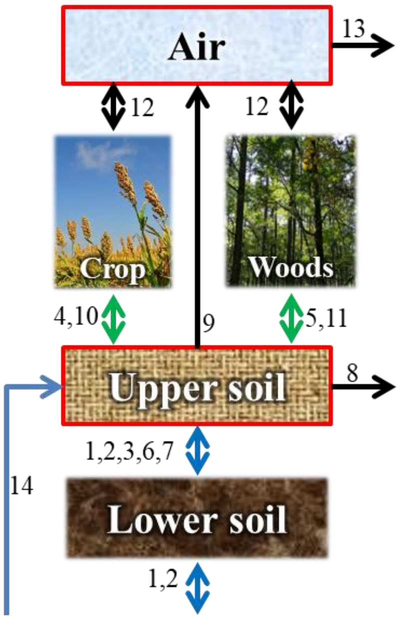

Media	No.	Process (outflow)
Lower Soil	1	Upward flow
	2	Downward flow
	3	Bioturbation
Upper soil	4	Crop uptake
	5	Tree uptake
	6	Downward flow
	7	Bioturbation
	8	Erosion
	9	Carbon degassing
Crop	10	Senescence
Woods	11	Senescence
Air	12	Photosynthesis
	13	Air flow
Groundwater	14	Well irrigation

Figure 12-3: The terrestrial landscape module.

Note 1: arrows in the figure indicate the direction of radionuclide transport and numbers on the arrows indicate the transport process numbers.

Note 2: radionuclide will release to soil through process 14 in well-water module.

Note 3: process 8 is connected to waterbody of the aquatic landscape module, and process 13 is connected to air.

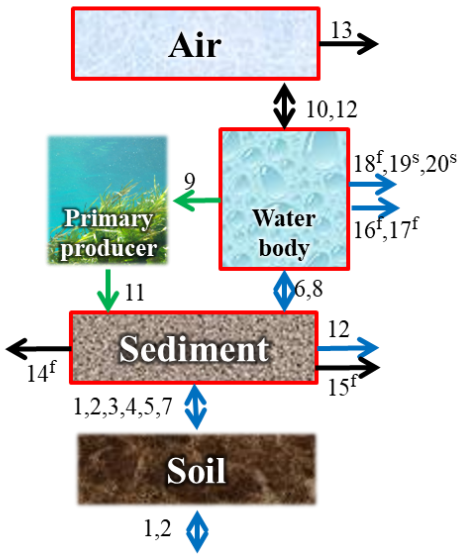

Media	No.	Process (outflow)
Soil	1	Upward flow
	2	Downward flow
	3	Bioturbation
Sediment	4	Downward flow
	5	Bioturbation
	6	Resuspension
	7	Net sedimentation
Waterbody	8	Sedimentation
	9	Uptake
	10	Carbon degassing
Primary producer	11	Senescence
Air	12	Carbon dissolving
	13	Air flow
Sediment (freshwater)	14^f	Sediment dredging
	15^f	Bed-load transport
Waterbody (freshwater)	16^f	Flooding
	17^f	Irrigation
	18^f	Surface runoff
Waterbody (sea)	19^s	Sea spray
	20^s	Marine current

Figure 12-4: The aquatic landscape module.

Note 1: superscript f indicates the freshwater ecosystem, and superscript s indicates the sea ecosystem.

Note 2: processes 14f, 16f, 19s, and 17f are connected to upper soil, process 15f is connected to sediment of the sea module, process 13 is connected to air, process 18f is connected to downstream waterbody or away from the system, and process 20s is away from the system.

12.2.4. Biosphere Dose Conversion Factor

The landscape module shown in Section 12.2.3 can be combined according to the release types shown in Table 12-1. The radionuclide activity concentration of each environment media could be calculated based on the constant release of 1 Bq/year for each radionuclide. Several potentially exposed groups are assumed according to their habits which may be exposed to radiation through exposure pathways corresponding to the landscape. The BDCF of the potentially exposed groups can be calculated, and the largest one in all cases was chosen.

The maximum BDCF of each release type chosen cautiously for each potentially exposed group is listed in Table 12-4. The result shows that the maximum BDCF value for all radionuclides is Pa-231 of the fruit grower, and the second-largest value is Ac-227 of the poultry farmer. The ingestion and inhalation dose conversion factors of Pa-231 are high, and its distribution coefficient (K_d) value is relatively low compared with the other radionuclides whose ingestion and inhalation dose conversion factors are also high (for example, Th-229, Th-230, and Cm-246). When the K_d values are high, the radionuclides are absorbed by the soil, and only a small portion reaches the upper soil along with the water cycle in the surface system. Therefore, the BDCF for Pa-231 is higher than other radionuclides. It should be noted that, although BCDF is high for several radionuclides, it doesn't mean their dose consequences in safety assessment are severe. Some of them may be absorbed and retarded in the near-field and far-field.

Several pessimistic assumptions are made in this assessment, so the BDCFs shown in this section are relatively large compared with the international reference (JNC, 2000; NUMO, 2021). These assumptions and their uncertainty are discussed in Section 12.2.6.

Table 12-4: BDCFs of the potentially exposed groups ($\frac{Sv/y}{Bq/y}$).

	R.G.	Sta.	F.V.	Cow	Pig	Pou.	F.F.	O.F.
C-14	3.3×10^{-12}	3.7×10^{-12}	3.4×10^{-12}	3.6×10^{-12}	5.6×10^{-12}	6.2×10^{-12}	4.2×10^{-12}	3.4×10^{-12}
Cl-36	2.5×10^{-12}	3.4×10^{-12}	4.4×10^{-12}	2.7×10^{-12}	3.4×10^{-12}	3.7×10^{-12}	2.5×10^{-12}	2.5×10^{-12}
Ni-59	3.5×10^{-14}	6.0×10^{-14}	6.0×10^{-14}	3.9×10^{-14}	4.6×10^{-14}	4.9×10^{-14}	3.5×10^{-14}	3.5×10^{-14}
Se-79	7.1×10^{-11}	8.8×10^{-11}	1.1×10^{-10}	9.3×10^{-11}	1.0×10^{-10}	1.1×10^{-10}	7.2×10^{-11}	7.1×10^{-11}
Sr-90	4.9×10^{-12}	1.1×10^{-11}	7.5×10^{-12}	5.1×10^{-12}	5.1×10^{-12}	5.3×10^{-12}	5.4×10^{-12}	5.1×10^{-12}
Zr-93	5.0×10^{-13}	1.3×10^{-12}	6.4×10^{-13}	5.0×10^{-13}	5.3×10^{-13}	5.0×10^{-13}	5.2×10^{-13}	5.1×10^{-13}
Nb-94	5.2×10^{-11}	5.2×10^{-11}	5.2×10^{-11}	5.2×10^{-11}	5.2×10^{-11}	5.2×10^{-11}	4.1×10^{-11}	4.0×10^{-11}
Tc-99	2.9×10^{-13}	5.7×10^{-13}	3.8×10^{-13}	3.3×10^{-13}	2.9×10^{-13}	4.0×10^{-13}	2.9×10^{-13}	2.9×10^{-13}
Pd-107	3.4×10^{-14}	5.6×10^{-14}	7.8×10^{-14}	3.4×10^{-14}	3.4×10^{-14}	3.4×10^{-14}	3.4×10^{-14}	3.4×10^{-14}
Sn-126	5.6×10^{-12}	8.5×10^{-12}	1.1×10^{-11}	5.7×10^{-12}	5.7×10^{-12}	5.8×10^{-12}	5.4×10^{-12}	5.3×10^{-12}
I-129	5.0×10^{-11}	8.5×10^{-11}	7.2×10^{-11}	5.5×10^{-11}	6.5×10^{-11}	6.5×10^{-11}	5.4×10^{-11}	5.1×10^{-11}
Cs-135	1.3×10^{-12}	1.9×10^{-12}	1.6×10^{-12}	1.4×10^{-12}	2.5×10^{-12}	1.6×10^{-12}	1.6×10^{-12}	1.3×10^{-12}
Cs-137	8.1×10^{-12}	1.1×10^{-11}	9.5×10^{-12}	8.7×10^{-12}	1.5×10^{-11}	9.8×10^{-12}	9.7×10^{-12}	8.2×10^{-12}
Th-232	9.4×10^{-11}	2.2×10^{-10}	1.3×10^{-10}	9.9×10^{-11}	1.0×10^{-10}	1.0×10^{-10}	9.6×10^{-11}	9.6×10^{-11}
U-236	2.2×10^{-11}	4.2×10^{-11}	3.0×10^{-11}	2.3×10^{-11}	3.1×10^{-11}	2.8×10^{-11}	2.3×10^{-11}	2.3×10^{-11}
Pu-240	4.1×10^{-11}	5.9×10^{-11}	1.0×10^{-10}	4.1×10^{-11}	4.1×10^{-11}	4.1×10^{-11}	4.3×10^{-11}	4.3×10^{-11}
Th-229	2.0×10^{-10}	4.8×10^{-10}	2.8×10^{-10}	2.1×10^{-10}	2.3×10^{-10}	2.3×10^{-10}	2.1×10^{-10}	2.1×10^{-10}
U-233	2.4×10^{-11}	4.5×10^{-11}	3.3×10^{-11}	2.5×10^{-11}	3.4×10^{-11}	3.1×10^{-11}	2.5×10^{-11}	2.5×10^{-11}
Np-237	1.8×10^{-11}	4.2×10^{-11}	2.9×10^{-11}	1.8×10^{-11}	1.8×10^{-11}	1.9×10^{-11}	1.9×10^{-11}	1.9×10^{-11}
Am-241	2.5×10^{-11}	6.4×10^{-11}	2.8×10^{-11}	2.6×10^{-11}	2.6×10^{-11}	2.7×10^{-11}	3.0×10^{-11}	2.6×10^{-11}
Cm-245	7.1×10^{-11}	1.7×10^{-10}	1.1×10^{-10}	7.5×10^{-11}	7.5×10^{-11}	7.6×10^{-11}	7.3×10^{-11}	7.3×10^{-11}
Pb-210	2.7×10^{-10}	5.0×10^{-10}	3.6×10^{-10}	2.7×10^{-10}	3.4×10^{-10}	3.6×10^{-10}	2.8×10^{-10}	2.7×10^{-10}
Ra-226	1.2×10^{-10}	2.5×10^{-10}	1.6×10^{-10}	1.2×10^{-10}	1.7×10^{-10}	1.4×10^{-10}	1.3×10^{-10}	1.2×10^{-10}
Th-230	8.7×10^{-11}	2.3×10^{-10}	2.3×10^{-10}	2.3×10^{-10}	2.3×10^{-10}	2.3×10^{-10}	8.8×10^{-11}	8.8×10^{-11}
U-234	2.3×10^{-11}	4.3×10^{-11}	3.2×10^{-11}	2.4×10^{-11}	3.3×10^{-11}	3.0×10^{-11}	2.4×10^{-11}	2.4×10^{-11}
U-238	2.1×10^{-11}	4.0×10^{-11}	2.9×10^{-11}	2.2×10^{-11}	3.0×10^{-11}	2.7×10^{-11}	2.2×10^{-11}	2.2×10^{-11}
Pu-238	3.7×10^{-11}	5.3×10^{-11}	9.2×10^{-11}	3.7×10^{-11}	3.7×10^{-11}	3.8×10^{-11}	3.9×10^{-11}	3.9×10^{-11}
Pu-242	1.2×10^{-10}	4.7×10^{-10}	5.1×10^{-10}	4.5×10^{-10}	4.5×10^{-10}	4.5×10^{-10}	1.2×10^{-10}	1.2×10^{-10}
Cm-246	7.1×10^{-11}	1.7×10^{-10}	1.1×10^{-10}	7.5×10^{-11}	7.5×10^{-11}	7.5×10^{-11}	7.3×10^{-11}	7.3×10^{-11}
Ac-227	4.2×10^{-10}	9.9×10^{-10}	6.0×10^{-10}	4.2×10^{-10}	4.2×10^{-10}	4.2×10^{-10}	4.5×10^{-10}	4.2×10^{-10}
Pa-231	5.7×10^{-10}	1.1×10^{-09}	1.5×10^{-09}	8.1×10^{-10}	8.1×10^{-10}	8.1×10^{-10}	5.7×10^{-10}	5.7×10^{-10}
U-235	2.2×10^{-11}	4.2×10^{-11}	3.0×10^{-11}	2.3×10^{-11}	3.1×10^{-11}	2.8×10^{-11}	2.3×10^{-11}	2.3×10^{-11}
Pu-239	4.8×10^{-11}	1.9×10^{-10}	2.0×10^{-10}	1.8×10^{-10}	1.8×10^{-10}	1.8×10^{-10}	4.9×10^{-11}	4.8×10^{-11}
Am-243	2.6×10^{-11}	6.7×10^{-11}	3.1×10^{-11}	2.9×10^{-11}	3.0×10^{-11}	3.0×10^{-11}	3.1×10^{-11}	2.7×10^{-11}

Note: The maximum value of each radionuclide is highlighted by yellow background.

12.2.5. Assessment of Radiological Effects on the Environment

In order to protect the biological diversity and the sustainability of natural resources, the radiological effect of the radionuclides released from the repository on the non-human biota should be evaluated. However, the dose limit of non-human biota is not required by domestic regulations, so the related evaluation methodology has not been developed. According to the suggestions from ICRP publication 108 and the results of the FASSET, ERICA, and PROTECT projects developed by the European atomic energy community (Euratom), assessment should be considered when candidate sites are confirmed. According to the experience of international projects (such as SKB), the impacts are much smaller than the regulatory requirements of environmental protection.

12.2.6. Uncertainties in the Risk Estimation

In order to cover the considerable uncertainty, several pessimistic assumptions are made in this assessment, and it results in the larger BDCFs. According to the BIOMASS-2020 (T. Lindborg, 2020) and Section 2.7, the uncertainty of the risk assessment includes three types, which is (1) System/scenario uncertainty, (2) Concept/model uncertainty, and (3) Data/ parameter uncertainty, discussed as follows:

(1) System/scenario uncertainty:

The system/scenario uncertainty in the biosphere assessment could be addressed by temporal and spatial aspects. The safety assessment timeframe for the disposal repository is one million years, and the landscape on the surface environment during this time is assumed to change with the periodic transition of the glacial cycle. In general, the exposure of the potentially exposed group at a specific time should be estimated by a radionuclide transport model built according to the landscape at that time. However, due to uncertainty of the length of the glacial cycle, uncertainty exists in the evaluation of landscape evolution at a specific time. In order to cover this kind of uncertainty, the maximum value of BDCFs of all landscape evolution periods is pessimistic selected for the following radiation risk assessment.

The spatial aspect of the system/scenario uncertainty is depended on the site characteristics. For example, if the candidate site is located in eastern Taiwan, the impact of the sea-level change on the landscape evolution is small because eastern Taiwan is close to the Ryukyu trench. The shoreline will change slightly when the sea-level falls, and the release location may still occur on the sea. However, if the candidate site is located in western Taiwan, the Taiwan Strait may become terrestrial land because of the sea-level fall. The release location may occur on the terrestrial or freshwater aquatic landscape and cause more severe consequences. In the reference case, a large-scale landscape change is assumed to consider the uncertainty of release location. However, evidence of the area and geometry of the biosphere object is not enough, so the smaller area is assumed pessimistically in this assessment to cover the considerable uncertainty. When the candidate site is confirmed in the future, the uncertainty could be reduced by estimating the catchment and depression area change caused by sea-level change according to the topography of land and sea bottom.

(2) Concept/model uncertainty:

In order to reduce the uncertainty of human error in biosphere modelling, the international guide was followed, and the example of reference biosphere was used for code verification. Also, the compartment model was used to perform biosphere assessment, and the radionuclide distribution inside the compartment was assumed to be homogeneous. This assumption causes the uncertainties of vertical transport and dispersion, leading to the instant surface arrival and the dilution of radionuclides. The uncertainties could be reduced by increasing the compartment number in the vertical direction and adjusting the compartment area and depth according to the detailed investigation and the in situ testing of the candidate site.

(3) Data/parameter uncertainty:

The parameters used in the biosphere assessment could be divided into two parts, the radionuclide-dependent data and the radionuclide-independent data. Uncertainty of the radionuclide-dependent data, which uses the international reference, has not been discussed. The radionuclide-independent data includes the human-related factors and the environmental parameters. The human-related data used in this assessment comes from the national data library. Although there may be an uncertainty of local habit difference, a higher food consumption rate is considered according to the suggestion of BIOMASS-6 to increase the confidence. The uncertainties in the environmental parameters are considerable because many data come from the different areas in Taiwan or even other countries due to the lack of local research, so several parameters are chosen pessimistically to cover the uncertainty. Especially the soil water flow data in the unsaturated zone, which affects the radionuclide distribution in the soil, will be a major source of parameter uncertainty in the biosphere assessment. Compared with SNFD 2017, the capillary rise process, which results in larger BDCFs, is added pessimistically to cover this uncertainty.

In summary, several pessimistic assumptions are made to cover the considerable uncertainty in this case. The relatively high BDCF result can not reveal the local characteristics. A detailed site investigation and site description model could be made to reduce the uncertainty in the future, and the complete uncertainty analysis of biosphere assessment could be done and fed back to the safety case.

12.3. Criticality

According to Chapter 7, when the canister cavity is full of water, the effective neutron multiplication factor should be less than 0.95. This is to ensure that the SNF can be maintained in a subcritical state, which can avoid criticality during disposal (safety function F3). Only intact canister case in the current phase is considered in this report. The long-term effect such as cast iron corrosion after water intrusion has not been considered yet.

MCNP program, a Monte Carlo method code, was used to track and record the migration history of neutrons for nuclear criticality analysis (LANL, 2018). It is assumed that the BWR and PWR canisters are fully loaded with SNF (12 SNF for the BWR canister, and 4 PWR SNF for the PWR canister), and the fuels are conservatively assumed to be fresh with maximum initial enrichment up to 5.0 U-235 wt%. Through sensitivity analysis, various parameters such as fuel type, canister geometry, material property and other parameters are evaluated for their influence on the effective neutron multiplication factor. After that, the most conservative parameter combination is used to maximize the effective neutron multiplication factor.

The nuclear criticality safety analysis model had been established. The model contains SNF, canister, buffer, and deposition hole and includes all types of SNF in Taiwan (8 types of BWR SNF and 2 types of PWR SNF). After performing a series of sensitivity studies of the reactivity effect on several parameters, the most conservative parameter combination for calculating the maximum neutron effective multiplication factor is as follows:

(1) Choose ATRIUM10 to represent SNF for BWR and OFA 17X17 to represent SNF for PWR.
(2) Iron content of the cast iron lining is 90%.
(3) Density of the cast iron lining is 7.1 g/cm^3.
(4) Iron content of the insert channels is 97.57%.
(5) Density of the insert channels is 7.85 g/cm^3.
(6) The fuel assemblies are displaced radially inward, as shown in Figure 12-6.
(7) Minimum c-c distance between compartments.
(8) Minimum insert channel size.
(9) Nominal insert channel tube wall thickness.
(10) Nominal insert cast iron diameter.
(11) Nominal copper shell thickness.
(12) Nominal insert channel length.

(13)Nominal length of copper canister.

(14)The temperature is 20 ℃.

The maximum neutron multiplication factor can be determined based on these most conservative parameter combinations listed above. Based on the analysis results, if the canister does not fail and can maintain its integrity, i.e., no water in the canister cavity, the maximum neutron effective multiplication factor is less than 0.3, so there is no doubt about nuclear criticality safety at all. If the canister fails and water enters, since hydrogen is an excellent neutron moderator, the probability of nuclear fission will increase. In fact, the canister is loaded with spent fuel instead of fresh fuel, which is a credit that has not been considered in the analysis model currently. A brief analysis result shows that the reactivity significantly reduces if burnup credit is taken. International nuclear criticality safety analysis of similar designs was referred to; the results show that it is extremely unlikely to achieve nuclear criticality. Therefore, further discussion will focus on the burnup credit to prove that if burnup credit is taken, then the neutron multiplication factor can still meet the requirements, which need to be less than 0.95, even if the canister fails and water enters.

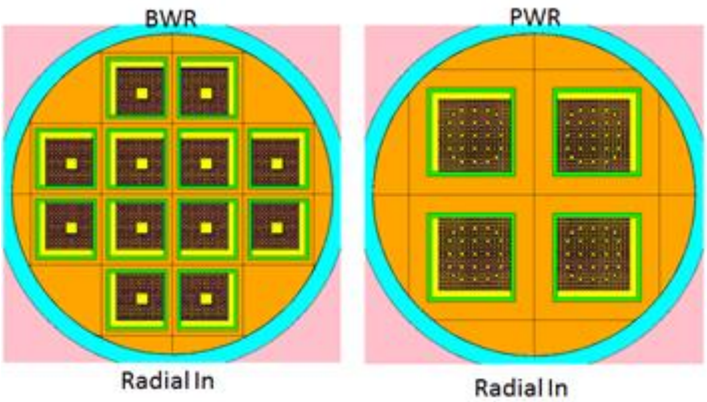

Figure 12-5:The radial-inward displaced fuel assemblies.

12.4. Radionuclide Transport and Dose Estimation

The purpose of the radionuclide transport calculation model is to calculate radionuclide transport through multi-barriers to the biosphere when a safety function of the canister fails.

GoldSim was used in the radionuclide transport calculation, and Figure 9-23 shows the schematic diagram. Two parts are included in this model:

(1) Near-field: Including the canister, buffer and backfill.

(2) Far-field: The rock and fractures within rock.

Two potential transport paths were considered in the near-field. When the canister is failed, the main transport path for radionuclides is from the canister to the fracture intersecting a deposition hole (Q1 path). Radionuclides diffuse through the buffer and the backfill to EDZ at the bottom of the disposal tunnel were also considered (Q2 path).

The natural decay of radionuclides is also included in the radionuclide transport model. If the radionuclide belongs to a certain decay chain, the daughter nuclides would also be included in the evaluation.

12.4.1. Estimation of Nuclide Transport in Near-Field

In near-field transport calculation, the compartment model has been used to describe the geometries, as shown in Figure 12-6, and the material characteristics of the void volume of the canister, the buffer and the backfill. The estimation was carried out based on the main processes, which include radionuclide transport (TWF17 and TWC15) and transport of radionuclides in the water phase (TWBu25 and TWBfT21), in cooperation with radioactive decay (TWF01), metal corrosion (TWF11), fuel dissolution (TWF12), dissolution of gap inventory (TWF13), speciation of radionuclides, colloid formation (TWF14), diffusive transport of species (TWBu11), sorption (including exchange of major ions) (TWBu12 and TWBfT11) and colloid transport (TWBu23).

The void volume in the canister was assumed to be 1 m^3 (SKB, 2010i). The groundwater will intrude into the canister when the canister is failed. The radionuclides will be released into groundwater in the void volume of the canister by the following mechanisms:

(1) Continuous release:

Radionuclides embedded in the fuel matrix are released into groundwater constantly once groundwater intrudes into the canister. The rate of continuous release was specified according to Table 8-1.

(2) Instant release:

Radionuclides located in the fuel-clad gap or grain boundaries will be released instantly upon contact with groundwater. The release fraction of the total radionuclide inventory was specified according to Table 8-4.

(3) Corrosion release:

The activated nuclides in metal are released constantly upon contact with groundwater. The release rate and release fraction of the total radionuclide inventory were specified according to Table 8-2 and Table 8-3.

The dissolved amount of radionuclide released in groundwater depends on the solubility limit of its element. Radionuclide will precipitate in the void volume of the canister if the amount in the water exceeds the solubility limit. The solubility limits of elements were specified according to Table 8-8 and Figure 8-2. The isotopes will share a solubility limit according to their fraction of the total amount.

Diffusion is the primary transport mechanism for radionuclides transported through the buffer and the backfill. The element specific effective diffusion coefficients are listed in Table 8-6. The diffusion-available porosity can be found in Table 8-7. The sorption of nuclides on materials is controlled by the partition coefficient (K_d), the values are specified according to Table 8-9 to Table 8-11. The transport of radionuclides from the near-field to the fracture in the far-field is dominated by advection. The near-field release rate of radionuclides was estimated by an equivalent flow rate (Q_{eq}). The equivalent flow rate, which are described in Chapter 9 (hydrogeological evolution), is an analytical solution of solute transport equivalent flow rate at the interface of near and far-field to avoid fine discretization of the near/far-field interface (Romero, 1995).

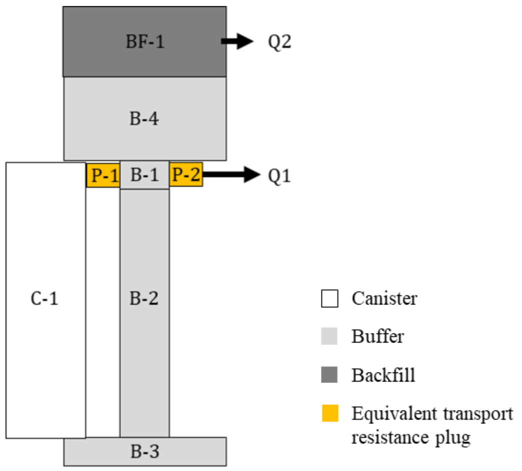

Figure 12-6: Materials of the compartments and the release paths in the near-field.

Note: B-1 to B-4 is compartment names representing the buffer. Bf-1 is the compartment name representing the backfill. C-1 is the compartment name representing the canister. P-1 and P-2 are compartment names representing the equivalent transport resistance plugs. Q1 and Q2 are release paths in the near-field.

12.4.2. Estimation of Nuclide Transport in Far-Field

The one-dimensional advection-dispersion equation coupling with matrix diffusion in the direction perpendicular to the advection has been adopted in simulation to estimate the migration of the radionuclides in the far-field. The estimation is carried out based on major processes, transport of radionuclides in the water phase (TWGe24), in cooperation with radioactive decay (TWF01), advective transport/mixing of dissolved species (TWGe11), diffusive transport of dissolved species in fractures and rock matrix (TWGe12), speciation and sorption (TWGe13) and colloidal processes (TWGe18).

The input parameters of the far-field transport calculation model include length (L), cross-sectional area (A) and flow rate (Q) of the channel. These parameters were calculated based on the results of Chapter 9 (flow-related transport resistance and advective travel time).

$L = vt_w$	(12- 1)
$A = 2bW = \dfrac{2WL}{Fv}$	(12- 2)
$Q = 2bW\dfrac{L}{t_w}$	(12- 3)

where,

A = cross-sectional area of the path, [m^2].

b = a half of aperture, [m].

F = flow related transport resistance, [yr/m].

L = length of the path, [m].

Q = flow rate of the path, [m^3/yr].

t_w = advective travel time, [yr].

v = velocity, [m/yr].

W = width of the path [m], arbitrarily assumed to be 1 m.

The Peclet number (P_e) is 10 (SKB, 2010h). In other studies carried out in hard rocks (Joyce, 2010), the modelling of hydrogeology suggests a limited correlation between high near-field groundwater flow (i.e. Q_{eq}) and low F values, and such correlations have not been considered in this study. Migration of radionuclides in rock matrix is mainly controlled by diffusion. The element-specific effective diffusion coefficients are listed in Table 8-6, and the available diffusion porosity is listed in Table 8-7. The maximum penetration depth for solute diffusion into the rock matrix is calculated based on the fracture spacing in the reference case (Section 4.3.2). The calculation equation for the maximum penetration depth is shown below (SKB, 2010i):

$$M_t = 0.5/P_{10} \tag{12- 4}$$

where,

M_t = maximum penetration depth, [m].

P_{10} = fracture intensity, [m^{-1}].

According to the calculation, the maximum penetration depth for radionuclide diffusion into the rock matrix is about 1.67 m. The sorption of nuclides on rock matrix is controlled by the partition coefficient (K_d). And K_d values are specified according to Table 8-9 and Table 8-11.

12.4.3. Description of the Biosphere

To estimate the dose consequences in the biosphere due to the releases of radionuclides from repository, the annual release activities of radionuclides calculated by the radionuclide transport calculation model were multiplied by BDCFs given in Section 12.2.4. The annual effective doses of nine potentially exposed groups in the biosphere were estimated.

12.4.4. Simplified Analytical Models

The analytical solutions of the near-field and far-field radionuclide transport models are derived based on works by Hedin (2002) to verify the results calculated by numerical models. The metal corrosion release of fuel and shared solubility limit of isotopes are taken into account in the analytical solutions. The main difference between the numerical solutions and analytical solutions for near-field is in the calculation of the annual release rate of radionuclides with the decay chain. The parent nuclides of Ra-226 and Pb-210, for example, were assumed totally precipitated in the void volume of the canister. However, this is unrealistic for some radionuclides if transport in the buffer is dominated by advection. Taking Pb-210 as an example, its parent nuclide Ra-226 is partly dissolved into groundwater and released due to the relatively high groundwater flow around the canister. This assumption could result in an overestimation. Besides, the redissolution of precipitated radionuclides was not considered in the analytical solutions. Therefore, compared with the numerical results, dose curves of some likely precipitable nuclides calculated by the analytical solutions are different.

The calculation of radionuclide transport in the fracture in the far-field depends on the release mechanism of the nuclides. For instance, the Cl-36 will be released into the void volume of the canister by continuous, instant and corrosion release. The release rate due to continuous release is calculated based on the works by Hedin (2002). The time of occurrence of the peak release rate due to instant and corrosion release is calculated by the following equation (Hedin, 2002):

$\tau_{geo} = \frac{R_f z}{v} - \frac{3}{4\lambda}\left(1 - \sqrt{1 + \left(\frac{2R_f L}{3A_R v}\right)^2 \lambda}\right)$	(12- 5)
$A_R = \frac{bR_f}{\sqrt{\epsilon_p D_e R_p}}$	(12- 6)
$R_f = 1 + \frac{K_f}{b}$	(12- 7)

$R_p = 1 + \frac{1-\epsilon_p}{\epsilon_p} K_d \rho$	(12- 8)

where,

τ_{geo} = the time of occurrence of the peak release rate, [yr].

D_e = effective diffusion coefficient in rock matrix, [m^2/yr].

ϵ_p = porosity of rock matrix, [-].

K_d = partition coefficient in rock matrix, [m^3/kg].

K_f = fracture partition coefficient (per unit surface area), [m].

λ = radioactive decay constant, [yr^{-1}].

ρ = density of rock matrix, [kg/m^3].

R_f = rock fracture wall retardation constant, [-].

R_p = rock matrix retardation constant, [-].

Peak release rate is calculated by the following equation (SKB, 2006b):

$\phi_{Peak\_Far} = M_0(IRF + CRF)/\tau$	(12- 9)
$\tau = F^2 D_e\left[\epsilon_p + \left(1-\epsilon_p\right)K_d\rho\right]2\sqrt{\pi}\left(\frac{e}{6}\right)^{\frac{3}{2}}$	(12- 10)

where,

ϕ_{Peak_Far} = peak release rate, [mol/yr].

CRF = corrosion release fraction, [-].

e = Euler’s number, [-].

IRF = instant release fraction, [-].

M_0 = inventory of radionuclide, [mol].

The difference between the numerical model and analytical solutions of far-field is that the analytical solutions only calculate the peak release rate and its occurrence time due to instant release and corrosion release of inventory.

Some cases will be carried out by numerical models and theanalytical solutions simultaneously. The results are presented in Sections 12.5.8 and 12.6.6.

12.4.5. Selection of the Radionuclides

There are thousands of radionuclides in SNF. However, the influence of most radionuclides on the radiation dose of the biosphere is insignificant. In order to improve the efficiency of simulation, the selection of radionuclides is based on radiotoxicity index, half-life and inventory.

According to the description in Section 4.2.3, SCALE/ORIGEN-S (ORNL, 2011) has been adopted to estimate the inventory of fission/activation products, actinides and other nuclides. A total of 34 critical nuclides were selected (Table 4-1):

12.5. Quantitative Assessment of Canister Failure due to Corrosion

12.5.1. Introduction

As mentioned in Section 11.8.1, canister failure due to corrosion might occur if solutes are transported by advection in the buffer. When a canister is failed, groundwater will intrude into the canister and carry radionuclides out from the canister. The nuclides dissolved in the groundwater will be transported to the biosphere through the geosphere, resulting in doses for the potential exposed group.

The purpose of this section is to describe the estimation methods, input parameters and results of radionuclide transport calculation models for the corrosion scenario.

12.5.2. Conceptualization of the Transport Conditions

As described in Chapter 11, the buffer surrounding the canister is eroded to a certain degree if the canister is failed due to corrosion. Under this condition, the mass transport in the buffer is dominated by advection. In this scenario, radionuclides the transport of radionuclides from the canister to fracture in the geosphere are controlled by the groundwater surrounding the canister. In the near-field radionuclide transport model, the mass transport rate at the interface of buffer and geosphere is described by the equivalent flow rate. If the advection occurs in buffer, the equivalent flow (Q_{eq_eroded}) around the deposition hole can be calculated by the following equation (SKB, 2010l):

$$Q_{eq\_eroded} = f_{conc} U_0 2 r_h h_{can} \tag{12- 11}$$

where,

Q_{eq_eroded} = equivalent flow rate for eroded buffer condition, [m^3/yr].

f_{conc} = flow concentration factor, [-].

U_0 = equivalent initial flux, [m/yr].

r_h = radius of the deposition hole, [m].

h_{can} = height of the canister, [m].

Due to the higher flow rate in the deposition hole with eroded buffer condition, the flow concentration factor is assumed to be 2 (SKB, 2010l). Besides, equivalent initial flux is specified according to the evaluated results of Chapter 9 (hydrogeological evolution). The radionuclides transport in the fractures in the far-field is described in Section 12.4.2.

12.5.3. Input Parameters for the Transport Models

The properties of materials are specified according to Section 8.3. In deterministic cases, the median value of flow-related data estimated in Section 9.3.6 and 9.4.6 have been specified (Table 12-5 and Figure 12-7). The flow-related data estimated by the hydrogeological model were evaluated under three sea-levels, including current sea-level, sea-level falls to -20 m, and sea-level falls to -120 m. In stochastic cases, the flow-related data were sampled by the Latin hyper-cube sampling method. In GoldSim, the probability distribution of an input parameter was divided into several intervals equally. After that, the interval was randomly sorted, and a value was sampled from each interval to ensure sampling uniformly from the probability distribution (GoldSim

Technology Group, 2014). The near-field and far-field radionuclide release rates would be multiplied by dose conversion factors of the reference group in the biosphere (Section 12.2) to estimate the influence of radiation.

Table 12-5: Median values of the flow-related parameters.

Path	Flow-related transport resistance [yr/m]	Advective travel time [yr]	Velocity [m/yr]	Equivalent flow rate [m^3/yr]	Equivalent initial flux [m/yr]
Q1	1.84×10^{7}	9.07×10^{2}	3.78	7.84×10^{-5}	2.09×10^{-5}
Q2	2.07×10^{7}	1.06×10^{3}	2.98	4.11×10^{-5}	4.25×10^{-4}

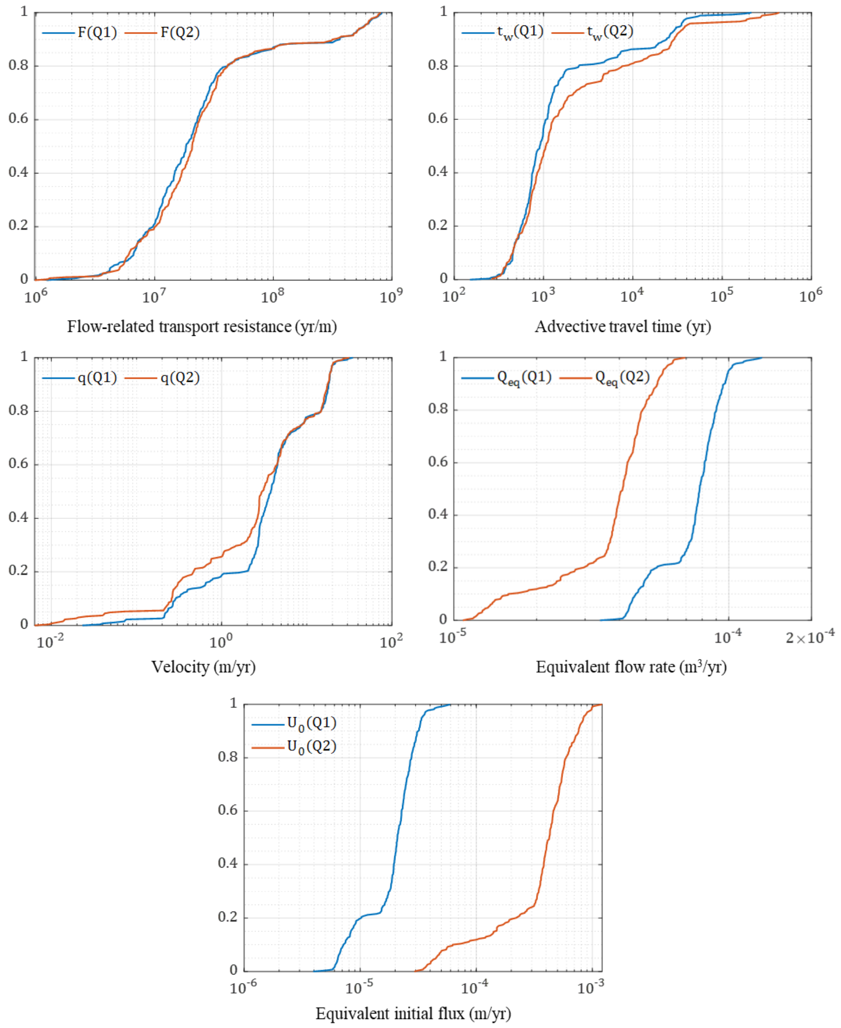

Figure 12-7: Cumulative density distribution of the flow-related parameters.

Note: the evaluation results of current sea-level 0 m, sea-level falls to -20 m, and sea-level falls to -120 m are included in the graphs.

12.5.4. Analyses of Basic Case

According to the analyses of Chapter 11, canister failure due to corrosion would not occur under the reference evolution. Therefore, the corrosion scenario is not taken into consideration as part of the basic scenario.

12.5.5. Analyses of Other Transport Conditions

Assuming advection condition in buffer occurs immediately after the repository is closed. On the other hand, the erosion time of the buffer is skipped (i.e., initial advection case in section 11.8.1). Therefore, taking the deposition hole, DH-2110, with the deepest corrosion depth of the copper canister, for example, the corrosion depth may increase about 1.90×10^{-1} mm. The containment safety function Can1 (providing a barrier against corrosion) will still be maintained under this condition. Therefore, this condition is not taken into account in the analysis of retardation.

12.5.6. Analyses of Variant Cases

Assuming that a canister will fail because of corrosion after 10^5 years post-closure. In this scenario, the buffer will be missing, and radionuclides will be transported from the canister to fracture by advection. The transport path Q1 will be the dominant transport path in this case. Under this condition, the deterministic and the stochastic cases were analyzed:

(1) Deterministic cases:

Figure 12-8 shows the near-field annual effective dose of the reference group for deterministic calculation of corrosion scenario with current sea-level. The near-field dose consequences were estimated by multiplying near-field release rates of different radionuclides by BDCFs. This means that the transport resistance for radionuclides in the far-field is neglected. It helps understand the contribution of transport resistance from the far-field. As shown in Figure 12-8, the peak doses that occur at early failure times are mainly induced by instant or metal corrosion release of inventory of Nb-94 and Cl-36. The release duration of instant and metal corrosion release are relatively short than the timescale for the safety assessment; the release rates of these 2 mechanisms are also faster than the release from the fuel matrix, as shown in Table 8-1 and Table 8-2. The peak annual effective dose is 2.92×10^{2} μSv/yr and is dominated by Pb-210 and Ra-226. The high amount of U-238 in the fuel constrains the release of its isotopes (U-233, U-234, U-235 and U-236) by the solubility limit in near-field. This also leads to the release increase of daughter nuclides of uranium isotopes (SKB, 2006b). The increased Th-230 will precipitate and generate Ra-226, leading to an increase in the release of Ra-226 and Pb-210. Most Ni-59 inventory (96%) will be released by metal corrosion and some of them are precipitated in the void volume of the canister during the first 1,000 years after canister failure. Therefore, a constant release rate of Ni-59 during a long-term period can be seen. The annual effective dose of Ni-59 will decrease after the precipitation amount is released or decays.

Figure 12-9 shows the far-field annual effective dose for the deterministic calculation of corrosion scenario with current sea-level. The red dash line is the dose corresponding to the risk limit, 14 μSv/yr, which is calculated based on the dose-to-risk conversion factor proposed by the ICRP-60 report, 7.30×10^{-2} Sv^{-1} (ICRP, 1991). Most of the radionuclides will be retarded by the far-field. The peak annual effective dose is 2.51×10^{-1} μSv/yr. And the dominant radionuclides will be Cl-36 and I-129. The retardation safety function of rock matrix in far-field is insignificant for these 2 nuclides (the partition coefficients of Cl-36 and I-129 are 0).

Figure 12-10 shows the near-field annual effective dose of the reference group for the deterministic calculation of corrosion scenario with sea-level falls to -120 m. The peak annual effective dose is 3.68×10^{2} μSv/yr. And the dominant radionuclides will be Pb-210 and Nb-94. Compared with the current sea-level case (see

Figure 12-8), the peak annual effective dose of Ra-226 is lower. This is due to the lower solubility limit of Ra-226 in water with low ion strength (3 orders of magnitude lower than the current sea-level). Figure 12-11 shows the far-field annual effective dose for the deterministic calculation of corrosion scenario with sea-level falls to -120 m. The peak annual effective dose is 3.38×10^{-1} μSv/yr. And the dominant radionuclides will be Cl-36 and I-129, which are similar to the case with the current sea-level (see Figure 12-9).

(2) Probabilistic cases:

In probabilistic cases, the data were sampled by the Latin hypercube method. Figure 12-12 shows the near-field mean annual effective dose of the reference group after 10,000 realizations. The peak mean annual effective dose is 4.07×10^{2} μSv/yr and the dominant radionuclides will be Pb-210 and Ra-226. The mean solubility limit of Ni-59 is higher than in deterministic cases. Therefore, the mean annual effective dose of Ni-59 is not limited by the solubility limit. Figure 12-13 shows the far-field mean annual effective dose of the reference group after 10,000 realizations. The peak mean annual effective dose is 3.57×10^{-1} μSv/yr. And the dominant radionuclides will be Cl-36 and I-129, which are similar to the deterministic cases. Figure 12-14 shows the far-field mean, median, 95^{th} and 99^{th} percentiles annual effective dose of the reference group in the biosphere. The 99^{th} percentile peak annual effective dose is 5.37 μSv/yr. This can help to understand how the dose consequences in the biosphere could be affected when the data uncertainties described in chapter 8 are taken into consideration.

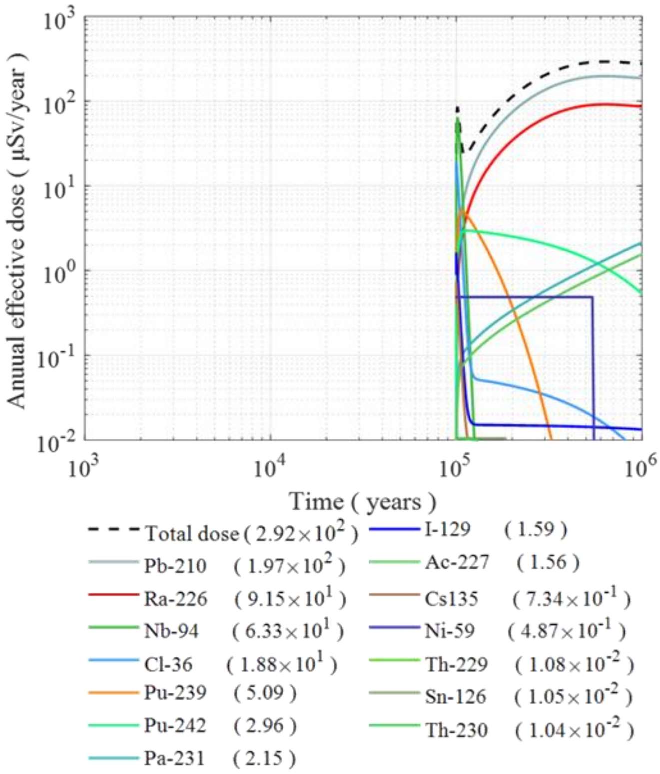

Figure 12-8: Near-field annual effective doses for corrosion variant case (current sea-level, deterministic case).

Note: the legends are sorted by the peak annual effective doses (µSv/yr) for radionuclides.

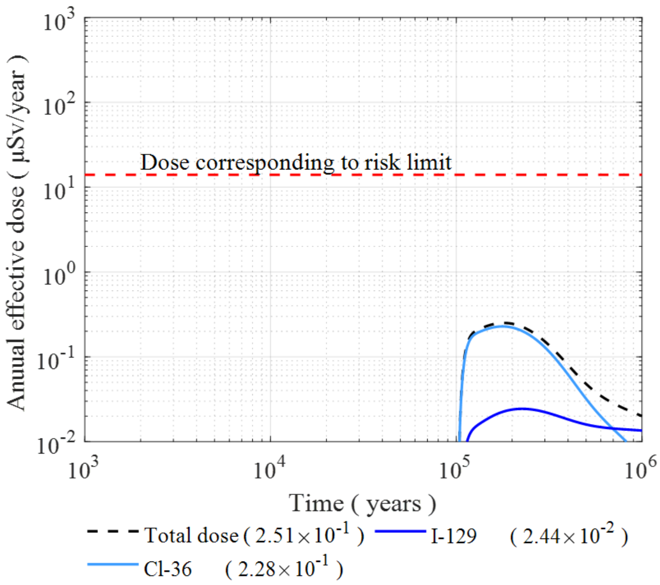

Figure 12-9: Far-field annual effective doses for corrosion variant case (current sea-level, deterministic case).

Note: the legends are sorted by the peak annual effective doses (µSv/yr) for radionuclides.

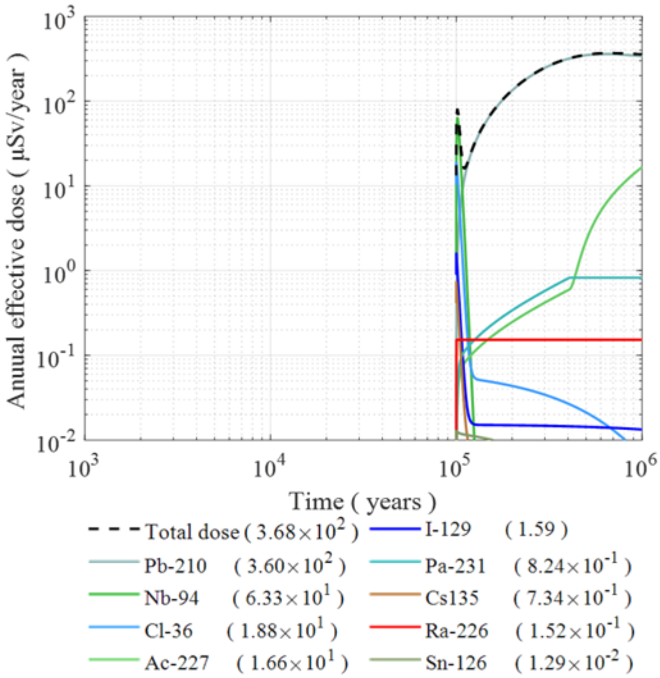

Figure 12-10: Near-field annual effective doses for corrosion variant case (sea-level falls to -120 m, deterministic case).

Note: the legends are sorted by the peak annual effective doses (μSv/yr) for radionuclides.

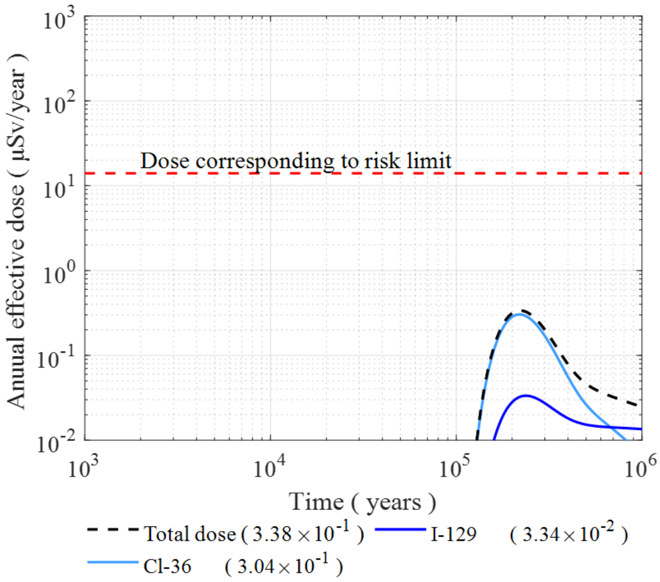

Figure 12-11: Far-field annual effective doses for corrosion variant case (sea-level falls to -120 m, deterministic case).

Note: the legends are sorted by the peak annual effective doses (μSv/yr) for radionuclides.

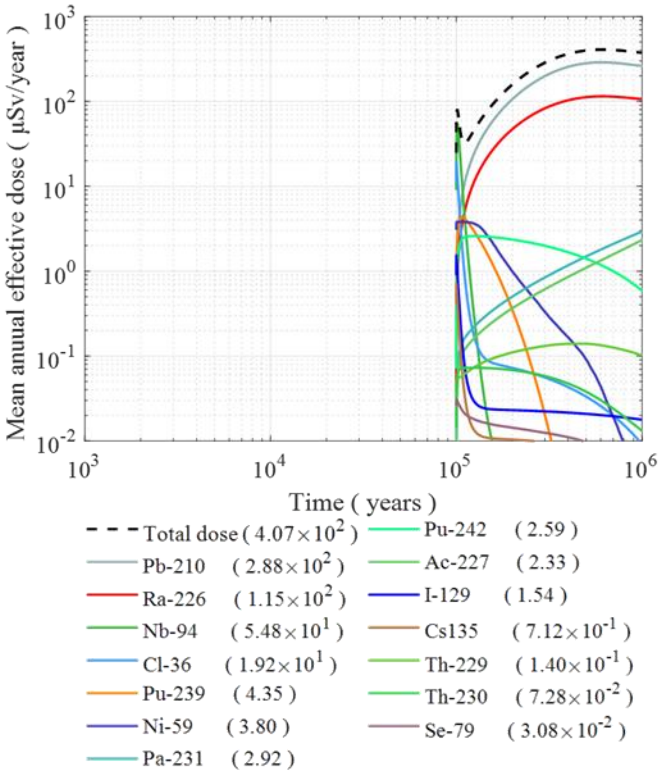

Figure 12-12: Near-field mean annual effective doses for corrosion variant case (probabilistic case).

Note: the legends are sorted by the peak annual effective doses (μSv/yr) for radionuclides.

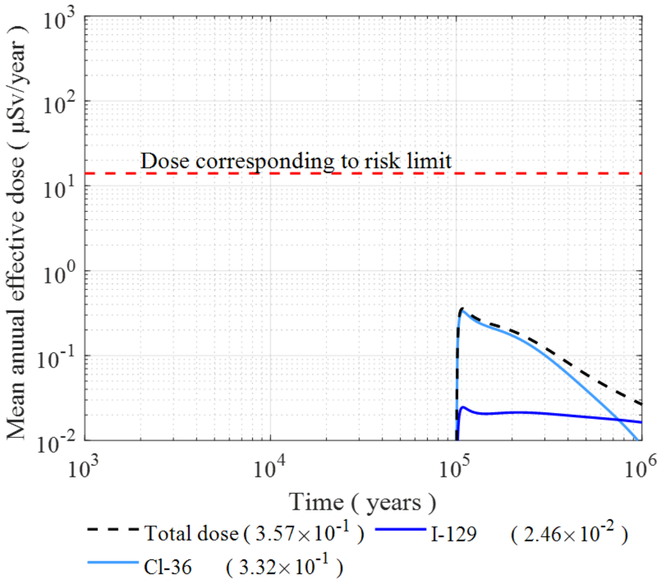

Figure 12-13: Far-field mean annual effective doses for corrosion variant case (probabilistic case).

Note: the legends are sorted by the peak annual effective doses (μSv/yr) for radionuclides.

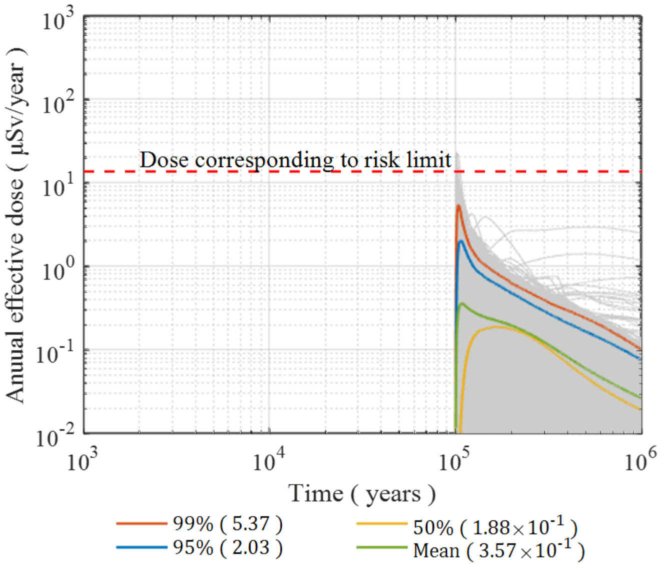

Figure 12-14: The mean value, medium value, and 95th and 99th percentiles of far-field annual effective doses for corrosion variant case (probabilistic case).

Note: the legends are sorted by peak annual effective doses (μSv/yr) of radionuclides and the grey lines indicate histories of different realizations.

12.5.7. Summary

Assuming that the corrosion containment safety function of a canister is jeopardized at an age of 10^5 years after closure of the repository. The advection occurs in the buffer. The deterministic calculation shows that the peak far-field effective annual doses of the reference group under different sea-levels are 2.51×10^{-1} μSv/yr and 3.38×10^{-1} μSv/yr dominated by Cl-36 and I-129. There was no significant difference between the two cases with respect to the influence on the reference group in the biosphere. The parameter uncertainties of barrier properties and flow-related data are taken into account in the probabilistic calculation. Figure 12-13 shows the stochastic calculation results, the 99th percentile peak annual effective dose is 5.37 μSv/yr. In some extreme cases, the peak annual effective dose might exceed the dose limit (14 μSv/yr). However, the corrosion containment safety function of the canister would not be jeopardized by corrosion over the safety assessment timescale according to the analyses of the containment safety function.

12.5.8. Calculation using the Analytical Models

As mentioned in Section 12.4.4, the simplified analytical solutions were used to verify the correctness of the results of near-field and far-field numerical models.

The calculation of the deterministic corrosion variant case with current sea-level data was conducted using the analytical solutions. Figure 12-15 shows the near-field annual effective dose calculated by the analytical solutions. The peak annual effective dose is 4.01×10^{2} μSv/yr dominated by Pb-210 and Nb-94. By comparing with Figure 12-8, it can be seen that the release rates of Pb-210 and Ra-226 are higher during the early stage of canister failure. As mentioned in Section 12.4.4, the parent nuclides of these 2 nuclides were assumed to be totally precipitated in the void volume of the canister and decayed to daughter nuclides. However, in fact, the parent nuclides of these 2 nuclides would not totally precipitate in the canister under the conditions of this case. The redissolution of precipitated nuclide was not taken into account in the analytical solutions. Therefore, the duration of constant release of Ni-59 is shorter. The main reason for the absence of Ac-227 in the figure is that contribution to activity from the decay of its parent nuclides was not taken into account in the calculation of the analytical solution.

Figure 12-16 shows the far-field annual effective dose calculated by the analytical solutions. Based on the instant release and corrosion release of the inventory, the peak value was calculated. The annual effective dose is 2.05×10^{-1} μSv/yr dominated by Cl-36 and I-129. The peak value is similar to the one in Figure 12-9. Tails of curves are caused by the continuous release of the inventory. And the results are in good agreement with the results estimated using the numerical models.

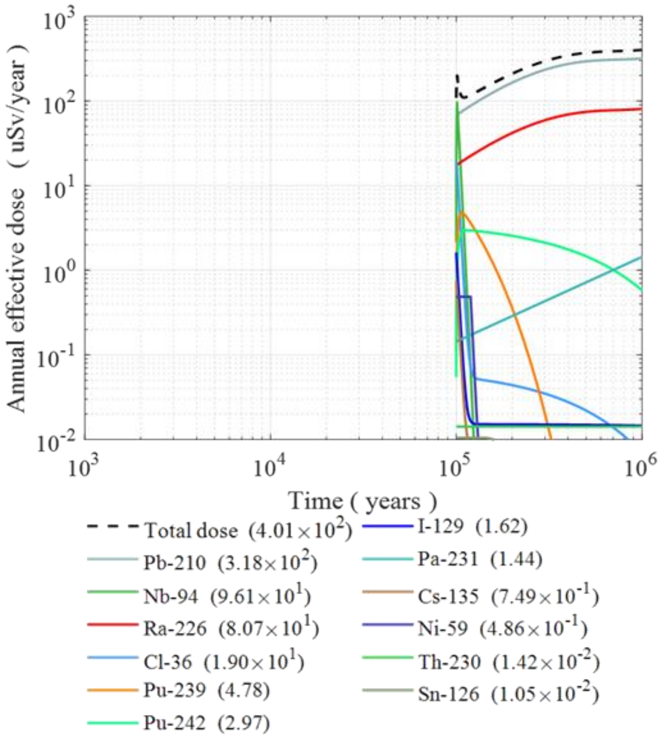

Figure 12-15: Near-field annual effective doses for corrosion variant case (current sea-level, deterministic case, and analytical model).

Note: the legends are sorted by the peak annual effective doses (μSv/yr) for radionuclides.

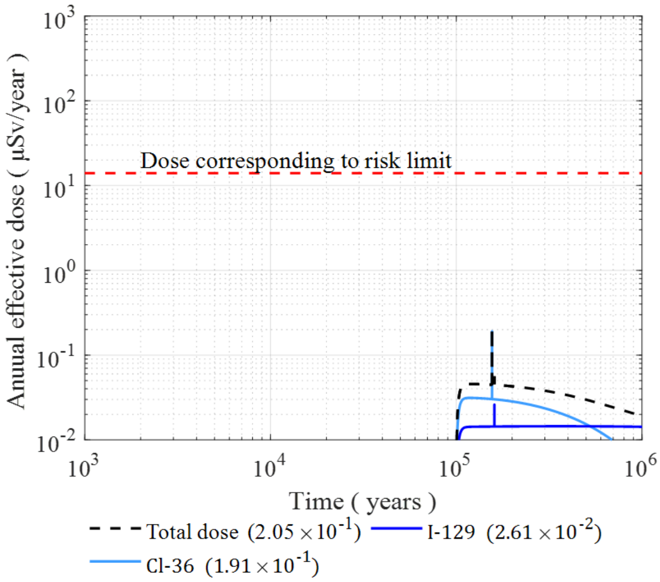

Figure 12-16: Far-field annual effective doses for corrosion variant case (current sea-level, deterministic case, and analytical model).

Note: the legends are sorted by the peak annual effective doses (μSv/yr) for radionuclides.

12.5.9. Sensitivity Analyses

A tornado chart (Figure 12-17) was used to identify sensitive parameters in the radionuclide transport calculation model. In calculation, upper bound, lower bound and central values are calculated with 95.5^{th}, 4.5^{th}, and 50.0^{th} percentiles of each parameter, respectively. The variables are sorted according to the calculated range. Therefore, the variable with the largest range is the top one of the chart. The lower the position of the chart, the smaller the range is. This method was used to identify the input parameters with a relatively high influence on the estimation target. In sensitivity analyses, the estimation target is the peak total annual effective dose from the far-field of the probabilistic calculation for the corrosion variant case. The result is shown in Figure 12-17. The flow-related transport resistance along the Q1 path, F (Q1), is the input parameter that affects the results the most. A higher flow-related transport resistance, a better retardation for nuclides transport in rock fracture in far-field. According to Section 12.5.6, the peak total dose released from the far-field is dominated by Cl-36 and I-129. Therefore, the instant release fractions (IRF) of these two nuclides are also affecting dose results. Besides, Cl-36 is an anionic nuclide, and diffusivity of Cl-36 in the rock matrix will depend on the effective diffusivity coefficient and diffusion-available porosity. A higher effective diffusivity coefficient, a lower release rate of Cl-36 due to more Cl-36 is contained in the rock matrix. However, this is a non-linear process, the nuclides diffused into the rock matrix can also re-enter the water in fracture. The fuel matrix dissolution rate affects the annual release amount of nuclides from the fuel matrix. A large amount of Cl-36 and I-129 is embedded in the fuel matrix; therefore, the fuel matrix dissolution rate also influences the results.

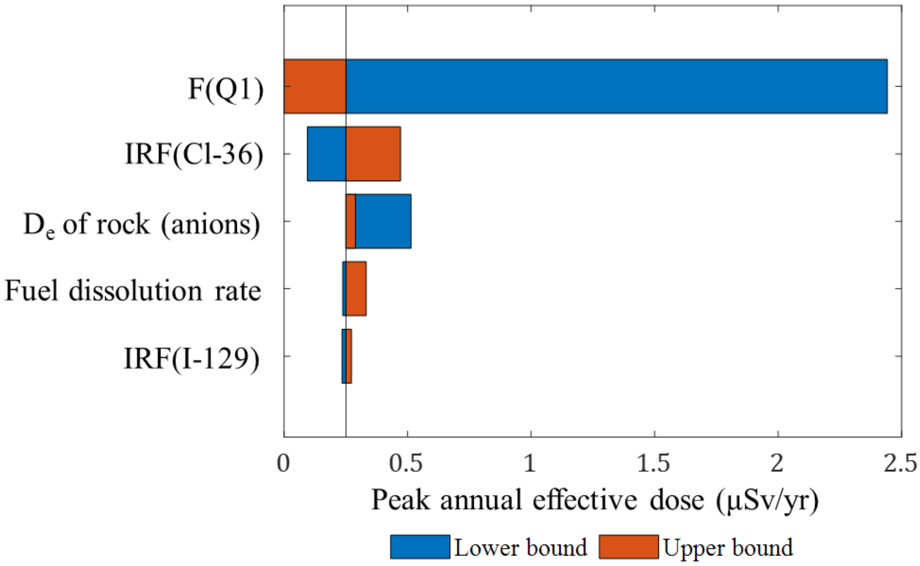

Figure 12-17: Results of the sensitivity analyses for corrosion variant case (probabilistic case).

12.6. Quantitative Assessment of Canister Failure due to Shear Force

According to the result analyzed in section 11.8.1, displacement of fractures in the repository of the reference case may occur when the repository is affected by earthquakes induced by faults or diffuse seismicity. And fracture displacement might accumulate. Therefore, assuming that a canister would fail if a fracture intersects the deposition hole and the accumulated displacement is larger than 5 cm. In this scenario, the retardation safety function of the buffer is maintained. The solute transport in the buffer is dominated by diffusion. The buffer thickness between the canister and wall of the deposition hole is assumed to reduce from 35 cm to 25 cm. After the canister fails, groundwater will fill up the void volume of the canister gradually. Though, the delay time between canister failure and onset of radionuclide transport will be around 100 years (SKB, 2011). If radionuclides are transported in fracture, they will transport to the biosphere through the geosphere by advection and might cause radiation dose to the potentially exposed groups.

12.6.1. Conceptualization of the Transport Conditions

Figure 12-18 shows the radionuclide transport calculation model in the shear load scenario. The transport resistance in the canister was neglected after the failure of the canister. As mentioned in Section 12.4.1, radionuclides in the canister will be released through three mechanisms when groundwater intrudes into the canister. The retardation safety function of the buffer will be intact; therefore, the dissolved radionuclides will be transported by diffusion from the void volume in the canister to the buffer (B-1). The radionuclides in buffer (B-1) will be transported by diffusion from buffer to backfill, i.e., from B-1 to B-4 and BF-1. The compartment dimensions are listed in Table 12-6. The buffer (B-1) and backfill (BF-1) are intersected by the Q1 path and Q2 path, respectively. The radionuclides released to rock fracture will mainly be controlled by the flow rate through the deposition hole and bottom of the backfill tunnel. The equivalent flow rate is the hydraulic boundary condition for the interface of near/far-field, which can be calculated by equation (9-4). The equivalent flow rates used in the calculation are listed in Table 12-5 and Figure 12-7. When radionuclides in the buffer diffuse into rock fracture through the Q1 path, most of the transport resistance will be located at the entrance of the rock fracture. In order to avoid detailed discretization, the buffer and the rock fracture are connected by an equivalent transport resistance plug (P-2)(Romero, 1995).

The length and area of the equivalent transport resistance plug are calculated by the following equations (SKB, 2010h):

$P_L = \left[1 - 1.35\log_{10}\left(\frac{b}{a}\right) + 1.6\log_{10}\left(\frac{d}{a}\right)\right] b$	(12- 12)
$P_A = \pi(2r_d)(2b)$	(12- 13)

where,

a = the height of the compartment in connection with the rock fracture, [m].

d = thickness the buffer, [m].

P_A = area of the equivalent transport resistance plug, [m^2].

P_L = length of the equivalent transport resistance plug, [m].

r_d = radius of deposition hole, [m].

The transport of radionuclides in rock fracture is described in Section 12.4.2.

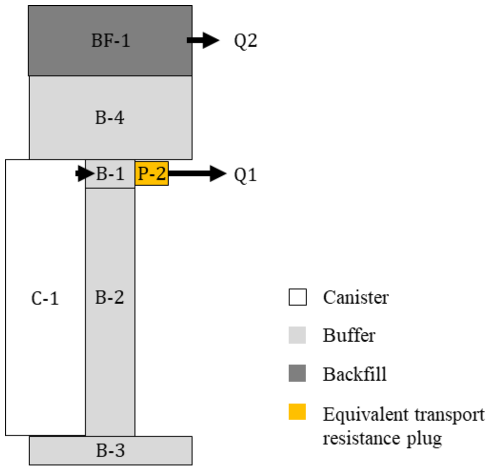

Figure 12-18: Compartments and release paths in the near-field for canister failure due to shear force.

Table 12-6: Geometry of the compartments in the near-field.

Number of compartment	Diameter [m]	Height [m]	Note
C-1	1.05	4.905	
B-1	1.75	5.00×10^{-1}	Thickness is 2.50×10^{-1} m. The compartment is horizontally divided into 6 sub-compartments of equal thickness, each thickness is about 4.17 cm.
B-2	1.75	4.405	Vertically divided into 2 sub-compartments. The height of upper part is 1.00 m, the lower part is 3.405 m.
B-3	1.75	5.00×10^{-1}	
B-4	1.75	1.50	The compartment was vertically divided into 3 sub-compartments, each has a height of 5.00×10^{-1} m.
BF-1	1.75	1.25	

12.6.2. Input Parameters for the Transport Models

The material properties used in radionuclide transport calculation are described in Section 8.3. The median values of flow-related data under current sea-level and sea-level fall to -20 m and -120 m are listed in Table 12-5. Estimation results in Sections 9.3.6 and 9.4.6 were used in the deterministic calculation. In stochastic calculation, the flow-related data are sampled by the Latin hypercube method. The influence to the reference group in the biosphere was evaluated by multiplying the near-field and far-field annual release rates with the dose conversion factors estimated in Section 12.2.

12.6.3. Analyses of Basic Case

According to Sections 9.4.5 and 11.7.2, the probabilistic evaluation of the distribution of the canister failure times resulted in 509 different values of failure time. The canister failure rate due to shear force increases over time. The earliest canister failure might occur at about 226,000 years after the repository closure. The expected number of canister failure is about 0.87 canisters. In deterministic calculation, assuming that one canister fails at the earliest possible failure time (about 226,000 years). In probabilistic calculation, possible failure times would be taken into account.

(1) Deterministic cases:

Figure 12-19 shows the near-field annual effective dose of the reference group for deterministic calculation of shear load scenario under current sea-level. The peak annual effective dose is 2.06 μSv/yr dominated by Cl-36 and I-129 after the canister is failed and dominated by Ra-226 in the longer term. Figure 12-20 shows the far-field annual effective dose for the deterministic calculation of shear load scenario with current sea-level. The peak annual effective dose is 1.59×10^{-1} μSv/yr dominated by Cl-36 and I-129. Other radionuclides are retarded or decaying.

Figure 12-21 shows the near-field annual effective dose of the reference group for deterministic calculation of shear load scenario when sea-level falls to -120 m. The peak annual effective dose is 9.57×10^{-1} μSv/yr dominated by Cl-36 and I-129. Compared to the results of the current sea-level, the peak annual effective dose is lower due to less diffusion. On the other hand, the annual effective doses of Ra-226 and Pu-242 are lower than those of the current sea-level case due to higher partition coefficients. Figure 12-22 shows the far-field annual effective dose for the deterministic calculation of the shear load scenario when sea-level falls to -120 m. The peak annual effective dose is 1.86×10^{-1} μSv/yr dominated by Cl-36 and I-129. It is similar to the results of the current sea-level case.

(2) Probabilistic cases:

In probabilistic cases, a failed canister was simulated and the data sets described in section 8.3 were sampled 100 times by the Latin hypercube method at each possible failure time. There are 509 possible failure times over the safety assessment timescale. Therefore, 50,900 realizations were implemented in this case. The mean annual effective doses were estimated by multiplying the near-field and the far-field doses with the expected number of failed canisters (8.72×10^{-1} canister).

Figure 12-23 shows the near-field mean annual effective dose of the reference group for the probabilistic calculation of the shear load scenario. The peak mean annual effective dose is 5.28×10^{-1} μSv/yr dominated by Ra-226. The parent nuclides Ra-226 and Th-230 will precipitate and decay in the void volume of the canister. This will lead to the gradual rising of the mean annual effective dose of Ra-226 in the near-field. Figure 12-24 shows the far-field mean annual effective dose of the reference group for the probabilistic calculation of the shear load scenario. The peak mean annual effective dose is 3.29×10^{-2} μSv/yr dominated by Cl-36 and I-129 The mean annual effective dose is increased over time, this is because the increasing canister failure rate (see Figure 9-56) and doses will be dominated by long-lived radionuclides. Figure 12-25 shows the far-field mean, median, 95th and 99th percentiles annual effective dose of the reference group in the biosphere. In this case, the uncertainty of the canister failure times was sampled, and 10,000 realizations were run. The results were multiplied by the expected canister failure number described above. The 99th percentile peak annual effective dose is 1.57×10^{-1} μSv/yr.

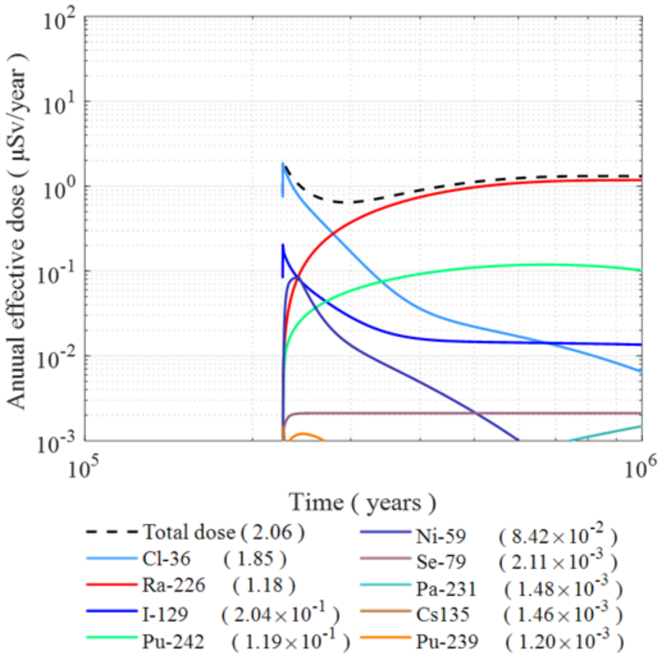

Figure 12-19: Near-field annual effective doses for shear load case (current sea-level, deterministic case).

Note: the legends are sorted by the peak annual effective doses. And the values in the brackets are the peak annual effective doses (µSv/yr).

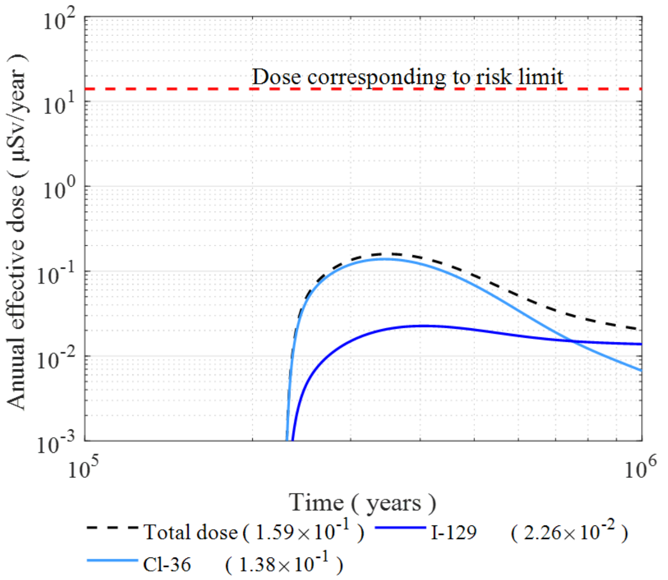

Figure 12-20: Far-field annual effective doses for shear load case (current sea-level, deterministic case).

Note: the legends are sorted by the peak annual effective doses. And the values in the brackets are the peak annual effective doses (µSv/yr).

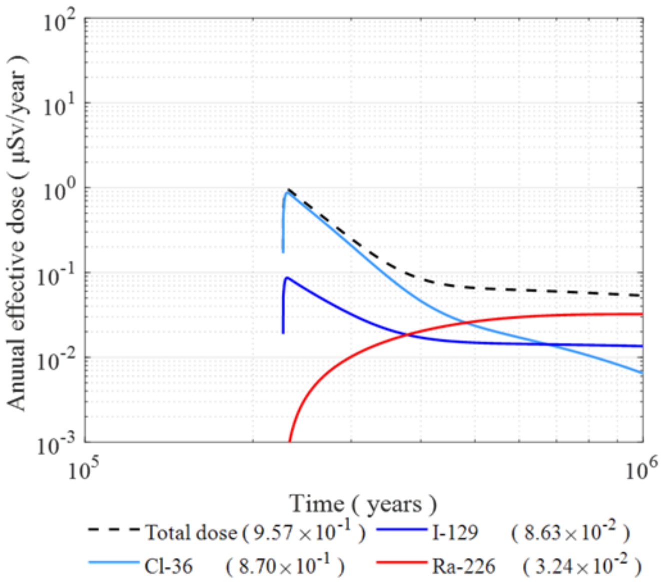

Figure 12-21: Near-field annual effective doses for shear load case (sea-level falls to -120 m, deterministic case).

Note: the legends are sorted by the peak annual effective doses. And the values in the brackets are the peak annual effective doses (μSv/yr).

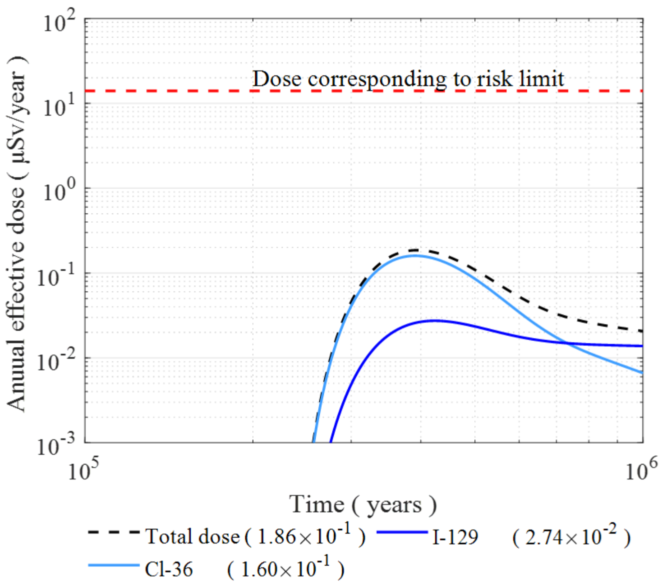

Figure 12-22: Far-field annual effective doses for shear load case (sea-level falls to -120 m, deterministic case).

Note: the legends are sorted by the peak annual effective doses. And the values in the brackets are the peak annual effective doses (μSv/yr).

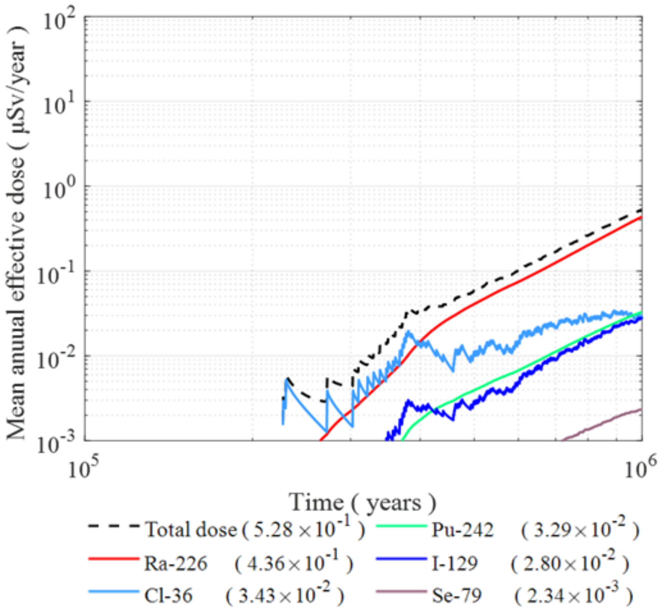

Figure 12-23: Near-field mean annual effective doses for shear load case (probabilistic case).

Note: the legends are sorted by the peak annual effective doses. And the values in the brackets are the peak annual effective doses (μSv/yr).

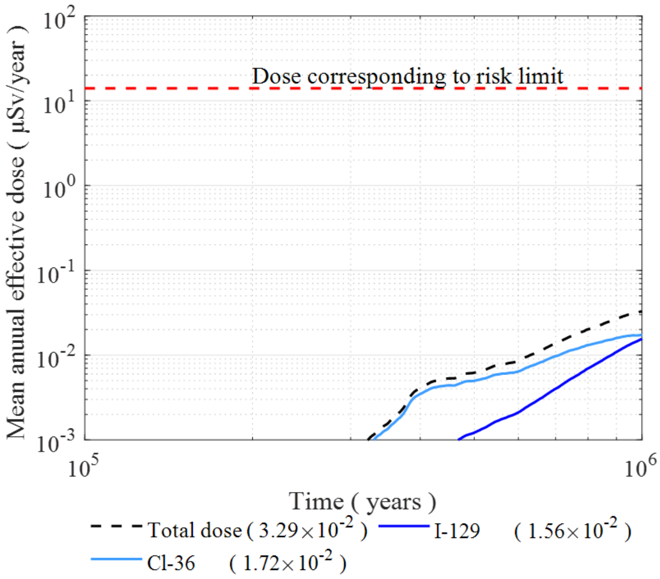

Figure 12-24: Far-field mean annual effective doses for shear load case (probabilistic case).

Note: the legends are sorted by the peak annual effective doses. And the values in the brackets are the peak annual effective doses (μSv/yr).

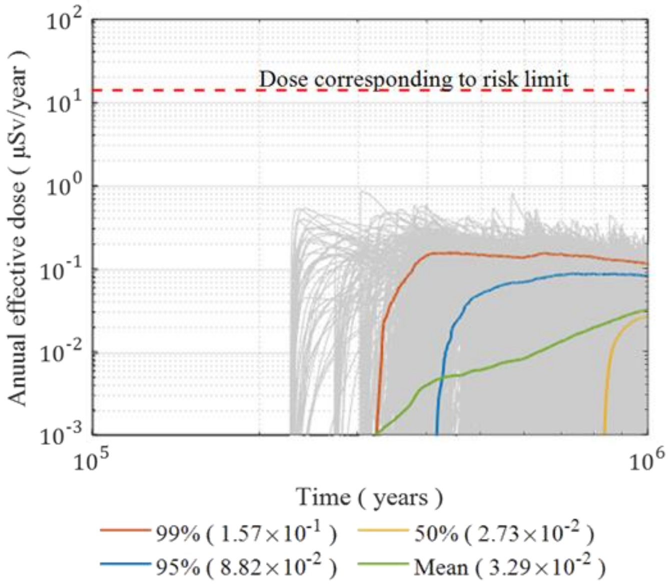

Figure 12-25: The mean value, medium value, and 95th and 99th percentiles of far-field annual effective doses for corrosion variant case (probabilistic case).

Note: the values in the brackets are the peak annual effective doses (μSv/yr) and the grey lines indicate histories of different realizations.

12.6.4. Analyses of Other Transport Conditions

In the deterministic and probabilistic calculation cases of the shear load scenario, the variations of transport properties have been taken into consideration. The transport resistance of the canister was neglected in the calculation cases. The thickness of the buffer surrounding the canister was assumed to be 25 cm in the basic case. And the buffer was neglected in the variant cases. The flow-related transport parameters, e.g., equivalent flow rate, flow-related transport resistance and advective transport time, estimated based on conditions under current sea-level and sea-level falls to -20 m and -120 m were used in the probabilistic calculation. The influence of shear displacement on flow-related transport parameters has not been estimated and therefore has not been considered in the calculation of current cases.

12.6.5. Analyses of Variant Cases

The shear displacement may increase the flow rate in the rock fracture and cause the buffer to be eroded. In order to estimate the influence of this phenomenon, assuming that the retardation safety function of the buffer is omitted after the failure of the containment safety function of the canister (i.e. initial advection case in section 11.8.1.). The other near-field transport conditions used in this case were the same as described in Section 12.5.2 and calculated probabilistically.

Figure 12-26 shows the near-field mean annual effective dose of the reference group. The peak annual effective dose is 8.59×10^{1} μSv/yr and is dominated by Pb-210 and Ra-226. Compared with the results of the basic case (buffer intact) (Figure 12-23), the near-field peak annual effective dose is increased approximately 176 times. The reason for this is the increment of the equivalent flow rate and the absence of buffer and its sorption. For instance, the mean annual effective dose of Pb-210 is significantly increased in this case, and the Pb-210 will significantly adsorb on buffer if the buffer exists (the mean K_d value of Pb-210 for buffer/backfill is 1.05×10^{2} m^3/kg). Figure 12-27 shows the far-field mean annual effective dose of the reference group in the biosphere. The peak annual effective dose is 3.89×10^{-2} μSv/yr and is dominated by Cl-36 and I-129. The other nuclides are retarded in the far-field.

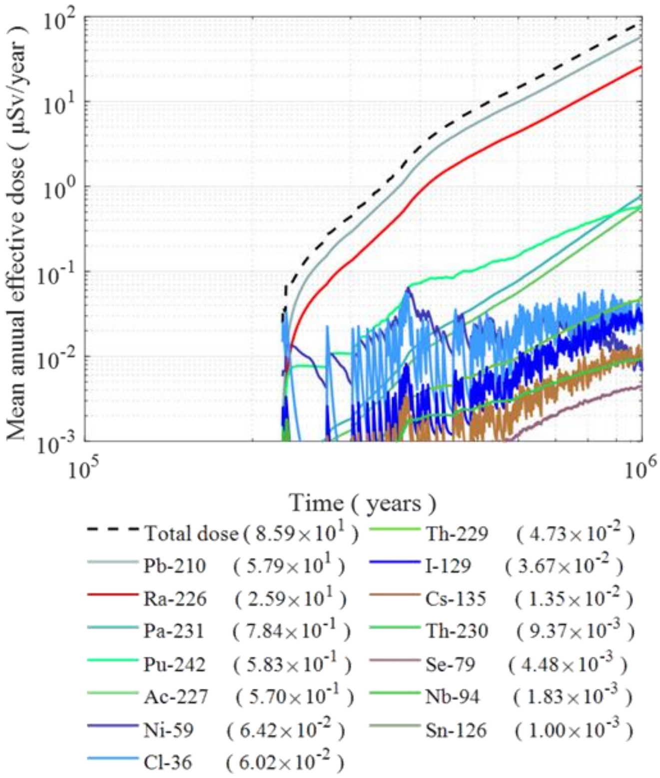

Figure 12-26: Near-field mean annual effective doses for shear load variant case (probabilistic case).

Note: the legends are sorted by the peak annual effective doses. And the values in the brackets are the peak annual effective doses (µSv/yr).

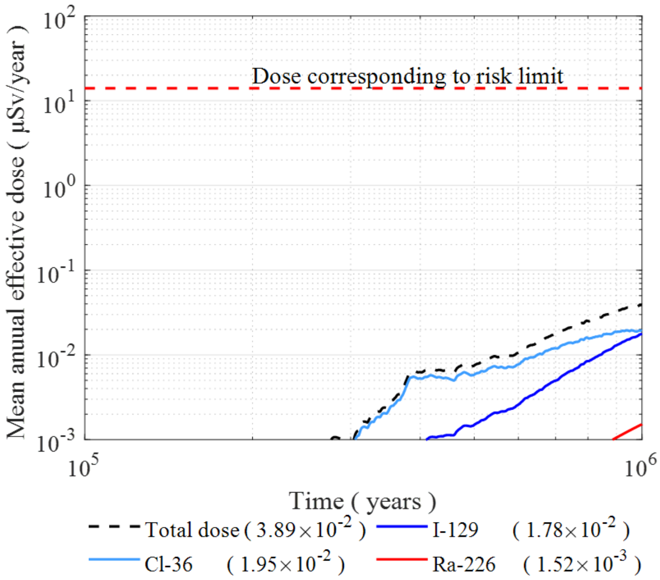

Figure 12-27: Far-field mean annual effective doses for shear load variant case (probabilistic case).

12.6.6. Calculation using the Analytical Models

As described in Section 12.4.4, the simplified analytical solutions were used to verify the results of numerical models for the near-field and the far-field. The deterministic calculation results of the basic case of shear load scenario with current sea-level have been verified using the analytical solutions, and the results are shown in this chapter.

Figure 12-28 shows the near-field annual effective doses calculated by the analytical solutions. The peak annual effective dose is 1.90 μSv/yr, and it is similar to the results of the numerical models. In the early stage of canister failure, the peak dose is dominated by Cl-36 and I-129; and Ra-226 in the longer term. Generally, the trends of dose curves for the dominating nuclides in the analytical results are similar to the numerical results (Figure 12-19).

Figure 12-29 shows the far-field annual effective doses calculated by the analytical solutions. The peak annual effective dose is 1.54×10^{-1} μSv/yr and is dominated by Cl-36 and I-129. By comparing with numerical results (Figure 12-20), it can be seen that the peak value of the total dose is similar. The tails of curves in the results of analytical solutions are in good agreement with results estimated with the numerical models.

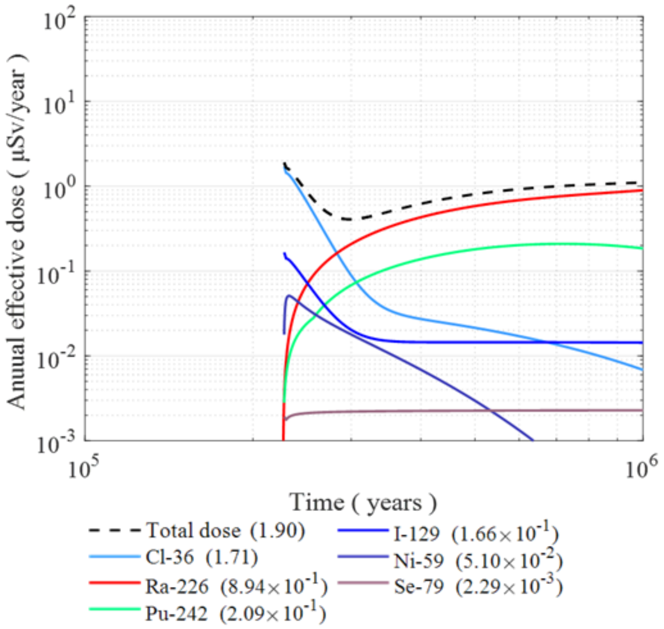

Figure 12-28: Near-field annual effective doses for shear load basic case (current sea-level, deterministic case, and analytical model).

Note: the legends are sorted by the peak annual effective doses. And the values in the brackets are the peak annual effective doses (μSv/yr).

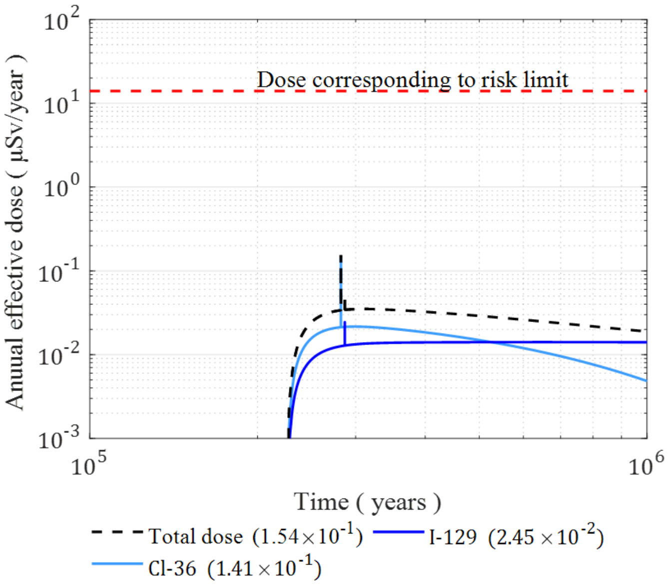

Figure 12-29: Far-field annual effective doses for shear load basic case (current sea-level, deterministic case, and analytical model).

Note: the legends are sorted by the peak annual effective doses. And the values in the brackets are the peak annual effective doses (μSv/yr).

12.6.7. Sensitivity Analyses

The method used to carry out the sensitivity analyses has been described in Section 12.5.10. The estimation target is the far-field peak total annual effective dose of probabilistic calculation for the basic case of shear load scenario. Figure 12-30 shows the results. The canister failure time is the input parameter most affecting the result. In this scenario, the peak annual effective doses are dominated by Cl-36 and I-129. The later the canister failure time, the lower the released activity of Cl-36. The fuel dissolution rates and the instant release fractions of Cl-36 and I-129 also have a certain degree of influence on the estimation target. When other conditions remain the same, a higher fuel dissolution rate or instant release fraction means that more inventory will be released into water. These two nuclides are readily soluble, therefore leading to a higher peak annual effective dose. As the results of sensitivity analyses for the corrosion scenario (Section 12.5.10), the flow-related transport resistance of the Q1 path has a large influence on the peak dose. It should be noted that when the 95.5th percentile of flow-related transport resistance of the Q1 path has been used in the calculation, the flow-related transport resistance of the Q2 path is the median value, leading to the release of radionuclides mainly through the Q2 path. However, the flow-related transport resistances of a deposition hole have a certain degree of correlation, see Figure 12-31; hence the dose results did not reflect the situation that would result from this phenomenon.

Currently, a correlation between the near-field groundwater flow (i.e., Q_{eq}) and F, which can be seen in other studies (Joyce, 2010), has not been observed. The limitation of the hydrogeology model in the reference case might be the reason for this. In the future, more attention will be paid to the correlation when developing the DFN model.

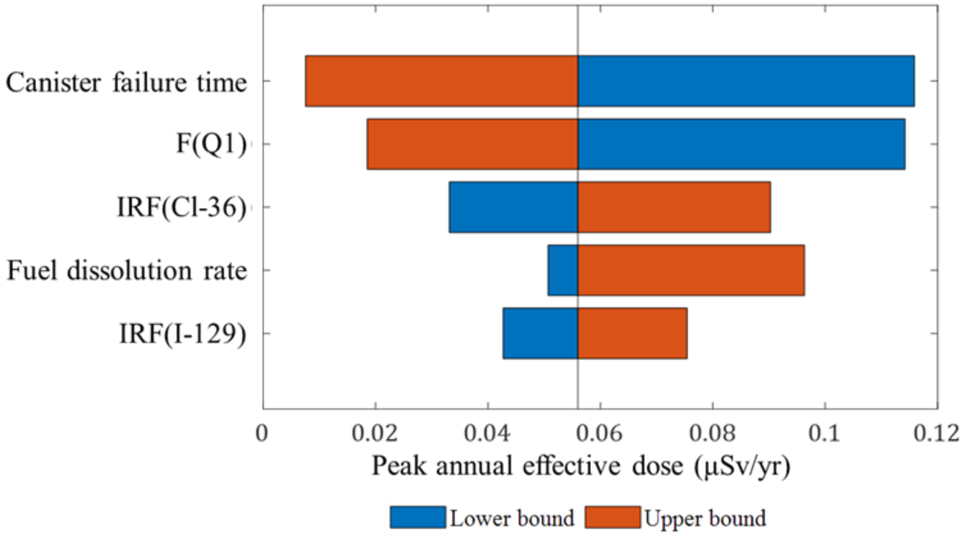

Figure 12-30: Results of the sensitivity analyses for shear load basic case (probabilistic case).

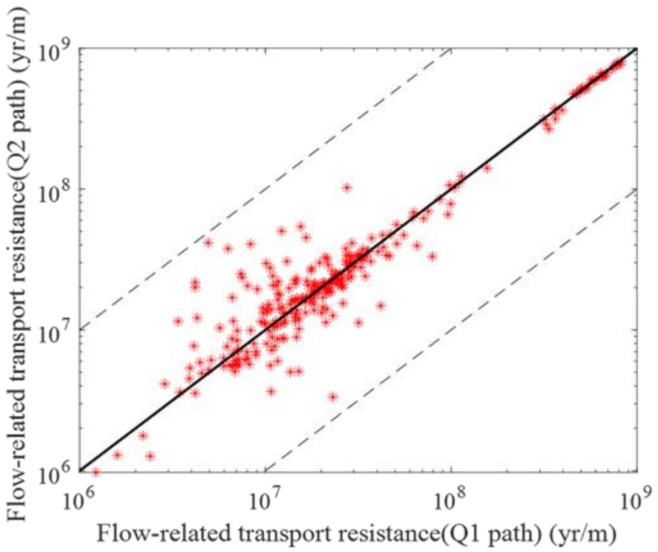

Figure 12-31: Flow-related transport resistance of Q1 and Q2 paths of each deposition hole (the evaluation results of current sea-level, sea-level -20 m, and sea-level -120 m).

Note: the dashed lines indicate difference by an order of magnitude.

12.7. Analyses of What-If Scenarios

The analyses of what-if scenarios are described in this chapter, including: (1) initial defect of canister, (2) colloid facilitated transport and (3) radionuclide transport in the gas phase.

12.7.1. Canister Failure due to Initial Defect

With the development of industrial technology and welding methods, and other relevant literature (SKB, 2011), it is believed that the possibility of occurrence of an initial pinhole in the copper shell of the canister is very low. However, this failure mode can be used to evaluate the retardation safety function of fuel, canister buffer and rock fracture. Therefore, the initial defect scenario analyses were carried out.

The estimation cases and assumptions are listed below and summarized as Table 12-7:

(1) Assuming that one canister has a penetrating small rounded pinhole in the copper shell when it is manufactured:

In this case, according to the estimations of SKB (SKB, 2010h), the radius of the rounded pinhole is 2×10^{-3} m, and a water-conducting channel takes more than 1,000 years to form (SKB, 2010h). Therefore, the duration between canister failure and onset of radionuclide transport (t_{Delay}) was assumed to take 1,000 years. Figure 12-6 shows how compartments are modelled by the near-field radionuclide transport calculation model in this scenario. The buffer is intact, and groundwater will intrude into the void volume in the canister and gradually fill it up. The radionuclides in the void volume of the canister are gradually transported by diffusion once the continuous water-conducting channel is formed. P-1 block is an equivalent transport resistance plug connecting between the pinhole and the buffer nearby the pinhole to avoid a detailed discretization. The length (P_L) and area (P_A) of the plug are calculated by the following equations (Romero, 1995):

$P_L = \frac{r_{hole}}{\sqrt{2}}$	(12- 14)
$P_A = \pi r_{hole}^2$	(12- 15)

where,

P_A = area of the equivalent transport resistance plug, [m^2].

P_L = length of the equivalent transport resistance plug, [m].

r_{hole} = radius of the initial pinhole, [m]

The other transport concept is the same as the shear load scenario (see Section 12.6.1) except for the buffer thickness. The buffer block, B-1, is not squeezed by shear force in this case; therefore, the buffer thickness is maintained as 35 cm.

(2) Assuming that one canister loses its containment safety function after the repository closure:

In this case, the area of the defect is 100 m^2 (SKB, 2010h), meaning that the canister does not have any transport resistance with respect to the radionuclides. The onset of radionuclide transport after canister failure (t_{Delay}) is 100 years after repository closure. The concept of radionuclide transport in the near-field is the same as the shear load scenario (Section 12.6.1) except for the buffer thickness. The thickness of B-1 block is 35 cm in this case.

(3) Assuming that one canister loses its containment safety function immediately after the repository closure, the advection occurs in the buffer surrounding the canister:

In this case, one canister will have a water-conducting channel after the closure, and the concept of radionuclide transport in the near-field will be the same as the corrosion scenario (Section 12.5.2).

(4) Based on case (3), neglecting the fuel dissolution rate and metal corrosion rate:

In this case, assuming that the inventory in one canister releases into the void volume of the canister immediately after the canister failure. The transport mechanism between the canister and rock fracture is dominated by advection.

The transport of radionuclides in rock fracture is described in Section 12.4.2. The flow-related data used in these cases are listed in Table 12-5. In this scenario, the deterministic data of the current sea-level have been used.

Figure 12-32 shows the near-field annual effective dose of initial pinhole case (1). The peak annual effective dose is 1.20×10^{-1} μSv/yr. The peak dose is dominated by C-14 and Cl-36 at the early stage. C-14 and Cl-36 are low K_d and likely soluble nuclides and some of these two nuclides (73.20% for C-14 and 10.10% for Cl-36) are instantly released or released by metal corrosion, leading to higher annual release rates of C-14 and Cl-36. The peak annual effective dose is dominated by Ra-226 in the late period. Figure 12-33 shows the far-field annual effective dose of the initial pinhole case (1). The peak annual effective dose is 5.69×10^{-2} μSv/yr and dominated by Cl-36 and I-129. The released activity of C-14 is low due to retardation and decay in rock fracture.

Figure 12-34 shows far-field annual effective doses of different cases. Comparing with case (1), the peak annual effective dose is increased 4.5 times if one canister loses its containment safety function after the repository closure. If the advection occurs in the buffer surrounding the canister (case 3), the far-field annual effective dose is maintained at a high level for a longer period due to a higher activity of nuclides released into rock fracture after the canister failure. If the release rate of fuel dissolution and metal corrosion is neglected (case 4), all of the inventory releases into the void volume of the canister, the peak annual effective dose is increased 60 times compared with case (1). Some of the nuclides, like uranium isotopes, are precipitated and decayed in water. On the contrary, readily soluble nuclides like Cl-36 and I-129 are released into rock fracture with high activity at the early stage. The continuous release mechanism of the fuel matrix was not taken into account in this case; therefore, the far-field release dose curve is dropped at the late period. The asterisks represent the peak annual effective doses and time of occurrence if all canisters in the repository failed under the same conditions. The doses are calculated by multiplying the peak annual effective dose of each case with the total canisters number in the repository (2,571 canisters). If the release rate of fuel dissolution and metal corrosion are taken into account, the peak annual effective dose does not exceed the background radiation in Taiwan (1.62 mSv/yr).

Table 12-7: Summarized cases for Canister failure due to initial defect

<table>
<tr><th>Case</th><th>Condition of fuel</th><th>Condition of canister</th><th>Condition of buffer</th></tr>
<tr><td>(1)</td><td rowspan="3">Radionuclides released from fuel according to the fuel dissolution rate and metal corrosion rate.</td><td>Small rounded pinhole in the copper shell.</td><td rowspan="2">Intact (i.e. nuclides diffuse in the buffer).</td></tr>
<tr><td>(2)</td><td rowspan="3">Large damage (i.e. the canister does not have any transport resistance with respect to the radionuclides).</td></tr>
<tr><td>(3)</td><td rowspan="2">Advection occurs in the buffer.</td></tr>
<tr><td>(4)</td><td>Neglecting the fuel dissolution rate and metal corrosion rate.</td></tr>
</table>

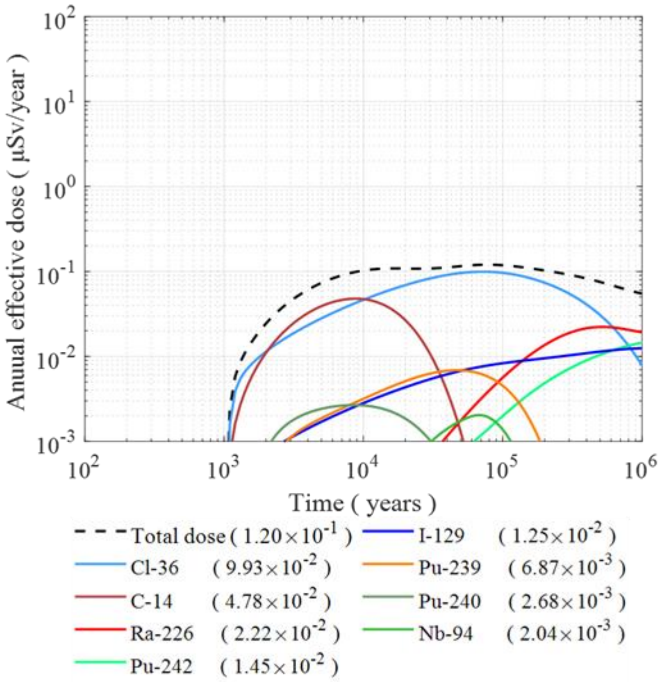

Figure 12-32: Near-field annual effective doses for initial canister defect case.

Note: the legends are sorted by the peak annual effective doses. And the values in the brackets are the peak annual effective doses (μSv/yr).

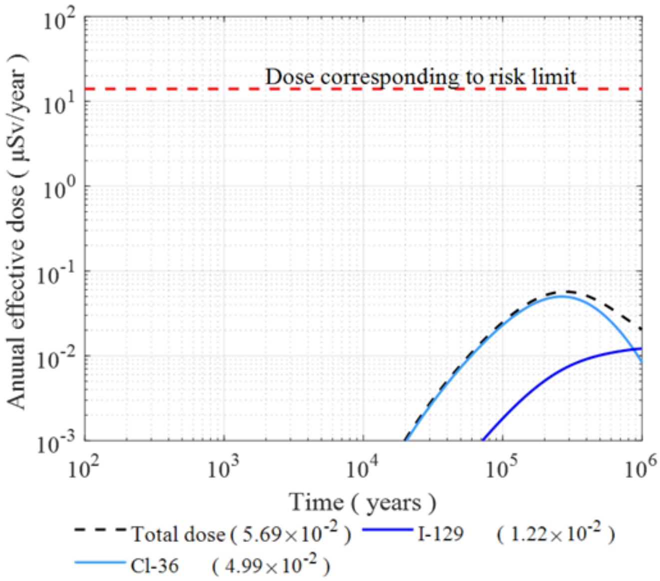

Figure 12-33: Far-field annual effective doses for initial canister defect case (1).

Note: the legends are sorted by the peak annual effective doses. And the values in the brackets are the peak annual effective doses (μSv/yr).

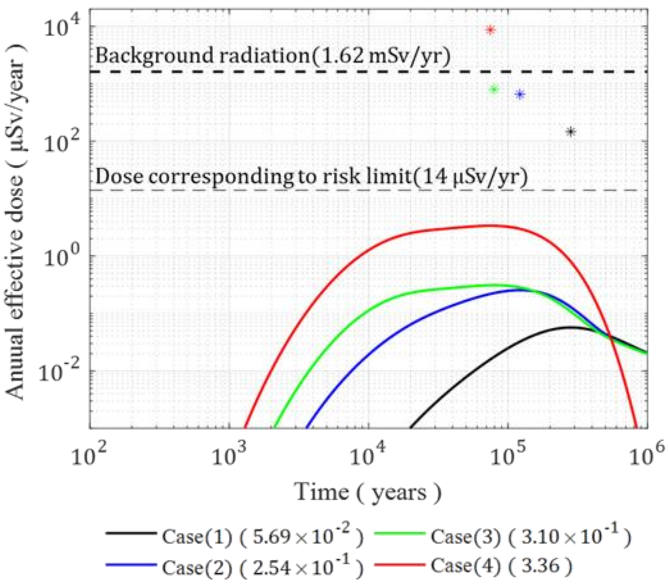

Figure 12-34: Far-field annual effective doses for initial canister defect case (1) to (4).

Note: the values in the brackets are the peak annual effective doses (μSv/yr) and the star signs indicate the peak annual effective doses and their corresponding time when all the 2,571 canisters are failed.

12.7.2. Colloid Facilitated Transport Case

As mentioned in Section 9.3.11, the buffer colloid might be produced when buffer erosion occurrs. The colloids will be transported by groundwater along the rock fracture. Colloids may act as carriers for radionuclides that have a high affinity for buffer. This transport mechanism need to be investigated and is crucial for radionuclides that are low soluble and not readily transported by the groundwater. Therefore, the analyses of colloid-facilitated transport cases were carried out.

In order to estimate the effect of colloid-facilitate transport in the far-field (geosphere), the effective diffusion coefficient (D_e) and retardation coefficient (R_m) of the rock matrix are replaced by the values calculated by the following equations (SKB, 2010h):

$D_{e,app} = \dfrac{D_e}{1 + m_c K_c}$	(12- 16)
$R_{m,app} = \dfrac{R_m}{1 + m_c K_c}$	(12- 17)

where,

$D_{e,app}$ = apparent effective diffusion coefficient of rock matrix, [m^2/yr].

K_c = partition coefficient for radionuclide sorption onto buffer, [m^3/kg].

m_c = concentration of buffer colloid in rock fracture, [kg/m^3].

$R_{m,app}$ = apparent retardation factor of rock matrix, [-].

According to the above equations, the retardation of rock matrix for radionuclides is low if the colloid concentration is high or the radionuclides have a high affinity for buffer colloids. In this scenario, assuming that the buffer colloid concentration is 10 kg/m^3. According to literature, this is a conservative value (SKB, 2010m).

The radionuclide transport calculation is based on the corrosion variant case (current sea-level) and the concentration of buffer colloid in rock fracture is 10 kg/m^3. Figure 12-35 (right-hand side) shows the far-field annual effective dose of the reference group. The peak annual effective dose is 2.63×10^{-1} μSv/yr. By comparing with left-hand side of Figure 12-35, i.e. without colloid in far-field, the annual effective doses of Pb-210, Sn-126 and Th-229 are increased. In contrast, Cl-36 and I-129 are not affected due to non-sorption onto buffer colloid.

In this section, a conservative estimation has been carried out to estimate the effect of colloids on the released doses. The mechanisms that may retard the buffer colloid were not taken into account in the calculation. For instance, filtration of colloids by sediments in rock fracture (SKB, 2010n).

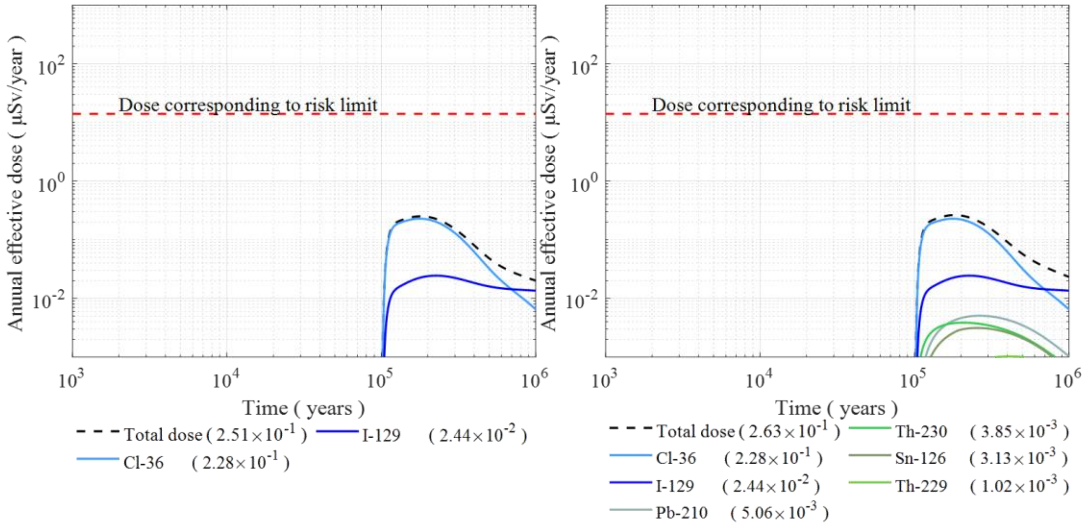

Figure 12-35: Far-field annual effective dose for corrosion variant case with (right) and without (left) colloid facilitated transport (current sea-level, deterministic case, and the concentration of colloid is 10 kg/m^3).

Note: the legends are sorted by the peak annual effective doses. And the values in the brackets are the peak annual effective doses (μSv/yr).

12.7.3. Radionuclide Transport in Gas Phase

The FEPs described in this section: Transport of radionuclides in a gas phase (TWBu26 and TWBfT22) and Transport of radionuclides in the gas phase (TWGe25).

If a canister is failed after the closure, the hydrogen will be produced by anaerobic corrosion of the cast iron lining. Due to the sealing properties of the saturated bentonite in buffer, hydrogen will be accumulated instead of being released continuously. When the accumulative rate is higher than the diffusive transport rate in the buffer, the gas pressure will be built up. In the corrosion scenario, the hydrogen will be carried away from the canister by advective flow. Therefore, the hydrogen gas cannot accumulate in the canister.

According to relevant literature (SKB, 2003), assuming that the gas breaks through the bentonite by fracturing when the internal gas pressure exceeds 20 MPa. The buffer would be sealed when the internal gas pressure is lower than 10 MPa. If the internal gas pressure is larger than 10 MPa after the gas breakthrough pulse, the gas will be released at the same rate as the gas formation rate. Under this condition, the geometry of the breach channel is unstable. The radionuclides (e.g., C-14 and Rn-222) could be transported in the gas phase to the biosphere through the breach channel and would be more rapid than in aqueous phase.

The occurrence time of gas breakthrough depends on the failure time of the canister and the corrosion rate of cast iron lining. According to literature, half of the gas in the canister will be released with the gaseous radionuclides when the gas pressure in the canister exceeds 20 MPa and breaks through. Assuming that half of the inventory of C-14 and Rn-222 in one canister is in the gaseous phase and will be released to the ground. The other half inventory of C-14 and Rn-222 will be released with continuously produced gas, and this release can be neglected because its impact is insignificant.

According to the calculation, if the breakthrough pulse occurs at 10,000 years after repository closure, the released inventory of C-14 and Rn-222 are 11 GBq and 4.69 GBq, respectively. If the breakthrough pulse occurs at 100,000 years after repository closure, the released inventory of C-14 and Rn-222 are 1.98×10^{-4} GBq and 35.91 GBq, respectively.

The C-14 could be released in form of methane (CH_4) or carbon dioxide (CO_2). The former one can be directly released into atmosphere or oxidized to carbon dioxide by soil organisms. C-14 may not be used in the biosphere if it is released as methane. C-14 will be metabolised by photosynthesis and enters the human food chain (SKB, 2006c). On the other hand, Rn-222 is a noble gas and rarely reacts with other elements since it is already stable.

According to the above descriptions, for C-14, the effects of inhalation and ingestion will be estimated. For Rn-222, only the radiation effects of inhalation will be estimated.

The dose consequence estimation method is based on SKB's reports (SKB, 2006d and SKB, 2006c). In estimation, the released activities of C-14 and Rn-222 are described above. The other parameters are the same as the SKB's report and are listed in Table 12-8 to Table 12-10. The estimated annual effective dose of the first year was divided by 50 years to calculate the annual mean life-time risk, and the results are shown in Table 12-11. The highest dose consequence, about 6.56 μSv/yr, is due to inhalation of Rn-222 indoors. The World Health Organization (WHO) recommends a reference level for the indoor radon concentration should not exceed 300 Bq/m^3. The corresponding annual effective dose is about 10 mSv/yr (WHO, 2009). The results of this scenario do not exceed this reference level.

Table 12-8: Parameters used in the case of radionuclide transport in gas phase.

Height of mixing layer [m]	Wind speed [m/s]	Release area [m^2]
2.00×10^{1}	2	1.00×10^{4}
Reference	SKB, 2006d	

Table 12-9: Parameters for dose estimation of C-14 ingestion.

Carbon content of air [g/m^3]	Dose conversion factor for Bq C-14/g C-12 [μSv/(Bq C-14/g C-12)]	Reduction factor of release area [-]
1.30×10^{-1}	5.29×10^{1}	1.00×10^{-1}
Reference	SKB, 2006d	

Table 12-10: Parameters for dose estimation of C-14 and Rn-222 inhalation.

Nuclide	Location	Inhalation rate [m^3/yr]	Dose factor [Sv/Bq]	Volume of house [m^3]	Area of house [m^2]	Ventilation rate [h^{-1}]	Occupancy factor [-]
C-14	Indoors	8.10×10^{3}	6.20×10^{-12}	1.00×10^{3}	1.00×10^{2}	2	5.00×10^{-1}
	Outdoors			-			
Nuclide	**Location**	**Dose factor [(μSv/yr)/(Bq/m^3)]**		**Volume of house [m^3]**	**Area of house [m^2]**	**Ventilation rate [h^{-1}]**	**Occupancy factor [-]**
Rn-222	Indoors	3.20×10^{1}		1.00×10^{3}	1.00×10^{2}	2	5.00×10^{-1}
	Outdoors	4.70×10^{1}		-			
Reference		SKB, 2006d					

Table 12-11: Annual mean life risk from C-14 and Rn-222 gaseous release from a single canister.

Pathway	Radionuclide	
	C-14	Rn-222
Ingestion(μSv/yr)	3.97×10^{-2}	-
Inhalation(outdoors) (μSv/yr)	4.90×10^{-5}	1.50×10^{-1}
Inhalation(indoors) (μSv/yr)	3.20×10^{-3}	6.56

12.8. Summation of the Risk

According to the descriptions in Chapter 11, the failure of safety function of withstanding shear force may occur in the safety assessment time period under the design-basis evolution. The expected number of failed canister is approximately 8.70×10^{-1} canisters. The retardation safety function of the buffer may be intact or defective when the containment safety function of the canister is failed. The analyses of combination conditions are shown in Section 12.6. The curves of annual effective dose are multiplied with dose-to-risk conversion factors, Figure 12-36 shows the results. The peak annual effective dose is higher when advection occurs in the buffer and is lower than the regulation limit, approximately 2 orders of magnitude. The annual effective dose will gradually increase over time, mainly because the nuclides that dominate the annual effective dose are long-lived, and the failure rate induced by the shear load will also increase over time (shown in Figure 9-28).

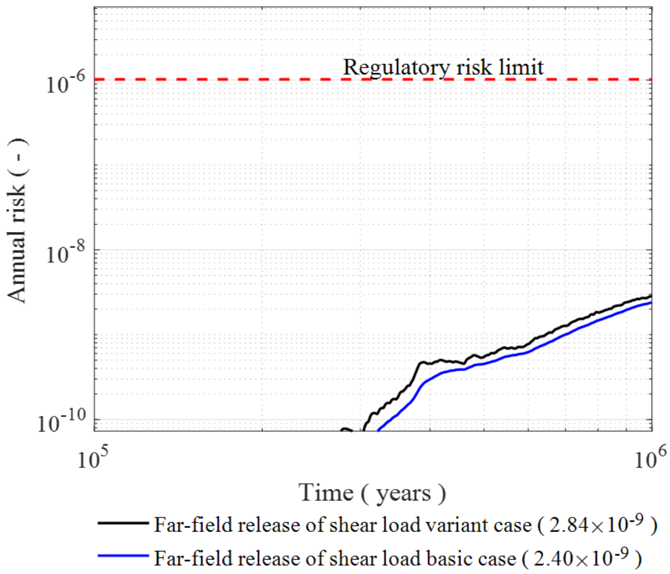

Figure 12-36: Annual risk from the repository.

Note: the values in the brackets are the peak annual risk (-).

12.9. Uncertainties of the Risk Assessment

Figure 12-25 shows the far-field annual effective doses when safety function indicator criterion Can3 is failed and when retardation safety function of the buffer is still intact. The uncertainties of parameters have been taken into consideration, including inventories of nuclides, release rates, properties of barriers and the parameters for nuclides in different materials. The flow-related data in the far-field were also taken into account. The 99^{th} annual effective dose is higher than the mean annual effective dose by approximately 5 times. The flow-related resistance (F) of a flow path is correlated with the advective travel time (t_w) and the flow-related data varied over time; these phenomena have not been taken into consideration in assessments. There are only 58 sets of flow-related data provided by the hydrogeological model for different deposition holes under the current sea-level, but 67 and 145 sets for sea-level drops 20 m and 120 m, respectively. This means that the results of probabilistic cases in this chapter tend toward the dose releases when the sea-level is lower than the current situation. The expected canister failure number was used to demonstrate canister failure due to loss of safety function Can3. The assumptions and effects for the estimations of canister failure will be described in Chapter 14.

In terms of scenario uncertainties, Figure 12-36 shows the annual risks for probabilistic calculation of shear load scenario with the uncertainties of the retardation safety function of the buffer. The difference in peak risk is not significant (approximately 1.2 times). In terms of the uncertainties of radionuclide transport calculation models with respect to risk estimation, the analytical solutions have been used to verify the correctness of the numerical results.

Biosphere conversion factors for 9 potentially exposed groups were estimated by the biosphere models. And far-field annual effective doses of these potentially exposed groups when the canisters are failed due to loss of safety function Can3 with advection condition in the buffer are shown in Figure 12-37. The fruit and vegetable grower group has the highest peak annual risk (4.59×10^{-9}), it is 1.6 times higher compared to the reference group. Figure 12-38 shows far-field annual effective doses of different nuclides of the group. Comparing with Figure 12-27, Cl-36 and I-129 are the main contributors to dose and risk; therefore, the difference is caused by the uncertainties of the intake of these two nuclides for a different potentially exposed group.

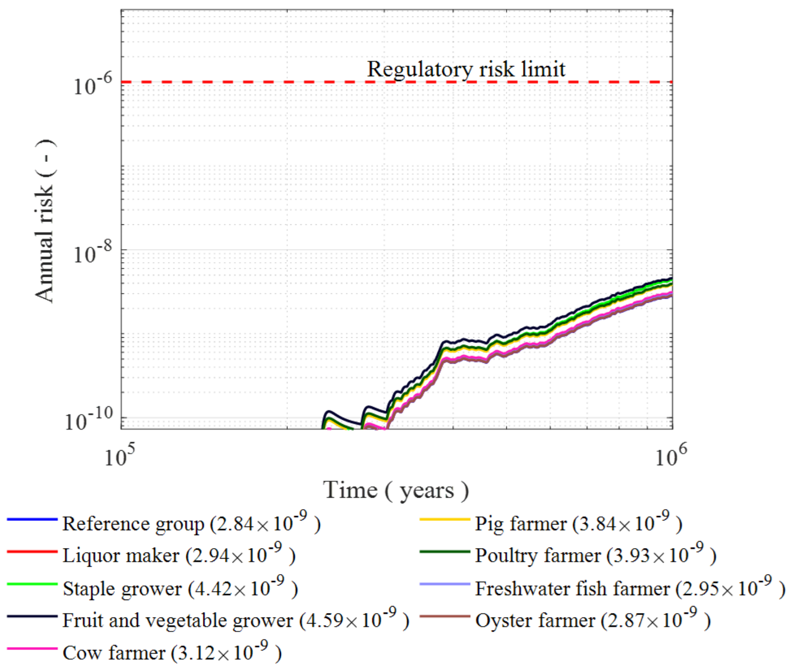

Figure 12-37: Annual risk of different PEGs of shear load variant case (probabilistic case).

Note: the values in the brackets are the peak annual risk (-).

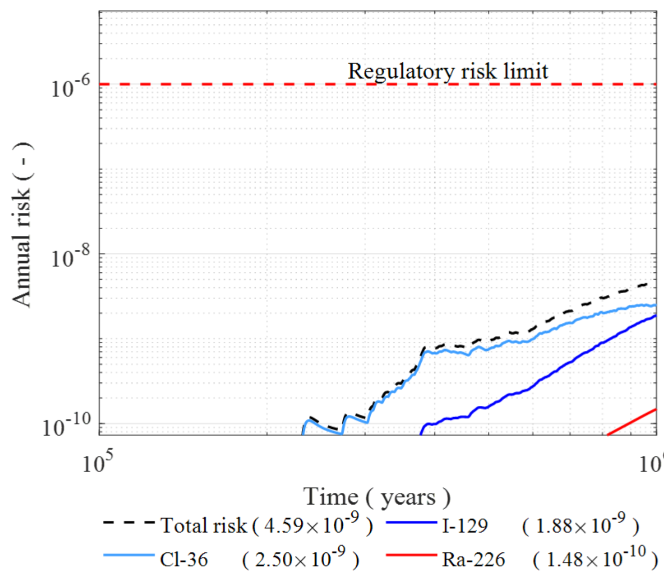

Figure 12-38: Annual risk of the "fruit and vegetable grower group" of shear load variant case (probabilistic case).

Note: the legends are sorted by the peak annual effective doses. And the values in the brackets are the peak annual risk (-).

12.10. Summary of the Retardation safety function Analyses

In general, radionuclides with relatively high instant release fractions, such as Cl-36, are more likely to dissolve in water and migrate in the buffer/backfill and fractures. About 8.6% of Cl-36 is instantly released after the containment safety function of the canister is failed. Cl-36 has a high solubility in water and cannot be absorbed by buffer/backfill and matrix of rock fracture; therefore, it can easily migrate in barriers. On the other hand, uranium is completely embedded in the fuel matrix and is hardly soluble in water and can be effectively absorbed by the barriers. Elements such as plutonium, thorium and americium share similar properties as uranium.

In Section 12.7.1, the effect of different canister failure conditions for peak annual effective doses of the reference group for early failure of the containment safety function of the canister under the same flow-related conditions is shown. A comparison of the release rate between the initial defect case (1) and case (2) shows that the smaller defect effectively reduces the release of radionuclides. If the advection occurs in buffer, it leads to a higher annual effective dose at an earlier time period, but the peak annual effective doses of case (2) and case (3) have insignificant differences. Mechanisms of fuel dissolution and metal corrosion mitigate the release of radionuclides after the failure of the containment safety function of the canister. The elements embedded in the fuel matrix have relatively low solubility limits, and they are constrained in the canister if fuel dissolution and metal corrosion are neglected. Meaning that neglecting these mechanisms has an insignificant effect on this kind of radionuclides. On the contrary, radionuclides that have a relatively high instant release fraction, e.g., Cl-36, it is totally dissolved and massively released during the early period if these mechanisms are neglected. Overall, the far-field peak annual effective dose is an order of magnitude higher for case (4) compared with other cases.

The radionuclides with a low partition coefficient released from near-field into rock fracture are not readily retarded by rock matrix (e.g. I-129 and Cl-36). The pulse-like release curves induced by Cl-36 and I-129 appear in the early period of near-field annual effective dose results are mitigated in the far-field due to the dispersion and matrix diffusion. On the contrary, radionuclides with high partition coefficient transport through the geosphere will be retarded. If the buffer colloids are existed in the geosphere (see Section 12.7.2), the transport of radionuclides with high buffer K_d value in the geosphere will be facilitated and will lead to an increase in the release rate. In the aspect of the geosphere, taking canister initial defect case (1) as an example, the peak annual effective dose of far-field release is decreased by about 46% compared to the near-field release if the radionuclides are transported through the geosphere.

12.11. Conclusion of Sensitivity Analyses

The results of sensitivity analysis for the shear-load and corrosion scenario have been described in Section 12.5.9 and Section 12.6.7. The results show that the annual effective doses of the two scenarios are strongly influenced by the flow-related transport resistance. The higher flow-related transport resistance leads to the lower peak annual effective dose. As an example, in the corrosion scenario, if upper and lower bounds of flow-related transport resistance are used in the calculation, there will be about five orders of magnitude difference in peak annual effective dose. Related parameters for the largest dose contributors (Cl-36 and I-129), e.g., instant release fraction and diffusion coefficient in rock matrix, also have a certain degree of influence on the peak dose. The sensitivity analysis of the peak annual effective dose to the failure time of the canister containment safety function is estimated by the probabilistic shear load case. The results show that the canister failure time also highly influences the peak dose. The longer time it takes for the canister to fail the lower the released activity of Cl-36.

13. Additional Analyses and Supporting Arguments

13.1. Introduction

The objective of this chapter is to the supplement demonstration of the long-term safety of the repository and the integrity of the safety assessment.

(1) In addition to the analysis of the main evolution scenarios of the repository in Chapter 12, analyses of other scenarios, including non-design basis evolution scenarios (Sections 13.2) and future human actions scenarios (Sections 13.3), are described in this chapter. And in Section 13.4, supplementary information on optimization will be discussed.

(2) In order to illustrate the integrity of the assessment, FEPs are excluded from the safety assessment and the reasons for exclusion will be described in Section 13.5.

(3) In Section 13.6, the radiotoxicity of the repository after the safety assessment timescale will be discussed, and a comparison with the level of natural uranium mines will be made. On the other hand, the natural analogue of the repository will be described in Section 13.7, so confidence in the long-term safety of the repository can be reinforced.

13.2. Future Human Actions Scenarios

13.2.1. Introduction

In order to avoid the possibility of human beings inadvertently invading the repository and being exposed to radiation from SNF, siting and design of the repository are carried out according to the following recommendations referred to SKB (2010o):

(1) The repository should be avoided in locations where natural resources are located.

(2) Depth of the repository should be set below the depth of the water supply and most of the underground facilities.

(3) After the repository is completed, the repository should be closed to make it difficult for personnel to enter.

(4) Within a reasonable and feasible extent, the repository should be supervised, and relevant data should be preserved.

In addition, during the supervision of the repository, human actions that may interfere with the supervision of the repository should also be restricted or kept within bounds. Although the repository site will be selected after strict site selection procedures, it is difficult to predict which resources may become economically valuable resources in the future. Therefore, when the repository is no longer under supervision and relevant data is lost, it may be caused by human intrusion due to exploration of minerals, water resources, or drilling for research purposes. Therefore, it is generally accepted internationally that it is necessary to consider the possible impact of future human actions in the design and safety assessment of the repository (NEA, 1995; ICRP, 1999).

13.2.2. Principles and Methods for Handling FHA

When assessing the scenario of future human actions, it will be conducted according to the following principles referred to SKB (2010o):

(1) Evaluating the situation after the post-closure repository.

(2) The assessment area is defined as the area near the repository.

(3) The assessment only considers unintentional human actions.

(4) This human action will weaken the safety function of the multiple barriers of the repository.

13.2.3. Description of the Study Cases

As mentioned in Section 10.3, the future human action scenarios will adopt a "typical" approach (NEA, 2016), and based on current knowledge and experience, a set of representative cases will be used for relevant evaluation. According to the analysis in Section 5.3, drilling operations are the only ones that will directly cause the canisters to be penetrated, causing radionuclides to further affect the human environment. Therefore, the drilling case is used as an analysis case of future human actions and refers to the SKB report for the scenario setting (SKB, 2010o).

Assume that 300 years after the post-closure of the repository, all relevant information about the repository has been lost; at the same time, it is assumed that the drilling technology is the same as today. The scenario of the analysis case is set as follows:

(1) Suppose that a canister in a repository was accidentally excavated during drilling operations, resulting in the canister being penetrated; at this time, the drilling operator discovered an abnormality and stopped the drilling operation.

(2) The SNF in the canister is brought to the surface along with the drilling water, resulting in a circular polluted area on the ground 1 and causing external exposure to the drilling operators.

(3) It is conservatively assumed that one month after drilling operations ceased, a family moved to a contaminated area, where they lived on their own in farming and received radiation doses.

13.2.4. Analysis of the Study Cases

Under the above scenario, the doses of drilling staff and residents under the drilling case were evaluated separately.

(1) Drilling staff:

Assuming that after the repository has been closed for 300 years, the repository has not been supervised and relevant information has been lost.

Unintentional drilling operations were carried out on the surface area of the repository, and the canister of the repository was accidentally excavated during the drilling operation, which caused one canister to be penetrated. At this time, the drilling operator found an abnormality and stopped the drilling operation.

According to current drilling technology, it is assumed that the drill bit used for drilling operations is 0.051 m in diameter and the drilling diameter is 0.056 m. Based on the ratio of the cross-sectional area of the drill bit to the surface area of the canister, the ratio of the number of fuel rods affected by the drilling operation is estimated to be about 3%.

The 3% of the SNF will be brought to the surface along with the drilling water and evenly distributed in the circular polluted area on the ground, which will affect the external exposure of drilling operators.

The results of the assessment of the drilling staff's dose are shown in Figure 13-1. It is assessed that a canister was destroyed by drilling 300 years after the closure of the repository. The dose rate received by the drilling operator was 2.6 mSv/hr, and the main dose contribution nuclear species was Am-241. If the drilling case occurred after the repository was closed for 1,000 years, the dose contribution of nuclear species would be Nb-94.

(2) Residents:

It is assumed that after the drilling operation occurs, the drilling well is abandoned and gradually filled with groundwater, causing the penetrated canister to continuously release radionuclides into the groundwater.

After one month of drilling operations, a family moved to a contaminated area and was self-sufficient in farming. The radiation impact that family members may receive is divided into two categories for discussion:

(a) Using contaminated well water:

The reference group received the dose from using contaminated well water for irrigation and drinking contaminated well water. The possible exposure pathways caused by using contaminated well water are as follows, the ingested dose from drinking contaminated well water, the in vitro exposure dose caused by soil contaminated by irrigation, and the ingested dose caused by ingesting contaminated crops. The results of the dose evaluation are shown in Figure 13-2.

The evaluation results show that if the drilling case occurred 300 years after the post-closure of the repository, the annual effective dose to the reference group caused by the use of contaminated well water was 0.38 mSv/yr, and the main dose contributor was Am-241.

(b) The use of soil contamination:

Suppose that after drilling operations, the soil containing SNF fragments is used for farming by residents. Assuming that the crop can be used for vegetables for 5 people, the farming area is 102 m^2, and the farming soil thickness is 0.25 m. The reference group spends 1 hour a day on the contaminated farmland and consumes 2.5% of the vegetables harvested from the farmland every year. For soil contaminated by SNF, the exposure pathways considered are the in vitro exposure dose caused by contaminated soil, the inhalation dose caused by the inhalation of suspended particles contaminated by radionuclides in the air, and the intake dose caused by ingesting contaminated vegetables. The results of the dose evaluation are shown in Figure 13-3.

The evaluation results show that if the drilling case occurred 300 years after the post-closure of the repository and the use of contaminated soil for farming, the annual effective dose to the reference group is 8.80 Sv/yr, and the main dose contributor is Pu-238; if the drilling case occurred after post-closure 500 years, the main dose contributor was Cl-36.

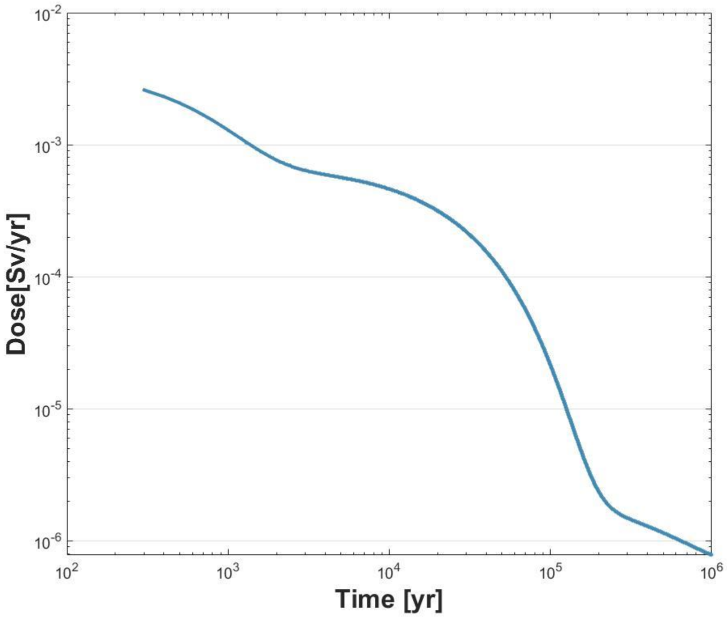

Figure 13-1: Dose estimation of the drilling staff when drilling occurred during post-closure 300 to 1 million years.

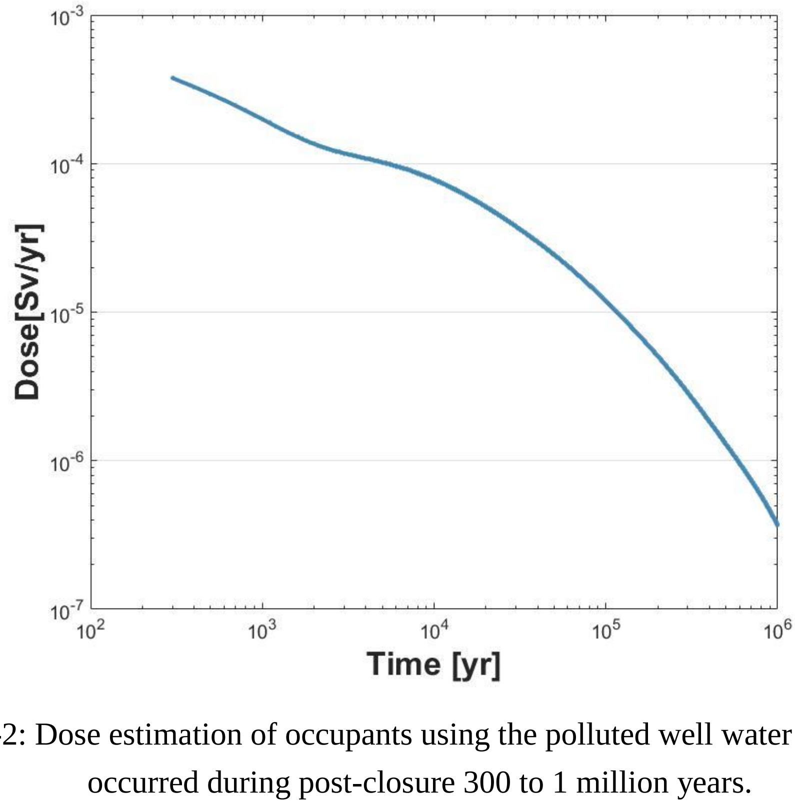

Figure 13-2: Dose estimation of occupants using the polluted well water when drilling occurred during post-closure 300 to 1 million years.

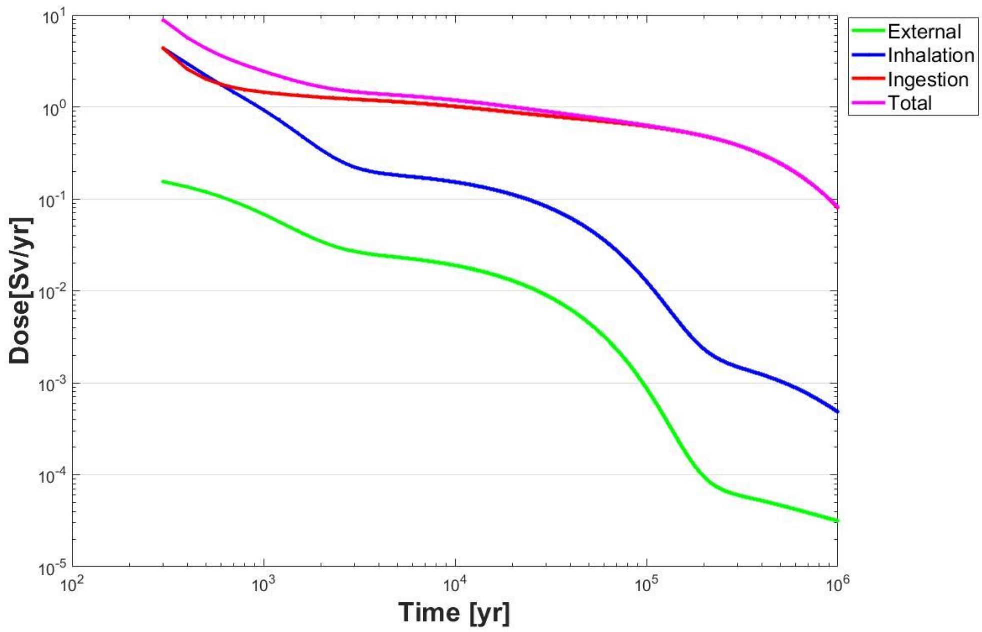

Figure 13-3: Dose estimation of farming using the contaminated soil when drilling occurred during post-closure 300 to 1 million years.

Note: Green line: external exposure dose; blue line: inhalation dose; red line: ingestion dose; purple line: total dose.

13.2.5. Incomplete Closure of the Repository

According to the recommendations of the relevant international literature (SSM, 2008), in assessing the possible impact of future human actions, it is also necessary to assess the possible impact on the repository after closure. Since the excavation and operation of the repository are phased operations, the discussion will be based on the incomplete closure of the repository.

After the disposal tunnels successively dispose of the canisters, they will be immediately backfilled and closed. It is unlikely that the disposal operations will be temporarily terminated and the disposal tunnels will be abandoned during the process, leaving the canisters on the ground. Therefore, it is more likely that when all the canisters have been disposed or all the disposal tunnels have been backfilled and closed, the repository is abandoned, leaving the repository in addition to the closed disposal tunnels, the rest (such as the main tunnel, etc.) is in an unclosed state. The above situation may occur when the repository is not completely closed due to political decisions. This plan has not yet evaluated the incomplete closure of the repository. The evaluation method can be developed and built with the plan in the future.

13.3. Non-Design-Basis Evolution Scenarios

In this chapter, although the probability of occurrence in the reference case is extremely small, possible radiation impact of the external factors (including uplift/denudation and volcanism) that may affect the long-term safety of the repository are described.

13.3.1. Uplift/Denudation

The safety assessment study of the Japanese uplift/denudation scenario (Wakasugi, 2017) and research of the Japan Atomic Energy Agency (JAEA) (JNC, 2000) were referred to in the report. Because the uplift rate and erosion rate are different in different regions, the range that can be covered in the diverse geological environment is limited.

Therefore, only stages in the assessment of uplift/denudation cases are briefly discussed in this report.

The uplift/denudation case is divided into 3 stages according to the depth of the repository:

(1) Stage 1:

Before reaching the weathered layer, canisters can maintain their containment safety function after closure. However, canisters uplift gradually at average velocity.

(2) Stage 2:

The second stage is when the repository enters the weathered layer until it reaches the ground surface. After the repository enters the weathered layer, the surrounding environment of the repository will change from a reducing environment to an oxidizing environment due to the shallow depth of the repository, which will accelerate the corrosion of the copper shell canister. With the uplift of the repository, the nuclides species still retained in the canister and the nuclides species released in the host rock will also migrate to the weathered layer due to the uplift/denudation effect.

(3) Stage 3:

The third stage is when the repository reaches the ground due to uplift/denudation from the weathered layer. In general, when the repository reaches the surface, the canister is exposed to the ground and will be detected by humans, and humans should take some intervention measures. However, in the Japanese uplift/denudation case study, the radiation damage caused by the uplift/denudation scenario to humans and the environment is conservatively evaluated, so any intervention measures are not considered.

13.3.2. Volcanism

According to the methods and assumptions of the volcano scenario in Chapter 10, the safety assessment method of the volcano case is briefly described. In accordance with Taiwan’s “Regulations on the Final Disposal of High-level Radioactive Waste and the Safety Management of Facilities” and “Specifications for Sites of High-level Radioactive

Waste Disposal Facilities" and other relevant regulations (please refer to Section 1.4), sites can completely avoid dangerous regions, where the volcanic activity occurred in 100,000 years or above magma, with potential risk.

Assuming that 100,000 years after the closure of the repository, it is affected by potential volcanic activity. The magma in the volcano channel penetrates the repository vertically from bottom to top, causing the containment safety function of some canisters to directly fail. The radionuclides in the canister are mixed in the magma and spread to the surface environment of the adjacent area around the volcano as the volcano erupts. After a period of time, the volcanic eruptions mixed with radionuclides will gradually sink to the surface, accumulate to a certain thickness, and mix evenly with the soil. Finally, through the exposure pathways of inhalation, ingestion, and external exposure, the radiation impact of the reference group of the potentially exposed group is evaluated.

13.4. Demonstration of Optimization of the Analyses and the Use of Best Available Techniques

13.4.1. Introduction

According to suggestions from literature (SKB, 2011; SSM, SSMFS 2008:37), it is necessary to ensure that the design and evaluation methods are optimized and BAT are adopted when developing a disposal program. Optimization means that siting, design, construction, operation and containment of the repository and the associated system components should have the capability to prevent, limit and retard the release of radionuclides from the multiple barrier system reasonably and feasibly.

The calculated risk should be the basis when choosing the best available technology. The radiation dose should be minimized reasonably, taking economic and social factors into account. That is the principle of ALARA (as low as reasonably achievable)(SKB, 2011). The scenarios which will affect the risk and the related safety functions are mainly conducted in the safety assessment, so the scenarios of canister corrosion and shear force would be the main focus.

Regarding two of the scenarios mentioned above, the factors that comprise of these scenarios will be examined from a design viewpoint, and the corresponding risks will be calculated. When actual conditions, uncertainties and economic feasibility are taken into consideration, the optimization goal can be achieved by iteration between design and risk assessment. In addition, the design which is deemed to not directly affect the risk assessment results (such as backfill, plug, and etc.) will be evaluated to ensure that there is no impact on safety functions and to confirm whether a better design can be improved its safety or not.

13.4.2. Potential Corrosion Failure

In the canister corrosion failure scenario, the safety function of providing a barrier against corrosion (Can 1) is the most important factor for risk calculation. According to the results in Chapters 9 and 11, the corrosion scenario will occur when the transport mechanism within the buffer changes from diffusion to advection. According to the literature (SKB, 2011) and results in Section 11.2.2, the factors that influence the transport mechanism within the buffer, include (1) buffer density; (2) backfill density; (3) type of bentonite; (4) ionic strength in the geosphere; (5) high groundwater flow in the geosphere.

Based on the safety assessment results of canister corrosion, the copper thickness of the canister still has enough margin to withstand the canister corrosion under a very pessimistic situation. It has no demand to adjust the copper thickness at this current stage. In addition, the buffer density has the ability to resist the transportation of corrodent within the buffer. So it has no demand to increase the density of the buffer.Thelayout and depth of the repository will influence groundwater flow rate and equivalent initial flux of the deposition holes; however, the equivalent initial flux of deposition holes based on the current layout and depth of the repository is too low to make a huge impact on canister corrosion. It has no demand to increase and adjust the copper thickness from the viewpoint of canister corrosion. In summary, the current design of buffer density and copper thickness can fulfill the safety function of Can 1, and the integrity of the canister can be maintained.

13.4.3. Potential Shear Force Failure

In the scenario of canister shear failure, the safety function Can3 is the most important factor for risk calculation. According to the literature (SKB, 2011) and results in Section 11.8, the main factors that may affect the shear force failure include: (1) strength of the cast iron lining and possible defect of the case iron lining; (2) mechanical properties of the copper shell; (3) density and property of the buffer; (4) implementation of FPC and EFPC.

When evaluating containment safety function related to shear force, FPC and EFPC, which are the basis for selecting the position of the deposition holes were also taken into account. Based on seismic characteristics and uncertainty, the expected value of canister failure due to shear force is 0.87 under cumulative shear displacement over the safety assessment timescale. It is shown that with the current design, the assessment results of potential shear force failure can be in line with the requirements of the regulations over the safety assessment timescale.

Conducting FPC and EFPC efficiently can reduce the risk of canister failure due to shear force. There is no motivation to take more restricted criterion, regarding to FPC and EFPC are pessimistic criteria (SKB, 2010f). Besides, in the excavation period, large fractures intersecting deposition holes could be detected in a detailed site investigation. Therefore, the risk can be further reduced.

13.4.4. Relevant Design Factors that Do Not Have Impact on the Risk

According to the risk analysis in Chapters 11 and 12, the factor not included in the scenario discussion under the framework of existing reference cases and reference design is isostatic load. It cannot be determined whether design optimization or development of the best available technology is required. The discussions are described as follows:

Based on the results of the swelling pressure of the buffer in Section 11.6.2 and strength of the canister in Section 11.6.3, the maximum swelling pressure of the buffer is about 8.23 MPa and the groundwater pressure is around 5 MPa under the framework of the existing reference cases and reference design. The possible maximum isostatic load to the canister will be 13.23 MPa. In addition, based on the results of mechanical influences due to buffer swelling, the design of the copper shell and the cast iron lining can withstand the external forces and maintain the integrity of the canister. The canister will encounter an additional external force of around 30 MPa in the glacial period of Nordic countries due to the ice sheet covering the surface of the repository; however, it shall not happen in the reference case. It shows that the current design has enough margin within the safety assessment timescale. Therefore, there is no need to adjust the design to provide more margin.

13.5. Impact on Scenarios and Risk Assessment after FEPs Screening

13.5.1. Introduction

By the SCREENING process of FEPs, one can ensure that important factors related to the long-term safety of the repository are included in the assessment.

By referring to the experience and implementation strategy of SKB SR-site in Sweden, overall safety assessment can start with checking technologies that are developed, developing and pending. Then, according to the progress of the plan, the implementation status of each technology and reasons for not including each in the safety assessment can be explained. Finally, FEPs analysis can be completed to explain the influence of the screening on scenario analysis and risk analysis.

The analysis in this section in terms of the main disposal components that have fuel (source term), canister, buffer, backfill and geosphere is discussed. The auxiliary components of the engineered barrier system, such as the central area, bottom plate, sealing and plug, are not primarily considered safety concerns and are not taken into account here. In addition, the boundary conditions related to climate affecting the geosphere, as well as climatic issues related to conditions and processes of the biosphere are discussed in climate and biosphere separately. There is no more discussion in this section. Therefore, to ensure that FEPs related to the long-term safety of the repository have been considered by re-examining previously neglected or labeled as irrelevant FEPs.

13.5.2. Source Term

The internal processes of the source term have been screened out and described as follows:

(1) Induced fission (criticality)

The acceptance criteria of a fuel assembly for the canister should ensure that the fuel cannot induce fission under the canister filled completely. At the same time, the criticality analysis of the failed canister showed that it was highly unlikely to reach a critical state. Therefore, meeting the acceptance criteria of fuel packaging, this effect can be reasonably neglected.

(2) Radiolysis/acidification of residual gas (intact canister)

In a sealed canister, the amount of water and air is limited. Therefore, stress corrosion cracking insertion is not possible because the limited water and air (nitrogen) content limits the formation of corrosive gases such as nitric acid and nitrite acid. Because water and air content are limited in the engineering design, it is reasonable to neglect this process.

13.5.3. Canister

The internal processes of the canister have been screened out and described as follows:

(1) Galvanic corrosion (failed canister):

This process describes the potential corrosion of cast iron lining when the canister fails. In canister design, the effect of potential corrosion is within a margin of error under the anaerobic reduction condition. In addition, since the cast iron lining is not regarded as a corrosion barrier, potential corrosion for cast iron lining can be neglected.

(2) Stress corrosion cracking:

In canister design, stress corrosion cracking of the copper canister was assessed to be negligible due to the very low expected concentration of SCC promoting agents and the insufficient availability of oxidants.

13.5.4. Buffer

The internal processes of the buffer have been screened out and described as follows:

Gas transport/dissolution (intact canister): if the canister is intact, it is expected that no gas will be generated due to corrosion. The gas originally existing in the pores of the buffer is also dissolved and diffused during the process of saturation. In addition, the pore water in the buffer may decompose into hydrogen and oxygen by radiolysis, but it cannot produce a large amount of gas. However, microbial processes may also lead to the formation of gaseous substances, but as long as the high swelling pressure is maintained in the buffer, the microbial process will be very low. Therefore, when the canister is intact, the process of gas transport/dissolution can be neglected.

13.5.5. Backfill

The internal processes of backfill have been screened out and described as follows. Because the constituent material is MX-80 bentonite which is the same as the buffer, part of the factors have been screened out in the same way as the buffer.

(1) Diffusive transport of species (early stage, intact canister):

Because advection is dominant in the unsaturated phase, diffusion can be neglected.

(2) Sorption (including ion-exchange) (early stage, intact canister):

There are no paths for transportation in backfill during the unsaturated phase. Therefore, the sorption process is negligible.

(3) Aqueous speciation and reactions (early stage, intact canister):

Geochemical processes are the same before and after the saturation. Therefore, aqueous speciations and reactions can be neglected before saturation. This process is the same in the buffer.

13.5.6. Geosphere

The internal processes of the geosphere have been screened out and described as follows:

Reactions between groundwater and rock matrix (excavation period, temperate climate): the main impact is caused by reactions of groundwater and minerals filled in the fractures. Because there is no significant changes in groundwater composition and matrix porosity during the entire operation period, therefore, this process can be neglected.

13.6. Safety of the Disposal System beyond One Million Years

Radiotoxicity of the SNF can drop to the level of natural uranium mines after one million years and continues to decrease gradually. Therefore, no risk calculation is required for the disposal system beyond the safety assessment timescale. On the other hand, the uncertainty of the evolution of the repository will increase over time; but by evidence given by natural analogues, the confidence in the long-term safety of the repository can still be proven.

13.7. Study of Natural Analogues

It can enhance the confidence in the technical assessment of the deep geological disposal concept by studying a natural system that is similar to the disposal system. The study of natural analogues is an important method to verify the results of the safety assessment of a deep geological repository as it overcomes the disadvantages inherent to laboratory experiments and in-situ testing in terms of time and spatial scales. These results can be used as a reference for the safety assessment of the deep geological repository (台電公司, 2019a).

Internationally, natural analogue research can be divided into three categories: (1) natural analogy for geological disposal, (2) natural analogy for metals, and (3) natural analogy for bentonite.

(1) Natural analogues for geological disposal

The natural analogues research of geological disposal focuses on proving that the host rock has the ability to restrict the migration of radionuclides. For example, the study of the Tono uranium deposit in Japan points out that the uranium deposit has been buried underground for more than 10 million years (Shinjo et al., 1997); Yoshida et al., 1994b). Uranium deposits in the Cigar Lake uranium deposit in Canada have been buried under clay for 1.3 billion years, but no mass transport of uranium is evident even with the natural processes stretching over the enormous time horizon (SKB, 1994). Natural nuclear fission chain reactions have occurred in the Oklo uranium deposit, located in the Gabonese Republic, an African country. The radionuclides produced by the reaction such as uranium, plutonium, cesium, strontium, etc., can still be retained in the clay surrounding the uranium deposit for over 20 million years (Hidaka and Holliger, 1998; Isobe et al., 1995).

(2) Natural analogues for metal

The canister materials for the disposal of high-level waste are not the same in different countries. For example, the copper-iron canister, which is consisted of an outer copper shell and cast iron lining, is used in Sweden and Finland. Japan is take carbon steel as a canister material. Titanium, nickel-based alloys, stainless steel, etc., are also considered as candidate materials in some countries. Since the metal production technology in the past was not as advanced as today, there are no corrosion data for modern materials such as titanium, nickel-based alloys, and stainless steel in nature to do natural analogue research. Most of the research are based on archaeological artifacts such as iron and copper.

The study of natural analogues for metals focuses on proving that the metals used in the canister have sufficient corrosion resistance. For example, native copper of different sizes was discovered in mudstone 170 million years ago in Devon, UK (Posiva, 2012). These native copper have been preserved in the clay matrix after the diagenetic reaction of the mudstone without further alteration. The natural clay matrix of the mudstone formation is not smectite-rich, nor has it been compacted to ensure a low permeability buffer around the copper. In such an environment, the native copper can still be preserved well, which shows that the copper can maintain its integrity for a long time in the natural environment.

Tylecote (1977) studied the durability of various bronzes and copper alloys (lead, tin, and bronze, etc.). The result shows that copper and copper alloys have good corrosion resistance and are suitable for making the canister. Bresle et al. (1983) also collected copper archaeological artifacts from five different regions (including Roman coins, metal vases, objects from the Swedish Bronze Age, 17th-century coins, lumps of native copper, etc.) for analysis. The objects were all of different ages, came from a wide range of environments and had differing compositions. All samples (excluding the native metal) indicated pitting factors of less than 3, which is smaller the factor (5) used in the KBS-3 assessment (SKB, 2010). The native metal had a pitting factor of 2 to 6.

The Swedish warship Kronan sank in the Baltic Sea in 1676. Some of the copper cannons on the ship were salvaged ashore in the 1980s. These cannons had a high copper content. The composition of these cannons is 96.3% copper, 3.3% tin, and a small amount of zinc, iron, etc. They were buried in the clay on the seabed and stayed in the extreme environment of the seabed for 300 years. By observing the corrosion degree of the copper cannons, it can be found that the cannon had suffered only minor corrosion, despite the oxidizing conditions (Hallberg, 1988).

The iron nails excavated from the Roman fortress at Inchtuthil have been buried underground for nearly 2,000 years. The iron nails remained intact when they were excavated, and only the outer layer was corroded (McConchie, 2014). The iron pillars of the ancient temple Chandra in Delhi, India, were built about 1,600 years ago. The outer pillar was corroded and formed a crust. The crust has high corrosion resistance and can protect the pillar against corrosion (Fayek and Brown, 2015).

The helmet crafted around 750 AD was excavated in the city of York, U.K. The helmet was made from iron, brass, bronze and silver. The helmet was found in clay soil and which formed a grey crust over the helmet. The interior of the helmet had been filled with thick clay. This environment had the effect of greatly reducing the amount of oxygen available, leading to the remarkable preservation of the helmet (Smart and Adams, 2006).

(3) Natural analogues for bentonite

The main component of bentonite is montmorillonite. Montmorillonite, once damped, has excellent swelling capacity. It can take advantage of its swelling capacity by filling the gap between the buffer blocks, the disposal pits and the surrounding host rock with this material. It also can achieve the purpose of adsorbing radionuclides. The performance of the buffer is determined by the content of montmorillonite. Therefore, the natural analogue study of bentonite focuses on proving that the montmorillonite mineral can maintain its structure and characteristics after long-term environmental changes. The related research topic includes the alteration of montmorillonite, the influence of pH on bentonite, the influence of salinity on bentonite, etc.

In order to understand the reaction of smectite-illite alteration, Velde and Vasseur (1992) studied sedimentary rock samples from four different regions (the Texas Gulf Coast in teh U.S., the Niigata

Basin in Japan, Los Angeles Basin in the U.S., and the Paris Basin in France) with ages ranging from 4 million to 210 million years. The result shows that the reaction rate at repository-relevant temperatures is very slow in relation to the timescale considered for a repository (about 1 million years) (SKB, 2011).

The Cyprus Natural Analogue Project (CNAP) is an international collaborative project involving NDA-RWMD (Nuclear Decommissioning Authority-Radioactive Waste Management Directorate, UK), Posiva (Finland) and SKB (Sweden). Cyprus has highly alkaline groundwater with a pH value of about 10 to 11 (generation age was about 800,000 years ago) and bentonite deposits (generation age was about 83 million years ago), which can be used to study the effect of alkaline groundwater on bentonite. The research has shown that only a few smectites would transform into other minerals when alkaline groundwater is in contact with bentonite for a long time. It is unlikely to impact the properties of the bentonite significantly. It can be used as an analogy to the relation between alkaline pore water caused by low-alkali cement materials in the repository and bentonite (Alexander, 2013).

Smellie (Posiva, 2012) studied the effect of high-salinity groundwater on the properties of bentonite, which is from a deposit in Wyoming, USA. The study pointed out that the groundwater in the repository had slowly become more saline over several million years, finally becoming a brine. Nevertheless, the bentonite of the mine was not found to be degraded due to the influence of salinity. It was shown that the Wyoming bentonite had been isolated from interaction with marine waters by thick, relatively impermeable marine clays. The bentonite/impermeable clay boundary shows no visible alteration. It possibly indicated that the bentonite is resistant to saline water interaction.

14. Conclusions

14.1. Introduction

Based on international experience, a reference case was established, and the Swedish KBS-3 disposal concept was adopted as the basis for the safety assessment. The assessment technologies of the first stage of the final disposal program have been improved, and a safety case and related assessment have been developed using an integrated quantification method so that the long-term safety of the repository can be ensured. The basis for the safety case of the repository is as the following:

(1) The repository will be built in long-term stable host rock with no valuable minerals, and it will be isolated from humans and near-surface activities. Therefore, changes in human society will not have a significant impact on the repository, and long-term climate changes on the ground will not have a direct influence on the repository either.

(2) The repository will be constituted by a multiple barriers system including engineered barriers and natural barriers. And safety functions of the system are isolation, containment, and retardation.

(3) The geological environment in which the repository is located should have an extremely low groundwater flow rate, good mechanical stability, suitable groundwater chemical conditions, and long-term stability. Also, the engineered barriers have been designed referring to mature international design with decades of experience.

(4) Through appropriate design requirements, the safety of the repository can be maintained, and the impact from thermal, hydrological, mechanical and chemical processes can be minimized to reduce the influence on the long-term safety of the repository.

14.2. Summary of the Assessment

Results of the preliminary safety case are summarized in this chapter. The results will be described in the aspects of control standards, climate related issues, and other issues related to barrier performance and confidence.

14.2.1. Comparison with the Control Standards

According to suggestions from the ICRP-122 report and the description in Section 10.2, the design basis evolution scenario is regarded as planned exposure and should be regulated by risk constraints or dose constraints. According to Chapter 11, within the safety assessment timescale of the repository, the containment safety function of the canisters is not likely to fail due to corrosion or the surrounding isostatic load. If the retardation capability of the buffer around the canisters is assumed to be ignored, radionuclides would be released into the biosphere and cause the highest annual risk to the fruit and vegetable farming group, as shown in Figure 12-38. In this case, however, the annual risk is still lower than the regulation limit (10^{-6}).

14.2.2. Climate-Related Issues

The following statement can be concluded through the assessment of climate change:

(1) Taiwan is located in the subtropical zone. In the next 1,000,000 years, the climate of the reference case will be between subtropical climate pattern and temperate climate pattern, with a cycle of 120,000 years (it is estimated that there are more than 8 glacial cycles). The annual average temperature of the surface will be between 17 ℃ and 23.8 ℃. And the temperature will not drop below 0°C. Moreover, the repository will be located at 500 m depth underground; therefore, it should not be affected by changes in surface temperature immediately. As a result, the possibility of buffer freezing was preliminarily excluded. Therefore, glacial climate and glacial overburdens are considered not to occur during the one million-year assessment time. This means that the increased hydrostatic pressures, the increased flow rates, the possible penetration of oxygenated groundwater to repository depth and the

profound alterations of biosphere conditions associated with a glacial climate did not have to be addressed in the safety assessment for the reference case.

(2) During the glacial cycle, global temperature will drop, leading to the expansion of glaciers and land area, which causes a decrease of the sea-level. The sea-level will cycle between the current height and -120 m, which will cause the reference case to cycle between the offshore island and coastal land. This will affect the salinity of the groundwater and cause the release point of the groundwater to cycle between sea and land. Detailed analysis results can be found in Chapter 9.

(3) As mentioned above, changes in the sea-level may affect landscape considered in the biosphere assessment. Therefore, in the development of biosphere objects in this report, different radionuclide models have been established, and biosphere dose conversion factors were calculated conservatively. Detailed analysis results can be found in Chapter 12.

14.2.3. Other Issues Related to Barrier Performance and Design

Over the timescale of safety assessment, the following statement can be concluded after the assessment:

(1) For the containment safety function of the canister, high transmissivity fractures will affect the release of the colloids and rock shear displacement of the repository and indirectly cause the canister to fail because of impact from corrosion and shear force. Thus, FPC and EFPC have been applied to determine the layout to avoid such an impact.

(2) During the operation period, the impact from colloid erosion of the buffer can be ignored. And in the initial period after closure, requirements from the safety function indicator criteria for swelling pressure can be fulfilled; therefore, advection in the buffer and canister sinking can be avoided. Besides, decay heat from the SNF will not jeopardize the integrity of the safety functions of the buffer.

However, mass loss of the buffer in one deposition hole might exceed 1,200 kg in the remaining glacial period after closure. Advection in the buffer might thus occur, and the corrosion rate of the canister might be accelerated.

(3) Seismic source parameters were applied in the shear displacement assessment. And canister failure number was calculated based on the results of intersected fractures over the safety assessment timescale.

(4) The design of each component is related to the conditions of the potential site. Therefore, performance and safety assessment of the site is needed to understand the performance and integrity of safety functions. Moreover, adjustment and optimization can be done accordingly.

14.2.4. Confidence

Confidence is the degree of confidence for evaluation results that can be used as the basis for applying for a construction license. The elements that can help improve overall confidence of the assessment results in this report are described as follows:

(1) Various research and technology development results are referred for long-term safety assessment of the repository in this report.

(2) By referring to domestic and international research, uncertainties of each factor have been analyzed, and long-term safety-related issues have been identified to implement a thorough assessment.

(3) Peer review and related quality assurance procedures are adopted to establish confidence in the analysis and assessment results.

Deep geological disposal technologies for SNF have been well developed around the world over decades. With increasing long-term safety research and understanding of relevant issues, people have comprehended more and more about how the canisters will fail and what key processes of canister failure are, such as copper corrosion, shear force failure and other potential factors. Based on previous research, the design of the deep geological repository in Taiwan and development of safety assessment are promoted in this program. According to the statement in this preliminary safety case report, confidence in the results of the safety assessment is sufficient for the current stage of the program. After the candidate disposal site is confirmed, repository design optimization can be adopted to enhance confidence in the results of the safety assessment.

14.3. Demonstration of the Compliance

14.3.1. Introduction

In order to verify the long-term safety of the repository and prove that it meets the requirements of relevant laws and regulations, demonstration of the compliance will be discussed according to the following aspects: safety concept of the repository, regulatory requirements, optimization of the design, confidence of the preliminary safety case, robustness of the assessment, and complements of the safety assessment.

14.3.2. Safety Concept

The main safety functions in this report are isolation, containment, and retardation. The safety function of isolation is mainly provided by the geosphere (host rock), and the safety functions of containment and retardation are provided by the geosphere and engineered barriers. The relevant discussion is described as follows:

(1) Isolation

Host rock outside the repository is able to isolate the radioactive waste for a long time. Uplift/denudation is supposed to be ruled out during siting process. However, it is still discussed in the non-design-basis evolution scenario.

(2) Containment

An intact canister provides the safety function of containment to the repository system. The containment safety function of the canister depends on the performance of the buffer (which can limit advection transport between the host rock and the canister) and also depends on the chemical, mechanical, hydrogeological and thermal conditions of the host rock. The integrity of the containment safety function of the repository under long-term evolution is discussed in Chapter 9, and interactions of containment safety function between components are summarized in Chapter 11.

According to the assessment results in Section 11.5, even if solute transport by advection in buffer, which results in an increase of canister copper shell corrosion, the canisters will still be able to maintain the containment safety function 1,000,000 years after closure.

According to the assessment results in Section 11.6, even and uneven loadings were taken into account, and the canister copper shell can still maintain its integrity. The integrity of the cast iron lining will not fail, which means the canisters can maintain containment safety function, and the canisters will not fail because of isostatic load 1,000,000 years post-closure.

According to the assessment results in Section 11.7, shear displacement caused by earthquakes will cause less than one canister to fail under probability analysis. That means most of the canisters can maintain containment safety function, and the canisters will not fail because of shear force in the safety assessment timescale.

In general, most of the canisters in the repository can maintain containment safety functions over the safety assessment timescale under the engineering design in this report.

(3) Retardation

When the containment safety function of the canister fails, the surrounding components could be affected. In Section 12.7.1, radiation impact on buffer retardation safety function integrity when the canister fails initially is discussed in case (2) and case (3). The results show that retardation safety functions of the buffer can delay the time of peak dose for tens of thousands of years. In addition, according to the assessment results in Section 12.6.3 and Section 12.6.5, if the canister fails in post-closure 230,000 years, retardation safety functions of the buffer can effectively retard radionuclides that are easy to be adsorbed.

In Section 12.5 and Section 12.6, a comparison of the annual effective dose caused by radionuclides released from the near-field and far-field shows that radionuclides that are easy to be adsorbed by host rock can be effectively retarded when released to the geosphere. However, radionuclides that are not easily adsorbed and with long half-lives will dominate the peak annual effective dose of the potentially exposed group in the biosphere. According to Section 12.9, the retardation safety function designed for the repository has been taken into account, and the peak annual risk caused by the repository will be less than the regulation limit (10^{-6}).

Evaluation of available hydrogeological information of the reference case has resulted in favorable results for the hydrogeological model. If more hydrogeological data from this site or other sites are acquired and more elaborate evaluations of these data are performed, less favorable results of the hydrogeological model could be obtained. As a result, an advection/corrosion scenario could become much more important in the overall risk assessment of the repository. This is in line with the findings of programs in other countries.

The containment safety function is to ensure the main safety function of the repository. Based on the assessment results, the containment safety function can be effectively maintained by the canister, engineered barriers and natural barriers over the safety assessment timescale. When a few containment safety functions fail, the retardation safety function of the repository can retard most of the radionuclides, and the requirements of the regulations can still be complied with. As a result, the safety of the repository can be ensured under the current engineering design.

14.3.3. Regulatory Requirements

Regarding radiation dose and risk that may be caused by the repository, relevant provisions of the “Regulations on the Final Disposal of High-Level Radioactive Waste and Safety Management of the Facilities” should be followed. Annual risk caused by radiation effect on individuals in the critical group outside the repository shall not exceed one in a million. As described in Chapter 10, the design-basis-evolution scenario should be regulated by risk constraints or dose constraints. The containment safety function and retardation safety function of the design-basis-evolution scenario are evaluated in Chapter 11 and Chapter 12, and compared in Section 14.2.1. While the uncertainty of parameters and scenarios was taken into account, the personal risk caused by the repository would be lower than 4.59×10^{-9} yr^{-1}, which is under regulatory limitation.

14.3.4. Optimization and Best Available Techniques

The design of the repository can improve the protection capacity of the repository through optimization within a reasonable and feasible range. Optimization needs to comply with the principle of as low as reasonably achievable (ALARA), and the calculated risk value must be used as the basis. Under the premise of economic and social factors, the possible radiation dose to humans should be minimized as much as possible. In the assessment, scenarios that affect the risk and safety function will be focused. In this report, a scenario of canister failure due to corrosion and a shear force scenario have been focused on. Potential risk corresponding to each scenario has been evaluated in safety assessment. For safety function Can1, the basic requirement of the safety function is to maintain the thickness of the copper shell. When the buffer is intact, factors that affect corrosion of the canister include the density of the buffer, the density of the backfill, analysis results of the evolution of the groundwater flow field, analysis results of the evolution of the geochemical conditions, etc. On the other hand, when the buffer is eroded, analysis results of the copper shell thickness of the canister and evolution of the groundwater flow field will affect calculation of the canister corrosion failure time. In the assessment of canister failure due to shear force, safety function Can3 will be the evaluation basis. Factors such as the strength and quality of the cast iron lining, mechanical properties of the copper shell, the density of the buffer, and implementation of deposition hole rejection criteria will influence the effect of shear force. Therefore, the results will be fed back to the specification of each component. During iteration, initial state of each component and assessment ability will be improved, and optimized feasible technology can be implemented.

From Section 13.4.2 and 13.4.3, currently, optimized technologies have been used of impact factors and possible processes of canister failure due to corrosion and shear force. However, the specification of each component and still be revised through the feedback of the following safety assessment. Also, uncertainty analysis of parameters and integrity analysis can be implemented to confirm whether ALARA is achieved.

14.3.5. Confidence

The long-term safety of the repository has been preliminarily analyzed in this report.

(1) Through identification of FEPs in Chapter 3, studies of their roles in Chapter 6 and evolution analysis of the repository in Chapter 9 can be used as representatives of overall confidence of the assessment and results.

(2) The long-term safety of the disposal concept has been confirmed through systematic identification of safety functions and safety function indicators (please refer to Chapter 7).

(3) A systematic approach has been taken to analyze the evolution of the repository at different times (please refer to Chapter 9). For control and evaluation methods for parameter uncertainty and data quality, please refer to Chapter 8. The results of evolution analysis

are divided into several scenarios for the assessment using safety functions as the basis (please refer to Chapter 10 to Chapter 12).

(4) Confidence of radionuclide migration and risk assessment can be confirmed by adopting simplified analytical models using the same input parameters as the ones used in the numerical models.

(5) The results of radionuclide migration and risk assessment are overestimated because of the adoption of several conservative assumptions (such as the number of canister failures and the consequences).

Relevant analysis results such as initial state description and long-term safety analysis are carried out in accordance with quality assurance procedures in Section 2.8 to ensure the quality of the related documents and results.

14.3.6. Robustness of the Assessment

A generic safety assessment method of NEA MeSA and a systematic safety assessment method developed based on the KBS-3 disposal concept were adopted and modified. And a reference case was established for the safety assessment. Through systematic scenarios selection, scenarios related to safety functions were defined. Relevant factors that will affect the safety functions were also considered. In addition, corresponding evaluation methods have been built based on international safety cases. Moreover, the effects of a combination of the scenarios were discussed. The long-term safety and comprehensiveness of the safety case have been confirmed.

14.3.7. Complements of the Safety Assessment

Supplementary requirements for the safety assessment include quality assurance, uncertainty management, and natural analogue, which are discussed as follows:

(1) Quality assurance

Nuclear Quality Assurance (NQA) guidelines published by the ASME were referred to for the implementation of the quality assurance project. In the process of safety assessment, the quality assurance system was mainly established in the formulation of FEPs, determination of model input parameters, the application process of the evaluation program, record keeping of the output results, and audit/improvement of the overall safety assessment process. This ensures traceability of the overall safety assessment process and provides confidence for the safety assessment results.

(2) Uncertainty management

In the process of safety assessment, there are various uncertainties, such as system/scenario uncertainty, concept/model uncertainty, and data uncertainty. In this report, the advanced international experience was referred to for the reduction of the degree of uncertainty that affects confidence in the safety assessment results. Specific measures are discussed in Section 2.7.

(3) Natural analogue

In the process of implementing safety assessment, international research information on natural analogue is referred to, including natural analogue of geological disposal such as Tono in Japan, Cigar Lake in Canada, and Oklo uranium deposit in Gabon; natural analogue of metal materials such as Devon in U.K., Kronan in Sweden, Inchtuthil in Italy; other natural analogues such as research plan in Cyprus and Wyoming bentonite plan in U.S.A. (please refer to Section 13.6). Mastery of relevant knowledge will help understand relevant mechanism of processes and help assess rationality of the safety assessment results on a long-term evolution scale.

14.4. Design Basis

14.4.1. Overview

The design basis is very important for the long-term safety of the repository. Through evaluation of the design basis, feedback to the design of the canister and other components can be made, and design requirements can also be developed. Once more detailed investigation data are obtained, and processes of the repository can be better understood, relevant design can be adjusted based on updated results of the safety assessment. In addition, the confidence of the design can be proven and the robustness of the repository can be demonstrated by the assessment of the design basis. Also, the degree of risk can be understood from analysis results other than design basis.

Based on the disposal concept of KBS-3, the design basis of shear displacement of the canister, corrosion of the canister and buffer are discussed.

14.4.2. Shear Displacement of the Canister

Canisters might be damaged because of shear displacement induced by earthquakes. In this report, earthquake-induced shear displacement, performance under shear displacement, repository layout, and EFPC were taken into account for the evaluation of canister failure probability due to shear force. The canister was assumed to fail when accumulating 5 cm of shear displacement. And 50,000 DFN realizations with the 300 m long disposal tunnel were applied for the evaluation. The results show that the occurrence of shear failure will be around 230,000 years after the closure. The probability of failure will be about 1/1,000,000. As for 1,000,000 years after the closure, the probability of failure will increase to about 1/3,000. Therefore, based on the design requirements and the evaluation results, the expected value of canister failure over the safety assessment timescale should be less than 1 canister.

14.4.3. Corrosion of the Canister

In the design base case of corrosion, limited corrosion and long-term corrosion were both taken into account. During the evaluation, the environmental parameters including the total amount of corrodent in the initial period after closure, hydrogeology and long-term evolution of groundwater composition at the disposal depth need to be considered.

The total amount of corrodent is for evaluation of limited corrosion, and the remaining ones are for evaluation of long-term corrosion. Therefore, when evaluating long-term corrosion, hydrogeological data at sea-level 0 m, -20 m and -120 m in nine glacial cycles were taken into consideration. Buffer erosion rate and groundwater composition were then calculated based on the hydrogeological data. The maximum corrosion depth of copper shell over the safety assessment timescale would be about 10.2 mm.

Currently, the assessment results are based on the current hydrogeological conceptual model of the reference case. Not all aspects of the hydrogeological units and DFN model have been captured yet. All of the calculation should be re-implemented when the hydrogeological conceptual model of the reference case changes. Besides, in order to reduce uncertainty, a benchmark case study including boundary conditions of hydrogeology for each period (such as salt water distribution) can be implemented in the future. And the impact of corrosion parameters such as buffer erosion range and groundwater chemical composition can also be evaluated.

14.4.4. Cases Related to the Buffer

The design basis of the buffer includes the chemical composition of the bentonite and its ability to withstand mechanical and thermal loads during the 10^6 years-assessment period.

Specification of the buffer shall be built in accordance with the design requirements. As described in Chapter 4, the buffer consists of pre-compact buffer components to be installed in the deposition hole. Buffer components include solid blocks installed above and below the canister, ring-shaped blocks installed around the canister, and pellets filled in the gap between the blocks and the rock surface of the deposition hole. The saturated density of the buffer in each part of the deposition hole was calculated according to the reference specification of buffer components and dimensions of the deposition hole. The results are shown in Figure 4-9. Saturated density of the buffer below the canister will be 2,039 kg/m^3, around the canister will be 2,023 kg/m^3, above the canister will be 2,049 kg/m^3, and the upper part with the connecting bevel will be 1,965 kg/m^3. The average saturated density will be around 2,019 kg/m^3, and the density of each part of the buffer in the deposition hole will be between 1,950 and 2,050 kg/m^3 after installation. Density-related design requirements in Chapter 4 are fulfilled. According to the test of swelling pressure and hydraulic conductivity of MX-80 bentonite, the swelling pressure is larger than 2 MPa, and the hydraulic conductivity is lower than 10^{-12} m/s under the abovementioned density conditions. Hence, design-related requirements in Table 4-5 are fulfilled.

14.5. Feedback to Reference Design and Design Premises

14.5.1. Introduction

The results of the safety assessment based on the KBS-3 disposal concept are fed back to the design of the repository from the viewpoint of safety.

14.5.2. Mechanical Stability of the Canister

The canister needs to withstand hydrostatic pressure caused by the deep groundwater. It also needs to withstand the swelling pressure of the buffer around the canister. Moreover, since the reference case is located in a seismically active zone, it is also necessary to consider the impact of earthquake-induced fracture shear displacement on the canisters. The canister is composed of cast iron lining and copper shell, and mechanical failure criteria were defined according to material properties. The safety margin of the canister was also evaluated. Therefore, the mechanical stability of the canister can be ensured.

As described in Section 4.2.4, mechanical design requirements of the canister include resistance to isostatic load, resistance to uneven swelling pressure, and resistance to rock shear force. Based on the analysis results in the previous sections, the mechanical stability of the canisters will not exceed the destruction criteria.

Relevant feedback to the mechanical stability of the canisters is as follows:

(1) The canister was designed when the comprehensive impact from swelling pressure of the buffer, hydrostatic pressure and ice pressure in the Nordic countries during the glacial period was taken into account. The design can withstand the isostatic load of 50 MPa. However, since the reference case is located in the subtropical zone and there should be no glacier coverage, the maximum isostatic load to the canister should be around 13.23 MPa. Therefore, the design against isostatic load should be conservative enough.
(2) The canister may be subjected to non-uniform isostatic load caused by uneven swelling pressure of the buffer in unsaturated and saturated period and non-uniform isostatic load caused by over-excavation or rock collapse of the deposition hole. The stress distribution of the copper shell and the cast iron lining was calculated based on different conditions. The results show that the maximum stress on the copper shell and the cast iron lining is less than the failure criteria of the materials. This can ensure the integrity of the canister.
(3) Earthquake-induced shear displacement, performance under shear displacement, repository layout, and EFPC were taken into account for the evaluation of canister failure probability due to shear force. The results show that the occurrence of shear failure will be around 230,000 years after the closure. The probability of failure will be about 1/1,000,000. And the probability of failure will rise to about 1/3,000 after 1,000,000 years after the closure. The expected value of canister failure over the safety assessment timescale should be less than 1 canister.

14.5.3. Provision of Corrosion Barrier

The copper shell thickness of the canister was evaluated when uncertainty during the manufacturing process of the copper shell, limited corrosion, and corrosion from sulfide in the groundwater were taken into account. The results show that after 1,000,000 years after the closure, there will still be about 36.8 mm of the copper shell. According to the analysis results, the copper shell canister can resist corrosion for at least 1 million years when the buffer is eroded; the thickness of the copper shell will still have enough margin even if the buffer is severely eroded. The thickness of the copper shell can be adjusted (reduce thickness) in subsequent optimization.

With respect to the five issues raised by the Swedish Land and Environmental Court, most of the issues have been solved in SKB TR-19-15 (SKB, 2019):

(1) Copper corrosion in pure water: a huge amount of work has been done to prove that copper corrosion in pure water is not an issue. And now, it is recognized by the Swedish regulator that copper corrosion in pure water is not an issue anymore.

(2) Pitting in the presence of sulfide, including any impact of sauna effect: multiple studies and arguments have shown that copper is not suspectable to corrosion in the presence of sulfide under repository conditions (the sulfide flux is too low to sustain pit growth ahead of the uniform corrosion front).

(3) Stress corrosion cracking in the presence of sulfide, including any impact of sauna effect: the sulfide flux is too low and SCC of copper will be discounted in the presence of sulfide under repository conditions.

(4) Hydrogen embrittlement: the only effect shown to be influential is the creep behavior. This behavior will only be accelerated under extreme conditions when the copper shell absorbs hydrogen.

(5) The impact of ionizing radiation on pitting, SCC, and hydrogen embrittlement: the radiation fields of the KBS-3 canister are very low that the impact can be ignored. Relevant studies are still going on in a European Union project and in Canada.

For future research and development, more attention is planned to be paid to the topics in SKB TR-19-15. In the short term, the sulfide generation mechanism under the saturated state of the buffer, including sulfide deposition and sulfate-reducing bacteria which produces sulfide will be the main focus. The establishment of a sulfide transport model and analysis of important parameters will be necessary.

In correlation analysis of copper shell corrosion, hydrogeological parameters and groundwater composition that constitute the transmission of corrodent are both identified as important parameters. Although the calculation results are based on the current hydrogeological conceptual model of the reference case, not all aspects of the hydrogeological units and DFN model have been captured yet. All of the calculation should be re-implemented once the hydrogeological conceptual model of the reference case changes. Subsequent discussion on the formation mechanism of sulfide in the saturated buffer can be used to establish a sulfide transport model. The influence of different corrodent on the corrosion of the canisters can also be evaluated using the copper shell corrosion evaluation model and related chemical kinetics under saturated buffer.

14.5.4. Material of the Canister

The canister is designed to be composed of a ductile copper shell on the outside and a high-strength cast iron insert, square channel tube, and lid on the inside. According to the test results of international literature, the insert and the tube are the main components to resist external force depending on their geometric shape and material strength. The strength of the external copper shell is lower, and it is easy to be bent and deformed under shear force or bending moment acts. But it has the ductility that can wrap the canister and provide a corrosion barrier for the canister.

14.5.5. Durability of the Buffer

The mass loss of buffer mainly due to erosion, will affect the safety function of the buffer during the one million years disposal period. Moreover, this is caused by extrusion, erosion by seeping water, and sedimentation. According to the evaluation results in Section 9.4.8, the erosion rate of the buffer is directly proportional to the fracture aperture, the velocity of seeping water, and the dip of the fracture, and inversely proportional to the cationic strength of groundwater. Therefore, in order to reduce the impact of these factors on the erosion rate of the buffer. First, the intersection of deposition holes and fractures should be avoided. Second, the region with lower groundwater flow velocity should be selected during long-term disposal to reduce the erosion effect caused by seeping water. Finally, the area with higher groundwater cation strength should be chosen.

Suitable hydrogeochemical conditions should be considered to avoid erosion caused by the low cationic strength of groundwater. In the engineering design, consideration should also be given to: (1) layout of the deposition holes should avoid the positions intersecting with fractures. Moreover, fracture locations with larger dip angles should also be avoided. (2) To establish suitable criteria for deposition holes and hydraulic characteristics to avoid the mass loss of buffer due to erosion.

14.5.6. Installed Buffer Mass

The hydraulic conductivity of the buffer needs to be less than 1×10^{-12} m/s and the swelling pressure of buffer need to be more than 2 MPa to fulfill the requirements of safety functions of the buffer, such as limiting advection and limiting microbial activity. And according to the experiment results of hydraulic conductivity and swelling pressure of MX-80 bentonite, density conditions required for the design requirements of material properties can be obtained. Besides, when the designed buffer specification and impact from the evolution of the repository were taken into account, mass loss of the buffer was conservatively estimated to be less than 1,200 kg. The aforementioned safety functions can be satisfied.

In addition, according to the buffer erosion analysis results (Section 11.2.2), the percentage of mass loss of the buffer in one deposition hole is around 3% within 100,000 years, indicating that the erosion effect is not severe. The current design of the buffer should be able to keep a certain degree of safety margin. When the safety margin needs to be improved, the density of the buffer can be increased, areas with high hydraulic conductivity can be avoided, or areas with higher groundwater cation constant can be chosen to reduce the erosion rate of the buffer.

14.5.7. Buffer Thickness

The thickness of the buffer is according to the design requirements of the deposition hole in Section 4.2.6. In order to fulfill the relevant design requirements, the buffer must provide sufficient swelling pressure and appropriate hydraulic conductivity. Therefore, according to Section 14.5.6, the buffer should have an appropriate dry density to make its properties achieve the design requirements. However, under the impact of long-term evolution, it is necessary to consider the loss of buffer due to erosion, which causes its density to decrease. Therefore, when evaluating the appropriate thickness design of the buffer, the results of Section 14.5.5 and Section 14.5.6 will be taken into consideration at the same time.

Mass loss of the buffer was calculated at different stages of evolution. Calculations take the velocity of seeping water, ionic strength, fracture aperture, and fracture dip into consideration under different hydrogeological evolution conditions. Therefore, according to the evaluation results, the currently designed buffer thickness, 35 cm, can provide approximately 200,000 to 300,000 years of service life. However, the erosion rate will be affected by parameters such as seeping water velocity, ionic strength, fracture aperture, and fracture dip; geological survey and model evaluation need to be focused on to well-understand the characteristics of the potential sites. An appropriate buffer design can be made by that. Moreover, the difference between the results from the two-region model and the regression formula of the KTH model is large, and it should be studied further in the future.

14.5.8. Mineralogical Composition of the Buffer

The reference material of the buffer is MX-80 bentonite. According to the experiment results, when the dry density of the buffer is larger than 1,450 kg/m^3, swelling pressure and hydraulic conductivity of the buffer can fulfill the design requirements such as limiting advection and reducing microbial activity.

In addition, the buffer composition should not have substances that may be harmful to the other engineered barriers. Therefore, in the composition of the buffer, the content of organic carbon should be less than 1 wt%, sulfide content should not exceed 0.5 wt% of the total mass, corresponding to approximately 1% of pyrite, and total sulfur content (including sulfide) should not exceed 1 wt%. The composition of MX-80 bentonite meets the above conditions and is not harmful to copper shell of the canister.

14.5.9. Backfill

The backfill is the material installed in the disposal tunnels to fill the empty space. The purpose and function of the backfill in the disposal tunnels are to provide mechanical support for the buffer, to maintain the volume of the buffer in the deposition hole, and to prevent a drop in the buffer density due to swelling out of the deposition hole. Therefore, the safety functions can be maintained. By filling the empty space in the disposal tunnels, backfill can restrict groundwater flow and reduce the harmful impact on the engineered barriers from the groundwater. The hydraulic conductivity of the backfill should be less than 10^{-10} m/s and the swelling pressure should be more than 0.1 MPa to fulfill relevant design requirements. For better operation efficiency and uniformity of the backfill, the backfill will be pre-pressed into blocks using uniaxial compression and stacked in the disposal tunnels. In order to fulfill the design requirements, the minimum allowable dry density of the backfill should be 1,408 kg/m^3 after the installation when the uncertainty of the operation is taken into account. The swelling pressure of the buffer and the backfill after saturation was evaluated using FLAC3D. From the results, the minimum swelling pressure of the backfill after saturation will be about 1.5 MPa. This fulfills the design requirements of swelling pressure.

In addition, backfill composition should have long-term chemical stability and will not affect groundwater composition. Therefore, in the composition of the backfill, the content of organic carbon should be less than 1 wt%, sulfide content should not exceed 0.5 wt% of the total mass corresponding to approximately 1% of pyrite, and total sulfur content (including sulfide) should not exceed 1 wt%. The composition of MX-80 bentonite meets the above conditions, and is not harmful to the copper shell of the canister.

14.5.10. Selecting of the Deposition Holes

Host rock around the deposition holes is the main natural barrier in the repository. When conditions of host rock are harmful to the EBS, the deposition hole selecting method can be applied to reduce risk. From the evaluation results, feedback to the selection of the deposition holes is as the following:

(1) Extend full perimeter criterion (EFPC)

EFPC could reduce intersections between the deposition holes and fractures to avoid potential conductive fractures and decrease the impact of shear displacement induced by earthquakes on the canister (SKB, 2006e). Section 9.4.5 shows that the canister failure rate due to shear displacement over the safety assessment timescale is quite low. It should be noted that EFPC will be the primary reason for the loss of deposition hole positions when it is applied. And since EFPC is a pessimistic criterion, relaxation of EFPC can be further discussed according to the characteristics of the candidate sites.

(2) Loss of deposition hole positions

The capacity of the layout provides about 11% redundancy for deposition-hole positions. However, when EFPC is applied, there will be about 4.2% loss of deposition-hole positions (loss of deposition-hole positions was calculated by a stochastic model based on limited site investigation data. The actual number can only be verified during the construction of the facility).

14.5.11. Hydraulic Characteristics of the wall of the Deposition Holes

Preliminary analysis results show that the hydrostatic pressure on the interface between the fracture and the deposition hole wall would be around 5.10 MPa to 5.30 MPa, and the velocity of groundwater in the fractures would be around 3.37×10^{-9} m/s to 3.40×10^{-8} m/s, the inflow of the deposition hole wall would be around 1.16×10^{-12} m^3/s to 3.15×10^{-11} m^3/s, and these meet the design requirements. Note that the calculation results are based on the current hydrogeological conceptual model of the reference case. Not all aspects of the hydrogeological units and the DFN model have been captured yet. All of the calculation shall be revised once the hydrogeological conceptual model of the reference case changes.

14.5.12. Placement of the Canisters

This section focuses on describing feedback from analysis regarding thermal evaluation. The design of spacing between deposition holes mainly follows the design requirements for long-term safety of the buffer and that temperature of the buffer should be less than 100°C. Based on Section 9.3.4, maximum temperature of the buffer at the top of the canister can fulfill the requirements. Thus, adjustment of the spacing is not necessary under safety aspects. Spacing between the deposition holes is 6 m in original KBS-3 design and current design of spacing between the deposition holes is 9 m for the reference case. Spacing adjustment and optimization for using the deposition area efficiently can be further discussed in the future.

14.5.13. Excavation Damage Zone Control

Due to the impact from the excavation damage zone, the risk of erosion of the buffer may increase. This will further affect the risk of corrosion of the canisters. When establishing design requirements, the maximum allowable transmissivity is 1×10^{-8} m^2/s for excavation damage zone caused by the planned excavation method, which is the drilling and blasting method (SKB, 2011). Before placing the canister into the deposition hole, the maximum allowable transmissivity of the excavation damage zone is 1×10^{-10} m^2/s, and the mechanical full face down-hole drilling technique is utilized. In addition, since the excavation damage zone is mainly located on the surface of the tunnel, it can be removed with construction methods and tools. Therefore, the impact can be conservatively taken into account when maximum allowable transmissivity is applied.

14.5.14. Shotcrete and Grouting Materials

The pore solution of concrete and mortar made of ordinary Portland cement has pH value between a pH 12 and pH 13. A high pH pore solution will jeopardize the safety functions of the buffer and change the waterproof characteristics of the buffer. It will also affect the transport properties of radionuclides in the repository. In order to lower the pH value of the concrete and reduce material degradation effectively, low-pH Pozzolanic materials will be used instead of cement materials. The low-pH concrete can be used as grouting and shotcrete materials for the repository. It has higher durability than ordinary Portland concrete and can therefore reach a pH value < 11, hydraulic conductivity < 10^{-8} m/s, and compressive strength > 280 kg/cm^2. Subsequent laboratory tests can be carried out for this low-pH concrete, and application methods, machines, and structures can also be studied in the future.

14.5.15. Repository Depth

Factors related to repository depth include hydrogeology characteristics, geochemical properties, long-term stability, construction and investigation technologies, the mechanical stability of the tunnels, and the influence of rock temperature on engineered barriers. According to the final disposal concept around the world, repository depth is typically between 300 m to 1,000 m underground.

Besides, according to Article 11.1 of the "Directions for Sites of High-Level Radioactive Waste Final Disposal Facility," the depth must be deeper than 300 m underground. Therefore, the repository of the reference case will be located at a depth of 500 m (tunnel floor). No significant impact has been found regarding the safety of the repository based on the assessment of the reference case. Currently, there is no urgent need for adjusting the design of repository depth, but optimization based on new evidences in the future can still be implemented.

14.5.16. Tunnels, Shafts, and Closure

Relevant design for tunnels, shafts, and closures is described in Chapter 4. Preliminary stress analysis results show that the smallest safety factor is located at the tunnel bottom during and after excavation. The results show that the tunnel will remain stable, and they also demonstrate that the requirements can be achieved. In the future, since technologies for tunnels, shafts and closures are well developed internationally, detailed design can be planned when specific sites are chosen and in-situ measurement data are acquired. Also, according to the seismic characteristics of Taiwan, analysis related to source loading on the tunnels and shafts and reinforcement measures when the rock has insufficient strength can be studied. An evaluation model for tunnel and shaft connection can be developed, and an analysis of the interactions and impact can be implemented thereby.

14.5.17. Backfill of Boreholes

During the construction period, boreholes will be drilled from the disposal tunnels to the host rock for detailed investigation. These boreholes should be sealed before the closure of the repository in order to avoid potential release paths. Therefore, there will be horizontal and upward-directed holes that need to be sealed. And the boreholes, tunnels and deposition holes should be checked so that they are not connected to each other when designing the repository layout.

The borehole sealing concept refers to the Sandwich-concept from the Swedish SKB (please see Section 4.2.12). A borehole with water-bearing fractures will be filled with permeable materials such as sand that will not significantly change the natural groundwater flow. On the other hand, the parts without water-bearing fractures will be sealed with bentonite. Quartz-based concrete (quartz sand and low pH cement) is positioned for a certain length in the transition zones between the bentonite and the sand to prevent interaction between different materials. In addition, copper plugs are installed between the materials to facilitate construction and prevent mixing between different materials (Sandén et al., 2018b).

The study regarding borehole seals has shown that the impact of unsealed seals of the boreholes is very moderate(Joyce, 2010), and when the hydraulic conductivity of the borehole seal is lower than 10^{-6} m/s, it is enough to let the groundwater flow similar to the surrounding rock mass (SKB, 2011; Luterkort et al., 2012). In the future, with the determination of the site and the detailed geological survey data, the impact of the borehole reference design on the groundwater flow in the disposal facility and the surrounding rock mass can be assessed, and the effectiveness of the design of the borehole seal can be confirmed.

14.6. Feedback to Detailed Site Investigation and SDM

A preliminary design of the repository has been completed in this report based on the initial state of the reference case. The corresponding safety assessment has been performed to ensure the long-term safety of the repository. In this chapter, feedback will be provided for field survey planning and the establishment of site descriptive model (SDM) to ensure the integrity of the design and integrity of safety assessment of the repository and reduce uncertainty.

SDM is the integration and evaluation method of geoscience information specifying site characteristics (Andersson et al., 2013) developed by the SKB. There are seven fields in the SDM, which are geology, thermal properties, rock mechanics, hydrology and hydrogeology, hydrogeochemistry, transport properties, and ecosystems.

Every field is independent but correlated to each other. Through SDM, characteristics of the sites can be understood more thoroughly.

14.6.1. Improvement in Characterization of Deformation Zones with Potential to Generate Large Earthquakes

The most important factors affecting fracture shear displacement induced by earthquakes are location, length, and area of faults and deformation zones, followed by slip rate, return period of the fault, and velocity structure. Among the aforementioned factors, the location of the fault and deformation zone will affect the distance between the fault and the fracture, as the length and area of the fault and deformation zone will affect the evaluation of the scale of the largest earthquake. If investigation data of these factors are not sufficient, uncertainty in the evaluation results of fracture shear displacement induced by earthquake may generate:

(1) Length of faults and deformation zone is easy to be incomprehensively understood due to insufficient survey data. For example, if a fault or deformation zone extends from land to sea, survey data might be insufficient, resulting in bad judgment on the fault length, and the potential magnitude of the largest earthquake might be underestimated. Therefore, analysis results of fracture displacement induced by an earthquake might be affected.

(2) Cumulative amount of earthquake-induced fracture displacement will be affected by the recurrence period of fault activity. Detailed information on the recurrence interval of fault activity can improve evaluation results of fracture displacement induced by earthquakes.

(3) Velocity structure will affect transferring of seismic waves. It is necessary to increase relevant data through a survey, to improve the evaluation results of the models.

(4) Fault fractured zone, deformation zone, and its surrounding areas are not suitable for setting up a repository. In addition, lateral uncertainty exists in the width of the fault fractured zone and the deformation zone because of the difference between the mechanical

properties of the rock mass and the geological structure. Therefore, the width of the fault fractured zone and the deformation zone is also an important parameter in the field survey.

In order to improve the above issues, besides location, length, width, area and other information of fault and deformation zone, the recurrence interval of fault activity and three-dimensional velocity structure of the survey area and the surrounding area should be focused on during the field survey. Other than that, data of land and sea can be integrated to describe the geometry and distribution of structure, recurrence interval of fault activity, and three-dimensional velocity structure of the area thoroughly.

14.6.2. Improvement in Means to Constrain the Size of Fractures Intersecting Deposition Holes

As mentioned previously, the integrity of the canister is potentially jeopardized by an earthquake if a large fracture shear displacement intersects the deposition hole. Although EFPC is applied for the selection of deposition holes to reduce this circumstance, loss of deposition positions will increase the footprint area of the repository. Additionally, more research and analysis need to be done for the practical efficiency and accuracy of EFPC in identifying fractures. As a result, the accuracy and degree of identification of the surrounding large fractures must be improved in field surveys for a better understanding of their spatial distribution and size. In addition, since the DFN recipe used for fracture assessment was obtained based on statistical analysis from field survey data with logarithmic linear distribution of fracture size, the fracture size is logarithmic linear distribution. Regarding fracture size distribution, it should be recognized that power-law distribution for conductive fractures and non-conductive fractures can be different. In subsequent research, dynamic simulation is suggested for generating fractures to obtain a logarithmic bilinear distribution of fracture size.

14.6.3. Reduce Uncertainties of the DFN Models

The DFN model is the basis for the assessment of hydrogeological evolution, earthquake-induced fracture shear displacement, and radionuclide transport. The DFN model is derived from statistical analysis of field survey data. Not all aspects of the DFN model of the reference case are captured yet. Therefore, the amount of ground surface facture investigation and borehole fracture investigation must be considered for field surveys in the future to reduce uncertainty caused by the lack of survey data. Besides, outcrop or boreholes should be deployed appropriately so that distribution of fracture characteristics can be estimated through interpolation and uncertainty of spatial heterogeneity can be reduced. If the aforementioned requirements are compromised because of the limitation of the quantity of the host rock or the environment, tunnel excavation or horizontal drilling should be adopted in each stage to increase data and reduce uncertainty. Additionally, tunnel wall mapping and pilot hole survey during the excavation period can also be adopted to decrease DFN uncertainty.

14.6.4. Identification of the Connected Water-Conducting Fractures

In hydrogeological evolution analysis, fracture connectivity of the DFN will be analyzed to identify connected water-conducting fractures. Therefore, an inflow of specific deposition holes can be calculated to evaluate the possible failure scenario of the canister and possible release path.

In this report, numerical simulation was used to identify connected water-conducting fractures. And accuracy of the numerical simulation can be improved by fracture investigation of the ground surface, borehole, and field test since not all aspects of the hydrogeological units and water-conducting fractures of the reference case are captured yet. Therefore, in field surveys in the future, long-term and large-scale in-situ pumping tests in boreholes should be incorporated to interpret connected water-conducting fractures. In order to meet the needs of in-situ pumping test, it is necessary to take deployment of drilling (which includes location, depth, angle and quantity), pumping equipment that can pump large amounts of water for a long time, and instruments for measuring and sealing various fractures into account when planning for field survey. When implementing a field survey, a preliminary interpretation of the distribution of the main water-conducting fracture can be made, and the layout of the repository can be modified accordingly. After the preliminary interpretation, drilling can be carried out for further investigation. Finally, a pumping test will be implemented for confirmation.

Numerical simulation for characterization of the connected water-conducting fractures can be done when more detailed field survey data are acquired. And distribution of three-dimensional connected water-conducting fractures in specific locations or regions will be analyzed, which refines the basis of hydrogeological evolution analysis and radionuclide transport assessment.

14.6.5. Hydraulic Characteristics of the Repository Volume

The hydraulic characteristics of the repository are related to the location and distribution of water-conducting structures and connected water-conducting fractures. Hydraulic characteristics of the repository under different boundary conditions can be understood based on the results of the hydrogeological analysis.

Since the hydraulic characteristics of the repository will be directly affected by the distribution of fractures and the amount of the inflow, it should be described in the SDM (such as the width of fracture aperture and the hydraulic conductivity). Currently, not all aspects of the DFN model for the reference case are captured. After candidate sites are confirmed, deterministic fracture distribution can be established based on the actual fracture trace and fracture parameters of the repository. And a comparison of investigation value and estimated value of fracture inflow can also be implemented.

14.6.6. Verification of Conformity of EDZ Design Premises

The method of controlling the development of EDZ is mainly related to the selection of the excavation method, operation quality of the excavation method and quality control. After the excavation operation begins, a detailed investigation plan and pilot construction are required to ensure that EDZ meets the design requirements of the maximum allowable transmissivity of 1×10^{-8} m^2/s (please refer to Section 14.4.12).

In field surveys in the future, the excavation method can be tested in areas with similar characteristics to the host rock. Over-excavation range and transmissivity of the surrounding rock after excavation can be measured. The depth and range of EDZ can be measured by non-destructive testing to confirm whether the EDZ meets the design requirements. In addition, based on the results of the field survey, suggestions for excavation methods can be provided, and parameters such as the extent of EDZ and the maximum transmissivity in SDM can be set accordingly.

14.6.7. Rock Mechanics

The mechanical property of rock will affect deformation and the location where damage could occur. This will further affect the layout and safety functions of the repository. The mechanical property of rock depends on the characteristics of the intact rock (such as the geometric distribution of different rock types, the strength and deformation characteristics of these rock types), and the nature and distribution of fractures (such as the geometric distribution of fractures and fracture zones). Mechanical interference can happen at different times or in different regions. The degree of impact from the interference may also be different, depending on the load condition.

In this report, a mechanical stability analysis of the repository layout has been developed based on the existing rock mechanics data. Since the data are limited, borehole surveys are suggested in field surveys in the future. The cores from borehole surveys can be characterized according to the following items:

(1) Measurement of initial stress of the rock at the planned disposal depth.
(2) Measurement of mechanical properties of the complete rock mass at the planned disposal depth.
(3) Risk analysis of extensive spalling or other rock fractures.
(4) Analysis of mechanical properties of a single fracture and fracture zone.

The development of rock mechanics distribution model is also suggested which can analyze the distribution of the initial stress. The model includes deformation and strength characteristics of intact rock mass, fracture areas and weakened areas in rock volume, rock mass unit composed of fracture and intact rock mass, rock quality related to construction feasibility, and related mechanical effects of rock stress and properties.

14.6.8. Thermal Properties

Thermal impact on the buffer is mainly affected by thermal conductivity, local temperature and layout of the repository. In field surveys in the future, borehole temperature and density, porosity, chemical properties, mineral composition, thermal conductivity, and heat content of the first core can be firstly confirmed. Therefore, unsuitable conditions can be excluded (such as high geothermal gradient, high initial temperature, and non-uniform thermal characteristics). In addition, through a detailed investigation, the uncertainty of spatial variability and thermal conductivity can be reduced. A more specific thermal spacing design can be proposed, which can improve the utilization of space effectively and reduce the excavation area and construction cost of the program.

As for SDM, the thermal property model should be established according to investigation data, including thermal property distribution, initial temperature of host rock, structure and rock type formation. And the SDM can be refined thereby.

14.6.9. Hydrogeochemistry

The chemical environment (including redox characteristics, salinity, and ionic strength) of the repository will affect the safety functions of the engineered barriers, such as the canister and buffer. Besides, the content of potassium, sulfide and ferrous iron in groundwater may also affect the chemical stability of the canister and buffer.

The distribution of hydrated species in groundwater has been estimated based on the analysis results of steady-state salinity distribution. Ionic strength, pH value, and concentration of sulfide and iron that may affect the safety functions of the buffer and the canister have been calculated as well.

In field survey in the future, the following survey items are suggested through drilling:

(1) Sampling and chemical logging.

(2) Sampling and chemical well logging during the core drilling process.

(3) At least one deep borehole for the hydrogeochemical survey.

(4) Long-term monitoring of chemical parameters.

(5) Investigation of fracture-filling minerals.

For building the hydrogeology descriptive model, in order to describe the chemical conditions of the host rock around the repository, the redox capacity of the disposal environment needs to be evaluated based on the content of divalent iron ions, pyrite, and sulfide in the rock and the groundwater, and the content of fractured minerals. The evaluation models which can qualitatively describe the effects of chemical substances and quantitatively describe the concentration of chemical substances are suggested to be established. Therefore, the redox condition of the repository can be estimated. Evaluation models that can describe chemical processes qualitatively and describe concentration quantitatively can also be built. At the same time, it can be integrated with hydrogeological analysis to implement the hydrogeochemical analysis.

14.6.10. Surface Biosphere

Geometric shapes and spatial connections of different biosphere objects have been defined to evaluate BDCFs according to relevant assumptions of the SDM and the analysis results of hydrogeological evolution.

If candidate sites are chosen, more detailed investigations (such as surface water bodies, climate change, soil sediments, and biological populations) related to the surface environment can be carried out and the result variation of biosphere assessment caused by the data uncertainty could figure out. The distribution of BDCFs could be sent to safety assessment to perform the overall uncertainty assessment to improve the confidence of the result.

First, natural changes and cycles can be understood by large-scale survey, surface measurement and deployment of monitoring stations. Then, research on candidate sites can be more focused on properties of chemical, morphology, hydrology, and biological populations for possible biosphere objects such as lakes, rivers, and oceans. In addition, data will be collected for stoichiometric analysis of the weathered layer and biological populations. Finally, partition coefficients (k_d) of the surface can be evaluated.

As for model evaluation, geographic information system (GIS) models can be established in the future by applying survey data. GIS can describe land use, biological group boundaries, and surface hydrology and sediment assessment models. In the biosphere, in addition to combining the analysis of near-surface groundwater and the analysis of surface water, a coupled analysis mode of deep groundwater and surface water can also be established. Therefore, uncertainty when analyzing the flux of land water and the uncertainty of biosphere models can be reduced. The abovementioned models and long-term evolution of the LDM (Landscapes Development Model) can be utilized to support safety assessment.

14.7. Feedback to R&D Program

Preliminary design and relevant safety assessment of the repository have been conducted based on the initial state of the reference case to ensure the long-term safety of the repository. Though, according to current investigation results, design, and the assessment results, feedback will be given to the planning of technology development in this chapter.

14.7.1. Source Term

(1) Nuclide inventory and decay heat:

The SCALE6 code package of analysis programs from the Oak Ridge National Laboratory is used to calculate the SNF inventory, and the SCALE6's library covers a wealth of international nuclear fuel-related data, which is complete and continuously updated and has been validated over many years with decay heat and nuclide inventory experiments, making it well suited for SNF characterization. On the other hand, the calculation of decay heats was performed using the conservative regulatory guideline RG3.54 published by the U.S. Nuclear Regulatory Commission, which also has some confidence.

In the SNFD 2017 report, it is conservatively assumed the fuel burnup and cooling time for the assessment of the inventory and decay of SNF. Therefore, in the SNFD2021 report, important parameters such as fuel design, operation history, discharged burnup, and cooling time were also considered, and an appropriate loading schedule plan was developed to refine the analysis and evaluation of decay heat and nuclide inventory.

At present, the calculation of nuclide inventory only takes into account the fission products and the actinides from the nuclear fission process. The activation products from the activation of structural materials in the fuel assembly or impurities in the fuel pellets can be further refined by collecting data on the element composition and impurity content of Taiwan’s SNF in the future. Since PWR control rods may be disposed of together with PWR SNF in the future, the activation products from the neutron activation of PWR control rods should also be considered. In addition, according to the international literature (SKB, TR-10-13, p42), the activation products generated from the crud of SNF during operation should also be considered in the calculation of the nuclide inventory. In addition to the complete consideration of activation products, the fission gas release (FGR) has an important impact on the instantaneous release rate of radionuclides, so it should be gradually included in the evaluation and calculation of the nuclide inventory in the follow-up.

(2) Nuclear Criticality Safety:

MCNP program was used in the nuclear criticality safety analysis. The MCNP is a particle migration simulation code that is widely used in nuclear criticality safety analysis. It also has many applications and verifications. In the future, MCNP will be the benchmark against criticality experiments to evaluate its confidence and conservativeness.

In the SNFD2017 report, there was no native nuclear criticality safety analysis, but an indirect comparison with international literature was performed. After the SNFD2017 report, domestic nuclear criticality safety analysis technology was established in the program. To begin with, the nuclear criticality safety analysis model for a canister is built, and the conservative parameter combination is determined through sensitivity analysis. The maximum neutron effective multiplication factor evaluation is therefore completed in a fresh-fuel-loaded configuration. According to the analysis results, the initial enrichment of the SNF in the BWR canister must be below

3.8 U-235 wt% to meet the regulations. And the initial enrichment of uranium-235 of the SNF in the PWR canister must be less than 2.4 U-235 wt% to meet the regulations. In the condition of initial enrichment up to 5.0 U-235 wt%, the current design can meet the regulation only if the burnup credit is taken. This report only considers intact canister case in the current phase; the long-term effects like cast iron corroding after water intrusion, will be considered in the future.

(3) Shielding analysis

In shielding analysis, SCALE and MCNP codes were used to calculate the radiation dose rates (including the absorbed dose rates and the effective dose rates) on the surface of the canister. These two codes are recommended by NUREG-1536 and NUREG-1567 to evaluate the radiation source terms and perform shielding analysis for ISFSIs (Independent Spent Fuel Storage Installations). According to the results of the analysis, the maximum absorbed dose rate on the surface of the canister is 0.142 ± 0.16% Gy/h, which complies with the design requirement of the canister. On the other hand, the maximum effective dose rate on the surface of the canister is 210.0 ± 0.16% mSv/h. By comparing with the international literature of a similar design of the canister (SKB, 2011, p167), the result of the evaluation is close and is within the same order of magnitude, and thus should have sufficient confidence. In addition, the development and calculation of the above-mentioned model have been executed under the QA project; therefore, the current evaluation result has already been provided with a certain degree of confidence.

Furthermore, based on the result of the evaluation, it is found that the effective dose rate on the surface of the canister is very high. Therefore, the canister should first be emplaced in a transport/storage cask with a sufficient shielding capability for loading, transferring, storing and disposing, in order to protect workers from radiations. The design of the transport/storage cask can be carried out in the following development, and the effective dose rates on the surface of the cask can be analyzed. Those can be used to calculate doses of workers for the excavation and operation, and relevant work schedule can thereby be established.

14.7.2. Canister

The technical development related to canistesr can be divided into: (1) heat transfer characteristics research of materials, (2) chemical and mechanical factor research, (3) corrosion mode (including stress corrosion) analysis, (4) corrosion resistance and failure evaluation, (5) isostatic load resistance evaluation. The detailed description of the above five parts be described as follows:

(1) Heat transfer characteristics research of materials:

The ANSYS Fluent three-dimensional numerical analysis software is used to calculate the heat transfer characteristics of the canister and the heat transfer analysis model of the SNF, taking into account the effects of heat conduction, heat convection, and heat radiation. ANSYS Fluent 3D numerical analysis software is an analysis program certified by ISO 9001 and has been recognized internationally. Its steady-state and transient numerical analysis capabilities have also been verified by the analytical solutions.

In the SNFD2017 report, the initial decay heat of the SNF in the canister was assigned to be 1,315 W, which was assumed to be evenly distributed among all the SNF in the canister. According to the evaluation results, the internal design of the canister has considered the decay heat generation of the SNF, and the appropriate spacing is designed to reduce the possible impact of the decay heat, and the heat energy is transferred to the outer surface of the canister, buffer and host rock. The development and calculation have all been implemented under the quality assurance project, which has a certain degree of confidence.

The following will establish a heat transfer analysis model which considers the non-uniform distribution of heat sources and calculates the temperature distribution and evolution of the SNF and the canister body based on the loading configuration plan.

(2) Chemical and mechanical factor research:

The collections of canister types and related data in various countries will be conducted, and the analysis based on the geological and environmental conditions of Taiwan will be carried out to assess the impact of the canister under different swelling pressures of the buffer and to conduct a complete evaluation of the different bentonite materials that may be used in Taiwan. In addition, the water quality analysis should be made to enhance the chemical impact research on the different states (under unsaturated, saturated, and advective).

In the mechanical factors, the experiment based on Taiwan’s groundwater condition should be established, and the stress-strain relation of bentonite in different conditions should be conducted. In addition, various optimization options on the conceptual design will also be used to establish the material parameters of cast iron, copper and other materials to make the relevant performance evaluation more credible.

(3) Corrosion mode (including stress corrosion) analysis

The corrosion analysis based on the hydrogeological and hydrogeochemical evolution has been involved in the calculation process, but the interaction with pore water is not included in the assessment. The factor not only affects the analysis of the corrosion of the canister but also influences the estimation of the bentonite erosion and radionuclides transport. Therefore, the groundwater chemical reaction model and the pore water evolution model will be involved in analyzing the chemical reaction of various ions and establishing the verification of the key mechanisms. The international cooperation will also be adopted, combined with a relevant international database and the results of the Taiwanese anaerobic environment test to establish relevant test data under Taiwanese groundwater quality conditions.

(4) Corrosion resistance and failure evaluation

A three dimensional near-field copper corrosion model with solute transport will be established to enhance the technique of canister failure probability analysis. Based on the laboratory scale evaluation, the corrosion model of sulfide produced by sulfate-reducing bacteria will also be established. Since each ion actually has a competitive effect when it reacts with copper, an advanced electrochemistry and probability distribution will be introduced to refine the evaluation technology.

(5) Isostatic load resistance evaluation

The long-term evolution of external factors such as tectonic stress, plate or fault movement will be fully considered, and the performance of the canister against isostatic load will be evaluated based on the regional characteristics of the host rock and the conceptual design. In addition, the model verification will be carried out for the numerical analysis model of multiple earthquakes and the analysis model of comprehensive erosion effect.

According to the evaluation results, the shear force caused by the earthquake is an important factor affecting the failure of the canister. Therefore, the follow-up will also consider the long-term changes in the phenomenon of tectonic stress, plate or fault movement and conduct seismic shear force evaluation. The evaluation of near-field hydraulic-mechanical effects caused by fault displacement to establish applicable design requirements will also be conducted.

14.7.3. Buffer and Backfill

Technical establishment related to buffer and backfill can be divided into two major subjects: (1) characteristics of buffer and backfill and (2) engineered barriers and near-field environmental impact. The subjects are described as follows:

(1) Characteristics of buffer and backfill:

Researches on the characteristics of buffer and backfill include four major issues: (a) properties of unsaturated bentonite, (b) saturation behavior of buffer and backfill, (c) properties and characteristics of buffer and backfill, and (d) laboratory-scale coupling tests. These issues are described as follows:

(a) Properties of unsaturated bentonite:

Unsaturated properties test of bentonite will be established. The relation between water content and suction of bentonite will be analyzed, and relevant values for evaluation of the saturation process of the buffer and backfill can be provided. Previously, the development of material characteristic tests in the saturation phase has been the main focus of the program in Taiwan. Soil-water characteristics curve of bentonite materials can be studied, and parameters required for buffer and backfill in behavior simulation of the resaturation process can be acquired.

(b) Saturation behavior of buffer and backfill:

Performance of buffer and backfill after the installation has been preliminarily evaluated in the program.

Model analysis and experimental technology will be developed, and the behavior of buffer and backfill after saturation in the repository, such as the hydraulic conductivity of the host rock, characteristics of the fractures, and properties of the buffer and backfill, will be analyzed.

Regarding the international evaluation of the long-term evolution of the repository (especially the complex effect of thermal-hydrological-mechanical coupling), TPC is actively participating in DECOVALEX (DEvelopment of COupled models and their VALidation against EXperiments) to improve understanding of coupled behavior and also provide calibration of the evaluation models.

In addition, to meet the needs of numerical model research, experiment technology of moisture transportation under thermal-hydrological coupling conditions of buffer and backfill can be improved, and the parameters of the evaluation models can be updated.

Numerical model research of disposal tunnel-scale can also be further developed. Thermal-hydrological-mechanical coupling conceptual model can be developed based on the results of parameter tests of unsaturated/saturated bentonite characteristics and laboratory-scale coupling tests. And model calibration can be provided hence.

(c) Properties and characteristics of buffer and backfill:

Test results of buffer and backfill characteristics (including thermal conductivity test, hydraulic conductivity test, swelling pressure test, triaxial mechanical test, etc.) will be used to develop numerical simulation technology. The initial performance of the buffer and backfill after installation can therefore be evaluated, and the coincidence of requirements of related safety functions and design requirements can be ensured.

Previously, basic property tests for MX-80 bentonite under different bentonite density conditions and different groundwater conditions have been implemented The tests include heat conduction properties test, hydraulic conductivity test, and swelling pressure test. Relevant test equipment and capabilities have been equipped in the program. In the future, tests can be carried out based on the analysis of the saturation behavior of the buffer and backfill to examine the parameters required for the development of the numerical model. And parameter calibration in the numerical model can be refined. In addition, tests of mechanical parameters, such as the elastoplastic model, will be carried out in line with the development of the numerical model to refine the simulation of mechanical behavior in the model.

(d) Laboratory-scale coupling tests:

Model tests will be performed to understand the coupling mechanism of the temperature distribution under the influence of heat, the moisture distribution after water intrusion, the swelling behavior of the bentonite material after absorbing water and its interaction, etc., and provide the relevant hypothesis and verification data of the numerical model. In the past, the experimental research of a small-scale thermal-hydrological-mechanical coupling test has been completed. Also, the behavior of bentonite materials subjected to the coupling of temperature, moisture and mechanics was analyzed by numerical simulation based on the experimental conditions and compared with the experimental results.

Based on the aforementioned test experience, a coupled test with a temperature gradient can be developed in the future. By establishing heating at one end and maintaining room temperature at the other end, to make the temperature move from the axial direction, and install temperature, humidity, and pressure transducers at the axial position. Therefore, the changes in temperature, humidity and pressure at different positions in the axial position of bentonite materials can be effectively measured. It can also provide a comparison between the numerical model of the saturation behavior analysis of the buffer and the backfill to confirm the rationality of the conceptual model and calibrate the parameters.

(e) Radionuclide transport under buffer advection condition:

Once the groundwater intrudes into a canister, the radionuclides in the canister may precipitate in the void volume of the canister and may present as a colloidal state. In the analysis of the retardation function of the corrosion scenario, the advection condition occurs in the buffer surrounding the canister. Therefore, colloid filtration of the buffer cannot be guaranteed. This phenomenon will be taken into account in the future by referring to international experience (SKB, 2010h), i.e., solubility limits of elements are not adopted in radionuclide transport calculation yet.

(f) Potential release path of near-field:

The potential release paths of near-field, Q1 and Q2 pathways, are included in the current radionuclide transport calculation model. However, according to international experience, a fracture intersecting the deposition tunnel also can be a potential release path, Q3 pathway, in the near-field (SKB, 2010h). This potential release path will be taken into account in further development.

(2) Engineered barrier and near-field environmental impact:

The engineered barrier and near-field environmental impact research mainly include three major objectives: (a) clay erosion experiments and evaluation, (b) near-field groundwater chemical characteristics/reaction research, and (c) microbial activity on the formation of sulfide in bentonite, etc., are described as follows:

(a) Clay erosion experiments and evaluation:

Relevant technologies for experimenting and model evaluation combined with conceptual design and host rock characteristics for analysis have been developed. And the degree of erosion of the buffer and the backfill under extreme conditions, as well as the impact on safety functions have been evaluated.

In the initial state after the repository is closed, the groundwater flow will form a channel in the bentonite and a continuing water flow and a consecutive erosion of bentonite particles. Piping and erosion tests have been established to evaluate the erosion impact caused by horizontal pipe flow. The test results are in line with the trends in international literature. Subsequent research can be further carried out on the upscale vertical piping and erosion test. Establish a vertical container similar to the deposition hole to observe the formation of pipe flow channels and the influence of erosion. In addition, flow rate, water composition, and other influencing factors will also be considered to study the formation of piping and the selfhealing ability of the buffer after the piping channels are closed.

After the buffer is saturated, chemical erosion is the main erosion behavior. Beginning in 2012, the BELBaR (Bentonite Erosion: effects on the Long term performance of the engineered Barrier and Radionuclide transport) project led by the European Union believed that the formation of colloids and loss of buffer mass would weaken the safety functions of the engineered barrier system and promote the transport of nuclides. At present, there have been related studies in the world, through experimental research and model development, to reduce the uncertainty caused by the instability factors between the colloid, the engineered barrier system, and the fractures of the host rock. At present, relevant research has been conducted through experimental research and model development to refine the safety assessment of the engineered barrier system under the long-term impact of rock fracture and groundwater. Relevant research is used to reduce the uncertainty caused by the instability factors between the engineered barrier system, the fractures of the host rock and the colloid.

Assessment methods for chemical erosion are also planned to be established. The follow-up research in the future will refer to the test methods of international research and conduct test research on the conditions of groundwater composition and other key conditions that affect chemical erosion in Taiwan. And improve the development of the evaluation model through comparison with test results.

(b) Near-field groundwater chemical characteristics/reaction research:

Hydro-chemical coupling model technologies such as water contamination, water-rock reaction, reaction conceptual model, etc. will be developed. And conceptual design and host rock characteristics to investigate groundwater quality changes under steady-state conditions will be combined with the models in order to provide evaluation applications such as erosion of the buffer and corrosion of the canisters.

After the repository closure, the buffer will be affected by the thermal gradient from the SNF decay heat, suction from the unsaturated buffer, and the hydraulic gradient from the hydrostatic pressure of the surrounding host rock. After saturation and cooling of the near-field, the interaction of groundwater and bentonite may cause changes in aqueous species in the bentonite porewater. And the redistribution of accessory minerals and the cation exchanger in the bentonite, which changes the chemical conditions in the porewater. Therefore, it is also necessary to evaluate the chemical evolution, such as the influence of salinity, the transformation of minerals, the cementation of bentonite, the oxygen consumption in the backfill, and the formation of colloids. And such as salinity, ionic strength, pH value, and reduction conditions that may indirectly affect safety functions require further analysis. Taiwan's groundwater quality conditions and bentonite and groundwater tests for verification of bentonite chemical analysis will be performed.

(c) Microbial activity on the formation of sulfide in bentonite:

The sulfide production by sulfate-reducing bacteria present initially in the buffer is one of the main sources of sulfide. The sulfide produced will cause corrosion of the copper shell of the canister. Therefore, we will continue to study the formation mechanism of sulfide in the buffer to provide relevant evaluation applications of the canister corrosion.

The National Tsing Hua University Nuclear Science & Technology Development Center has been incorporated to conduct sulfate-reducing bacteria activity tests. The establishment of procedures for strain cultivation, preparation of test samples mixed with bacteria, and analysis of bacteria survival rate have been completed. In addition, a buffer diffusion test was carried out to analyze the diffusion coefficient of sulfate under different conditions. It can be used to estimate the diffusion parameters of sulfides and to evaluate the impact of sulfides in the buffer. Subsequent studies will continue to carry out long-term sulfate-reducing bacteria activity tests to evaluate the corrosion rate of the copper shell caused by the bacteria.

(d) Radionuclide transport under buffer advection condition:

Once the groundwater intrudes into a canister, the radionuclides in the canister may precipitate in the void volume of the canister and may present as colloidal state. In the analysis of the retardation function of the corrosion scenario, the advection condition occurs in the buffer surrounding the canister. Therefore, colloid filtration of the buffer cannot be guaranteed. This phenomenon will be taken into account by referring to international experience (SKB, 2010h), i.e., solubility limits of elements are not adopted in radionuclide transport calculation.

With respect to the five issues raised by the Land and Environmental Court, most of the issues have been resolved in SKB TR-19-15(SKB, 2019, ch10):

(a) Copper corrosion in pure water

Huge amounts of work have been done on copper corrosion in pure water, and even the Swedish regulator does not see this as an issue any more.

(b) Pitting in the presence of sulfide, including any impact of the sauna effect

Through multiple studies and arguments that copper is not suspectable to corrosion in the presence of sulfide under repository conditions (the sulfide flux is too low to sustain pit growth ahead of the uniform corrosion front)

(c) Stress corrosion cracking in the presence of sulfide, including any impact of the sauna effect

The sulfide flux too low discount SCC of copper in the presence of sulfide under repository conditions

(d) Hydrogen embrittlement

The only effects that have been shown have been on the creep behaviour, but only at accelerated rates by H-charging under extreme conditions

(e) The impact of ionising radiation on pitting, SCC, and hydrogen embrittlement

The radiation fields for the KBS-3 canister are too low to be of concern. Work on this is going on in an EU project and in Canada.

Regarding the corrosion future R&D, the topics from SKB TR-19-15 will continue to be paid attention to. In addition, for the short term, the sulfide generation mechanism under the saturated state of the buffer material will be discussed, including sulfide deposition and sulfate-reducing bacteria to produce sulfide; it is necessary to analyze important parameters and establish a sulfide transport model.

14.7.4. Geosphere

Flow-related parameters calculated by the hydrogeology model should have a certain degree of correlation which is varied with time. In order to include the impact of the correlation in the radionuclide transport calculation, an evaluation model will be developed in the future by referring to international experience (SKB, 2010h; POSIVA, 2014).

The establishment of technology related to the geosphere focuses on geochemical analysis of radionuclides and coupling analysis of the groundwater flow. It can be divided into: (1) geochemical reaction analysis of radionuclides in the host rock; (2) parallel verification of hydraulic-mechanical coupling analysis of fracture shear force displacement, and (3) coupling analysis of groundwater flow and radionuclides transport. They are described as follows:

(1) Geochemical reaction analysis of radionuclides in the host rock

After the canister fails, radionuclides in SNF will dissolve in the groundwater, then transport in rock fractures. During transport, geochemical reactions can occur, and these reactions will further affect the transport behavior of the radionuclides. A constant distribution coefficient was used when analyzing the geochemical reactions of radionuclides in the host rock. However, the safety assessment time scale of the repository is 1 million years, and geochemical conditions may change with external climate conditions which can then affect the geochemical reaction of radionuclides in the host rock. Therefore, geochemical model analysis technology will be established, the geochemical reaction between radionuclides and the mineral composition of the host rock will be analyzed, and distribution coefficients between radionuclides and the host rock under different environmental conditions will be estimated, so that influence of adsorption behavior of radionuclides under long-term evolution can be taken into account. In addition, the far-field dynamic distribution coefficients will be used to conduct radionuclide transport calculation and parameter sensitivity analysis of radionuclide activity, so that evaluation results can reflect the impact of climate evolution more realistically.

(2) Parallel verification of hydraulic-mechanical coupling analysis of fracture shear displacement

Thermal-hydraulic-mechanical-chemical multi-physical field coupling is the core technology for performing evolution analysis and safety assessment of the repository. Internationally, in order to evaluate the long-term evolution of the repository, the development of THMC coupling analysis is continuously carried out. For example, in DECOVALEX international cooperation test plan, international coupling tests and model verification through a number of large-scale tests are carried out. The effectiveness and accuracy of the THMC coupling analysis are improved through comparison between the evaluation results of the numerical models. TPC will actively participate in the DECOVALEX international cooperation test project. Through parallel verification with the international analysis data, the reliability of Taiwan's relevant analysis technology will be improved.

In 2019 Task B of the DECOVALEX International Cooperation Test Project, fracture reactivation in clay layer due to increase of water pressure which in turn leads to re-slip and deformation of fractures or faults, was discussed through the fault slip test in Mont Terri Underground Laboratory in Switzerland. The main research purposes are as follows:

(a) Critical driving water pressure required for fracture reactivation was evaluated.

(b) The relation between the change in the size of the space and water pressure after the fractures are reactivated was evaluated.

TPC will plan to establish a hydraulic-mechanical coupling assessment model of fractures through the following steps:

(a) A conceptual numerical model of rock with fractures will be established. And a comparison of the analysis results with the results of other teams in DECOVALEX Task B will be performed to conduct a benchmark test which will be seen as a basis for the next stage of the analysis.

(b) In FM1 mode, fluid can only flow in the initial fractures. As the fractures expand according to the Mohr-Coulomb failure criterion, fluid will flow along the cracked fractures. In FM2 mode, fluid can flow freely in the fractures regardless of the cracking situation. The evaluation results based on these two modes will be compared.

(c) A simple single fracture mode (only secondary fault) will be established, and parameters will be adjusted so that they can be verified with in-situ measurement data.

(d) A complex multi-fracture model (including main fault and secondary fault) will be established, and the evaluation results will be compared with the analysis results of other teams in Task B. Also, they will be verified with in-situ measurement data.

(3) Coupling analysis of groundwater flow and radionuclide transport

GDSA (general disposal system analysis) is a general method used in evaluating the long-term evolution of the disposal environmental conditions¸ so that the performance of the repository can be analyzed. In the future, TPC will apply PFLOTRAN as the analyzing program of reactive transport.

PFLOTRAN program includes coupling mechanisms of thermal, hydrological, and chemical. It can simulate three-dimensional porous media multiphase flow, geochemical coupling transport, simulated transport, etc. And it also conforms to the current development trend of groundwater flow and radionuclide transport coupling analysis.

14.7.5. Biosphere

BDCF of potentially exposed groups was calculated when uncertainty caused by climate evolution and changes in the surface environment and human lifestyles was taken into account through biosphere assessment.

According to the results, if radionuclides are released into the sea, the radioactive impact on humans will be much smaller; on the other hand, if radionuclides are released into freshwater bodies or well-water, the radioactive impact on humans will be more severe. In general, crop and livestock farmers are the critical groups in most of the assessment cases. From the assessment results, it can be assumed that when the sea-level drops and the repository becomes far away from the sea, the probability of radionuclides released into freshwater bodies becomes higher. This will cause higher doses to humans (especially for the crop and livestock farmers).

In the future, when candidate sites are selected, evaluation of landscape evolution and release location can be the main focus. The geographic information system can also be established based on the regional fine-grid digital elevation model of the land and the sea bottom. This can be combined with surface hydrological code to delineate biosphere objects based on the long-term evolution of terrain and waterbody. Besides, the mechanism of the water balance system of the unsaturated zone should also be studied by applying in-situ experiments and evaluation models. Radionuclide transports inside the unsaturated zone can therefore be better described, and confidence of the biosphere assessment can be improved. Finally, studies and research results will be collected continuously, so that the comprehensiveness of biosphere assessment can be better improved.

14.7.6. Climate

Climate evolution analysis of the reference case has been implemented based on the development of international global climate models. When a candidate site is selected in the future, a smaller-scale climate evolution analysis can be carried out, and regional climate characteristics such as rainfall, wind field, temperature and so on can be evaluated using simulation experiments of global and regional climate models, so that accuracy of climate evolution analysis can be improved.

14.8. Conclusion Relevant to Safety Assessment Methodology

After implementation of the preliminary assessment in this report, the safety assessment methodology described in Chapter 2 is ensured to conform to general principles of safety assessment methods used in the world. And the methodology can be applied to the long-term safety assessment of the repository.

14.8.1. Steps of the Methodology

As described in Section 2.2, the NEA MeSA method has been adopted and modified in the preliminary safety case report (see Figure 2-1). The main components of the processes include: (1) assessment context, (2) assessment basis, (3) safety assessment, (4) synthesis evidence, arguments and analyses, and (5) other elements.

Based on the safety case method and geological characteristics of the reference case, the preliminary design concept of the repository system has been developed, and a post-closure safety assessment has been implemented. It can be seen that the safety case method can be applied to relevant assessment regarding the long-term safety of the repository in Taiwan.

14.8.2. Quality Assurance

This report refers to the Nuclear Quality Assurance (NQA) guidelines published by the ASME to implement the quality assurance project of the program. Related quality assurance procedures have also been established for the safety assessment in this report (such as input parameter source and confidence check, model/code verification and validation, and assessment model flow control). Key checkpoints have also been documented as quality records in order to improve traceability. In addition, while implementing the quality assurance system, the safety assessment will be continually reviewed and improved through internal discussion and external audit at the same time so that the effectiveness and efficiency of the safety assessment can be improved and confidence and integrity of the assessment results can be assured.

14.8.3. Expert Judgements

Expert judgment for the safety assessment was introduced in this report. Discussion and advice on the analysis results of the FEPs are the main focus of the task. The Taiwan FEPs database has been established, taking the internationally agreed FEPs list provided by the NEA of OECD and research results from other experienced countries. Through interdisciplinary external experts’ discussion of the database, potential impact factors of the disposal system can be more clearly defined, and the integrity of the long-term safety assessment of the repository can be further ensured.

15. References

台灣電力公司(2010)，我國用過核子燃料最終處置初步技術可行性評估報告(SNFD2009報告)，台灣電力公司。

台灣電力公司(2017)，用過核子燃料最終處置計畫潛在處置母岩特性調查與評估階段—我國用過核子燃料最終處置技術可行性評估報告—技術支援報告(3) 安全評估，TPC-SNFD2017-TSR03。

台灣電力公司(2017)，用過核子燃料最終處置計畫潛在處置母岩特性調查與評估階段—我國用過核子燃料最終處置技術可行性評估報告—SNFD2017報告，TPC-SNFD2017。

台灣電力公司(2018a)，用過核子燃料最終處置計畫，台灣電力公司核能後端營運處；行政院原子能委員會放射性物料管理局，2020年核定版。

台灣電力公司(2018b)我國用過核子燃料最終處置初步技術可行性評估報告(SNFD2017報告)，台灣電力公司。

台灣電力公司(2019)，用過核子燃料最終處置計畫潛在處置母岩特性調查與評估階段－我國用過核子燃料最終處置技術可行性評估報告－SNFD2017報告，TPC-SNFD2017-V1。

台灣電力公司(2019a)，用過核子燃料最終處置計畫候選場址評選與核定階段107年度成果報告(修訂二版)，台灣電力公司。

Åkesson, M., Kristensson, O., Börgesson, L., Ann Dueck Clay Technology (2010), THM modelling of buffer, backfill and other system components, Critical processes and scenarios, SKB, TR-10-11.

Alexander, W. R., Milodowski, A. E., Pitty, A. F., Hardie, S. M. L., Kemp, S. J., Rushton, J. C., Siathas, A., Siathas, A., Mackenzie, A. B., Korkeakoski, P., Norris, S., Sellin, P. and Rigas, M. (2013), Bentonite reactivity in alkaline solutions: interim results of the Cyprus Natural Analogue Project (CNAP), Clay Minerals, vol. 48, pp. 235-249.

Andersson, E. (2010), The limnic ecosystems at Forsmark and Laxemar-Simpevarp, SKB TR-10-02.

Andersson, J., Skagius, K., Winberg, A., Lindborg, T., and Strom, A., 2013, Site-descriptive Modelling for a Final Repository for Spent Nuclear Fuel in Sweden, Environ Earth Sci (2013) 69:1045–1060.

ASTM Standard E1269, (2011), Standard test method for determining specific heat capacity by differential scanning calorimetry, ASTM International, West Conshohocken, PA.

Atomic energy council (1997) [In Chinese: 原子能委員會(1997)放射性廢料管理方針，中華民國77年9月16日台科字第25776號令發布，中華民國86年9月2日台科字第33951號令修正。]

Atomic energy council (2002) [In Chinese: 原子能委員會(2002)游離輻射防護法，中華民國91年12月23日行政院院臺科字第0910064739號令發布。]

Atomic energy council (2010) [In Chinese: 原子能委員會(2010)放射性物料管理法，中華民國91年12月25日總統華總一義字第09100248760號令發布。]

Atomic energy council (2011) [In Chinese: 原子能委員會(2011)放射性物料管理法施行細則，中華民國92年7月30日行政院原子能委員會會物字第0920018935號令發布，中華民國108年11月21日行政院原子能委員會會物字第10800134611號令修正。]

Atomic energy council (2013) [In Chinese: 原子能委員會(2013)高放射性廢棄物最終處置及其設施安全管理規則，中華民國94年8月30日會物字第0940028885號令發布，中華民國102年1月18日會物字第1020001007號令修正。]

Atomic energy council (2017) [In Chinese: 原子能委員會(2017)高放射性廢棄物最終處置設施場址規範，中華民國104年4月24日會物字第1040013356號令發布，中華民國106年3月29日會物字第1060039311號令修正。]

Atomic energy council (2019) [In Chinese: 原子能委員會(2019)核子保防作業辦法，中華民國92年9月10日行政院原子能委員會會綜

字第0920023127號令發布，中華民國108年7月25日行政院原子能委員會會綜字第10800084831號令修正。]

Atomic energy council (2020) [In Chinese: 原子能委員會(2020)放射性廢棄物處理貯存最終處置設施建造執照申請審核辦法，中華民國93年4月7日行政院原子能委員會會物字第0930010683號令發布，中華民國109年8月7日行政院原子能委員會會物字第1090008779號令修正。]

Bäckblom, G. (2008), Excavation damage and disturbance in crystalline rock – results from experiments and analyses, Swedish Nuclear Fuel and Waste Management Company, SKB, TR-08-08.

Barton, N. (2013), Shear strength criteria for rock, rock joints, rockfill and rock masses: Problems and some solutions, Journal of Rock Mechanics and Geotechnical Engineering, Vol. 5, No. 1, pp. 249-261.

Becker D-A, Buhmann D, Storck R, Alonso J, Cormenzana J-L, Hugi M, van Gemert F, O'Sullivan P, Laciok A, Marivoet J, Sillen X, Nordman H, Vieno T, Niemeyer M (2002), Testing of safety and performance indicators (SPIN). EUR 19965 EN, European Commission.

BMUB (2010), Safety Requirements Governing the Final Disposal of Heat-Generating Radioactive Waste.

Bresle, A., Saers, J. and Arrhenius, B. (1983), Studies in pitting corrosion on archaeological bronzes, SKB Technical Report, TR 83-05, SKB, Stockholm, Sweden.

Brown, E. T., (1981), Rock characterization testing and monitoring – ISRM suggested method, Pergamon Press Ltd., U.K.

Bulgaria Government (2004), Regulation for Save Management of Radioactive Waste, Adopted by the Council of Ministers Decree No. 198.

Chang, C. P. (2016) [In Chinese: 張中白 (2016) 臺灣島的災害宿命，台灣學系列講座，2016/03/11，臺灣學研究中心；2020/07/14

Chang, C. S., Kuo, T. J., Lin, W., Chang, Y. T. and Lee, Y. H. (2005) [In Chinese: 張傳聖、郭泰融、林蔚、張育德、李奕亨(2005)我國用過核子燃料長程處置-潛在處置母岩特性調查與評估階段-潛在處置母岩特性調查(93年計畫)－跨孔試驗與量測(含K區KMBH04鑽探報告)，台灣電力公司委辦計畫，SNFD-ERL-90-220，工業技術研究院。]

Chang, Y. W., Chien, W. Y. and Chiu, S. P. (2010) [In Chinese: 張毓文、簡文郁、邱世彬(2010)金、馬及澎湖地區之設計地震研擬，國家地震工程研究中心，共76頁。]

Chen, C. H., Shieh, Y. N., Lee, T., Chen, C. H. and Mertzman, S. A. (1990), Nd-Sr-O isotopic evidence for source contamination and an unusual mantle component under Luzon Arc, Geochimica et Cosmochimica Acta, Vol. 54, pp. 2473–2483.

Chen, C. J., Wu, Y. C. and Lo, H. T (2017) [In Chinese: 陳麒任、吳元傑、羅晞廷(2017)用過核子燃料最終處置計畫潛在處置母岩特性調查與評估階段--發展功能/安全評估技術(104-107年度計畫)--處置設施佈置研究報告，台灣電力公司委辦計畫，SNFD-03-IPR-015，核能研究所。]

Chen, H. Y., Hsu, H. H., Lee, L. Y. and Chen Y. M. (2018) [In Chinese: 陳宏宇、許晃雄、林李耀、陳永明(2018)臺灣氣候的過去與未來-臺灣氣候變遷科學報告2017-物理現象與機制-重點摘錄。30頁。]

Chen, W. S., Yu, H. S., Yui, T. F., Chung, S. L., Lin, C. H., Lin, C. W., Yu, N. T., Wu, Y. M. and Wang, K. L. (2016)][In Chinese: 陳文山、俞何興、俞震甫、鍾孫霖、林正洪、林啟文、游能悌、吳逸民、王國龍(2016)，臺灣地質概論，中華民國地質學會出版，共204頁。]

Cheng, S. N., Chiang, C. H. and Chen, Y. L. (2011) [In Chinese: 鄭世楠、江嘉豪、陳燕玲(2011)台灣地區歷史地震資料的建置，中央氣象局地震技術報告彙編，第60卷，第427-448頁。]

Chiang, L. W. and Yu, C. C. (2019a) [In Chinese: 蔣立為、余錦昌(2009a)用過核子燃料最終處置計畫潛在處置母岩特性調查與評估階段--潛在處置母岩特性調查(97~99年度計畫) --區域性地下水量估算技術資料蒐集成果報告，工研院執行/台灣電力公司委辦，SNFD-EEL-90-270 / SNFD-ITRI-TR2009-0270。]

Chiang, L. W., Lin, W., Chien, C. M. and Yu, C. C. (2006) [In Chinese: 蔣立為、林蔚、錢正明、余錦昌(2006)用過核子燃料最終處置計畫潛在處置母岩特性調查與評估階段--潛在處置母岩特性調查(94~96年度計畫)--技術發展ー跨孔追蹤稀釋試驗成果報告，工研院執行/台灣電力公司委辦，SNFD-EEL-90-243 / SNFD-ITRI-TR2006-0243。]

Chiu, L. W., Huang, C. H. and Wu, C. C. (2015) [In Chinese: 邱立文、黃群修、吳俊奇(2015)第四次全國森林資源調查，行政院農委會林務局委託報告。]

Chiu, Y. C. and Chang, C. T. (2019) [In Chinese: 邱筠捷、張清土(2019)用過核子燃料最終處置計畫潛在處置母岩特性調查與評估階段-發展功能/安全評估技術(104-107年度計畫)，腐蝕氣體對緩衝材料影響研究報告，SNFD-06-IPR-004-03，核能研究所。]

Chu, C. F., Hsu, H. W., Huang, Z. L., Wu, C. C., Chang, H. K. (2005) [In Chinese: 朱金芳、徐錫偉、黃宗林、吳建春、張先康(2005)，福州市活斷層探測與地震危險性評價，中國城市活斷層探測叢書，科學出版社。]

Chuang, W. S. (1988) [In Chinese: 莊文星(1988)，臺灣新生代晚期火山岩之定年與地球化學研究，國立臺灣大學，海洋研究所，博士論文，共231頁。]

Chuang, Y. F. (2018) [In Chinese: 莊怡芳(2018)回填材料設計需求與施工技術報告(修訂一版)，用過核子燃料最終處置計畫潛在處置母岩特性調查與評估階段發展功能/安全評估技術(104-107年度計畫)，SNFD-06-IPR-003-02，核能研究所。]

Chuang, Y. F. (2020) [In Chinese: 莊怡芳(2020)緩衝材料設計(60個日曆天成果說明)，用過核子燃料最終處置計畫─108年度成果報告及109年度工作計畫，SNFD-B05-OTH-108-001，核能研究所。]

Chung, S. L., Sun, S. S., Tu, K., Chen, C. H. and Lee, C. Y. (1994), Late Cenozoic basaltic volcanism around the Taiwan Strait, SE China: Product of lithosphere-asthenosphere interaction during continental extension, Chemical Geology, Vol. 112, pp. 1–20.

Chung, S. L., Yang, T. F., Lee, C. Y. and Chen, C. H. (1995), The igneous provinciality in Taiwan: Consequence of continental rifting superimposed by Luzon and Ryukyu subduction systems, Journal of Southeast Asian Earth Sciences, Vol. 11, Issue 2, pp. 73–80.

CNSC (2006), Assessing the Long Term Safety of Radioactive Waste Management, Canadian Nuclear Safety Commission, Regulatory Guide G-320.

CNSC (2021), Safety Case for the Disposal of Radioactive Waste, Canadian Nuclear Safety Commission, Waste Management, Volume III, REGDOC-2.11.1, Version 2.

Cornell, C. A., and Van Marke, E. H. (1969), The major influence on seismic risk, Proceedings Third World Conference on Earthquake Engineering, Sandiago, Chile, A-1, 69-93.

Czech Republic (2002), Regulation No.307/2002 Coll. of the State Office for Nuclear Safety of 13 June 2002 on Radiation Protection.

Directorate-General of Budget, Accounting and Statistics, Executive Yuan (2017) [In Chinese: 行政院主計總處(2017)，104年農林漁牧業普查報告金門縣報告，行政院主計總處。]

ENSI (2009), Specific design principles for deep geological repositories and requirements for the safety case, Guideline for Swiss nuclear installations G03/e.

EPRI (2010a), EPRI Review of Geologic Disposal for Used Fuel and High Level Radioactive Waste: Volume I II -Review of National Repository Programs, Electric Power Research Institute, No. 1021614.

EPRI (2010b), EPRI Review of Geologic Disposal for Used Fuel and High Level Radioactive Waste: Volume II -U.S. Regulations for Geologic Disposal, Electric Power Research Institute, No. 1021384.

Faure, G. (1991), Principle and applications of inorganic geochemistry, Macmillan.

Fayek, M. and Brown, J. (2015), Natural and anthropogenic analogues for high-level nuclear waste disposal repositories: a review, A report to the Canadian Nuclear Safety Commission (CNSC), RSP-310.

Food and drug administration (2017) [In Chinese: 食品藥物管理署(2017)國家攝食資料庫。2020/10/29 取自 http://tnfcds.cmu.edu.tw/index.php?action=about]

Golder Associates Inc. (2009), Upscaling from Discrete Fracture Network Models to Equivalent Porous Media Models.

GoldSim Technology Group (2017), GoldSim Contaminant Transport Module User's Guide, Version 7.0, Copyright GoldSim Technology Group LLC, 1998-2017.

Green Engineering Technology Research Center, Kao Yuan University (2011) [In Chinese: 高苑科技大學綠功能技術研發中心(2011)國家重要濕地碳匯功能調查計畫總結報告書，內政部營建署城鄉發展分署委託報告。]

Gutenberg, R., and C.F. Richter, (1944). Frequency of earthquakes in California, Bulletin of the Seismological Society of America, 34, p185-p188.

Hallberg, R.O. (1988), Inferences from a corrosion study of a bronze cannon, applied to high level nuclear waste disposal, Applied Geochemistry. Vol. 3, Issue 3, pp. 273-280.

Hedin, A. (2002), Integrated Analytic Radionuclide Transport Model for a Spent Nuclear Fuel Repository in Saturated Fractured Rock, Nuclear Technology, Vol. 138, pp. 179-205.

Hedström, M., Hansen E. E., and Nilsson, U. (2015), Montmorillonite phase behaviour, Relevance for buffer erosion in dilute groundwater, Technical Report TR-15-7, SWEDISH NUCLEAR FUEL AND WASTE MANAGEMENT CO

Hicks, T. W. (2005), Review of SKB's Code Documentation and Testing, SKI Report 2005:05.

Hidaka, H. and Holliger, P. (1998), Geochemical and Neutronic Characteristics of the Natural Fossil Fission Reactors at Oklo and Bangombe, Gabon, Geochim. Cosmochim. Acta, Vol. 62, pp. 89-108.

Holmboe M, Wold S, and Jonsson M (2010), Colloid diffusion in compacted bentonite: microstructural constraints, Clays and Clay Minerals 58, 532–541.

Hsiao, Y. H. and Chang, C. T. (2019) [In Chinese: 蕭宇翔、張清土(2019)緩衝材料熱-水-力-化耦合特性研究報告，用過核子燃料最終處置計畫潛在處置母岩特性調查評估階段-發展功能/安全評估技術。]

Hsieh, C. L., Chien, C. M., Chao, C. H. and Wang, P. H. (1996) [In Chinese: 謝傳禮、翦知湣、趙泉鴻、汪品先(1996)末次盛冰期中國海古地理輪廓及其氣候效應，第四紀研究，第16卷，第1期，第1–10頁。]

Hsieh, M. H. and Wu, Y. C. (2018) [In Chinese: 謝孟修、吳元傑(2018)用過核子燃料最終處置計畫潛在處置母岩特性調查與評估階段--發展功能/安全評估技術(104-107年度計畫)—隧道封塞設計報告，台灣電力公司委辦計畫，SNFD-03-IPR-033，核能研究所。]

Hsieh, M. L., Lai, T. H., Wu, L. C., Lu, W. C., Liu, H. T. and Liew, P. M. (2006), Eustatic Sea-Level Change of 11-5 ka in Western Taiwan, Constrained by Radiocarbon Dates of Core Sediments. TAO, Vol. 17, No. 2, pp. 353-370.

Hsieh, P. S. and Lin, W. (2012) [In Chinese: 謝佩珊、林蔚(2012)用過核子燃料最終處置計畫-潛在處置母岩特性調查與評估階段-潛在處置母岩特性調查(99-101年度計畫)-K區花崗岩岩心礦物組成

特性分析─FY99~101計畫執行成果報告，台灣電力公司委辦計畫，SNFD-GEL-90-288，工業技術研究院

Hsu, N. C., Kuo, C. T., Chu, E. S., Wang, H. C., Chiang, C. J., Chang, T. H., Wu, C. M., Fu, T. C. and Kao, W. Y. (1991) [In Chinese: 徐年盛、郭振泰、朱文生、王曉中、江崇榮、張德鑫、吳呈懋、傅大章、高尉明(1991)放射性廢料設施及其附近地區地下水流及水質傳輸模擬之研究(一)，台大土木工程研究所水利組，水利79013。]

Huang, C. C., Liu, C. C. and Wen, C. K. (2006) [In Chinese: 黃家勤、劉正千、溫清光(2006)流域非點源污染對於感潮河段動態水質影響之研究，臺南大學環境生態研究所，行政院國家科學委員會專題研究計畫。]

Hung, C.C., Wu, Y.C., and King, F. (2017), Corrosion assessment of canister for the disposal of spent nuclear fuel in crystalline rock in Taiwan, Corrosion Engineering, Science and Technology, VOL. 52, NO. S1, pp. 194–199.

Hungary Government (2003), Decree 47/2003 (VI II. 8.) ESZCSM of the Minister of Health, Social and Family Affairs on certain issues of interim storage and final disposal of radioactive wastes, and on certain radiohygiene issues of naturally occurring radioactive materials concentrating during industrial activity.

IAEA (2003), Reference Biosphere for Solid Radioactive Waste Disposal: Report of BIOMASS Theme 1 of BIOsphere Modelling and ASSessment Programme, IAEA-BIOMASS-6, International Atomic Energy Agency, Vienna.

IAEA (2010), Seismic Hazards in Site Evaluation for Nuclear Installations, International Atomic Energy Agency, Safety Standards Series, Specific Safety Guide, No. SSG-9, 60p.

IAEA (2012), The Safety Case and Safety Assessment for the Disposal of Radioactive Waste, International Atomic Energy Agency, Safety Standards Series, Specific Safety Guide, No. SSG-23, 120p.

ICRP (1991), 1990 Recommendations of the International Commission on Radiological Protection, ICRP Publication 60.

ICRP (1999), Radiation protection recommendations as applied to the disposal of long-lived solid radioactive waste, ICRP Publication 81.

ICRP (2013), Radiological Protection in Geological Disposal of Long-lived Solid Radioactive Waste, ICRP Publication 122. Ann. ICRP 42(3).

INER (2017a) [In Chinese: 核能研究所(2017a)用過核子燃料最終處置計畫潛在處置母岩特性調查與評估階段—我國用過核子燃料最終處置技術可行性評估報告—技術支援報告(2)處置設計與工程技術，核能研究所。]

INER (2017b) [In Chinese: 核能研究所(2017b)用過核子燃料最終處置計畫潛在處置母岩特性調查與評估階段—我國用過核子燃料最終處置技術可行性評估報告—技術支援報告(3)，核能研究所。]

INER (2018) [In Chinese: 核能研究所(2018)用過核子燃料最終處置計畫潛在處置母岩特性調查與評估階段—發展功能/安全評估技術(104-107年度計畫)，深層地質環境中重要核種於岩體裂隙之吸附反應與擴散行為研究報告。]

INER (2020a) [In Chinese: 核能研究所(2020a)區域特性調查技術精進技術報告，用過核子燃料最終處置計畫—108年度成果報告及109年度工作計畫技術服務案，台灣電力公司委辦計畫，SNFD-B03-IPR-001-02，行政院原子能委員會核能研究所。]

INER (2020b) [In Chinese: 核能研究所(2020b)處置設施工程設計及安全評估技術精進技術報告，用過核子燃料最終處置—108年度成果報告及109年度工作計畫技術服務案，台灣電力公司委辦計畫，SNFD-B02-IPR-001-02，行政院原子能委員會核能研究所。]

INER (2020c) [In Chinese: 核能研究所(2020c)地下設施配置設計(60個日曆天成果說明)，用過核子燃料最終處置—108年度成果報告及109年度工作計畫，SNFD-B04-OTH-108-002，行政院原子能委員會核能研究所。]

INER (2020d) [In Chinese: 核能研究所(2020d)廢棄物罐設計(60個日曆天成果說明)，用過核子燃料最終處置—108年度成果報告及109年度工作計畫，SNFD-B04-OTH-108-001，行政院原子能委員會核能研究所。]

INER (2020e) [In Chinese: 核能研究所(2020e)廢棄物罐抗圍壓性能評估(90個日曆天成果說明)，用過核子燃料最終處置—108年度成果報告及109年度工作計畫，SNFD-B04-OTH-108-003，行政院原子能委員會核能研究所。]

IPCC (2007), Climate Change 2007: Synthesis Report. Contribution of Working Groups I, II and III to the Fourth Assessment Report of the Intergovernmental Panel on Climate Change [Core Writing Team, Pachauri, R.K and Reisinger, A. (eds.)]. IPCC, Geneva, Switzerland, 104 pp.

IPCC (2013), Climate Change 2013: The Physical Science Basis. Contribution of Working Group I to the Fifth Assessment Report of the Intergovernmental Panel on Climate Change [Stocker, T.F., D. Qin, G. K. Plattner, M. Tignor, S.K. Allen, J. Boschung, A. Nauels, Y. Xia, V. Bex and P.M. Midgley (eds.)]. Cambridge University Press, Cambridge, United Kingdom and New York, NY, USA.

IPCC (2021): Summary for Policymakers. In: Climate Change 2021: The PhysicalScience Basis. Contribution of Working Group I to the Sixth Assessment Report of theIntergovernmental Panel on Climate Change [Masson-Delmotte, V., P. Zhai, A. Pirani,S. L. Connors, C. Pean, S. Berger, N. Caud, Y. Chen, L. Goldfarb, M. I. Gomis, M.Huang, K. Leitzell, E. Lonnoy, J.B.R. Matthews, T. K. Maycock, T. Waterfield, O.Yelekci, R. Yu and B. Zhou (eds.)]. Cambridge University Press. In Press.

Isobe, H., Ohnuki, T., Murakami, T. and Gauthier-Lafeye, F. (1995), Migration Behaviour of Uranium under Oxidizing Condition in the Oklo Natural Reactor Zone 2, Gabon, Sci. Bas. Nucl. Was. Manag. XVIII, pp. 1211-1218.

ITRI (2015)[In Chinese: 工研院(2015)，用過核子燃料最終處置計畫潛在處置母岩特性調查與評估階段－潛在處置母岩特性調查(104-107年度計畫)－SNFD2017參考案例及數據彙整說明報告表二:地質概念模式及特性數據，台灣電力公司委辦計畫，SNFD-ITRI-TR2015-0001，工業技術研究院。]

JNC (2000), H12 Project to Establish the Scientific and Technical Basis for HLW Disposal in Japan, Project Overview Report, 2nd Progress Report on Research and Development for the Geological Disposal of HLW in Japan, JNC Technical Report TN1410 2000-001, Japan Nuclear Cycle Development Institute, Tokai-mura Japan.

Joyce, S., Applegate, D., Hartley, L., Hoek, J., Swan, D., Marsic, N., and Follin, S. (2010), Groundwater flow modelling of periods with temperate climate conditions – Forsmark, SKB R-09-20.

Kana, D.D., Brady, B.H.G., Vanzant, B.W., and Nair, P.K. (1991), Critical Assessment of Seismic and Geomechanics Literature Related to a High-Level Nuclear Waste underground Repository, NUREG/CR-5440, Washington, DC: Nuclear Regulatory Commission.

Kawamura, K., Parrenin, F., Lisiecki, L., Uemura, R., Vimeux, F., Severinghaus, J., Hutterli, M., Nakazawa, T., Aoki, S., Jouzel, J., Raymo, M., Matsumoto, K., Nakata, H., Motoyama, H., Fujita, S., Goto-Azuma, K., Fujii, Y. and Watanabe, O. (2007) Northern Hemisphere forcing of climatic cycles in Antarctica over the past 360,000 years. Nature Vol. 448, pp. 912–916.

King F., Ahonen L., Taxén C., Vuorinen U. and Werme L. (2001), Copper corrosion under expected conditions in a deep geologic repository, Swedish Nuclear Fuel and Waste Management Company Report, SKB, TR-01-23.

King, F. and Litke, CD. (1992), Development of a Container Failure Function for Copper, Atomic Energy of Canada Limited Whiteshell Nuclear Research Establishment Pinava, Manitoba, Canada, pp. 274-289.

Kuo, T. J., Chang, C. S., Tung, L. T., Lee, Y. H., Chen, W. S. and Huang, Y. T. (2003) [In Chinese: 郭泰融、張傳聖、董倫道、李奕亨、陳文山、黃炎聰(2003)我國用過核燃料長程處置潛在處置母岩特性調查與評估階段-潛在處置母岩特性調查(91年計畫)－K區地球物理井測(BH1及BH2孔)報告，台灣電力公司委辦計畫，SNFD-ERL-90-195，工業技術研究院。]

Kurosawa S, Yui M, and Yoshikawa H, (1997), Experimental study of colloid filtration by compacted bentonite, In Gray W J, Triay I R (eds), Scientific basis for nuclear waste management XX: symposium held in Boston, Massachusetts, USA, 2–6 December 1996. Pittsburgh, PA: Materials Research Society. (Materials Research Society Symposium Proceedings 465), 963–970.

Lallemand, S., Theunissen, T., Schnürle, P., Lee, C.S., Liu, C.S. and Font, Y. (2013), Indentation of the Philippine Sea plate by the Eurasia plate in Taiwan: Details from recent marine seismological experiments, Tectonophysics, Vol. 594, pp. 60–79.

LANL (2018), Monte Carlo N–Particle® Transport Code System Version 6.2, Los Alamos National Laboratory, CCC-850.

Lee, S. W., Chien, K. L. and Chang, C. T. (2018) [In Chinese: 李思偉、簡光勵、張清土 (2018)，地下水化學組成對緩衝材料/回填材料影響研究報告，用過核子燃料最終處置計畫潛在處置母岩特性調查與評估階段發展功能/安全評估技術(104-107年度計畫)，SNFD-06-IPR-008-01，核能研究所。]

Lee, Y. H., Chen, W. S., Kuo, T. R. and Lin, W. (2007) [In Chinese: 李奕亨、陳文山、郭泰融、林蔚(2007)，用過核子燃料最終處置計畫-潛在處置母岩特性調查與評估階段-潛在處置母岩特性調查(94~96年度計畫)－地球物理孔內調查94~96年執行成果報告，台灣電力公司委辦計畫，SNFD-EEL-90-236，工業技術研究院。]

Lee, Y. H., Chen, W. S., Kuo, T. R. and Lin, W. (2009) [In Chinese: 李奕亨、陳文山、郭泰融、林蔚(2009)，用過核子燃料最終處置潛在處置母岩特性調查與評估階段潛在處置母岩特性調查(97-99

年度計畫)－KMBH06裂隙特性量測與分析-地球物理孔內調查與分析執行成果報告，台灣電力公司委辦計畫，SNFD-EEL-90-264，工業技術研究院。]

Lin, H. C. and Lee, L. H. (2011) [In Chinese: 林幸助、李麗華(2011)，金門國家公園沿海濕地碳通量調查計畫，金門國家公園管理處委託國立中興大學辦理報告。]

Lin, W., Chang, W. T. and Chang, C. S. (2003) [In Chinese: 林蔚、張育德、張傳聖(2003)我國用過核子燃料長程處置-潛在處置母岩特性調查與評估階(91年計畫)－K區花崗岩特性分析，台灣電力公司委辦計畫，SNFD-ERL-90-190，工業技術研究院。]

Lin, W., Chen, W. S. and Yang, M. T. (2005) [In Chinese: 林蔚、陳文山、楊明宗(2005)我國用過核子燃料長程處置潛在處置母岩特性調查與評估階段ー潛在處置母岩特性調查計畫- 潛在處置母岩特性調查，台灣電力公司委辦計畫，SNFD-ERL-90-219，工業技術研究院。]

Lin, W., Chien, C. M., Chiang, L.W., Chen, W. S. and Lin, C. K. (2007) [In Chinese: 林蔚、錢正明、蔣立為、陳文山、林鎮國(2007)用過核子燃料最終處置計畫潛在處置母岩特性調查與評估階段-潛在處置母岩特性調查(94~96年度計畫)-KMBH01-02-04地下地質概念模式報告，台灣電力公司委辦計畫，SNFD-EEL-90-247，工研院能資所。]

Lin, W., Chien, C. M., Kuo, T. R., Chen, W. S., Liao, C.W. and Lin, C. K. (2007) [In Chinese: 林蔚、錢正明、郭泰融、陳文山、廖啟雯、林鎮國(2007)K區潛在處置母岩地質概念模式評估--94~96 年執行成果報告，SNFD-ERL-90-242，工研院能資所。]

Lin, W., Lee, C. Y., Yang, H, C. and Chen, C. H. (2011) [In Chinese: 林蔚、李寄嵎、楊小青、陳正宏(2011)，台灣地質圖說明書-金門，五萬分之一地質圖幅，第77號，經濟部中央地質調查所。]

Lin, W., Lin, C. K., Chien, C. M., Chiang, L.W., Chang, Y.T., Yang, M.T., Yu, J.C. Chen, J. H. and Su, Y. H. (2007) [In Chinese: 林

蔚、林鎮國、錢正明、蔣立為、張育德、楊明宗、余錦昌、陳榮輝、蘇毓秀(2007)，用過核子燃料最終處置－潛在處置母岩特性調查(94~96年度計畫)－鑽探報告，台灣電力公司委辦計畫，SNFD-EEL-90-235，工業技術研究院。]

Lin, W., Lin, C. K., Chien, C. M., Hsieh, P. S., Chiang, L. W., Chang, Y. T., Chen, W. S., Lee, Y. H., Kuo, T. R., Liou, C. C., Chang, C. C. and Huang, S. Y. (2012) [In Chinese: 林蔚、林鎮國、錢正明、謝佩珊、蔣立為、張育德、陳文山、李奕亨、郭泰融、劉智超、張濟權、黃淞洋(2012)用過核子燃料最終處置計畫潛在處置母岩特性調查與評估階段－潛在處置母岩特性調查(99-101年度計畫)－K區調查成果(1999-2010)彙編，台灣電力公司委辦計畫，SNFD-GEL-90-290，工業技術研究院。]

Lindborg, T. (2010), Landscape Forsmark – data, methodology and results for SR-Site, SKB TR-10-05.

Liu, C. C. and Tien, N. C. (2015) [In Chinese: 劉智超、田能全(2015)我國用過核子燃料長程處置潛在處置母岩特性調查與評估階段--潛在處置母岩特性調查(101-103年度計畫)--花崗岩物性、熱及力學特性分析FY101~103執行成果報告，工研院執行/台灣電力公司委辦，SNFD-ITRI-90-311 / SNFD-ITRI-TR2015-0311。]

Liu, P. M. (2003) [In Chinese:劉平妹(2003)，乾溼冷暖孢粉知道，科學發展，第369期，第18–23頁。]

Luterkort, D., Gylling, B., and Johansson, R. (2012), Closure of the Spent Fuel Repository in Forsmark, Studies of alternative concepts for sealing of ramp, shafts and investigation boreholes, Technical Report TR-12-08, Swedish Nuclear Fuel and Waste Management Co.

Masurat, P., Eriksson, S. and Pedersen, K. (2010), Microbial sulphide production in compacted Wyoming bentonite MX-80 under in situ conditions relevant to a repository for high-level radioactive waste, Applied Clay Science, Vol. 47, pp 58–64.

McConchie, M. (2014), Five iron nails from the Roman hoard at Inchtuthil, Australian National University, from https://slll.cass.anu.edu.au/occasional-papers.

Ministry of Labor (2017) [In Chinese: 勞動部(2017)106年國際勞動統計，行政院勞動部。]

Murray-Wallace, C.V. and Woodroffe, W.D. (2014), Quaternary Sea-Level Changes – A Global Perspective, Cambridge University Press, 504p.

NDA/RWM/153 (2017), RWM, Geological Disposal. Methods for Management and Quantification of Uncertainty. NDA Report NDA/RWM/153, Radioactive Waste Management.

NEA (1995), Future human actions at disposal sites: a report from the NEA Working Group on Assessment of Future Human Actions at Radioactive Waste Disposal Sites, p18.

NEA (1997a), Disposal of Radioactive Waste. The Probabilistic System Assessment Group: History and Achievements, 1985-1994, OECD, Paris.

NEA (2005), Dverstorp, B., et al. "Management of uncertainty in safety cases and the role of risk." NEA News 23.1 (2005): 14-17.

~~NEA (2012), "Indicators in the Safety Case: A Report of the Integration Group on the Safety Case (IGSC)", OECD Publishing, Paris.~~

NEA (2012a), Methods for Safety Assessment of Geological Disposal Facilities for Radioactive Waste, Outcomes of the NEA MeSA Initiative, Radioactive Waste Management 2012.

NEA (2012b), "Indicators in the Safety Case: A Report of the Integration Group on the Safety Case (IGSC)", OECD Publishing, Paris.

NEA (2016), Scenario Development Workshop Synopsis, Integration Group for the Safety Case, Radioactive Waste Management, NEA/RWM/R(2015)3, March 2016.

NEA (2020), "Two decades of Safety Case Development: An IGSC 20th Anniversary Brochure."

Neretnieks, I., Liu, L. and Moreno, L. (2010), Mass transfer between waste canister and water seeping in rock fractures, Swedish Nuclear Fuel and Waste Management Company, SKB, TR-10-42.

NUMO (2021), わが国における安全な地層処分の実現－適切なサイトの選定に向けたセーフティケースの構築－, NUMO-TR-20-03付属書 6-1, 原子力発電環境整備機構.

OECD/NEA (2007), Regulating the Long- term Safety of Geological Disposal: Towards a Common Understanding of the Main Objectives and Bases of Safety Criteria, NEA No. 6182.

ORNL (2011), Scale: A Comprehensive Modeling and Simulation Suite for Nuclear Safety Analysis and Design, ORNL/TM-2005/39, Version 6.1, June 2011. Available from Radiation Safety Information Computational Center at Oak Ridge National Laboratory as CCC-785.

Pan, C.Y (2016) [In Chinese:離島結晶岩測試區地震危害度分析報告，用過核子燃料最終處置計畫潛在處置母岩特性調查與評估階段--發展功能/安全評估技術(104-107年度計畫)，台灣電力公司委辦計畫，核能研究所。]

POSIVA (2012), Safety case for the disposal of spent nuclear fuel at Olkiluoto – complementary considerations 2012, Posiva report, POSIVA 2012-11.

POSIVA (2013), Human Intruder Dose Assessment for Deep Geological Disposal, Working Report 2013-23.

POSIVA (2014), Radionuclide Transport in the Repository Near-Field and Far-Field, POSIVA, POSIVA 2014-02.

POSIVA (2019), POSIVA 2018-02, Nummi, Olli. "Plan for Uncertainty Assessment in the Safety Case for the Operating Licence Application.".

POSIVA and SKB (2017), Safety functions, performance targets and technical design requirements for a KBS-3V repository – Conclusions and recommendations form a joint SKB and POSIVA working group, POSIVA Oy and Swedish Nuclear Fuel and Waste Management Company, POSIVA-SKB-Report-01.

Rohling, E.J., Fenton, M., Jorissen, F.J., Bertrand, P., Ganssen, G., and Caulet, J.P. (1998), Magnitudes of sea-level lowstands of the past 500,000 years, Nature, Vol. 394, pp. 162–165.

Romero, L. (1995), Fast Multiple-Path Model to Calculate Radionuclide Release from the Near Field of a Repository, Volume 112, Nuclear Technology.

Ruddiman, W.F. (2008), Earth's Climate: Past and Future, 2nd edition, W.H. Freeman and Company. pp. 465

Sandén T, Nilsson U, Johannesson L-E, Hagman P, Nilsson G. (2018b), Sealing of investigation boreholes. Full scale field test and large-scale laboratory tests, Swedish Nuclear Fuel and Waste Management Company, SKB TR-18-18.

Sandén, T. and Börgesson, L. (2008), Deep repository-engineered barrier system, Piping and erosion in tunnel backfill, Laboratory tests to understand processes during early water uptake, Clay Technology AB, Swedish Nuclear Fuel and Waste Management Company, SKB, R-06-72.

Sandén, T. and Börgesson, L. (2010), Early effects of water inflow into a deposition hole, Laboratory tests results, Swedish Nuclear Fuel and Waste Management Company, SKB, R-10-70.

Sandén, T., Börgesson, L., Dueck, A., Goudarzi, R., and Lönnqvist, M. (2008), Deep repository-Engineered barrier system, Erosion and sealing processes in tunnel backfill materials investigated in laboratory, Clay Technology AB, Swedish Nuclear Fuel and Waste Management Company, SKB, R-08-135.

Sandén, T., Marjavaara P., and Fritzell, A, (2018a).Water Handling During Backfilling. Development report (Posiva SKB Report 05). POSIVA Oy and Swedish Nuclear Fuel and Waste Management Co.

SEPA and NIEA (2009), Geological Disposal Facilities on Land for Solid Radioactive Wastes: Guidance on Requirements for Authorisation.

Shih, Y. H., Chen, L. C. and Tsai, T. L. (2018) [In Chinese: 施宇鴻、陳亮丞、蔡翠玲(2018)，膠體於工程障壁及岩體裂隙之傳輸行為評估研究報告，台灣電力公司研究報告，SNFD-05-IPR-003-03。]

Shimazaki, K. (1986), Small and Large Earthquakes: The Effects of the Thickness of Seismogenic, Geophysical Monograph Series, Earthquake Source Mechanics, Vol. 37, pp. 209-216.

Shinjo, N., Yoshida, H. and Ota, K. (1997), An Analogue Study on Nuclide Migration in Tsukiyoshi Fault, Tono Uranium Deposit, Proc. Migration 97, pp. 94-95.

Siame, L., Chu, H.T., Carcaillet, J., Bourlès, D., Braucher, R., Lu, W.C., Angelier, J., and Dussouliez, Ph. (2007), Glacial retreat history of Nanhuta Shan (north-east Taiwan) from preserved glacial features: The cosmic ray exposure perspective, Quaternary Sciences Reviews, Vol. 26, pp. 2185–2200.

SKB (1994), Final report of the AECL/SKB Cigar Lake Analog Study, TR-94-04.

SKB (2003), Gas migration in KBS-3 buffer bentonite Sensitivity of test parameters to experimental boundary conditions, Swedish Nuclear Fuel and Waste Management Company, SKB, TR-03-02.

SKB (2004), Deep repository. Underground design premises, Edition D1/1, Swedish Nuclear Fuel and Waste Management Company, SKB, R-04-60.

SKB (2006a), Geosphere process report for the safety assessment SR-Can, TR-06-19.

SKB (2006b), Long-term safety for KBS-3 repositories at Forsmark and Laxemar – a first evaluation. Main report of the SR-Can project. SKB, TR-06-09.

SKB (2006c), The ecosystem models used for dose assessments in SR-Can, Swedish Nuclear Fuel and Waste Management Company, SKB, R-06-81.

SKB (2006d), The biosphere at Forsmark Data, assumptions and models used in the SR-Can assessment, Swedish Nuclear Fuel and Waste Management Company, SKB, R-06-82

SKB (2008), Excavation damage and disturbance in crystalline rock – results from experiments and analyses.SKB, TR-08-08.

SKB (2009a), Design premises for a KBS-3V repository based on results from the safety assessment SR-Can and some subsequent analyses, Swedish Nuclear Fuel and Waste Management Company, SKB, TR-09-22.

SKB (2009b), Underground design Forsmark. Layout D2, Swedish Nuclear Fuel and Waste Management Company, SKB, R-08-116.

SKB (2009c), Strategy for thermal dimensioning of the final repository for spent nuclear fuel, Swedish Nuclear Fuel and Waste Management Company, SKB, R-09-04.

SKB (2009d), Uneven swelling pressure on the canister simplified load cases derived from uneven wetting, rock contours and buffer density distribution, Document ID 1206894.

SKB (2010a), Spent nuclear fuel for disposal in the KBS-3 repository, Swedish Nuclear Fuel and Waste Management Company, SKB, TR-10-13.

SKB (2010b), Heikki Raiko, Rolf Sandström, Design analysis report for the canister, Swedish Nuclear Fuel and Waste Management Company, SKB, TR-10-28.

SKB (2010c), Design, production and initial state of buffer, Technical Report, Swedish Nuclear Fuel and Waste Management Company, SKB, TR-10-15.

SKB (2010d), Buffer, backfill and closure process report for the safety assessment SR-Site, Swedish Nuclear Fuel and Waste Management Company, SKB, TR-10-47.

SKB (2010e), Design, production and initial stat of the backfill and plug in deposition tunnels, Swedish Nuclear Fuel and Waste Management Company, SKB, TR-10-16.

SKB (2010f), Full perimeter intersection criteria, definitions and implementations in SR-Site, Swedish Nuclear Fuel and Waste Management Company, SKB, TR-10-21.

SKB (2010g), Groundwater Flow Modelling of the Excavation and Operational Phases, Swedish Nuclear Fuel and Waste Management Company, SKB, R-09-19.

SKB (2010h), Radionuclide transport report for the safety assessment SR-Site, Swedish Nuclear Fuel and Waste Management Company, SKB, TR-10-50.

SKB (2010i), Data report for the safety assessment SR-Site, Swedish Nuclear Fuel and Waste Management Company, SKB, R-10-52.

SKB (2010j), Design, Construction and Initial State of the Underground Openings, Swedish Nuclear Fuel and Waste Management Company, SKB, TR-10-18.

SKB (2010k), SR-Site Groundwater Flow Modelling Methodology, Setup and Results, Swedish Nuclear Fuel and Waste Management Company, SKB, R-09-22.

SKB (2010l), Corrosion calculations report for the safety assessment SR-Site, Swedish Nuclear Fuel and Waste Management Company, SKB, TR-10-66.

SKB (2010l), Design, production and initial state of the canister, Swedish Nuclear Fuel and Waste Management Company, SKB, TR-10-14.

SKB (2010m), Sorption of prioritized elements on montmorillonite colloids and their potential to transport radionuclides, Swedish Nuclear Fuel and Waste Management Company, SKB, TR-10-20.

SKB (2010n), Geosphere process report for the safety assessment SR-Site, Swedish Nuclear Fuel and Waste Management Company, SKB, TR-10-48.

SKB (2010o), Handling of future human actions in the safety assessment SR-Site, SKB, Technical Report TR-10-53.

SKB (2011), Long-term safety for the final repository for spent nuclear fuel at Forsmark -Main report of the SR-Site project Volume III, Swedish Nuclear Fuel and Waste Management Company, SKB TR-11-01.

SKB (2016), Clay erosion – impact of flocculation and gravitation, SKB, TR-16-11.

SKB (2017), Clay erosion - impact of flocculation and gravity, Swedish Nuclear Fuel and Waste Management Company, SKB, TR-16-11.

SKB, (2019). Supplementary information on canister integrity issues, TR-19-15.

Smart, N.R. and Adams, R. (2006), Natural analogues for expansion due to the anaerobic corrosion of ferrous materials, SKB Technical Report, TR-06-44, Stockholm, Sweden.

SSI (1998), The Swedish Radiation Protection Institute's Regulations on the Protection of Human Health and the Environment in connection wi th the Final Management of Spent Nuclear Fuel and Nuclear Waste, SSI FS 1998:1.

SSM (2008), Strålsäkerhetsmyndighetens föreskrifter och allmänna råd om säkerhet vid slutförvaring av kärnämne och kärnavfall (The Swedish Radiation Safety Authority's Regulations concerning Safety in connection with the Disposal of Nuclear Material and Nuclear Waste) (in Swedish). Stockholm: Strålsäkerhetsmyndigheten (Swedish Radiation Safety Authority). (SSMFS 2008:21)

SSM (2008b) , The Swedish Radiation Safety Authority's Regulations concerning the Protection of Human Health and the Environment in connection with the Final Management of Spent Nuclear Fuel and Nuclear Waste, SSMFS 2008:37.

STUK (2001), Long-term safety of disposal of spent nuclear fuel. Guide YVL 8.4. STUK (Radiation and Nuclear Safety Authority), Finland.

STUK (2013), Disposal of nuclear waste, Guide YVL D.5.

STUK (2014a), Guide YVL D.5. Disposal of nuclear waste. Radiation and Nuclear Safety Authority, Helsinki, Finland. ISBN 978-952-309-128-3.

STUK (2018), Disposal of Nuclear Waste, Radiation and Nuclear Safety Authority, GUIDE YVL D.5.

Stumm W., and Morgan, J. J. (1981), Aquatic Chemistry, 2nd ed. John Wiley and Sons.

Svensson, U. (2010), DarcyTools, Version 3.4, Verification, validation and demonstration, Swedish Nuclear Fuel and Waste Management Company, SKB, R-10-71.

Svensson, U. and Ferry, M. (2010), DarcyTools, Version 3.4, User's guide, Swedish Nuclear Fuel and Waste Management Company, SKB, R-10-72.

Svensson, U., Ferry, M., and Kuylenstierna, H. O. (2010), DarcyTools, Version 3.4 - Concepts, methods andequations, Swedish Nuclear Fuel and Waste Management Company, SKB, R-07-38.

Tien, N. C. and Liou, C. C. (2010) [In Chinese: 田能全、劉智超(2010)，用過核子燃料最終處置計畫潛在處置母岩特性調查與評估階段－潛在處置母岩特性調查(97-99年度計畫)－岩塊試驗97-99年執行成果報告，台灣電力公司委辦計畫，SNFD-EEL-90-275，工業技術研究院。]

Tien, N. C., Liou, C. C. and Huang, S. Y. (2012) [In Chinese: 田能全、劉智超、黃淞洋(2012)，用過核子燃料最終處置計畫-潛在處置母岩特性調查與評估階段-潛在處置母岩特性調查(99-101年度計畫)－岩塊熱傳試驗FY99-101年執行成果報告，台灣電力公司委辦計畫，SNFD-GEL-90-293，工業技術研究院。]

TraCE-21ka (2011), Simulation of Transient Climate Evolution over the last 21,000 years, NCAR; Retrieved 2019/10/2 from https://www.earthsystemgrid.org/dataset/ucar.cgd.ccsm.trace.html.

Tylecote, R. F. (1977), Durable Materials for Seawater: the Archaeological Evidence, The International Journal of Nautical Archaeology and Underwater Exploration, Vol.6, pp.269-283.

U.S. National Oceanic and Atmospheric Administration (NOAA) (2012), Oyster Reef Habitat, 2020/10/22 from https://www.fisheries.noaa.gov/national/habitat-conservation/oyster-reef-habitat

US NRC (1999), Spent Fuel Generation in an Independent Spent Fuel Storage Installation, Regulatory Guide 3.54, Revision 1.

US NRC (2007), A performance-Based Approach to Define the Site-Specific Earthquake Ground Motion, Regulatory Guide 1.208.

US NRC (2010), Technical Basis for the Proposed Expansion of the Regulatory Guide 3.54, “Decay Heat Generation in an Independent Spent Fuel Storage Installation,CR-6999, NUREG/CR-6999.

Velde, B. and Vasseur, G. (1992), Estimation of the diagenetic smectite to illite transformation in time-temperature space. American Mineralogist, Vol. 77, pp. 967-976.

Wang, K.L., Chung, S.L., O'Reilly S.Y., Sun, S.S., Shinjo, R., and Chen, C.H. (2004), Geochemical constraints for the genesis of post-collisional magmatism and the geodynamic evolution of the northern Taiwan region, Journal of Petrology, Vol. 45, Issue 5, pp. 975–1011.

Water Resource Agency (2017)[In Chinese: 水利署(2017)，106年水權統計-水權年報-一般水權登記引用水量-地下水，水利署。]

Wells, D. L. and Coppersmith, K. J. (1994), New empirical relationships among magnitude, rupture length, rupture width, rupture area, and surface displacement. Bull. Seism. Soc. Am, 84(4), pp. 974-1002.

Wen, K. L., Chien, W. Y., Chang, Y. W., Lin, C. M. and Kuo, C. H. (2011) [In Chinese: 溫國樑、簡文郁、張毓文、林哲民、郭俊翔(2011)面震源與衰減律參數研究及核電廠地盤反應量測，行政院原子能委員會核能研究所委辦計畫，國家地震工程研究中心。]

WHO (2009), WHO handbook on indoor randon: a public health perspective, World Health Organization.

Wu, W. N. and Zhao, L. (2013), Delineating seismogenic structures by a revised best estimate method: application to the Taiwan orogenic belt. J. Seismology, Vol. 17, pp. 545-556.

Xu, H., Qiu, X., Zhao, M., Sun, J., and Zhu, J. (2006), Characteristics of the crustal structure and hypocentral tectonics in the epicentral area of Nan'ao earthquake(M7.5), the northeastern South China Sea, Chinese Science Bulletin, Vo1. 51, Supp. II, pp. 95-106.

Yang, M. P., Chang, C. T. Hsiao, Y. H. and Chuang, Y. F. (2017) [In Chinese: 楊孟北，張清土，蕭宇翔、莊怡芳(2017)，緩衝材料基本性質研究報告，SNFD-06-IPR-001-03，核能研究所。]

Yang, M. T., Liu, C. H., Shen, C. N., Lin, C. T., Yang. M. S. and Lu, C.Y. (2003) [In Chinese: 楊明宗、柳志錫、沈振南、林棋財、楊敏順、呂金玉(2003)，我國用過核燃料長程處置潛在處置母岩特

性調查與評估階段--潛在處置母岩特性調查計畫(91年計畫)--K區(BH1及BH2)岩石力學報告，台灣電力公司委辦計畫，SNFD-ERL-90-199，工業技術研究院。]

Yen, Y. T. and Ma, K. F. (2011), Source-Scaling Relationship for M 4.6–8.9 Earthquakes, Specifically for Earthquakes in the Collision Zone of Taiwan, Bulletin of the Seismological Society of America, Vol. 101, No. 2, pp. 464–481, doi: 10.1785/0120100046.

Yokoyama, Y., K. Lambeck, De Deckker P., P Johnston, LK Fifield (2000), Timing of the Last Glacial Maximum from observed sea-level minima. Nature Vol. 406, pp. 713–716.

Yoshida, H., Kodama, K. and Ota, K. (1994), Role of Microscopic Flow-paths on Nuclide Migration in Sedimentary rocks, A Case Study form the Tono Uranium Deposit, Central Japan, Radiochim. Acta, Vol. 66/67, pp. 505-511.

Yu, S. B., Chen, H. Y., Kuo, L. C. (1997), Velocity field of GPS stations in the Taiwan area. Tectonophysics, Vol. 274, pp.41–59.

Zhou, J., Chen, J. T., Luo, M. H., Lee, M. A., Hsu, H. H., Kong, J. C., Tsou, C. H., Lu, M. M., Hong, C. W., Chen, Z. D., Cheng, C. T. (2017) [In Chinese: 周佳、陳佳婷、羅敏輝、李明安、許晃雄、洪志誠、鄒治華、盧孟明、洪致文、陳正達、鄭兆尊(2017)，臺灣氣候變遷科學報告2017-物理現象與機制。臺灣氣候變遷推估與資訊平台建置計畫。666頁。]

Appendix A: Process models for terrestrial module

Medium	No.	Process	Object	Expression	Parameter
Lower soil (L)	1	Upward flow	Upper soil	$\lambda_{LU,flow}=\frac{F_{LU,ter}}{d_{Lsoil}*\theta_{w,Lsoil}*R_{i,Lsoil}}$ $R_{i,Lsoil}=1+\frac{(1-\theta_{t,Lsoil})\rho_{Lsoil}}{\theta_{w,Lsoil}}K_{d,i,Lsoil}$ BIOMASS-6(2003, p338)	$\lambda_{ji,k}$：Transfer coefficients inputs to compartment *i* from compartment *j* by *k* process (1/yr) $F_{ji,ter}$：Flow from compartment j to compartment *i* of terrestrial module (m/yr) d_i：Thickness of compartment *i* (m) $\theta_{w,i}$：Water filled porosity of compartment *i* $\theta_{t,i}$：Total porosity of compartment *i* ρ_{Lsoil}：Grain density of compartment *i* (kg/m^3) R_i：Retardation coefficient of compartment *i* $K_{d,i}$：Sorption coefficient of compartment *i* (m^3/kg) BT_{LU}：Bioturbation rate (kgdw/m^2/yr) PP_i：Primary production of compartment *i* (kg/m2/yr) CR_i：Concentration ratio factor from root uptake to compartment *i* (mg/kgfw)/(mg/kgdw) Er_i：Erosion rate for the compartment *i* (m/yr) $Degas_i$：Degassing rate of compartment *i* (kgC/m^2/yr) DIC_i：Dissolved inorganic carbon in compartment *i* (kgC/m^3) $Bioloss_i$：Biomass loss rate of compartment *i* (kgDW/m^2/y) $Biomass_i$：Total biomass of compartment *i* (kgDW/m^2) NPP_t：Net primary production of compartment *i* (kg/m^2/yr) $mixH_t$：CO_2 Mixing height of terrestrial region (m) $C_{C,air}$：Carbon concentration in air (kg/m^3) vwind：wind speed (m/s) area：region area (m^2) Q_{IRR}：Well-water irrigation rate (m^3/yr) V_{well}：Well capacity (m^3)
	2	Downward flow	Deep soil	$\lambda_{LO,flow}==\frac{F_{LO,ter}}{d_{Lsoil}*\theta_{w,Lsoil}*R_{i,Lsoil}}$ $R_{i,Lsoil}=1+\frac{(1-\theta_{t,Lsoil})\rho_{Lsoil}}{\theta_{w,Lsoil}}K_{d,i,Lsoil}$ BIOMASS-6(2003, p338)	
	3	Bioturbation	Upper soil	$\lambda_{LU,Bio}=\frac{BT_{LU}}{\rho_{Lsoil}*d_{Lsoil}}$ POSIVA(2014, p33)	
Upper soil (U)	4	Root uptake (crop)	Crop	$\lambda_{Ucrop,root}=\frac{PP_{crop}*CR_{crop}}{(1-\theta_{t,Usoil})*\rho_{Usoil}*d_{Usoil}}$ BIOMASS-6(2003, p339)	
	5	Root uptake (tree)	Woods	$\lambda_{Uwood,root}=\frac{PP_{tree}*CR_{tree}}{(1-\theta_{t,Usoil})*\rho_{Usoil}*d_{Usoil}}$ BIOMASS-6(2003, p339)	
	6	Downward flow	Lower soil	$\lambda_{UL,\mathrm{flow}}=\frac{F_{UL,ter}}{d_{Usoil}*\theta_{w,Usoil}*R_{i,Usoil}}$ $R_{i,Usoil}=1+\frac{(1-\theta_{t,Usoil})\rho_{Usoil}}{\theta_{w,Usoil}}K_{d,i,Usoil}$ BIOMASS-6(2003, p338)	
	7	Bioturbation	Lower soil	$\lambda_{ULBio}=\frac{BT_{UL}}{\rho_{Usoil}*d_{Usoil}}$ POSIVA(2014, p33)	
Upper soil	8	Erosion	Water body	$\lambda_{UW,Er}=\frac{Er_U}{d_{Usoil}}$ BIOMASS-6(2003, p338)	$\lambda_{ji,k}$：Transfer coefficients inputs to compartment *i* from compartment *j* by *k* process (1/yr)

Medium	No.	Process	Object	Expression	Parameter
	9	Carbon degassing	Air	$\lambda_{Air,degas} = \frac{Degas_t}{DIC_t * d_{Usoil}}$ Avila et al. (2008, p108)	$F_{ji,ter}$：Flow from compartment *j* to compartment *i* of terrestrial module (m/yr) d_i：Thickness of compartment *i* (m) $\theta_{w,i}$：Water filled porosity of compartment *i* $\theta_{t,i}$：Total porosity of compartment *i* ρ_{Lsoil}：Grain density of compartment *i* (kg/m^3) $R_{i,j}$：Retardation coefficient of compartment *j* for radionuclide *i* $K_{di,j}$：Sorption coefficient of compartment *j* for radionuclide *i* (m^3/kg) BT_{ji}：Bioturbation rate from compartment *j* to compartment *i* ($kgdw/m^2/yr$) PP_i：Primary production of compartment *i* (kg/m2/yr) CR_i：Concentration ratio factor from root uptake to compartment *i* (mg/kgfw)/(mg/kgdw) Er_i：Erosion rate for the compartment *i* (m/yr) $Degas_i$：Degassing rate of compartment *i* ($kgC/m^2/yr$) DIC_i：Dissolved inorganic carbon in compartment *i* (kgC/m^3) $Bioloss_i$：Biomass loss rate of compartment *i* ($kgDW/m^2/y$) $Biomass_i$：Total biomass of compartment *i* ($kgDW/m^2$) NPP_t：Net primary production of compartment *i* ($kg/m^2/yr$) $mixH_t$：CO_2 Mixing height of terrestrial region (m) $C_{C,air}$：Carbon concentration in air (kg/m^3) vwind：wind speed (m/s) area：region area (m^2) Q_{IRR}：Well-water irrigation rate (m^3/yr) V_{well}：Well capacity (m^3)
Cropland (crop)	10	Senescence/ Litter fall fall	Upper soil	$\lambda_{cropU,loss} = \frac{Bioloss_{crop}}{Biomass_{crop}}$ POSIVA(2014, p33)	
Woods (wood)	11	Senescence/ Litter fall	Upper soil	$\lambda_{woodU,loss} = \frac{Bioloss_{tree}}{Biomass_{crop}}$ POSIVA(2014, p33)	
Air	12	photosynthesis	Woods and crop	$\lambda_{\mathrm{Air,phosyn}} = \frac{\mathrm{NPP_t}}{\mathrm{mixH_t} * \mathrm{C_{C,air}}}$ POSIVA(2014, p33)	
	13	Air flow	Air or sink	$\lambda_{\mathrm{air,air}} = \frac{\mathrm{v_{wind}}}{\sqrt{\mathrm{area}/\pi}}$ POSIVA(2014, p33)	
Well-water (well)	14	Irrigation	Upper soil	$\lambda_{wellU,irr} = \frac{Q_{IRR}}{V_{well}}$ JNC(2000, pD-4)	

Reference for Appendix A.
IAEA (2003), Reference Biosphere for Solid Radioactive Waste Disposal: Report of BIOMASS Theme 1 of BIOsphere Modelling and ASSessment Programme, IAEA-BIOMASS-6, International Atomic Energy Agency, Vienna.
POSIVA (2014), Radionuclide Transport and Dose Assessment for Humans in the Biosphere Assessment BSA-2012, POSIVA.
Avila, R. and Ekström, P. A., (2010), Landscape dose conversion factors used in the safety assessment SR-Site, SKB TR-10-06.

Appendix B: Process models for aquatic module

General processes for aquatic module					
Medium	**No.**	**Process**	**Object**	**Expression**	**Parameter**
Soil (S)	1	Upward flow	Sediment	$\lambda_{SSed,flow} = \frac{F_{SSed,w}}{d_{soilw} * \theta_{w,soilw} * R_{i,soilw}}$ $R_{i,soilw} = 1 + \frac{(1-\theta_{t,soilw})\rho_{soilw}}{\theta_{w,soilw}} K_{di,soilw}$ BIOMASS-6(2003, p338)	$\lambda_{ji,k}$：Transfer coefficients inputs to compartment *i* from compartment *j* by *k* process (1/yr) $F_{ji,w}$：Flow from compartment *j* to compartment *i* of aquatic module (m/yr) d_i：Thickness of compartment *i* (m) $\theta_{w,i}$：Water filled porosity of compartment *i* $\theta_{t,i}$：Total porosity of compartment *i* ρ_i：Grain density of compartment *i* (kg/m^3) $R_{i,j}$：Retardation coefficient of compartment *j* for radionuclide *i* $K_{di,j}$：Sorption coefficient of compartment *j* for radionuclide *i* (m^3/kg) BT_{ji}：Bioturbation rate from compartment *j* to compartment *i* (kgdw/m^2/yr) PP_i：Primary production of compartment *i* (kg/m2/yr) CR_i：Concentration ratio factor from root uptake to compartment *i* (mg/kgfw)/(mg/kgdw) $Resus_{ji}$：Resuspension rate from compartment *j* to compartment *i* (kg/m^2/y) $NetSed_{ji}$：Net sedimentation rate from compartment *j* to compartment *i* (kg/m^2/yr) $Sedi_{ji}$：Sedimentation rate from compartment *j* to compartment *i* (kgdw/m^2/yr) C_{SS}：Suspend solid concentration in waterbody (kg/m^3) $Degas_i$：Degassing rate of compartment *i* (kgC/m^2/yr) DIC_i：Dissolved inorganic carbon in compartment *i* (kgC/m^3) $Bioloss_i$：Biomass loss rate of compartment *i* (kgDW/m^2/y) $Biomass_i$：Total biomass of compartment *i* (kgDW/m^2) $Dissolve_i$：Carbon dissolving rate of compartment *i* (kgC/m^2/yr) $C_{C,air}$：Carbon concentration in air (kg/m^3) vwind：wind speed (m/s) area：region area (m^2)
	2	Downward flow	Deep soil	$\lambda_{SO,flow} = \frac{F_{SO,w}}{d_{soilw} * \theta_{w,soilw} * R_{i,soilw}}$ $R_{i,soilw} = 1 + \frac{(1-\theta_{t,soilw})\rho_{soilw}}{\theta_{w,soilw}} K_{d,i,soilw}$ BIOMASS-6(2003, p338)	
	3	Bioturbation	Sediment	$\lambda_{SSedBio} = \frac{BT_{SSed}}{\rho_{soilw} * d_{soilw}}$ POSIVA(2014, p29)	
Sediment (Sed)	4	Downward flow	Soil	$\lambda_{SedS,flow} = \frac{F_{SedS,w}}{d_{sed} * \theta_{w,sed} * R_{i,sed}}$ $R_{i,sed} = 1 + \frac{(1-\theta_{t,sed})\rho_{sed}}{\theta_{w,sed}} K_{d,i,sed}$ BIOMASS-6(2003, p338)	
	5	Bioturbation	Soil	$\lambda_{SedS,Bio} = \frac{BT_{SedS}}{\rho_{sed} * d_{sed}}$ POSIVA(2014, p29)	

Sediment (Sed)	6	Resuspension	Waterbody	$\lambda_{sedw,resus} = \frac{Resus_{sed}}{\rho_{sed} * d_{sed}}$ POSIVA(2014, p29)	$\lambda_{ji,k}$：Transfer coefficients inputs to compartment *i* from compartment *j* by *k* process (1/yr) $F_{ji,w}$：Flow from compartment *j* to compartment *i* of aquatic module (m/yr) d_i：Thickness of compartment *i* (m) $\theta_{w,i}$：Water filled porosity of compartment *i* $\theta_{t,i}$：Total porosity of compartment *i* ρ_i：Grain density of compartment *i* (kg/m^3) $R_{i,j}$：Retardation coefficient of compartment *j* for radionuclide *i* $K_{di,j}$：Sorption coefficient of compartment *j* for radionuclide *i* (m^3/kg) BT_{ji}：Bioturbation rate from compartment *j* to compartment *i* (kgdw/m^2/yr) PP_i：Primary production of compartment *i* (kg/m2/yr) CR_i：Concentration ratio factor from root uptake to compartment *i* (mg/kgfw)/(mg/kgdw) $Resus_{ji}$：Resuspension rate from compartment *j* to compartment *i* (kg/m^2/y) $NetSed_{ji}$：Net sedimentation rate from compartment *j* to compartment *i* (kg/m^2/yr) $Sedi_{ji}$：Sedimentation rate from compartment *j* to compartment *i* (kgdw/m^2/yr) C_{SS}：Suspend solid concentration in waterbody (kg/m^3) $Degas_i$：Degassing rate of compartment *i* (kgC/m^2/yr) DIC_i：Dissolved inorganic carbon in compartment *i* (kgC/m^3) $Bioloss_i$：Biomass loss rate of compartment *i* (kgDW/m^2/y) $Biomass_i$：Total biomass of compartment *i* (kgDW/m^2) $Dissolve_i$：Carbon dissolving rate of compartment *i* (kgC/m^2/yr) $C_{C,air}$：Carbon concentration in air (kg/m^3) vwind：wind speed (m/s) $area_i$：region area of landscape *i* (m^2)
	7	Net sedimentation	Soil	$\lambda_{seds,netsed} = \frac{NetSed_{sed}}{\rho_{sed} * d_{sed}}$ POSIVA(2014, p29)	
Waterbody (w)	8	Sedimentation	Sediment	$\lambda_{Sedw,sedi} = \frac{Sedi_w}{d_w} * \frac{K_{d,i,ss}}{R_w}$ $R_{i,w} = 1 + K_{d,i,ss} * C_{ss}$ ss: suspended solids POSIVA(2014, p29)	
	9	Uptake	Primary production	$\lambda_{wpp,uptake} = \frac{PP_w * CR_w}{d_w * R_{i,w}}$ $R_{i,w} = 1 + K_{d,i,ss} * C_{ss}$ POSIVA(2014, p29)	
	10	Degassing	Air	$\lambda_{wair,degas} = \frac{Degas_w}{DIC_w * d_w}$ Avila et al. (2008, p108)	
Primary production (PP)	11	Senescence	Sediment	$\lambda_{ppsed,loss} = \frac{Bioloss_w}{Biomass_w}$ POSIVA(2014, p29)	
Air	12	Carbon dissolving	Waterbody	$\lambda_{airw,dissolve} = \frac{Dissolve_w}{mixH_t * C_{C,air}}$ Avila et al. (2008, p109)	
	13	Air flow	Air or Sink	$\lambda_{air,air} = \frac{v_{wind}}{\sqrt{area_{ter}/\pi}}$ POSIVA(2014, p29)	
Freshwater specific processes for aquatic module					
Medium	**No.**	**Process**	**Object**	**Expression**	**Parameter**
Sediment (Sed)	14	Dredging	Upper soil	$\lambda_{dig,sed,fw} = Digsed_{fw}$ JNC(2000, pD-2)	

Medium	No.	Process	Object	Expression	Parameter
	15	Bed-load	Sea Sediment	$\lambda_{bedload,r} = \frac{K_{d,i,sed} * Bedload_r}{R_{i,sed} * \theta_{r,sed}}$ JNC(2000, pD-3)	$\lambda_{ji,k}$：Transfer coefficients inputs to compartment *i* from compartment *j* by *k* process (1/yr) $Digsed_{fw}$：Dredging rate of freshwater sediment(1/yr) $R_{i,j}$：Retardation coefficient of compartment *j* for radionuclide *i* $K_{di,j}$：Sorption coefficient of compartment *j* for radionuclide *i* (m^3/kg) $\theta_{w,i}$：Water filled porosity of compartment *i* $Flood_{fw}$：Flooding rate of freshwater waterbody(m^3/yr) d_i：Thickness of compartment *i* (m) $area_i$：region area of landscape *i* (m^2) Irr_{fw}：Irrigation rate (m/yr) $outflow_i$：Outflow of the catchment (m^3/yr) F_{pre}：Precipitation (m/yr) F_{runoff}：Surface runoff (m/yr)
Waterbody (w)	16	Flooding	Upper soil	$\lambda_{flooding,fw} = \frac{Flood_{fw}}{d_w * area_w}$ JNC(2000, pD-1)	
	17	Irrigation	Upper soil	$\lambda_{irr,fw} = \frac{Irr_{fw} * area_{crop}}{d_w * area_{fw}}$ JNC(2000, pD-1)	
	18	River flow	Water body	$\lambda_{flow,fw} = \frac{outflow_i}{d_{fw} * area_{fw}}$ $outflow_i = outflow_{i-1} + (F_{pre} * area_{fw}) + (F_{runoff} * area_{ter})$ (Derived)	
Sea specific processes for aquatic module					
Medium	**No.**	**Process**	**Object**	**Expression**	**Parameter**
Waterbody (w)	19	Sea-spray	Upper soil	$\lambda_{\mathrm{seaspray},s} = seaspray_s * sspinhance_s$ JNC(2000, pD-4)	$\lambda_{ji,k}$：Transfer coefficients inputs to compartment *i* from compartment *j* by *k* process (1/yr) $seaspray_s$：Sea spray rate (1/yr) $sspinhance_s$：Sea spray enhancement factor $outflow_i$：Outflow of the catchment (m^3/yr) d_i：Thickness of compartment *i* (m) $area_i$：region area of landscape *i* (m^2) F_{pre}：Precipitation (m/yr) F_{runoff}：Surface runoff (m/yr)
	20	Marine discharge	Sink	$\lambda_{\mathrm{seatosink}} = \frac{outflow_i}{d_s * area_s}$ $outflow_i = outflow_{i-1} + (F_{pre} * area_{fw}) + (F_{pre} * area_s) + (F_{runoff} * area_{ter})$ (Derived)	

Reference for Appendix B

IAEA (2003), Reference Biosphere for Solid Radioactive Waste Disposal: Report of BIOMASS Theme 1 of BIOsphere Modelling and ASSessment Programme, IAEA-BIOMASS-6, International Atomic Energy Agency, Vienna.

POSIVA (2014), Radionuclide Transport and Dose Assessment for Humans in the Biosphere Assessment BSA-2012, POSIVA.

Avila, R. and Ekström, P. A., (2010), Landscape dose conversion factors used in the safety assessment SR-Site, SKB TR-10-06.

JNC (2000), H12: Project to Establish the Scientific and Technical Basis for HLW Disposal in Japan – Supporting report 3, Japan Nuclear Cycle Development Institute, JNC TN1410 2000-004.

Appendix C: Ingestion exposure pathways model for dose calculation model

<table>
<tr><th>Pathways</th><th>Medium</th><th>Expression</th><th>Parameter</th></tr>
<tr><td>Water</td><td>Waterbody</td><td>$D_{i,ingw}=DCF_{i,ing}*ING_w*C_{i,w}$</td><td rowspan="14">$D_{i,j}$：The annual individual dose from the pathway j by radionuclide i (Sv/y)
$DCF_{i,j}$：Ingestion dose conversion factor of radionuclide i for pathway j (Sv/Bq)
ING_i：Human's ingestion rate of food i (m^3/y)
$C_{i,j}$：concentration of radionuclide i in medium j(Bq/m^3)
$F_{p1,i}$ ：External contamination due to soil, food processing retained fraction of radionuclide i
$F_{p2,i}$ ：Internal food processing retained fraction of radionuclide i
$F_{p3,i}$ ：External food processing retained fraction of radionuclide i
$CF_{i,j}$：Concentration factor of radionuclide i for medium j (mg/kgfw)/(mg/kgdw)
S_{crop} ：Crop soil contamination(kgdw/ kgfw)
$\theta_{t,i}$：Total porosity of compartment i
θ_i：Wet soil porosity of compartment i
ρ_i：Grain density of compartment i (kg/m^3)
I_{crop} ：Interception factor for crop
V_{irr}：Irrigation rate
$F_{i,tr}$ ：Translocation factor of radionuclide i
Y ：Crop annual yield (kg/y)
W_i ：Weathering rate of radionuclide i (y^{-1})
T ：Time from irrigation to harvest (y)
$TF_{ing,i,j}$：Animal product transfer factor from ingestion of radionuclide i for animal j (d/kg)
$TF_{inh,i,j}$：Animal product transfer factor from inhalation of radionuclide i for animal j (d/kg)
$INGA_i$：Ingestion rate for animal i (kgfw/d)
$INGWA_i$：Water ingestion rate for animal i (m^3/d)
$INGSA_i$：Soil ingestion rate for animal i (m^3/d)
$R_{i,j}$：Retardation coefficient of compartment j for radionuclide i
$K_{di,j}$：Sorption coefficient of compartment j for radionuclide i (m^3/kg)</td></tr>
<tr><td>Root vegetable</td><td>Upper Soil,</td><td rowspan="4">$D_{i,ingcrop}=DCF_{i,ing}*ING_{crop}*C_{i,crop}$
$C_{i,crop}=\frac{(F_{i,p2}CF_{i,crop}+F_{i,p1}S_{crop})C_{i,U}}{(1-\theta_{t,U})\rho_U}+I_{crop}V_{irr}C_{i,w}\left(\frac{e^{-W_iT}F_{i,p3}+F_{i,p2}F_{i,tr}}{Y}\right)$
IAEA(2003, p340)
$C_{C-14,crop}=\frac{C_{C14,air}}{C_{C,air}}\times C_{sC,corp}$
(Derived)</td></tr>
<tr><td>Green vegetable</td><td>Upper Soil, Waterbody</td></tr>
<tr><td>Grain</td><td>Upper Soil, Waterbody</td></tr>
<tr><td>Fruit</td><td>Upper Soil, Waterbody</td></tr>
<tr><td>Beef</td><td>Upper Soil, Waterbody, Air</td><td rowspan="7">$D_{i,ingprod}=DCF_{i,ing}*ING_{prod}*C_{i,prod}$
$C_{i,prod}=TF_{ing,i,prod}\left(C_{i,crop}INGA_i+C_{i,w}INGWA_i+\frac{C_{i,U}INGSA_i}{(1-\theta_{t,U})\rho_U+\theta_U\rho_w}\right)$
$+TF_{inh,i,prod}\left(BR_aO_a(C_{i,airs}+C_{C14,air})\right)$
$TF_{inh,i,prod}=TF_{ing,i,prod}\frac{f_L+f_Cf_1(inh)}{f_1(ing)}$
$C_{i,airs}=\frac{C_{i,s}(R-1)dust_s}{(1-\theta_{t,U})\rho_UR_U}$
$R=1+\frac{(1-\theta_{t,U})\rho K_{d,i,s}}{\theta_U}$
IAEA(2003, p341)</td></tr>
<tr><td>Pork</td><td>Upper Soil, Waterbody, Air</td></tr>
<tr><td>Chicken</td><td>Upper Soil, Waterbody, Air</td></tr>
<tr><td>Milk</td><td>Upper Soil, Waterbody, Air</td></tr>
<tr><td>Pig offal</td><td>Upper Soil, Waterbody, Air</td></tr>
<tr><td>Egg</td><td>Upper Soil, Waterbody, Air</td></tr>
<tr><td>Freshwater fish</td><td>Waterbody (freshwater)</td><td rowspan="2">$D_{i,ingaqfood}=DCF_{i,ing}*ING_{aqfood}*C_{i,aqfood}$
$C_{i,aqfood}=FF_{sed}C_{i,w}CF_{i,aqfood}$
$FF_{sed}=\frac{1}{1+K_{d,i,sed}\alpha_s}$
IAEA(2003, p446-p447)
$C_{C-14,aqfood}=\frac{C_{C14,water}}{DIC}\times C_{sC,aqfood}$
(Derived)</td></tr>
<tr><td>Oyster</td><td>Waterbody (Sea)</td></tr>
</table>

			BR_a ：Animal breathing rate (m^3/hr) O_a ：Animal occupancy (hr/d) f_L ：Fraction of inhaled activity reaching the systemic circulation f_C ：Fraction of inhaled activity that is cleared to the gastrointestinal tract $f_{1(inh)}$：Fraction of inhaled activity, cleared to the gastrointestinal tract $f_{1(ing)}$：fraction of ingested activity reaching the body fluids $dust_s$ ：Dust level in the air (kg/m^3) FF_{sed} ：Fraction of activity in the filtered lake water $CF_{i,aqfood}$：Crop concentration factor of radionuclide *i* for water food (Bq/kgfw)/(Bq/l) $C_{sC,aqfood}$：Stable carbon concentration of water food(gC/kg) DIC_i：Dissolved inorganic carbon in compartment *i* (kgC/m^3)

Reference for Appendix C

IAEA (2003), Reference Biosphere for Solid Radioactive Waste Disposal: Report of BIOMASS Theme 1 of BIOsphere Modelling and ASSessment Programme, IAEA-BIOMASS-6, International Atomic Energy Agency, Vienna.

Appendix D: Inhalation and external exposure pathways model for dose calculation model

<table>
<tr><th>Pathways</th><th>Medium</th><th>Expression</th><th>Parameter</th></tr>
<tr><td>Dust inhalation (soil)</td><td>Upper soil</td><td>$D_{i,inh}=DCF_{i,inh}*BR*OS*C_{i,air}$
$C_{i,airs}=\frac{C_{i,U}(R_{i,U}-1)\mathrm{dust}_s}{(1-\theta_t)\rho R_{i,s}}$
$R_{i,s}=1+\frac{(1-\theta_{ts})\rho_s K_{d,i,s}}{\theta_s}$
IAEA(2003, p338-p342)</td><td rowspan="6">$D_{i,j}$：The annual individual dose from the pathway *j* by radionuclide *i* (Sv/y)
$DCF_{i,j}$：Ingestion dose conversion factor of radionuclide *i* for pathway *j* (Sv/Bq)
$C_{i,j}$：concentration of radionuclide *i* in medium *j*(Bq/m^3)
$R_{i,j}$：Retardation coefficient of compartment *j* for radionuclide *i*
$K_{di,j}$：Sorption coefficient of compartment *j* for radionuclide *i* (m^3/kg)
$\theta_{t,i}$：Total porosity of compartment *i*
ρ_i：Grain density of compartment *i* (kg/m^3)
$dust_s$ ：Dust level in the air (kg/m^3)
O_i：Human occupancy for compartment *i* (hr/d)
AIRaero：Concentration of aerosol in air (m^3/m^3)</td></tr>
<tr><td>Dust inhalation (sediment)</td><td>Sediment</td><td>$C_{i,airsed}=\frac{C_{i,sed}(R_{i,sed}-1)\mathrm{dust}_{sed}}{(1-\theta_{tsed})\rho_{sed}R_{i,sed}}$
$R_{i,sed}=1+\frac{(1-\theta_{tsed})\rho_{sed}K_{d,i,sed}}{\theta_{sed}}$
(Derived)</td></tr>
<tr><td>Aerosol inhalation (waterbody)</td><td>Waterbody</td><td>$D_{inhaero}=DCF_{inh}\,BR\,O_w\,\mathrm{AIR}_{aero}\,C_{i,w}$
IAEA(2003, p344)</td></tr>
<tr><td>External- soil</td><td>Upper soil</td><td>$D_{i,exts}=DCF_{ext}*O_s*C_{i,s}$
IAEA(2003, p343)</td></tr>
<tr><td>External- sediment</td><td>Sediment</td><td>$D_{i,extsed}=DCF_{ext}*O_{sed}*C_{i,sed}$
IAEA(2003, p343)</td></tr>
<tr><td>External-immerse</td><td>Waterbody</td><td>$D_{i,immw}=DCF_{i,imw}*O_w*C_{i,w}$
IAEA(2003, p343)</td></tr>
</table>

Reference for Appendix D

IAEA (2003), Reference Biosphere for Solid Radioactive Waste Disposal: Report of BIOMASS Theme 1 of BIOsphere Modelling and ASSessment Programme, IAEA-BIOMASS-6, International Atomic Energy Agency, Vienna.

Appendix E: Dataset for Biosphere Assessment

(1) Radionuclides considered in the biosphere assessment

Chain	Nuclide	Atomic weight (g/mol)	Half-live (y)	Daughter
Fission/ Activation products	C-14	14.0032	5.70×10^{3}	-
	Cl-36	35.9683	3.01×10^{5}	-
	Ni-59	58.9343	7.60×10^{4}	-
	Se-79	78.9185	2.95×10^{5}	-
	Sr-90	89.9077	2.89×10^{1}	-
	Zr-93	92.9065	1.61×10^{6}	-
	Nb-94	93.9073	2.03×10^{4}	-
	Tc-99	98.9063	2.11×10^{5}	-
	Pd-107	106.905	6.50×10^{6}	-
	Sn-126	125.908	2.30×10^{5}	-
	I-129	128.905	1.57×10^{7}	-
	Cs-135	134.906	2.30×10^{6}	-
	Cs-137	136.907	3.01×10^{1}	-
4N	Th-232	232.038	1.40×10^{10}	-
	U-236	236.046	2.34×10^{7}	Th-232
	Pu-240	240.054	6.56×10^{3}	U-236
4N+1	Th-229	229.032	7.93×10^{3}	-
	U-233	233.040	1.59×10^{5}	Th-229
	Np-237	237.048	2.14×10^{6}	U-233
	Am-241	241.057	4.32×10^{2}	Np-237
	Cm-245	245.065	8.42×10^{3}	Am-241
4N+2	Pb-210	209.984	2.22×10^{1}	Po-210
	Ra-226	226.025	1.60×10^{3}	Pb-210
	Th-230	230.033	7.54×10^{4}	Ra-226
	U-234	234.041	2.45×10^{5}	Th-230
	U-238	238.051	4.47×10^{9}	U-234
	Pu-238	238.05	8.77×10^{1}	U-234
	Pu-242	242.059	3.75×10^{5}	U-238
	Cm-246	246.067	4.71×10^{3}	Pu-242
4N+3	Ac-227	227.028	2.18×10^{1}	-
	Pa-231	231.036	3.28×10^{4}	Ac-227
	U-235	235.044	7.04×10^{8}	Pa-231
	Pu-239	239.052	2.41×10^{4}	U-235
	Am-243	243.061	7.37×10^{3}	Pu-239

(2) Sorption coefficients of soil (m^3/kg)

	Best est.	Min.	Max.	Data source
C-14	1.00×10^{-1}	0.00	1.00×10^{-1}	Kato and Suzuki(2008, p42)
Cl-36	3.00×10^{-4}	4.00×10^{-5}	1.20×10^{-3}	IAEA(2010, p33)，All soils
Ni-59	2.80×10^{-1}	3.00×10^{-3}	7.20×10^{0}	IAEA(2010, p31)，All soils
Se-79	2.00×10^{-1}	4.00×10^{-3}	2.10×10^{0}	IAEA(2010, p33)，All soils
Sr-90	5.20×10^{-2}	4.00×10^{-4}	6.50×10^{0}	IAEA(2010, p31)，All soils
Zr-93	4.10×10^{-1}	2.00×10^{-3}	1.00×10^{1}	IAEA(2010, p33)，All soils
Nb-94	1.50×10^{0}	1.60×10^{-1}	8.40×10^{0}	IAEA(2010, p33)，All soils
Tc-99	2.30×10^{-4}	1.00×10^{-5}	1.10×10^{-2}	IAEA(2010, p33)，All soils
Pd-107	1.80×10^{-1}	5.50×10^{-2}	6.70×10^{-1}	IAEA(2010, p33)，All soils
Sn-126	1.60×10^{0}	1.30×10^{-1}	3.10×10^{1}	IAEA(2010, p33)，All soils
I-129	6.90×10^{-3}	1.00×10^{-5}	5.80×10-1	IAEA(2010, p31)，All soils
Cs-135	1.20×10^{0}	4.30×10^{-3}	3.80×10^{2}	IAEA(2010, p31)，All soils
Cs-137	1.20×10^{0}	4.30×10^{-3}	3.80×10^{2}	IAEA(2010, p31)，All soils
Th-232	1.90×10^{0}	1.80×10^{-2}	2.50×10^{2}	IAEA(2010, p31)，All soils
U-236	2.00×10^{-1}	7.00×10^{-4}	6.70×10^{1}	IAEA(2010, p31)，All soils
Pu-240	7.40×10^{-1}	3.20×10^{-2}	9.60×10^{0}	IAEA(2010, p33)，All soils
Th-229	1.90×10^{0}	1.80×10^{-2}	2.50×10^{2}	IAEA(2010, p31)，All soils
U-233	2.00×10^{-1}	7.00×10^{-4}	6.70×10^{1}	IAEA(2010, p31)，All soils
Np-237	3.50×10^{-2}	1.30×10^{-3}	1.20×10^{0}	IAEA(2010, p33)，All soils
Am-241	2.60×10^{0}	5.00×10^{-2}	1.10×10^{2}	IAEA(2010, p33)，All soils
Cm-245	9.30×10^{0}	1.90×10^{-1}	5.20×10^{1}	IAEA(2010, p33)，All soils
Pb-210	2.00×10^{0}	2.50×10^{-2}	1.30×10^{2}	IAEA(2010, p33)，All soils
Ra-226	2.50×10^{0}	1.20×10^{-2}	9.50×10^{2}	IAEA(2010, p33)，All soils
Th-230	1.90×10^{0}	1.80×10^{-2}	2.50×10^{2}	IAEA(2010, p31)，All soils
U-234	2.00×10^{-1}	7.00×10^{-4}	6.70×10^{1}	IAEA(2010, p31)，All soils
U-238	2.00×10^{-1}	7.00×10^{-4}	6.70×10^{1}	IAEA(2010, p31)，All soils
Pu-238	7.40×10^{-1}	3.20×10^{-2}	9.60×10^{0}	IAEA(2010, p33)，All soils
Pu-242	7.40×10^{-1}	3.20×10^{-2}	9.60×10^{0}	IAEA(2010, p33)，All soils
Cm-246	9.30×10^{0}	1.90×10^{-1}	5.20×10^{1}	IAEA(2010, p33)，All soils
Ac-227	1.70×10^{0}	4.50×10^{-1}	5.40×10^{0}	IAEA(2010, p33)，All soils
Pa-231	2.00×10^{0}	5.40×10^{-1}	6.60×10^{0}	IAEA(2010, p33)，All soils
U-235	2.00×10^{-1}	7.00×10^{-4}	6.70×10^{1}	IAEA(2010, p31)，All soils
Pu-239	7.40×10^{-1}	3.20×10^{-2}	9.60×10^{0}	IAEA(2010, p33)，All soils
Am-243	2.60×10^{0}	5.00×10^{-2}	1.10×10^{2}	IAEA(2010, p33)，All soils
Po-210	2.10×10-1	1.20×10-2	7.00×10^{0}	IAEA(2010, p33)，All soils

(3) Sorption coefficients of freshwater sediment (m^3/kg)

	Best est.	Min.	Max.	Data source
C-14	1.00×10^{-1}	0.00	2.00×10^{0}	Kato and Suzuki(2008, p42)
Cl-36	1.00×10^{0}	0.00	1.00×10^{0}	Kato and Suzuki(2008, p42)
Ni-59	1.00×10^{1}	4.00×10^{-3}	1.00×10^{1}	Kato and Suzuki(2008, p42)
Se-79	1.00×10^{-2}	4.00×10^{-3}	5.00×10^{0}	Kato and Suzuki(2008, p42)
Sr-90	5.00×10^{-1}	3.00×10^{-3}	1.00×10^{0}	Kato and Suzuki(2008, p42)
Zr-93	1.00×10^{1}	5.00×10^{-3}	1.00×10^{1}	Kato and Suzuki(2008, p42)
Nb-94	1.00×10^{1}	1.00×10^{-2}	1.00×10^{2}	Kato and Suzuki(2008, p42)
Tc-99	1.00×10^{-1}	0.00	2.00×10^{-1}	Kato and Suzuki(2008, p42)
Pd-107	2.00×10^{0}	4.00×10^{-3}	1.00×10^{1}	Kato and Suzuki(2008, p42)
Sn-126	1.00×10^{1}	5.00×10^{-3}	5.00×10^{1}	Kato and Suzuki(2008, p42)
I-129	1.00×10^{-1}	0.00	3.00×10^{-1}	Kato and Suzuki(2008, p42)
Cs-135	2.00×10^{0}	1.00×10^{0}	3.00×10^{1}	Kato and Suzuki(2008, p42)
Cs-137	2.00×10^{0}	1.00×10^{0}	3.00×10^{1}	Kato and Suzuki(2008, p42)
Th-232	5.00×10^{3}	7.00×10^{-1}	5.00×10^{3}	Kato and Suzuki(2008, p42)
U-236	5.00×10^{-2}	5.00×10^{-2}	3.00×10^{0}	Kato and Suzuki(2008, p42)
Pu-240	1.00×10^{2}	1.00×10^{-2}	1.00×10^{2}	Kato and Suzuki(2008, p42)
Th-229	5.00×10^{3}	7.00×10^{-1}	5.00×10^{3}	Kato and Suzuki(2008, p42)
U-233	5.00×10^{-2}	5.00×10^{-2}	3.00×10^{0}	Kato and Suzuki(2008, p42)
Np-237	5.00×10^{-1}	1.00×10^{-2}	5.00×10^{1}	Kato and Suzuki(2008, p42)
Am-241	1.00×10^{2}	1.00×10^{-2}	1.00×10^{3}	Kato and Suzuki(2008, p42)
Cm-245	1.00×10^{2}	1.00×10^{1}	1.00×10^{2}	Kato and Suzuki(2008, p42)
Pb-210	1.00×10^{1}	1.00×10^{-2}	1.00×10^{1}	Kato and Suzuki(2008, p42)
Ra-226	1.00×10^{0}	5.00×10^{-1}	3.00×10^{1}	Kato and Suzuki(2008, p42)
Th-230	5.00×10^{3}	7.00×10^{-1}	5.00×10^{3}	Kato and Suzuki(2008, p42)
U-234	5.00×10^{-2}	5.00×10^{-2}	3.00×10^{0}	Kato and Suzuki(2008, p42)
U-238	5.00×10^{-2}	5.00×10^{-2}	3.00×10^{0}	Kato and Suzuki(2008, p42)
Pu-238	1.00×10^{2}	1.00×10^{-2}	1.00×10^{2}	Kato and Suzuki(2008, p42)
Pu-242	1.00×10^{2}	1.00×10^{-2}	1.00×10^{2}	Kato and Suzuki(2008, p42)
Cm-246	1.00×10^{2}	1.00×10^{1}	1.00×10^{2}	Kato and Suzuki(2008, p42)
Ac-227	1.00×10^{2}	1.00×10^{-2}	1.00×10^{3}	Kato and Suzuki(2008, p42)
Pa-231	5.00×10^{3}	1.00×10^{0}	5.00×10^{3}	Kato and Suzuki(2008, p42)
U-235	5.00×10^{-2}	5.00×10^{-2}	3.00×10^{0}	Kato and Suzuki(2008, p42)
Pu-239	1.00×10^{2}	1.00×10^{-2}	1.00×10^{2}	Kato and Suzuki(2008, p42)
Am-243	1.00×10^{2}	1.00×10^{-2}	1.00×10^{3}	Kato and Suzuki(2008, p42)
Po-210	1.00×10^{1}	1.00×10^{-2}	1.00×10^{1}	Kato and Suzuki(2008, p42)

(4) Sorption coefficients of sea sediment (m^3/kg)

	Best est.	Min.	Max.	Data source
C-14	1.00×10^{-1}	1.00×10^{-1}	1.00×10^{1}	Kato and Suzuki(2008, p41)
Cl-36	1.00×10^{-4}	3.00×10^{-5}	1.00×10^{-1}	Kato and Suzuki(2008, p41)
Ni-59	2.00×10^{1}	1.00×10^{1}	5.00×10^{2}	Kato and Suzuki(2008, p41)
Se-79	1.00×10^{0}	0.00	1.00×10^{1}	Kato and Suzuki(2008, p41)
Sr-90	1.00×10^{0}	1.00×10^{-1}	5.00×10^{0}	Kato and Suzuki(2008, p41)
Zr-93	1.00×10^{1}	1.00×10^{-1}	5.00×10^{3}	Kato and Suzuki(2008, p41)
Nb-94	1.00×10^{1}	1.00×10^{0}	1.00×10^{3}	Kato and Suzuki(2008, p41)
Tc-99	1.00×10^{-1}	1.00×10^{-2}	1.00×10^{1}	Kato and Suzuki(2008, p41)
Pd-107	5.00×10^{1}	1.00×10^{1}	5.00×10^{2}	Kato and Suzuki(2008, p41)
Sn-126	1.00×10^{1}	2.00×10^{-2}	2.00×10^{2}	Kato and Suzuki(2008, p41)
I-129	2.00×10^{-2}	0.00	1.00×10^{-1}	Kato and Suzuki(2008, p41)
Cs-135	3.00×10^{0}	1.00×10^{-1}	2.00×10^{1}	Kato and Suzuki(2008, p41)
Cs-137	3.00×10^{0}	1.00×10^{-1}	2.00×10^{1}	Kato and Suzuki(2008, p41)
Th-232	5.00×10^{3}	1.00×10^{2}	1.00×10^{4}	Kato and Suzuki(2008, p42)
U-236	5.00×10^{-1}	1.00×10^{-1}	5.00×10^{0}	Kato and Suzuki(2008, p42)
Pu-240	2.00×10^{3}	1.00×10^{1}	2.00×10^{4}	Kato and Suzuki(2008, p42)
Th-229	5.00×10^{3}	1.00×10^{2}	1.00×10^{4}	Kato and Suzuki(2008, p42)
U-233	5.00×10^{-1}	1.00×10^{-1}	5.00×10^{0}	Kato and Suzuki(2008, p42)
Np-237	2.00×10^{0}	2.00×10^{-1}	5.00×10^{1}	Kato and Suzuki(2008, p42)
Am-241	2.00×10^{3}	1.00×10^{2}	2.00×10^{4}	Kato and Suzuki(2008, p42)
Cm-245	2.00×10^{3}	1.00×10^{2}	2.00×10^{4}	Kato and Suzuki(2008, p42)
Pb-210	2.00×10^{2}	1.00×10^{1}	1.00×10^{4}	Kato and Suzuki(2008, p42)
Ra-226	5.00×10^{0}	5.00×10^{-1}	5.00×10^{2}	Kato and Suzuki(2008, p42)
Th-230	5.00×10^{3}	1.00×10^{2}	1.00×10^{4}	Kato and Suzuki(2008, p42)
U-234	5.00×10^{-1}	1.00×10^{-1}	5.00×10^{0}	Kato and Suzuki(2008, p42)
U-238	5.00×10^{-1}	1.00×10^{-1}	5.00×10^{0}	Kato and Suzuki(2008, p42)
Pu-238	2.00×10^{3}	1.00×10^{1}	2.00×10^{4}	Kato and Suzuki(2008, p42)
Pu-242	2.00×10^{3}	1.00×10^{1}	2.00×10^{4}	Kato and Suzuki(2008, p42)
Cm-246	2.00×10^{3}	1.00×10^{2}	2.00×10^{4}	Kato and Suzuki(2008, p42)
Ac-227	2.00×10^{3}	1.00×10^{1}	1.00×10^{4}	Kato and Suzuki(2008, p42)
Pa-231	5.00×10^{3}	1.00×10^{2}	1.00×10^{4}	Kato and Suzuki(2008, p42)
U-235	5.00×10^{-1}	1.00×10^{-1}	5.00×10^{0}	Kato and Suzuki(2008, p42)
Pu-239	2.00×10^{3}	1.00×10^{1}	2.00×10^{4}	Kato and Suzuki(2008, p42)
Am-243	2.00×10^{3}	1.00×10^{2}	2.00×10^{4}	Kato and Suzuki(2008, p42)
Po-210	2.00×10^{2}	1.00×10^{1}	1.00×10^{4}	Kato and Suzuki(2008, p42)

(5) Sea-spray enhancement factor

	Best est.	Min.	Max.	Data source
C-14	1	1	3	Kato and Suzuki(2008, p39)
Cl-36	1	1	3	Kato and Suzuki(2008, p39)
Ni-59	1	1	3	Kato and Suzuki(2008, p39)
Se-79	1	1	3	Kato and Suzuki(2008, p39)
Sr-90	1	1	3	Kato and Suzuki(2008, p39)
Zr-93	1	1	3	Kato and Suzuki(2008, p39)
Nb-94	1	1	3	Kato and Suzuki(2008, p39)
Tc-99	1	1	3	Kato and Suzuki(2008, p39)
Pd-107	1	1	3	Kato and Suzuki(2008, p39)
Sn-126	1	1	3	Kato and Suzuki(2008, p39)
I-129	10	3	50	Kato and Suzuki(2008, p39)
Cs-135	1	1	3	Kato and Suzuki(2008, p39)
Cs-137	1	1	3	Kato and Suzuki(2008, p39)
Th-232	10	3	50	Kato and Suzuki(2008, p39)
U-236	10	3	50	Kato and Suzuki(2008, p39)
Pu-240	10	3	50	Kato and Suzuki(2008, p39)
Th-229	10	3	50	Kato and Suzuki(2008, p39)
U-233	10	3	50	Kato and Suzuki(2008, p39)
Np-237	10	3	50	Kato and Suzuki(2008, p39)
Am-241	10	3	50	Kato and Suzuki(2008, p39)
Cm-245	10	3	50	Kato and Suzuki(2008, p39)
Pb-210	10	3	50	Kato and Suzuki(2008, p39)
Ra-226	10	3	50	Kato and Suzuki(2008, p39)
Th-230	10	3	50	Kato and Suzuki(2008, p39)
U-234	10	3	50	Kato and Suzuki(2008, p39)
U-238	10	3	50	Kato and Suzuki(2008, p39)
Pu-238	10	3	50	Kato and Suzuki(2008, p39)
Pu-242	10	3	50	Kato and Suzuki(2008, p39)
Cm-246	10	3	50	Kato and Suzuki(2008, p39)
Ac-227	10	3	50	Kato and Suzuki(2008, p39)
Pa-231	10	3	50	Kato and Suzuki(2008, p39)
U-235	10	3	50	Kato and Suzuki(2008, p39)
Pu-239	10	3	50	Kato and Suzuki(2008, p39)
Am-243	10	3	50	Kato and Suzuki(2008, p39)
Po-210	10	3	50	Kato and Suzuki(2008, p39)

(6) Soil to plant concentration factors for terrestrial landscape

	Cropland (grain) (Bq/kg)/(Bq/kg)	Data source	Woods (mg/kg)/(mg/kg)	Data source
C-14	-	-	-	-
Cl-36	5.00×10^{0}	JAEA(2008, p31)	3.80×10^{0}	POSIVA(2014a, p739)
Ni-59	5.00×10^{-2}	JAEA(2008, p31)	-	N/A
Se-79	1.00×10^{0}	JAEA(2008, p31)	3.50×10^{-2}	POSIVA(2014a, p739)
Sr-90	8.00×10^{-2}	JAEA(2008, p31)	3.60×10^{-2}	IAEA(2010, p101)
Zr-93	5.00×10^{-3}	JAEA(2008, p31)	-	N/A
Nb-94	1.00×10^{-2}	JAEA(2008, p31)	3.00×10^{-3}	POSIVA(2014a, p739)
Tc-99	1.00×10^{1}	JAEA(2008, p31)	-	N/A
Pd-107	2.00×10^{-1}	JAEA(2008, p31)	-	N/A
Sn-126	2.00×10^{-1}	JAEA(2008, p31)	-	N/A
I-129	1.00×10^{-1}	JAEA(2008, p31)	2.10×10^{-2}	POSIVA(2014a, p739)
Cs-135	2.00×10^{-2}	JAEA(2008, p31)	1.08×10^{-2}	IAEA(2010, p101)
Cs-137	2.00×10^{-2}	JAEA(2008, p31)	1.08×10^{-2}	IAEA(2010, p101)
Th-232	5.00×10^{-4}	JAEA(2008, p31)	-	N/A
U-236	1.00×10^{-4}	JAEA(2008, p31)	-	N/A
Pu-240	3.00×10^{-5}	JAEA(2008, p31)	-	N/A
Th-229	5.00×10^{-4}	JAEA(2008, p31)	-	N/A
U-233	1.00×10^{-4}	JAEA(2008, p31)	-	N/A
Np-237	3.00×10^{-4}	JAEA(2008, p31)	-	N/A
Am-241	1.00×10^{-5}	JAEA(2008, p31)	-	N/A
Cm-245	1.00×10^{-1}	JAEA(2008, p31)	-	N/A
Pb-210	1.00×10^{-2}	JAEA(2008, p31)	-	N/A
Ra-226	4.00×10^{-2}	JAEA(2008, p31)	-	N/A
Th-230	5.00×10^{-4}	JAEA(2008, p31)	-	N/A
U-234	1.00×10^{-4}	JAEA(2008, p31)	-	N/A
U-238	1.00×10^{-4}	JAEA(2008, p31)	-	N/A
Pu-238	3.00×10^{-5}	JAEA(2008, p31)	-	N/A
Pu-242	3.00×10^{-5}	JAEA(2008, p31)	-	N/A
Cm-246	1.00×10^{-1}	JAEA(2008, p31)	-	N/A
Ac-227	1.00×10^{-3}	JAEA(2008, p31)	-	N/A
Pa-231	4.00×10^{-2}	JAEA(2008, p31)	-	N/A
U-235	1.00×10^{-4}	JAEA(2008, p31)	-	N/A
Pu-239	3.00×10^{-5}	JAEA(2008, p31)	-	N/A
Am-243	1.00×10^{-5}	JAEA(2008, p31)	-	N/A
Po-210	2.00×10^{-4}	JAEA(2008, p31)	-	N/A

(7) Soil to plant concentration factors for aquatic landscape

	Freshwater m3/kg	Data source	Sea L/kg	Data source
C-14	-	-	-	-
Cl-36	7.10×10^{-1}	POSIVA(2014a, p771)	5.00×10^{-2}	IAEA(2004, p51-p52)
Ni-59	7.70×10^{-1}	IAEA(2010, p122)	2.00×10^{3}	IAEA(2004, p51-p52)
Se-79	5.50×10^{0}	POSIVA(2014a, p771)	1.00×10^{3}	IAEA(2004, p51-p52)
Sr-90	4.10×10^{-1}	IAEA(2010, p122)	1.00×10^{1}	IAEA(2004, p51-p52)
Zr-93	-	-	3.00×10^{3}	IAEA(2004, p51-p52)
Nb-94	3.40×10^{1}	POSIVA(2014a, p771)	3.00×10^{3}	IAEA(2004, p51-p52)
Tc-99	5.50×10^{-3}	IAEA(2010, p122)	3.00×10^{4}	IAEA(2004, p51-p52)
Pd-107	-	-	1.00×10^{3}	IAEA(2004, p51-p52)
Sn-126	-	-	2.00×10^{5}	IAEA(2004, p51-p52)
I-129	1.30×10^{-1}	IAEA(2010, p122)	1.00×10^{4}	IAEA(2004, p51-p52)
Cs-135	9.70×10^{-2}	IAEA(2010, p122)	5.00×10^{1}	IAEA(2004, p51-p52)
Cs-137	9.70×10^{-2}	IAEA(2010, p122)	5.00×10^{1}	IAEA(2004, p51-p52)
Th-232	-	-	2.00×10^{2}	IAEA(2004, p51-p52)
U-236	2.10×10^{-1}	IAEA(2010, p122)	1.00×10^{2}	IAEA(2004, p51-p52)
Pu-240	2.60×10^{1}	IAEA(2010, p122)	4.00×10^{3}	IAEA(2004, p51-p52)
Th-229	-	-	2.00×10^{2}	IAEA(2004, p51-p52)
U-233	2.10×10^{-1}	IAEA(2010, p122)	1.00×10^{2}	IAEA(2004, p51-p52)
Np-237	7.20×10^{0}	IAEA(2010, p122)	5.00×10^{1}	IAEA(2004, p51-p52)
Am-241	3.70×10^{0}	IAEA(2010, p122)	8.00×10^{3}	IAEA(2004, p51-p52)
Cm-245	9.00×10^{0}	IAEA(2010, p122)	5.00×10^{3}	IAEA(2004, p51-p52)
Pb-210	1.90×10^{0}	IAEA(2010, p122)	1.00×10^{3}	IAEA(2004, p51-p52)
Ra-226	2.90×10^{0}	IAEA(2010, p122)	1.00×10^{2}	IAEA(2004, p51-p52)
Th-230	-	-	2.00×10^{2}	IAEA(2004, p51-p52)
U-234	2.10×10^{-1}	IAEA(2010, p122)	1.00×10^{2}	IAEA(2004, p51-p52)
U-238	2.10×10^{-1}	IAEA(2010, p122)	1.00×10^{2}	IAEA(2004, p51-p52)
Pu-238	2.60×10^{1}	IAEA(2010, p122)	4.00×10^{3}	IAEA(2004, p51-p52)
Pu-242	2.60×10^{1}	IAEA(2010, p122)	4.00×10^{3}	IAEA(2004, p51-p52)
Cm-246	9.00×10^{0}	IAEA(2010, p122)	5.00×10^{3}	IAEA(2004, p51-p52)
Ac-227	-	-	1.00×10^{3}	IAEA(2004, p51-p52)
Pa-231	-	-	1.00×10^{2}	IAEA(2004, p51-p52)
U-235	2.10×10^{-1}	IAEA(2010, p122)	1.00×10^{2}	IAEA(2004, p51-p52)
Pu-239	2.60×10^{1}	IAEA(2010, p122)	4.00×10^{3}	IAEA(2004, p51-p52)
Am-243	3.70×10^{0}	IAEA(2010, p122)	8.00×10^{3}	IAEA(2004, p51-p52)
Po-210	-	-	1.00×10^{3}	IAEA(2004, p51-p52)

(8) Data for terrestrial module

Parameters		Value	Data source
Geometry			
Thickness (m)	Upper soil	0.15	Derive from SNFD 2017
	Lower soil	0.15	Derive from SNFD 2017
	Deep soil	0.5	Lindborg, 2010, p80
Area ratio	Crop land	0.63	Local government
	Woods	0.37	Forestry Bureau
Soil properties			
Grain density (kg/m^3)	Upper soil	2,700	Derive from SNFD 2017
	Lower soil	2,700	Derive from SNFD 2017
	Deep soil	2,700	Derive from SNFD 2017
Total porosity	Upper soil	0.7	Derive from SNFD 2017
	Lower soil	0.4	Derive from SNFD 2017
	Deep soil	0.1	Derive from SNFD 2017
Wet soil porosity	Upper soil	0.4	Derive from SNFD 2017
	Lower soil	0.3	Derive from SNFD 2017
	Deep soil	0.06	Derive from SNFD 2017
Bulk density (kg/m^3)	Upper soil	810	Grain density *(1- Total porosity)
	Lower soil	1,620	Grain density *(1- Total porosity)
	Deep soil	2,430	Grain density *(1- Total porosity)
Hydrological parameters			
Upward flow (m/yr)	Lower soil	0.109	POSIVA(2013, p99)，(cropland F23upp)
	Deep soil	0.012	POSIVA(2013, p99)，(cropland F12upp)
Downward flow (m/yr)	Upper soil	0.284	POSIVA(2013, p99)，(cropland F32down)
	Lower soil	0.067	SNFD 2021
Precipitation (m/yr)		1.077	SNFD 2021
Irrigation-well (m^3/yr)		124,446	Water resources agency
Well-water capacity(m^3)		189,182	Taiwan water corporation
Biological parameters			
Biomass (kg/m^2)	Crop	0.196	Local government
	Woods	15.01	Forestry Bureau
Biomass production ($kg/m^2/yr$)	Crop	0.196	Equal to biomass
	Woods	0.64	Forestry Bureau
Biomass loss rate ($kg/m^2/yr$)	Crop	0.196	Equal to biomass
	Woods	0.368	Forestry Bureau
Net primary production ($kg/m^2/yr$)	Crop	0.122	POSIVA(2014a, p701)
	Woods	0.432	Forestry Bureau
Terrestrial process parameters			
Bioturbation ($kg/m^2/yr$)	Upper soil	2	POSIVA(2014a, p712)
	Lower soil	2	POSIVA(2014a, p712)
Erosion (m/yr)		1.70E-04	IAEA(2003, p338)
C-14 related parameters			
Degassing rate ($kgC/m^2/yr$)		0.044	Löfgren(2010, p361)
Dissolved Inorganic Carbon (kgC/m^3)		0.086	Löfgren(2010, p348)
Carbon concentration in air (kg/m^3)		0.2	IAEA(2010, p139)
Wind speed (m/s)		2.99	Central Weather Bureau

(9) Data for aquatic module

Parameter		Value	Data source
Geometry			
Thickness (Lake) (m)	Waterbody	5	Derive from SNFD 2017
	Sediment	0.5	Derive from SNFD 2017
	Soil	0.3	Derive from SNFD 2017
Area (Lake) (km2)		0.15	Local government
Thickness (River) (m)	Waterbody	2	NUMO-SC20-SR6-1, 2020, p34 (table-7)
	Sediment	0.4	NUMO-SC20-SR6-1, 2020, p34 (table-7)
	Soil	0.3	NUMO-SC20-SR6-1, 2020, p34 (table-7)
Area (River) (km2)		0.025	NUMO-SC20-SR6-1, 2020, p34 (table-7)
Thickness (Sea) (m)	Waterbody	5	NUMO-SC20-SR6-1, 2020, p34 (table-7)
	Sediment	0.5	NUMO-SC20-SR6-1, 2020, p34 (table-7)
	Soil	0.3	NUMO-SC20-SR6-1, 2020, p34 (table-7)
Area (Sea) (km2)		2	NUMO-SC20-SR6-1, 2020, p34 (table-7)
Soil properties			
Grain density (Lake) (kg/m^3)	Sediment	2,650	Derive from SNFD 2017
	Soil	2,650	Derive from SNFD 2017
Grain density (River) (kg/m^3)	Sediment	2,600	Derive from SNFD 2017
	Soil	2,600	Derive from SNFD 2017
Grain density (Sea) (kg/m^3)	Sediment	2,700	Derive from SNFD 2017
	Soil	2,700	Derive from SNFD 2017
Total porosity (Lake)	Sediment	0.96	Andersson(2010, p385)
	Soil	0.4	Assume the same with lower soil
Total porosity (River)	Sediment	0.96	Andersson(2010, p385)
	Soil	0.4	Assume the same with lower soil
Total porosity (Sea)	Sediment	0.96	Andersson(2010, p385)
	Soil	0.4	Assume the same with lower soil
Wet soil porosity (Lake)	Sediment	0.07	Andersson(2010, p385)
	Soil	0.3	Assume the same with lower soil
Water-filled porosity (River)	Sediment	0.07	Andersson(2010, p385)
	Soil	0.3	Assume the same with lower soil
Water-filled porosity (Sea)	Sediment	0.07	Andersson(2010, p385)
	Soil	0.3	Assume the same with lower soil
Bulk density (Lake) (kg/m^3)	Sediment	1,590	Grain density *(1- Total porosity)
	Soil	2,430	Grain density *(1- Total porosity)
Bulk density (River) (kg/m^3)	Sediment	1,560	Grain density *(1- Total porosity)
	Soil	2,430	Grain density *(1- Total porosity)
Bulk density (Sea) (kg/m^3)	Sediment	1,620	Grain density *(1- Total porosity)
	Soil	2,430	Grain density *(1- Total porosity)
Hydrological parameters			
Upward flow (Lake) (m/yr)	Sediment	0.01	POSIVA(2013, p99)(w-F34upp)
	Soil	0.075	POSIVA(2013, p99)(w-F23upp)
	Deep soil	0.008	POSIVA(2013, p99)(w-F12upp)
Upward flow (River) (m/yr)	Sediment	0.01	POSIVA(2013, p99)(w-F34upp)
	Soil	0.075	POSIVA(2013, p99)(w-F23upp)
	Deep soil	0.008	POSIVA(2013, p99)(w-F12upp)
Upward flow (Sea) (m/yr)	Sediment	0.01	POSIVA(2013, p99)(w-F34upp)
	Soil	0.075	POSIVA(2013, p99)(w-F23upp)
	Deep soil	0.008	POSIVA(2013, p99)(w-F12upp)
Downward flow (Lake) (m/yr)	Sediment	0.343	POSIVA(2013, p99)(w-F43down ave.)
	Soil	0.061	POSIVA(2013, p99)(w-F32down ave.)
	Deep soil	0.068	SNFD 2021
Downward flow (River) (m/yr)	Sediment	0.327	POSIVA(2013, p99)(w-F43down min.)
	Soil	0.048	POSIVA(2013, p99)(w-F32down min.)
	Deep soil	0.068	SNFD 2021

Downward flow (Sea) (m/yr)	Sediment	0.380	POSIVA(2013, p99)(w-F43down max.)
	Soil	0.088	POSIVA(2013, p99)(w-F32down max.)
	Deep soil	0.068	SNFD 2021
Irrigation rate (m/yr)		0.461	Derived from local data
Flooding rate (m^3/yr)		100	JNC(2000, pF-3)
Marine discharge (m^3/yr)		1×10^{10}	JNC(2000, pF-3)
Precipitation (m/yr)		1.077	SNFD 2021
Biological parameters			
Biomass (kg/m^2)	Lake	0.92	Equal to biomass production
	River	0.2482	Equal to biomass production
	Sea	0.106	National park
Biomass production (kg/m^2/yr)	Lake	0.92	Construction and planning Agency
	River	0.2482	National Science Council
	Sea	0.106	Equal to Biomass
Biomass loss rate (kg/m^2/yr)	Lake	0.92	Equal to biomass production
	River	0.2482	Equal to biomass production
	Sea	0.106	Equal to Biomass
Aqutic process parameters			
Bioturbation (fresh) (kg/m^2/yr)	Sediment	4	POSIVA(2014a, p716)
	Soil	4	POSIVA(2014a, p716)
Bioturbation (sea) (kg/m^2/yr)	Sediment	6.5	POSIVA(2014a, p716)
	Soil	6.5	POSIVA(2014a, p716)
Gross Sedimentation (kg/m^2/yr)	Lake	1.1	POSIVA(2014a, p589)
	River	8.8	POSIVA(2014a, p590)
	Sea	3.1	POSIVA(2014a, p595)Table 15-12
Resuspension (kg/m^2/yr)	Lake	0.8	POSIVA(2014a, p589)Table 15-4
	River	8.8	POSIVA(2014a, p590)
	Sea	1.3	POSIVA(2014a, p595)Table 15-13
Net sedimentation (kg/m^2/yr)	Lake	0.3	Sedimentation - Resuspension
	River	0	Sedimentation - Resuspension
	Sea	1.8	Sedimentation - Resuspension
Suspend solid concentration (kg/m^3)	Lake	0.007	POSIVA(2014a, p632)Table16-2
	River	0.013	POSIVA(2014a, p635)Table16-8
	Sea	0.003	POSIVA(2014a, p637)Table16-14
Sea spray rate (m^3/yr)		3×10^5	Kato and Suzuki(2008, p39)
Bed-load transport (kg/yr)		1.60×10^5	JNC(2000, pF-3)
Dredging of sediments (m^3/yr)		1.6	JNC(2000, pF-3)
C-14 related parameters			
Degassing rate (gC/m^2/yr)	Freshwater	40.3	Construction and planning Agency
	Sea	30.6	Construction and planning Agency
Carbon uptake rate (gC/m^2/yr)	Freshwater	11.1	SKB TR 10-02 (2010, p403)
	Sea	23.0	Construction and planning Agency
Dissolved Inorganic Carbon (kgC/m^3)	Lake	0.0033	POSIVA(2014a, p645)
	River	0.0074	POSIVA(2014a, p647)
	Sea	0.017	POSIVA(2014a, p649)
Carbon concentration in air (kg/m^3)		0.2	IAEA(2010, p139)
The height of mixing layer (m)		9.5	SKB TR 10-06 (2010, p52)
Wind speed (m/s)		2.99	Central Weather Bureau

(10) Nuclide-independent data for dose model

Parameter		Value	Data source
Consumption rate			
Water (m^3/yr)		0.73	Health Promotion Administration
Crop (kg/yr)	Root	22.00	Food and Drug Administration
	Green	33.42	Food and Drug Administration
	Grain	20.45	Food and Drug Administration
	Fruit	64.08	Food and Drug Administration
Livestock meat (kg/yr)	Beef	4.87	Food and Drug Administration
	Pork	21.24	Food and Drug Administration
	Chicken	11.41	Food and Drug Administration
Livestock product (kg/yr)	Milk	19.45	Food and Drug Administration
	Offal	0.94	Food and Drug Administration
	Egg	12.13	Food and Drug Administration
Freshwater Fish (kg/yr)		4.03	Food and Drug Administration
Oyster (kg/yr)		1.35	Food and Drug Administration
Soil (kg/yr)		0.083	IAEA(2003, p345)
Sediment (kg/yr)		0.208	Derive from NOAA
Crop			
Crop soil contamination (kgdw/kgfw)	Root	2.0×10^{-04}	Smith et al.(1996, p5-25)
	Green	1.3×10^{-04}	Smith et al.(1996, p5-p25)
	Grain	1.3×10^{-04}	Smith et al.(1996, p5-p25)
	Fruit	2.0×10^{-04}	Smith et al.(1996, p5-p25)
Crop annual yield (kg/m^2/yr)	Root	1.87	Local Government
	Green	2.19	Local Government
	Grain	9.8E-02	Local Government
	Fruit	1.15	Local Government
Time from irrigation to harvest (yr)	Root	4.0×10^{-02}	IAEA(2003, p356)
	Green	4.2×10^{-02}	嚴士濳(2015，p20)
	Grain	5.6×10^{-02}	Council of Agriculture
	Fruit	8.3×10^{-02}	Council of Agriculture
Irrigation rate (m/yr)	Root	0.16	嚴士濳(2015，p21)
	Green	9.5E-02	Brouwer et al.(1986, p61)(table 14)
	Grain	0.38	嚴士濳(2015，p21)
	Fruit	1.34	Council of Agriculture
Stable carbon content of crop			
Root (g/kg)		46	IAEA(2010, p140)(Root crops)
Green (g/kg)		30	IAEA(2010, p140)(Leafy and non-leafy vegetables)
Grain (g/kg)		390	IAEA(2010, p140)(Cereals)
Fruit (g/kg)		62	IAEA(2010, p140)(Fruit)
Livestock			
Animal consumption rate (Grain) (kgfw/d)	Cow	20	Local data
	Pig	10	Kato and Suzuki(2008, p38)
	Chicken	0.3	
Animal water consumption rate (m^3/d)	Cow	7.0×10^{-02}	Kato and Suzuki(2008, p38)
	Pig	5.0×10^{-02}	
	Chicken	5.0×10^{-04}	
Animal soil consumption rate (kg/d)	Cow	0.6	Kato and Suzuki(2008, p38)
	Pig	0.2	
	Chicken	0.02	
Animal breathing rate (m^3/hr)	Cow	5.4	Kato and Suzuki(2008, p28)
	Pig	0.5	
	Chicken	0.01	
Animal occupancy (h/d)	Cow	24	Assumed.
	Pig	24	

	Chicken	24	
Water density (kg/m^3)		1,000	IAEA(2003, p356)
Dust in air (kg/m^3)		2.0×10^{-6}	IAEA(2003, p356)
Water food			
Suspend solid concentration (kg/m^3)	Freshwater	7.0×10^{-3}	POSIVA(2014a, p632)
	Sea	3.0×10^{-3}	POSIVA(2014a, p637)
Stable carbon in water (gC/kg)		117	IAEA(2010, p134)
Breathing			
Breathing rate (m^3/hr)		1.7	IAEA(2003, p356)
Concentration of aerosol (m^3/m^3)		1.0×10^{-11}	IAEA(2003, p356)
Dust in air (kg/m^3)		2.0×10^{-6}	JAEA(2008, p41)
External			
Occupancy (h/yr)		8,760	Assumed.

(11) Dose conversion factor

	Ingestion Sv/Bq	Inhalation Sv/Bq	External(Sv/h)/(Bq/m^3)	
			Soil	Water immerse
C-14	5.80×10^{-10}	5.80×10^{-9}	2.60×10^{-19}	1.60×10^{-18}
Cl-36	9.30×10^{-10}	7.30×10^{-9}	4.60×10^{-17}	1.60×10^{-16}
Ni-59	6.30×10^{-11}	4.40×10^{-10}	0.00	0.00
Se-79	2.90×10^{-9}	6.80×10^{-9}	3.50×10^{-19}	2.20×10^{-18}
Sr-90	2.80×10^{-8}	1.60×10^{-7}	1.40×10^{-17}	5.30×10^{-17}
Zr-93	1.10×10^{-9}	3.30×10^{-9}	0.00	0.00
Nb-94	1.70×10^{-9}	4.90×10^{-8}	1.80×10^{-13}	6.10×10^{-13}
Tc-99	6.40×10^{-10}	1.30×10^{-8}	2.40×10^{-18}	1.10×10^{-17}
Pd-107	3.70×10^{-11}	5.90×10^{-10}	0.00	0.00
Sn-126	4.70×10^{-9}	2.80×10^{-8}	2.90×10^{-15}	1.70×10^{-14}
I-129	1.10×10^{-7}	9.80×10^{-9}	2.50×10^{-16}	3.20×10^{-15}
Cs-135	2.00×10^{-9}	8.60×10^{-9}	7.40×10^{-19}	4.00×10^{-18}
Cs-137	1.30×10^{-8}	3.90×10^{-8}	1.50×10^{-17}	5.40×10^{-17}
Th-232	2.30×10^{-7}	2.50×10^{-5}	1.00×10^{-17}	7.20×10^{-17}
U-236	4.70×10^{-8}	8.70×10^{-6}	4.10×10^{-18}	4.20×10^{-17}
Pu-240	2.50×10^{-7}	1.60×10^{-8}	2.90×10^{-18}	4.00×10^{-17}
Th-229	4.90×10^{-7}	2.40×10^{-4}	6.20×10^{-15}	3.10×10^{-14}
U-233	5.10×10^{-8}	5.80×10^{-7}	2.70×10^{-17}	1.30×10^{-16}
Np-237	1.10×10^{-7}	5.00×10^{-5}	1.50×10^{-15}	8.30×10^{-15}
Am-241	2.00×10^{-7}	9.60×10^{-5}	8.50×10^{-16}	6.70×10^{-15}
Cm-245	2.10×10^{-7}	9.90×10^{-5}	6.50×10^{-15}	3.20×10^{-14}
Pb-210	6.90×10^{-7}	5.60×10^{-6}	4.70×10^{-17}	4.70×10^{-16}
Ra-226	2.80×10^{-7}	9.50×10^{-6}	6.20×10^{-16}	2.50×10^{-15}
Th-230	2.10×10^{-7}	1.00×10^{-4}	2.30×10^{-17}	1.40×10^{-16}
U-234	4.90×10^{-8}	9.40×10^{-6}	7.80×10^{-18}	6.30×10^{-17}
U-238	4.50×10^{-8}	8.00×10^{-6}	1.90×10^{-18}	2.90×10^{-17}
Pu-238	2.30×10^{-7}	1.10×10^{-4}	3.00×10^{-18}	4.10×10^{-17}
Pu-242	2.40×10^{-7}	1.10×10^{-4}	2.50×10^{-18}	3.30×10^{-17}
Cm-246	2.10×10^{-7}	9.80×10^{-5}	2.30×10^{-18}	3.80×10^{-17}
Ac-227	1.10×10^{-6}	5.50×10^{-4}	9.60×10^{-18}	4.70×10^{-17}
Pa-231	7.10×10^{-7}	1.40×10^{-4}	3.70×10^{-15}	1.40×10^{-14}
U-235	4.70×10^{-8}	8.50×10^{-6}	1.40×10^{-14}	5.70×10^{-14}
Pu-239	2.50×10^{-7}	1.20×10^{-4}	5.70×10^{-18}	3.40×10^{-17}
Am-243	2.00×10^{-7}	9.60×10^{-5}	2.70×10^{-15}	1.80×10^{-14}
Po-210	4.50×10^{-7}	2.30×10^{-6}	1.00×10^{-18}	3.30×10^{-18}
Data source	Atomic energy council	Atomic energy council	Eckerman and Ryman(1993, p166)	Eckerman and Ryman(1993, p76)

(12) Food processing fraction

	Root			Green			Grain			Fruit		
	Fp1	Fp2	Fp3	Fp1	Fp2	Fp3	Fp1	Fp2	Fp3	Fp1	Fp2	Fp3
C-14	1	1	1	1	1	1	1	1	1	1	1	1
Cl-36	1	0.6	1	1	0.6	1	1	0.4	1	1	1	1
Ni-59	1	1	1	1	1	1	1	1	1	1	1	1
Se-79	1	1	1	1	1	1	1	1	1	1	1	1
Sr-90	0.9	1	0.9	1	1	1	0.6	1	0.6	1	1	1
Zr-93	1	1	1	1	1	1	1	1	1	1	1	1
Nb-94	1	1	1	1	1	1	1	1	1	1	1	1
Tc-99	1	1	1	1	1	1	1	1	1	1	1	1
Pd-107	1	1	1	1	1	1	1	1	1	1	1	1
Sn-126	1	1	1	1	1	1	1	1	1	1	1	1
I-129	1	1	1	0.8	1	0.8	1	1	1	0.8	1	0.8
Cs-135	0.9	0.9	0.9	1	0.9	1	0.6	0.4	0.6	1	1	1
Cs-137	0.9	0.9	0.9	1	0.9	1	0.6	0.4	0.6	1	1	1
Th-232	1	1	1	1	1	1	1	1	1	1	1	1
U-236	1	1	1	1	1	1	1	1	1	1	1	1
Pu-240	1	1	1	1	1	1	0.2	1	0.2	1	1	1
Th-229	1	1	1	1	1	1	1	1	1	1	1	1
U-233	1	1	1	1	1	1	1	1	1	1	1	1
Np-237	1	1	1	1	1	1	1	1	1	1	1	1
Am-241	1	1	1	1	1	1	0.2	1	0.2	1	1	1
Cm-245	1	1	1	1	1	1	1	1	1	1	1	1
Pb-210	1	1	1	1	1	1	0.6	1	0.6	1	1	1
Ra-226	1	1	1	1	1	1	1	1	1	1	1	1
Th-230	1	1	1	1	1	1	1	1	1	1	1	1
U-234	1	1	1	1	1	1	1	1	1	1	1	1
U-238	1	1	1	1	1	1	1	1	1	1	1	1
Pu-238	1	1	1	1	1	1	0.2	1	0.2	1	1	1
Pu-242	1	1	1	1	1	1	0.2	1	0.2	1	1	1
Cm-246	1	1	1	1	1	1	1	1	1	1	1	1
Ac-227	1	1	1	1	1	1	1	1	1	1	1	1
Pa-231	1	1	1	1	1	1	1	1	1	1	1	1
U-235	1	1	1	1	1	1	1	1	1	1	1	1
Pu-239	1	1	1	1	1	1	0.2	1	0.2	1	1	1
Am-243	1	1	1	1	1	1	0.2	1	0.2	1	1	1
Po-210	0.5	1	0.5	1	1	1	1	1	1	1	1	1
Data source	IAEA(2010, p147)		=FP1	IAEA(2010, p147)		=FP1	IAEA(2010, p147-p148)		=FP1	IAEA(2010, p147)		=FP1

(Fp1: External-soil, Fp2: Internal, Fp3: External-interception)

(13) Interception factor for crop

	Root	Green	Grain	Fruit
C-14	6.70×10^{-1}	5.90×10^{-1}	7.11×10^{-1}	5.00×10^{-1}
Cl-36	6.70×10^{-1}	5.90×10^{-1}	7.11×10^{-1}	5.00×10^{-1}
Ni-59	6.70×10^{-1}	5.90×10^{-1}	7.11×10^{-1}	5.00×10^{-1}
Se-79	6.70×10^{-1}	5.90×10^{-1}	7.11×10^{-1}	5.00×10^{-1}
Sr-90	6.70×10^{-1}	5.90×10^{-1}	8.04×10^{-1}	5.00×10^{-1}
Zr-93	6.70×10^{-1}	5.90×10^{-1}	7.11×10^{-1}	5.00×10^{-1}
Nb-94	6.70×10^{-1}	5.90×10^{-1}	7.11×10^{-1}	5.00×10^{-1}
Tc-99	6.70×10^{-1}	5.90×10^{-1}	7.11×10^{-1}	5.00×10^{-1}
Pd-107	6.70×10^{-1}	5.90×10^{-1}	7.11×10^{-1}	5.00×10^{-1}
Sn-126	6.70×10^{-1}	5.90×10^{-1}	7.11×10^{-1}	5.00×10^{-1}
I-129	6.70×10^{-1}	5.90×10^{-1}	8.53×10^{-1}	5.00×10^{-1}
Cs-135	6.70×10^{-1}	5.90×10^{-1}	7.11×10^{-1}	5.00×10^{-1}
Cs-137	6.70×10^{-1}	5.90×10^{-1}	7.11×10^{-1}	5.00×10^{-1}
Th-232	6.70×10^{-1}	5.90×10^{-1}	7.11×10^{-1}	5.00×10^{-1}
U-236	6.70×10^{-1}	5.90×10^{-1}	7.11×10^{-1}	5.00×10^{-1}
Pu-240	6.70×10^{-1}	5.90×10^{-1}	7.11×10^{-1}	5.00×10^{-1}
Th-229	6.70×10^{-1}	5.90×10^{-1}	7.11×10^{-1}	5.00×10^{-1}
U-233	6.70×10^{-1}	5.90×10^{-1}	7.11×10^{-1}	5.00×10^{-1}
Np-237	6.70×10^{-1}	5.90×10^{-1}	7.11×10^{-1}	5.00×10^{-1}
Am-241	6.70×10^{-1}	5.90×10^{-1}	7.11×10^{-1}	5.00×10^{-1}
Cm-245	6.70×10^{-1}	5.90×10^{-1}	7.11×10^{-1}	5.00×10^{-1}
Pb-210	6.70×10^{-1}	5.90×10^{-1}	7.11×10^{-1}	5.00×10^{-1}
Ra-226	6.70×10^{-1}	5.90×10^{-1}	7.11×10^{-1}	5.00×10^{-1}
Th-230	6.70×10^{-1}	5.90×10^{-1}	7.11×10^{-1}	5.00×10^{-1}
U-234	6.70×10^{-1}	5.90×10^{-1}	7.11×10^{-1}	5.00×10^{-1}
U-238	6.70×10^{-1}	5.90×10^{-1}	7.11×10^{-1}	5.00×10^{-1}
Pu-238	6.70×10^{-1}	5.90×10^{-1}	7.11×10^{-1}	5.00×10^{-1}
Pu-242	6.70×10^{-1}	5.90×10^{-1}	7.11×10^{-1}	5.00×10^{-1}
Cm-246	6.70×10^{-1}	5.90×10^{-1}	7.11×10^{-1}	5.00×10^{-1}
Ac-227	6.70×10^{-1}	5.90×10^{-1}	7.11×10^{-1}	5.00×10^{-1}
Pa-231	6.70×10^{-1}	5.90×10^{-1}	7.11×10^{-1}	5.00×10^{-1}
U-235	6.70×10^{-1}	5.90×10^{-1}	7.11×10^{-1}	5.00×10^{-1}
Pu-239	6.70×10^{-1}	5.90×10^{-1}	7.11×10^{-1}	5.00×10^{-1}
Am-243	6.70×10^{-1}	5.90×10^{-1}	7.11×10^{-1}	5.00×10^{-1}
Po-210	6.70×10^{-1}	5.90×10^{-1}	7.11×10^{-1}	5.00×10^{-1}
Data source	IAEA(2010, p13)Radish	IAEA(2010, p13)Chinese cabbage	IAEA(2010, p13)Rice	Kato and Suzuki(2008, p42)

(14) Crop translocation factor

	Root	Data source	Green	Data source
C-14	4.00×10^{-1}	Kato and Suzuki(2008, p37)	5.80×10^{-1}	Kato and Suzuki(2008, p36)
Cl-36	1.90×10^{-1}	Kato and Suzuki(2008, p37)	1.90×10^{-1}	Kato and Suzuki(2008, p36)
Ni-59	3.90×10^{-2}	Kato and Suzuki(2008, p37)	3.70×10^{-1}	Kato and Suzuki(2008, p36)
Se-79	6.80×10^{-2}	Kato and Suzuki(2008, p37)	3.00×10^{-1}	Kato and Suzuki(2008, p36)
Sr-90	5.00×10^{-3}	IAEA(2010, p22)	2.00×10^{-1}	Kato and Suzuki(2008, p36)
Zr-93	5.30×10^{-1}	Kato and Suzuki(2008, p37)	1.30×10^{-1}	Kato and Suzuki(2008, p36)
Nb-94	5.30×10^{-1}	Kato and Suzuki(2008, p37)	5.20×10^{-1}	Kato and Suzuki(2008, p36)
Tc-99	1.10×10^{-1}	Kato and Suzuki(2008, p37)	2.80×10^{-1}	Kato and Suzuki(2008, p36)
Pd-107	3.90×10^{-2}	Kato and Suzuki(2008, p37)	3.70×10^{-1}	Kato and Suzuki(2008, p37)
Sn-126	2.20×10^{-1}	Kato and Suzuki(2008, p37)	2.20×10^{-1}	Kato and Suzuki(2008, p37)
I-129	7.40×10^{-2}	Kato and Suzuki(2008, p37)	6.10×10^{-1}	Kato and Suzuki(2008, p37)
Cs-135	4.60×10^{-2}	IAEA(2010, p22)	1.90×10^{-1}	Kato and Suzuki(2008, p37)
Cs-137	4.60×10^{-2}	IAEA(2010, p22)	1.90×10^{-1}	Kato and Suzuki(2008, p37)
Th-232	2.90×10^{-1}	Kato and Suzuki(2008, p37)	2.90×10^{-1}	Kato and Suzuki(2008, p37)
U-236	4.30×10^{-2}	Kato and Suzuki(2008, p37)	4.30×10^{-2}	Kato and Suzuki(2008, p37)
Pu-240	4.30×10^{-2}	Kato and Suzuki(2008, p37)	4.30×10^{-2}	Kato and Suzuki(2008, p37)
Th-229	2.90×10^{-1}	Kato and Suzuki(2008, p37)	2.90×10^{-1}	Kato and Suzuki(2008, p37)
U-233	4.30×10^{-2}	Kato and Suzuki(2008, p37)	4.30×10^{-2}	Kato and Suzuki(2008, p37)
Np-237	2.90×10^{-1}	Kato and Suzuki(2008, p37)	2.90×10^{-1}	Kato and Suzuki(2008, p37)
Am-241	2.90×10^{-1}	Kato and Suzuki(2008, p37)	2.90×10^{-1}	Kato and Suzuki(2008, p37)
Cm-245	1.10×10^{-1}	Kato and Suzuki(2008, p37)	1.10×10^{-1}	Kato and Suzuki(2008, p37)
Pb-210	2.20×10^{-1}	Kato and Suzuki(2008, p37)	2.20×10^{-1}	Kato and Suzuki(2008, p37)
Ra-226	9.90×10^{-2}	Kato and Suzuki(2008, p37)	9.90×10^{-2}	Kato and Suzuki(2008, p37)
Th-230	2.90×10^{-1}	Kato and Suzuki(2008, p37)	2.90×10^{-1}	Kato and Suzuki(2008, p37)
U-234	4.30×10^{-2}	Kato and Suzuki(2008, p37)	4.30×10^{-2}	Kato and Suzuki(2008, p37)
U-238	4.30×10^{-2}	Kato and Suzuki(2008, p37)	4.30×10^{-2}	Kato and Suzuki(2008, p37)
Pu-238	4.30×10^{-2}	Kato and Suzuki(2008, p37)	4.30×10^{-2}	Kato and Suzuki(2008, p37)
Pu-242	4.30×10^{-2}	Kato and Suzuki(2008, p37)	4.30×10^{-2}	Kato and Suzuki(2008, p37)
Cm-246	1.10×10^{-1}	Kato and Suzuki(2008, p37)	1.10×10^{-1}	Kato and Suzuki(2008, p37)
Ac-227	2.90×10^{-1}	Kato and Suzuki(2008, p37)	2.90×10^{-1}	Kato and Suzuki(2008, p37)
Pa-231	2.90×10^{-1}	Kato and Suzuki(2008, p37)	2.90×10^{-1}	Kato and Suzuki(2008, p37)
U-235	4.30×10^{-2}	Kato and Suzuki(2008, p37)	4.30×10^{-2}	Kato and Suzuki(2008, p37)
Pu-239	4.30×10^{-2}	Kato and Suzuki(2008, p37)	4.30×10^{-2}	Kato and Suzuki(2008, p37)
Am-243	2.90×10^{-1}	Kato and Suzuki(2008, p37)	2.90×10^{-1}	Kato and Suzuki(2008, p37)
Po-210	2.20×10^{-1}	Kato and Suzuki(2008, p37)	2.20×10^{-1}	Kato and Suzuki(2008, p37)
	Grain	Data source	Fruit	Data source
C-14	4.00×10^{-1}	Kato and Suzuki(2008, p36)	2.00×10^{-1}	Kato and Suzuki(2008, p36)
Cl-36	1.90×10^{-1}	Kato and Suzuki(2008, p36)	1.10×10^{-1}	Kato and Suzuki(2008, p36)

Ni-59	3.90×10^{-2}	Kato and Suzuki(2008, p36)	1.60×10^{-1}	Kato and Suzuki(2008, p36)
Se-79	6.80×10^{-2}	Kato and Suzuki(2008, p36)	1.20×10^{-1}	Kato and Suzuki(2008, p36)
Sr-90	1.20×10^{-2}	IAEA(2010, p20)	4.40×10^{-3}	IAEA(2010, p22)
Zr-93	5.60×10^{-2}	Kato and Suzuki(2008, p36)	6.20×10^{-2}	Kato and Suzuki(2008, p36)
Nb-94	5.60×10^{-2}	Kato and Suzuki(2008, p36)	6.20×10^{-1}	Kato and Suzuki(2008, p36)
Tc-99	1.20×10^{-1}	Kato and Suzuki(2008, p36)	1.20×10^{-1}	Kato and Suzuki(2008, p36)
Pd-107	1.70×10^{-1}	Kato and Suzuki(2008, p36)	1.60×10^{-1}	Kato and Suzuki(2008, p36)
Sn-126	1.00×10^{-1}	Kato and Suzuki(2008, p36)	1.10×10^{-1}	Kato and Suzuki(2008, p36)
I-129	2.80×10^{-1}	Kato and Suzuki(2008, p36)	3.30×10^{-1}	Kato and Suzuki(2008, p36)
Cs-135	2.70×10^{-2}	IAEA(2010, p19)	4.60×10^{-2}	IAEA(2010, p22)
Cs-137	2.70×10^{-2}	IAEA(2010, p19)	4.60×10^{-2}	IAEA(2010, p22)
Th-232	1.30×10^{-1}	Kato and Suzuki(2008, p36)	1.30×10^{-1}	Kato and Suzuki(2008, p36)
U-236	1.60×10^{-1}	Kato and Suzuki(2008, p36)	1.90×10^{-1}	Kato and Suzuki(2008, p36)
Pu-240	1.60×10^{-1}	Kato and Suzuki(2008, p36)	3.00×10^{-6}	IAEA(2010, p22)
Th-229	1.30×10^{-1}	Kato and Suzuki(2008, p36)	1.30×10^{-1}	Kato and Suzuki(2008, p36)
U-233	1.60×10^{-1}	Kato and Suzuki(2008, p36)	1.90×10^{-1}	Kato and Suzuki(2008, p36)
Np-237	2.00×10^{-1}	Kato and Suzuki(2008, p36)	2.10×10^{-1}	Kato and Suzuki(2008, p36)
Am-241	1.30×10^{-1}	Kato and Suzuki(2008, p36)	5.00×10^{-6}	Kato and Suzuki(2008, p36)
Cm-245	2.00×10^{-1}	Kato and Suzuki(2008, p36)	2.10×10^{-1}	Kato and Suzuki(2008, p36)
Pb-210	2.00×10^{-2}	IAEA(2010, p20)	1.10×10^{-1}	Kato and Suzuki(2008, p36)
Ra-226	8.00×10^{-2}	Kato and Suzuki(2008, p36)	7.30×10^{-2}	Kato and Suzuki(2008, p36)
Th-230	1.30×10^{-1}	Kato and Suzuki(2008, p36)	1.30×10^{-1}	Kato and Suzuki(2008, p36)
U-234	1.60×10^{-1}	Kato and Suzuki(2008, p36)	1.90×10^{-1}	Kato and Suzuki(2008, p36)
U-238	1.60×10^{-1}	Kato and Suzuki(2008, p36)	1.90×10^{-1}	Kato and Suzuki(2008, p36)
Pu-238	1.60×10^{-1}	Kato and Suzuki(2008, p36)	3.00×10^{-6}	IAEA(2010, p22)
Pu-242	1.60×10^{-1}	Kato and Suzuki(2008, p36)	3.00×10^{-6}	IAEA(2010, p22)
Cm-246	2.00×10^{-1}	Kato and Suzuki(2008, p36)	2.10×10^{-1}	Kato and Suzuki(2008, p36)
Ac-227	2.00×10^{-1}	Kato and Suzuki(2008, p36)	2.10×10^{-1}	Kato and Suzuki(2008, p36)
Pa-231	2.00×10^{-1}	Kato and Suzuki(2008, p36)	2.10×10^{-1}	Kato and Suzuki(2008, p36)
U-235	1.60×10^{-1}	Kato and Suzuki(2008, p36)	1.90×10^{-1}	Kato and Suzuki(2008, p36)
Pu-239	1.60×10^{-1}	Kato and Suzuki(2008, p36)	3.00×10^{-6}	IAEA(2010, p22)
Am-243	1.30E-01	Kato and Suzuki(2008, p36)	5.00×10^{-6}	IAEA(2010, p22)
Po-210	1.00E-01	Kato and Suzuki(2008, p36)	1.10×10^{-1}	Kato and Suzuki(2008, p36)

(15) Crop weathering rate (1/yr)

	Root	Data source	Green	Data source
C-14	18	Kato and Suzuki(2008, p39)	18	Kato and Suzuki(2008, p40)
Cl-36	18	Kato and Suzuki(2008, p39)	18	Kato and Suzuki(2008, p40)
Ni-59	18	Kato and Suzuki(2008, p39)	18	Kato and Suzuki(2008, p40)
Se-79	18	Kato and Suzuki(2008, p39)	18	Kato and Suzuki(2008, p40)
Sr-90	18	Kato and Suzuki(2008, p39)	18	Kato and Suzuki(2008, p40)
Zr-93	18	Kato and Suzuki(2008, p39)	18	Kato and Suzuki(2008, p40)
Nb-94	18	Kato and Suzuki(2008, p39)	18	Kato and Suzuki(2008, p40)
Tc-99	18	Kato and Suzuki(2008, p39)	18	Kato and Suzuki(2008, p40)
Pd-107	18	Kato and Suzuki(2008, p39)	18	Kato and Suzuki(2008, p40)
Sn-126	18	Kato and Suzuki(2008, p39)	18	Kato and Suzuki(2008, p40)
I-129	18	Kato and Suzuki(2008, p39)	18	Kato and Suzuki(2008, p40)
Cs-135	18	Kato and Suzuki(2008, p39)	18	Kato and Suzuki(2008, p40)
Cs-137	18	Kato and Suzuki(2008, p39)	18	Kato and Suzuki(2008, p40)
Th-232	18	Kato and Suzuki(2008, p39)	18	Kato and Suzuki(2008, p40)
U-236	18	Kato and Suzuki(2008, p39)	18	Kato and Suzuki(2008, p40)
Pu-240	18	Kato and Suzuki(2008, p39)	51	Kato and Suzuki(2008, p40)
Th-229	18	Kato and Suzuki(2008, p39)	18	Kato and Suzuki(2008, p40)
U-233	18	Kato and Suzuki(2008, p39)	18	Kato and Suzuki(2008, p40)
Np-237	18	Kato and Suzuki(2008, p39)	51	Kato and Suzuki(2008, p40)
Am-241	18	Kato and Suzuki(2008, p39)	51	Kato and Suzuki(2008, p40)
Cm-245	18	Kato and Suzuki(2008, p39)	18	Kato and Suzuki(2008, p40)
Pb-210	18	Kato and Suzuki(2008, p39)	18	Kato and Suzuki(2008, p40)
Ra-226	18	Kato and Suzuki(2008, p39)	18	Kato and Suzuki(2008, p40)
Th-230	18	Kato and Suzuki(2008, p39)	18	Kato and Suzuki(2008, p40)
U-234	18	Kato and Suzuki(2008, p39)	18	Kato and Suzuki(2008, p40)
U-238	18	Kato and Suzuki(2008, p39)	18	Kato and Suzuki(2008, p40)
Pu-238	18	Kato and Suzuki(2008, p39)	51	Kato and Suzuki(2008, p40)
Pu-242	18	Kato and Suzuki(2008, p39)	51	Kato and Suzuki(2008, p40)
Cm-246	18	Kato and Suzuki(2008, p39)	18	Kato and Suzuki(2008, p40)
Ac-227	18	Kato and Suzuki(2008, p39)	18	Kato and Suzuki(2008, p40)
Pa-231	18	Kato and Suzuki(2008, p39)	18	Kato and Suzuki(2008, p40)
U-235	18	Kato and Suzuki(2008, p39)	18	Kato and Suzuki(2008, p40)
Pu-239	18	Kato and Suzuki(2008, p39)	51	Kato and Suzuki(2008, p40)
Am-243	18	Kato and Suzuki(2008, p39)	51	Kato and Suzuki(2008, p40)
Po-210	18	Kato and Suzuki(2008, p39)	18	Kato and Suzuki(2008, p40)
	Grain	**Data source**	**Fruit**	**Data source**
C-14	8.4	Kato and Suzuki(2008, p39)	18	Kato and Suzuki(2008, p39)
Cl-36	8.4	Kato and Suzuki(2008, p39)	18	Kato and Suzuki(2008, p39)

Ni-59	8.4	Kato and Suzuki(2008, p39)	18	Kato and Suzuki(2008, p39)
Se-79	8.4	Kato and Suzuki(2008, p39)	18	Kato and Suzuki(2008, p39)
Sr-90	12	IAEA(2010, p18)	18	Kato and Suzuki(2008, p39)
Zr-93	8.4	Kato and Suzuki(2008, p39)	18	Kato and Suzuki(2008, p39)
Nb-94	8.4	Kato and Suzuki(2008, p39)	18	Kato and Suzuki(2008, p39)
Tc-99	8.4	Kato and Suzuki(2008, p39)	18	Kato and Suzuki(2008, p39)
Pd-107	8.4	Kato and Suzuki(2008, p40)	18	Kato and Suzuki(2008, p39)
Sn-126	8.4	Kato and Suzuki(2008, p40)	18	Kato and Suzuki(2008, p39)
I-129	18	IAEA(2010, p18)	18	Kato and Suzuki(2008, p39)
Cs-135	7.2	IAEA(2010, p18)	18	Kato and Suzuki(2008, p39)
Cs-137	7.2	IAEA(2010, p18)	18	Kato and Suzuki(2008, p39)
Th-232	8.4	Kato and Suzuki(2008, p40)	18	Kato and Suzuki(2008, p39)
U-236	8.4	Kato and Suzuki(2008, p40)	18	Kato and Suzuki(2008, p39)
Pu-240	21.1	IAEA(2010, p18)	5.9	IAEA(2010, p18)
Th-229	8.4	Kato and Suzuki(2008, p40)	18	Kato and Suzuki(2008, p39)
U-233	8.4	Kato and Suzuki(2008, p40)	18	Kato and Suzuki(2008, p39)
Np-237	51	Kato and Suzuki(2008, p40)	51	Kato and Suzuki(2008, p39)
Am-241	51	Kato and Suzuki(2008, p40)	51	Kato and Suzuki(2008, p39)
Cm-245	8.4	Kato and Suzuki(2008, p40)	18	Kato and Suzuki(2008, p39)
Pb-210	8.4	Kato and Suzuki(2008, p40)	18	Kato and Suzuki(2008, p39)
Ra-226	8.4	Kato and Suzuki(2008, p40)	18	Kato and Suzuki(2008, p39)
Th-230	8.4	Kato and Suzuki(2008, p40)	18	Kato and Suzuki(2008, p39)
U-234	8.4	Kato and Suzuki(2008, p40)	18	Kato and Suzuki(2008, p39)
U-238	8.4	Kato and Suzuki(2008, p40)	18	Kato and Suzuki(2008, p39)
Pu-238	21.1	IAEA(2010, p18)	5.9	IAEA(2010, p18)
Pu-242	21.1	IAEA(2010, p18)	5.9	IAEA(2010, p18)
Cm-246	8.4	Kato and Suzuki(2008, p40)	18	Kato and Suzuki(2008, p39)
Ac-227	8.4	Kato and Suzuki(2008, p40)	18	Kato and Suzuki(2008, p39)
Pa-231	8.4	Kato and Suzuki(2008, p40)	18	Kato and Suzuki(2008, p39)
U-235	8.4	Kato and Suzuki(2008, p40)	18	Kato and Suzuki(2008, p39)
Pu-239	21.1	IAEA(2010, p18)	5.9	IAEA(2010, p18)
Am-243	51	Kato and Suzuki(2008, p40)	51	Kato and Suzuki(2008, p39)
Po-210	8.4	Kato and Suzuki(2008, p40)	18	Kato and Suzuki(2008, p39)

(16) Soil to crop concentration factor (Bq/kg)/(Bq/kg)

	Root	Data source	Green	Data source
C-14	-	-	-	-
Cl-36	1.20×10^{1}	IAEA(2010, p64)	2.60×10^{1}	IAEA(2010, p64)
Ni-59	3.00×10^{-2}	Kato and Suzuki(2008, p32)	3.00×10^{-2}	Kato and Suzuki(2008, p31)
Se-79	1.00×10^{0}	Kato and Suzuki(2008, p32)	1.00×10^{0}	Kato and Suzuki(2008, p31)
Sr-90	1.40×10^{-1}	IAEA(2010, p74)	9.80×10^{-1}	IAEA(2010, p74)
Zr-93	4.00×10^{-3}	IAEA(2010, p42)	4.00×10^{-3}	IAEA(2010, p42)
Nb-94	1.70×10^{-2}	IAEA(2010, p42)	1.70×10^{-2}	IAEA(2010, p42)
Tc-99	1.90×10^{0}	IAEA(2010, p74)	7.20×10^{-1}	IAEA(2010, p74)
Pd-107	2.00×10^{-1}	Kato and Suzuki(2008, p32)	2.00×10^{-1}	Kato and Suzuki(2008, p31)
Sn-126	1.00×10^{-1}	Kato and Suzuki(2008, p32)	1.00×10^{-1}	Kato and Suzuki(2008, p31)
I-129	5.60×10^{-2}	IAEA(2010, p74)	3.00×10^{-2}	IAEA(2010, p74)
Cs-135	1.50×10^{-2}	IAEA(2010, p74)	3.80×10^{-2}	IAEA(2010, p74)
Cs-137	1.50×10^{-2}	IAEA(2010, p74)	3.80×10^{-2}	IAEA(2010, p74)
Th-232	1.90×10^{-5}	IAEA(2010, p74)	3.40×10^{-5}	IAEA(2010, p68)
U-236	4.70×10^{-2}	IAEA(2010, p68)	4.80×10^{-2}	IAEA(2010, p68)
Pu-240	4.60×10^{-3}	IAEA(2010, p74)	1.10×10^{-3}	IAEA(2010, p74)
Th-229	1.90×10^{-5}	IAEA(2010, p74)	3.40×10^{-5}	IAEA(2010, p68)
U-233	4.70×10^{-2}	IAEA(2010, p68)	4.80×10^{-2}	IAEA(2010, p68)
Np-237	2.20×10^{-2}	IAEA(2010, p42)	2.70×10^{-2}	IAEA(2010, p42)
Am-241	6.70×10^{-4}	IAEA(2010, p42)	2.70×10^{-4}	IAEA(2010, p42)
Cm-245	8.50×10^{-4}	IAEA(2010, p64)	1.40×10^{-3}	IAEA(2010, p64)
Pb-210	2.40×10^{-3}	IAEA(2010, p68)	3.70×10^{-1}	IAEA(2010, p68)
Ra-226	9.80×10^{-2}	IAEA(2010, p74)	2.70×10^{-2}	IAEA(2010, p74)
Th-230	1.90×10^{-5}	IAEA(2010, p74)	3.40×10^{-5}	IAEA(2010, p68)
U-234	4.70×10^{-2}	IAEA(2010, p68)	4.80×10^{-2}	IAEA(2010, p68)
U-238	4.70×10^{-2}	IAEA(2010, p68)	4.80×10^{-2}	IAEA(2010, p68)
Pu-238	4.60×10^{-3}	IAEA(2010, p74)	1.10×10^{-3}	IAEA(2010, p74)
Pu-242	4.60×10^{-3}	IAEA(2010, p74)	1.10×10^{-3}	IAEA(2010, p74)
Cm-246	8.50×10^{-4}	IAEA(2010, p42)	1.40×10^{-3}	IAEA(2010, p42)
Ac-227	1.00×10^{-3}	Kato and Suzuki(2008, p32)	1.00×10^{-3}	Kato and Suzuki(2008, p31)
Pa-231	4.00×10^{-2}	Kato and Suzuki(2008, p32)	4.00×10^{-2}	Kato and Suzuki(2008, p31)
U-235	4.70×10^{-2}	IAEA(2010, p68)	4.80×10^{-2}	IAEA(2010, p68)
Pu-239	4.60×10^{-3}	IAEA(2010, p74)	1.10×10^{-3}	IAEA(2010, p74)
Am-243	6.70×10^{-4}	IAEA(2010, p42)	2.70×10^{-4}	IAEA(2010, p42)
Po-210	5.80×10^{-3}	IAEA(2010, p42)	7.40×10^{-3}	IAEA(2010, p42)
	Grain	**Data source**	**Fruit**	**Data source**
C-14	-	-	-	-
Cl-36	3.60×10^{1}	IAEA(2010, p64)	5.00×10^{0}	Kato and Suzuki(2008, p30)

Ni-59	2.70×10^{-2}	IAEA(2010, p42)	1.00×10^{-2}	Kato and Suzuki(2008, p31)
Se-79	1.00×10^{0}	Kato and Suzuki(2008, p31)	5.00×10^{-1}	Kato and Suzuki(2008, p31)
Sr-90	5.10×10^{-2}	IAEA(2010, p74)	1.00×10^{-1}	IAEA(2010, p74)
Zr-93	1.00×10^{-3}	IAEA(2010, p42)	4.00×10^{-3}	IAEA(2010, p42)
Nb-94	1.40×10^{-2}	IAEA(2010, p42)	8.00×10^{-3}	IAEA(2010, p42)
Tc-99	3.00×10^{-2}	IAEA(2010, p74)	3.00×10^{-1}	IAEA(2010, p74)
Pd-107	2.00×10^{-1}	Kato and Suzuki(2008, p31)	2.00×10^{-1}	Kato and Suzuki(2008, p31)
Sn-126	2.00×10^{-1}	Kato and Suzuki(2008, p31)	1.00×10^{-1}	Kato and Suzuki(2008, p31)
I-129	1.50×10^{-4}	IAEA(2010, p74)	1.20×10^{-3}	IAEA(2010, p74)
Cs-135	3.00×10^{-3}	IAEA(2010, p74)	2.00×10^{-2}	IAEA(2010, p74)
Cs-137	3.00×10^{-3}	IAEA(2010, p74)	2.00×10^{-2}	IAEA(2010, p74)
Th-232	6.30×10^{-5}	IAEA(2010, p68)	5.30×10^{-6}	IAEA(2010, p68)
U-236	1.80×10^{-2}	IAEA(2010, p68)	4.40×10^{-2}	IAEA(2010, p68)
Pu-240	3.00×10^{-5}	Kato and Suzuki(2008, p31)	8.20×10^{-4}	IAEA(2010, p74)
Th-229	6.30×10^{-5}	IAEA(2010, p68)	5.30×10^{-6}	IAEA(2010, p68)
U-233	1.80×10^{-2}	IAEA(2010, p68)	4.40×10^{-2}	IAEA(2010, p68)
Np-237	2.90×10^{-3}	IAEA(2010, p42)	1.80×10^{-2}	IAEA(2010, p42)
Am-241	2.20×10^{-5}	IAEA(2010, p42)	3.70×10^{-5}	IAEA(2010, p68)
Cm-245	2.30×10^{-5}	IAEA(2010, p42)	3.20×10^{-4}	IAEA(2010, p42)
Pb-210	2.50×10^{-3}	IAEA(2010, p68)	7.00×10^{-3}	IAEA(2010, p68)
Ra-226	3.50×10^{-3}	IAEA(2010, p68)	1.00×10^{-1}	IAEA(2010, p68)
Th-230	6.30×10^{-5}	IAEA(2010, p68)	5.30×10^{-6}	IAEA(2010, p68)
U-234	1.80×10^{-2}	IAEA(2010, p68)	4.40×10^{-2}	IAEA(2010, p68)
U-238	1.80×10^{-2}	IAEA(2010, p68)	4.40×10^{-2}	IAEA(2010, p68)
Pu-238	3.00×10^{-5}	Kato and Suzuki(2008, p31)	8.20×10^{-4}	IAEA(2010, p74)
Pu-242	3.00×10^{-5}	Kato and Suzuki(2008, p31)	8.20×10^{-4}	IAEA(2010, p74)
Cm-246	2.30×10^{-5}	IAEA(2010, p42)	3.20×10^{-4}	IAEA(2010, p42)
Ac-227	1.00×10^{-3}	Kato and Suzuki(2008, p31)	5.00×10^{-5}	Kato and Suzuki(2008, p31)
Pa-231	4.00×10^{-2}	Kato and Suzuki(2008, p31)	4.00×10^{-2}	Kato and Suzuki(2008, p31)
U-235	1.80×10^{-2}	IAEA(2010, p68)	4.40×10^{-2}	IAEA(2010, p68)
Pu-239	3.00×10^{-5}	Kato and Suzuki(2008, p31)	8.20×10^{-4}	IAEA(2010, p74)
Am-243	2.20×10^{-5}	IAEA(2010, p42)	3.70×10^{-5}	IAEA(2010, p68)
Po-210	2.40×10^{-4}	IAEA(2010, p42)	1.90×10^{-4}	IAEA(2010, p42)

(17) Animal product transfer factor from ingestion (d/kg)

	Beef	Data source	Pork	Data source
C-14	1.20×10^{-1}	Kato and Suzuki(2008, p28)	5.80×10^{-1}	Kato and Suzuki(2008, p30)
Cl-36	4.30×10^{-2}	Kato and Suzuki(2008, p28)	2.20×10^{-1}	Kato and Suzuki(2008, p30)
Ni-59	3.00×10^{-2}	Kato and Suzuki(2008, p28)	4.10×10^{-2}	Kato and Suzuki(2008, p30)
Se-79	5.40×10^{-1}	Kato and Suzuki(2008, p28)	3.20×10^{-1}	IAEA(2010, p95)
Sr-90	1.30×10^{-3}	IAEA(2010, p93)	2.50×10^{-3}	IAEA(2010, p95)
Zr-93	1.20×10^{-6}	IAEA(2010, p93)	3.50×10^{-3}	Kato and Suzuki(2008, p30)
Nb-94	2.60×10^{-7}	IAEA(2010, p93)	1.00×10^{-3}	Kato and Suzuki(2008, p30)
Tc-99	6.00×10^{-3}	IAEA(2010, p93)	1.00×10^{-4}	Kato and Suzuki(2008, p30)
Pd-107	7.10×10^{-5}	IAEA(2010, p93)	3.60×10^{-5}	Kato and Suzuki(2008, p30)
Sn-126	1.90×10^{-3}	IAEA(2010, p93)	4.40×10^{-3}	Kato and Suzuki(2008, p30)
I-129	6.70×10^{-3}	IAEA(2010, p93)	4.10×10^{-2}	IAEA(2010, p95)
Cs-135	2.20×10^{-2}	IAEA(2010, p93)	2.00×10^{-1}	IAEA(2010, p95)
Cs-137	2.20×10^{-2}	IAEA(2010, p93)	2.00×10^{-1}	IAEA(2010, p95)
Th-232	2.30×10^{-4}	IAEA(2010, p93)	4.60×10^{-3}	Kato and Suzuki(2008, p30)
U-236	3.90×10^{-4}	IAEA(2010, p93)	4.40×10^{-2}	IAEA(2010, p95)
Pu-240	1.10×10^{-6}	IAEA(2010, p93)	8.30×10^{-5}	Kato and Suzuki(2008, p30)
Th-229	2.30×10^{-4}	IAEA(2010, p93)	4.60×10^{-3}	Kato and Suzuki(2008, p30)
U-233	3.90×10^{-4}	IAEA(2010, p93)	4.40×10^{-2}	IAEA(2010, p95)
Np-237	1.20×10^{-4}	Kato and Suzuki(2008, p28)	4.50×10^{-5}	Kato and Suzuki(2008, p30)
Am-241	5.00×10^{-4}	IAEA(2010, p93)	1.00×10^{-3}	Kato and Suzuki(2008, p30)
Cm-245	9.80×10^{-5}	IAEA(2010, p93)	9.90×10^{-5}	Kato and Suzuki(2008, p30)
Pb-210	7.00×10^{-4}	IAEA(2010, p93)	3.10×10^{-2}	Kato and Suzuki(2008, p30)
Ra-226	1.70×10^{-3}	IAEA(2010, p93)	3.50×10^{-2}	Kato and Suzuki(2008, p30)
Th-230	2.30×10^{-4}	IAEA(2010, p93)	4.60×10^{-3}	Kato and Suzuki(2008, p30)
U-234	3.90×10^{-4}	IAEA(2010, p93)	4.40×10^{-2}	IAEA(2010, p95)
U-238	3.90×10^{-4}	IAEA(2010, p93)	4.40×10^{-2}	IAEA(2010, p95)
Pu-238	1.10×10^{-6}	IAEA(2010, p93)	8.30×10^{-5}	Kato and Suzuki(2008, p30)
Pu-242	1.10×10^{-6}	IAEA(2010, p93)	8.30×10^{-5}	Kato and Suzuki(2008, p30)
Cm-246	9.80×10^{-5}	IAEA(2010, p93)	9.90×10^{-5}	Kato and Suzuki(2008, p30)
Ac-227	1.60×10^{-4}	Kato and Suzuki(2008, p28)	1.70×10^{-4}	Kato and Suzuki(2008, p30)
Pa-231	5.00×10^{-5}	Kato and Suzuki(2008, p28)	1.10×10^{-4}	Kato and Suzuki(2008, p30)
U-235	3.90×10^{-4}	IAEA(2010, p93)	4.40×10^{-2}	IAEA(2010, p95)
Pu-239	1.10×10^{-6}	IAEA(2010, p93)	8.30×10^{-5}	Kato and Suzuki(2008, p30)
Am-243	5.00×10^{-4}	IAEA(2010, p93)	1.00×10^{-3}	Kato and Suzuki(2008, p30)
Po-210	4.00×10^{-3}	Kato and Suzuki(2008, p28)	3.10×10^{-2}	Kato and Suzuki(2008, p30)
	Chicken	**Data source**	**Milk**	**Data source**
C-14	2.30×10^{1}	Kato and Suzuki(2008, p28)	1.00×10^{-2}	Kato and Suzuki(2008, p29)
Cl-36	8.70×10^{0}	Kato and Suzuki(2008, p28)	1.70×10^{-2}	Kato and Suzuki(2008, p29)

Ni-59	1.70×10^{0}	Kato and Suzuki(2008, p28)	9.50×10^{-4}	IAEA(2010, p89)
Se-79	9.70×10^{0}	IAEA(2010, p95)	4.00×10^{-3}	IAEA(2010, p89)
Sr-90	2.00×10^{-2}	IAEA(2010, p95)	1.30×10^{-3}	IAEA(2010, p89)
Zr-93	6.00×10^{-5}	IAEA(2010, p95)	3.60×10^{-6}	IAEA(2010, p89)
Nb-94	3.00×10+	IAEA(2010, p95)	4.10×10^{-7}	IAEA(2010, p89)
Tc-99	1.20×10^{0}	Kato and Suzuki(2008, p29)	7.50×10^{-3}	Kato and Suzuki(2008, p30)
Pd-107	1.40×10^{-3}	Kato and Suzuki(2008, p29)	2.50×10^{-4}	Kato and Suzuki(2008, p30)
Sn-126	1.80×10+	Kato and Suzuki(2008, p29)	1.00×10^{-3}	Kato and Suzuki(2008, p30)
I-129	8.70×10^{-3}	IAEA(2010, p95)	5.40×10^{-3}	IAEA(2010, p89)
Cs-135	2.70×10^{0}	IAEA(2010, p95)	4.60×10^{-3}	IAEA(2010, p89)
Cs-137	2.70×10^{0}	IAEA(2010, p95)	4.60×10^{-3}	IAEA(2010, p89)
Th-232	1.80×10^{-1}	Kato and Suzuki(2008, p29)	5.00×10^{-6}	Kato and Suzuki(2008, p30)
U-236	7.50×10^{-1}	IAEA(2010, p95)	1.80×10^{-3}	IAEA(2010, p89)
Pu-240	1.00×10^{-1}	Kato and Suzuki(2008, p29)	1.00×10^{-5}	IAEA(2010, p89)
Th-229	1.80×10^{-1}	Kato and Suzuki(2008, p29)	5.00×10^{-6}	Kato and Suzuki(2008, p30)
U-233	7.50×10^{-1}	IAEA(2010, p95)	1.80×10^{-3}	IAEA(2010, p89)
Np-237	1.70×10^{-3}	Kato and Suzuki(2008, p29)	5.00×10^{-6}	Kato and Suzuki(2008, p30)
Am-241	1.00×10^{-1}	Kato and Suzuki(2008, p29)	4.20×10^{-7}	IAEA(2010, p89)
Cm-245	4.00×10^{-3}	Kato and Suzuki(2008, p29)	9.00×10^{-6}	Kato and Suzuki(2008, p30)
Pb-210	1.20×10^{0}	Kato and Suzuki(2008, p29)	1.90×10^{-4}	IAEA(2010, p89)
Ra-226	4.80×10^{-1}	Kato and Suzuki(2008, p29)	3.80×10^{-4}	IAEA(2010, p89)
Th-230	1.80×10^{-1}	Kato and Suzuki(2008, p29)	5.00×10^{-6}	Kato and Suzuki(2008, p30)
U-234	7.50×10^{-1}	IAEA(2010, p95)	1.80×10^{-3}	IAEA(2010, p89)
U-238	7.50×10^{-1}	IAEA(2010, p95)	1.80×10^{-3}	IAEA(2010, p89)
Pu-238	1.00×10^{-1}	Kato and Suzuki(2008, p29)	1.00×10^{-5}	IAEA(2010, p89)
Pu-242	1.00×10^{-1}	Kato and Suzuki(2008, p29)	1.00×10^{-5}	IAEA(2010, p89)
Cm-246	4.00×10^{-3}	Kato and Suzuki(2008, p29)	9.00×10^{-6}	Kato and Suzuki(2008, p30)
Ac-227	6.60×10^{-3}	Kato and Suzuki(2008, p29)	4.00×10^{-7}	Kato and Suzuki(2008, p30)
Pa-231	4.10×10^{-3}	Kato and Suzuki(2008, p29)	5.00×10^{-6}	Kato and Suzuki(2008, p30)
U-235	7.50×10^{-1}	IAEA(2010, p95)	1.80×10^{-3}	IAEA(2010, p89)
Pu-239	1.00×10^{-1}	Kato and Suzuki(2008, p29)	1.00×10^{-5}	IAEA(2010, p89)
Am-243	1.00×10^{-1}	Kato and Suzuki(2008, p29)	4.20×10^{-7}	IAEA(2010, p89)
Po-210	2.40×10^{0}	IAEA(2010, p95)	2.10×10^{-4}	IAEA(2010, p89)
	Pig offal	**Data source**	**Egg**	**Data source**
C-14	5.80×10^{-1}	Assume the same with pork	2.30×10^{1}	Kato and Suzuki(2008, p29)
Cl-36	2.20×10^{-1}	Assume the same with pork	8.70×10^{0}	Kato and Suzuki(2008, p29)
Ni-59	4.10×10^{-2}	Assume the same with pork	1.70×10^{0}	Kato and Suzuki(2008, p29)
Se-79	3.20×10^{-1}	Assume the same with pork	1.60×10^{1}	IAEA(2010, p96)
Sr-90	2.50×10^{-3}	Assume the same with pork	3.50×10^{-1}	IAEA(2010, p96)
Zr-93	3.50×10^{-3}	Assume the same with pork	2.00×10^{-4}	IAEA(2010, p96)
Nb-94	1.00×10^{-3}	Assume the same with pork	1.00×10^{-3}	IAEA(2010, p96)

Tc-99	1.00×10^{-4}	Assume the same with pork	1.20×10^{0}	Kato and Suzuki(2008, p29)
Pd-107	3.60×10^{-5}	Assume the same with pork	1.40×10^{-3}	Kato and Suzuki(2008, p29)
Sn-126	4.40×10^{-3}	Assume the same with pork	1.80×10^{-1}	Kato and Suzuki(2008, p29)
I-129	4.10×10^{-2}	Assume the same with pork	2.40×10^{0}	IAEA(2010, p96)
Cs-135	2.00×10^{-1}	Assume the same with pork	4.00×10^{-1}	IAEA(2010, p96)
Cs-137	2.00×10^{-1}	Assume the same with pork	4.00×10^{-1}	IAEA(2010, p96)
Th-232	4.60×10^{-3}	Assume the same with pork	1.80×10^{-1}	Kato and Suzuki(2008, p29)
U-236	4.40×10^{-2}	Assume the same with pork	1.10×10^{0}	IAEA(2010, p96)
Pu-240	8.30×10^{-5}	Assume the same with pork	1.20×10^{-3}	IAEA(2010, p96)
Th-229	4.60×10^{-3}	Assume the same with pork	1.80×10^{-1}	Kato and Suzuki(2008, p29)
U-233	4.40×10^{-2}	Assume the same with pork	1.10×10^{0}	IAEA(2010, p96)
Np-237	4.50×10^{-5}	Assume the same with pork	1.70×10^{-2}	Kato and Suzuki(2008, p29)
Am-241	1.00×10^{-3}	Assume the same with pork	3.00×10^{-3}	IAEA(2010, p96)
Cm-245	9.90×10^{-5}	Assume the same with pork	4.00×10^{-2}	Kato and Suzuki(2008, p29)
Pb-210	3.10×10^{-2}	Assume the same with pork	1.20×10^{0}	Kato and Suzuki(2008, p29)
Ra-226	3.50×10^{-2}	Assume the same with pork	2.50×10^{-1}	Kato and Suzuki(2008, p29)
Th-230	4.60×10^{-3}	Assume the same with pork	1.80×10^{-1}	Kato and Suzuki(2008, p29)
U-234	4.40×10^{-2}	Assume the same with pork	1.10×10^{0}	IAEA(2010, p96)
U-238	4.40×10^{-2}	Assume the same with pork	1.10×10^{0}	IAEA(2010, p96)
Pu-238	8.30×10^{-5}	Assume the same with pork	1.20×10^{-3}	IAEA(2010, p96)
Pu-242	8.30×10^{-5}	Assume the same with pork	1.20×10^{-3}	IAEA(2010, p96)
Cm-246	9.90×10^{-5}	Assume the same with pork	4.00×10^{-2}	Kato and Suzuki(2008, p29)
Ac-227	1.70×10^{-4}	Assume the same with pork	1.60×10^{-2}	Kato and Suzuki(2008, p29)
Pa-231	1.10×10^{-4}	Assume the same with pork	4.10×10^{-3}	Kato and Suzuki(2008, p29)
U-235	4.40×10^{-2}	Assume the same with pork	1.10×10^{0}	IAEA(2010, p96)
Pu-239	8.30×10^{-5}	Assume the same with pork	1.20×10^{-3}	IAEA(2010, p96)
Am-243	1.00×10^{-3}	Assume the same with pork	3.00×10^{-3}	IAEA(2010, p96)
Po-210	3.10×10^{-2}	Assume the same with pork	1.10×10^{0}	IAEA(2010, p96)

(18) Water to water food concentration factor (L/Kg)

	Freshwater fish	Data source	Oyster	Data source
C-14	-	-	-	-
Cl-36	9.50×10^{1}	IAEA(2010, p124)	5.00×10^{-2}	IAEA(2004, p46)
Ni-59	7.10×10^{1}	IAEA(2010, p124)	2.00×10^{3}	IAEA(2004, p46)
Se-79	6.90×10^{3}	IAEA(2010, p124)	9.00×10^{3}	IAEA(2004, p46)
Sr-90	2.00×10^{2}	JNC(2000, pF15)	1.00×10^{1}	IAEA(2004, p46)
Zr-93	9.50×10^{1}	IAEA(2010, p124)	5.00×10^{3}	IAEA(2004, p46)
Nb-94	3.00×10^{2}	JNC(2000, pF15)	1.00×10^{3}	IAEA(2004, p46)
Tc-99	2.00×10^{1}	JNC(2000, pF15)	5.00×10^{2}	IAEA(2004, p46)
Pd-107	2.00×10^{1}	JNC(2000, pF15)	3.00×10^{2}	IAEA(2004, p46)
Sn-126	1.00×10^{3}	JNC(2000, pF15)	5.00×10^{5}	IAEA(2004, p46)
I-129	6.50×10^{2}	IAEA(2010, p124)	1.00×10^{1}	IAEA(2004, p46)
Cs-135	3.00×10^{3}	IAEA(2010, p124)	6.00×10^{1}	IAEA(2004, p46)
Cs-137	3.00×10^{3}	IAEA(2010, p124)	6.00×10^{1}	IAEA(2004, p46)
Th-232	1.90×10^{2}	IAEA(2010, p124)	1.00×10^{3}	IAEA(2004, p46)
U-236	2.40×10^{0}	IAEA(2010, p124)	3.00×10^{1}	IAEA(2004, p46)
Pu-240	4.00×10^{0}	JNC(2000, pF15)	3.00×10^{3}	IAEA(2004, p46)
Th-229	1.90×10^{2}	IAEA(2010, p124)	1.00×10^{3}	IAEA(2004, p46)
U-233	2.40×10^{0}	IAEA(2010, p124)	3.00×10^{1}	IAEA(2004, p46)
Np-237	1.00×10^{1}	JNC(2000, pF15)	4.00×10^{2}	IAEA(2004, p46)
Am-241	8.00×10^{2}	JNC(2000, pF15)	1.00×10^{3}	IAEA(2004, p46)
Cm-245	3.00×10^{1}	JNC(2000, pF15)	1.00×10^{3}	IAEA(2004, p46)
Pb-210	3.70×10^{2}	IAEA(2010, p124)	5.00×10^{4}	IAEA(2004, p46)
Ra-226	2.10×10^{2}	IAEA(2010, p124)	1.00×10^{2}	IAEA(2004, p46)
Th-230	1.90×10^{2}	IAEA(2010, p124)	1.00×10^{3}	IAEA(2004, p46)
U-234	2.40×10^{0}	IAEA(2010, p124)	3.00×10^{1}	IAEA(2004, p46)
U-238	2.40×10^{0}	IAEA(2010, p124)	3.00×10^{1}	IAEA(2004, p46)
Pu-238	4.00×10^{0}	JNC(2000, pF15)	3.00×10^{3}	IAEA(2004, p46)
Pu-242	4.00×10^{0}	JNC(2000, pF15)	3.00×10^{3}	IAEA(2004, p46)
Cm-246	3.00×10^{1}	JNC(2000, pF15)	1.00×10^{3}	IAEA(2004, p46)
Ac-227	8.00×10^{2}	JNC(2000, pF15)	1.00×10^{3}	IAEA(2004, p46)
Pa-231	1.00×10^{1}	JNC(2000, pF15)	5.00×10^{2}	IAEA(2004, p46)
U-235	2.40×10^{0}	IAEA(2010, p124)	3.00×10^{1}	IAEA(2004, p46)
Pu-239	4.00×10^{0}	JNC(2000, pF15)	3.00×10^{3}	IAEA(2004, p46)
Am-243	8.00×10^{2}	JNC(2000, pF15)	1.00×10^{3}	IAEA(2004, p46)
Po-210	5.00×10^{1}	JNC(2000, pF15)	2.00×10^{4}	IAEA(2004, p46)

Reference for Appendix E

Central Weather Bureau (2015)，中華民國104年氣候資料年報第一部分-地面資料，中央氣象局。
Central Weather Bureau (2016)，中華民國105年氣候資料年報第一部分-地面資料，中央氣象局。
Central Weather Bureau (2017)，中華民國106年氣候資料年報第一部分-地面資料，中央氣象局。
Water Resources Agency (2017)，106年水權統計-水權年報-一般水權登記引用水量-地下水，水利署。

Atomic energy council (2005)，游離輻射防護安全標準附表三。
邱立文、黃群修、吳俊奇(2015)，第四次全國森林資源調查，Forestry Bureau。
金門Liquor factory(2019)，金酒Q&A之Q2。2019/10/29取自http://www.kkl.com.tw/tc/faq.aspx。
金門縣政府(2018)，金門新聞，Local government。2019/10/29取自 https://www.kinmen.gov.tw/News_Content2.aspx?n=98E3CA7358C89100&sms=BF7D6D478B935644&s=7C817756AF19774A&Create=1。
金門縣政府主計處(2017)，中華民國一O六年八月份金門縣統計月報，Local government。
Food and Drug Administration (2017)，食品營養成分資料庫。2019/10/29取自 https://consumer.fda.gov.tw/Food/TFND.aspx?nodeID=178。
高苑科技大學綠功能技術研發中心(2011)，國家重要濕地碳匯功能調查計畫總結報告書，Construction and planning Agency。
國民健康署(2019)，對抗夏季，笑「喝」呵，國民健康署預防熱傷害衛教專區，Health Promotion Administration。
國立中興大學(2011)，金門國家公園沿海濕地碳通量調查計畫，National park。
張雅玲(2016)，紅龍果品種特性及栽培管理，Council of Agriculture。
黃玶吉(2017)，用過核子燃料最終處置計畫潛在處置母岩特性調查與評估階段—發展功能/安全評估技術(104-107年度計畫)—生物圈劑量轉換因子研究報告，台灣電力公司委辦計畫，SNFD-04-IPR-008-03，Institute of Nuclear Energy，SNFD-2017。
黃家勤、劉正千、溫清光(2006)，流域非點源污染對於感潮河段動態水質影響之研究，臺南大學環境生態研究所，National Science Council。
楊藹華(2014)，高粱栽培與管理，Council of Agriculture。
潘文涵(2016)，國民營養健康狀況變遷調查(102-105年)，Health Promotion Administration。
鄭祈全(2014)，森林淨初級生產力之遙測估算，Taiwan J For Sci 29(4): 251-66，Forestry Bureau。
謝政融(2015)，探討『火龍果』水足跡之研究ー以台東地區為例，Council of Agriculture。
嚴士潛(2015)，灌溉原理與實用，城邦印書館三版一刷。
Andersson, E., (2010), The limnic ecosystems at Forsmark and Laxemar-Simpevarp, SKB TR-10-02.
Avila, R., Ekström, P. A., (2010), Landscape dose conversion factors used in the safety assessment SR-Site, SKB TR-10-06.
Brouwer C. and Heibloem, M. (1986), Irrigation Water Management: Irrigation Water Needs, FAO Land and Water Development Division.
Eckerman, K. F. and Ryman, J. C. (1993), "External exposure to radionuclides in air, water and soil", FEDERAL GUIDANCE REPORT No. 12, EPA-402-R-93-081.
IAEA (2010), Handbook of Parameter Values for the Prediction of Radionuclide Transfer in Terrestrial and Freshwater Environments, technical reports series NO.472, International Atomic Energy Agency, Vienna.
IAEA (2004), Sediment Distribution Coefficients and Concentration Factors for Biota in the Marine Environment, technical reports series NO.422, International Atomic Energy Agency, Vienna.
IAEA (2003), Reference Biosphere for Solid Radioactive Waste Disposal: Report of BIOMASS Theme 1 of BIOsphere Modelling and ASSessment Programme, IAEA-BIOMASS-6, International Atomic Energy Agency, Vienna.
JNC (2000), H12: Project to Establish the Scientific and Technical Basis for HLW Disposal in Japan – Supporting report 3, Japan Nuclear Cycle Development Institute, JNC TN1410 2000-004.
Kato, T. and Suzuki, Y. (2008), Identification of significant parameters through sensitivity analysis in biosphere assessment of geological disposal, JAEA-Research 2008-021.
Lindborg, T. (2010), Landscape Forsmark – data, methodology and results for SR-Site, SKB TR-10-05.
Löfgren, A., EcoAnalytica (2010), The terrestrial ecosystems at Forsmark and Laxemar-Simpevarp, SKB TR-10-01.
POSIVA (2013), Surface and Near-Surface Hydrological Modelling in the Biosphere Assessment BSA-2012, POSIVA 2012-30.
POSIVA (2014), Data Basis for the Biosphere Assessment BSA-2012, POSIVA 2012-28.
Smith, G. M., Watkins, B. M., Little, R. H., Jones, H. M.and Mortimeer, A. M. (1996), Biosphere Modeling and Dose Assessment for Yucca Mountain, EPRI TR-107190 3294-18.